

# Advances and New Perspectives in Marine Biotechnology

## Volume 1: Marine Animals & Plants

Edited by

Paul F. Long, Bernie Degnan and  
Pabulo H. Rampelotto

Printed Edition of the Special Issue Published in *Marine Drugs*



MDPI

[www.mdpi.com/journal/marinedrugs](http://www.mdpi.com/journal/marinedrugs)

Paul F. Long, Bernie Degnan and Pabulo H. Rampelotto (Eds.)

# **Advances and New Perspectives in Marine Biotechnology**

## **Volume 1: Marine Animals & Plants**



This book is a reprint of the special issue that appeared in the online open access journal *Marine Drugs* (ISSN 1660-3397) in 2014 (available at: [http://www.mdpi.com/journal/marinedrugs/special\\_issues/marine-biotechnology](http://www.mdpi.com/journal/marinedrugs/special_issues/marine-biotechnology)).

*Guest Editors*

Paul F. Long  
Institute of Pharmaceutical Science & Department of Chemistry  
King's College London  
Franklin-Wilkins Building, 150 Stamford Street  
London SE1 9NH, United Kingdom

Bernie Degan  
School of Biological Sciences  
The University of Queensland  
Brisbane, Queensland 4072, Australia

Pabulo H. Rampelotto  
Center of Biotechnology and PPGBCM  
Federal University of Rio Grande do Sul  
Bento Gonçalves Avenue, P.O. Box 15005  
91501-970, Porto Alegre—RS, Brazil

*Editorial*  
MDPI AG  
Klybeckstrasse 64  
Basel, Switzerland

*Office Publisher*  
Shu-Kun Lin

*Managing Editor*  
Alicia Li

**1. Edition 2015**

MDPI • Basel • Beijing • Wuhan • Barcelona

ISBN 978-3-03842-105-4 Volume 1-2 (Hbk)  
ISBN 978-3-03842-108-5 Volume 1-2 (PDF)

ISBN 978-3-03842-106-1 Volume 1 (Hbk) ISBN 978-3-03842-109-2 Volume 1 (PDF)

ISBN 978-3-03842-107-8 Volume 2 (Hbk) ISBN 978-3-03842-110-8 Volume 2 (PDF)

Articles in this volume are Open Access and distributed under the Creative Commons Attribution license (CC BY), which allows users to download, copy and build upon published articles even for commercial purposes, as long as the author and publisher are properly credited, which ensures maximum dissemination and a wider impact of our publications. The book taken as a whole is © 2015 MDPI, Basel, Switzerland, distributed under the terms and conditions of the Creative Commons by Attribution (CC BY-NC-ND) license (<http://creativecommons.org/licenses/by-nc-nd/4.0/>).

# Table of Contents

List of Contributors.....	VII
About the Guest Editors.....	XVI
Preface.....	XVII

**Matteo Francavilla, Massimo Franchi, Massimo Monteleone and Carmela Caroppo**

The Red Seaweed *Gracilaria gracilis* as a Multi Products Source

Reprinted from: *Mar. Drugs* **2013**, 11(10), 3754–3776

<http://www.mdpi.com/1660-3397/11/10/3754> ..... 1

**Atsushi Furuta, Kazi Abdus Salam, Idam Hermawan, Nobuyoshi Akimitsu,**

**Junichi Tanaka, Hidenori Tani, Atsuya Yamashita, Kohji Moriishi,**

**Masamichi Nakakoshi, Masayoshi Tsubuki, Poh Wee Peng, Youichi Suzuki,**

**Naoki Yamamoto, Yuji Sekiguchi, Satoshi Tsuneda and Naohiro Noda**

Identification and Biochemical Characterization of Halisulfate 3 and Suvanine as Novel

Inhibitors of Hepatitis C Virus NS3 Helicase from a Marine Sponge

Reprinted from: *Mar. Drugs* **2014**, 12(1), 462–476

<http://www.mdpi.com/1660-3397/12/1/462> ..... 25

**Eric H. Andrianasolo, Liti Haramaty, Eileen White, Richard Lutz and Paul Falkowski**

Mode of Action of Diterpene and Characterization of Related Metabolites from the Soft

Coral, *Xenia elongate*

Reprinted from: *Mar. Drugs* **2014**, 12(2), 1102–1115

<http://www.mdpi.com/1660-3397/12/2/1102> ..... 40

**Xiaohong Wang, Heinz C. Schröder, Vladislav Grebenjuk, Bärbel Diehl-Seifert,**

**Volker Mailänder, Renate Steffen, Ute Schloßmacher and Werner E. G. Müller**

The Marine Sponge-Derived Inorganic Polymers, Biosilica and Polyphosphate, as

Morphogenetically Active Matrices/Scaffolds for the Differentiation of Human Multipotent

Stromal Cells: Potential Application in 3D Printing and Distraction Osteogenesis

Reprinted from: *Mar. Drugs* **2014**, 12(2), 1131–1147

<http://www.mdpi.com/1660-3397/12/2/1131> ..... 54

- Isabel Rodríguez Amado, José Antonio Vázquez, Pilar González, Diego Esteban-Fernández, Mónica Carrera and Carmen Piñeiro**  
 Identification of the Major ACE-Inhibitory Peptides Produced by Enzymatic Hydrolysis of a Protein Concentrate from Cuttlefish Wastewater  
 Reprinted from: *Mar. Drugs* **2014**, 12(3), 1390–1405  
<http://www.mdpi.com/1660-3397/12/3/1390> ..... 71
- Nathan J. Kenny, Yung Wa Sin, Xin Shen, Qu Zhe, Wei Wang, Ting Fung Chan, Stephen S. Tobe, Sebastian M. Shimeld, Ka Hou Chu and Jerome H. L. Hui**  
 Genomic Sequence and Experimental Tractability of a New Decapod Shrimp Model, *Neocaridina denticulate*  
 Reprinted from: *Mar. Drugs* **2014**, 12(3), 1419–1437  
<http://www.mdpi.com/1660-3397/12/3/1419> ..... 87
- Ge Liu, Ming Liu, Jianteng Wei, Haijuan Huang, Yuyan Zhang, Jin Zhao, Lin Xiao, Ning Wu, Lanhong Zheng and Xiukun Lin**  
 CS5931, a Novel Polypeptide in *Ciona savignyi*, Represses Angiogenesis via Inhibiting Vascular Endothelial Growth Factor (VEGF) and Matrix Metalloproteinases (MMPs)  
 Reprinted from: *Mar. Drugs* **2014**, 12(3), 1530–1544  
<http://www.mdpi.com/1660-3397/12/3/1530> ..... 106
- Veronica Piazza, Ivanka Dragić, Kristina Sepčić, Marco Faimali, Francesca Garaventa, Tom Turk and Sabina Berne**  
 Antifouling Activity of Synthetic Alkylpyridinium Polymers Using the Barnacle Model  
 Reprinted from: *Mar. Drugs* **2014**, 12(4), 1959–1976  
<http://www.mdpi.com/1660-3397/12/4/1959> ..... 121
- Stefano Varrella, Giovanna Romano, Adrianna Ianora, Matt G. Bentley, Nadia Ruocco and Maria Costantini**  
 Molecular Response to Toxic Diatom-Derived Aldehydes in the Sea Urchin *Paracentrotus lividus*  
 Reprinted from: *Mar. Drugs* **2014**, 12(4), 2089–2113  
<http://www.mdpi.com/1660-3397/12/4/2089> ..... 139
- Qiang Liu, Di Wu, Na Ni, Huixia Ren, Chuanming Luo, Chengwei He, Jing-Xuan Kang, Jian-Bo Wan and Huanxing Su**  
 Omega-3 Polyunsaturated Fatty Acids Protect Neural Progenitor Cells against Oxidative Injury  
 Reprinted from: *Mar. Drugs* **2014**, 12(5), 2341–2356  
<http://www.mdpi.com/1660-3397/12/5/2341> ..... 164

**Hideki Kanda, Yuichi Kamo, Siti Machmudah, Wahyudiono and Motonobu Goto**

Extraction of Fucoxanthin from Raw Macroalgae excluding Drying and Cell Wall Disruption by Liquefied Dimethyl Ether

Reprinted from: *Mar. Drugs* **2014**, 12(5), 2383–2396

<http://www.mdpi.com/1660-3397/12/5/2383> ..... 180

**Hsiao-Che Kuo, Hao-Hsuan Hsu, Chee Shin Chua, Ting-Yu Wang, Young-Mao Chen and Tzong-Yueh Chen**

Development of Pedigree Classification Using Microsatellite and Mitochondrial Markers for Giant Grouper Broodstock (*Epinephelus lanceolatus*) Management in Taiwan

Reprinted from: *Mar. Drugs* **2014**, 12(5), 2397–2407

<http://www.mdpi.com/1660-3397/12/5/2397> ..... 194

**Swarna Oli, Usama Ramadan Abdelmohsen, Ute Hentschel and Tanja Schirmeister**

Identification of Plakortide E from the Caribbean Sponge *Plakortis halichondroides* as a Trypanocidal Protease Inhibitor using Bioactivity-Guided Fractionation

Reprinted from: *Mar. Drugs* **2014**, 12(5), 2614–2622

<http://www.mdpi.com/1660-3397/12/5/2614> ..... 205

**Yadollah Bahrami, Wei Zhang and Chris Franco**

Discovery of Novel Saponins from the Viscera of the Sea Cucumber *Holothuria lessona*

Reprinted from: *Mar. Drugs* **2014**, 12(5), 2633–2667

<http://www.mdpi.com/1660-3397/12/5/2633> ..... 214

**Si-Mei Long, Feng-Yin Liang, Qi Wu, Xi-Lin Lu, Xiao-Li Yao, Shi-Chang Li, Jing Li, Huanxing Su, Ji-Yan Pang and Zhong Pei**

Identification of Marine Neuroactive Molecules in Behaviour-Based Screens in the Larval Zebrafish

Reprinted from: *Mar. Drugs* **2014**, 12(6), 3307–3322

<http://www.mdpi.com/1660-3397/12/6/3307> ..... 250

**Bao Nguyen, Jean-Pierre Le Caer, Gilles Mourier, Robert Thai, Hung Lamthanh, Denis Servent, Evelyne Benoit and Jordi Molgó**

Characterization of a Novel *Conus bandanus* Conopeptide Belonging to the M-Superfamily Containing Bromotryptophan

Reprinted from: *Mar. Drugs* **2014**, 12(6), 3449–3465

<http://www.mdpi.com/1660-3397/12/6/3449> ..... 267

- Jabin R. Watson, Timothy C. R. Brennan, Bernard M. Degnan, Sandie M. Degnan and Jens O. Krömer**  
 Analysis of the Biomass Composition of the Demosponge *Amphimedon queenslandica* on Heron Island Reef, Australia  
 Reprinted from: *Mar. Drugs* **2014**, 12(6), 3733–3753  
<http://www.mdpi.com/1660-3397/12/6/3733> ..... 284
- Elango Jeevithan, Bin Bao, Yongshi Bu, Yu Zhou, Qingbo Zhao and Wenhui Wu**  
 Type II Collagen and Gelatin from Silvertip Shark (*Carcharhinus albimarginatus*) Cartilage: Isolation, Purification, Physicochemical and Antioxidant Properties  
 Reprinted from: *Mar. Drugs* **2014**, 12(7), 3852–3873  
<http://www.mdpi.com/1660-3397/12/7/3852> ..... 305
- Natalya V. Ageenko, Konstantin V. Kiselev, Pavel S. Dmitrenok and Nelly A. Odintsova**  
 Pigment Cell Differentiation in Sea Urchin Blastula-Derived Primary Cell Cultures  
 Reprinted from: *Mar. Drugs* **2014**, 12(7), 3874–3891  
<http://www.mdpi.com/1660-3397/12/7/3874> ..... 328
- Natalia V. Zhukova**  
 Lipids and Fatty Acids of Nudibranch Mollusks: Potential Sources of Bioactive Compounds  
 Reprinted from: *Mar. Drugs* **2014**, 12(8), 4578–4592  
<http://www.mdpi.com/1660-3397/12/8/4578> ..... 346
- Fatih Karadeniz, Jung-Ae Kim, Byul-Nim Ahn, Myeong Sook Kwon and Chang-Suk Kong**  
 Effect of *Salicornia herbacea* on Osteoblastogenesis and Adipogenesis *in Vitro*  
 Reprinted from: *Mar. Drugs* **2014**, 12(10), 5132–5147  
<http://www.mdpi.com/1660-3397/12/10/5132> ..... 361
- Ingrid Richter and Andrew E. Fidler**  
 Marine Invertebrate Xenobiotic-Activated Nuclear Receptors: Their Application as Sensor Elements in High-Throughput Bioassays for Marine Bioactive Compounds  
 Reprinted from: *Mar. Drugs* **2014**, 12(11), 5590–5618  
<http://www.mdpi.com/1660-3397/12/11/5590> ..... 378

# List of Contributors

**Usama Ramadan Abdelmohsen:** Department of Botany II, Julius-von-Sachs-Institute for Biological Sciences, University of Würzburg, Julius-von-Sachs Platz 3, Würzburg 97082, Germany; Department of Pharmacognosy, Faculty of Pharmacy, Minia University, Minia 61519, Egypt.

**Natalya V. Ageenko:** Cytotechnology Laboratory, A.V. Zhirmunsky Institute of Marine Biology, FEB RAS, Vladivostok 690041, Russia; Far Eastern Federal University, Sukhanova Str. 8, Vladivostok 690950, Russia.

**Byul-Nim Ahn:** Department of Organic Material Science and Engineering, Pusan National University, Busan 609-735, Korea.

**Nobuyoshi Akimitsu:** Radioisotope Center, The University of Tokyo, 2-11-16 Yayoi, Bunkyo-ku, Tokyo 113-0032, Japan.

**Isabel Rodríguez Amado:** Group of Recycling and Valorisation of Waste Materials (REVAL), Marine Research Institute (IIM-CSIC), r/Eduardo Cabello, 6. Vigo, Galicia 36208, Spain.

**Eric H. Andrianasolo:** Center for Marine Biotechnology, Institute of Marine and Coastal Sciences, Rutgers, The State University of New Jersey, New Brunswick, NJ 08901, USA.

**Yadollah Bahrami:** Department of Medical Biotechnology, School of Medicine, Flinders University, Adelaide 5001, SA 5042, Australia; Centre for Marine Bioproducts Development, Flinders University, Adelaide 5001, SA 5042, Australia; Australian Seafood Cooperative Research Centre, Mark Oliphant Building, Science Park, Adelaide 5001, SA 5042, Australia; Medical Biology Research Center, Kermanshah University of Medical Sciences, Kermanshah 6714415185, Iran.

**Bin Bao:** Department of Marine Pharmacology, College of Food Science and Technology, Shanghai Ocean University, Shanghai 201306, China.

**Evelyne Benoit:** Neurobiology and Development Laboratory, Research Unit # 3294, Institute of Neurobiology Alfred Fessard # 2118, National Center for Scientific Research, Gif sur Yvette Cedex 91198, France.

**Matt G. Bentley.** Dove Marine Laboratory, School of Marine Science and Technology, Newcastle University, Newcastle upon Tyne, UK.

**Sabina Berne:** Department of Biology, Biotechnical Faculty, University of Ljubljana, Večna pot 111, Ljubljana 1000, Slovenia.

**Timothy C. R. Brennan:** Systems and Synthetic Biology Group, Australian Institute for Bioengineering and Nanotechnology, University of Queensland, Brisbane, Queensland 4072, Australia.

**Yongshi Bu:** Department of Marine Pharmacology, College of Food Science and Technology, Shanghai Ocean University, Shanghai 201306, China.

**Carmela Caroppo :** Institute for Coastal Marine Environment, National Research Council, via Roma 3, Taranto 74121, Italy.



**Mónica Carrera:** Institute of Molecular Systems Biology (IMSB), ETH Zürich, Zürich 8093, Switzerland.

**Ting Fung Chan:** School of Life Sciences, The Chinese University of Hong Kong, Shatin, Hong Kong, China.

**Tzong-Yueh Chen:** Laboratory of Molecular Genetics, Institute of Biotechnology, College of Bioscience and Biotechnology, National Cheng Kung University, Tainan 70101, Taiwan; Translational Center for Marine Biotechnology, National Cheng Kung University, Tainan 70101, Taiwan; Agriculture Biotechnology Research Center, National Cheng Kung University, Tainan 70101, Taiwan; University Center of Bioscience and Biotechnology, National Cheng Kung University, Tainan 70101, Taiwan; Research Center of Ocean Environment and Technology, National Cheng Kung University, Tainan 70101, Taiwan.

**Young-Mao Chen:** Laboratory of Molecular Genetics, Institute of Biotechnology, College of Bioscience and Biotechnology, National Cheng Kung University, Tainan 70101, Taiwan; Translational Center for Marine Biotechnology, National Cheng Kung University, Tainan 70101, Taiwan; Agriculture Biotechnology Research Center, National Cheng Kung University, Tainan 70101, Taiwan.

**Ka Hou Chu:** School of Life Sciences, The Chinese University of Hong Kong, Shatin, Hong Kong, China.

**Maria Costantini:** Stazione Zoologica Anton Dohrn, Villa Comunale, Naples 80121, Italy

**Bernard M. Degnan:** School of Biological Science, University of Queensland, Brisbane, Queensland 4072, Australia.

**Sandie M. Degnan:** School of Biological Science, University of Queensland, Brisbane, Queensland 4072, Australia.

**Bärbel Diehl-Seifert:** NanotecMARIN GmbH, 55128 Mainz, Germany.

**Pavel S. Dmitrenok:** Laboratory of Instrumental and Radioisotope Methods of Analysis, G.B. Elyakov Pacific Institute of Bioorganic Chemistry, FEB RAS, Vladivostok 690022, Russia.

**Ivanka Dragič:** Department of Biology, Biotechnical Faculty, University of Ljubljana, Večna pot 111, Ljubljana 1000, Slovenia.

**Diego Esteban-Fernández:** Department of Chemistry, Humboldt-Universität zu Berlin, Brook-Taylor Strasse 2, Berlin 12489, Germany.

**Marco Faimali:** ISMAR—CNR Institute of Marine Science, U.O.S. Genova, Via De Marini 6, 16149 Genova, Italy.

**Paul Falkowski:** Center for Marine Biotechnology, Institute of Marine and Coastal Sciences, Rutgers, The State University of New Jersey, New Brunswick, NJ 08901, USA.

**Andrew E. Fidler:** Environmental Technology Group, Cawthron Institute, Private Bag 2, Nelson 7012, New Zealand; Maurice Wilkins Centre for Molecular Biodiscovery, University of Auckland, Auckland 1142, New Zealand; Institute of Marine Science, University of Auckland, Auckland 1142, New Zealand.

**Matteo Francavilla:** STAR-Agroenergy Research Group, University of Foggia, via Gramsci 89/91, Foggia 71121, Italy; Institute of Marine Science, National Research Council, via Pola 4, Lesina 71010, Italy.

**Massimo Franchi:** Institute of Marine Science, National Research Council, via Pola 4, Lesina 71010, Italy.

**Chris Franco:** Department of Medical Biotechnology, School of Medicine, Flinders University, Adelaide 5001, SA 5042, Australia; Centre for Marine Bioproducts Development, Flinders University, Adelaide 5001, SA 5042, Australia; Australian Seafood Cooperative Research Centre, Mark Oliphant Building, Science Park, Adelaide 5001, SA 5042, Australia.

**Atsushi Furuta:** Department of Life Science and Medical Bioscience, Waseda University, 2-2 Wakamatsu-cho, Shinjuku-ku, Tokyo 162-8480, Japan; Biomedical Research Institute, National Institute of Advanced Industrial Science and Technology (AIST), 1-1-1 Higashi, Tsukuba, Ibaraki 305-8566, Japan.

**Francesca Garaventa:** ISMAR—CNR Institute of Marine Science, U.O.S. Genova, Via De Marini 6, 16149 Genova, Italy.

**Pilar González:** Group of Recycling and Valorisation of Waste Materials (REVAL), Marine Research Institute (IIM-CSIC), r/Eduardo Cabello, 6. Vigo, Galicia 36208, Spain.

**Motonobu Goto:** Japan Science and Technology Agency, Chiyoda, Tokyo 102-0076, Japan

**Vladislav Grebenjuk:** ERC Advanced Investigator Grant Research Group, Institute for Physiological Chemistry, University Medical Center, Johannes Gutenberg University, Duesbergweg 6, D-55128 Mainz, Germany.

**Liti Haramaty:** Center for Marine Biotechnology, Institute of Marine and Coastal Sciences, Rutgers, The State University of New Jersey, New Brunswick, NJ 08901, USA.

**Chengwei He:** State Key Laboratory of Quality Research in Chinese Medicine, Institute of Chinese Medical Sciences, University of Macau, Macao 999078, China.

**Ute Hentschel:** Department of Botany II, Julius-von-Sachs-Institute for Biological Sciences, University of Würzburg, Julius-von-Sachs Platz 3, Würzburg 97082, Germany.

**Idam Hermawan:** Department of Chemistry, Biology and Marine Science, University of the Ryukyus, Nishihara, Okinawa 903-0213, Japan.

**Hao-Hsuan Hsu:** Laboratory of Molecular Genetics, Institute of Biotechnology, College of Bioscience and Biotechnology, National Cheng Kung University, Tainan 70101, Taiwan; Translational Center for Marine Biotechnology, National Cheng Kung University, Tainan 70101, Taiwan; Agriculture Biotechnology Research Center, National Cheng Kung University, Tainan 70101, Taiwan.

**Haijuan Huang:** Qingdao University of Science and Technology, Qingdao 266042, China.

**Jerome H. L. Hui:** School of Life Sciences, The Chinese University of Hong Kong, Shatin, Hong Kong, China.

**Adrianna Ianora:** Stazione Zoologica Anton Dohrn, Villa Comunale, Naples 80121, Italy.

**Elango Jeevithan:** Department of Marine Pharmacology, College of Food Science and Technology, Shanghai Ocean University, Shanghai 201306, China.

**Yuichi Kamo:** Department of Chemical Engineering, Nagoya University, Furo-cho, Chikusa-ku, Nagoya 464-8603, Japan.

**Hideki Kanda:** Department of Chemical Engineering, Nagoya University, Furo-cho, Chikusa-ku, Nagoya 464-8603, Japan; Japan Science and Technology Agency, Chiyoda, Tokyo 102-0076, Japan.

**Jing-Xuan Kang:** Laboratory for Lipid Medicine and Technology, Massachusetts General Hospital and Harvard Medical School, Boston, MA 02114, USA.

**Fatih Karadeniz:** Marine Biotechnology Center for Pharmaceuticals and Foods, Silla University, Busan 617-736, Korea.

**Nathan J. Kenny:** School of Life Sciences, The Chinese University of Hong Kong, Shatin, Hong Kong, China; Department of Zoology, University of Oxford, Oxford OX1 3PS, UK.

**Jung-Ae Kim:** Marine Biotechnology Center for Pharmaceuticals and Foods, Silla University, Busan 617-736, Korea; Department of Food and Nutrition, College of Medical and Life Science, Silla University, Busan 617-736, Korea.

**Konstantin V. Kiselev:** Laboratory of Biotechnology, Institute of Biology and Soil Sciences, FEB RAS, Vladivostok 690022, Russia.

**Chang-Suk Kong:** Department of Food and Nutrition, College of Medical and Life Science, Silla University, Busan 617-736, Korea.

**Jens O. Krömer:** Centre for Microbial Electrosynthesis (CEMES), Advanced Water Management Centre, University of Queensland, Brisbane, Queensland 4072, Australia.

**Hsiao-Che Kuo:** Laboratory of Molecular Genetics, Institute of Biotechnology, College of Bioscience and Biotechnology, National Cheng Kung University, Tainan 70101, Taiwan; Translational Center for Marine Biotechnology, National Cheng Kung University, Tainan 70101, Taiwan; Agriculture Biotechnology Research Center, National Cheng Kung University, Tainan 70101, Taiwan.

**Myeong Sook Kwon:** Department of Food and Nutrition, College of Medical and Life Science, Silla University, Busan 617-736, Korea.

**Hung Lamthanh:** Neurobiology and Development Laboratory, Research Unit # 3294, Institute of Neurobiology Alfred Fessard # 2118, National Center for Scientific Research, Gif sur Yvette Cedex 91198, France; Institute of Biotechnology and Environment, University of Nha Trang, Nha Trang, Khanh Hoa 57000, Vietnam.

**Jean-Pierre Le Caer:** Research Unit # 2301, Natural Product Chemistry Institute, National Center for Scientific Research, Gif sur Yvette Cedex 91198, France.

**Jing Li:** School of Chemistry & Chemical Engineering, Sun Yat-sen University, Guangzhou 510275, China.

**Shi-Chang Li:** School of Chemistry & Chemical Engineering, Sun Yat-sen University, Guangzhou 510275, China.

**Feng-Yin Liang:** Department of Neurology, National Key Clinical Department and Key Discipline of Neurology, Guangdong Key Laboratory for Diagnosis and Treatment of Major Neurological Diseases, The First Affiliated Hospital, Sun Yat-sen University, Guangzhou 510080, China.

**Xiukun Lin:** Department of Pharmacology, Capital Medical University, Beijing 100069, China.

**Ge Liu:** Institute of Oceanology, Chinese Academy of Sciences, 7 Nanhai Road, Qingdao 266071, China; The University of Chinese Academy of Sciences, Beijing 100049, China.

**Ming Liu:** Key Laboratory of Marine Drugs, Ministry of Education, School of Medicine and Pharmacy, Ocean University of China, Qingdao 266003, China.

**Qiang Liu:** State Key Laboratory of Quality Research in Chinese Medicine, Institute of Chinese Medical Sciences, University of Macau, Macao 999078, China.

**Si-Mei Long:** Department of Neurology, National Key Clinical Department and Key Discipline of Neurology, Guangdong Key Laboratory for Diagnosis and Treatment of Major Neurological Diseases, The First Affiliated Hospital, Sun Yat-sen University, Guangzhou 510080, China.

**Xi-Lin Lu:** Department of Neurology, National Key Clinical Department and Key Discipline of Neurology, Guangdong Key Laboratory for Diagnosis and Treatment of Major Neurological Diseases, The First Affiliated Hospital, Sun Yat-sen University, Guangzhou 510080, China.

**Chuanming Luo:** State Key Laboratory of Quality Research in Chinese Medicine, Institute of Chinese Medical Sciences, University of Macau, Macao 999078, China.

**Richard Lutz:** Center for Marine Biotechnology, Institute of Marine and Coastal Sciences, Rutgers, The State University of New Jersey, New Brunswick, NJ 08901, USA.

**Siti Machmudah:** Department of Chemical Engineering, Nagoya University, Furo-cho, Chikusa-ku, Nagoya 464-8603, Japan; Department of Chemical Engineering, Sepuluh Nopember Institute of Technology, Kampus ITS Sukolilo, Surabaya 60111, Indonesia.

**Volker Mailänder:** Max Planck Institute for Polymer Research, Ackermannweg 10, 55129 Mainz, Germany; Medical Clinic, University Medical Center, Johannes Gutenberg University, Langenbeckstr. 1, D-55131 Mainz, Germany.

**Jordi Molgó:** Neurobiology and Development Laboratory, Research Unit # 3294, Institute of Neurobiology Alfred Fessard # 2118, National Center for Scientific Research, Gif sur Yvette Cedex 91198, France.

**Massimo Monteleone:** STAR-Agroenergy Research Group, University of Foggia, via Gramsci 89/91, Foggia 71121, Italy.

**Kohji Moriishi:** Department of Microbiology, Division of Medicine, Graduate School of Medicine and Engineering, University of Yamanashi, 1110 Shimokato, Chuo-shi, Yamanashi 409-3898, Japan.

**Gilles Mourier:** Molecular Engineering of Proteins, Institute of Biology and Technology Saclay, Atomic Energy Commission, Gif sur Yvette Cedex 91191, France.

**Werner E. G. Müller:** ERC Advanced Investigator Grant Research Group, Institute for Physiological Chemistry, University Medical Center, Johannes Gutenberg University, Duesbergweg 6, D-55128 Mainz, Germany.

**Masamichi Nakakoshi:** Institute of Medical Chemistry, Hoshi University, 2-4-41 Ebara, Shinagawa-ku, Tokyo 142-8501, Japan.

**Bao Nguyen:** Neurobiology and Development Laboratory, Research Unit # 3294, Institute of Neurobiology Alfred Fessard # 2118, National Center for Scientific Research, Gif sur Yvette Cedex 91198, France; Institute of Biotechnology and Environment, University of Nha Trang, Nha Trang, Khanh Hoa 57000, Vietnam.

**Na Ni:** State Key Laboratory of Quality Research in Chinese Medicine, Institute of Chinese Medical Sciences, University of Macau, Macao 999078, China.

**Naohiro Noda:** Department of Life Science and Medical Bioscience, Waseda University, 2-2 Wakamatsu-cho, Shinjuku-ku, Tokyo 162-8480, Japan; Biomedical Research Institute, National Institute of Advanced Industrial Science and Technology (AIST), 1-1-1 Higashi, Tsukuba, Ibaraki 305-8566, Japan.

**Nelly A. Odintsova:** Cytotechnology Laboratory, A.V. Zhirmunsky Institute of Marine Biology, FEB RAS, Vladivostok 690041, Russia; Far Eastern Federal University, Sukhanova Str. 8, Vladivostok 690950, Russia.

**Swarna Oli:** Institute of Pharmacy and Biochemistry, Johannes Gutenberg-University of Mainz, Staudinger Weg 5, Mainz 55128, Germany.

**Ji-Yan Pang:** School of Chemistry & Chemical Engineering, Sun Yat-sen University, Guangzhou 510275, China.

**Zhong Pei:** Department of Neurology, National Key Clinical Department and Key Discipline of Neurology, Guangdong Key Laboratory for Diagnosis and Treatment of Major Neurological Diseases, The First Affiliated Hospital, Sun Yat-sen University, Guangzhou 510080, China.

**Poh Wee Peng:** Department of Microbiology, Yong Loo Lin School of Medicine, National University of Singapore, Center for Translational Medicine, 14 Medical Drive, #15-02, Level 15, Singapore 117599, Singapore.

**Veronica Piazza:** ISMAR—CNR Institute of Marine Science, U.O.S. Genova, Via De Marini 6, 16149 Genova, Italy.

**Carmen Piñeiro:** Scientific Instrumentation Service (SICIM), Marine Research Institute (IIM-CSIC), r/ Eduardo Cabello, 6. Vigo, Galicia 36208, Spain.

**Huixia Ren:** State Key Laboratory of Quality Research in Chinese Medicine, Institute of Chinese Medical Sciences, University of Macau, Macao 999078, China.

**Ingrid Richter:** Environmental Technology Group, Cawthron Institute, Private Bag 2, Nelson 7012, New Zealand; School of Biological Science, Victoria University of Wellington, P.O. Box 600, Wellington 6140, New Zealand.

**Giovanna Romano:** Stazione Zoologica Anton Dohrn, Villa Comunale, Naples 80121, Italy.

**Nadia Ruocco:** Stazione Zoologica Anton Dohrn, Villa Comunale, Naples 80121, Italy.

**Kazi Abdus Salam:** Radioisotope Center, The University of Tokyo, 2-11-16 Yayoi, Bunkyo-ku, Tokyo 113-0032, Japan.

**Tanja Schirmeister:** Institute of Pharmacy and Biochemistry, Johannes Gutenberg-University of Mainz, Staudinger Weg 5, Mainz 55128, Germany.

**Ute Schloßmacher:** ERC Advanced Investigator Grant Research Group, Institute for Physiological Chemistry, University Medical Center, Johannes Gutenberg University, Duesbergweg 6, D-55128 Mainz, Germany.

**Heinz C. Schröder:** ERC Advanced Investigator Grant Research Group, Institute for Physiological Chemistry, University Medical Center, Johannes Gutenberg University, Duesbergweg 6, D-55128 Mainz, Germany.

**Yuji Sekiguchi:** Biomedical Research Institute, National Institute of Advanced Industrial Science and Technology (AIST), 1-1-1 Higashi, Tsukuba, Ibaraki 305-8566, Japan.

**Kristina Sepčič:** Department of Biology, Biotechnical Faculty, University of Ljubljana, Večna pot 111, Ljubljana 1000, Slovenia.

**Denis Servent:** Molecular Engineering of Proteins, Institute of Biology and Technology Saclay, Atomic Energy Commission, Gif sur Yvette Cedex 91191, France.

**Xin Shen:** School of Life Sciences, The Chinese University of Hong Kong, Shatin, Hong Kong, China.

**Sebastian M. Shimeld:** Department of Zoology, University of Oxford, Oxford OX1 3PS, UK.

**Chee Shin Chua:** Laboratory of Molecular Genetics, Institute of Biotechnology, College of Bioscience and Biotechnology, National Cheng Kung University, Tainan 70101, Taiwan.

**Yung Wa Sin:** School of Life Sciences, The Chinese University of Hong Kong, Shatin, Hong Kong, China.

**Renate Steffen:** ERC Advanced Investigator Grant Research Group, Institute for Physiological Chemistry, University Medical Center, Johannes Gutenberg University, Duesbergweg 6, D-55128 Mainz, Germany.

**Huanxing Su:** State Key Laboratory of Quality Research in Chinese Medicine, Institute of Chinese Medical Sciences, University of Macau, Macao 999078, China.

**Youichi Suzuki:** Department of Microbiology, Yong Loo Lin School of Medicine, National University of Singapore, Center for Translational Medicine, 14 Medical Drive, #15-02, Level 15, Singapore 117599, Singapore.

**Junichi Tanaka:** Department of Chemistry, Biology and Marine Science, University of the Ryukyus, Nishihara, Okinawa 903-0213, Japan.

**Hidenori Tani:** Research Institute for Environmental Management Technology, National Institute of Advanced Industrial Science and Technology (AIST), 16-1 Onogawa, Tsukuba, Ibaraki 305-8569, Japan.

**Robert Thai:** Molecular Engineering of Proteins, Institute of Biology and Technology Saclay, Atomic Energy Commission, Gif sur Yvette Cedex 91191, France.

**Stephen S. Tobe:** Department of Cell and Systems Biology, University of Toronto, Toronto M5S 3G5, Canada.

**Masayoshi Tsubuki:** Institute of Medical Chemistry, Hoshi University, 2-4-41 Ebara, Shinagawa-ku, Tokyo 142-8501, Japan.

**Satoshi Tsuneda:** Department of Life Science and Medical Bioscience, Waseda University, 2-2 Wakamatsu-cho, Shinjuku-ku, Tokyo 162-8480, Japan.

**Tom Turk:** Department of Biology, Biotechnical Faculty, University of Ljubljana, Večna pot 111, Ljubljana 1000, Slovenia.

**Stefano Varrella:** Stazione Zoologica Anton Dohrn, Villa Comunale, Naples 80121, Italy

**José Antonio Vázquez:** Group of Recycling and Valorisation of Waste Materials (REVAL), Marine Research Institute (IIM-CSIC), r/Eduardo Cabello, 6. Vigo, Galicia 36208, Spain.

**Wahyudiono:** Department of Chemical Engineering, Nagoya University, Furo-cho, Chikusa-ku, Nagoya 464-8603, Japan.

**Jian-Bo Wan:** State Key Laboratory of Quality Research in Chinese Medicine, Institute of Chinese Medical Sciences, University of Macau, Macao 999078, China.

**Ting-Yu Wang:** Laboratory of Molecular Genetics, Institute of Biotechnology, College of Bioscience and Biotechnology, National Cheng Kung University, Tainan 70101, Taiwan; Translational Center for Marine Biotechnology, National Cheng Kung University, Tainan 70101, Taiwan.

**Wei Wang:** School of Life Sciences, The Chinese University of Hong Kong, Shatin, Hong Kong, China.

**Xiaohong Wang:** ERC Advanced Investigator Grant Research Group, Institute for Physiological Chemistry, University Medical Center, Johannes Gutenberg University, Duesbergweg 6, D-55128 Mainz, Germany.

**Jabin R. Watson:** School of Biological Science, University of Queensland, Brisbane, Queensland 4072, Australia.

**Jianteng Wei:** Lanzhou Institute of Chemical Physics, Chinese Academy of Sciences, Lanzhou 730000, China.

**Eileen White:** The Cancer Institute of New Jersey, 195 Little Albany Street, New Brunswick, NJ 08903, USA.

**Di Wu:** State Key Laboratory of Quality Research in Chinese Medicine, Institute of Chinese Medical Sciences, University of Macau, Macao 999078, China.

**Ning Wu:** Institute of Oceanology, Chinese Academy of Sciences, 7 Nanhai Road, Qingdao 266071, China.

**Qi Wu:** Department of Neurology, National Key Clinical Department and Key Discipline of Neurology, Guangdong Key Laboratory for Diagnosis and Treatment of Major Neurological Diseases, The First Affiliated Hospital, Sun Yat-sen University, Guangzhou 510080, China.

**Wenhui Wu:** Department of Marine Pharmacology, College of Food Science and Technology, Shanghai Ocean University, Shanghai 201306, China.

**Lin Xiao:** Qingdao Agricultural University, Qingdao 266109, China.

**Naoki Yamamoto:** Department of Microbiology, Yong Loo Lin School of Medicine, National University of Singapore, Center for Translational Medicine, 14 Medical Drive, #15-02, Level 15, Singapore 117599, Singapore.

**Atsuya Yamashita:** Department of Microbiology, Division of Medicine, Graduate School of Medicine and Engineering, University of Yamanashi, 1110 Shimokato, Chuo-shi, Yamanashi 409-3898, Japan.

**Xiao-Li Yao:** Department of Neurology, National Key Clinical Department and Key Discipline of Neurology, Guangdong Key Laboratory for Diagnosis and Treatment of Major Neurological Diseases, The First Affiliated Hospital, Sun Yat-sen University, Guangzhou 510080, China.

**Wei Zhang:** Department of Medical Biotechnology, School of Medicine, Flinders University, Adelaide 5001, SA 5042, Australia; Centre for Marine Bioproducts Development, Flinders University, Adelaide 5001, SA 5042, Australia; Australian Seafood Cooperative Research Centre, Mark Oliphant Building, Science Park, Adelaide 5001, SA 5042, Australia

**Yuyan Zhang:** Qingdao University of Science and Technology, Qingdao 266042, China.

**Jin Zhao:** Department of Biotechnology, Zhengzhou University, Zhengzhou 450001, China.

**Qingbo Zhao:** Department of Marine Pharmacology, College of Food Science and Technology, Shanghai Ocean University, Shanghai 201306, China.

**Qu Zhe:** School of Life Sciences, The Chinese University of Hong Kong, Shatin, Hong Kong, China.

**Lanhong Zheng:** Yellow Sea Fisheries Research Institute, Chinese Academy of Fishery Sciences, Qingdao 266071, China.

**Yu Zhou:** Department of Marine Pharmacology, College of Food Science and Technology, Shanghai Ocean University, Shanghai 201306, China.

**Natalia V. Zhukova:** Institute of Marine Biology, Far East Branch, Russian Academy of Sciences, Vladivostok 690041, Russia; School of Biomedicine, Far Eastern Federal University, Vladivostok 690950, Russia.



## About the Guest Editors



**Paul F. Long** is a Reader in Pharmacognosy at King's College London. Dr Long has been a Visiting Scientist at the Australian Institute of Marine Science and is currently a Visiting International Research Professor at the University of São Paulo, Brazil. Dr Long's research uses a combination of bioinformatics, laboratory, and field experimental approaches. He is currently interested in understanding the molecular mechanisms underpinning the generation of toxin diversification in cnidarian venoms.



**Bernie Degan** is an Australian Laureate Fellow and Professor at the Centre for Marine Sciences and the School of Biological Sciences at The University of Queensland (UQ) in Brisbane, Australia. He jointly heads the Marine Genomics Lab at UQ, which seeks to understand, through the study of a wide range of marine invertebrates, the genomic mechanisms that underpin the formation and evolution of animals. He was the Director and co-Chair of the 10th International Marine Biotechnology Conference, which was held in Brisbane in 2013. Most of the papers in this edited book come from this conference.



**Pabulo Henrique Rampelotto** is a molecular biologist currently developing his research at the Federal University of Rio Grande do Sul. His work is developed in collaboration with the biotech company, Neoprospecta Microbiome Technologies. Prof. Rampelotto is the founder and Editor-in-Chief of the Springer Book Series “Grand Challenges in Biology and Biotechnology.” He is also an Editor-in-Chief, Associate Editor, Guest Editor, and member of the editorial board of several scientific journals in the field of Life Sciences and Biotechnology. He is best known for his leadership and eminent work as Guest Editor of several successful Special Issues. In his Special Issues, some of the most distinguished team leaders in the field have published their works, ideas, and findings.

# Preface

As the Century of Biology begins to bear fruit, through the translation of predictive biological understanding into applications that enhance the human condition and maintain biodiversity, the almost infinite potential of marine biological resources will be unlocked. Although Marine Biotechnology already has delivered products for medicine, food, bioenergy, nanomaterials, and bioremediation, less than 5% of our vast oceanic environment has been explored. Marine Biotechnology is a scientifically and economically expanding enterprise that is poised to harness the enormous but uncharted functional diversity of marine life, with its novel and rich array of biodesigns and biosynthetic capabilities. From this pursuit comes new genes, chemicals, materials, and inspirations for the benefit of industry, nutrition, and medicine, and which enable the sustainable use and management of the world's oceans. This Special Issue in *Marine Drugs* highlights the cutting-edge developments in Marine Biotechnology with a collection of papers written by authors who are leading experts in the field, including selected papers from the 10th International Marine Biotechnology Conference (IMBC-2013), the premier meeting in marine biotechnology, which is held under the auspices of the International Marine Biotechnology Association.

Paul F. Long, Bernie Degnan, Pabulo H. Rampelotto  
*Guest Editors*



# The Red Seaweed *Gracilaria gracilis* as a Multi Products Source

Matteo Francavilla, Massimo Franchi, Massimo Monteleone and Carmela Caroppo

**Abstract:** In recent years seaweeds have increasingly attracted interest in the search for new drugs and have been shown to be a primary source of bioactive natural compounds and biomaterials. In the present investigation, the biochemical composition of the red seaweed *Gracilaria gracilis*, collected seasonally in the Lesina Lagoon (Southern Adriatic Sea, Lesina, Italy), was assayed by means of advanced analytical techniques, such as gas-chromatography coupled with mass spectrometry and spectrophotometric tests. In particular, analysis of lipids, fatty acids, sterols, proteins, phycobiliproteins and carbohydrates as well as phenolic content, antioxidant and radical scavenging activity were performed. In winter extracts of *G. gracilis*, a high content of R-phycoerythrin together with other valuable products such as arachidonic acid (PUFA  $\omega$ -6), proteins and carbohydrates was observed. High antioxidant and radical scavenging activities were also detected in summer extracts of the seaweed together with a high content of total phenols. In conclusion, this study points out the possibility of using *Gracilaria gracilis* as a *multi products source* for biotechnological, nutraceutical and pharmaceutical applications even although more investigations are required for separating, purifying and characterizing these bioactive compounds.

Reprinted from *Mar. Drugs*. Cite as: Francavilla, M.; Franchi, M.; Monteleone, M.; Caroppo, C. The Red Seaweed *Gracilaria gracilis* as a Multi Products Source. *Mar. Drugs* **2013**, *11*, 375463776.

## 1. Introduction

The marine world, due to its phenomenal biodiversity, is a rich natural resource of many biologically active compounds [1,2]. Many marine organisms live in complex habitats exposed to extreme conditions and, in adapting to new environmental surroundings, they produce a wide variety of primary and secondary metabolites which cannot be found in other organisms. Marine-based bioactive compounds can be derived from a vast array of sources, including marine plants, macro- and microalgae, microorganisms, and sponges, all of which contain their own unique set of biomolecules [3].

Macroalgae, known also as seaweeds, produce many biologically active phytochemicals, which include among others, carotenoids, terpenoids, xanthophylls, chlorophylls, phycobilins, polyunsaturated fatty acids, polysaccharides, vitamins, sterols, tocopherol and phycocyanins [4]. Seaweeds represent 23.4% of the tonnage and 9.7% of the value of the global (marine, brackish water, and freshwater) aquaculture production, estimated at 59.4 million tonnes and \$ 70.3 billion in 2004 [5,6]. They are used as food, fodder, feed and fertilizer [7] and many of the bioactive compounds produced by the macroalgae are known to have potential beneficial use in healthcare [8,9].

*Gracilaria* Greville genus (Gracilariales, Rhodophyta) is represented by more than 300 species of which 160 have been accepted taxonomically. The macroalgae belonging to this genus are important for industrial and biotechnological uses and are considered economically valuable

resources, because of their ability to achieve high yields of commercially valuable biomass [10]. In fact, they contain, besides other compounds, phycocolloids, the main source of agar-agar, which is a gelatinous non-toxic colloidal carbohydrate present in the cell wall and intercellular spaces of the algae and has wide use in the preparation of food, ice creams, jellies, soups, bacteriological samples and cosmetics [7,11]. These algae are also sources of important bioactive metabolites with antibiotic activity; but also sources of different prostaglandins and other substances that may be toxic to humans by causing gastrointestinal disorders and lethality [4].

During the period 1970–1990, in the Mediterranean Lesina Lagoon (Southern Adriatic Sea, Lesina, Foggia, Italy) local fishermen used to harvest the red seaweed *Gracilaria gracilis* (Stackhouse) Steentoft, Irvine *et* Farnham (as *Gracilaria confervoides* Greville) [12,13]. The biomass, after the sun drying process, was sold to some private companies as raw material for agar extraction. The harvested algal biomass reached 100 t dried weight per year [14]. Unfortunately, the over-exploitation of this natural resource contributed to a drastic reduction in production of *Gracilaria* biomass. As a consequence, other seaweeds not economically valuable, like *Valonia aegagropila*, *Chaetomorpha* sp. grew quickly in the Lesina Lagoon, reaching sometimes bloom conditions [15,16].

After this period, some field experiments aimed at re-establishing stable coverage of *Gracilaria gracilis* were carried out successfully in the Lesina Lagoon. These studies pointed out not only an increase in *Gracilaria* biomass (around 1200 t wet weight per year), but also the nutrient uptake capacity of this species in the area of its re-colonization in the lagoon [17]. This aspect is particularly interesting taking into account that *Gracilaria* could also represent a bio-remediator useful to control the risk of eutrophication in this coastal lagoon.

Recently, Francavilla *et al.* [18] found that *Gracilaria* harvested in the Lesina Lagoon could be used as an interesting source of natural porous material with several biotechnological applications. Moreover, Buldarin *et al.* [19] found that microwave (MW)-mediated pyrolysis of this macroalga produced chemical rich bio-oils which are rich in aromatics, sugars and other high value chemicals.

In the light of those results and of worldwide great interest in algae biomass as a source of bioactive compounds (for the nutraceutical, pharmaceutical and cosmetic industry) and new biomaterials, the aim of this work was to screen (for the first time, to the best of our knowledge) the biochemical composition of *Gracilaria gracilis* collected in the Lesina Lagoon, with the idea of taking into account the algal biomass as a hypothetical *multi product source*. In particular, the analysis of lipids, fatty acids, sterols, protein, phycobiliproteins, carbohydrates, as well as phenolic content, antioxidant and radical scavenging activity were performed. Moreover, because biochemical composition depends on many environmental and seasonal factors [20,21], *Gracilaria* was collected seasonally in order to evaluate if there were significant differences in the biochemical composition of this species.

## 2. Results and Discussion

### 2.1. Lipids and Fatty Acids (FAMES)

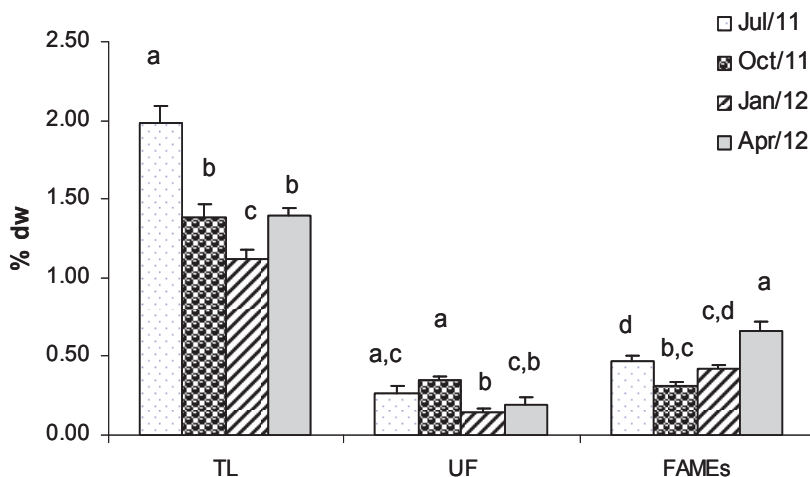
Lipids are a large group of natural compounds which includes fats, waxes, sterols, fat-soluble vitamins (such as vitamins A, D, E and K), monoglycerides, diglycerides, phospholipids, carotenoids and others [22]. They play many biological functions including energy storage, structural components of cell membranes, and signalling molecules. Although humans and other mammals use various biosynthetic pathways to both break down and synthesize lipids, some essential lipids can be obtained only from diet [22].

Figure 1 shows the concentration of total lipids (TL), unsaponified fraction (UF) and fatty acids (FAMES) extracted from *Gracilaria* seaweed. The biomass sampled in July showed the highest lipid content which represented 1.98% dry weight. The lowest concentration in TL was found in winter (January, 1.12% dry weight), whereas intermediate concentrations were found in *Gracilaria* sampled in October and April (1.38% and 1.40% dry weight, respectively). Statistical analyses confirmed that TL values were significantly different in all the seasons, only with comparable values in fall and spring (Figure 1). The detected concentrations were very similar to those measured by other authors in *Gracilaria* sp. [23,24] and confirmed the low lipid content in red seaweeds. Therefore, its contribution as a food energy source appears to be low.

The unsaponified fraction of total lipids, which includes waxes, sterols, fat-soluble vitamins and carotenoids, generally was low and ranged between 0.35% dry weight in October and 0.15% dry weight in January (Figure 1). In this case Tukey's test showed significant differences only in the samples collected in autumn and winter (Figure 1).

With regard to the total amount of FAMES in *Gracilaria*, the highest concentration was observed in biomass collected in April (0.67% dry weight) whereas the lowest concentration was in October (0.31% dry weight). Statistical analyses showed significant differences in terms of FAMES content between samples collected in April and those sampled in the other months (Figure 1). No significant differences were found between samples collected in summer and winter, while samples collected in winter were similar ( $p > 0.05$ ) to those collected in autumn. Fatty acids are precursors in the biosynthesis of eicosanoids, which are important bioregulators of many cellular processes [25–27]. Eicosapentaenoic (EPA) and docosahexaenoic (DHA) polyunsaturated  $\omega$ -3 fatty acids are known to: (i) have capacities for cardioprotection; (ii) reduce triacylglycerol and cholesterol levels; (iii) have antiinflammatory and anticancer effects [28]. FAMES composition in *Gracilaria*, a mixture of 31 compounds, showed significant variation between the analysed seasons (Table 1).

**Figure 1.** Mean concentration (% dry weight) of Total Lipids (TL), Unsaponified fraction (UF) and Fatty Acids Methyl Esters (FAMES) extracted from *G. gracilis*. Different superscripts (a–d) indicate significant difference ( $p < 0.05$ ).



**Table 1.** Fatty Acids composition (% w/w of total amount of fatty acids) of *G. gracilis* sampled in four different seasons.

Fatty Acids Methyl Esters	Structure	Fatty Acid Content (%)			
		11 July	11 October	12 January	12 April
Methyl decanoate	C10:0	0.05 <sup>a</sup>	0.03 <sup>b</sup>	nd	0.03 <sup>b</sup>
Methyl undecanoate	C11:0	0.01	nd	nd	nd
Methyl dodecanoate	C12:0	0.28 <sup>a</sup>	0.35 <sup>a</sup>	0.06 <sup>b</sup>	0.12 <sup>c</sup>
Methyl tridecanoate	C13:0	0.06 <sup>a</sup>	0.07 <sup>a</sup>	0.02 <sup>b</sup>	0.03 <sup>b</sup>
Methyl 9-tetradecanoate	9-C14:1	0.02 <sup>a</sup>	0.39 <sup>b</sup>	0.74 <sup>c</sup>	0.55 <sup>d</sup>
Methyl tetradecanoate	C14:0	5.48 <sup>a</sup>	5.55 <sup>a</sup>	3.48 <sup>b</sup>	5.13 <sup>a</sup>
<i>cis</i> -10 Pentadecenoic Acid Methyl Ester	10-C15:1	nd	0.15 <sup>a</sup>	0.03 <sup>b</sup>	0.04 <sup>b</sup>
Pentadecanoic Acid Methyl Ester	C15:0	1.03 <sup>a</sup>	1.32 <sup>b</sup>	0.52 <sup>c</sup>	0.53 <sup>c</sup>
Palmitoleic Acid Methyl Ester	9-C16:1	3.84 <sup>a</sup>	8.19 <sup>b</sup>	2.21 <sup>c</sup>	8.81 <sup>d</sup>
Palmitic Acid Methyl Ester	C16:0	25.67 <sup>a</sup>	38.13 <sup>b</sup>	28.55 <sup>c</sup>	29.29 <sup>c</sup>
<i>cis</i> -10 Heptadecenoic Acid Methyl Ester	10-C17:1	0.14 <sup>a</sup>	1.12 <sup>b</sup>	0.23 <sup>c</sup>	0.24 <sup>c</sup>
Heptadecanoic Acid Methyl Ester	C17:0	0.64 <sup>a</sup>	1.14 <sup>b</sup>	0.20 <sup>c</sup>	0.30 <sup>c</sup>
Linolenic Acid Methyl Ester	C18:3 <i>n</i> -3	0.42 <sup>a</sup>	0.23 <sup>b</sup>	0.09 <sup>c</sup>	3.88 <sup>d</sup>
Linoleic Acid Methyl Ester	C18:2 <i>n</i> -6 <i>c</i>	4.85 <sup>a</sup>	2.49 <sup>b</sup>	1.33 <sup>c</sup>	4.14 <sup>d</sup>
Oleic Acid Methyl Ester	C18:1 <i>n</i> -9 <i>c</i>	10.78 <sup>a</sup>	8.79 <sup>b</sup>	5.76 <sup>c</sup>	9.12 <sup>b</sup>
Elaidic Acid Methyl Ester	C18:1 <i>n</i> -9 <i>t</i>	4.16 <sup>a</sup>	6.15 <sup>b</sup>	3.22 <sup>c</sup>	2.02 <sup>d</sup>
Stearic Acid Methyl Ester	C18:0	3.35 <sup>a</sup>	3.62 <sup>a</sup>	1.87 <sup>b</sup>	2.30 <sup>c</sup>

**Table 1. Cont.**

Arachidonic Acid Methyl Ester	C20:4 <i>n</i> -6	33.27 <sup>a</sup>	16.05 <sup>b</sup>	47.78 <sup>c</sup>	38.30 <sup>d</sup>
<i>cis</i> -5-8-11-14-17-Eicosapentaenoic Acid Methyl Ester	C20:5 <i>n</i> -3	1.13 <sup>a</sup>	1.84 <sup>b</sup>	0.24 <sup>c</sup>	3.93 <sup>d</sup>
<i>cis</i> -11,14,17-Eicosatrienoic Acid Methyl Ester	C20:3 <i>n</i> -3	2.48 <sup>a</sup>	1.23 <sup>b</sup>	2.07 <sup>c</sup>	2.82 <sup>a</sup>
<i>cis</i> -11,14-Eicosdienoic Acid Methyl Ester	11,14-C20:2	0.32 <sup>a</sup>	0.25 <sup>b</sup>	0.23 <sup>b,c</sup>	0.19 <sup>c</sup>
<i>cis</i> -8,11,14-Eicosatrienoic Acid Methyl Ester	8,11,14-C20:3 <i>n</i> -6	nd	0.32 <sup>a</sup>	0.71 <sup>b</sup>	nd
<i>cis</i> -11 Eicosenoic Acid Methyl Ester	11-C20:1	0.28	nd	nd	nd
Arachidic Acid Methyl Ester	C20:0	0.15 <sup>a</sup>	0.40 <sup>b</sup>	0.08 <sup>c</sup>	0.61 <sup>d</sup>
Heneicosanoic Acid Methyl Ester	C21:1	0.02 <sup>a</sup>	0.02 <sup>a</sup>	0.04 <sup>b</sup>	0.02 <sup>a</sup>
<i>cis</i> -4,7,10,13,16,19-Docosahexaenoic Acid Methyl Ester	C22:6 <i>n</i> -3	0.23 <sup>a</sup>	0.43 <sup>b</sup>	0.03 <sup>c</sup>	0.12 <sup>d</sup>
Erucic Acid Methyl Ester	C22:1 <i>n</i> -9	0.65 <sup>a</sup>	0.34 <sup>b</sup>	0.19 <sup>c</sup>	0.13 <sup>c</sup>
Docosanoic Acid Methyl Ester	C22:0	0.26 <sup>a</sup>	0.38 <sup>b</sup>	0.09 <sup>c</sup>	0.19 <sup>d</sup>
Tricosanoic Acid Methyl Ester	C23:0	0.08 <sup>a</sup>	0.16 <sup>b</sup>	0.02 <sup>c</sup>	0.02 <sup>c</sup>
<i>cis</i> -15-Tetracosenoic Acid Methyl Ester	15-C24:1	0.09 <sup>a</sup>	0.31 <sup>b</sup>	0.15 <sup>c</sup>	0.15 <sup>c</sup>
Tetracosanoic Acid Methyl Ester	C24:0	0.27 <sup>a</sup>	0.56 <sup>b</sup>	0.05 <sup>c</sup>	0.15 <sup>d</sup>
TOTAL (mg g <sup>-1</sup> dry weight)		4.71 <sup>a</sup>	3.14 <sup>b</sup>	4.18 <sup>a</sup>	6.67 <sup>c</sup>
SFA (% w/w)		37.33 <sup>a</sup>	51.71 <sup>b</sup>	34.94 <sup>c</sup>	34.19 <sup>c</sup>
MUFA (% w/w)		19.98 <sup>a</sup>	25.31 <sup>b</sup>	12.54 <sup>c</sup>	18.60 <sup>a</sup>
PUFA (% w/w)		42.70 <sup>a</sup>	22.52 <sup>b</sup>	51.77 <sup>c</sup>	47.18 <sup>a</sup>
PUFA $\omega$ 6 (% w/w)		38.12 <sup>a</sup>	18.86 <sup>b</sup>	49.82 <sup>c</sup>	37.51 <sup>a</sup>
PUFA $\omega$ 3 (% w/w)		4.26 <sup>a</sup>	3.73 <sup>a,b</sup>	2.43 <sup>b</sup>	9.51 <sup>c</sup>
$\omega$ 6/ $\omega$ 3		8.96 <sup>a</sup>	5.06 <sup>b</sup>	20.48 <sup>c</sup>	3.95 <sup>b</sup>

SFA: Saturated Fatty Acids; MUFA: Mono-Unsaturated Fatty Acids; PUFA: Poly-Unsaturated Fatty Acids.  $\omega$ 6/ $\omega$ 3: ratio of  $\omega$ 6 and  $\omega$ 3 Fatty Acids; nd: not detected. <sup>a-d</sup> Row wise values with different superscripts of this type indicate significant difference ( $p < 0.05$ ).

In July, the most abundant FAMES were arachidonic acid (AA-C20:4 *n*-6) and palmitic acid (PA-C16:0). AA reached the highest relative concentration during winter time (January, 48%). The lowest content in AA was found in October (16%) whereas intermediate concentrations were observed in July and April (33% and 38% respectively). Tukey's test revealed significant differences in AA concentration in samples collected in all the seasons (Table 1). Concerning PA, its highest concentration was detected in October (38%) when AA was less concentrated. The lowest value was observed in July (26%). Statistical analyses confirmed significant differences in terms of PA concentration only in these two periods (Table 1). Other abundant fatty acids monitored in *Gracilaria* were: tetradecanoic acid (C14:0), palmitoleic acid (9-C16:1), stearic acid (C18:0), oleic acid (C18:1*n*-9c), elaidic acid (C18:1*n*-9t) and linoleic acid (C18:2*n*-6c). PUFAs (Poly-Unsaturated Fatty Acids) were 52% by total FAMES in January, when also the lowest content in MUFAs (Mono Unsaturated Fatty Acids) and SFAs (Saturated Fatty Acids) was found (20% and 37%, respectively) (Table 1). In October, concentration of PUFAs decreased to 23% and concentration of MUFAs and SFAs reached their highest values (25% and 52%, respectively). In



April, when the highest content in FAMES was found (0.67% dry weight), PUFAs were 47% of total FAMES and MUFAs and SFAs represented 19% and 34% respectively. Arachidonic acid and linoleic acid were the only two PUFAs  $\omega$ -6 present in *Gracilaria*, whereas linolenic acid (C18:3n-3), eicosapentanoic acid (C20:5n-3), eicosatrienoic acid (C20:3n-3) and docosahexanoic acid (C22:6n-3) were the PUFAs  $\omega$ -3 detected.

Statistical analysis showed that in *Gracilaria* biomass the concentrations of palmitoleic acid, elaidic acid, linoleic acid, eicosapentanoic acid and docosahexanoic acid were significantly different in all the seasons. Also the other fatty acids showed significant differences in their concentration but in a reduced number of seasons (Table 1).

Recently, the importance of the  $\omega$ -6/ $\omega$ -3 ratio has been discussed in scientific reports. The original value 1 of the ratio  $\omega$ -6/ $\omega$ -3 involved the balance of intake of both polyunsaturated  $\omega$ -6 and  $\omega$ -3 fatty acids. The high dietary intake of  $\omega$ -6 fatty acids from a diet rich in vegetable oils causes detrimental turnover of the balance ratio ( $\omega$ -6/ $\omega$ -3) to  $\omega$ -3 fatty acids. This ratio is 50 in Europe and the United States, and 12 in Japan, which is compared to 1 for Greenland Eskimos due to their higher consumption of fish fatty acids [29]. A huge intake of  $\omega$ -6 fatty acids and an excessively high  $\omega$ -6/ $\omega$ -3 ratio promotes the pathogenesis of cardiovascular, inflammatory, and autoimmune diseases and cancer [30]. The WHO currently recommends a  $\omega$ -6/ $\omega$ -3 ratio lower than 10. The  $\omega$ -6/ $\omega$ -3 ratio in *Gracilaria* extracts was constantly below this limit. The lowest value was found in samples collected in April when the highest amount of FAMES was found too. Only in January was this ratio higher than 10 because of the high concentration of AA (48%, Table 1). Therefore, taking into account all the results in terms of FAMES, content of PUFAs and  $\omega$ -6/ $\omega$ -3 ratio, *Gracilaria* biomass seems to be an interesting candidate as source of PUFAs and AA if it is harvested in spring, according also to the results reported by MacArtain *et al.* [31].

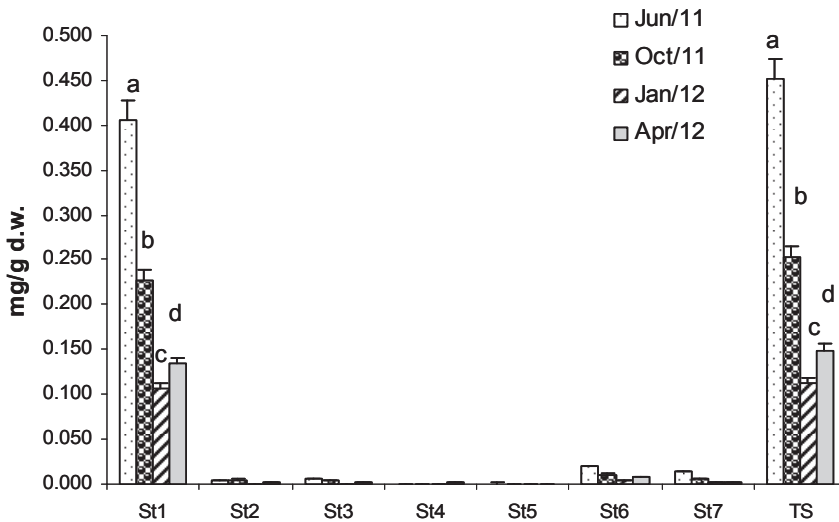
## 2.2. Sterols

The composition of the sterols fraction extracted from *Gracilaria* was investigated in order to explore if phytosterols, sterols with C<sub>28</sub> and C<sub>29</sub> structure, were present. This is because of the great interest in these compounds for their bioactivity and promising nutraceutical and pharmaceutical use. In fact, they are precursors of some bioactive molecules (e.g., ergosterol is a precursor of Vitamin D<sub>2</sub>) and have also been shown to lower total and LDL cholesterol levels in humans by inhibiting cholesterol absorption from the intestine [32]. Moreover, phytosterols possess anti-inflammatory activity and may be characterized by anti-cancer and anti-oxidative activities [33].

Total sterols (TS) concentration, analysed in the unsaponified fraction, was 0.45 mg/g dry weight of biomass in July (Figure 2). This value decreased drastically in January when TS was 0.11 mg/g dry weight cholesterol and TS concentrations were statistically different in all the samples of *Gracilaria* (Figure 2). Seven sterols were identified and corresponded respectively to: cholesterol (*St*<sub>1</sub>), (22*Z*)-ergosta-7,22-dien-3 $\beta$ -ol (*St*<sub>2</sub>), (24*R*)-methylcholest-5-en-3 $\beta$ -ol (*St*<sub>3</sub>), ergostan-5 $\alpha$ -3 $\beta$ -ol (*St*<sub>4</sub>), (24*S*) stigmasta 5,22-dien-3 $\beta$ -ol (*St*<sub>5</sub>), Stigmast-5-en-3 $\beta$ -ol (*St*<sub>6</sub>) and stigmastan-5 $\alpha$ -3 $\beta$ -ol (*St*<sub>7</sub>). Unfortunately, cholesterol was the most abundant, representing about 90% of TS. *St*<sub>6</sub> and *St*<sub>7</sub>, two phytosterols, were 4% and 3% of TS respectively, whereas the remaining sterols were only in

traces. Therefore, unfortunately, *Gracilaria* biomass cannot be considered as a source of phytosterols for nutraceutical applications because of the high content of cholesterol.

**Figure 2.** Concentration (mg g<sup>-1</sup> dry weight of biomass) of Total Sterol (TS) and sterols identified in *G. gracilis*. Cholesterol (*St*<sub>1</sub>), (22*Z*)-ergosta-7,22-dien-3 $\beta$ -ol (*St*<sub>2</sub>), (24*R*)-methylcholest-5-en-3 $\beta$ -ol (*St*<sub>3</sub>), ergostan-5 $\alpha$ -3 $\beta$ -ol (*St*<sub>4</sub>), (24*S*) stigmasta 5,22-dien-3 $\beta$ -ol (*St*<sub>5</sub>), Stigmast-5-en-3 $\beta$ -ol (*St*<sub>6</sub>) and stigmastan-5 $\alpha$ -3 $\beta$ -ol (*St*<sub>7</sub>). Different superscripts (a–d) indicate significant difference ( $p < 0.05$ ).



### 2.3. Proteins

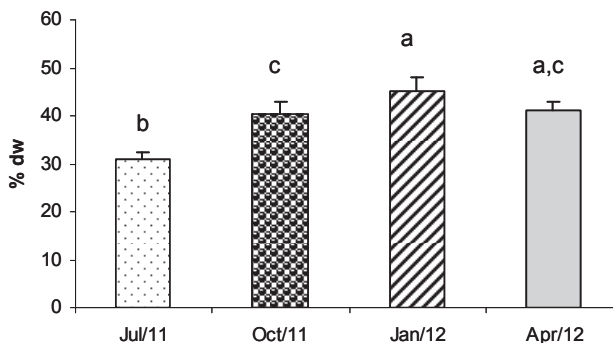
Macroalgae are a unique source of proteins although the content is very variable. Proteins are composed of different amino acids and hence the nutritional quality can be determined basically by the content, proportion and availability of these amino acids. Proteins can have antibacterial, antioxidant, immunostimulating, antithrombotic and anti-inflammatory activities; they can be used for prevention and treatment of hypertension, diabetes and hepatitis among other positive effects in the organism. All these health promoting effects make these compounds of great relevance as nutraceuticals [22]. Analyses of total protein in algae are often done in order to search for new sources of protein supplements. In *Gracilaria* species the protein content found ranged from 5.6% to 30% [34–38].

In this study, *Gracilaria* showed a very interesting protein concentration (Figure 3). In particular the protein content observed in January was 45% dry weight. This value decreased in October and April (about 41% dry weight) and reached the lowest concentration in summer (July, 31% dry weight).

Tukey's test revealed that the protein concentrations were significantly different in all the seasons, except for the samples collected in April when the concentrations were significantly

different only with respect to the value detected in July (Figure 3). Therefore, macroalgal biomass is a very promising source of protein if it is harvested in winter and spring.

**Figure 3.** Concentration (% dry weight) of total proteins in *G. gracilis*. Different superscripts (a–d) indicate significant difference ( $p < 0.05$ ).



#### 2.4. Phycobiliproteins

The phycobiliproteins are proteins with linear tetrapyrrole prosthetic groups (bilins) that, in their functional state, are covalently linked to specific cysteine residues of the proteins. These proteins are found in cyanobacteria (blue-green algae), in a class of biflagellate unicellular eukaryotic algae (cryptomonads), and in Rhodophyta (red algae). In all of them the phycobiliproteins act as photosynthetic accessory pigments.

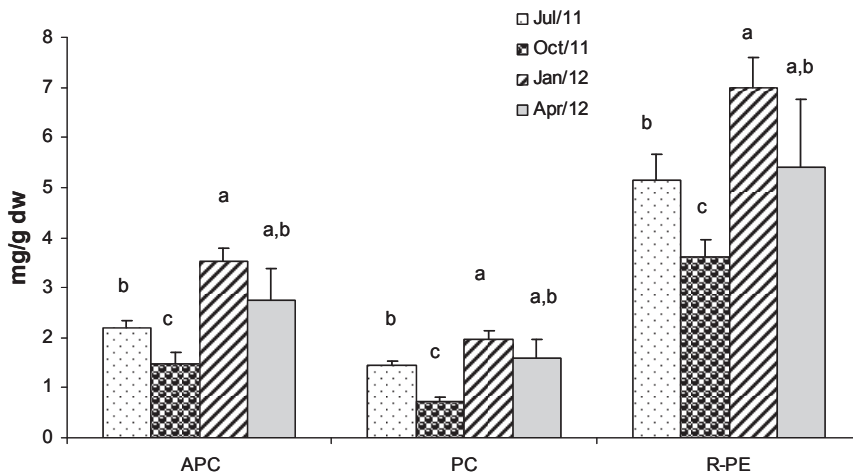
Figure 4 shows the concentrations of phycobiliproteins in *Gracilaria* extracts. R-phycoerythrin (R-PE) is the most abundant with a concentration which ranged between 7 mg/g dry weight in January and 3.6 mg/g dry weight in October. Allophycocyanin (APC) showed lower concentration than R-PE which ranged between 3.5 mg/g dry weight and 1.5 mg/g dry weight, in January and October respectively. Phycocyanin (PC) was the less abundant phycobiliprotein showing a concentration that ranged from 3 mg/g dry weight (d.w.) in January to 0.7 mg/g d.w. in October. Generally, the highest concentrations of the three phycobiliproteins were found in biomass sampled in winter time when light radiation and nutrient concentration in the lagoon are favourable for the biosynthesis of these metabolites [17].

Statistical analyses showed significant differences in terms of phycobiliprotein concentration in all the seasons, except for samples collected in April when the concentrations were significantly different only with respect to the values detected in October (Figure 4).

Phycobiliproteins can be used as very useful fluorescent probes because of their excellent spectroscopic properties [39,40], stability, high absorption coefficients, and high quantum yields. They are highly soluble in water and exhibit a large Stokes shift which is very important for detection [41]. Phycobiliproteins are attractive since they are not harmful to humans if they are applied to an external surface or ingested. They are already used as photosensitizers for treatment of tumors and have potential to substitute Photofrin (a kind of light sensitive agent in photodynamic therapy) in common use which is purified from animal blood [42]. Phycobiliproteins are also widely

used as natural colorants for food and cosmetics. For their wide usage phycobiliproteins have a great economic potential [43,44]. The concentration of R-PE found in *Gracilaria* harvested in winter is very interesting from a biotechnological point of view. Therefore, the algal biomass could be proposed as a novel industrial source of R-PE. Actually, purified R-PE is a very expensive compound which costs about 50 euro per mg (AnaSpec, Inc., Fremont, CA, USA).

**Figure 4.** Concentration ( $\text{mg g}^{-1}$  dry weight) of phycobiliproteins in *G. gracilis*. Allophycocyanin (APC), phycocyanin (PC) and R-phycoerythrin (R-PE). Different superscripts (a–d) indicate significant difference ( $p < 0.05$ ).



### 2.5. Fractionated Extraction of Algal Biomass for Antioxidant Assays and Analysis of Total Phenolic Content

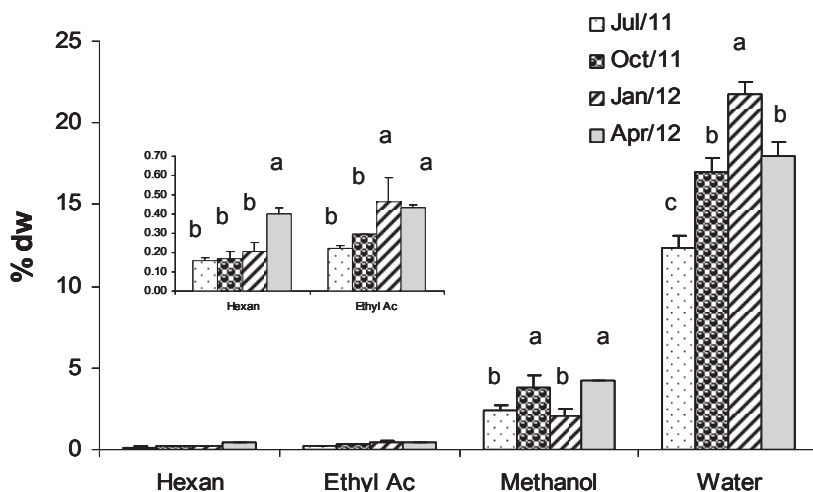
Figure 5 shows concentrations of *Gracilaria* extracts obtained by using four solvents with increasing polarity: *n*-hexane, ethyl acetate, methanol and water (at 80 °C). Results evidenced that the higher the solvent polarity the higher the concentration of extract. Therefore, the highest concentration was found using water (21% dry weight), whereas the lowest one was found using *n*-hexane (0.16% d.w.). Statistically significant differences were detected mainly in the water extracts during all the seasons, except in April when values were comparable with those observed in October (Figure 5). Methanol and ethyl acetate showed intermediate concentrations (4.2% and 0.43% dry weight in April respectively). Generally, extracts of biomass in winter were more concentrated than extracts of biomass in other seasons. Exceptions were represented by the *n*-hexane and methanol extracts that showed the highest concentration in April (0.40% dry weight). Interestingly, in the same sample the highest concentrations of FAMES were also found, which might have been extracted by *n*-hexane.

The dried extracts, dissolved in methanol, were used for antioxidant assays and analysis of phenolic content.

## 2.6. Antioxidant Activity Assays

Reactive oxygen species such as hydroxyl, super oxide and peroxy radicals produced in human tissue cells are responsible for extensive oxidative damage that leads to age related degenerative conditions, cancer and a wide range of other human diseases [45,46].

**Figure 5.** Concentration (% dry weight) of extracts of *G. gracilis* obtained by using four solvents with increasing polarity: *n*-hexane, ethyl acetate, methanol and deionized water (at 80 °C). Different superscripts (a–d) indicate significant difference ( $p < 0.05$ ).



Many researchers have found different types of antioxidants in various species of higher plants [47,48]. However, seaweeds also are considered to be an interesting source of antioxidant compounds. In fact, several researchers have reported the antioxidant properties of both brown and red seaweeds from across the globe [49–52]. Further, the evidence available in the literature suggests the potential protective effects of seaweeds against oxidative stress in target tissues and lipid oxidation in food [53]. To date no reports have identified *Gracilaria gracilis* as a source of antioxidant compounds. While there are two reports of *Gracilaria edulis* showing antioxidant activity it is not possible to compare the antioxidant results reported here and those reported in *Gracilaria edulis* as different extractions methods were used [51,54].

Many authors have stressed the need to carry out more than one type of antioxidant activity measurement to take into account the various mechanisms of antioxidant action [52,55], as no single assay will accurately reflect all of the radical sources or all antioxidants in a mixed or complex system [56].

Three different antioxidant assays were carried out in this study to test the activity of *Gracilaria* extracts: FRAP, ABTS and DPPH assays.

### 2.6.1. Ferric-Reducing Antioxidant Power (FRAP) Assay

The four seasonal extracts showed a high variability in antioxidant activity (as  $\mu\text{mol Trolox g}^{-1}$  extract) (Table 2). Analysing the biomass sampled in July, the highest activity ( $809 \mu\text{mol Trolox g}^{-1}$ ) was found in the ethyl acetate extract. The *n*-hexane extract showed an intermediate value ( $370 \mu\text{mol Trolox g}^{-1}$ ) whereas in the methanol and water fraction the lowest antioxidant activities were found ( $100$  and  $13 \mu\text{mol Trolox g}^{-1}$ , respectively). Interestingly, these values decreased to about 60%–70% in extracts of biomass sampled in October. In fact, the antioxidant activity was  $312 \mu\text{mol Trolox g}^{-1}$  in the ethyl acetate extract,  $114 \mu\text{mol Trolox g}^{-1}$  in hexane,  $27 \mu\text{mol Trolox g}^{-1}$  in methanol and  $9 \mu\text{mol Trolox g}^{-1}$  in the water extract.

**Table 2.** Ferric-reducing antioxidant power (FRAP) ( $\mu\text{mol Trolox g}^{-1}$  extract) of extracts obtained from *G. gracilis* sampled in four different seasons ( $n = 3$ ).

Date	Extracts				
	HE	EA	ME	WT	CTR (BHT)
July/11	$370.74 \pm 18.5^a$	$808.90 \pm 40.4^a$	$99.90 \pm 5.0^a$	$13.32 \pm 0.7^a$	$1917.93 \pm 95.9$
October/11	$114.28 \pm 5.7^b$	$312.47 \pm 15.6^b$	$26.90 \pm 1.3^b$	$9.06 \pm 0.5^b$	
January/12	$189.23 \pm 9.5^c$	$62.02 \pm 3.1^c$	$53.05 \pm 2.7^c$	$9.19 \pm 0.5^b$	
April/12	$117.24 \pm 5.9^b$	$29.82 \pm 1.5^d$	$50.14 \pm 2.5^c$	$14.61 \pm 0.7^a$	

All the values are mean  $\pm$  SD; SD: standard deviation. HE: *n*-Hexan; EA: Ethyl Acetate; ME: methanol; WT: Water ( $80^\circ\text{C}$ ); CTR: Control (butylated hydroxytoluene). <sup>a-d</sup> Column wise values with different superscripts of this type indicate significant difference ( $p < 0.05$ ).

Statistical analyses evidenced significant differences in all the seasons with regard to the ethyl acetate extracts. In the *n*-hexane and methanol extracts differences were evidenced in all the seasons except in April when values were comparable with those detected in October and January, respectively. In water extracts values showed a lower seasonality (Table 2).

Comparing these results with a known and commercial antioxidant, butylated hydroxytoluene (BHT), we found that the ethyl acetate extract (of July) had 42% antioxidant activity by BHT ( $1918 \mu\text{mol Trolox g}^{-1}$ ) (Table 2).

### 2.6.2. ABTS Assay

Results of ABTS antioxidant assay are reported in Table 3 (as  $\text{mmol Trolox g}^{-1}$  extract). Similar to that found using FRAP assay, the highest activity was found in the ethyl acetate extract of biomass sampled in July ( $0.43 \text{ mmol Trolox g}^{-1}$ ). However, this activity decreased only marginally in April ( $0.34 \text{ mmol Trolox g}^{-1}$ ). The hexane extract showed the highest activity in April ( $0.26 \text{ mmol Trolox g}^{-1}$ ) and the lowest in October ( $0.07 \text{ mmol Trolox g}^{-1}$ ). Interestingly, in the methanol and water extracts of *Gracilaria* seaweed the lowest antioxidant activities were found. They ranged between  $0.06$  and  $0.02 \text{ mmol Trolox g}^{-1}$  for methanol extracts and between  $0.15$  and  $0.05 \text{ mmol Trolox g}^{-1}$  for water extracts. As already observed for the FRAP assay, Tukey's test showed significant differences in all the seasons with regard to the ethyl acetate extracts. In the *n*-hexane extracts differences were evidenced in all the seasons except in October when values

were comparable with those detected in July. In the methanol and water extracts values showed a lower seasonality (Table 3).

Surprisingly, antioxidant activity of ethyl acetate extracts for July and April were higher than the activity of gallic acid (0.28 mmol Trolox g<sup>-1</sup>) used as control.

### 2.6.3. DPPH Assay

Table 4 shows the scavenging activity of extracts of *Gracilaria* biomass at different concentrations. EC<sub>50</sub> value (mg extract mL<sup>-1</sup>), the effective concentration at which 50% of the DPPH radicals were scavenged, is used to compare the scavenging activity of extracts.

**Table 3.** Antioxidant activity (mmol Trolox g<sup>-1</sup> extract) of extracts obtained from *G. gracilis* sampled in four different seasons measured using ABTS assay ( $n = 3$ ).

Date	Extracts				
	HE	EA	ME	WT	CTR (GA)
July/11	0.09 ± 0.02 <sup>a</sup>	0.43 ± 0.04 <sup>a</sup>	0.06 ± 0.01 <sup>a</sup>	0.07 ± 0.02 <sup>a</sup>	0.28 ± 0.04
October/11	0.07 ± 0.01 <sup>a</sup>	0.18 ± 0.02 <sup>b</sup>	0.02 ± 0.01 <sup>b</sup>	0.05 ± 0.01 <sup>a</sup>	
January/12	0.16 ± 0.03 <sup>b</sup>	0.26 ± 0.02 <sup>c</sup>	0.06 ± 0.02 <sup>a</sup>	0.10 ± 0.03 <sup>a,b</sup>	
April/12	0.26 ± 0.03 <sup>c</sup>	0.34 ± 0.03 <sup>d</sup>	0.03 ± 0.01 <sup>b</sup>	0.15 ± 0.03 <sup>b</sup>	

All the values are mean ± SD; SD: standard deviation; HE: *n*-Hexan; EA: Ethyl Acetate; ME: methanol; WT: Water (80 °C); CTR: Control (gallic acid). <sup>a-d</sup> Column wise values with different superscripts of this type indicate significant difference ( $p < 0.05$ ).

The ethyl acetate extract of seaweed sampled in July showed the highest scavenging effect, corresponding to the lowest EC<sub>50</sub> (0.82 mg mL<sup>-1</sup>) (Table 4). The hexane extract of the same sample of biomass (July), showed intermediate EC<sub>50</sub> value (1.1 mg mL<sup>-1</sup>) and methanol showed the highest value (2.94 mg mL<sup>-1</sup>). At the concentrations tested, it was not possible to measure the EC<sub>50</sub> of the water extract. Therefore, we reported EC<sub>40</sub>, the concentration at which 40% of the DPPH radicals were scavenged. The EC<sub>40</sub> of the water extract of July was 10 mg mL<sup>-1</sup>.

**Table 4.** DPPH radical scavenging activity (EC<sub>50</sub> value, mg extract mL<sup>-1</sup> methanol) in extracts of *G. gracilis* sampled in four different seasons ( $n = 3$ ).

Date	Extracts				
	HE	EA	ME	WT	CTR (BHT)
11 July	1.1 ± 0.06 <sup>a</sup>	0.82 ± 0.04 <sup>a</sup>	2.94 ± 0.15 <sup>a</sup>	10 ± 0.50 <sup>*</sup>	0.67 ± 0.03
11 October	3.43 ± 0.17 <sup>b</sup>	2.55 ± 0.13 <sup>b</sup>	5.73 ± 0.29 <sup>b</sup>	30.4 ± 1.52 <sup>*</sup>	
12 January	3.32 ± 0.17 <sup>b</sup>	3.47 ± 0.17 <sup>c</sup>	9.72 ± 0.49 <sup>c</sup>	33.17 ± 1.66 <sup>a</sup>	
12 April	4.29 ± 0.21 <sup>c</sup>	7.03 ± 0.35 <sup>d</sup>	8.72 ± 0.44 <sup>c</sup>	35.03 ± 1.75 <sup>a</sup>	

All the values are mean ± SD; SD: standard deviation; HE: *n*-Hexan; EA: Ethyl Acetate; ME: methanol; WT: Water (80 °C); CTR: Control (gallic acid). <sup>a-d</sup> Column wise values with different superscripts of this type indicate significant difference ( $p < 0.05$ ). <sup>\*</sup> EC<sub>40</sub> value (mg extract mL<sup>-1</sup> methanol).

The extracts of *Gracilaria* sampled in other months showed higher EC<sub>50</sub> values than the sample for July (Table 4). In fact, the EC<sub>50</sub> of the ethyl acetate extract of biomass sampled in October was

2.55 mg mL<sup>-1</sup>, hexane extract was 3.43 mg mL<sup>-1</sup> and methanol extract was 5.73 mg mL<sup>-1</sup>. The EC<sub>40</sub> of water extract was 30.4 mg mL<sup>-1</sup>. These values increased in the samples for January and April.

Also the DPPH assay confirmed what already had been observed for the ABTS and FRAP assays. In fact statistical analysis revealed a marked seasonality regarding ethyl acetate extracts. With regard to the *n*-hexane extracts, samples collected in October and January showed comparable values, but significantly different with respect to those collected in the other seasons. Also methanol extracts were characterized by significant differences except for samples collected in spring which were found to be similar to samples collected in winter (Table 4).

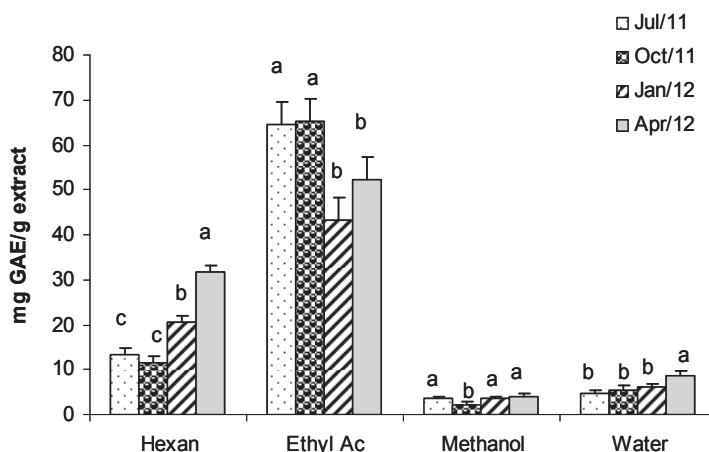
Finally, similar to that which we found for ABTS assay, the EC<sub>50</sub> radical scavenging activity of the ethyl acetate extract of *Gracilaria* sampled in July was very similar to the scavenging activity of BHT used as control (Table 4).

### 2.7. Total Phenolic Content

Phenols are an important group of natural products with antioxidant and other biological activities [57]. These compounds play an important role in algal cell defence against abiotic and biotic stress. Many of them possess antioxidant, antimicrobial and antiviral activities that are important for the protection of algal cells against stress conditions.

Several authors have recently published results regarding the total phenol content and antioxidant activity of algae [51,52].

**Figure 6.** Total Phenolic content (mg GAE g<sup>-1</sup> dry weight extract) in extracts of *G. gracilis*. Different superscripts (a–d) indicate significant difference ( $p < 0.05$ ).



The phenolic content in extracts of *Gracilaria* was very variable even if a marked seasonality was not so evident, as statistical analyses evidenced (Figure 6). The highest concentration was found in the ethyl acetate extract (65 mg GAE g<sup>-1</sup> of extract in July and October), whereas the lowest one was found in the methanol extract (2.3 mg GAE g<sup>-1</sup> of extract in October). Hexane and water extracts showed intermediate values of phenolic content that ranged from 11.56 to 31.8 mg



GAE g<sup>-1</sup> and from 4.7 to 8.8 mg GAE g<sup>-1</sup> respectively. Interestingly, the phenolic content that we found in ethyl acetate extracts of *Gracilaria gracilis* in July and October was higher than the value reported by Ganesan *et al.* [51] for *Gracilaria edulis* (16.26 mg GAE g<sup>-1</sup> of extract).

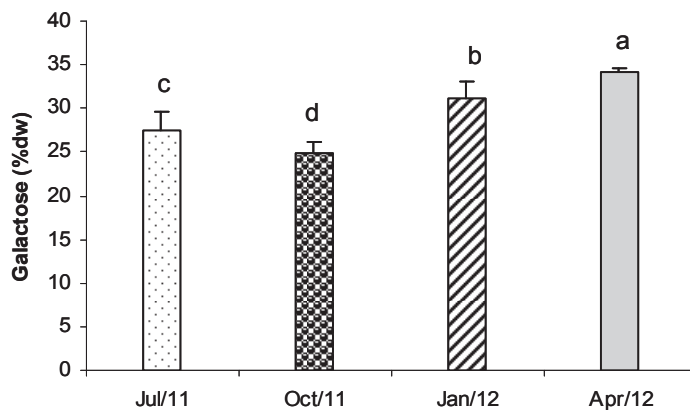
The overlapping of FRAP, TEAC and DPPH assays with the Total Phenols content highlights a positive correlation. In other words, it seems that the antioxidant and scavenging activity is related to phenolic compounds soluble in *n*-hexane and ethyl acetate.

### 2.8. Total Carbohydrates

Carbohydrates perform numerous essential roles in living beings [22]. Monosaccharides are the major source of energy for metabolism while polysaccharides serve for storage of energy and can act as structural components. Furthermore, they have been shown to have other beneficial health effects, including their prebiotic effect and antioxidant or anti-inflammatory activity [58].

In Figure 7 the concentration of total carbohydrates detected in *Gracilaria* is represented. In April, the average carbohydrates content was 34.1% dry weight, while in October it was 24.8% dry weight. In July and January intermediate concentrations were found (27.5% and 31.1% dry weight respectively). Values showed significant differences in all the tested samples (Figure 7). The seasonal variation and the carbohydrate contents that were found in *Gracilaria* biomass were very similar to those reported by Marinho-Soriano and Bourret [59] for the same species collected in the Thau lagoon (France).

**Figure 7.** Total carbohydrate content (% dry weight biomass) in *G. gracilis* extract. Different superscripts (a–d) indicate significant difference ( $p < 0.05$ ).



## 3. Experimental Section

### 3.1. Biomass Sampling

*Gracilaria gracilis* was collected from the western area of the Lesina lagoon, where a stable coverage of this seaweed was found (41.866470° N, 15.363350° E). About 3 Kg of wet biomass were sampled in July and October 2011 and January and April 2012, respectively. Algal biomass

was washed with distilled water and their epiphytes removed. The fresh seaweed was placed in a freezer ( $-20\text{ }^{\circ}\text{C}$ ) immediately after collection. The cleaned seaweed was freeze-dried at  $-110\text{ }^{\circ}\text{C}$  for 3 days and then ground to fine powder and stored in airtight containers at  $-20\text{ }^{\circ}\text{C}$ .

### 3.2. Lipid Extraction

Lipids from the macroalgal pellets were extracted according to Bligh and Dyer [60]. Briefly, 0.5 g of freeze-dried algal biomass were homogenized for 2 min at 12,000 rpm in a mixture of chloroform and methanol (2:1, v/v, 25 mL) using a Kinematica GmgH homogenizer. The mixture was centrifuged and the solid residue re-suspended in a chloroform/methanol mixture (25 mL). Homogenization continued for a further 2 min and the solution was centrifuged again and washed with fresh solvent (25 mL). The combined supernatants were cleaned using a saturated NaCl water solution and the chloroform phase was recovered using a separatory funnel. The water phase was extracted several times with chloroform until the organic solvent was colourless. The chloroform phase was combined and dried with sodium sulphate overnight. The solvent was removed on a rotary evaporator (Büchi Rotavapor) and the purified lipids were weighed.

### 3.3. Saponification of Lipids for Sterols Analysis

Lipids (50 mg under  $\text{N}_2$ ) were saponified by refluxing in 20 mL of a 5% (w/v) KOH methanol/water (4:1, v/v) solution for 2 h. The refluxed mixture was then transferred into a separatory funnel, and the reflux bottle was washed with 40 mL of Milli-Q water. The unsaponified matter in the combined solution was then extracted four times with 20 mL of *n*-hexane. The hexane phases were then combined, dried with sodium sulphate overnight, filtered and evaporated. Sterols content in the unsaponified fraction was analysed by means of GC-MS.

### 3.4. Sterols Analysis by Gaschromatography-Mass Spectrometry (GC-MS)

Purified sterols fraction of *Gracilaria* biomass was analysed by gas chromatography-mass spectrometry as previously described by Francavilla *et al.* [61]. A Varian Saturn 2200 GC/MS/MS ion trap (Varian Analytical Instruments, Walnut Creek, CA, USA) was used. The GC/MS was equipped with a Varian 3800 CP gas chromatograph (GC). A CP-Sil-8 (30 m  $\times$  250  $\mu\text{m}$   $\times$  0.25  $\mu\text{m}$ ) fused silica column (Varian Analytical Instruments, Walnut Creek, CA, USA) was installed in the GC and helium was used as carrier gas at a constant flow rate of 1.0 mL  $\text{min}^{-1}$ .

### 3.5. Fatty Acids Methyl Esters (FAMES) Analysis

Hydroalcolic residue of extraction process of unsaponified fraction was acidified until pH 1 by adding HCl 2 M and extracted 3 times with 25 mL of *n*-hexane. The hexane phases were then combined, dried with sodium sulphate anhydrous, filtered and evaporated. The yellowish viscous liquid obtained (Fatty Acids) was treated with 10 mL of freshly prepared 5% methanolic HCl in a pyrex screw-topped tube. This mixture was carefully mixed and the tube was closed under nitrogen and then heated for 2 h in an oven at  $60\text{ }^{\circ}\text{C}$ . After cooling to room temperature, 5 mL of 6%

aqueous  $K_2CO_3$  were added and the mixture was extracted 4 times with 20 mL of *n*-hexane. The hexane phases were then combined, dried with sodium sulphate anhydrous, filtered and evaporated. The process yielded a yellowish viscous liquid (Fatty Acids Methyl Esters) that was weighed and stored at  $-20\text{ }^\circ\text{C}$  until GC-MS analysis.

FAMEs were analysed by means of the same GC-MS/MS equipment described above for sterols analysis, but with a different column temperature regime:  $140\text{ }^\circ\text{C}$  for 5 min, followed by a  $2\text{ }^\circ\text{C}/\text{min}$  ramp up to  $240\text{ }^\circ\text{C}$ , followed by 5 min at  $240\text{ }^\circ\text{C}$ . The injector temperature was  $250\text{ }^\circ\text{C}$  and the injected volume was  $0.2\text{ }\mu\text{L}$ .

FAME peaks were identified by comparison of their retention times and mass spectra with those of a standard mixture (PUFA C4-C24, Supelco, Bellafonte, PA, USA) whereas they were quantified by using calibration curves made with PUFA C4-C24 standard (Supelco, Bellafonte, PA, USA) and using C15:0 FAME (Supelco, Bellafonte, PA, USA) as internal standard.

### 3.6. Protein Extraction and Analysis

An amount of 50 mg of freeze dried algal sample mixed with 50 mg of alumina was ground manually with pestle and mortar. The mixture was suspended in 5 mL of lysis buffer (0.1 N NaOH, 0.05 M EDTA, 2% SDS, 2%  $\beta$ -mercaptoethanol) [62] for 20 min. After the incubation with buffer, samples were ground for 5 min using a Potter homogeniser (Marconi, model MA099) and kept at room temperature. The mixture was transferred in a centrifuge glass tube and 5 mL of lysis buffer were added to rinse the homogeniser and recover all water-ground material. After this step, samples were centrifuged at  $21\text{ }^\circ\text{C}$ ,  $15,000\times g$  for 20 min. Supernatants were collected for protein assay. The final volume of the extract was 10.0 mL. The extract was diluted (1:100) in MilliQ water for spectrophotometric analysis according to the Lowry method [63]. The spectrophotometer was blanked with MilliQ water to which was added lysis buffer in the same dilution rate of the samples. Calibration curves were prepared using bovine serum albumin (BSA) (Sigma Co., St. Louis, MO, USA) at the maximum concentration of  $100\text{ }\mu\text{g mL}^{-1}$ .

### 3.7. Phycobiliprotein Extraction and Analysis

An amount of 0.5 g of freeze dried algal sample mixed with 0.5 g of alumina was ground manually with pestle and mortar. The mixture was suspended in 10 mL of 1 M acetic acid–sodium acetate buffer (pH 5.5) with 0.01% of sodium azide for 30 min in the dark. After the incubation with buffer, samples were ground for 5 min using a Potter homogeniser (Marconi, model MA099). The mixture was transferred to a centrifuge glass tube centrifuged at  $5\text{ }^\circ\text{C}$ ,  $15,000\times g$  for 20 min. Supernatant was collected and the pellet was extracted three times again with buffer as described. Supernatants were combined and the final volume of the extract was about 40.0 mL. Phycobiliproteins (identified as R-phycoerythrin R-PE, phycocyanin PC and allophycocyanin APC) were quantified by spectrophotometry according to Kursar *et al.* [64].

The absorbance of the aqueous supernatants was determined at 498.5, 614.0, and 651.0 nm and their APC, PC, and R-PE contents were calculated as  $\mu\text{g mL}^{-1}$  using the following Equations (1):

$$\begin{aligned} \text{APC} &= 181.3A_{651} - 22.3A_{614} \\ \text{PC} &= 151.1A_{614} - 99.1A_{651} \\ \text{R-PE} &= 155.8A_{498.5} - 40.0A_{614} - 10.5A_{651} \end{aligned} \quad (1)$$

### 3.8. Fractionated Extraction of Algal Biomass

The extraction procedure of Hajimahmoodi *et al.* [65] was performed. Four solvents with different polarity were used to perform the extractions. They were conveniently selected in order to perform selective extraction of compounds (or better, group of compounds) with different polarities, according to the principle “*similia solunt similibus*”. Briefly, a precisely weighed amount (2 g) of ground dried algal biomass was homogenized at 17,000 rpm, using a Kinematica GmgH homogenizer, twice each time with 20 mL of *n*-hexane at room temperature for 1 min followed by centrifugation. Further extractions in a similar manner were performed sequentially on the pellet using ethyl acetate, methanol and then deionized water (at 80 °C). The isolated supernatants for each solvent were combined. Hexane, ethyl acetate and methanol extracts were evaporated under vacuum and the dried samples were weighed, dissolved in 1 mL of methanol and stored at -20 °C until analysis. The water extract was freeze dried, weighed and dissolved in 5 mL of methanol. The four extracts were used for antioxidant activity assay and analysis of the total phenolic content.

### 3.9. Antioxidant Activity Assays

#### 3.9.1. Reducing Power: The FRAP Assay

The FRAP (ferric-reducing antioxidant power) assay is based on the reduction of a ferric-tripyridyl triazine complex to its ferrous-blue-coloured form in the presence of antioxidants [66]. Briefly, the FRAP reagent contained 5 mL of a TPTZ (2,4,6-tripyridyl-*S*-triazine) solution ( $10 \text{ mmol L}^{-1}$ ) in HCl ( $40 \text{ mmol L}^{-1}$ ) plus 5 mL of  $\text{FeCl}_3$  ( $20 \text{ mmol L}^{-1}$ ) and 50 mL of acetate buffer ( $0.3 \text{ mol L}^{-1}$ , pH 3.6). It was freshly prepared and warmed to 37 °C. A 100  $\mu\text{L}$  sample of each extract (hexane, ethyl acetate, methanol and water) was mixed with 3 mL of FRAP reagent and the absorbance of the reaction mixture was measured at 593 nm after incubation at 37 °C for 10 min. The results could be expressed in micromole of Fe (II), (+) catechin, vitamin C, Trolox or BHT equivalent [67]. For the present study, the standard curve was constructed using Trolox solution (1–30  $\mu\text{M}$ ) and the results were expressed as  $\mu\text{mol Trolox g}^{-1}$  dry weight of extract. Butylated hydroxytoluene (BHT) whose concentration was  $0.1 \text{ mg mL}^{-1}$  was used as positive control.

#### 3.9.2. ABTS Assay

The antioxidant activities of seaweed extracts were also measured by using the ABTS [2-2'-azino-bis (3-ethylbenz-thiazoline-6-sulfonic acid)] assay as described by Matanjun *et al.* [52]. ABTS is a chromogen (colourless) that would be converted to blue-green coloured  $\text{ABTS}^+$  radical cation by an oxidative reagent.  $\text{ABTS}^+$  could also be reduced to its colourless form by antioxidant. The absorbance

was measured spectrophotometrically at 645 nm as a function of concentration and the scavenging percentage of ABTS<sup>+</sup> was calculated relative to Trolox, a water-soluble analogue of vitamin E used as an antioxidant standard.

Briefly, ABTS<sup>+</sup> radical cation was generated by a reaction of 7 mM sample with 2.45 mM potassium persulphate. The reaction mixture was allowed to stand in the dark for 16 h at room temperature. A working solution was prepared by diluting 3 mL of ABTS stock solution with 57 mL phosphate buffered saline (PBS, 5 mM, pH 7.4). A volume of 2 mL of this working solution was dispensed to test tubes. Addition of 200  $\mu$ L diluted methanolic extracts (10  $\mu$ L of extract was diluted with 190  $\mu$ L of methanol, dilution 1:20) initiated the reaction and absorbance was read after exactly 6 min. Gallic acid (GA) at the concentration of 0.1 mg mL<sup>-1</sup> was used as positive control. The results were expressed as mmol Trolox g<sup>-1</sup> dry weight of extract.

### 3.9.3. DPPH Radical Scavenging Activity

This activity was detected by the method of Hu *et al.* [68]. An aliquot of each sample (30  $\mu$ L, 0.5–30 mg/mL) in acetone/MeOH (1/1, v/v) was mixed with 200  $\mu$ L of 100  $\mu$ M DPPH (2,2-diphenyl-2-picrylhydrazyl hydrate) prepared with methanol. The mixture was shaken vigorously and then left to stand at room temperature for 60 min in the dark. The absorbance was measured spectrophotometrically at 520 nm against an acetone/MeOH (1/1, v/v) blank. The lower absorbance indicated the stronger scavenging activity. EC<sub>50</sub> value (mg extract mL<sup>-1</sup>), the effective concentration at which 50% of the DPPH radicals were scavenged, was obtained from the plot of scavenging activity against the concentration of extract. The scavenging activity was calculated based on the percentage of DPPH radical scavenged using the follow Equation (2) [50]:

$$\text{Scavenging effect (\%)} = [1 - (A_{\text{sample}} - A_{\text{sample blank}})/A_{\text{control}}] \times 100 \quad (2)$$

where the  $A_{\text{control}}$  is the absorbance of the control (DPPH solution without extract), the  $A_{\text{sample}}$  is the absorbance of the test extract (DPPH solution plus test extract), and the  $A_{\text{sample blank}}$  is the absorbance of the extract only (extract without DPPH solution). Butylated hydroxytoluene (BHT), a synthetic antioxidant, was used as positive control.

### 3.10. Determination of Total Phenolic Content

Total phenolics were colorimetrically determined using Folin-Ciocalteu reagent as described by Velioglu *et al.* [69] with slight modifications. The extract (200  $\mu$ L) was mixed with 1.5 mL of Folin-Ciocalteu reagent (previously diluted tenfold with distilled water) and allowed to stand at room temperature for 5 min. A 1.5 mL sodium bicarbonate solution (60 g L<sup>-1</sup>) was added to the mixture. After incubation for 90 min at room temperature, the absorbance was measured at 750 nm. Total phenolics were quantified by a calibration curve obtained from measuring the absorbance of known concentrations of gallic acid standard solutions (25–150  $\mu$ g mL<sup>-1</sup> in 50% methanol). The results were calculated as gallic acid equivalent (GAE) g<sup>-1</sup> dry weight of extract.

### 3.11. Total Carbohydrates

Total carbohydrate content was assayed by the phenolsulphuric acid method [70] after extraction with 2.5 N HCl for 3 h at 100 °C. The results were calculated from a galactose standard curve and reported as % dry weight of algal biomass.

### 3.12. Statistical Analyses

All the experiments were repeated three times. Unless otherwise stated, all data were expressed as mean  $\pm$  standard deviation (SD). The means of all the parameters were examined for significance by analysis of variance (ANOVA) using the software JMP version 9 (SAS Institute Inc., Cary, NC, USA). When *F* values showed significance, individual means were compared using Tukey's honest significant difference (HSD). Significant differences were considered when  $p < 0.05$ .

## 4. Conclusions

*Gracilaria gracilis* of Lesina Lagoon is a natural marine biomass which has already been found interesting for several applications including agar, as mesoporous material and for bio-oils production. The results of this study highlight that this marine biomass seems to be also a promising source of R-phycoerythrin if it is harvested in winter time. In the same season, the red seaweed also contains a high amount of other valuable products including arachidonic acid (PUFA  $\omega$ -6), proteins and carbohydrates. High antioxidant and radical scavenging activity, comparable to that of commercial antioxidants compounds, was found in biomass harvested in summer time when the highest concentration of total phenols was also detected. However, more investigations are required for separating, purifying and characterizing these bioactive compounds. Furthermore, it will be necessary to deepen the knowledge of the biology of this macroalga in the Lesina Lagoon, by considering the life cycle and the reproductive peaks to optimize the exploitation of the species and to safeguard its presence in the lagoon.

In conclusion, this study pointed out the possibility of using *Gracilaria gracilis* as a *multi products source* for biotechnological, nutraceutical and pharmaceutical applications according to the new concept of "Biorefinery". Nevertheless, it will be very important to investigate the economic and environmental affordability and sustainability of *Gracilaria* natural resource by means of Life Cycle Assessment.

## Acknowledgments

Matteo Francavilla gratefully acknowledges the European Commission, Directorate-General for Research & Innovation, for funding the project "STAR AgroEnergy" (FP7 Regpot 2011-1, Grant Agreement No. 286269) as well as Fondazione Cassa di Risparmio di Puglia for funding the project MADLENA.

## Conflicts of Interest

The authors declare no conflict of interest.

## References

1. Molinski, T.F.; Dalisay, D.S.; Lievens, S.L.; Saludes, J.P. Drug development from marine natural products. *Nat. Rev. Drug Discov.* **2009**, *8*, 69–85.
2. Lordan, S.; Ross, R.P.; Stanton, C. Marine bioactives as functional food ingredients: Potential to reduce the incidence of chronic diseases. *Mar. Drugs* **2011**, *9*, 1056–1100.
3. Rasmussen, R.S.; Morrissey, M.T. Marine biotechnology for production of food ingredients. *Adv. Food Nutr. Res.* **2007**, *52*, 237–292.
4. De Almeida, C.L.F.; de S. Falcão, H.; de M. Lima, G.R.; de A. Montenegro, C.; Lira, N.S.; de Athayde-Filho, P.F.; Rodrigues, L.C.; de Souza, M.F.V.; Barbosa-Filho, J.M.; Batista, L.M. Bioactivities from marine algae of the genus *Gracilaria*. *Int. J. Mol. Sci.* **2011**, *12*, 4550–4573.
5. Food and Agriculture Organization of the United Nations. In *Year Book of Fishery and Aquaculture Statistics (2006)*; Food and Agricultural Organisation of the United Nations: Rome, Italy, 2008; Volume 98, p. 57.
6. Bourgoignon, N.; Stiger-Pouvreau, V. Red and Brown Macroalgae along the French Coasts, Metropole and Overseas Departements and Territories. In *Handbook of Marine Macroalgae: Biotechnology and Applied Phycology*, 1st ed.; Se-Kwon, K., Ed.; JohnWiley & Sons, Ltd.: New Delhi, India, 2012; pp. 58–105.
7. Ghosh, R.; Banerjee, K.; Mitra, A. Eco-Biochemical Studies of Common Seaweeds in the Lower Gangetic Delta. In *Handbook of Marine Macroalgae: Biotechnology and Applied Phycology*, 1st ed.; Se-Kwon, K., Ed.; JohnWiley & Sons, Ltd.: New Delhi, India, 2012; pp. 45–57.
8. Smit, A.J. Medicinal and pharmaceutical uses of seaweed natural products: A review. *J. Appl. Phycol.* **2004**, *16*, 245–262.
9. Kadam, S.; Prabhasankar, P. Marine foods as functional ingredients in bakery and pasta products. *Food Res. Int.* **2010**, *43*, 1975–1980.
10. Capo, T.R.; Jaramillo, J.C.; Boyd, A.E.; Lapointe, B.E.; Serafy, J.E. Sustained high yields of *Gracilaria* (Rhodophyta) grown in intensive large-scale culture. *J. Appl. Phycol.* **1999**, *11*, 143–147.
11. Kerton, F.M.; Liu, Y.; Omania, K.W.; Hawboldt, K. Green chemistry and the ocean-based biorefinery. *Green Chem.* **2013**, *15*, 860–871.
12. Trotta, P. On the Rhodophyta *Gracilaria confervoides* Grev. in Lesina lagoon: Field Survey and *in Vitro* Culture. In Proceedings of the International Congress Phytodepuration and Biomass Utilization, Parma, Italy, 15–16 May 1981; pp. 91–96.
13. D’Adamo, R.; Cecere, E.; Fabbrocini, A.; Petrocelli, A.; Sfriso, A. The Lagoons of Lesina and Varano. In *Flora and Vegetation of the Italian Transitional Water Systems*; Cecere, E., Petrocelli, A., Izzo, G., Sfriso, A., Eds.; Spinea, CORILA, Multigraph: Venezia, Italy, 2009; pp. 159–171.

14. Trotta, P. La pesca, la qualità delle acque, gli scarichi in laguna. In Proceedings of the Conference La laguna di Lesina: Quali prospettive, Quali soluzioni, Lesina (FG), Italy, 11 December 1994; pp. 11–21.
15. Manini, E.; Fiordelmondo, C.; Gambi, C.; Pusceddu, A.; Danovaro, R. Benthic microbial loop functioning in coastal lagoons: A comparative approach. *Oceanol. Acta* **2003**, *26*, 27–38.
16. Nonnis Marzano, C.; Scalera Liaci, L.; Franchini, A.; Gravina, F.; Mercurio, M.; Corriero, G. Distribution, persistence and change in the macrobenthos of the lagoon of Lesina (Apulia, southern Adriatic Sea). *Oceanol. Acta* **2003**, *26*, 57–66.
17. Francavilla, M. Riabilitazione delle acque lagunari salmastre attraverso la gestione di praterie di macroalghe di valore commerciale. Ph.D. Thesis, Università di Foggia, Facoltà di Agraria, Foggia, Italy, 2007.
18. Francavilla, M.; Pineda, A.; Lin, C.S.K.; Franchi, M.; Trotta, P.; Romero, A.A.; Luque, R. Natural porous agar materials from macroalgae. *Carbohydr. Polym.* **2013**, *92*, 1555–1560.
19. Budarin, V.L.; Zhao, Y.; Gronnow, M.J.; Shuttleworth, P.S.; Breeden, S.W.; Macquarrie, D.J.; Clark, J.H. Microwave-mediated pyrolysis of macro-algae. *Green Chem.* **2011**, *13*, 2330–2333.
20. Dawczynski, C.; Schubert, R.; Jahreis, G. Amino acids, fatty acids, and dietary fibre in edible seaweed products. *Food Chem.* **2007**, *103*, 891–899.
21. Bocanegra, A.; Bastida, S.; Benedí, J.; Ródenas, S.; Sánchez-Muniz, F.J. Characteristics and nutritional and cardiovascular-health properties of seaweeds. *J. Med. Food* **2009**, *12*, 236–258.
22. Bernal, J.; Mendiola, J.A.; Ibañez, E.; Cifuentes, A. Advanced analysis of nutraceuticals. *J. Pharm. Biomed. Anal.* **2011**, *55*, 758–774.
23. Burtin, P. Nutritional value of seaweeds. *Electron. J. Environ. Agric. Food Chem.* **2003**, *2*, 498–503.
24. Mišurcová, L. Chemical Composition of Seaweeds. In *Handbook of Marine Macroalgae: Biotechnology and Applied Phycology*, 1st ed.; Se-Kwon, K., Ed.; JohnWiley & Sons, Ltd.: New Delhi, India, 2012; pp. 181–182.
25. Gressler, V.; Yokoya, N.Y.; Fujii, M.T.; Colepicolo, P.; Mancini Filho, J.; Pavan Torres, R.; Pinto, E. Lipid, fatty acid, protein, amino acid and ash contents in four Brazilian red algae species. *Food Chem.* **2010**, *120*, 585–590.
26. Benatti, P.; Peluso, G.; Nicolai, R.; Calvani, M. Polyunsaturated fatty acids: Biochemical, nutritional and epigenetic properties. *J. Am. Coll. Nutr.* **2004**, *23*, 281–302.
27. Von Schacky, C. The role of Omega-3 fatty acids in cardiovascular disease. *Curr. Atheroscler. Rep.* **2003**, *5*, 139–145.
28. Maeda, H.; Tsukui, T.; Sashima, T.; Hosokawa, M.; Miyashita, K. Seaweed carotenoid, fucoxanthin, as multi-functional nutrient. *Asia Pac. J. Clin. Nutr.* **2008**, *17*, 196–199.
29. Simopoulos, A.P. Omega-3 fatty acids in inflammation and autoimmune diseases. *J. Am. Coll. Nutr.* **2002**, *21*, 495–505.
30. Simopoulos, A.P. The importance of the omega-6/omega-3 fatty acid ratio in cardiovascular diseases and other chronic diseases. *Exp. Biol. Med.* **2008**, *233*, 674–688.



31. MacArtain, P.; Gill, C.I.R.; Brooks, M.; Campbell, R.; Rowland, I.R. Nutritional value of edible seaweeds. *Nutr. Rev.* **2007**, *65*, 535–543.
32. Fernandes, P.; Cabral, J.M.S. Phytosterols: Applications and recovery. *Bioresour. Technol.* **2007**, *98*, 2335–2350.
33. Platt, D.; Pelled, D.; Shulman, A. Oils Enriched with Diacylglycerols and Phytosterolesters for Use in the Reduction of Cholesterol and Tryclycerides. PCT Patent WO2004069150, 23 September 2004.
34. McDermid, K.J.; Stuercke, B. Nutritional composition of edible Hawaiian seaweeds. *J. Appl. Phycol.* **2003**, *15*, 513–524.
35. Marrion, O.; Fleurence, J.; Schwertz, A.; Guéant, J.-L.; Mamelouk, L.; Ksouri, J.; Villaume, C. Evaluation of protein *in vitro* digestibility of *Palmaria palmata* and *Gracilaria verrucosa*. *J. Appl. Phycol.* **2005**, *17*, 99–102.
36. Renaud, S.M.; Luong-Van, J.T. Seasonal variation in the chemical composition of tropical Australian marine macroalgae. *J. Appl. Phycol.* **2006**, *18*, 381–387.
37. Wen, X.; Peng, C.; Zhou, H.; Lin, Z.; Lin, G.; Chen, S.; Li, P. Nutritional composition and assessment of *Gracilaria lemaneiformis* Bory. *J. Integr. Plant Biol.* **2006**, *48*, 1047–1053.
38. Marinho-Soriano, E.; Câmara, M.R.; Cabral, T.M.; Carneiro, M.A.A. Preliminary evaluation of the seaweed *Gracilaria cervicornis* (Rhodophyta) as a partial substitute for the industrial feeds used in shrimp (*Litopenaeus vannamei*) farming. *Aquac. Res.* **2007**, *38*, 182–187.
39. Vernon, T.O.; Alexander, N.; Glazer, A.N.; Stryer, L. Fluorescent phycobiliprotein conjugates for analyses of cells and molecules. *J. Cell Biol.* **1982**, *93*, 981–986.
40. Ayyagari, M.S.; Pande, R.; Kamtekar, S.; Marx, K.A.; Tripathy, S.K.; Gao, H.; Kumar, J.; Akkara, J.A.; Kaplan, D.L. Molecular assembly of proteins and conjugated polymers: Toward development of biosensors. *Biotechnol. Bioeng.* **1995**, *45*, 116–125.
41. Glazer, A.N. Light harvesting by phycobilisome. *Annu. Rev. Biophys. Biophys. Chem.* **1985**, *14*, 47–77.
42. Li, G.W.; Wang, G.C.; Li, Z.G.; Tseng, C.K. Biological effect of R-phycoerythrin-mediated photosensitization on DNA. *Prog. Biochem. Biophys.* **2000**, *27*, 621–624.
43. Niu, J.F.; Wang, G.C.; Tseng, C.K. Method for large-scale isolation and purification of R-phycoerythrin from red alga *Polysiphonia urceolata* Grev. *Protein Expr. Purif.* **2006**, *49*, 23–31.
44. Bermejo, R.; Ruiz, E.; Acién, F.G. Recovery of B-phycoerythrin using expanded bed adsorption chromatography: Scale-up of the process. *Enzym. Microb. Technol.* **2007**, *40*, 927–933.
45. Reaven, P.D.; Witzum, J.L. Oxidised LDL in atherogenesis. Role of dietary modification. *Annu. Rev. Nutr.* **1996**, *16*, 51–71.
46. Aruoma, I.O. Antioxidant action of plant foods. Use of oxidative DNA damage, as a tool for studying antioxidant efficacy. *Free Radic. Res.* **1999**, *30*, 419–427.
47. Shon, M.Y.; Kim, T.H.; Sung, N.J. Antioxidants and free radical scavenging activity of *Phellinus baumii* (Phellius of Hymenochaetaeaceae) extracts. *Food Chem.* **2003**, *82*, 593–597.
48. Kumaran, A.; Karunakaran, R.J. *In vitro* antioxidant properties of methanol extracts of five *Phyllanthus* species from India. *Food Sci. Technol.* **2007**, *40*, 344–352.

49. Kuda, T.; Tsunekawa, M.; Goto, H.; Araki, Y. Antioxidant properties of four edible algae harvested in the Noto Peninsula, Japan. *J. Food Compos. Anal.* **2005**, *18*, 625–633.
50. Duan, X.J.; Zhang, W.W.; Li, X.M.; Wang, B.G. Evaluation of antioxidant property of extract and fractions obtained from a red alga, *Polysiphonia urceolata*. *Food Chem.* **2006**, *95*, 37–43.
51. Ganesan, P.; Chandini, S.K.; Kumar, C.S.; Bhaskar, N. Antioxidant properties of methanol extract and its solvent fractions obtained from selected Indian red seaweeds. *Bioresour. Technol.* **2008**, *99*, 2717–2723.
52. Matanjun, P.; Mohamed, S.; Mustapha, N.M.; Muhammad, K.; Ming, C.H. Antioxidant activities and phenolics content of eight species of seaweeds from north Borneo. *J. Appl. Phycol.* **2008**, *20*, 367–373.
53. Yuan, Y.V.; Bone, D.E.; Carrington, M.F. Antioxidant activity of dulse (*Palmaria palmate*) extract evaluated *in vitro*. *Food Chem.* **2005**, *91*, 485–494.
54. Murugan, K.; Iyer, V.V. Antioxidant and Antiproliferative Activities of Marine Algae, *Gracilaria edulis* and *Enteromorpha linguata*, from Chennai Coast. *Int. J. Cancer Res.* **2012**, *8*, 15–26.
55. Frankel, E.N.; Meyer, A.S. The problems of using one-dimensional methods to evaluate multifunctional food and biological antioxidants. *J. Sci. Food Agric.* **2000**, *80*, 1925–1941.
56. Prior, R.; Wu, X.; Schaich, K. Standardized methods for the determination of antioxidant capacity and phenolics in foods and dietary supplements. *J. Agric. Food Chem.* **2005**, *53*, 4290–4302.
57. Onofrejevá, L.; Vašičková, J.; Klejdusa, B.; Stratil, P.; Mišurcová, L.; Kráčmar, S.; Kopecký, J.; Vaceka, J. Bioactive phenols in algae: The application of pressurized-liquid and solid-phase extraction techniques. *J. Pharm. Biomed. Anal.* **2010**, *51*, 464–470.
58. Wijesekara, I.; Pangestuti, R.; Kima, S.-K. Biological activities and potential health benefits of sulfated polysaccharides derived from marine algae. *Carbohydr. Polym.* **2011**, *84*, 14–21.
59. Marinho-Soriano, E.; Bourret, E. Effects of season on the yield and quality of agar from *Gracilaria* species (Gracilariaceae, Rhodophyta). *Bioresour. Technol.* **2003**, *90*, 329–333.
60. Bligh, E.G.; Dyer, W.J. A rapid method of total lipid extraction and purification. *Can. J. Biochem. Physiol.* **1959**, *37*, 911–917.
61. Francavilla, M.; Trotta, P.; Luque, R. Phytosterols from *Dunaliella tertiolecta* and *Dunaliella salina*: A potentially novel industrial application. *Bioresour. Technol.* **2010**, *101*, 4144–4150.
62. Von der Haar, T. Optimized protein extraction for quantitative proteomics of yeasts. *PLoS One* **2007**, *2*, e1078.
63. Lowry, O.H.; Rosebrough, N.J.; Farr, A.L.; Randall, R.J. Protein measurement with the Folin phenol reagent. *J. Biol. Chem.* **1951**, *193*, 265–275.
64. Kursar, T.A.; van der Meer, J.; Alberte, R.S. Light harvesting system of red alga *Gracilaria tikvahiae*. I. biochemical analyses of pigment mutations. *Plant Physiol.* **1983**, *73*, 353–360.
65. Hajimahmoodi, M.; Faramarzi, M.A.; Mohammadi, N.; Soltani, N.; Oveisi, M.R.; Nafissi-Varcheh, N. Evaluation of antioxidant properties and total phenolic contents of some strains of microalgae. *J. Appl. Phycol.* **2010**, *22*, 43–50.

66. Benzie, I.F.F.; Strain, J.J. The ferric reducing ability of plasma as a power: The FRAP assay. *Anal. Biochem.* **1976**, *239*, 70–76.
67. Katalinic, V.; Milos, M.; Kulisic, T.; Jukic, M. Screening of 70 medicinal plant extracts for antioxidant capacity and total phenols. *Food Chem.* **2006**, *94*, 550–557.
68. Hu, C.C.; Lin, J.T.; Lu, F.J.; Chou, F.P.; Yang, D.J. Determination of carotenoids in *Dunaliella salina* cultivated in Taiwan and antioxidant capacity of the algal carotenoid extract. *Food Chem.* **2008**, *109*, 439–446.
69. Velioglu, Y.S.; Mazza, G.; Gao, L.; Oomah, B.D. Antioxidant activity and total phenolics in selected fruits, vegetables and grain products. *J. Agric. Food Chem.* **1998**, *46*, 4113–4117.
70. Dubois, M.; Gilles, K.A.; Hamilton, J.K.; Rebers, P.A.; Smith, F. Colorimetric method for determination of sugars and related substances. *Anal. Chem.* **1956**, *28*, 350–356.

# Identification and Biochemical Characterization of Halisulfate 3 and Suvanine as Novel Inhibitors of Hepatitis C Virus NS3 Helicase from a Marine Sponge

Atsushi Furuta, Kazi Abdus Salam, Idam Hermawan, Nobuyoshi Akimitsu, Junichi Tanaka, Hidenori Tani, Atsuya Yamashita, Kohji Moriishi, Masamichi Nakakoshi, Masayoshi Tsubuki, Poh Wee Peng, Youichi Suzuki, Naoki Yamamoto, Yuji Sekiguchi, Satoshi Tsuneda and Naohiro Noda

**Abstract:** Hepatitis C virus (HCV) is an important etiological agent that is responsible for the development of chronic hepatitis, liver cirrhosis, and hepatocellular carcinoma. HCV nonstructural protein 3 (NS3) helicase is a possible target for novel drug development due to its essential role in viral replication. In this study, we identified halisulfate 3 (hal3) and suvanine as novel NS3 helicase inhibitors, with  $IC_{50}$  values of 4 and 3  $\mu$ M, respectively, from a marine sponge by screening extracts of marine organisms. Both hal3 and suvanine inhibited the ATPase, RNA binding, and serine protease activities of NS3 helicase with  $IC_{50}$  values of 8, 8, and 14  $\mu$ M, and 7, 3, and 34  $\mu$ M, respectively. However, the dengue virus (DENV) NS3 helicase, which shares a catalytic core (consisting mainly of ATPase and RNA binding sites) with HCV NS3 helicase, was not inhibited by hal3 and suvanine, even at concentrations of 100  $\mu$ M. Therefore, we conclude that hal3 and suvanine specifically inhibit HCV NS3 helicase via an interaction with an allosteric site in NS3 rather than binding to the catalytic core. This led to the inhibition of all NS3 activities, presumably by inducing conformational changes.

Reprinted from *Mar. Drugs*. Cite as: Furuta, A.; Salam, K.A.; Hermawan, I.; Akimitsu, N.; Tanaka, J.; Tani, H.; Yamashita, A.; Moriishi, K.; Nakakoshi, M.; Tsubuki, M.; *et al.* Identification and Biochemical Characterization of Halisulfate 3 and Suvanine as Novel Inhibitors of Hepatitis C Virus NS3 Helicase from a Marine Sponge. *Mar. Drugs* **2014**, *12*, 462-476.

## 1. Introduction

An estimated 150 million people worldwide are chronically infected with the hepatitis C virus (HCV), a major etiological agent responsible for the development of chronic hepatitis, liver cirrhosis, and hepatocellular carcinoma (World Health Organization, 2013). The current standard therapy is based mainly on a triple combination of pegylated interferon- $\alpha$ , ribavirin, and a recently approved NS3 serine protease inhibitor (such as telaprevir), which increases the viral clearance rate to >70% [1,2]. However, because of severe side effects, the emergence of drug-resistant HCV mutations, and drug-drug interactions [3,4], the development of novel direct-acting antivirals that target the viral or host proteins involved in HCV replication are needed urgently. HCV nonstructural protein 3 (NS3) helicase has been considered as a novel antiviral target owing to its essential role in viral replication [5,6].

HCV is a member of the *Flaviviridae* family of positive-stranded RNA viruses. The viral genome contains a single open reading frame encoding a polyprotein that is processed by virus-encoded and

host cellular proteases into structural and nonstructural proteins. The structural proteins (core protein [C], and the envelope glycoproteins E1 and E2) build up the virus particle, whereas the nonstructural proteins p7 and NS2 support particle assembly without being incorporated into the viral particles [7,8]. The remaining nonstructural proteins (NS3, NS4A, NS4B, NS5A, and NS5B) form a complex with viral RNA to support viral replication [9]. NS3 is a multifunctional enzyme with serine protease and NTPase/helicase domains at the *N*- and *C*-termini, respectively [10]. The NS3 helicase can unwind double-stranded RNA (dsRNA), double-stranded DNA, and RNA/DNA heteroduplexes in a 3'–5' direction by using a nucleoside triphosphate as the energy source [11–14]. Although the exact role of NS3 helicase in the viral life cycle remains unclear, a fully functional NS3 helicase is required for replication of the HCV replicon [5] and for HCV replication in chimpanzees [15], suggesting that NS3 helicase inhibitors could be potential therapeutic agents. However, no HCV NS3 helicase inhibitors have yet been entered into clinical trials, at least in part due to similarities between NS3 and cellular RNA helicases [8].

HCV NS3 helicase is part of the family of viral DExH proteins; the NS3/NPH-II family that encompasses helicases from positive-stranded RNA viruses [16–18]. These closely related helicases share a catalytic core that consists mainly of NTPase and nucleic acid binding sites, as well as many other structural and functional features. Indeed, dengue virus (DENV) NS3 helicase, another viral DExH protein, and HCV NS3 helicase share highly conserved amino acid sequences, and consequently have similar conformational structures [19]. Thus, if a compound inhibits HCV NS3 helicase, it may also inhibit DENV NS3 helicase [20–22]. Assessing the inhibitory specificity can provide useful information to understand whether inhibitors target the NTPase, nucleic acid binding, or other allosteric sites of NS3 helicase.

HCV NS3 helicase inhibitors function by inhibiting NTP binding, nucleic acid binding, NTP hydrolysis or NDP release, the coupling of NTP hydrolysis to the translocation and unwinding of nucleic acids, or unwinding by sterically blocking helicase translocation [6]. In addition, owing to an interdependent linkage between NS3 helicase and serine protease activities [23–25], the inhibition of NS3 serine protease may also lead to the inhibition of NS3 helicase. Compounds that intercalate into the strands of double-stranded nucleic acids could also inhibit NS3 helicase [26].

Naturally occurring products are an important source of structurally diverse and biologically active secondary metabolites. The diversity of organisms in the marine environment has provided new drugs in almost all therapeutic areas [27–29]. To date, seven therapeutic agents derived from the marine environment are used as anticancer, antiviral, pain control, and hypertriglyceridemia agents [27]. The chemical structure has been isolated for two of these compounds, whereas the remaining five are synthetic agents based on marine products. An additional 13 agents are in phase 1, 2, or 3 clinical trials. Therefore, natural marine products include a number of highly significant lead compounds that are driving new drug development.

In this study, we screened extracts from marine organisms for NS3 helicase inhibitors using a fluorescence helicase assay based on photoinduced electron transfer (PET), as described in our previous study [30]. During purification, halisulfate 3 (hal3) and suvanine, which were isolated from marine sponge extracts, were identified as novel NS3 helicase inhibitors with IC<sub>50</sub> values in the low micromolar range. The inhibitory effects of hal3 and suvanine against the other helicase-related

activities of NS3 (ATPase, RNA binding, and serine protease activities) were also assessed. Finally, the inhibitory activities of hal3 and suvanine against DENV NS3 helicase were determined to characterize the binding sites of hal3 and suvanine.

## 2. Results and Discussion

To obtain novel NS3 helicase inhibitors, extracts from marine organisms were screened using a fluorescence helicase assay based on PET. Forty-three extracts prepared from marine organisms were screened, and 11 were identified that inhibited the helicase activity >50% (samples 4, 10, 13, 14, 17, 19, 21, 22, 25, 26, and 37) (Table 1), suggesting that these extracts contained NS3 helicase inhibitors. Of these extracts, sample 10 exhibited the strongest inhibition of NS3 helicase, and abolished its activity completely. Therefore, this extract was purified to isolate and concentrate the inhibitory components. After several purification steps, the inhibitory components were identified as hal3 and suvanine (Figure 1) by comparing their NMR spectra with those reported previously [31,32] for each compound (Supplementary Figures S1–S4). Hal3 and suvanine inhibited NS3 helicase activity in a dose-dependent manner, with IC<sub>50</sub> values of 4 and 3 μM, respectively (Figure 2A,B).

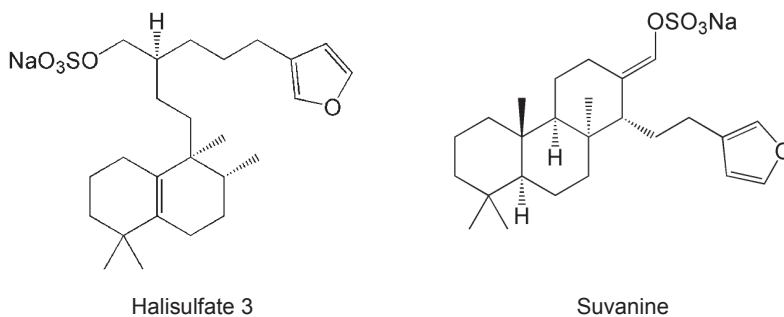
**Table 1.** Inhibitory effects of extracts from marine organisms on hepatitis C virus (HCV) nonstructural protein 3(NS3) helicase activity.

No.	NS3 Helicase Activity (% of Control) *	Marine Organism	Species
1	92	Sponge	<i>Unidentified</i>
2	74	Soft coral	<i>Briareum</i>
3	57	Tunicate	<i>Unidentified</i>
<u>4</u>	<u>36</u>	<u>Sponge</u>	<u><i>Liosina</i></u>
5	54	Sponge	<i>Unidentified</i>
6	71	Sponge	<i>Xestospongia</i>
7	77	Sponge	<i>Epipolasis</i>
8	110	Sponge	<i>Unidentified</i>
9	86	Sponge	<i>Strongylophora</i>
<b>10</b>	<b>0</b>	<b>Sponge</b>	<b><i>Unidentified</i></b>
11	83	Sponge	<i>Stylotella aurantium</i>
12	78	Sponge	<i>Epipolasis</i>
<u>13</u>	<u>25</u>	<u>Sponge</u>	<u><i>Unidentified</i></u>
<u>14</u>	<u>43</u>	<u>Sponge</u>	<u><i>Hippospongia</i></u>
15	75	Sponge	<i>Unidentified</i>
16	85	Sponge	<i>Unidentified</i>
<u>17</u>	<u>49</u>	<u>Sponge</u>	<u><i>Xestospongia testudinaria</i></u>
18	69	Sponge	<i>Unidentified</i>
<u>19</u>	<u>40</u>	<u>Sponge</u>	<u><i>Theonella</i></u>
20	64	Sponge	<i>Unidentified</i>
<u>21</u>	<u>44</u>	<u>Sponge</u>	<u><i>Unidentified</i></u>
<u>22</u>	<u>46</u>	<u>Sponge</u>	<u><i>Petrosia</i></u>

**Table 1. Cont.**

23	72	Tunicate	<i>Unidentified</i>
24	61	Sponge	<i>Unidentified</i>
<b><u>25</u></b>	<b><u>50</u></b>	<b><u>Tunicate</u></b>	<b><u><i>Didemnum molle</i></u></b>
<b><u>26</u></b>	<b><u>33</u></b>	<b><u>Sponge</u></b>	<b><u><i>Unidentified</i></u></b>
27	67	Sponge	<i>Unidentified</i>
28	87	Soft coral	<i>Unidentified</i>
29	62	Sponge	<i>Unidentified</i>
30	60	Sponge	<i>Unidentified</i>
31	85	Sponge	<i>Cinachyra</i>
32	70	Sponge	<i>Liosina</i>
33	68	Sponge	<i>Unidentified</i>
34	58	Sponge	<i>Unidentified</i>
35	72	Sponge	<i>Stylotella</i>
36	57	Sponge	<i>Unidentified</i>
<b><u>37</u></b>	<b><u>39</u></b>	<b><u>Sponge</u></b>	<b><u><i>Unidentified</i></u></b>
38	72	Tunicate	<i>Didemnum</i>
39	62	Sponge	<i>Unidentified</i>
40	71	Jellyfish	<i>Unidentified</i>
41	74	Sponge	<i>Unidentified</i>
42	52	Tunicate	<i>Unidentified</i>
43	67	Annelid	<i>Unidentified</i>

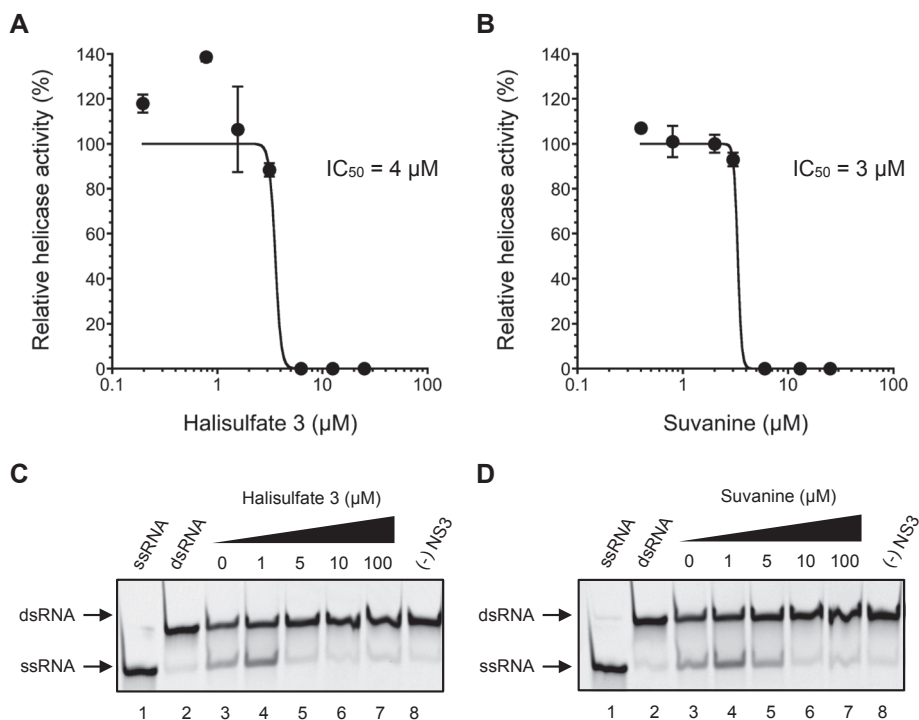
\* NS3 helicase activity in the presence of extract is expressed as a percentage of control in the absence of extract (100%); The sample with the strongest inhibition against NS3 helicase is in bold, underlined font; samples with relatively strong inhibition against NS3 helicase (<50%) are underlined.

**Figure 1.** Structures of halisulfate 3 (hal3) and suvanine.

The inhibitory effects of hal3 and suvanine were confirmed using a gel-based helicase assay. The helicase activity was calculated as the ratio of the signal intensity derived from single-stranded (ssRNA) in the sample containing the inhibitor to the control sample (lacking the inhibitor but containing DMSO vehicle). Similar to the results of the fluorescence helicase assay, hal3 and suvanine inhibited helicase-catalyzed RNA unwinding in a dose-dependent manner (Figure 2C,D). Therefore, these data clearly indicate that hal3 and suvanine exert inhibitory effects. Hal3 and suvanine were identified in 1988 [33] and 1985 [34], respectively. They have similar distinguishing

structural features of a sulfated side chain and a furan moiety at the terminus of the molecule (Figure 1). Although some bioactivities for hal3 and suvanine have been reported, this report is the first that identifies these compounds as helicase inhibitors. In addition, bioactive effects of hal3 alone have not been reported. A mixture of halisulfates 2–5 (hal3 and its analogues) showed antimicrobial activity against *S. aureus*, *C. albicans*, and *B. subtilis*. Moreover, a mixture of halisulfates 2–4 inhibited PMA-induced inflammation in a mouse ear edema assay and inhibited phospholipase A<sub>2</sub> [31]. Suvanine is a serine protease inhibitor [35] and an antagonist of the mammalian bile acid sensor farnesoid-X-receptor [36]. In addition, suvanine interferes with heat shock protein 60, a chaperone involved in the inflammatory response, giving evidence for its anti-inflammatory properties [37].

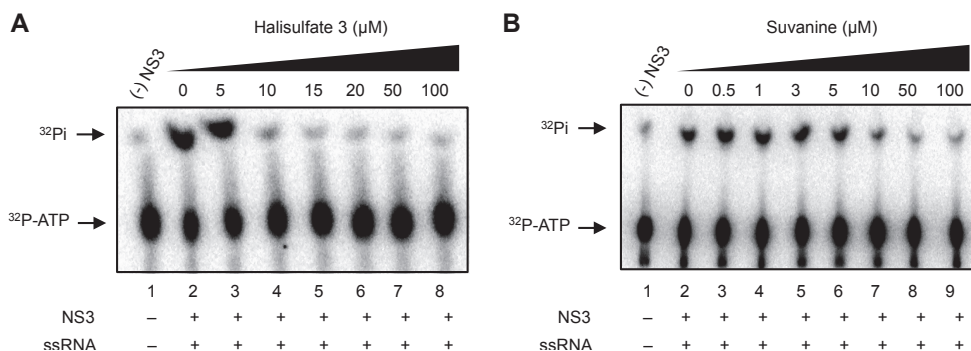
**Figure 2.** Inhibition of NS3 helicase-catalyzed RNA unwinding activity by hal3 and suvanine. **(A,B)** Inhibition curves of hal3 and suvanine generated using a fluorescence helicase assay. The NS3 helicase activities of samples containing inhibitor were calculated relative to control samples containing DMSO vehicle rather than inhibitor. The data are presented as mean  $\pm$  standard deviation of three replicates; **(C,D)** Gel images representing the inhibitory effects of hal3 and suvanine in a gel-based helicase assay. Fluorescence-labeled ssRNA and dsRNA were applied to lanes 1 and 2, respectively. The dsRNA was incubated with NS3 in the presence of increasing concentrations of inhibitor (lanes 3–7, 0–100  $\mu$ M). Lane 8 shows the control reaction in the absence of NS3.





As the unwinding ability of NS3 helicase is dependent on ATP hydrolysis, the amount of inorganic phosphate (Pi) released from radioisotope-labeled ATP was measured to determine the effects of hal3 and suvanine on the ATPase activity of NS3 (Figure 3). The released Pi was separated by thin-layer chromatography and visualized using autoradiography. The density of the upper spots corresponding to Pi, which represents ATPase activity, decreased dose-dependently for both hal3 and suvanine. The ATPase activity was calculated as the ratio of the signal intensity derived from the released Pi in the sample containing inhibitor to that in the control sample (lacking the inhibitor but containing DMSO vehicle). The IC<sub>50</sub> values of hal3 and suvanine were calculated to be 8 and 7  $\mu$ M, respectively. As this concentration range is similar to that in which RNA unwinding was inhibited (Figure 2), it is likely that hal3 and suvanine inhibit NS3 helicase via the inhibition of ATPase activity.

**Figure 3.** Effects of hal3 and suvanine on NS3 ATPase activity demonstrated by autoradiography of an ATPase assay using [ $\gamma$ -<sup>32</sup>P] ATP. Lane 1 contains the control reaction without NS3. Lanes 2–8 (A) and 2–9 (B) show the ATP hydrolysis reaction with poly(U) RNA at increasing concentrations (0–100  $\mu$ M) of hal3 and suvanine, respectively.



As RNA binding is required for NS3 helicase activity, the effects of hal3 and suvanine on NS3 RNA binding activity were examined by gel mobility shift assay (Figure 4). As a control, the non-specific binding of ssRNA to bovine serum albumin (BSA) was assessed (lane 2). The density of the upper bands corresponding to the NS3-ssRNA complex, which represents NS3 RNA binding activity, decreased dose-dependently in the presence of both hal3 and suvanine. RNA binding activity was calculated as the ratio of the signal intensity derived from the NS3-ssRNA complex in the sample containing the inhibitor to that in the control sample (lacking the inhibitor but containing DMSO vehicle). The IC<sub>50</sub> values of hal3 and suvanine were calculated to be 8 and 3  $\mu$ M, respectively. The data presented in Figures 2 and 4 reveal that the NS3 helicase and RNA binding activities decrease at similar inhibitor concentration ranges for hal3 and suvanine, suggesting that the inhibition of NS3 helicase by these compounds is associated with RNA binding activity.

It was reported that the helicase activity of NS3 is interdependently linked to its serine protease activity [23–25]. Therefore, we examined the effects of hal3 and suvanine on NS3 serine protease activity using a fluorescence serine protease assay (Figure 5). Serine protease activity decreased in

a dose-dependent manner in the presence of hal3 and suvanine, with  $IC_{50}$  values of 14 and 34  $\mu\text{M}$ , respectively. Although the inhibition of the serine protease activity seems to be rather modest compared with that of the ATPase and RNA binding activities (Figures 3 and 4), the inhibition of NS3 helicase by hal3 and suvanine is likely to be also related to serine protease activity.

**Figure 4.** Effects of hal3 and suvanine on NS3 RNA binding activity, assessed by autoradiography of a gel mobility shift assay using  $^{32}\text{P}$ -labeled ssRNA. Lanes 1 and 2 contain control reactions consisting of heat-denatured ssRNA and 300 nM BSA instead of NS3, respectively. Lanes 3–9 (A) and 3–10 (B) show the RNA binding reaction with increasing concentrations (0–100  $\mu\text{M}$ ) of hal3 and suvanine, respectively.

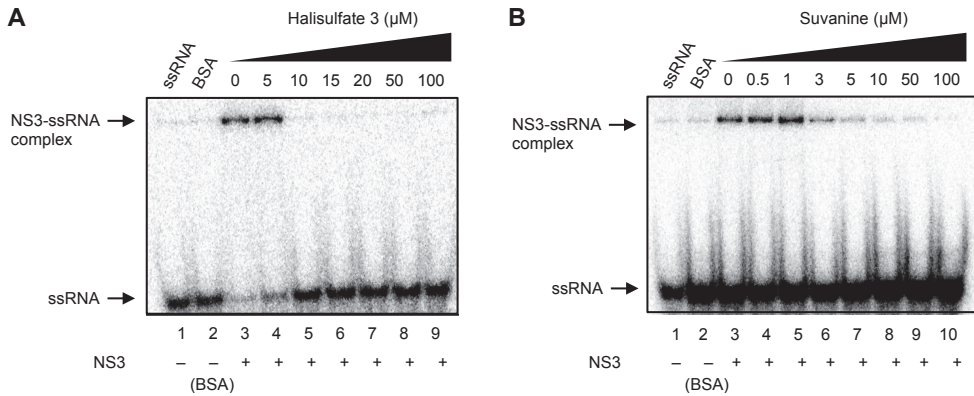
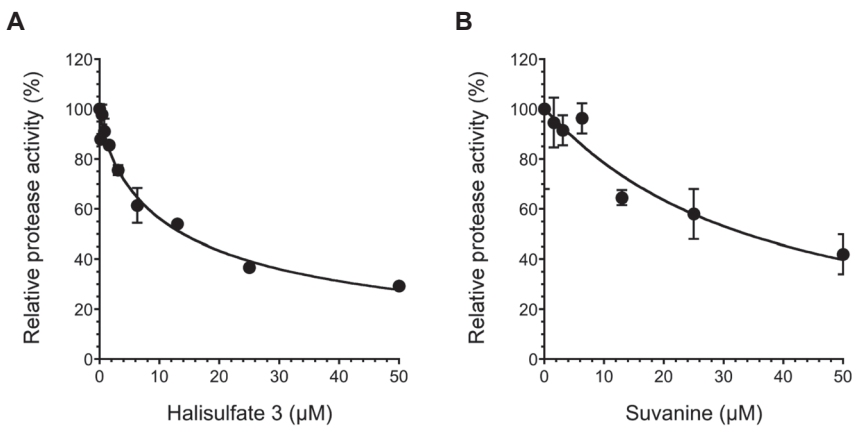


**Figure 5.** Effects of hal3 (A) and suvanine (B) on NS3 serine protease activity. The NS3 serine protease activity of samples containing inhibitor was calculated relative to control samples containing DMSO vehicle rather than inhibitor. The data are presented as means  $\pm$  standard deviation of three replicates.

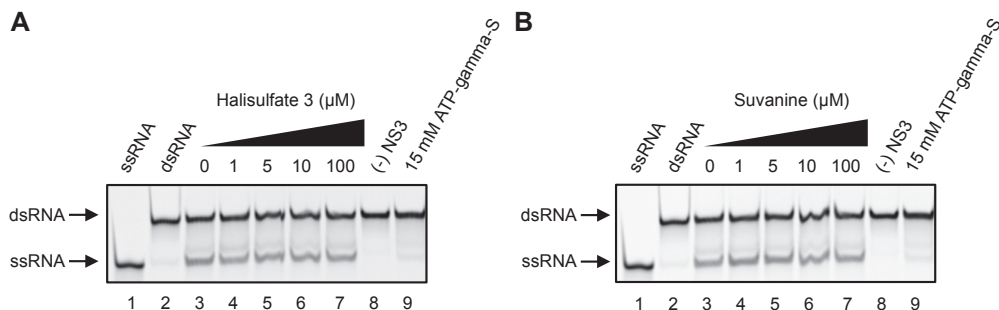


The catalytic cores of DENV and HCV NS3 helicases, which consist predominantly of ATPase and RNA binding sites, share almost identical folds and extensive structural similarity [38]. Because the substrate specificity of DENV and HCV NS3 helicases is similar [39], the dsRNA

substrate and capture strand of the gel-based HCV NS3 helicase assay were also used for the gel-based DENV NS3 helicase assay (Figure 6), and helicase activity was calculated as described above. Hal3 and suvanine did not abolish DENV NS3 helicase activity, even in the presence of 100  $\mu\text{M}$  of each inhibitor. This finding suggests that the inhibitory effects of hal3 and suvanine are specific to HCV NS3 helicase, and that these inhibitors bind less efficiently to any site in DENV NS3 helicase, including the catalytic core.

This study demonstrated that hal3 and suvanine inhibit the ATPase, RNA binding, and serine protease activities of NS3 (Figures 3–5). Taken together with observations that hal3 and suvanine did not inhibit DENV NS3 helicase (Figure 6), it is likely that these inhibitors do not bind to the catalytic core that contains the ATPase activity and RNA binding sites. Therefore, we conclude that hal3 and suvanine inhibit HCV NS3 helicase via interactions with allosteric sites of NS3. This likely induces conformational changes in NS3, inhibiting or abolishing its activities. Compounds with inhibitory activities against both helicase and serine protease activities have been reported previously [40]; however, there are only a small number of studies, and detailed inhibitory mechanisms are yet to be elucidated. The possible allosteric sites to which hal3 and suvanine bind could be an interface that forms between the helicase and protease domains of NS3. Indeed, a novel small-molecule binding site at the interface between these two domains was reported recently [41]. Furthermore, the inhibitory specificity of hal3 and suvanine against HCV NS3 helicase might be explained by structural differences between HCV and DENV NS3 helicases. A specific beta-strand tethers the C terminus of the helicase domain to the protease domain of HCV NS3, maintaining it in a compact conformation that differs from the extended conformation of DENV NS3 helicase [42]. As only HCV NS3 helicase forms an interface between the helicase and protease domains, the specificity of hal3 and suvanine for HCV NS3 helicase would be explained by the binding of hal3 and suvanine to the interface of HCV NS3.

**Figure 6.** Effects of hal3 (A) and suvanine (B) on DENV NS3 helicase activity, assessed using a gel-based helicase assay. Fluorescence-labeled ssRNA and dsRNA were applied to lanes 1 and 2, respectively. The dsRNA was incubated with NS3 in the presence of increasing concentrations of inhibitor (lanes 3–7, 0–100  $\mu\text{M}$ ). Lanes 8 and 9 contain the control reaction mixtures in the absence of NS3, and in the presence of 15 mM ATP- $\gamma$ -S as an inhibition control, respectively.



### 3. Experimental Section

#### 3.1. Preparation of Extracts from Marine Organisms

Specimens of marine organisms were collected by scuba diving in Okinawa, Japan, and Sorong, Indonesia, and kept frozen until use. The specimens were chopped into small pieces, and soaked in acetone for 20 h followed by methanol for 6 h. The acetone and methanol solutions were then combined and concentrated, and residual materials were separated into ethyl acetate and aqueous layers; each layer was then dried to obtain residues.

#### 3.2. Screening for HCV NS3 Helicase Inhibitors

The PET-based fluorescence helicase assay was performed as described previously [30]. The dsRNA substrate was prepared by annealing the 5' BODIPY FL-labeled fluorescence strand (5'-CUAUUACCUCCACCCUCAUAACCUUUUUUUUUUUUUU-3') to the quencher strand (5'-GGUUAUGAGGGUGGAGGUAUAG-3') at a 1:2 molar ratio. The dsRNA substrate contains the 3'-overhang that is necessary for the NS3 helicase to bind RNA prior to duplex unwinding. The capture strand (5'-CTATTACCTCCACCCTCATAACC-3'), which is complementary to the quencher strand, prevents the unwound duplexes from reannealing. None of the capture, quencher, or fluorescence strands are self-complementary. The fluorescence strand was purchased from J-Bio 21 Corporation (Tokyo, Japan), and was labeled with BODIPY FL at the 5'-end via an aminoethylphosphate linker with a six-carbon spacer. The quencher and capture strands were purchased from Japan Bio Services (Saitama, Japan). The reaction mixture contained 25 mM MOPS-NaOH (pH 6.5), 3 mM MgCl<sub>2</sub>, 2 mM dithiothreitol, 4 U RNasin (Promega, Madison, WI, USA), 50 nM dsRNA substrate, 100 nM capture strand, 5 mM ATP, a marine organism extract, and 240 nM NS3 in a total reaction volume of 20 μL. Each marine organism extract diluted in DMSO was added to the reaction mixture at a final concentration of 17.5–32.5 μg/mL. The full-length HCV NS3 protein with serine protease and NTPase/helicase activities was expressed and purified as described previously [43].

The reaction was started by the addition of HCV NS3 helicase, and was performed at 37 °C for 30 min using a LightCycler 1.5 (Roche Diagnostics, Basel, Switzerland). The fluorescence intensity was recorded every 5 s from 0 to 5 min, and then every 30 s from 5 to 30 min. Helicase activity was calculated as the initial reaction velocity relative to control (in the absence of a marine extract, but presence of DMSO vehicle). The IC<sub>50</sub> was calculated using KaleidaGraph (Synergy Software, Reading, PA, USA) by fitting plots of % activity vs. [I] using Equation (1) unless otherwise noted [44]:

$$\% \text{ Activity} = \frac{100}{1 + ([I]/IC_{50})^h} \quad (1)$$

where  $h$  is the Hill coefficient, and  $[I]$  is the inhibitor concentration.

### 3.3. Gel-Based HCV NS3 Helicase Assay

A gel-based helicase assay was performed on HCV NS3 helicases using an Alexa Fluor 488-labeled dsRNA strand and capture strand with the same nucleic acid sequences described in Section 3.2. The dsRNA substrate was prepared by annealing the 5' Alexa Fluor 488-labeled strand (5'-CUAAUACCUCACCCUCAUAACCUUUUUUUUUUUUUU-3') to the complementary strand (5'-GGUUAUGAGGGUGGAGGUAUAG-3') at a 1:2 molar ratio. The same capture strand described in Section 3.2 was used. All nucleic acid strands were purchased from Japan Bio Services (Saitama, Japan). The reaction mixture for HCV NS3 helicase contained the same components as described in Section 3.2, with increasing concentrations of hal3 or suvanine in a reaction volume of 20  $\mu$ L. The reaction was started by the addition of HCV NS3 helicase, and performed at 37 °C for 60 min using a GeneAmp PCR System 2700 (Applied Biosystems, Foster City, CA, USA). The reaction was stopped by the addition of 5  $\mu$ L of helicase termination buffer containing 10 mM Tris-HCl (pH 7.5), 50 mM EDTA, 30% glycerol, 0.06% bromophenol blue, and 0.12% Orange G. The inhibition of NS3 helicase was analyzed on a 20% native Tris/borate/EDTA (TBE) polyacrylamide gel, and labeled RNAs were visualized using Typhoon 9210 (GE Healthcare, Waukesha, WI, USA). The helicase activity was calculated as the ratio of the signal intensity derived from ssRNA in the sample containing inhibitor to that in the control sample containing DMSO vehicle instead of inhibitor.

### 3.4. ATPase Assay

NS3 ATPase activity was determined directly by monitoring [ $\gamma$ -<sup>32</sup>P] ATP hydrolysis by thin-layer chromatography, as described previously [45,46]. The reaction mixture contained 25 mM MOPS-NaOH (pH 7.0), 1 mM dithiothreitol, 5 mM MgCl<sub>2</sub>, 5 mM CaCl<sub>2</sub>, 1 mM [ $\gamma$ -<sup>32</sup>P] ATP (Muromachi Yakuhin, Tokyo, Japan), 300 nM NS3, 0.1  $\mu$ g/ $\mu$ L poly (U) ssRNA (Sigma-Aldrich, St. Louis, MO, USA), and increasing concentrations of hal3 or suvanine in a volume of 10  $\mu$ L. The reaction was conducted at 37 °C for 10 min, and stopped by the addition of 10 mM EDTA. Two microliters of each reaction mixture was then spotted onto a polyethyleneimine cellulose sheet (Merck, Darmstadt, Germany) and developed in 0.75 M LiCl/1 M formic acid solution for 20 min. The cellulose sheet was dried, and the released [ $\gamma$ -<sup>32</sup>P] phosphoric acid was visualized using an Image Reader FLA-9000 and quantified using Multi Gauge software V 3.11 (Fujifilm, Tokyo, Japan). ATPase activity was calculated as the ratio of the signal intensity derived from the released Pi in the sample containing inhibitor to that in the control sample containing DMSO vehicle instead of inhibitor.

### 3.5. RNA Binding Assay

NS3 RNA binding activity was determined by gel mobility shift assay, as described previously [45,46]. The ssRNA (5'-UGAGGUAGUAGGUUGUAUAGU-3') synthesized by Gene Design (Osaka, Japan) was labeled at the 5'-end with [ $\gamma$ -<sup>32</sup>P] ATP (Muromachi Yakuhin, Tokyo, Japan) using T4 polynucleotide kinase (Toyobo, Osaka, Japan) at 37 °C for 60 min, and purified using the phenol-chloroform extraction method. The reaction mixture contained 30 mM Tris-HCl

(pH 7.5), 100 mM NaCl, 2 mM MgCl<sub>2</sub>, 1 mM dithiothreitol, 20 U RNasin Plus (Promega), 300 nM NS3, 0.1 nM <sup>32</sup>P-labeled ssRNA, and increasing concentrations of inhibitor in a volume of 20 μL. The reaction was performed at room temperature for 15 min. An equal volume of a dye solution containing 0.025% bromophenol blue and 10% glycerol in 0.5× TBE was then added to each reaction mixture, and samples were loaded onto a 6% native-polyacrylamide gel. The labeled RNA bands were visualized using an Image Reader FLA-9000 and quantified using Multi Gauge software V 3.11 (Fujifilm, Tokyo, Japan). RNA binding activity was calculated as the ratio of the signal intensity derived from the NS3-ssRNA complex in the sample containing hal3 or suvanine to that in the control sample containing DMSO vehicle rather than inhibitor.

### 3.6. Serine Protease Assay

A fluorescence NS3 serine protease assay, based on fluorescence resonance energy transfer, was conducted using reagents provided in a SensoLyte™ 520 HCV protease assay kit (AnaSpec, San Jose, CA, USA), as described previously [30]. Briefly, NS3 protein with a two-fold excess of the NS4A cofactor peptide Pep4AK was prepared in 1× assay buffer provided with the kit. HCV NS3/4A protease was mixed with increasing concentrations of inhibitor, and incubated at 37 °C for 15 min. The reaction was started by the addition of 5-FAM/QXL 520 substrate in a 20 μL total reaction volume containing 240 nM HCV NS3/4A protease and increasing concentrations of hal3 or suvanine. Reactions were then incubated at 37 °C for 120 min on a LightCycler 1.5 (Roche Diagnostics, Basel, Switzerland), and the fluorescence intensity was recorded every min for 120 min. NS3 serine protease activity was calculated as the initial reaction velocity in the sample containing inhibitor relative to the control sample containing DMSO vehicle rather than inhibitor.

### 3.7. Gel-Based DENV NS3 Helicase Assay

A gel-based helicase assay was performed using DENV NS3 helicases, and the Alexa Fluor 488-labeled dsRNA strand and capture strand with the same nucleic acid sequences described in the Section 3.3. DENV NS3 helicase requires a single stranded 3' overhang to unwind dsRNA substrates in the 3' to 5' direction [39]; therefore, the substrate specificities of the DENV and HCV NS3 helicases are the same. The reaction mixture contained 50 mM Tris-HCl (pH 7.4), 1 mM DTT, 0.5% Tween 20, 0.25 μg/mL BSA, 2 mM MgCl<sub>2</sub>, 4 U RNasin (Promega), 5 mM ATP, 50 nM dsRNA substrate, 300 nM capture strand, an inhibitor, and 240 nM DENV NS3 in a total volume of 20 μL. DENV NS3 helicase was prepared as described previously [47]. The reaction was started by the addition of DENV NS3 helicase, and was performed at 37 °C for 60 min using a GeneAmp PCR System 2700 (Applied Biosystems, Foster City, CA, USA). The reaction was then stopped by the addition of 5 μL helicase termination buffer that contained 10 mM Tris-HCl (pH 7.5), 50 mM EDTA, 30% glycerol, 0.06% bromophenol blue, and 0.12% Orange G. The inhibition of DENV NS3 helicase was analyzed on a 20% native TBE polyacrylamide gel, and the labeled RNAs were visualized using Typhoon 9210 (GE Healthcare, Waukesha, WI, USA). The helicase activity was calculated as the ratio of the signal intensity from ssRNA in the sample containing inhibitor to that in the control sample containing DMSO vehicle instead of inhibitor.

#### 4. Conclusions

This study demonstrated that hal3 and suvanine isolated from a marine sponge inhibited NS3 helicase by suppressing the ATPase, RNA binding, and serine protease activities. Moreover, DENV NS3 helicase, which shares a catalytic core consisting mainly of ATPase and RNA binding activity sites with HCV NS3 helicase, was not inhibited by hal3 or suvanine. Therefore, it can be concluded that hal3 and suvanine inhibit HCV NS3 helicase specifically through interaction with an allosteric site of NS3 rather than the catalytic core, leading to the inhibition of all NS3 activities, presumably by inducing conformational changes. As such, it is possible that hal3 and suvanine are less likely to inhibit other cellular helicases that share a similar catalytic core to HCV NS3 helicase. This provides potentially useful information on advanced drug design strategies to identify novel NS3 helicase inhibitors that are expected to be more specific and less toxic. Experiments to address whether resistant HCV mutants emerge with the use of these compounds are underway in our laboratory.

#### Acknowledgments

The authors thank S. Nishikawa (AIST) for his kind gift of the expression plasmid pT7/His-NS3 containing the *N*-terminal His-tagged full-length HCV NS3. The Global COE Program “Center for Practical Chemical Wisdom” of the Ministry of Education, Culture, Sports, Science and Technology (MEXT) of Japan partially supported this study. This work was also partly supported by NUS SoM Start-up Grant (R-182-000-160-733, R-182-000-160-133) to NY.

#### Conflicts of Interest

The authors declare no conflict of interest.

#### References

1. Ghany, M.G.; Nelson, D.R.; Strader, D.B.; Thomas, D.L.; Seeff, L.B. An update on treatment of genotype 1 chronic hepatitis C virus infection: 2011 practice guideline by the American Association for the Study of Liver Diseases. *Hepatology* **2011**, *54*, 1433–1444.
2. Liang, T.J.; Ghany, M.G. Current and future therapies for hepatitis C virus infection. *N. Engl. J. Med.* **2013**, *368*, 1907–1917.
3. Sarrazin, C.; Hézode, C.; Zeuzem, S.; Pawlotsky, J.-M. Antiviral strategies in hepatitis C virus infection. *J. Hepatol.* **2012**, *56*, S88–S100.
4. Scheel, T.K.H.; Rice, C.M. Understanding the hepatitis C virus life cycle paves the way for highly effective therapies. *Nat. Med.* **2013**, *19*, 837–849.
5. Lam, A.M.I.; Frick, D.N. Hepatitis C virus subgenomic replicon requires an active NS3 RNA helicase. *J. Virol.* **2006**, *80*, 404–411.
6. Kwong, A.D.; Rao, B.G.; Jeang, K.-T. Viral and cellular RNA helicases as antiviral targets. *Nat. Rev. Drug Discov.* **2005**, *4*, 845–853.

7. Bartenschlager, R.; Penin, F.; Lohmann, V.; André, P. Assembly of infectious hepatitis C virus particles. *Trends Microbiol.* **2011**, *19*, 95–103.
8. Bartenschlager, R.; Lohmann, V.; Penin, F. The molecular and structural basis of advanced antiviral therapy for hepatitis C virus infection. *Nat. Rev. Microbiol.* **2013**, *11*, 482–496.
9. Lohmann, V.; Körner, F.; Koch, J.-O.; Herian, U.; Theilmann, L.; Bartenschlager, R. Replication of subgenomic hepatitis C virus RNAs in a hepatoma cell line. *Science* **1999**, *285*, 110–113.
10. Gallinari, P.; Brennan, D.; Nardi, C.; Brunetti, M.; Tomei, L.; Steinkühler, C.; de Francesco, R. Multiple enzymatic activities associated with recombinant NS3 protein of hepatitis C virus. *J. Virol.* **1998**, *72*, 6758–6769.
11. Kim, D.W.; Gwack, Y.; Han, J.H.; Choe, J. C-terminal domain of the hepatitis C virus NS3 protein contains an RNA helicase activity. *Biochem. Biophys. Res. Commun.* **1995**, *215*, 160–166.
12. Tai, C.-L.; Chi, W.-K.; Chen, D.-S.; Hwang, L.-H. The helicase activity associated with hepatitis C virus nonstructural protein 3 (NS3). *J. Virol.* **1996**, *70*, 8477–8484.
13. Gwack, Y.; Kim, D.W.; Han, J.H.; Choe, J. Characterization of RNA binding activity and RNA helicase activity of the hepatitis C virus NS3 protein. *Biochem. Biophys. Res. Commun.* **1996**, *225*, 654–659.
14. Gwack, Y.; Kim, D.W.; Han, J.H.; Choe, J. DNA helicase activity of the hepatitis C virus nonstructural protein 3. *Eur. J. Biochem.* **1997**, *250*, 47–54.
15. Kolykhalov, A.A.; Mihalik, K.; Feinstone, S.M.; Rice, C.M. Hepatitis C virus-encoded enzymatic activities and conserved RNA elements in the 3' nontranslated region are essential for virus replication *in vivo*. *J. Virol.* **2000**, *74*, 2046–2051.
16. Hall, M.C.; Matson, S.W. Helicase motifs: The engine that powers DNA unwinding. *Mol. Microbiol.* **1999**, *34*, 867–877.
17. Gorbalenya, A.E.; Koonin, E.V. Helicases: Amino acid sequence comparisons and structure-function relationships. *Curr. Opin. Struct. Biol.* **1993**, *3*, 419–429.
18. Jankowsky, E. *RNA Helicases*; Royal Society of Chemistry: London, UK, 2010; pp. 168–188.
19. Frick, D.N.; Lam, A.M.I. Understanding helicases as a means of virus control. *Curr. Pharm. Des.* **2006**, *12*, 1315–1338.
20. Borowski, P.; Deinert, J.; Schalinski, S.; Bretner, M.; Ginalski, K.; Kulikowski, T.; Shugar, D. Halogenated benzimidazoles and benzotriazoles as inhibitors of the NTPase/helicase activities of hepatitis C and related viruses. *Eur. J. Biochem.* **2003**, *270*, 1645–1653.
21. Zhang, N.; Chen, H.-M.; Koch, V.; Schmitz, H.; Liao, C.-L.; Bretner, M.; Bhadti, V.S.; Fattom, A.I.; Naso, R.B.; Hosmane, R.S.; *et al.* Ring-expanded (“fat”) nucleoside and nucleotide analogues exhibit potent *in vitro* activity against *Flaviviridae* NTPases/helicases, including those of the West Nile virus, hepatitis C virus, and Japanese encephalitis virus. *J. Med. Chem.* **2003**, *46*, 4149–4164.
22. Borowski, P.; Heising, M.V.; Miranda, I.B.; Liao, C.-L.; Choe, J.; Baier, A. Viral NS3 helicase activity is inhibited by peptides reproducing the Arg-rich conserved motif of the enzyme (motif VI). *Biochem. Pharmacol.* **2008**, *76*, 28–38.



23. Frick, D.N.; Ginzburg, O.; Lam, A.M.I. A method to simultaneously monitor hepatitis C virus NS3 helicase and protease activities. *Methods Mol. Biol.* **2010**, *587*, 223–233.
24. Dahl, G.; Sandström, A.; Akerblom, E.; Danielson, U.H. Effects on protease inhibition by modifying of helicase residues in hepatitis C virus nonstructural protein 3. *FEBS J.* **2007**, *274*, 5979–5986.
25. Frick, D.N. The hepatitis C virus NS3 protein: A model RNA helicase and potential drug target. *Curr. Issues Mol. Biol.* **2007**, *9*, 1–20.
26. Belon, C.A.; Frick, D.N. Helicase inhibitors as specifically targeted antiviral therapy for hepatitis C. *Future Virol.* **2009**, *4*, 277–293.
27. Mayer, A.M.S.; Glaser, K.B.; Cuevas, C.; Jacobs, R.S.; Kem, W.; Little, R.D.; McIntosh, J.M.; Newman, D.J.; Potts, B.C.; Shuster, D.E. The odyssey of marine pharmaceuticals: A current pipeline perspective. *Trends Pharmacol. Sci.* **2010**, *31*, 255–265.
28. Gerwick, W.H.; Moore, B.S. Lessons from the past and charting the future of marine natural products drug discovery and chemical biology. *Chem. Biol.* **2012**, *19*, 85–98.
29. Newman, D.J.; Cragg, G.M. Natural products as sources of new drugs over the 30 years from 1981 to 2010. *J. Nat. Prod.* **2012**, *75*, 311–335.
30. Furuta, A.; Salam, K.A.; Akimitsu, N.; Tanaka, J.; Tani, H.; Yamashita, A.; Moriishi, K.; Nakakoshi, M.; Tsubuki, M.; Sekiguchi, Y.; *et al.* Cholesterol sulfate as a potential inhibitor of hepatitis C virus NS3 helicase. *J. Enzym. Inhib. Med. Chem.* **2013**, doi:10.3109/14756366.2013.766607.
31. Müller, E.L.; Faulkner, D.J. Absolute configuration of halisulfate 3 from the sponge *Ircinia* sp. *Tetrahedron* **1997**, *53*, 5373–5378.
32. Manes, L.V.; Crews, P.; Kernan, M.R.; Faulkner, D.J.; Fronczek, F.R.; Gandour, R.D. Chemistry and revised structure of suvanine. *J. Org. Chem.* **1988**, *53*, 570–575.
33. Kernan, M.R.; Faulkner, D.J. Sesterterpene sulfates from a sponge of the family Halichondriidae. *J. Org. Chem.* **1988**, *53*, 4574–4578.
34. Manes, L.V.; Naylor, S.; Crews, P.; Bakus, G.J. Suvanine, a novel sesterterpene from an *Ircinia* marine sponge. *J. Org. Chem.* **1985**, *50*, 284–286.
35. Kimura, J.; Ishizuka, E.; Nakao, Y.; Yoshida, W.Y.; Scheuer, P.J.; Kelly-Borges, M. Isolation of 1-methylherbipoline salts of halisulfate-1 and of suvanine as serine protease inhibitors from a marine sponge, *Coscinoderma mathewsi*. *J. Nat. Prod.* **1998**, *61*, 248–250.
36. Di Leva, F.S.; Festa, C.; D'Amore, C.; de Marino, S.; Renga, B.; D'Auria, M.V.; Novellino, E.; Limongelli, V.; Zampella, A.; Fiorucci, S. Binding mechanism of the farnesoid X receptor marine antagonist suvanine reveals a strategy to forestall drug modulation on nuclear receptors. Design, synthesis, and biological evaluation of novel ligands. *J. Med. Chem.* **2013**, *56*, 4701–4717.
37. Cassiano, C.; Monti, M.C.; Festa, C.; Zampella, A.; Riccio, R.; Casapullo, A. Chemical proteomics reveals heat shock protein 60 to be the main cellular target of the marine bioactive sesterterpene suvanine. *ChemBioChem* **2012**, *13*, 1953–1958.
38. Singleton, M.R.; Dillingham, M.S.; Wigley, D.B. Structure and mechanism of helicases and nucleic acid translocases. *Annu. Rev. Biochem.* **2007**, *76*, 23–50.

39. Wang, C.-C.; Huang, Z.-S.; Chiang, P.-L.; Chen, C.-T.; Wu, H.-N. Analysis of the nucleoside triphosphatase, RNA triphosphatase, and unwinding activities of the helicase domain of dengue virus NS3 protein. *FEBS Lett.* **2009**, *583*, 691–696.
40. Ndjomou, J.; Kolli, R.; Mukherjee, S.; Shadrack, W.R.; Hanson, A.M.; Sweeney, N.L.; Bartczak, D.; Li, K.; Frankowski, K.J.; Schoenen, F.J.; *et al.* Fluorescent primuline derivatives inhibit hepatitis C virus NS3-catalyzed RNA unwinding, peptide hydrolysis and viral replicase formation. *Antivir. Res.* **2012**, *96*, 245–255.
41. Saalau-Bethell, S.M.; Woodhead, A.J.; Chessari, G.; Carr, M.G.; Coyle, J.; Graham, B.; Hiscock, S.D.; Murray, C.W.; Pathuri, P.; Rich, S.J.; *et al.* Discovery of an allosteric mechanism for the regulation of HCV NS3 protein function. *Nat. Chem. Biol.* **2012**, *8*, 920–925.
42. Ding, S.C.; Kohlway, A.S.; Pyle, A.M. Unmasking the active helicase conformation of nonstructural protein 3 from hepatitis C virus. *J. Virol.* **2011**, *85*, 4343–4353.
43. Tani, H.; Akimitsu, N.; Fujita, O.; Matsuda, Y.; Miyata, R.; Tsuneda, S.; Igarashi, M.; Sekiguchi, Y.; Noda, N. High-throughput screening assay of hepatitis C virus helicase inhibitors using fluorescence-quenching phenomenon. *Biochem. Biophys. Res. Commun.* **2009**, *379*, 1054–1059.
44. Copeland, R.A. *Evaluation of Enzyme Inhibitors in Drug Discovery*; John Wiley & Sons: New York, NY, USA, 2005; pp. 111–140.
45. Salam, K.A.; Furuta, A.; Noda, N.; Tsuneda, S.; Sekiguchi, Y.; Yamashita, A.; Moriishi, K.; Nakakoshi, M.; Tsubuki, M.; Tani, H.; *et al.* Inhibition of hepatitis C virus NS3 helicase by manoalide. *J. Nat. Prod.* **2012**, *75*, 650–654.
46. Salam, K.A.; Furuta, A.; Noda, N.; Tsuneda, S.; Sekiguchi, Y.; Yamashita, A.; Moriishi, K.; Nakakoshi, M.; Tsubuki, M.; Tani, H.; *et al.* Psammaphin A inhibits hepatitis C virus NS3 helicase. *J. Nat. Med.* **2013**, *67*, 765–772.
47. Takahashi, H.; Takahashi, C.; Moreland, N.J.; Chang, Y.-T.; Sawasaki, T.; Ryo, A.; Vasudevan, S.G.; Suzuki, Y.; Yamamoto, N. Establishment of a robust dengue virus NS3-NS5 binding assay for identification of protein-protein interaction inhibitors. *Antivir. Res.* **2012**, *96*, 305–314.

# Mode of Action of Diterpene and Characterization of Related Metabolites from the Soft Coral, *Xenia elongata*

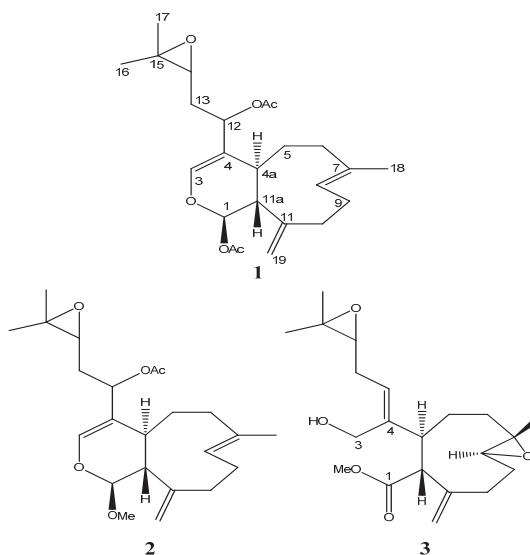
Eric H. Andrianasolo, Liti Haramaty, Eileen White, Richard Lutz and Paul Falkowski

**Abstract:** Chemical and biological investigation of the cultured marine soft coral *Xenia elongata* led to the isolation of two new diterpenes (**2**, **3**). Their structures were elucidated using a combination of NMR and mass spectrometry. Biological evaluations and assessments were determined using the specific apoptosis induction assay based on genetically engineered mammalian cell line D3 deficient in Bak and Bax and derived from a mouse epithelial cell. The diterpenes induce apoptosis in low micromolar concentrations. The results indicate that the previously isolated compound (**1**) affects cell in a manner similar to that of HSP90 and HDAC inhibitors and in a manner opposite of PI3 kinase/mTOR inhibitors. Compound (**3**) inhibits selectively HDAC6 in high micromolar concentrations.

Reprinted from *Mar. Drugs*. Cite as: Andrianasolo, E.H.; Haramaty, L.; White, E.; Lutz, R.; Falkowski, P. Mode of Action of Diterpene and Characterization of Related Metabolites from the Soft Coral, *Xenia elongata*. *Mar. Drugs* **2014**, *12*, 110261115.

## 1. Introduction

Natural products are the most reliable and rich source of new anticancer entities. Over the past 30 years, nearly 63% of anticancer drugs introduced to the pharmaceutical development market are natural products or can be traced from a natural products origin [1,2]. The soft coral of the genus *Xenia elongata* has produced interesting biological molecules, specifically apoptosis inducer compounds [3,4]. These molecules embed a framework of nine-membered rings and a particular arrangement of functional groups with multiple stereocenters. These structural features limit the range of chemical reactions that are applicable to their synthesis. There is little in the existing synthetic literature to define an effective strategy for the synthesis of these molecules [5]. The first total synthesis of an optically active xenicane diterpene has not yet been achieved [5,6]. In our ongoing effort to discover and develop new marine natural product biomedicinals, and in order to explore the diversity of natural products from the soft coral *Xenia elongata*, chemical and biological investigation of this organism were undertaken. Two novel diterpenes (**2**, **3**) were isolated and, remarkably, these new diterpenes induce apoptosis and, more importantly, **3** is 10-fold more active than the most active and previously isolated compound **1** (Figure 1). The detail mode of action of **1** by analysis of MCF-7 breast cancer treated with **1** was also reported here. HDAC inhibitory assay of **3** was also displayed and discussed.

**Figure 1.** Structure of compounds **1**, **2** and **3**.

## 2. Results and Discussion

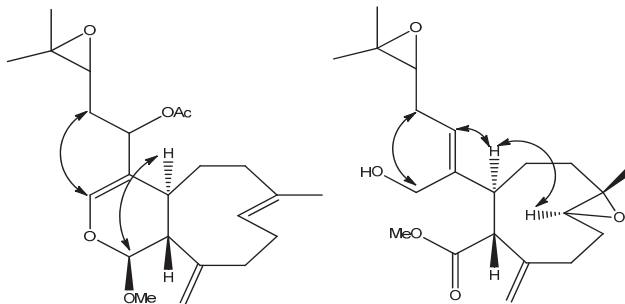
Live colonies of *Xenia elongata* were grown in the coral laboratory at the Marine Biotechnology Center, Institute of Marine and Coastal Sciences, Rutgers University. For extraction, 200 g of the colonies were isolated and frozen. A methanol (or dichloromethane) soluble fraction was extracted from frozen coral tissue, lyophilized and dissolved in DMSO. The extract that induced apoptosis was subsequently fractionated and purified by analytical RPHPLC. Using this strategy, compounds with proapoptotic activity were isolated from the whole tissue extracts. Chemical structures of the two compounds (**2** and **3**) were ascertained by standard spectroscopic techniques as described below.

The molecular formula of **2** was established as  $C_{23}H_{34}O_5$  on the basis of HRESIMS ( $m/z$  413.2299  $[M + Na]^+$  calcd. for  $C_{23}H_{34}O_5Na$ , 413.2298). This indicated a difference of 28 mass units and probably a carbonyl group, compared to compound **1** [3]. The  $^1H$  NMR (Supplementary Figure S1) of **2** indicated clearly the existence of the following functional groups: an 1-methoxydihydropyran moiety [ $\delta$  5.35 (d,  $J = 1.4$  Hz), H-1 and 6.51 (s), H-3], a terminal methylene [ $\delta$  5.05 (s) and 5.15 (s), H-19, H-19'], two methyls  $\alpha$  to oxygen [ $\delta$  1.33 (s), H-16, H-17], an epoxy signal at [ $\delta$  2.75 (dd,  $J = 5.9, 6.2$  Hz), H-14] and a vinyl methyl group [1.60 (s), H-18]. The NMR spectra of compounds **1** and **2** were compared in  $CDCl_3$  and were found to be similar, with the exception of the carbon at C-1 [ $\delta$  99.3] (Supplementary Figure S2) for **2** instead of C-1 [ $\delta$  91.7] for **1** in addition to that **2** has one less carbonyl signal, suggesting that a methoxy group is attached to C-1 in **2** instead of acetate group in **1**. The deshielding effect of the methoxy group to the carbon at C-1 position is more pronounced compared to the deshielding effect of an acetate group to the carbon at the same position.

The relative stereochemistry of **2** was established with the same method as described in our previous work [3] which is based on ROESY data (Supplementary Figure S3), coupling constant analyses and chemical shifts comparison to **1** and xeninculin [7], tsitsixenicin A [8,9] and related

compounds [7,9]. The coupling constant ( $J = 12$  Hz) between H-4a and H-11a suggests a trans ring junction. The small coupling constant ( $J = 1.4$  Hz) between H-1 and H-11a would favor the  $\alpha$ -position for H-1 if the six-member ring was in a quasi-boat conformation. A closer look of the crystal structure of xenicin and essentially the six-member ring, which is also present in **2**, suggests that H-1, if it is in the  $\alpha$ -position, should display ROESY cross peak correlation to H-4a. In order to verify this suggestion, a high scan ROESY experiment was performed. Careful analysis of the ROESY data, particularly in the cross region of H-1 and H-4a, revealed unambiguously that these two protons display a ROESY cross peak correlation (Figure 2). Based on this result, it appears that the configurations at C-1, C-4a, and C-11a in compound **2** are essentially the same as those in **1** and xeniculic acid, in which the protons H-1 and H-4a are on the  $\alpha$  face of the ring and the proton H-11a is oriented on the  $\beta$ -side. This observation confirmed that the stereochemistry of this proton at H-1 position is well conserved and common to any molecule with dihydropyran moiety in the xenicane diterpene class. Previous attempts to establish the stereochemistry of an acetate group at C-12 in xenicane diterpenes by chemical transformations and spectroscopy have failed [9,10], and therefore the stereochemistry at C-12 remains unassigned. This information suggested that the acetate group attached to C-12 is very reactive and probably leads to further transformation of the molecule as described by the proposed rearrangement in Scheme 1. From the above results, the structure of **2** was formulated as shown.

**Figure 2.** Selected ROESY cross peaks for compounds (**2**) and (**3**).

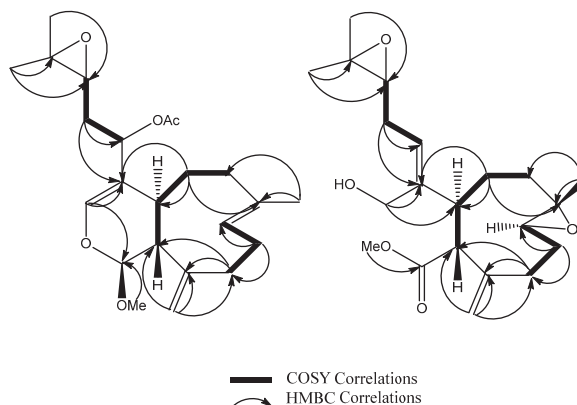


A molecular formula of  $C_{21}H_{32}O_5$  for **3** was determined from HRESIMS data (Supplementary Figure S4 Low resolution).  $^1H$  NMR (Supplementary Figure S5) of **3** indicated the presence of two epoxy signals at  $[\delta 2.80$  (dd,  $J = 11.5, 3.2$  Hz), H-8] and  $[\delta 2.76$  (dd,  $J = 7.2, 6.1$  Hz), H-14], one methyl  $\alpha$  to oxygen  $[\delta 1.16$  (s), H-18] and a terminal methylene  $[\delta 5.00$  (s) and  $5.20$  (s), H-19, H-19']. The presence of two equivalent protons at  $\delta [3.72, d(6)]$ , H-3 for an isolated methylene attached to oxygen indicated that **3** has a primary alcohol functional group at C-3 which also revealed that the dihydropyran moiety presents in **1** and **2** is absent in **3**. The NMR data of **3** were analogous to those of diterpene xenitacin isolated from the Formosan soft coral *Xenia umbellata* [4] except that xenitacin had an acetate group attached to C-3 instead of a hydroxy group for **3** at C-3 (Supplementary Figure S6).

The relative stereochemistry of **3** was investigated with the aid of a ROESY spectrum. The *Z*-configuration was assigned to  $\Delta^{4(12)}$  double bond based on the observed ROESY cross peak

between H-12 [ $\delta$  5.45] and H-4a [ $\delta$  3.29]. The configuration of the two chiral centers at C-4a and C-11a was deduced by ROESY data and comparison with those of xenitacin [4]. The large coupling constant ( $J = 12$  Hz) between H-4a [ $\delta$  3.29] and H-11a [ $\delta$  3.45] suggests that they have a configuration opposite to each other [4]. The observed ROESY cross peak between H-4a [ $\delta$  3.29] and H-8 [ $\delta$  2.80] (Figure 2, Supplementary Figure S7) suggests that they have similar configuration to xenitacin [4]. Therefore the structure of **3** was established as shown. Key HMBC and selected COSY correlations were established for **2** and **3** in order to assign all carbons framework in their structures (Figure 3 and Supplementary Figures S8–S13).

**Figure 3.** Key HMBC and selected COSY correlations for compounds (**2**) and (**3**).

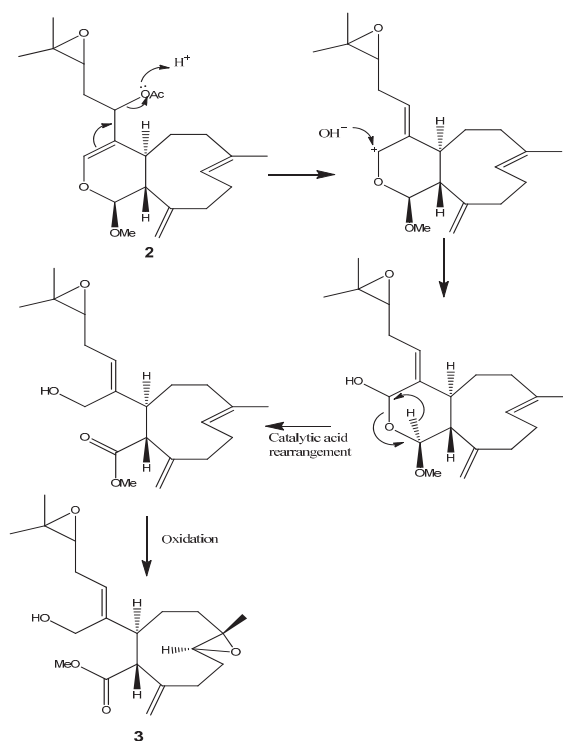


In order to assess the pro-apoptotic activities of these compounds as a marker for their potential anticancer efficacy, methanol soluble fractions of *Xenia* extracts were tested for apoptosis induction in an MTT assay using the apoptosis competent W2 and apoptosis resistant D3 cells, as described in our previous work [3]. Compounds **2** and **3** induce measurable cell death in W2 but not in D3 cells (Supplementary Figures S14 and S15). To quantify apoptosis induction, viability was determined using an MTT assay [11]. Measurements were taken at time 0 and 48 h after addition of compounds in different concentrations. Viability was calculated as the difference between time 0 (addition of compound) and 48 h. Apoptosis induction was defined as at least 20% death of W2 cells and a 10% or higher growth of D3 cells by MTT assay. The optimal concentration of the compounds for apoptosis induction was determined based on the dose response of the two cells lines by MTT assay. The results reveal a significant induction of apoptosis by the whole tissue extract and by individual compounds (11.5  $\mu$ M for **2** and 1.2  $\mu$ M for **3**), with the most remarkable induction shown by compound **3** (1.2  $\mu$ M) which is ten times more active than compound **1** previously characterized [3]. Treatment of W2 and D3 cells with 0.1  $\mu$ M staurosporine, a protein kinase inhibitor and potent inducer of apoptosis, was included as a positive control for apoptosis induction and for comparison. Thus, the diterpenes we have isolated and characterized effectively and specifically activate apoptosis in immortalized mammalian epithelial cells.

There are efforts underway to synthesize optically active xenicane diterpene [12] and work is in progress for the synthesis of diterpene from *Xenia elongata*. One synthetic compound (Supplementary

Figure S16) from this work which has the same structure of **3** but does not have the side chain was also tested for comparison of activity. The result revealed that this synthetic compound did not induce apoptosis, which suggested that the side chain is critical for the activity. It is also reported before that a similar structure, xenitacin, isolated from the Formosan soft coral *Xenia umbellata* [4], is the most active compound in its group in a cytotoxicity assay against P-388, HT-29 and A549 cells [4]. These bioactivity results may suggest that a conversion or rearrangement toward the most active structure may undergo within the organism itself or even in the cell in order to increase the efficacy of affecting or killing cancer cells. A proposed conversion or rearrangement of **2** to **3** is displayed (Scheme 1). It is also possible that **1** will convert to **2** by enzymatic reaction of deacetylation followed by methylation and then **2** will be converted to **3**.

**Scheme 1.** Proposed rearrangement of **2** under acidic conditions, to give **3**.



In order to determine the mode of action of diterpenes from *Xenia elongata*, a connectivity analysis for MCF-7 breast cancer cells treated with compound **1** was performed. The objective is to analyze changes in gene expression in a breast cancer cell line exposed to a soft coral diterpene, which is compound **1** in this experiment, and to compare the resulting signature to perturbagen signatures in the Connectivity Map [13].

To prepare a 0.12 M stock solution in DMSO, 1.6 mg of **1** was used. Proliferating MCF-7 breast cancer cells were treated in triplicate with either a 120  $\mu$ M final concentration of **1** (final DMSO concentration 0.1%), or were left untreated for 8 h. Cells were harvested before the RNA was

extracted then purified, reverse transcribed, and hybridized to an Affymetrix array by the CINJ Transcriptional Profiling Core. The resulting gene expression data were analyzed.

Expression levels of 22,277 genes in three untreated and three treated samples were obtained using an Affymetrix array. For this initial analysis, the 11,400 genes were used for which all six samples provided clearly measurable signals. (Genes for which any sample was determined to be “A” or “M” were excluded, and only those for which all six were called “P” by the Affymetrix software were kept).

The package “siggenes” [14] was used in the bioconductor set of gene expression packages for the R statistical system. Two different methods were considered for obtaining the most differentially expressed genes. The first method is known as “significance analysis of arrays” or “SAM” and was first proposed by Tusher *et al.* [15]. This method computes a modified t-statistic comparing treated to control samples for each gene. It then identifies differentially expressed genes so that the false discovery rate (FDR) is a pre-specified value. The second method, known as “Empirical Bayes Analysis of Microarrays” or “EBAM” [16] also computes the modified t-statistic. Unlike SAM, however, it computes the posterior probability that each gene is differentially expressed. Each of the two methods can be used to create a list of genes that are differentially expressed. The two lists will generally be different, although there is usually some overlap.

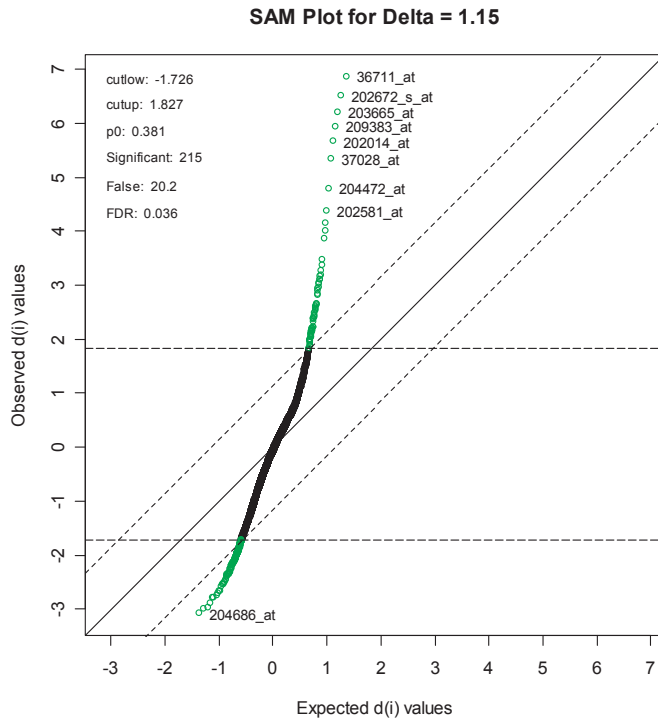
For the SAM method, the parameter delta was set to 1.15. This produced an FDR of 3.58%, and resulted in a list of 215 genes, of which an estimated 20 genes are falsely declared to be differentiated. A SAM plot is given in Figure 4, with some of the genes labeled. A complete list is given in Supplementary Table S1.

For the EBAM method, the required posterior probability was set to 0.7, which resulted in an FDR of 15.4%, to generate a list of about the same number of genes (211). An EBAM plot of posterior probabilities is given in Figure 5, and a complete list of differentially expressed genes is given in Supplementary Table S2. A list of the 61 genes that are present on both lists is given in Supplementary Table S3. One gene, with code “36711\_at,” is clearly at the top of both lists. This protein is a novel MAFF (v-maf musculoaponeurotic fibrosarcoma (avian) oncogene family, protein F)-LIKE protein.

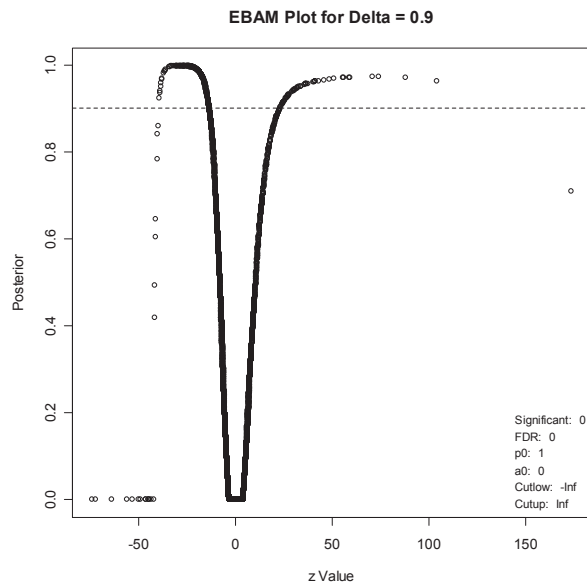
The diterpene connectivity scores for the 453 “instances” (representing treatment of various cell lines with 164 different compounds) are shown in Supplementary Tables S4 and S5. Common drug targets among the mostly highly connected instances include the proteasome, calmodulin, and histone deacetylases (HDACs). The presence of structurally distinct compounds that yield high connectivity scores suggests that the diterpene **1** acts as a proteasome and calmodulin inhibitor. Conversely, instances associated with the most highly ranked negative scores (corresponding to a gene expression profile similar to a reversal of the diterpene signature) include compounds that target the PI3 kinase/mTOR pathway. Additional inferences can be made from “permuted results” provided by the connectivity analysis (Table 1). In particular, analysis of permuted results supports the idea that the diterpene **1** is affecting cells in a manner similar to that of HSP90 and HDAC inhibitors and in a manner opposite to that of PI3 kinase/mTOR inhibitors. Note that the proteasome inhibitors are not included in the permuted results because they are represented by single instances.



**Figure 4.** SAM Plot, with some genes labeled.



**Figure 5.** EBAM plot. The points above the dotted line correspond to genes with a posterior probability of 0.9 of being differentially expressed.

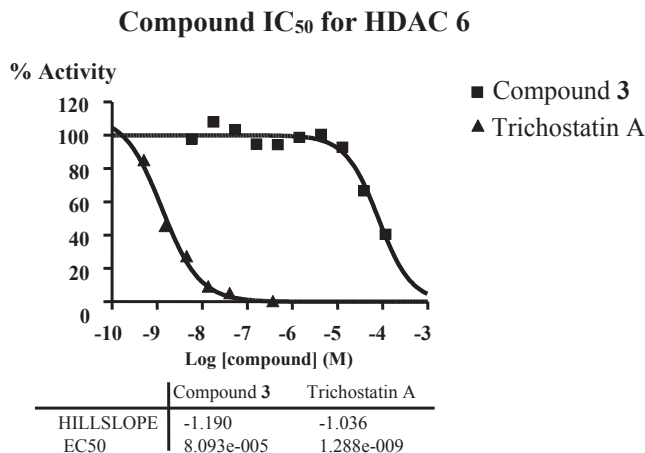


**Table 1.** Permuted results.

Rank	CMAP name	Score	N	Enrichment	<i>P</i> value	Target
1	sirolimus	-0.254	10	-0.770	0.0000	mTOR
2	17-allylamino-geldanamycin	0.496	18	0.611	0.0000	HSP90
3	trichostatin A	0.565	12	0.714	0.0000	HDACs
4	LY-294002	-0.038	17	-0.506	0.0001	PI3 kinase
5	geldanamycin	0.544	6	0.759	0.0004	HSP90
6	5253409	0.748	2	0.971	0.0009	?
7	5224221	0.758	2	0.967	0.0015	?
8	vorinostat	0.684	2	0.956	0.0032	HDAC
9	tetraethylene-pentamine	-0.084	6	-0.662	0.0055	proteases
10	wortmannin	-0.248	8	-0.565	0.0071	PI3 kinase

Each row in the table summarizes the performance of all instances produced with the same perturbagen. The table displays the cmap name for those perturbagens, the arithmetic mean of the connectivity scores for each of those instances (labeled “score”), the number of those instances (labeled “*n*”), a measure of the enrichment of those instances in the list of all instances ordered by descending order of connectivity score and up score (labeled “enrichment”) and a permutation *p*-value for that enrichment score (labeled “*p*”). Enrichment scores and *p*-values are not provided for perturbagens represented by only one instance or where the mean of the connectivity scores for their instances is zero.

In order to verify the predicted mode of action of diterpene from connectivity analysis, HDAC inhibitory assays were performed. Given the availability of compound material and the structural similarity of all isolated diterpenes, only compound **3** was subjected to enzymatic inhibition test against the class I (HDAC1, HDAC2, HDAC3 and HDAC8), the class II A (HDAC4, HDAC5, HDAC7 and HDAC9) and the class II B (HDAC6) enzymes. HDAC inhibitors Trichostatin A (TSA) and TMP269 (TMP) were used as reference compounds. The results showed that compound **3** up to 50 or 100  $\mu$ M did not significantly inhibit the class I (HDAC1, Supplementary Table S6; HDAC2, Supplementary Table S7; HDAC3, Supplementary Table S8; HDAC8, Supplementary Table S9) as well as the class II A (HDAC4, Supplementary Table S10; HDAC5, Supplementary Table S11; HDAC7, Supplementary Table S12; HDAC9, Supplementary Table S13), though compound **3** inhibited class II B HDAC6 with IC<sub>50</sub> around 80  $\mu$ M (Figure 6, Supplementary Table S14). The predicted mode of action of diterpene was verified. HDAC6 appears to be the key deacetylase regulating Hsp90; treatment of breast cancer cells with Hsp90 inhibitors or HDAC inhibitor (vorinostat) induces breast cancer cell differentiation [17]. Cell death signaling is complex and it is clear that there are multiple alternate pathways, especially in cancer cell types. The HDAC6 inhibition pathway is among several pathways that the diterpene may trigger simultaneously, thus explaining the difference of potency between the apoptosis induction assay and the HDAC6 inhibition assay.

**Figure 6.** Inhibition of HDAC6 by compound 3, IC<sub>50</sub> around 80  $\mu$ M.

### 3. Experimental Section

#### 3.1. General Experimental Procedures

Optical rotations were measured on JASCO P 1010 polarimeter. FT-IR spectra were obtained employing Hewlett Packard 8452A and Nicolet 510 instruments. All NMR spectra were recorded on a Bruker Avance DRX300 and DPX400 spectrometers. Spectra were referenced to residual solvent signal with resonances at  $\delta_{H/C}$  7.26/77.1 (CDCl<sub>3</sub>). ESI MS data were acquired on a Waters Micromass LCT Classic mass spectrometer and Varian 500-MS LC Ion Trap. HPLC separations were performed using Waters 510 HPLC pumps, a Waters 717 plus autosampler, and Waters 996 photodiode array detector. All solvents were purchased as HPLC grade.

#### 3.2. Extraction and Isolation Procedures

The organism was purchased from Ocean Reef Aquariums (ORA). Live colonies of *Xenia elongata* were kept in optimal growing conditions (Salinity 34 g/L, temperature 25 °C, light [min. 250  $\mu$ E m<sup>-2</sup> s<sup>-1</sup> and max. 500  $\mu$ E m<sup>-2</sup> s<sup>-1</sup>], pH 8.2–8.4) in the coral laboratory at the Marine Biotechnology Center, Institute of Marine and Coastal Sciences, Rutgers University. A voucher specimen is available as collection number SC/XE/Apr-04 System 1A. The soft coral was stored at –80 °C after addition of liquid nitrogen before workup. The material (80 g) was extracted three times, first with CH<sub>2</sub>Cl<sub>2</sub> and then with MeOH, to give a nonpolar crude organic extract (259.2 mg) and a polar crude organic extract (537.9 mg). A portion of these two extracts (30 mg each) was tested for apoptosis induction. The polar crude organic extract was found active and subjected to fractionation by solid phase extraction cartridge (Reverse-phase C18) to give three fractions using a stepwise gradient of H<sub>2</sub>O-MeOH as solvent system. The fraction eluting with 15% H<sub>2</sub>O and 85% MeOH had apoptosis induction activity. This fraction was further chromatographed on analytical RP HPLC (Phenomenex luna C8, 250  $\times$  4.60 mm) using a gradient elution (starting with 80% water and

20% CH<sub>3</sub>CN, flow rate 1 mL/min) to yield successively 3.1 mg of **2** ( $t_R = 27$  min), 2.6 mg of **3** ( $t_R = 33$  min). The extract/compound weight percents are 0.57% and 0.48% for **2** and **3**, respectively.

Compound **2**:  $[\alpha]_D^{22.5} -58$  ( $c$  0.87, CHCl<sub>3</sub>); IR  $\nu_{max}$  (neat) 3075, 2970, 2930, 2860, 1736, 1670, 1608, 1445, 1370, 1236, 1155, 1015, 950, 870, 835, 790 cm<sup>-1</sup>; <sup>1</sup>H NMR and <sup>13</sup>C NMR, see Table 2; HRESIMS  $m/z$  413.2299 (calcd. for C<sub>23</sub>H<sub>34</sub>O<sub>5</sub>Na, 413.2298).

**Table 2.** NMR Spectroscopic Data of Compound **2** <sup>1</sup>H (300 MHz, CDCl<sub>3</sub>) and <sup>13</sup>C (75 MHz, CDCl<sub>3</sub>).

Compound 2			
Position	$\delta_C$	$\delta_H$	HMBC
1	99.3 CH	5.35, d (1.4)	3, 4a
3	142.7 CH	6.51, s	1, 4, 4a, 12
4	112.6 qC		
4a	35.7 CH	2.19, dd (8, 12)	3, 4, 5, 11
5	31.0 CH <sub>2</sub>	1.50, m 1.95, m	4a, 6
6	40.1 CH <sub>2</sub>	2.08, m 2.22, m	5, 7, 8
7	135.5 qC		
8	124.6 CH	5.25, t (5.8)	9
9	24.7 CH <sub>2</sub>	2.45, m 2.08, m	8, 10
10	35.7 CH <sub>2</sub>	2.30, m	11, 19
11	150.0 qC		
11a	55.1 CH	1.70, dd (1.2,12)	1, 4a, 11
12	70.8 CH	4.85, dd (5.8, 6.1)	3, 4, 4a, 13, 14, CO
13	31.9 CH <sub>2</sub>	1.98, m 2.00, m	12, 14
14	62.8 CH	2.75, dd (5.9, 6.2)	13
15	60.1 qC		
16	18.9 CH <sub>3</sub>	1.33, s	14, 15, 17
17	24.7 CH <sub>3</sub>	1.33, s	14, 15, 16
18	17.7 CH <sub>3</sub>	1.60, s	6, 7, 8
19	119.8 CH <sub>2</sub>	5.05, s 5.15, s	10, 11, 11a
CH <sub>3</sub> of CH <sub>3</sub> COO	21.0 CH <sub>3</sub>	2.09, s	CO
CO of CH <sub>3</sub> COO	170.9 qC		
CH <sub>3</sub> of CH <sub>3</sub> O	51.5 CH <sub>3</sub>	3.52, s	1

Compound **3**:  $[\alpha]_D^{22.5} +12$  ( $c$  0.13, CHCl<sub>3</sub>); IR  $\nu_{max}$  (neat) 3075, 2970, 1740, 1730, 1600, 1370, 1240 cm<sup>-1</sup>; <sup>1</sup>H NMR and <sup>13</sup>C NMR, see Table 3; HRESIMS  $m/z$  365.2325 (calcd. for C<sub>21</sub>H<sub>33</sub>O<sub>5</sub>, 365.2328).

### 3.3. Biological Evaluation—Apoptosis Induction

Apoptosis induction in the presence of compounds (**2**, **3**) was carried out in the following manner. W2 (apoptosis competent) and D3 (apoptosis defective) cells were plated in 96- and 6-well plates and incubated for 24 h, after which they were evenly spread at about 50% confluency. At this time, compounds dissolved in DMSO and diluted in growth medium (DMEM) were added

to the cells at various concentrations. DMSO concentration was kept at 0.5% in all wells. Plates were incubated for 24, 48 and 72 h. Cell viability was determined using a modification of the MTT assay [11], where the reduction of yellow tertazolium salt (MTT—3-(4,5-dimethylthiazol-2-yl)-2,5) to purple formazan indicates mitochondrial activity, and thus cell viability. Cells were incubated with 0.5 mg/mL MTT for 3 h. Supernatant was aspirated and DMSO was added to dissolve the formazan crystals. After 30 min incubation at 37 °C, with shaking, absorbance was read at 570 nm on a Spectra MAX 250 (Molecular Devices) plate reader. Differential growth from time 0 to 48 h was calculated. Starurosporine, an apoptosis inducer, and DMSO were used as positive and negative controls, respectively.

**Table 3.** NMR Spectroscopic Data of Compound 3 <sup>1</sup>H (300 MHz, CDCl<sub>3</sub>) and <sup>13</sup>C (75 MHz, CDCl<sub>3</sub>).

<b>Compound 3</b>			
<b>Position</b>	<b>δ<sub>C</sub></b>	<b>δ<sub>H</sub></b>	<b>COSY</b>
1	172.4 qC		
3	65.5 CH <sub>2</sub>	3.72, d(6)	
4	138.1 qC		
4a	38.3 CH	3.29, m	5, 11a
5	28.7 CH <sub>2</sub>	1.55, m 1.73, m	4a, 6
6	38.3 CH <sub>2</sub>	1.17, m 1.99, m	5
7	59.7 qC		
8	63.8 CH	2.80, dd (11.5, 3.2)	9
9	27.2 CH <sub>2</sub>	2.13, m 1.43, m	8, 10
10	26.2 CH <sub>2</sub>	2.13, m 2.34, m	9
11..	143.0 qC		
11a	60.6 CH	3.45, d (12.0)	4a
12	126.6 CH	5.45, dd (10.1, 7.2)	13
13	28.1 CH <sub>2</sub>	2.30, m 2.38, m	12, 14
14	63.3 CH	2.76, dd (7.2, 6.1)	13
15	58.8 qC		
16	19.0 CH <sub>3</sub>	1.29, s	
17	24.6 CH <sub>3</sub>	1.32, s	
18	18.8 CH <sub>3</sub>	1.21, s	
19	121.1 CH <sub>2</sub>	5.00, s 5.20, s	
CH <sub>3</sub> O	51.6 CH <sub>3</sub>	3.50, s	

### 3.4. Connectivity Analyses

Cells were harvested and RNA extracted using TRIzol Reagent, (Invitrogen, Carlsbad, CA, USA) and RNeasy kit (Qiagen Sciences, MD, USA). RNA was purified, reverse transcribed, and hybridized to an Affymetrix U133 2.0 array by the CINJ Transcriptional Profiling Core. The resulting gene expression data were analyzed. Two methods were used to identify the most differentially expressed genes in the treated *versus* control groups. The first method (significance analysis of arrays) was set at a false discovery rate of 3.58%, and yielded 215 genes. A subset of

these 215 genes, including 145 with at least a 3-fold difference in expression (58 upregulated by treatment, 87 downregulated), was defined as the diterpene signature, and was used for the connectivity analysis supplementary (Supplementary Table S5). The diterpene signature was compared to 453 gene expression profiles present in the Connectivity Map [13]. For each of the 453 profiles, a connectivity score was calculated (based on the Kolmogorov–Smirnov statistic), which represents the relative similarity of the profile to the diterpene signature.

### 3.5. HDAC Inhibition Assay

#### 3.5.1. Class I

In singlet 10-dose IC<sub>50</sub> mode with 3-fold serial dilution starting at 50 μM against 4 HDACs (HDAC1, HDAC2, HDAC3 and HDAC8), 0.5 mg of Compound **3** was tested.

HDAC reference compound Trichostatin A (TSA) and TMP 269 were tested in a 10-dose IC<sub>50</sub> with 3-fold serial dilution starting at 10 μM.

Substrate for HDAC1, 2 and 3: Fluorogenic peptide from p53 residues 379–382 (RHKK(Ac)AMC).

Substrate for HDAC8: Fluorogenic peptide from p53 residues 379–382 (RHK(Ac)K(Ac)AMC).

Data pages include raw data, % Enzyme activity (relative to DMSO controls), and curve fits. Curve fits were performed where the enzyme activities at the highest concentration of compounds were less than 65%. IC<sub>50</sub> values were calculated using the GraphPad Prism 4 program based on a sigmoidal dose-response equation. The blank (DMSO) value was entered as  $1.0 \times 10^{-12}$  of concentration for curve fitting.

#### 3.5.2. Class II A and Class II B

In singlet 10-dose IC<sub>50</sub> mode with 3-fold serial dilution starting at 100 μM against 5 HDACs [II A (HDAC4, HDAC5, HDAC7, and HDAC9) IIB (HDAC6)], 0.5 mg of Compound **3** was tested.

HDAC reference compounds Trichostatin A (TSA) and TMP269 (TMP) were tested in a 10-dose IC<sub>50</sub> with 3-fold serial dilution starting at 10 μM.

Substrate for HDAC 6: Fluorogenic peptide from p53 residues 379–382 (RHKK(Ac)AMC).

Substrate for HDAC 4,5,7 and 9: Fluorogenic HDAC Class2a Substrate (Trifluoroacetyl Lysine, Ac-LGK(TFA)-AMC).

IC<sub>50</sub> values were calculated using the GraphPad Prism 4 program based on a sigmoidal dose-response equation. The blank (DMSO) value was entered as  $1.0 \times 10^{-12}$  of concentration for curve fitting.

#### 3.5.3. Class II B for IC<sub>50</sub> Calculation

0.5 mg of Compound **3** was tested in duplicate 10-dose IC<sub>50</sub> mode with 3-fold serial dilution starting at 120 μM against 1 HDAC (HDAC6).

HDAC reference compounds Trichostatin A (TSA) was tested in a 10-dose IC<sub>50</sub> with 3-fold serial dilution starting at 10 μM.

Substrate for HDAC6: Fluorogenic peptide from p53 residues 379–382 (RHKK(Ac)AMC).

IC<sub>50</sub> values were calculated using the GraphPad Prism 4 program based on a sigmoidal dose-response equation. The blank (DMSO) value was entered as  $1.0 \times 10^{-12}$  of concentration for curve fitting.

#### 4. Conclusions

The compounds described here represent novel natural products with specific proapoptotic, and therefore potential anticancer, activities. This work describes the mode of action of diterpene from the soft coral *Xenia elongata* using connectivity analysis for MCF-7 cells treated with a coral diterpene. The coral diterpene is affecting cells in a manner similar to that of HSP90 and HDAC inhibitors and in a manner opposite to that of PI3 kinase/mTOR inhibitors. The vast majority of human solid tumors are of epithelial origin, and defects in apoptosis, mostly upstream of Bax and Bak, play important roles in both tumor suppression and mediation of chemotherapeutic response. Consequently, efforts are increasingly focused on developing drugs that can re-activate the apoptotic pathway. The compounds identified here induce apoptosis upstream of Bax and Bak and may have a potential for use as anticancer agents that exploit the apoptosis pathway in tumor cells. Furthermore, the diterpene selectively inhibits HDAC6 and represents a new model structure of selective HDAC inhibitors which will contribute to the development of HDAC practical isoform selective [18]. Future work will likely focus on the identification of the protein targeted by the coral diterpene and the optimization of essential pharmacophores.

#### Acknowledgments

We thank Murugesan Gounder and Eric Rubin from Robert Wood Johnson Medical School and Cancer Institute of New Jersey for the connectivity analysis. We also thank Dirk Moore from Biometrics Cancer Institute of New Jersey for gene expression analysis. We acknowledge Michael Drahl and Tony Wang for making the synthetic compound available. This research was funded by Rutgers University through an Academic Excellence award to Paul Falkowski and Richard Lutz.

#### Conflicts of Interest

The authors declare that there is no conflict of interest.

#### References

1. Newman, D.J.; Cragg, G.M. Natural products as sources of new drugs over the last 25 years. *J. Nat. Prod.* **2007**, *70*, 461–477.
2. Simmons, T.L.; Andrianasolo, E.H.; McPhail, K.; Flatt, P.; Gerwick, W.H. Marine natural products as anticancer drugs. *Mol. Cancer Ther.* **2005**, *4*, 333–342.

3. Andrianasolo, E.H.; Haramaty, L.; Degenhardt, K.; Mathew, R.; White, E.; Lutz, R.; Falkowski, P. Induction of apoptosis by diterpenes from the soft coral *Xenia elongata*. *J. Nat. Prod.* **2007**, *70*, 1551–1557.
4. Duh, C.-Y.; El-Gamal, A.A.H.; Chiang, C.-Y.; Chu, C.-J.; Wang, S.-K.; Dai, C.-F. New cytotoxic xenia diterpenoids from the formosan soft coral *Xenia umbellata*. *J. Nat. Prod.* **2002**, *65*, 1882–1885.
5. Pollex, A.; Hiersemann, M. Catalytic asymmetric claisen rearrangement in natural product synthesis: Synthetic studies toward (–)-xeniolide F. *Org. Lett.* **2005**, *7*, 5705–5708.
6. Mushti, C.S.; Kim, J.-H.; Corey, E.J. Total synthesis of antheliolide A. *J. Am. Chem. Soc.* **2006**, *128*, 14050–14052.
7. Kashman, Y.; Groweiss, A. New diterpenoids from the soft corals *Xenia macrospiculata* and *Xenia obscuronata*. *J. Org. Chem.* **1980**, *45*, 3814–3824.
8. Davies-Coleman, M.T.; Beukes, D.R. Ten years of marine natural products research at Rhodes University. *S. Afr. J. Sci.* **2004**, *100*, 539–543.
9. Hooper, G.J.; Davies-Coleman, M.T.; Schleyer, M. New diterpenes from the South African soft coral *Eleutherobia aurea*. *J. Nat. Prod.* **1997**, *60*, 889–893.
10. Coval, S.J.; Scheuer, P.J.; Matsumoto, G.K.; Clardy, J. Two new xenicin diterpenoids from the octocoral *Anthelia edmondsoni*. *Tetrahedron* **1984**, *40*, 3823–3828.
11. Mosmann, T. Rapid colorimetric assay for cellular growth and survival: Application to proliferation and cytotoxicity assays. *J. Immunol. Meth.* **1983**, *65*, 55–63.
12. Drahl, M.A.; Akhmedov, N.G.; Williams, L.J. Selective conversion of an enantioenriched cyclonadienone to the xeniolide, xenibellol, and florldide cores: An integrated routing strategy. *Tetrahedron Lett.* **2011**, *52*, 325–328.
13. Connectivity MAP 02. Available online: <http://www.broad.mit.edu/cmap/> (accessed on 12 December 2007).
14. Schwender, H.; Krause, A.; Ickstadt, K. Identifying Interesting Genes with siggenes. *RNews* **2006**, *6*, 45–50.
15. Tusher, V.G.; Tibshirani, R.; Chu, G. Significance analysis of microarrays applied to the ionizing radiation response. *Proc. Natl. Acad. Sci. USA* **2001**, *98*, 5116–5121.
16. Efron, B.; Tibshirani, R.; Storey, J.D.; Tusher, V. Empirical bayes analysis of a microarray experiment. *J. Am. Statist. Assoc.* **2001**, *96*, 1151–1160.
17. Thomas, S.; Munster, P.N. Histone deacetylase inhibitor induced modulation of anti-estrogen therapy. *Cancer Lett.* **2009**, *280*, 184–191.
18. Su, H.; Altucci, L.; You, Q. Competitive or noncompetitive, that's the question: Research toward histone deacetylase inhibitors. *Mol. Cancer Ther.* **2008**, *7*, 1007–1012.



## The Marine Sponge-Derived Inorganic Polymers, Biosilica and Polyphosphate, as Morphogenetically Active Matrices/Scaffolds for the Differentiation of Human Multipotent Stromal Cells: Potential Application in 3D Printing and Distraction Osteogenesis

Xiaohong Wang, Heinz C. Schröder, Vladislav Grebenjuk, Bärbel Diehl-Seifert, Volker Mailänder, Renate Steffen, Ute Schloßmacher and Werner E. G. Müller

**Abstract:** The two marine inorganic polymers, biosilica (BS), enzymatically synthesized from ortho-silicate, and polyphosphate (polyP), a likewise enzymatically synthesized polymer consisting of 10 to >100 phosphate residues linked by high-energy phosphoanhydride bonds, have previously been shown to display a morphogenetic effect on osteoblasts. In the present study, the effect of these polymers on the differential differentiation of human multipotent stromal cells (hMSC), mesenchymal stem cells, that had been encapsulated into beads of the biocompatible plant polymer alginate, was studied. The differentiation of the hMSCs in the alginate beads was directed either to the osteogenic cell lineage by exposure to an osteogenic medium (mineralization activation cocktail; differentiation into osteoblasts) or to the chondrogenic cell lineage by incubating in chondrocyte differentiation medium (triggering chondrocyte maturation). Both biosilica and polyP, applied as Ca<sup>2+</sup> salts, were found to induce an increased mineralization in osteogenic cells; these inorganic polymers display also morphogenetic potential. The effects were substantiated by gene expression studies, which revealed that biosilica and polyP strongly and significantly increase the expression of bone morphogenetic protein 2 (BMP-2) and alkaline phosphatase (ALP) in osteogenic cells, which was significantly more pronounced in osteogenic *versus* chondrogenic cells. A differential effect of the two polymers was seen on the expression of the two collagen types, I and II. While collagen Type I is highly expressed in osteogenic cells, but not in chondrogenic cells after exposure to biosilica or polyP, the upregulation of the steady-state level of collagen Type II transcripts in chondrogenic cells is comparably stronger than in osteogenic cells. It is concluded that the two polymers, biosilica and polyP, are morphogenetically active additives for the otherwise biologically inert alginate polymer. It is proposed that alginate, supplemented with polyP and/or biosilica, is a suitable biomaterial that promotes the growth and differentiation of hMSCs and might be beneficial for application in 3D tissue printing of hMSCs and for the delivery of hMSCs in fractures, surgically created during distraction osteogenesis.

Reprinted from *Mar. Drugs*. Cite as: Wang, X.; Schröder, H.C.; Grebenjuk, V.; Diehl-Seifert, B.; Mailänder, V.; Steffen, R.; Schloßmacher, U.; Müller, W.E.G. The Marine Sponge-Derived Inorganic Polymers, Biosilica and Polyphosphate, as Morphogenetically Active Matrices/Scaffolds for the Differentiation of Human Multipotent Stromal Cells: Potential Application in 3D Printing and Distraction Osteogenesis. *Mar. Drugs* **2014**, *12*, 1131-1147.

## 1. Introduction

Bone formation is a complex process involving several cell lineages and growth factors, as well as an ordered scaffold, comprising a fibrillar organic network. The major categories of bone cells are the bone forming osteoblasts and the bone resorbing osteoclasts. In addition, osteocytes are found in mature bone, which do not divide and are derived from osteoprogenitors. Finally, lining cells cover the bone surface. During bone formation, a controlled cross-talk and coupling between the major cells takes place that maintains the balance between the anabolic osteoblasts and the catabolic osteoclasts [1]. While human osteoblasts derive from multipotent stromal cells (hMSC), previously also termed mesenchymal stem cells, osteoclasts differentiate from the monocyte/macrophage hematopoietic lineage and develop and adhere onto bone matrix.

Human MSCs (hMSCs), discovered in 1968 by Friedenstein [2], have the capacity to readily differentiate into the osteogenic, chondrogenic, adipogenic or myogenic cell lineage, depending on the activation of specific transcription factors. They can be efficiently expanded in culture; even after million-fold expansion, they retain the ability to differentiate (see [3]). Since hMSCs are very contact inhibited, they need to be expanded *ex vivo*. hMSCs are considered to be very promising candidates for bone and cartilage regeneration [4], due to their high osteogenic differentiation capacity. A promising approach to accelerate the healing of bone defects, including fractures created during bone lengthening by distraction osteogenesis (DO), might be the delivery of autologous MSCs directly to the damaged site [5]. This approach would provide a new strategy to manage the major, well-known problems caused by the common treatment of bone defects by autogenic bone grafting (e.g., [6]). At present, the most promising method for the application of MSCs appears to be the injection/delivery of the cells, embedded into platelet lysate from whole blood-derived pooled platelet concentrates and apheresis-derived platelet concentrates for the isolation and expansion of human bone marrow mesenchymal stromal cells [7]. Even though this technique sounds straightforward, it is presently difficult to deliver the cells to the desired location. Furthermore, a suitable, more solid-state matrix for embedding the MSCs during the injection process would improve the desired outcome.

Likewise important is the composition of a morphogenetically active scaffold for the three-dimensional (3D) growth of MSCs. A solution for formulating a suitable scaffold for MSCs would provide the basis for a future 3D printing/bioprinting of cells and human tissue/organs [8]. As a first step to reach this goal, the application of 3D printing in prosthetics, for the fabrication of human tissue bioprints inserted into lesions created during DO, is proposed. DO is an established and widely used technique for regenerating endogenous bone in orthopedic and maxillofacial surgery [9]. This surgical procedure aims to elicit a controlled regenerative process by the application of an active mechanical strain in order to initiate and enhance the biological response in the injured tissues to form new bone tissue. The regeneration process during DO includes four distinct stages [10]: (i) osteotomy; (ii) the latency phase, comprising the period between osteotomy and distraction (during this period, soft callus is formed); (iii) the distraction phase, during which traction is applied to transport bone; the formation of new immature woven and parallel-fibered bone islands commences; (iv) the consolidation phase, during which maturation and corticalization

of the regenerating bone occurs. During the distraction phase, a dynamic microenvironment is established, characterized by an increased angiogenesis, which is paralleled and followed by an increased proliferation of spindle-shaped fibroblasts. In turn, collagen (mostly Type I) is formed alongside the angiogenic centers, allowing intramembranous, but not endochondral, ossification [11]. Besides an intense osteoblastic differentiation activity [12], occasionally, also, trans-differentiation processes of chondroblasts, as well as of fibroblasts into osteoblasts have been reported. During the distraction phase, as well as during the consolidation phase, the high expression of the genes encoding for the bone morphogenetic proteins 2 and 4 (BMP-2 and BMP-4) has been described [13]. A series of complications associated with DO has been reported that, besides intra-operative difficulties, include, in particular, intra-distraction complications, which arise during distraction, as well as post-distraction complications, which concern the late problems arising during the period of splinting, e.g., malunion or relapse [14].

Recently, we developed a morphogenetically active scaffold, based on biosilica-alginate hydrogel [8,15]. Alginates, polysaccharides, allow the fabrication of a variety of biomaterials suitable for tissue engineering, e.g., gels and fibers, and are suitable vehicles for injectable solutions as pastes [16]. If those alginates are enriched with biosilica, the fabricated hydrogel has been shown to provide a morphogenetically active scaffold for bone-related SaOS-2 cells *in vitro* [8]. Biosilica is a naturally occurring polymer used by the oldest metazoans, the sponges (phylum: Porifera), as elements for their spicule formation (reviewed in [17,18]). A likewise polymeric inorganic material is polyphosphate (polyP), which occurs in any living organisms and at high concentrations in sponges, as well (see [17]).

Based on initial studies [19,20], we discovered that biosilica, enzymatically formed from ortho-silicate by the enzyme silicatein [18], displays an inductive anabolic bone-forming effect on SaOS-2 cells. This polymer causes a significant shift of the OPG-RANKL (osteoprotegerin: receptor activator of nuclear factor- $\kappa$ B ligand) ratio [21], resulting in an inhibition of the differentiation pathway of pre-osteoclasts into mature osteoclasts. In addition to an increased mineralization, biosilica has been shown to increase the expression of BMP-2 in SaOS-2 cells [22]. Finally, biosilica shows osteogenic potential [21]. These data have been supported recently [23] using hMSCs.

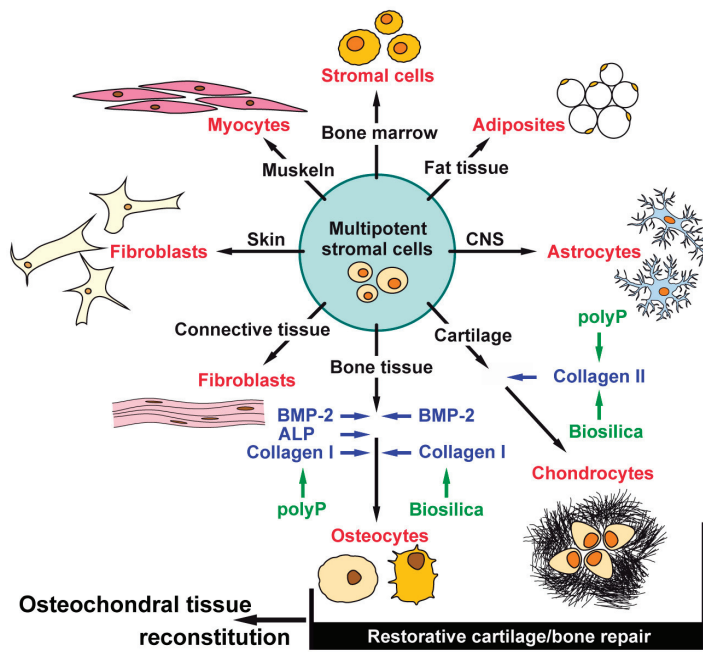
PolyP is known to act as a storage substance of energy, a chelator for metal cations, a phosphate donor for sugars and adenylate kinase and an inducer of apoptosis; in addition, it is involved in mineralization processes of bone tissue (reviewed in [17]). Moreover, polyP acts as a modulator of gene expression, e.g., in the osteoblast-like cell lines, MC3T3-E1 and SaOS-2 cells, and in hMSCs, and causes an increased expression of the genes encoding for osteocalcin, osterix, bone sialoprotein, BMP-2 and tissue nonspecific alkaline phosphatase, all proteins that are crucial for bone formation ([15]; reviewed in [24]).

The available data indicate that both SaOS-2 cells and hMSCs, after encapsulation into alginate hydrogels, can retain their proliferation and differentiation-promoting activity if the matrix had been supplemented with biosilica and polyP. hMSCs can differentiate into several lineages (Figure 1), dependent on the inducers added to the assay system [25]. Osteogenic differentiation is triggered by incubation in medium/fetal calf serum (FCS), supplemented with dexamethasone, ascorbic acid and sodium  $\beta$ -glycerophosphate. Chondrogenic differentiation occurs in medium/serum,

supplemented with transforming growth factor- $\beta$ 1, insulin, transferrin, dexamethasone and ascorbic acid. Adipogenic differentiation is promoted by medium/FCS, indomethacin, dexamethasone and 3-isobutyl-1-methylxanthine and insulin. Neurogenic differentiation is favored if the cells are incubated with  $\beta$ -mercaptoethanol.

The hMSCs provide a suitable cell source for osteochondral tissue reconstruction [26], required for an acceleration of the ossification processes during OD or after the transplantation of 3D tissue-like implants (Figure 1). Figure 1 also highlights recent findings that biosilica and polyP acts in an organic scaffold, like alginate, as a morphogenetically active inorganic polymer.

**Figure 1.** Multipotent differentiation of human multipotent stromal cells (hMSC). Specific transcription factors determine both the commitment and the differentiation of hMSCs towards the osteogenic, chondrogenic, adipogenic or myogenic lineage. The osteogenic and the chondrogenic lineages are involved in the restorative repair of bone and cartilage tissue (osteochondral tissue reconstitution). Biosilica and polyphosphate (polyP) display anabolic, morphogenetic effects on those two differentiation lines.



### Biosilica and polyP: morphogenetically active inorganic polymers

In the present study, we studied the differentiation of hMSCs towards the osteocyte and chondrocyte lineages. Both cell lineages are involved in bone formation and cartilage repair, two processes intimately involved in bone growth [27]. In turn, hMSCs are, due to their osteogenic and chondrogenic potential, attractive candidates for restorative cartilage/bone repair. Chondrocytes are known to express high levels of collagen Type II, while osteoblasts express collagen Type I [28]. Here, we used hMSCs to elucidate the morphogenetic potential of the two polymers of marine

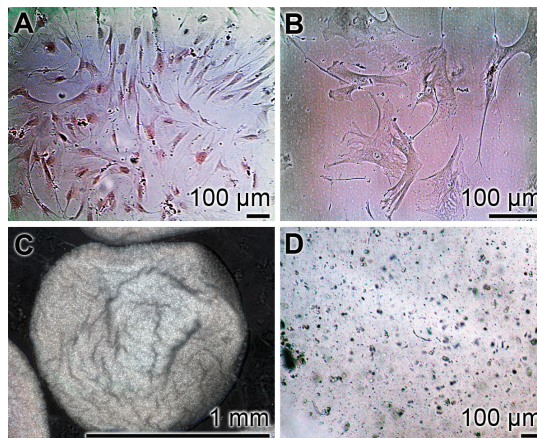
origin, biosilica and polyP, with respect to their differentiation capacity on the osteogenic differentiation, as well as on the chondrogenic differentiation lineage. The data show that these two polymers display a morphogenetic effect on both cell lineages.

## 2. Results and Discussion

### 2.1. Cultivation of hMSCs and Encapsulation into Alginate Beads

hMSCs were incubated in an  $\alpha$ -MEM/FCS medium, as described in “Experimental Section”. They show the characteristic plastic adherent properties (higher passage number) (Figure 2A,B). The hMSCs were subsequently induced to osteoblast- or chondrocyte-like cells and encapsulated into alginate beads of a diameter of  $\sim 1$  mm. At the beginning, the cells were scattered within the alginate; after five days, the newly divided cells aggregate together and form clumps (Figure 2C,D).

**Figure 2.** Light microscopic images of hMSCs, cultured in a monolayer (A and B), adherent to the plastic surface. The hMSCs induced to the osteogenic or the chondrogenic lineages were embedded into alginate beads (C and D).



### 2.2. Mineralization of the Cells, Triggered to Osteogenic Differentiation

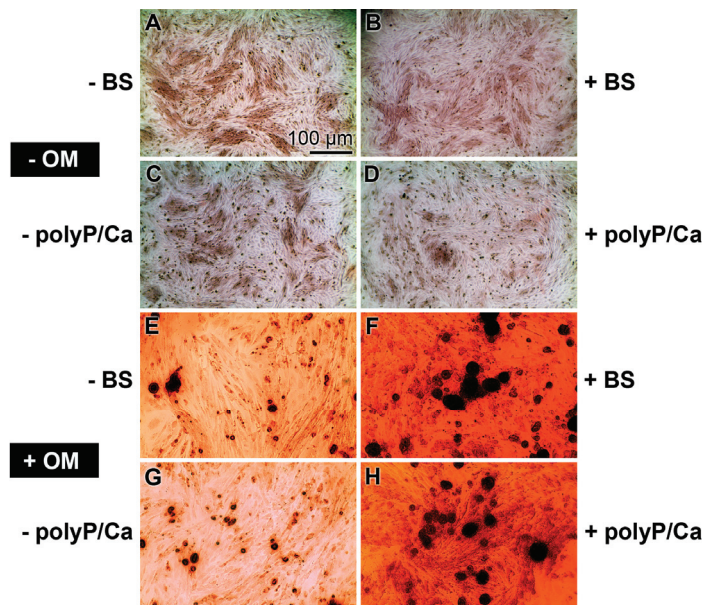
The hMSCs were encapsulated into alginate, either free of additional components “control-alginate” or containing either enzymatically synthesized biosilica “BS-alginate” or polyP ( $\text{Ca}^{2+}$  salt) “polyP-alginate”. In our previous studies we used 100 to 400  $\mu\text{M}$  prehydrolyzed TEOS (tetraethyl orthosilicate), together with silicatein [29] and polyP in the range of 50 to 100  $\mu\text{M}$  [30] to activate cell metabolism and the gene expression of osteoblasts. In the present study, we exposed the hMSCs to 200  $\mu\text{M}$  prehydrolyzed TEOS, together with 20  $\mu\text{g/mL}$  of silicatein or to 50  $\mu\text{M}$  polyP ( $\text{Ca}^{2+}$  salt).

The hMSCs were incubated as “control-alginate”, as “BS-alginate” or as “polyP-alginate” beads for 10 days in medium/serum in the absence or in the presence of osteogenic medium. This cocktail is composed of dexamethasone, ascorbic acid and sodium  $\beta$ -glycerophosphate [22], in order to trigger the hMSCs to form the osteogenic differentiation lineage. During the incubation of the

biosilica-containing or polyP-containing beads, those polymers (biosilica or polyP) were present also in the medium at the same concentrations.

After a 10-day's incubation period, the alginate matrix was partially de-cross-linked with Na-citrate for 15 min. Then, the cells were transferred to a microscope slide and stained with Alizarin Red S. The results show that the cells, not treated with osteogenic medium, are not stained, irrespective of whether they were exposed to biosilica or to polyP or remained without these polymers (Figure 3A–D). However, the intensity of the red staining of the cells increased strongly if the cells were incubated with osteogenic medium (Figure 3E–H). The level of intensity further increased if the hMSCs were incubated, in addition to osteogenic medium (Figure 3E,G), either with biosilica or with polyP (Ca<sup>2+</sup> salt) (Figure 3F,H).

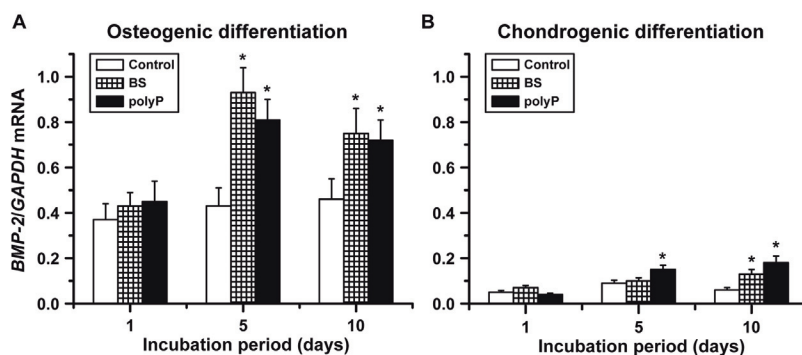
**Figure 3.** Induction of mineralization of hMSCs, embedded in alginate matrix, if incubated in the presence of osteogenic medium (OM), composed of dexamethasone, ascorbic acid and sodium  $\beta$ -glycerophosphate. The hMSCs were transferred to alginate beads and were incubated in the absence of osteogenic medium (–OM) or the presence of osteogenic medium (+OM) for 10 days. In two series of experiments, the cultures remained either without biosilica (–BS) or without polyP (Ca<sup>2+</sup> salt) (–polyP/Ca) or were exposed to those polymers (+BS; +polyP/Ca). Subsequently, the cross-linkages of alginate matrix were partially dissolved with Na-citrate and reacted with Alizarin Red S. The cells exposed to osteogenic medium and either biosilica or polyP (Ca<sup>2+</sup> salt) (+OM +BS; +OM +polyP/Ca) showed the strongest staining intensity to the dye. All images are in the same magnification; the scale is shown in (A).



### 2.3. Osteogenic versus Chondrogenic Differentiation: Effect of Biosilica and PolyP on BMP-2 Expression

Earlier, we reported that both biosilica and polyP cause *BMP-2* gene induction in SaOS-2 cells, if they grow in liquid medium [22]. In the present study, using alginate-encapsulated hMSCs, we exposed the beads either to osteogenic medium, to induce osteogenic differentiation, or to chondrocyte differentiation medium, to direct hMSCs to differentiation in the chondrogenic direction. The two sets of bead cultures were kept in the absence (“control-alginate”) or the presence of either biosilica (“BS-alginate”) or polyP ( $\text{Ca}^{2+}$  salt) (“polyP-alginate”). Samples were taken after one day, five days or 10 days. The alginate matrix around the cells was solubilized, and the released cells were subjected to real-time RT (reverse transcription)-PCR (qRT-PCR) to quantitatively determine the expression level of *BMP-2*. The expression was correlated to the expression of the house-keeping gene, *GAPDH*.

**Figure 4.** Levels of *BMP-2* transcripts in hMSCs after (A) induction with osteogenic medium to the osteogenic lineage or (B) triggering to form the chondrogenic lineage with chondrocyte differentiation medium (CDM). The cells were embedded into alginate beads and exposed to biosilica (BS; squared bars) or polyP ( $\text{Ca}^{2+}$  salt; closed bars) (polyP), as described in “Experimental Section”; the controls (open bars) did not receive those polymers (BS or polyP). Samples of beads were collected at Day 1, Day 5 and Day 10, after starting the experiments. The cells were released from the alginate matrix and, after isolation of the RNA, subjected to real-time RT (reverse transcription)-PCR (qRT-PCR). The expression level of *BMP-2* was normalized to the expression of *GAPDH*. Data are expressed as mean values  $\pm$  SD for four independent experiments. Differences between the groups were evaluated using the unpaired *t*-test. \*  $p < 0.05$ .



The experiments revealed that in the osteoblasts lineage, a high steady-state level of *BMP-2* transcription occurred already after five days if the cells in the beads were exposed either to biosilica or to polyP ( $\text{Ca}^{2+}$  salt). This increase is about two-fold, if compared to control cultures. After an extended incubation for 10 days, the transcription level drops to 1.5-fold, with respect to the controls (Figure 4A). In contrast, the expression level of *BMP-2* in the chondrogenic lineage is

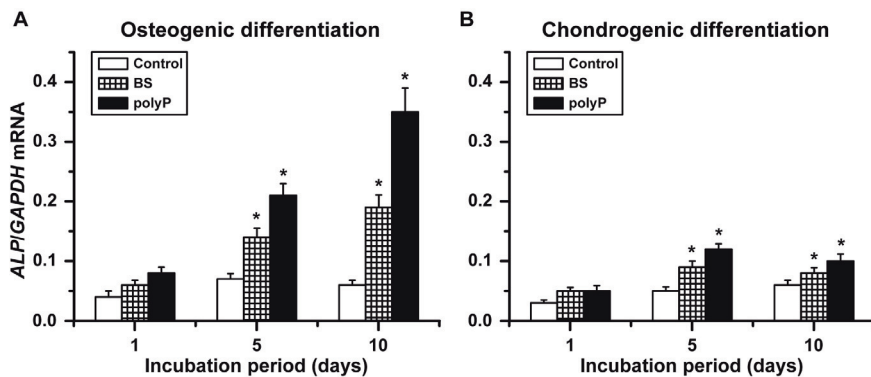
low, and (measured in the controls) it is approximately 15% of the level seen in the osteogenic lineage. If the cells/beads are exposed for five days or 10 days to biosilica or polyP ( $\text{Ca}^{2+}$  salt), the level of *BMP-2* in the chondrogenic lineage increases only up to about 25% of the levels found in the osteogenic lineage (Figure 4B).

#### 2.4. Osteogenic versus Chondrogenic Differentiation: Expression of ALP

As expected, the basal level of the *ALP* expression is already about 1.4-fold higher in the osteogenic cells (Figure 5A), compared to the transcription level in the chondrogenic cells (Figure 5B). This level is significantly increased to two-fold after the five-day incubation period in the presence of biosilica or in the presence of polyP ( $\text{Ca}^{2+}$  salt) to three-fold. After an incubation period of 10 days, this increase is even enhanced; the level in the presence of polyP ( $\text{Ca}^{2+}$  salt) is 5.9-fold compared to the controls.

Furthermore, chondrocytes contain the ALP that cleaves pyrophosphate [31], even though at a lower level. The overall *ALP* transcription level in chondrogenic cells is up to about 30% lower compared to the osteogenic cells (Figure 5B). The inducing activity of both biosilica and polyP ( $\text{Ca}^{2+}$  salt) in chondrogenic cells is significant. However, compared to the osteogenic cells, the level of induction is about three-fold lower in chondrogenic cells.

**Figure 5.** The induction *alkaline phosphatase (ALP)* gene in alginate-encapsulated hMSCs induced to either (A) the osteogenic lineage or (B) the chondrogenic lineage. The cells in those beads were incubated in the absence (controls; open bars), or the presence of either biosilica (BS; squared bars) or polyP ( $\text{Ca}^{2+}$  salt) (polyP; closed bars). \*  $p < 0.05$ .



#### 2.5. Osteogenic versus Chondrogenic Differentiation: Expression of Collagen Type I

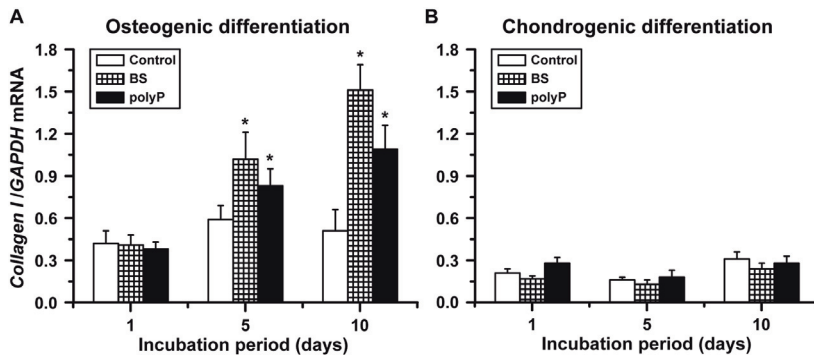
Osteoblasts can be differentiated in their expression levels of the collagen isoforms. While during osteogenic differentiation, the *collagen type I* gene undergoes a strong and increased expression [15,32], chondrocytes express primarily *collagen type II* [33].

The steady-state expression of the *collagen type I* gene is higher in the osteogenic cells (Figure 6A), compared to the chondrogenic cells (Figure 6B). If the osteogenic cells are exposed to



both biosilica and polyP ( $\text{Ca}^{2+}$  salt), an increased steady-state mRNA level is seen at Day 5 and Day 10; this increase is more pronounced in cultures supplemented with biosilica. No significant alteration of the *collagen type I* transcription level was measured in response to biosilica or polyP ( $\text{Ca}^{2+}$  salt) in chondrogenic cells (Figure 6B).

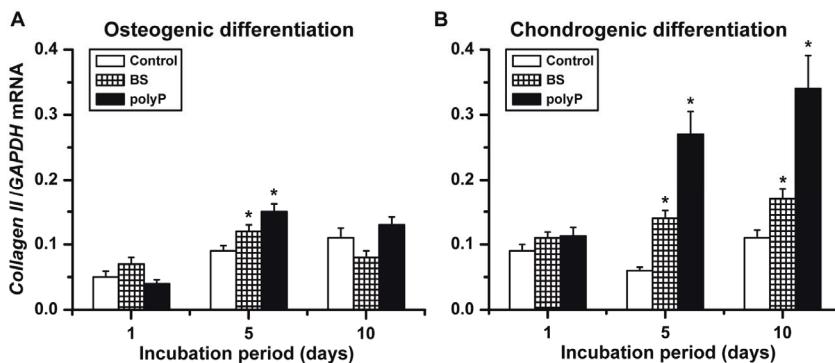
**Figure 6.** Effect of biosilica or polyP ( $\text{Ca}^{2+}$  salt) on the expression level of *collagen type I*. The osteogenic cells (A) or the chondrogenic cells (B) were incubated with biosilica, or with polyP ( $\text{Ca}^{2+}$  salt) or remained untreated (controls). \*  $p < 0.05$ .



## 2.6. Osteogenic versus Chondrogenic Differentiation: Expression of the Collagen Type II

The overall gene expression level of *collagen type II* in osteogenic cells (Figure 7A) is about half the one measured in the chondrogenic cells (Figure 7B). The inductive effect of biosilica and polyP ( $\text{Ca}^{2+}$  salt) is low in osteogenic cells, compared to the one measured for chondrogenic cells. Biosilica and polyP ( $\text{Ca}^{2+}$  salt) cause, at Day 5, a significant *collagen type II* gene induction in osteogenic cells. This increase of the steady-state expression of *collagen type II* is low in osteogenic cells compared to the expression seen for chondrogenic cells.

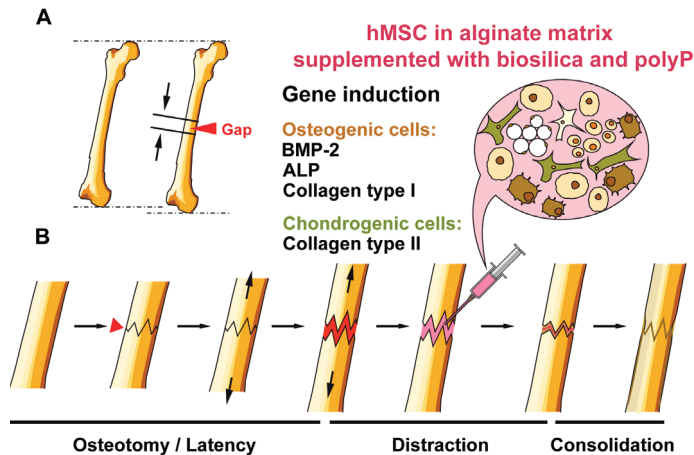
**Figure 7.** Gene expression of *collagen type II* in osteogenic cells (A) versus chondrogenic cells (B). As marked, the induced hMSCs were incubated with either biosilica, or polyP ( $\text{Ca}^{2+}$  salt) or remained without these polymers (controls). \*  $p < 0.05$ .



## 2.7. Discussion

The major challenge to realize an effective 3D printing of custom-built tissue implants is the development of a suitable morphogenetically active scaffold that allows the cells to be embedded to communicate with each other and to direct the individual cells to undergo differentiation into functional “terminally”-differentiated cells. Those cross-talking cells in a fluid/solid matrix will not only fill the space within the damaged tissue, but will also facilitate the replacement of the implanted material by physiologically developing cell assemblies, giving rise to spatially organized multicomponent tissues and structures. Alginate has been found to be a promising matrix for cells, potentially to be used for 3D printing [34]; this plant-derived polymer is, however, morphogenetically inactive. However, if alginate is enriched with organic cytokines/morphogens, e.g., BMP-2 [35], this inert matrix acquires the potency to facilitate the differentiation of stem cells *in vitro*. A further approach, which is likewise physiological, but by far less expensive, is to substitute the organic growth factors in the alginate with inorganic polymers, e.g., biosilica or polyP. Both inorganic polymers are physiologically formed in metazoans [24,36].

**Figure 8.** Distraction osteogenesis scheme. (A) The healthy part of the bone is broken into two segments with an external instrument. A distraction gap is formed; (B) distraction osteogenesis phases: osteotomy/latency, distraction, consolidation. During the distraction phase, hMSCs, embedded into alginate, are proposed to be injected into the fracture zone. These supplements are hoped to accelerate the velocity of bone formation under shortening the consolidation period. This alginate matrix is proposed to be supplemented with the morphogenetically active inorganic polymers, biosilica and polyP.



Besides 3D tissue printing, a morphogenetically active matrix is also needed to accelerate the regeneration step during DO. This technique, DO, requires a long time, during which the external fixator is attached at the limb during the consolidation phase. To ameliorate the medical, psychological, social and financial problems for the patient, successful attempts have been made to administer organic cytokines/morphogens, e.g., BMP-2, to accelerate bone formation [37]. During

the first phase of DO/osteotomy, the latency period, distraction starts under the formation of soft callus and initiation of bone repair processes [14] (Figure 8). During the distraction phase and the subsequent consolidation period, the bone-lacking gap is filled with bone cells until the bone is solidified and the fractures are healed.

The present study shows that both biosilica and polyP provide hMSC-containing alginate hydrogels with a morphogenetic/osteogenic potential, resulting in an increased growth and differentiation potential of the osteoblasts and their precursor cells. In detail, the genes encoding BMP-2, ALP and collagen Type I are induced, three functional and structural prerequisites for a functional activity of the osteoblasts. Furthermore, BMP-2 is known to induce ectopic bone formation and increases bone repair in several animal models. BMP-2 and the related morphogens, BMP-4 and BMP-7, promote cell differentiation into osteoblasts (see [38]). ALP, for a long time already implicated in biomineralization, is a feature of the osteoblast phenotype [39]. Moreover, experimental evidence is available that ALP, which is associated with cell membranes and matrix vesicles, is involved in bio-seed formation during hydroxyapatite formation (see [40]). *Collagen type I* gene expression precedes ALP formation in osteoblasts and in a back-circuit, promotes osteoblast differentiation from precursor cells [41].

Biosilica and polyP also act in a stimulatory manner on the differentiation of hMSCs to chondrogenic cells. Both polymers have been shown to induce in hMSCs, embedded into alginate, the gene encoding for collagen Type II. This fibrillar structural protein, again in a back-circle, promotes chondrogenic differentiation from hMSCs [42].

### 3. Experimental Section

#### 3.1. Isolation and Cultivation of Human MSCs

The hMSCs were isolated using previously described methods [25,43]. The human cells were obtained, after approval from the ethics committee, from bone marrow aspirations after informed consent of the donors. The deep-frozen, preserved hMSCs were thawed, and  $1 \times 10^6$  cells were suspended in one 75-cm<sup>2</sup> flask (Cat. no. 658175; Greiner, Frickenhausen, Germany) and cultivated in  $\alpha$ -MEM (Cat. no. F0915; Biochrom, Berlin, Germany), supplemented with 20% fetal calf serum (FCS; Gibco Invitrogen, Carlsbad, CA, USA), as well as with 0.5 mg/mL of gentamycin, 100 units penicillin and 100  $\mu$ g/mL of streptomycin, as well as 1 mM pyruvate (Sigma, Taufkirchen, Germany). The characteristics of the hMSCs with respect to their osteoblast, as well as adipogenic and chondrogenic differentiation potentials, have been given in detail [25,43]. The incubation was performed in a humidified incubator at 37 °C and 5% CO<sub>2</sub>. After 2 days, the non-adherent cells were discarded, and the adherent cells continued to be incubated with  $\alpha$ -MEM/FCS. Then, the culture medium was renewed every 3 days. At ~80% confluence, the cells were suspended using a 0.25% trypsin/0.02% EDTA solution (Sigma) and plated at a concentration of ~5000 cells/cm<sup>2</sup>. The cultures were split at a ratio of 1:3 every 5 to 6 days after the first passage. Those cells were used for the experiments, mainly for encapsulation into alginate.

The assays for staining the cells were performed in 24-well plates (Cat. no. 662160; Greiner), while the experiments with cells subjected to qRT-PCR were performed either in 48-well plates

(Cat. no. 677102; Greiner) or in 25-cm<sup>2</sup> flasks (Cat. no. 690175; Greiner). At the time of harvesting the cells, the cultures were approximately 80% confluent.

### 3.2. Preparation of Alginate/Silica and Alginate/PolyP (Ca<sup>2+</sup> Salt) Composite Hydrogel Beads

Adherent cells from ~80% confluent cultures were released from the plates and suspended in 1.2% (w/v) alginate (Na-alginate, Cat. no. CAA W20,150-2, low viscosity, dissolved in PBS, pH 7.4; Sigma) and processed as described [34]. In brief, the cell-hydrogel suspensions were passed through a needle (dimension: 0.45 × 6 × 23 mm) attached to a 1 mL syringe and dropped into a 1.5% (w/v) CaCl<sub>2</sub> solution. After 5 min, the approximately 1 mm-large beads were washed three times in saline and then twice in  $\alpha$ -MEM medium. The beads (approximately 60 beads/well) were placed into 24-well plates (Nunc, Langensfeld, Germany) and incubated in 3 mL of  $\alpha$ -MEM/FCS in the presence of the respective induction medium. Those cultures were termed “control-alginate”.

After termination of the experiments, the cells were released from the beads by washing twice with PBS and transferring them into 2 mL of 55 mM Na-citrate; after 30 min at 37 °C, the cells were collected by centrifugation (900× g, 5 min; [34,44]) and used for quantitative real-time RT-PCR determinations. For staining the cells with Alizarin Red S, the period for de-cross-linking of alginate with Na-citrate was shortened to 15 min. Then, the cells were stained.

Where indicated, the alginate beads were supplemented with biosilica or with polyP. Biosilica was prepared as described [29]. Prehydrolyzed TEOS (tetraethyl orthosilicate; Sigma) in a concentration of 200  $\mu$ M was added to 20  $\mu$ g/mL of recombinant silicatein; these components were added to the alginate matrix. After each medium change, prehydrolyzed TEOS/recombinant silicatein was added again to the medium. The biosilica-containing beads were termed “BS-alginate”. In a control experiment, silicatein was replaced in the assays by 20  $\mu$ g/mL of bovine serum albumin (BSA); those beads displayed no effect on the expression of the genes selected in the present study (data not shown). The beads were incubated for up to 10 days.

Na-polyP (average chain of approximately 40 phosphate units) was obtained from Chemische Fabrik Budenheim (Budenheim, Germany). To compensate for any effect, caused by a potential chelating activity of polyP to Ca<sup>2+</sup>, the polymer was mixed together with CaCl<sub>2</sub> in a stoichiometric ratio of 2:1 (polyP:CaCl<sub>2</sub>), as described [30]; the salt, designated as “polyP (Ca<sup>2+</sup> salt)”, was added to the beads and the medium at a concentration of 50  $\mu$ M. Incubation was again for up to 10 days. The beads containing polyP were termed “polyP-alginate”.

### 3.3. Differentiation Assays in Vitro

Osteogenic differentiation of hMSCs, encapsulated into hydrogel beads, was performed by exposure of the cells to the osteogenic medium, as described [22]. Osteogenic medium contained in the  $\alpha$ -MEM/FCS, dexamethasone (Sigma), ascorbic acid (Sigma) and sodium  $\beta$ -glycerophosphate (Sigma). As end-point marker for osteoblasts, the extent of mineralization based on Alizarin Red S staining, as well as the gene expression levels of selected marker genes was determined.

Chondrogenic differentiation of the stem cells was induced in  $\alpha$ -MEM/FCS supplemented with chondrocyte differentiation medium, as described [3,27]. It consists of premix tissue culture

supplement (Becton Dickinson, Heidelberg, Germany), dexamethasone, ascorbate-2-phosphate, pyruvate and transforming growth factor- $\beta$ 1 (Sigma), human insulin (Sigma) and transferrin (Sigma).

The described experiments were performed after having transferred the hMSCs to the respective activation medium.

The cells/beads were inspected with light microscopically using either a Keyence BZ-8000 epifluorescence microscope or a Keyence VK-8710K, color 3D laser microscope (Neu-Isenburg, Germany).

### 3.4. Mineralization Assay with Alizarin Red S

Mineralization by differentiated hMSCs was qualitatively assessed by staining the cell cultures on the coverslips with 10% Alizarin Red S, after fixation with ethanol [45].

### 3.5. Quantitative Real-Time RT-PCR (qRT-PCR) Analysis

The technique of quantitative real-time RT (reverse transcription)-PCR (qRT-PCR) was applied to determine the levels of transcription of the following genes: *BMP-2* (*bone morphogenetic protein-2*; NM\_001200.2) Fwd: 5'-ACCCTTTGTACGTGGACTTC-3' (nt<sub>1681</sub> to nt<sub>1700</sub>); and Rev: 5'-GTGGAGTTCAGATGATCAGC-3' (nt<sub>1785</sub> to nt<sub>1804</sub>; 124 bp); *ALP* (*alkaline phosphatase*; NM\_000478.4) Fwd: 5'-TGCAGTACGAGCTGAACAGGAACA-3' (nt<sub>1141</sub> to nt<sub>1164</sub>); and Rev: 5'-TCCACCAAATGTGAAGACGTGGGA-3' (nt<sub>1418</sub> to nt<sub>1395</sub>; 278 bp); *COL1* (*collagen type I*; NM\_000088) Fwd: 5'-TATGGGACCCCAAGGACCAAAAGG-3' (nt<sub>1122</sub> to nt<sub>1145</sub>); and Rev: 5'-TTTTCCATCTGACCCAGGGGAACC-3' (nt<sub>1234</sub> to nt<sub>1257</sub>) (136 bp); *COL2A1* (*collagen type II, alpha 1* (COL2A1), transcript variant 1, mRNA: NM\_001844) Fwd: 5'-TCCATTCATCCCACCC TCTCAC-3' (nt<sub>4755</sub> to nt<sub>4776</sub>); and Rev: 5'-TTTCTGCCTCTGCCTTGACC-3' (nt<sub>4902</sub> to nt<sub>4882</sub>; 148 bp). As a reference gene, GAPDH (glyceraldehyde 3-phosphate dehydrogenase; NM\_002046.3) (Fwd: 5'-CCGTCTAGAAAAACCTGCC-3' (nt<sub>845</sub> to nt<sub>863</sub>); and Rev: 5'-GCCAAATTCGTTG TCATACC-3' (nt<sub>1059</sub> to nt<sub>1078</sub>; 215 bp)) was used.

The cells were released from the hydrogel samples and collected by centrifugation. After RNA extraction using the TRIzol reagent (Invitrogen GmbH, Darmstadt, Germany), the samples were subjected to qRT-PCR. For that, 2  $\mu$ L of the appropriate dilution were employed as a template in the 30  $\mu$ L qRT-PCR assays. All reactions were run with an initial denaturation at 95 °C for 3 min, followed by 40 cycles, each with 95 °C for 20 s, 58 °C for 20 s, 72 °C for 20 s and 80 °C for 20 s. Fluorescence data were collected at the 80 °C step. The runs were performed in an iCycler (Bio-Rad, Hercules, CA, USA). The mean  $C_t$  values and efficiencies were calculated by applying the iCycler software (Bio-Rad); the estimated PCR efficiencies were in the range of 93%–103%. Expression levels were correlated to the GAPDH reference gene to determine relative expression, as described [21].

### 3.6. Further Analyses

The results were statistically evaluated using the paired Student's *t*-test [46]. DNA content was determined by application of the PicoGreen method, as described [45], using calf thymus DNA as a standard.

## 4. Conclusion

In conclusion, for the two inorganic polymers, biosilica and polyP, which are abundantly found in marine organisms, our findings extend our earlier results obtained with (almost) terminally differentiated osteoblasts (reviewed in [17]), establishing that, both inorganic polymers, biosilica and polyP, are potent morphogenetically active additives of the alginate matrix.

## Acknowledgments

We thank Sandra Ritz (Max-Planck-Institute for Polymer Research, Mainz, Germany) for supplying us with the hMSCs, as well as for introducing us to the technique of stem cell cultivation. W.E.G.M. is a holder of an ERC Advanced Investigator Grant (no. 268476 BIOSILICA), as well as of an ERC proof-of-concept grant (no. 324564; Silica-based nanobiomedical approaches for treatment of bone diseases). This work was supported by grants from the European Commission (no. 311848 "SPECIAL", and large-scale integrating project no. FP7-KBBE-2010-4-266033 "BlueGenics", as well as European-Chinese Research Staff Exchange Cluster PIRSES-GA-2009-246987 "MarBioTec\*EU-CN\*"), the International Human Frontier Science Program, the German Bundesministerium für Bildung und Forschung, International Bureau (no. CHN 09/1AP, German-Chinese Joint Lab on Bio-Nano-Composites), and the BiomaTiCS research initiative of the University Medical Center, Mainz.

## Conflicts of Interest

The authors declare no conflict of interest.

## References

1. Parra-Torres, A.Y.; Valdés-Flores, M.; Orozco, L.; Velázquez-Cruz, R. Molecular Aspects of Bone Remodeling. In *Topics in Osteoporosis*; InTech: Rijeka, Croatia, 2013; pp. 1–27.
2. Friedenstein, A.J.; Petrakova, K.V.; Kurolesova, A.I.; Frolova, G.P. Heterotopic of bone marrow. Analysis of precursor cells for osteogenic and hematopoietic tissues. *Transplantation* **1968**, *6*, 230–247.
3. Pittenger, M.F.; Mackay, A.M.; Beck, S.C.; Jaiswal, R.K.; Douglas, R.; Mosca, J.D.; Moorman, M.A.; Simonetti, D.W.; Craig, S.; Marshak, D.R. Multilineage potential of adult human mesenchymal stem cells. *Science* **1999**, *284*, 143–147.
4. Beyth, S.; Schröder, J.; Liebergall, M. Stem cells in bone diseases: Current clinical practice. *Br. Med. Bull.* **2011**, *99*, 199–210.

5. Sunay, O.; Can, G.; Cakir, Z.; Denek, Z.; Kozanoglu, I.; Erbil, G.; Yilmaz, M.; Baran, Y. Autologous rabbit adipose tissue-derived mesenchymal stromal cells for the treatment of bone injuries with distraction osteogenesis. *Cytotherapy* **2013**, *15*, 690–702.
6. Panetta, N.J.; Gupta, D.M.; Slater, B.J.; Kwan, M.D.; Liu, K.J.; Longaker, M.T. Tissue engineering in cleft palate and other congenital malformations. *Pediatr. Res.* **2008**, *63*, 545–551.
7. Gessmann, J.; Köller, M.; Godry, H.; Schildhauer, T.A.; Seybold, D. Regenerate augmentation with bone marrow concentrate after traumatic bone loss. *Orthop. Rev.* **2012**, *4*, e14.
8. Müller, W.E.G.; Schröder, H.C.; Feng, Q.L.; Schloßmacher, U.; Link, T.; Wang, X.H. Development of a morphogenetically active scaffold for three-dimensional growth of bone cells: Biosilica/Alginate hydrogel for SaOS-2 cell cultivation. *J. Tissue Engin. Regener. Med.* **2013**, doi:10.1002/term.1745.
9. Ilizarov, G.A. Clinical application of the tension–stress effect for limb lengthening. *Clin. Orthop. Relat. Res.* **1990**, *250*, 8–26.
10. Cope, J.B.; Samchukov, M.L.; Cherkashin, A.M. Mandibular distraction osteogenesis: A historic perspective and future directions. *Am. J. Orthod. Dentofacial Orthop.* **1999**, *115*, 448–460.
11. Jazrawi, L.M.; Majeska, R.J.; Klein, M.L.; Kagel, E.; Stromberg, L.; Einhorn, T.A. Bone and cartilage formation in an experimental model of distraction osteogenesis. *J. Orthop. Trauma* **1998**, *12*, 111–116.
12. Sato, M.; Yasui, N.; Nakase, T.; Kawahata, H.; Sugimoto, M.; Hirota, S.; Kitamura, Y.; Nomura, S.; Ochi, T. Expression of bone matrix proteins mRNA during distraction osteogenesis. *J. Bone Miner. Res.* **1998**, *13*, 1221–1231.
13. Matsubara, H.; Hogan, D.E.; Morgan, E.F.; Mortlock, D.P.; Einhorn, T.A.; Gerstenfeld, L.C. Vascular tissues are a primary source of BMP2 expression during bone formation induced by distraction osteogenesis. *Bone* **2012**, *51*, 168–180.
14. Hegab, A.F.; Shuman, M.A. Distraction osteogenesis of the maxillofacial skeleton: biomechanics and clinical implications. *Sci. Rep.* **2012**, *1*, 1–12.
15. Müller, W.E.G.; Wang, X.H.; Grebenjuk, V.; Diehl-Seifert, B.; Steffen, R.; Schloßmacher, U.; Trautwein, A.; Neumann, S.; Schröder, H.C. Silica as a morphogenetically active inorganic polymer: effect on the BMP-2-dependent and RUNX2-independent pathway in osteoblast-like SaOS-2 cells. *Biomater. Sci.* **2013**, *1*, 669–678.
16. Andersen, T.; Strand, B.L.; Formo, K.; Alsberg, E.; Christensen, B.E. Alginates as biomaterials in tissue engineering. *Carbohydr. Chem.* **2012**, *37*, 227–258.
17. Wang, X.H.; Schröder, H.C.; Wiens, M.; Ushijima, H.; Müller, W.E.G. Bio-silica and bio-polyphosphate: Applications in biomedicine (bone formation). *Curr. Opin. Biotechnol.* **2012**, *23*, 570–578.
18. Müller, W.E.G.; Schröder, H.C.; Burghard, Z.; Pisignano, D.; Wang, X.H. Silicateins—A novel paradigm in bioinorganic chemistry: Enzymatic synthesis of inorganic polymeric silica. *Chem. Eur. J.* **2013**, *19*, 5790–5804.
19. Carlisle, E.M. Silicon: An essential element for the chick. *Science* **1972**, *178*, 619–621.

20. Schwarz, K.; Milne, D.B. Growth-promoting effects of silicon in rats. *Nature* **1972**, *239*, 333–334.
21. Wiens, M.; Wang, X.H.; Schröder, H.C.; Kolb, U.; Schloßmacher, U.; Ushijima, H.; Müller, W.E.G. The role of biosilica in the osteoprotegerin/RANKL ratio in human osteoblast-like cells. *Biomaterials* **2010**, *31*, 7716–7725.
22. Wiens, M.; Wang, X.H.; Schloßmacher, U.; Lieberwirth, I.; Glasser, G.; Ushijima, H.; Schröder, H.C.; Müller, W.E.G. Osteogenic potential of bio-silica on human osteoblast-like (SaOS-2) cells. *Calcif. Tissue Int.* **2010**, *87*, 513–524.
23. Han, P.; Wu, C.; Xiao, Y. The effect of silicate ions on proliferation, osteogenic differentiation and cell signalling pathways (WNT and SHH) of bone marrow stromal cells. *Biomater. Sci.* **2013**, *1*, 379–392.
24. Müller, W.E.G.; Albert, O.; Schröder, H.C.; Wang, X.H. Bio-inorganic nanomaterials for biomedical applications (Bio-silica and polyphosphate). In *Handbook of Nanomaterials Properties*; Bhushan, B., Luo, D., Schrickler, S., Sigmund, W., Zauscher, S., Eds.; Springer-Press: Berlin, Germany, 2014; in press.
25. Pittenger, M.F.; Martin, B.J. Mesenchymal stem cells and their potential as cardiac therapeutics. *Circ. Res.* **2004**, *95*, 9–20.
26. Caplan, A.I. Mesenchymal stem cells. *J. Orthop. Res.* **1991**, *9*, 641–50.
27. Solchaga, L.A.; Penick, K.J.; Welter, J.F. Chondrogenic differentiation of bone marrow-derived mesenchymal stem cells: tips and tricks. *Methods Mol. Biol.* **2011**, *698*, 253–278.
28. Deshmukh, K.; Sawyer, B.D. Synthesis of collagen by chondrocytes in suspension culture: modulation by calcium, 3':5'-cyclic AMP, and prostaglandins. *Proc. Natl. Acad. Sci. USA* **1977**, *74*, 3864–3868.
29. Schlossmacher, U.; Wiens, M.; Schröder, H.C.; Wang, X.H.; Jochum, K.P.; Müller, W.E.G. Silintaphin-1: Interaction with silicatein during structureguiding biosilica formation. *FEBS J.* **2011**, *278*, 1145–1155.
30. Müller, W.E.G.; Wang, X.H.; Diehl-Seifert, B.; Kropf, K.; Schloßmacher, U.; Lieberwirth, I.; Glasser, G.; Wiens, M.; Schröder, H.C. Inorganic polymeric phosphate/polyphosphate as an inducer of alkaline phosphatase and a modulator of intracellular Ca<sup>2+</sup> level in osteoblasts (SaOS-2 cells) *in vitro*. *Acta Biomater.* **2011**, *7*, 2661–2671.
31. Xu, Y.; Pritzker, K.P.; Cruz, T.F. Characterization of chondrocyte alkaline phosphatase as a potential mediator in the dissolution of calcium pyrophosphate dihydrate crystals. *J. Rheumatol.* **1994**, *21*, 912–919.
32. Reffitt, D.M.; Ogston, N.; Jugdaohsingh, R.; Cheung, H.F.; Evans, B.A.; Thompson, R.P.; Powell, J.J.; Hampson, G.N. Orthosilicic acid stimulates collagen type 1 synthesis and osteoblastic differentiation in human osteoblast-like cells *in vitro*. *Bone* **2003**, *32*, 127–135.
33. Ma, H.L.; Hung, S.C.; Lin, S.Y.; Chen, Y.L.; Lo, W.H. Chondrogenesis of human mesenchymal stem cells encapsulated in alginate beads. *J. Biomed. Mater. Res. A* **2003**, *64*, 273–281.



34. Schloßmacher, U.; Schröder, H.C.; Wang, X.H.; Feng, Q.; Diehl-Seifert, B.; Neumann, S.; Trautwein, A.; Müller, W.E.G. Alginate/silica composite hydrogel as a potential morphogenetically active scaffold for three-dimensional tissue engineering. *RSC Adv.* **2013**, *3*, 11185–11194.
35. Lim, H.J.; Ghim, H.D.; Choi, J.H.; Chung, H.Y.; Lim, J.O. Controlled release of BMP-2 from alginate nanohydrogels enhanced osteogenic differentiation of human bone marrow stromal cells. *Macromol. Res.* **2010**, *18*, 787–792.
36. Wang, X.H.; Schröder, H.C.; Diehl-Seifert, B.; Kropf, K.; Schloßmacher, U.; Wiens, M.; Müller, W.E.G. Dual effect of inorganic polymeric phosphate/polyphosphate on osteoblasts and osteoclasts *in vitro*. *J. Tissue Eng. Regen. Med.* **2013**, *7*, 767–776.
37. Mandu-Hrit, M.; Haque, T.; Lauzier, D.; Kotsioprifitis, M.; Rauch, F.; Tabrizian, M.; Henderson, J.E.; Hamdy, R.C. Early injection of OP-1 during distraction osteogenesis accelerates new bone formation in rabbits. *Growth Factors* **2006**, *24*, 172–183.
38. Osyczka, A.M.; Diefenderfer, D.L.; Bhargava, G.; Leboy, P.S. Different effects of BMP-2 on marrow stromal cells from human and rat bone. *Cells Tissues Organs* **2004**, *176*, 109–119.
39. Fedarko, N.S.; Bianco, P.; Vetter, U.; Robey, P.G. Human bone cell enzyme expression and cellular heterogeneity: Correlation of alkaline phosphatase enzyme activity with cell cycle. *J. Cell Physiol.* **1990**, *144*, 115–121.
40. Golub, E.E.; Boesze-Battaglia, K. The role of alkaline phosphatase in mineralization. *Curr. Opin. Orthop.* **2007**, *18*, 444–448.
41. Shi, S.; Kirk, M.; Kahn, A.J. The role of type I collagen in the regulation of the osteoblast phenotype. *J. Bone Miner. Res.* **1996**, *11*, 1139–1145.
42. Chen, C.W.; Tsai, Y.H.; Deng, W.P.; Shih, S.N.; Fang, C.L.; Burch, J.G.; Chen, W.H.; Lai, W.F. Type I and II collagen regulation of chondrogenic differentiation by mesenchymal progenitor cells. *J. Orthop. Res.* **2005**, *23*, 446–453.
43. Lorenz, M.R.; Holzapfel, V.; Musyanovych, A.; Nothelfer, K.; Walther, P.; Frank, H.; Landfester, K.; Schrezenmeier, H.; Mailänder, V. Uptake of functionalized, fluorescent-labeled polymeric particles in different cell lines and stem cells. *Biomaterials* **2006**, *27*, 2820–2828.
44. Shoichet, M.S.; Li, R.H.; White, M.L.; Winn, S.R. Stability of hydrogels used in cell encapsulation: An *in vitro* comparison of alginate and agarose. *Biotechnol. Bioeng.* **1996**, *50*, 374–381.
45. Schröder, H.C.; Borejko, A.; Krasko, A.; Reiber, A.; Schwertner, H.; Müller, W.E.G. Mineralization of SaOS-2 cells on enzymatically (Silicatein) modified bioactive osteoblast-stimulating surfaces. *J. Biomed. Mat. Res. B* **2005**, *75B*, 387–392.
46. Sachs, L. *Angewandte Statistik*; Springer: Berlin, Germany, 1984; p. 242.

# Identification of the Major ACE-Inhibitory Peptides Produced by Enzymatic Hydrolysis of a Protein Concentrate from Cuttlefish Wastewater

Isabel Rodríguez Amado, José Antonio Vázquez, Pilar González, Diego Esteban-Fernández, Mónica Carrera and Carmen Piñeiro

**Abstract:** The aim of this work was the purification and identification of the major angiotensin converting enzyme (ACE) inhibitory peptides produced by enzymatic hydrolysis of a protein concentrate recovered from a cuttlefish industrial manufacturing effluent. This process consisted on the ultrafiltration of cuttlefish softening wastewater, with a 10 kDa cut-off membrane, followed by the hydrolysis with alcalase of the retained fraction. Alcalase produced ACE inhibitors reaching the highest activity ( $IC_{50} = 76.8 \pm 15.2 \mu\text{g mL}^{-1}$ ) after 8 h of proteolysis. Sequential ultrafiltration of the 8 h hydrolysate with molecular weight cut-off (MWCO) membranes of 10 and 1 kDa resulted in the increased activity of each permeate, with a final  $IC_{50}$  value of  $58.4 \pm 4.6 \mu\text{g mL}^{-1}$ . Permeate containing peptides lower than 1 kDa was separated by reversed-phase high performance liquid chromatography (RP-HPLC). Four fractions (A–D) with potent ACE inhibitory activity were isolated and their main peptides identified using high performance liquid chromatography coupled to an electrospray ion trap Fourier transform ion cyclotron resonance-mass spectrometer (HPLC-ESI-IT-FTICR) followed by comparison with databases and *de novo* sequencing. The amino acid sequences of the identified peptides contained at least one hydrophobic and/or a proline together with positively charged residues in at least one of the three C-terminal positions. The  $IC_{50}$  values of the fractions ranged from 1.92 to  $8.83 \mu\text{g mL}^{-1}$ , however this study fails to identify which of these peptides are ultimately responsible for the potent antihypertensive activity of these fractions.

Reprinted from *Mar. Drugs*. Cite as: Amado, I.R.; Vázquez, J.A.; González, P.; Esteban-Fernández, D.; Carrera, M.; Piñeiro, C. Identification of the Major ACE-Inhibitory Peptides Produced by Enzymatic Hydrolysis of a Protein Concentrate from Cuttlefish Wastewater. *Mar. Drugs* **2014**, *12*, 139061405.

## 1. Introduction

Cardiovascular diseases (CVD) are the main cause of death globally, accounting for approximately 17 million deaths a year, nearly one third of the total [1]. According to the World Health Organization, most cardiovascular diseases can be prevented by addressing risk factors, such as tobacco use, unhealthy diet and obesity, physical inactivity, high blood pressure, diabetes, and raised lipids [2]. Among all CVD, complications of hypertension account for 9.4 million deaths worldwide every year [3] and are the most common risk factors of heart diseases. Thus, hypertension is now considered a major health problem worldwide.

Blood pressure is regulated by the renin-angiotensin system, wherein, the angiotensin converting enzyme (ACE) hydrolyses biologically inactive angiotensin I to the potent vasoconstrictor angiotensin II, responsible for the increase in the arterial pressure. At present, the renin-angiotensin

system has become a key target for drugs combating hypertension [4] and, more specifically, various synthetic ACE inhibitors are widely used to treat cardiovascular disorders. However, these synthetic drugs have been described to have some side effects [5] and, thus, natural sources of ACE inhibitors are being investigated as a milder but effective alternative for the control of high blood pressure. Among the origins of these molecules are food-derived peptides from different sources, such as cheese whey [6], gelatin [7], and different meat and fish proteins [8].

Marine biodiversity is a valuable source of molecules with diverse biological activities. Hence, interest has focused on the search of bioactive compounds, including ACE inhibitors, from marine sources. Peptides with ACE-inhibitory activity have been isolated from different marine species including shrimp [9], sole [10], cuttlefish [11,12], and salmon [13], among others.

However, a more sustainable alternative providing high-value bioactive compounds is the use of fish byproducts. Among waste materials, fish processing wastewaters have been recently studied as starting materials to obtain ACE inhibitory peptides. Recently a functional concentrate from industrial shrimp (*Penaeus* spp.) cooking juice with antioxidative and antihypertensive (ACE-inhibitory) capacity has been obtained by Pérez-Santín *et al.* [14]. In addition, a screening study of different cuttlefish industrial processing wastewaters demonstrated the great potential of ultrafiltration (UF)-fractionation followed by proteolysis of cuttlefish protein concentrates as a source of peptide mixtures with antihypertensive and antioxidant activity [15].

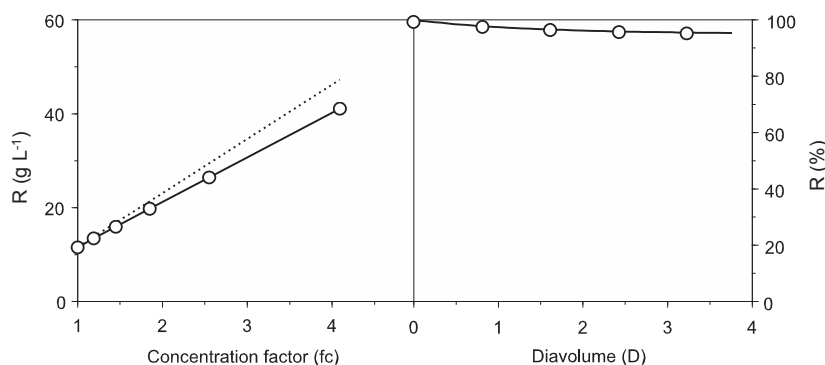
The purpose of the present study was to purify and identify the major ACE inhibitory peptides produced by enzymatic hydrolysis of proteins recovered by UF from cuttlefish softening wastewater. For that purpose, the ACE inhibitory peptides from a cuttlefish byproduct hydrolysate were fractionated by sequential ultrafiltration using 10 and 1 molecular weight cut-off (MWCO) membranes. The most active fractions in the 1 kDa permeate were isolated by reversed-phase high performance liquid chromatography (RP-HPLC), their ACE-inhibitory activity quantified and the main peptides were identified by mass spectrometry.

## 2. Results and Discussion

### 2.1. Protein Recovery by Ultrafiltration-Diafiltration (UF-DF)

The wastewater used in this work was the result of successive cooking operations using the same water in order to obtain a high initial protein concentration. For this reason, the protein content was significantly higher than others previously reported for cuttlefish processing effluents [16,17]. Protein concentration in cuttlefish softening wastewater was  $11.5 \pm 0.34 \text{ g L}^{-1}$  and reached  $95.42 \pm 1.22 \text{ g L}^{-1}$  of protein content after ultrafiltration-diafiltration (UF-DF) at 10 kDa. As can be seen in Figure 1, Equation (1) was able to simulate the DF process and parameter determinations were always significant (Student's *t* test,  $\alpha = 0.05$ ). Results of UF-DF using this cut-off membrane showed protein retentions higher than 95% of the initial protein content in the retentate and an overall concentration factor (fc) above 4.0.

**Figure 1.** Protein recovery from cuttlefish wastewater by UF-DF at 10 kDa molecular weight cut-off (MWCO). Left: concentration of retained protein in linear relation with the volumetric concentration factor (fc) showing experimental data (points) and theoretical profiles (discontinuous line). Right: Progress of protein (○) retention with the increase of diavolume from DF process (D). For clarity, confidence intervals (in all cases less than 5% of the experimental mean value;  $\alpha = 0.05$ ;  $n = 2$ ) were omitted. Equation (1) was used to fit the experimental data.



This result slightly improves previously published data in the treatment of cuttlefish effluents using membrane technology. An 85% reduction in the chemical oxygen demand (COD) of cuttlefish processing wastewater was observed after nanofiltration using a 550 Da cellulose acetate membrane [16]. On the other hand, a similar protein retention rate (78%) was reported in the microfiltration associated to ultrafiltration (15 kDa MWCO) of cuttlefish effluents using ceramic membranes [17]. All these studies consistently indicate a great efficiency of membrane technology for protein concentration. The use of these byproducts as a source of protein contributes to improving depuration of industrial wastewaters, reducing the treatment costs, and decreasing their contaminating effects.

## 2.2. ACE Inhibitory Activity of Cuttlefish Hydrolysate and Their UF Fractions

To obtain the ACE inhibitors, the cuttlefish protein concentrate was hydrolysed using alcalase according to optimal conditions previously reported for this substrate [12]. The extent of protein degradation by the proteolytic enzyme was estimated by assessing the degree of hydrolysis (DH) (Equation (2)). According to this calculation a high DH was observed from the beginning of the digestion, reaching a final value of  $37.8\% \pm 0.4\%$  after 8 h of proteolysis (Table 1).

Indeed, the highest levels of hydrolysis were greater than those obtained from cuttlefish muscle [18] and other seafood species [13] using this enzyme. As reported before [12], this difference might be attributed to the thermal treatment of proteins recovered by UF, which tends to increase the susceptibility of proteins to enzymatic hydrolysis due to their partial denaturation.

**Table 1.** Degrees of hydrolysis (DH) after 0.5, 2, and 8 h digestion with alcalase of a cuttlefish wastewater protein concentrate. Angiotensin converting enzyme (ACE) inhibitory activity ( $I_{ACE}$  (%)) and  $IC_{50}$  values ( $\mu\text{g mL}^{-1}$ ) of these hydrolysates, as well as retentates obtained by 10 and 1 kDa membrane and permeate of 1 kDa from the 8 h hydrolysate.  $I_{ACE}$  (%) was calculated by Equation (3). Mean values and standard deviations from triplicate samples are shown.

Values of DH, $I_{ACE}$ (%) and $IC_{50}$ for Hydrolysis and UF Processes				
		DH (%)	$I_{ACE}$ (%)	$IC_{50}$ ( $\mu\text{g mL}^{-1}$ )
		–	$37.8 \pm 0.4$	$292.5 \pm 20.3$
Hydrolysis	0.5 h	$17.5 \pm 0.2$	$76.2 \pm 3.2$	$214.4 \pm 27.3$
	2 h	$23.8 \pm 1.8$	$80.4 \pm 2.3$	$122.5 \pm 13.1$
	8 h	$36.4 \pm 0.9$	$92.1 \pm 0.6$	$76.8 \pm 15.2$
Ultrafiltration	10 kDa retentate	–	$83.3 \pm 0.6$	$273.9 \pm 30.1$
	1 kDa retentate	–	$94.6 \pm 2.9$	$235.6 \pm 20.2$
	1 kDa permeate	–	$68.0 \pm 1.4$	$58.4 \pm 4.6$

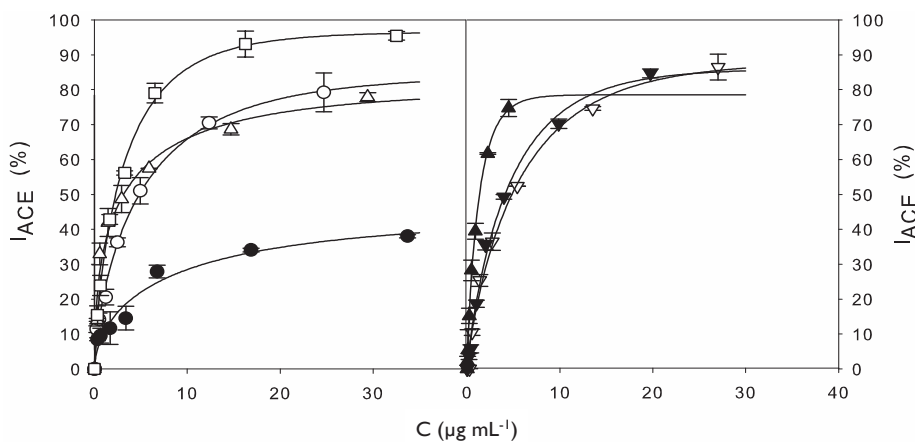
ACE inhibitory activity improved with increasing time of hydrolysis, reaching maximal values ( $92.1\% \pm 0.6\%$ ) after 8 h of proteolysis (Table 1). In addition, a direct relationship between ACE inhibitory activity and DH was observed in a study evaluating the ACE inhibitory activities of cuttlefish muscle protein hydrolysates prepared by treatment with various bacterial proteases [18]. In fact, the authors obtained a lower inhibitory activity ( $51.5\% \pm 1.5\%$ ) from a cuttlefish protein hydrolysate prepared using alcalase with a DH of 12.5%, *i.e.*, three-fold lower than the DH reported in the present study. However, it must be noted that hydrolysis conditions and calculation methods for the DH and ACE inhibitory varied between both studies, making difficult the direct comparison of the results.

To calculate  $IC_{50}$  values, dose-response curves (Figure 2) were plotted and accurately fitted by Equation (4), with coefficients of determination greater than 0.98.

Equation (4) allowed the direct determination of  $IC_{50}$  values using mathematical nonlinear fitting. The estimation of  $IC_{50}$  values using this model is more precise than direct interpolation or linear regression and allows the objective comparison between samples. This equation was consistent (Fisher's  $F$  test;  $p < 0.05$ ) and parameter estimations were always significant (Student's  $t$  test,  $\alpha = 0.05$ ) (data not shown). According to this approach,  $IC_{50}$  decreased with increasing time of hydrolysis reaching the lowest value (maximal ACE inhibitory activity) after 8 h of hydrolysis. These differences revealed that the use of alcalase was efficient in releasing peptides with ACE inhibitory activity from cuttlefish protein concentrate. In fact, this endoprotease has been widely employed for the production of potent marine derived ACE inhibitors from sources as diverse as the algae *Chlorella ellipsoidea* [19], salmon byproducts [20], seaweed pipefish muscle protein [21], the sea cucumber *Acaudina molpadioidea* [22], and lizard fish [23]. This enzyme is also less expensive than others commercially available, thus, being a good candidate for the industrial production of bioactive hydrolysates from marine byproducts. Values of  $IC_{50}$  for ACE inhibitory

activity of whole cuttlefish hydrolysates have been previously reported for various digestive proteases [11], including alcalase [18]. These values ranged from 1.19 to 2.31 mg mL<sup>-1</sup>, however the direct comparison with IC<sub>50</sub> values in the present study (Table 1) is not possible due to differences in the hydrolysis conditions but, also, in the methodology employed for ACE inhibitory activity determination and calculation.

**Figure 2.** Left: Experimental data (symbols) for ACE-inhibitory activity of cuttlefish softening wastewater protein concentrate before (●) and after hydrolysis with alcalase for 0.5 h (○), 2 h (△), and 8 h (□). Right: Experimental data (symbols) for ACE-inhibitory activity of 10 kDa (▽) and 1 kDa (▼) retentates and 1 kDa permeate (▲) from the 8 h hydrolysate. The dose-response curves (lines) were obtained by modeling experimental data to the Equation (4).



The 8 h hydrolysate, which led to the highest ACE inhibitory activity (lowest IC<sub>50</sub>), was fractionated in an attempt to isolate the active peptides. The use of UF has proven to be a valuable resource for hydrolysate fractionation, significantly decreasing the IC<sub>50</sub> value of peptide mixtures obtained from different sources [6,24–26]. For this reason, the 8 h hydrolysate was sequentially ultrafiltered through membranes at 10 and 1 kDa MWCO (Figure 3). Then, permeate and retentates ACE inhibitory activity was determined. As summarized in Table 1, the lowest IC<sub>50</sub> value was associated to 1 kDa permeate ( $58.4 \pm 4.6 \mu\text{g mL}^{-1}$ ), indicating that the maximum contribution to ACE-inhibitory activity is due to the peptides with MW below 1 kDa. Similarly, the ACE inhibitory activity was significantly higher in the lowermost MW fraction (<1 kDa) from collagenous residues from squid skins hydrolyzed with esperase [25].

This observation is in good agreement with previous studies reporting greater *in vitro* activity of low than high molecular weight peptides from different protein origin [13,18].

### 2.3. Identification of Major ACE Inhibitory Peptides

The ACE inhibitory peptides in the 1 kDa permeate from cuttlefish hydrolysate were separated by RP-HPLC on a C18 column. The chromatogram (Figure 4) was divided into sixty-five fractions

(2 mL) that were freeze-dried and their ACE inhibitory activity determined after resuspension in milliQ water and pH adjustment to 7.0. Four fractions showing the highest activity were collected separately under optimized separation conditions that allowed a better resolution of the peaks, *i.e.*, lower flow rate and a narrower acetonitrile gradient. The separation procedure was successively repeated to obtain a sufficient protein concentration for further analysis. The most active fractions (Figure 4A–D) were freeze-dried and their ACE inhibitory activity and IC<sub>50</sub> values determined (Table 2).

**Figure 3.** Process of ACE inhibitory peptide production from a protein enriched fraction recovered from cuttlefish wastewater by UF-DF at 10 kDa (Step 1) followed by hydrolysis with alcalase (0.4% v/v) for 8 h at 55 °C (Step 2). Then, the hydrolysate was fractionated using a sequentially UF through membranes of 10 (Step 3) and 1 kDa (Step 4). UFP: Permeates of UF; UFR: retentates of UF.

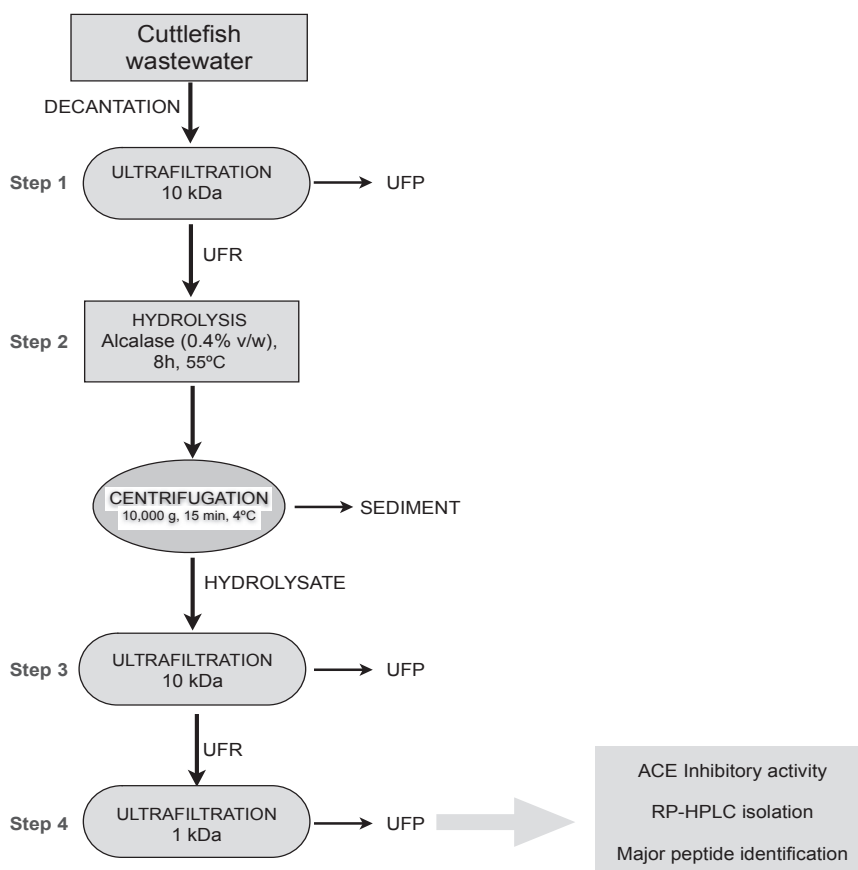
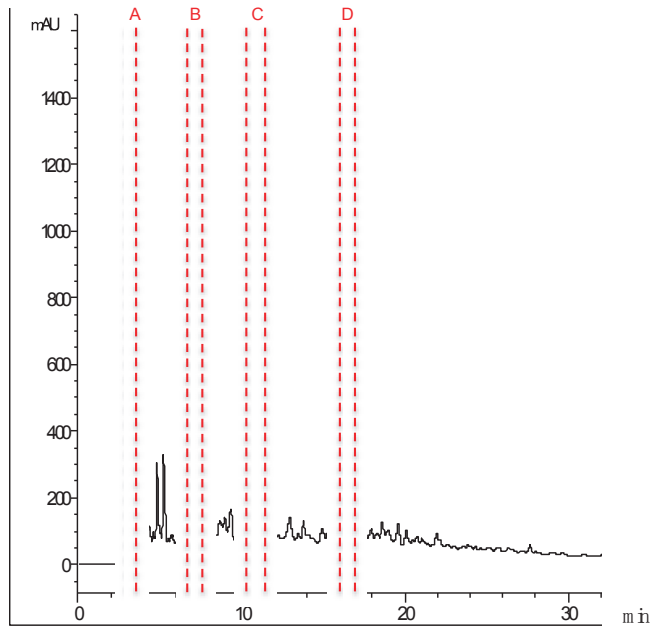


**Figure 4.** Peptide profile of the 8 h hydrolysate that was permeated through the 1 kDa ultrafiltration membrane after RP-HPLC separation. Lines indicate the peaks corresponding to the four active fractions (A–D).



The chemical characterization of each RP-HPLC fraction was carried out using mass spectrometry, in order to identify the main peptides contributing to the ACE inhibitory activity measured in these samples. According to these results (Table 2), among the four fractions only two (C and D) matched the protein databases and the other two fractions (A and B) had to be sequenced *de novo*.

The peptides identified in the fractions C and D are derived from muscular protein fragments of the cuttlefish mantle. Softening of fish muscle consists on the heating and addition of salts to solubilize myofibrillar proteins, improving the water-fat-retention and leading to acceptable rigidity/elasticity of the muscle gels [27]. Thus, as expected and since the cuttlefish hydrolysate was prepared from a protein concentrate recovered from softening wastewater, myofibrillar proteins, such as troponin, actin, and myosin were identified as protein sources from the identified peptides (Table 2). Antihypertensive peptides isolated from other squid proteins hydrolysates, such as collagen [27] and gelatin [7,28], have also been reported. These studies identified peptide sequences of the major ACE inhibitory fractions with a high content in proline, glycine, and leucine residues and suggesting the presence of this last amino acid could play an important role in the ACE-inhibitory activity [28].



**Table 2.** Major identified peptides corresponding to the four more active fractions after semi-preparative fractionation by reversed-phase high performance liquid chromatography (RP-HPLC) of the 1 kDa ultrafiltration permeate from the 8 h hydrolysate. The IC<sub>50</sub> (μg mL<sup>-1</sup>) value and the protein source of these fractions are shown.

Fraction	Peptides	Protein Source	Mass (Da)	IC <sub>50</sub> (μg mL <sup>-1</sup> )
A	GNALVFLLP		943.57	1.92 ± 0.40
	FALASSLVN		921.53	
	SPSIAPAL		755.40	
	GLFAAHRK		899.54	
	FTPESLAI		877.50	
	DAAIKTLTK		960.60	
	MMQLRKA		877.50	
	RALKIPAM		899.54	
	FTVKPVSR		933.59	
	SSSKAKKKP		960.60	
	KAVPIAIL		824.58	
	TRAASCP		705.30	
	INKAVTGLK		943.57	
	PEGSIRP		755.40	
B	VEDAEVGKK		974.52	4.00 ± 0.19
	FAGDDAPRA		919.43	
	AGSVNKSK		790.44	
	KAGSELGL		774.44	
	QSLEVSK		790.43	
	KEAEVSK		790.43	
	GAEVTVSK		790.43	
	QEVSLSK		790.43	
	AGEVSLSK		790.43	
	NFGCSVK		754.35	
	SVCGGFGK		754.35	
	AGDDPAR		701.32	
C	ADQSEGALQK	Myosin HC	1045.5	8.63 ± 0.86
	ISEQEASQR	Tropmyosin	1046.5	
	LGEGGRSTHE	Myosin HC	1041.5	
	RLKEAENR	Actin	981.5	
	TDQLGEGGRS	Myosin HC	1018.5	
D	DEDATGVIR	Tn C	974.47	7.18 ± 2.44
	GTDPEDALRN	Myosin RLC	1086.49	
	GVNLEDKRS	Myosin HC	1087.56	
	LTEAPLNPK	Actin	981.55	
	REDIDGNIK	Myosin LCK	1058.54	

As is known, peptide sequence greatly contributes to its biological activity. The structure–function relationship for ACE inhibitory peptides is not fully characterized, although recently published papers deal with the structure-activity relationships of di and tripeptides [29,30]. Some of the

information available about this topic indicates that the three amino acids in the *C*-terminal peptide sequence are particularly important for their binding to ACE, as they might interact with the active site of the enzyme [31]. For instance, this enzyme prefers hydrophobic amino acids, including aromatic residues (phenylalanine, tryptophan, and tyrosine) and branched chain amino acids (valine, leucine, and isoleucine) in one of the three positions of the *C*-terminal [32]. In this study, all of the peptides identified in the four potent ACE inhibitory fractions contained at least one hydrophobic residue, being the most abundant branched chain amino acids (Table 2).

On the other hand, ACE has low affinity for peptides with dicarboxylic amino acids in this position or those containing the amino acid proline in the penultimate position [33], although proline in final or penultimate position of the *C*-terminal peptide sequence promotes enzyme binding [34]. In fact, several identified ACE inhibitory peptides had a proline residue in one of these positions of *C*-terminal, although this is neither sufficient nor essential to confer activity [18]. Furthermore, the positively charged amino acids, such as arginine and lysine at the *C*-terminal sequences were also reported to contribute towards ACE inhibitory or antihypertensive effect [35]. As can be seen in Table 2, among the identified peptides many of them contained one of these residues in the *C*-terminal. This was especially evident in fraction B, where ten of the twelve peptides identified contained lysine or arginine in last position. In agreement with other published papers, these findings confirm that peptide sequences are greatly important to define their ACE inhibitory activity ( $IC_{50}$  values). However, the differences in the composition of the peptides identified in this study fail to explain the differences found in the ACE inhibitory activity and, thus, further studies are needed to define which of these peptides are ultimately responsible for the potent antihypertensive activity of these fractions.

### 3. Experimental Section

#### 3.1. Cuttlefish Processing Wastewater

Wastewater from the softening treatment during industrial manufacturing of cuttlefish was kindly provided by Frinova S.A., (Porriño, Galicia, Spain). The average content of suspended solids of this water was ranged among 0.3–0.7 g L<sup>-1</sup> and the solid residue was around 10–15 g L<sup>-1</sup>. The water was decanted to discard the particulate matter, sampled for analytical determinations, and stored at –20 °C until further use.

#### 3.2. Total Protein Analysis

Protein concentration was determined by the bicinchoninic acid assay (BCA, Pierce, Rockford, IL, USA) using bovine serum albumin as standard. Briefly, 200 µL of the BCA working reagent were mixed with 25 µL of sample. The mixture was incubated for 30 min at 37 °C and the absorbance taken at 562 nm using a Multiskan Spectrum Microplate Spectrophotometer (Thermo Scientific, Waltham, MA, USA).

### 3.3. Ultrafiltration-Diafiltration Process

Cleaned cuttlefish wastewater was subjected to ultrafiltration-diafiltration using a Prep/Scale-TFF polyethersulfone cartridge (Millipore Corporation, Bedford, MA, USA) of 10 kDa molecular weight cut-off (MWCO). The operation mode was the following: an initial phase of ultrafiltration (UF) at 40 °C with total recirculation of retentate was performed, immediately followed by a diafiltration (DF) process. During UF, the inlet pressure remained constant to determine the flow rate drops due to the increased concentration of protein in the retentate and to possible membrane fouling. The final retentate (after DF) was frozen at -20 °C for further hydrolysis and permeate from the DF phase was discarded.

For the modeling of the membrane process, we assumed that in the DF with constant volume (filtration flow = water intake flow), the concentration (or the total amount) of a permeable solute in the retentate followed first order kinetics [15]:

$$R = R_f + R_0 \exp[-(1-s)D] \quad (1)$$

where,  $R$  is the concentration of permeable protein in the retentate (% from the level at initial DF),  $R_0$  the initial concentration (%),  $R_f$  is the final and asymptotic concentration (%),  $D$  is the relative diavolume (volume of added water/constant retentate volume) and  $s$  is the specific retention of protein with variation between 0 (the solute is filtered as the solvent) and 1 (the solute is totally retained). Thus, using normalized values (%):  $R_0 + R_f = 100$ , being  $R_0 = 0$  if all protein is permeable.

### 3.4. Preparation of Enzymatic Hydrolysates

The cuttlefish wastewater concentrate (retentate) was pre-incubated at 55 °C for 10 min prior to enzymatic hydrolysis using Alcalase 2.4 L from Novo Co. (Novozyme Nordisk, Bagsvaerd, Denmark). The enzyme to substrate ratio (E/S) was 0.4% (v/w) in relation to retentate weight and the reaction was performed in a temperature-controlled water bath under constant magnetic stirring [12]. Samples were taken after 0.5, 2, and 8 h of hydrolysis, boiled for 15 min to inactivate the protease and then cooled in an ice-water bath for at least 30 min. Hydrolysates were centrifuged at 10,000×  $g$  for 15 min (4 °C) in an Avanti J-26 XP centrifuge (Beckman Coulter, Inc., Miami, FL, USA) and supernatants were stored at -20 °C until further analysis of their degree of hydrolysis and antihypertensive activity.

### 3.5. Degree of Hydrolysis Determination

The degree of hydrolysis (DH) was defined as the ratio of the released tyrosine to the initial tyrosine in the retentate [12], according to the following expression:

$$DH = \frac{C_t - C_0}{C_0} \times 100 \quad (2)$$

where,  $C_t$  is the tyrosine concentration ( $\text{g L}^{-1}$ ) of the hydrolysate at time  $t$  and  $C_0$  is the tyrosine concentration ( $\text{g L}^{-1}$ ) of the sample at time zero. Tyrosine was measured by the method described in Barker and Worgan [36].

### 3.6. Angiotensin I-Converting Enzyme (ACE) Inhibition Assay

The antihypertensive activity was determined using a modified version of the method described by Shalaby *et al.* [37] with *N*-[3-(2-Furyl) acryloyl]-L-phenylalanyl-glycyl-glycine (FAPGG) as substrate. Briefly, 10  $\mu\text{L}$  of sample were mixed with 10  $\mu\text{L}$  of ACE solution ( $0.5 \text{ U mL}^{-1}$ ) in each well of a 96-well microtiter plate. The reaction was started by adding 150  $\mu\text{L}$  of substrate (0.88 mM FAPGG in 50 mM Tris-HCl, pH 7.5, 0.3 M NaCl) pre-heated at 37 °C. The absorbance at 340 nm (A340) was acquired at time intervals of 30 s for 30 min in a Multiskan Spectrum Microplate Spectrophotometer (Thermo Scientific, Waltham, MA, USA). The control consisted of samples containing 10  $\mu\text{L}$  of buffer (50 mM Tris-HCl, pH 7.5, 0.3 M NaCl) instead of protein hydrolysate. Samples and controls were performed in triplicate.

ACE-inhibitory capacity ( $I_{ACE}$ ) was calculated as a function of the average slope of decrease in absorbance with time and expressed as percent of enzyme inhibition according to the following expression:

$$I_{ACE} (\%) = \left[ 1 - \frac{\rho A_h}{\rho A_c} \right] \times 100 \quad (3)$$

where,  $I_{ACE}$  is the ACE-inhibitory capacity (%),  $\rho A_h$  is the slope of decrease in A340 in the presence of inhibitor (hydrolysate) and  $\rho A_c$  is the slope of decrease in A340 in the absence of inhibitor (control).

For the calculation of the protein concentration causing a 50% ACE inhibition ( $IC_{50}$ ), dose-response curves were obtained assaying different concentrations of hydrolysates.  $IC_{50}$  values were calculated by fitting the dose-response curves of  $I_{ACE}$  vs. protein concentration to a mechanistic model developed by Estévez *et al.* [6]:

$$I_{ACE} = 100K \left( 1 - \frac{(K_m + S)}{\left( S + K_m \left( 1 + \frac{C(K_m + S)}{IC_{50}K_m(2K - 1)} \right) \right)} \right) \quad (4)$$

where,  $K$  is the maximum  $I_{ACE}$  (%),  $C$  is the protein concentration ( $\mu\text{g mL}^{-1}$ ) and  $IC_{50}$  is the concentration for semi-maximum response ( $\mu\text{g mL}^{-1}$ ).  $K_m$  is the Michaelis–Menten constant of FAPGG and  $S$  is the concentration of this substrate in the assay, respectively. Both  $K_m$  and  $S$  are constants under these experimental conditions, with values of 182  $\mu\text{g mL}^{-1}$  and 310  $\mu\text{g mL}^{-1}$ , respectively [6].

### 3.7. Isolation of Major ACE-Inhibitory Peptides

The 8-h-hydrolysate was further ultrafiltered to remove peptides with high molecular weight. UF were carried out in a stirred UF cell module (Millipore Corporation, Bedford, MA, USA) under a nitrogen flow pressure of 40 psi at room temperature using separately 10 and 1 kDa MWCO membranes (Millipore Corporation, Bedford, MA, USA). Firstly, the hydrolysate was ultrafiltrate using a 10 kDa MWCO membrane followed by further fractionation of the 10 kDa permeate through a 1 kDa MWCO membrane. Samples from 10 and 1 kDa retentates and 1 kDa permeate were collected and protein concentration and ACE-inhibitory activity ( $IC_{50}$ ) were determined.

The 1 kDa permeate was separated by RP-HPLC on an Agilent 1200 series system (Agilent, Waldbronn, Germany) using an ACE 5 C18 column (10 × 250 mm, 5  $\mu$ m). Peptides were eluted and monitored at 220 nm using water containing 0.1% trifluoroacetic acid (TFA) (mobile phase A) and acetonitrile with 0.1% TFA (mobile phase B), with a linear gradient of acetonitrile (0%–50% v/v) during 50 min. The ACE inhibitory activity was determined in 2 mL fractions collected at a flow rate of 2.5 mL  $min^{-1}$ . Those fractions showing the highest ACE inhibitory activity were collected using an Agilent Zorbax Eclipse C18 column (4.6 × 250 mm, 5  $\mu$ m) with a linear gradient of acetonitrile (5%–30% v/v) at a flow rate of 0.75 mL  $min^{-1}$  during 30 min. According to the chromatographic peptide profile obtained, four fractions from ten samples were defined and collected manually, frozen at  $-80\text{ }^{\circ}C$ , and lyophilized for further protein quantitation, antihypertensive activity determination, and mass spectrometry identification analysis.

### 3.8. Mass Spectrometry Analysis of ACE-Inhibitory Peptides

The freeze-dried fractions were diluted in 1 mL of 1% ACN, 0.1% formic acid (FA) and 2  $\mu$ L aliquots were analyzed using a C18 column coupled to an electrospray ion trap Fourier transform ion cyclotron resonance-mass spectrometer (ESI-IT-FTICR, Thermo Fisher Scientific, Bremen, Germany). A data dependent fragmentation method consisting of cycles of high resolution full scan spectra followed by ion trap fragmentation and detection of the five most intense masses was used for identification purposes. The chromatographic system (Agilent 1200 series, Waldbronn, Germany) was equipped with an Agilent SB C-18 column (0.5 × 150 mm, 5  $\mu$ m). A very slow elution program, namely, 0/5, 6/5, 7/10, 32/40, 34/90 (min/%B, being mobile phase A 5% ACN, 0.1% FA and mobile phase B pure ACN, 0.1% FA), at a flow of 20  $\mu$ L  $min^{-1}$ , was optimized to enhance the separation of the low hydrophobic species fractionated in the previous semi-preparative chromatographic dimension.

### 3.9. Mass Spectrometry Data Processing

MS/MS spectra were searched using SEQUEST-SORCERER™ 2 package (Sage-N Research Inc., Milpitas, CA, USA), against the UniProt/SwissProt database (release 2012\_10; 455.545 entries), which also included their respective decoy sequences. The following constraints were used for the searches: semi-tryptic cleavage with up to two missed cleavage sites and tolerances 1.0 Da for precursor ions and 0.5 Da for MS/MS fragments ions. The variable modifications allowed were methionine oxidation (m), carbamidomethylation of Cys and acetylation of the *N*-terminus of the

protein (*N*-Acyl). The database search results were subjected to statistical analysis with the PeptideProphet algorithm (v.4.4) [38]. The FDR was kept below 1%.

*De novo* sequencing was performed by manual interpretation of the ion series of the spectra with aid of the software packages: DeNovoX (Thermo Scientific, Waltham, MA, USA) and PEAKS Studio 6.0 (Bioinformatics Solutions Inc., Waterloo, Ontario, Canada). The parameters used for both programs were as follows: selection of the peptide charge (1+, 2+, 3+), tolerances of 0.3–0.5 Da for precursor and fragments ions, use or not of trypsin or Glu-C as proteases and three variable modifications: Methionine oxidation (m), carbamidomethylation of Cys and acetylation of the *N*-terminus of the protein (*N*-Acyl).

#### 4. Conclusions

In this study, ACE inhibitory peptides were produced from cuttlefish byproduct protein hydrolysate using a combination of membrane technology (UF-DF) and enzyme proteolysis using alcalase. The sequential ultrafiltration with two membranes cut-offs (10 and 1 kDa) led to recover a remarkable antihypertensive activity. The most bioactive peptides were subsequently separated by means of RP-HPLC and characterized by HPLC-ESI-IT-FTICR. The procedure developed in the present work demonstrated to be a feasible biotechnological approach to produce antihypertensive peptides from marine wastes and to help in the depuration and valorization of wastewaters generated by marine food processing. Nevertheless, further studies (peptide synthesis, re-chromatography of the HPLC fractions, *etc.*) are needed in order to identify which among these peptide mixtures are responsible for the observed activity.

#### Acknowledgements

We wish to thank to Margarita Nogueira and Ana Durán for their excellent technical assistance. We also thank to Almudena Pena for the kindly supply of the cuttlefish wastewater. The company Frinova S.A. funded this study (Contract N° 20090732 co-financed by CDTI). The authors also thank the Unit of Information Resources for Research (URICI-CSIC) for the co-funding of this publication in Open Access format.

#### Author Contributions

I.R.A. performed the experiments and wrote the text; J.A.V. supervised the experiments and corrected the manuscript; P.G. supervised the project; D.E.F. characterized the peptides by HPLC-ESI-IT-FTICR; M.C. processed the mass spectrometry data and C.P. separated the peptides by RP-HPLC and corrected the manuscript.

#### Conflicts of Interest

The authors declare no conflict of interest.

## References

1. World Health Organization. *Causes of Death 2008: Data Sources and Methods*; World Health Organization: Geneva, Switzerland, 2011. Available online: [http://www.who.int/healthinfo/global\\_burden\\_disease/cod\\_2008\\_sources\\_methods.pdf](http://www.who.int/healthinfo/global_burden_disease/cod_2008_sources_methods.pdf) (accessed on 20 October 2013).
2. World Health Organization. *A Global Brief on Hypertension. Silent Killer, Global Public Health Crisis*; World Health Organization: Geneva, Switzerland, 2013. Available online: [http://apps.who.int/iris/bitstream/10665/79059/1/WHO\\_DCO\\_WHD\\_2013.2\\_eng.pdf](http://apps.who.int/iris/bitstream/10665/79059/1/WHO_DCO_WHD_2013.2_eng.pdf) (accessed on 14 December 2013).
3. Lim, S.S.; Vos, T.; Flaxman, A.D.; Danaei, G.; Shibuya, K.; Adair-Rohani, H.; Al Mazroa, M.A.; Amann, M.; Anderson, H.R.; Andrews, K.G.; *et al.* A comparative risk assessment of burden of disease and injury attributable to 67 risk factors and risk factor clusters in 21 regions, 1990–2010: A systematic analysis for the Global Burden of Disease Study 2010. *Lancet* **2012**, *380*, 2224–2260.
4. Fang, H.; Luo, M.; Sheng, Y.; Li, Z.; Wu, Y.; Liu, C. The antihypertensive effect of peptides: A novel alternative to drugs? *Peptides* **2008**, *29*, 1062–1071.
5. Israïli, Z.H.; Hall, W.D. Cough and angioneurotic edema associated with angiotensin-converting enzyme inhibitor therapy. A review of the literature and pathophysiology. *Ann. Int. Med.* **1992**, *117*, 234–242.
6. Estévez, N.; Fuciños, P.; Sobrosa, A.C.; Pastrana, L.; Pérez, N.; Rúa, M.L. Modeling the angiotensin-converting enzyme inhibitory activity of peptide mixtures obtained from cheese whey hydrolysates using concentration-response curves. *Biotechnol. Prog.* **2012**, *28*, 1197–1206.
7. Alemán, A.; Pérez-Santín, E.; Bordenave-Juchereau, S.; Arnaudin, I.; Gómez-Guillén, M.C.; Montero, P. Squid gelatin hydrolysates with antihypertensive, anticancer and antioxidant activity. *Food Res. Int.* **2011**, *44*, 1044–1051.
8. Ryan, J.T.; Ross, R.P.; Bolton, D.; Fitzgerald, G.F.; Stanton, C. Bioactive peptides from muscle sources: Meat and fish. *Nutrients* **2011**, *3*, 765–791.
9. He, H.; Chen, X.; Sun, C.; Zhang, Y.; Gao, P. Preparation and functional evaluation of oligopeptide-enriched hydrolysate from shrimp (*Acetes chinensis*) treated with crude protease from *Bacillus* sp. SM98011. *Bioresour. Technol.* **2006**, *97*, 385–390.
10. Jung, W.-K.; Mendis, E.; Je, J.-Y.; Park, P.-J.; Son, B.W.; Kim, H.C.; Choi, Y.K.; Kim, S.-K. Angiotensin I-converting enzyme inhibitory peptide from yellowfin sole (*Limanda aspera*) frame protein and its antihypertensive effect in spontaneously hypertensive rats. *Food Chem.* **2006**, *94*, 26–32.
11. Balti, R.; Nedjar-Arroume, N.; Bougatef, A.; Guillochon, D.; Nasri, M. Three novel angiotensin I-converting enzyme (ACE) inhibitory peptides from cuttlefish (*Sepia officinalis*) using digestive proteases. *Food Res. Int.* **2010**, *43*, 1136–1143.
12. Amado, I.R.; Vázquez, J.A.; González, M.P.; Murado, M.A. Production of antihypertensive and antioxidant activities by enzymatic hydrolysis of protein concentrates recovered by ultrafiltration from cuttlefish processing wastewaters. *Biochem. Eng. J.* **2013**, *76*, 43–54.

13. Kristinsson, H.G.; Rasco, B.A. Biochemical and functional properties of Atlantic salmon (*Salmo salar*) muscle proteins hydrolyzed with various alkaline proteases. *J. Agric. Food Chem.* **2000**, *48*, 657–666.
14. Pérez-Santín, E.; Calvo, M.M.; López-Caballero, M.E.; Montero, P.; Gómez-Guillén, M.C. Compositional properties and bioactive potential of waste material from shrimp cooking juice. *LWT-Food Sci. Technol.* **2013**, *54*, 87–94.
15. Murado, M.A.; Fraguas, J.; Montemayor, M.I.; Vázquez, J.A.; González, P. Preparation of highly purified chondroitin sulphate from skate (*Raja clavata*) cartilage by-products. Process optimization including a new procedure of alkaline hydroalcoholic hydrolysis. *Biochem. Eng. J.* **2010**, *49*, 126–132.
16. Ferjani, E.; Ellouze, E.; Ben Amar, R. Treatment of seafood processing wastewaters by ultrafiltration-nanofiltration cellulose acetate membranes. *Desalination* **2005**, *177*, 43–49.
17. Ellouze, E.; Ben Amar, R.; Ben Salah, A.H. Cross-flow microfiltration using ceramic membranes applied to the cuttlefish effluents treatment: Effect of operating parameters and the addition of pre or post-treatment. *Desalination* **2005**, *177*, 229–240.
18. Balti, R.; Nedjar-Arroume, N.; Adjé, E.Y.; Guillochon, D.; Nasri, M. Analysis of novel angiotensin I-converting enzyme inhibitory peptides from enzymatic hydrolysates of cuttlefish (*Sepia officinalis*) muscle proteins. *J. Agric. Food Chem.* **2010**, *58*, 3840–3846.
19. Ko, S.-C.; Kang, N.; Kim, E.-A.; Kang, M.C.; Lee, S.-H.; Kang, S.-M.; Lee, J.-B.; Jeon, B.-T.; Kim, S.-K.; Park, S.-J.; *et al.* A novel angiotensin I-converting enzyme (ACE) inhibitory peptide from a marine *Chlorella ellipsoidea* and its antihypertensive effect in spontaneously hypertensive rats. *Process Biochem.* **2012**, *47*, 2005–2011.
20. Ahn, C.-B.; Jeon, Y.-J.; Kim, Y.-T.; Je, J.-Y. Angiotensin I converting enzyme (ACE) inhibitory peptides from salmon byproduct protein hydrolysate by alcalase hydrolysis. *Process Biochem.* **2012**, *47*, 2240–2245.
21. Wijesekara, I.; Qian, Z.-J.; Ryu, B.; Ngo, D.-H.; Kim, S.-K. Purification and identification of antihypertensive peptides from seaweed pipefish (*Syngnathus schlegeli*) muscle protein hydrolysate. *Food Res. Int.* **2011**, *44*, 703–707.
22. Zhao, Y.; Li, B.; Dong, S.; Liu, Z.; Zhao, X.; Wang, J.; Zeng, M. A novel ACE inhibitory peptide isolated from *Acaudina molpadioidea* hydrolysate. *Peptides* **2009**, *30*, 1028–1033.
23. Wu, S.; Sun, J.; Tong, Z.; Lan, X.; Zhao, Z.; Liao, D. Optimization of hydrolysis conditions for the production of angiotensin-I converting enzyme-inhibitory peptides and isolation of a novel peptide from lizard fish (*Saurida elongata*) muscle protein hydrolysate. *Mar. Drugs* **2012**, *10*, 1066–1080.
24. Hyun, C.-K.; Shin, H.-K. Utilization of bovine blood plasma proteins for the production of angiotensin I converting enzyme inhibitory peptides. *Process Biochem.* **2000**, *36*, 65–71.
25. Je, J.-Y.; Park, P.-J.; Kwon, J.Y.; Kim, S.-K. A novel Angiotensin I converting enzyme inhibitory peptide from Alaska Pollack (*Theragra chalcogramma*) frame protein hydrolysate. *J. Agric. Food Chem.* **2004**, *52*, 7842–7845.



26. Alemán, A.; Gómez-Guillén, M.C.; Montero, P. Identification of ACE-inhibitory peptides from squid skin collagen after *in vitro* gastrointestinal digestion. *Food Res. Int.* **2013**, *54*, 790–795.
27. Gordon, A.; Barbut, S. Effect of chloride salts on protein extraction and interfacial protein film formation in meat batters. *J. Sci. Food Agric.* **1992**, *58*, 227–238.
28. Alemán, A.; Giménez, B.; Pérez-Santín, E.; Gómez-Guillén, M.C.; Montero, P. Contribution of Leu and Hyp residues to antioxidant and ACE-inhibitory activities of peptide sequences isolated from squid gelatin hydrolysate. *Food Chem.* **2011**, *125*, 334–341.
29. He, R.; Ma, H.; Zhao, W.; Qu, W.; Zhao, J.; Luo, L.; Zhu, W. Modeling the QSAR of ACE-inhibitory peptides with ANN and its applied illustration. *Int. J. Pept.* **2012**, *2012*, 1–9.
30. Wu, J.; Aluko, R. E.; Nakai, S. Structural requirements of angiotensin I converting enzyme inhibitory peptides: Quantitative structure-activity relationship study of Di- and Tripeptides. *J. Agric. Food Chem.* **2006**, *54*, 732–738.
31. Ondetti, M.A.; Cushman, D.W. Enzymes of the renin-angiotensin system and their inhibitors. *Ann. Rev. Biochem.* **2012**, *51*, 283–308.
32. Mullally, M.M.; Meisel, H.; FitzGerald, R.J. Identification of a novel angiotensin-I-converting enzyme inhibitory peptide corresponding to a tryptic fragment of bovine  $\beta$ -lactoglobulin. *FEBS Lett.* **1997**, *402*, 99–101.
33. FitzGerald, R.J.; Meisel, H. Milk protein-derived peptide inhibitors of angiotensin-I-converting enzyme. *Br. J. Nutr.* **2000**, *84*, S33–S37.
34. Haque, E.; Chand, R. Antihypertensive and antimicrobial bioactive peptides from milk proteins. *Eur. Food Res. Technol.* **2008**, *227*, 7–15.
35. Cheung, H.-S.; Wang, F.-L.; Ondetti, M.; Sabo, E.; Cushman, D. Binding of peptide substrates and inhibitors of angiotensin-converting enzyme: Importance of the COOH-terminal dipeptide sequences. *J. Biol. Chem.* **1980**, *255*, 401–407.
36. Barker, T.W.; Worgan, J.T. The utilisation of palm oil processing effluents as substrates for microbial protein production by the fungus *Aspergillus oryzae*. *Appl. Microbiol. Biotechnol.* **1981**, *11*, 234–240.
37. Shalaby, S.M.; Zakora, M.; Otte, J. Performance of two commonly used angiotensin-converting enzyme inhibition assays using FA-PGG and HHL as substrates. *J. Dairy Res.* **2006**, *73*, 178–186.
38. Keller, A.; Nesvizhskii, A.I.; Kolker, E.; Aebersold, R. Empirical statistical model to estimate the accuracy of peptide identifications made by MS/MS and database search. *Anal. Chem.* **2002**, *74*, 5383–5392.

# Genomic Sequence and Experimental Tractability of a New Decapod Shrimp Model, *Neocaridina denticulata*

Nathan J. Kenny, Yung Wa Sin, Xin Shen, Qu Zhe, Wei Wang, Ting Fung Chan, Stephen S. Tobe, Sebastian M. Shimeld, Ka Hou Chu and Jerome H. L. Hui

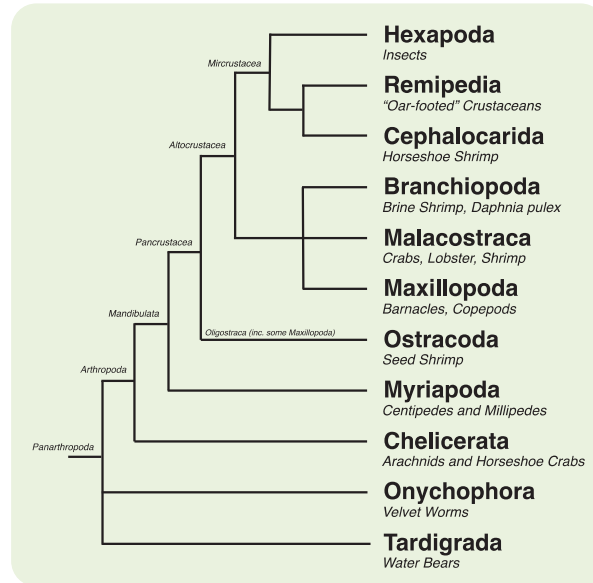
**Abstract:** The speciose Crustacea is the largest subphylum of arthropods on the planet after the Insecta. To date, however, the only publically available sequenced crustacean genome is that of the water flea, *Daphnia pulex*, a member of the Branchiopoda. While *Daphnia* is a well-established ecotoxicological model, previous study showed that one-third of genes contained in its genome are lineage-specific and could not be identified in any other metazoan genomes. To better understand the genomic evolution of crustaceans and arthropods, we have sequenced the genome of a novel shrimp model, *Neocaridina denticulata*, and tested its experimental malleability. A library of 170-bp nominal fragment size was constructed from DNA of a starved single adult and sequenced using the Illumina HiSeq2000 platform. Core eukaryotic genes, the mitochondrial genome, developmental patterning genes (such as Hox) and microRNA processing pathway genes are all present in this animal, suggesting it has not undergone massive genomic loss. Comparison with the published genome of *Daphnia pulex* has allowed us to reveal 3750 genes that are indeed specific to the lineage containing malacostracans and branchiopods, rather than *Daphnia*-specific ( $E$ -value:  $10^{-6}$ ). We also show the experimental tractability of *N. denticulata*, which, together with the genomic resources presented here, make it an ideal model for a wide range of further aquacultural, developmental, ecotoxicological, food safety, genetic, hormonal, physiological and reproductive research, allowing better understanding of the evolution of crustaceans and other arthropods.

Reprinted from *Mar. Drugs*. Cite as: Kenny, N.J.; Sin, Y.W.; Shen, X.; Zhe, Q.; Wang, W.; Chan, T.F.; Tobe, S.S.; Shimeld, S.M.; Chu, K.H.; Hui, J.H.L. Genomic Sequence and Experimental Tractability of a New Decapod Shrimp Model, *Neocaridina denticulata*. *Mar. Drugs* **2014**, *12*, 141961437.

## 1. Introduction

Crustaceans are found worldwide in marine and terrestrial environments and are of great scientific and commercial importance. However, they are relatively underrepresented at the genomic level [1,2]. The Crustacea is conventionally divided into six classes [3], the Branchiopoda, Cephalocarida, Maxillopoda, Ostracoda, Remipedia and Malacostraca (which includes decapods, isopods, amphipods and stomatopods) (Figure 1), with an approximate number of 67,000 described living species [4]. Recent phylogenetic investigation has revealed that the Hexapoda, a group that includes the Insecta, is in fact nested within the crustaceans [5,6]. This renders the subphylum “Crustacea” paraphyletic, and the number of extant insect species is excluded from the number of crustacean species given above.

**Figure 1.** Simplified pancrustacean phylogeny, after [5]. Note some smaller, cryptic clades are not shown, including some members of the Maxillopoda, which are paraphyletically grouped with the Ostracoda (e.g., Branchiura and Pentastomida). Phylogenetic analysis is presently conflicted on the closest sister group to the Hexapoda: [5] places the Xenocarida as the outgroup to the Hexapoda, whereas [6] places the Branchiopods in this position.



Extant published sequence resources in the Crustacea outside the Insecta are limited to that of a branchiopod, *Daphnia pulex* [7]. Although this animal is an important ecotoxicological model, its genome exhibits apparently high levels of gene duplication and loss and thus is not always suitable for use as an outgroup for comparison to the Insecta. Further, a single genome in the Crustacea also severely limits the conclusions that can be drawn as to the gain and loss of characters across the Pancrustacea, as current transcriptomic and expressed sequence tag (EST) resources will always only reflect the transcriptomic content of the specific tissues and time points sampled [1]. The provision of additional models to compare within the Crustacea is therefore a priority, given the importance of arthropods to the economy and a range of scientific spheres of investigation.

Malacostraca contains a number of orders, including the Amphipoda, Isopoda and Decapoda. A species within the Amphipoda, *Parhyale hawaiiensis*, has already been used in developmental investigations [8], and isopods are familiar, due to the ubiquity of the common woodlouse, which is often used as a behavioural and environmental model [9]. The most economically important malacostracan crustaceans, however, belong to the order Decapoda. Decapods are both wild-caught and farmed and provide an important global food source. They are also ecologically vital as detritivores for environmental stability [10,11]. With an estimated 15,000 living crab, crayfish, shrimp, lobster and related species [12], the diversity of body plans and novelties seen in the

Decapoda, including appendages, feeding mouthparts and segments, make them interesting models to study in evolutionary and developmental biology.

The cherry shrimp, *Neocaridina denticulata* (De Haan, 1844), is suggested as an excellent laboratory model within Decapoda—an experimentally tractable [13–15], cosmopolitan [16] and phylogenetically well-placed species [17]. It also has a limited history of use as a crustacean ecotoxicological model [13,14] and as a model of recent invasion [18]. The draft genome sequence of *N. denticulata denticulata* (De Haan, 1844) is presented here as a resource of benefit to a wide range of scientific investigations, including genomic, developmental, ecotoxicological, evolutionary, physiological and reproductive research. As another outgroup to the Insecta, it provides another lineage to that of the water flea, *D. pulex*, for comparison, and will allow further understanding of crustacean and arthropod biology. In addition, this species can be easily cultured and maintained in the laboratory [15], where insights gleaned from this species will be applicable to marine decapods and of much commercial utility for crustacean aquaculture and food safety. As such, this genomic resource will be of service to a range of scientific investigations worldwide.

## 2. Results and Discussion

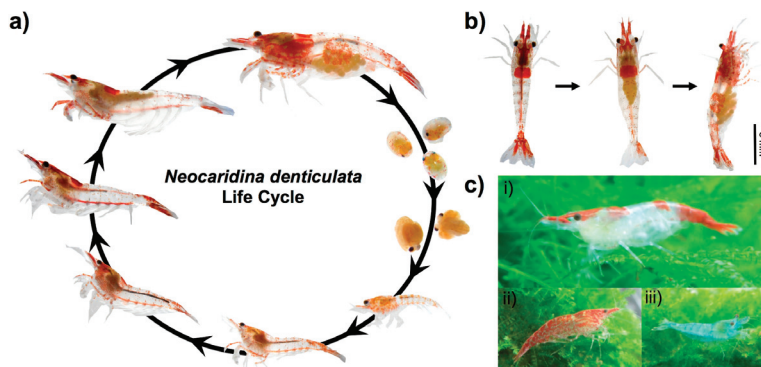
### 2.1. Animal Culture and Lifecycle

*Neocaridina* shrimp are native to many freshwater areas of East and Southeast Asia, tolerant of a wide range of conditions, commercially used for human consumption as a food flavouring agent and include a variety of colour forms (Figure 2c), and have spread around the world courtesy of the aquarium trade [19]. We have chosen *N. denticulata* for further study as it has much potential to become a model for aquacultural, developmental, ecotoxicological, food safety, genetic, hormonal, physiological and reproductive studies in the laboratory.

The start-up of culture and maintenance of *N. denticulata* is straightforward. Animals can be acquired commercially from the aquarium trade in a variety of colour morphs (Figure 2c). They can be kept in small freshwater tanks at room temperature, with simple filtration and aeration facilities sufficient for survival and reproduction. The native environments of *N. denticulata* generally are medium-soft and slightly alkaline (pH 7–7.5). However, *N. denticulata* can survive in a pH of 6.5–8.0 [14,19,20]. Optimum water temperature is 22–24 °C, and while shrimp are tolerant of a range of five degrees above and below this [15], temperatures should not be allowed to change rapidly or markedly. Low-powered filtration systems are recommended to aid the survival of juvenile shrimp, and a sponge filter is adequate, provided uneaten food is removed from tanks at regular intervals. Similar to other arthropods, *N. denticulata* is, however, sensitive to heavy metals and the use of insecticides, and care should be taken not to expose the culture tanks to airborne pollutants [15]. *N. denticulata* will thrive on a variety of foodstuffs [19], and we have had good results with several commercially available shrimp feed formulations. The provision of hiding spaces or plant material, such as Java Moss (Hypnaceae) is recommended, as decapods are known to be cannibalistic of tank mates during ecdysis [21], and plants can provide an alternative food source for the shrimp, both directly and as a substrate for algal growth.

Sexual maturity of the female can be observed through the transparent carapace and body instead of sacrificing the animal to measure the gonadosomatic index (ovary weight divided by total body weight) (Figure 2b). Breeding occurs in summer in subspecies in colder climates, whereas warm-weather subpopulations breed year-round [19]. Mating occurs shortly after ecdysis, following which the female lays her eggs, fertilizing them as they are laid; they are then attached to her pleopods (swimmerets). Approximately 20–30 eggs with sizes ranging from 0.57 to 1.08 mm [22] are laid simultaneously and are carried externally [15], where they are amenable to injection or manipulation (see Section 2.8). The eggs hatch at around 30 days post-mating, depending on water temperature [23]. *N. denticulata* grow to 7.3–28.5 mm in length, with both male and female *N. denticulata* attaining sexual maturity at 4–6 months of age [15,22]. Generation time is therefore relatively short compared to other shrimps or decapods and is similar to that of other model organisms, such as zebrafish and medaka, but faster than that of the frog, *Xenopus laevis*.

**Figure 2.** (a) The lifecycle of *N. denticulata*; and (b) the appearance of gravid female (left, dorsal view; right, side view) compared to a female without eggs (centre, dorsal view). The scale bar represents 5 mm on three adult shrimp in (b). (c) Some of the colour forms available commercially. (i) Red patched; (ii) punctate red patterning; and (iii) blue.



## 2.2. Genomic Sequencing

Genomic DNA from a single adult *N. denticulata denticulata* (De Haan, 1844) was extracted and sequenced on a single lane of the Illumina HiSeq2000 platform, as described in the experimental section. Basic read metrics relating to this sequencing are shown in Table 1. FastQC was run to ascertain read quality, with excellent results, and median Phred quality scores greater than 34 through to the last base in both reads (Supplementary Figure S1). No over-represented sequences were detected in our analysis. Raw sequence data have been uploaded to NCBI's SRA (Bioproject PRJNA224755, Biosample SAMN02384679, experiment SRX375172, reads SRR1027643). After an initial assembly trial, Bowtie [24] was used to determine actual fragment size and the standard deviation for future use.

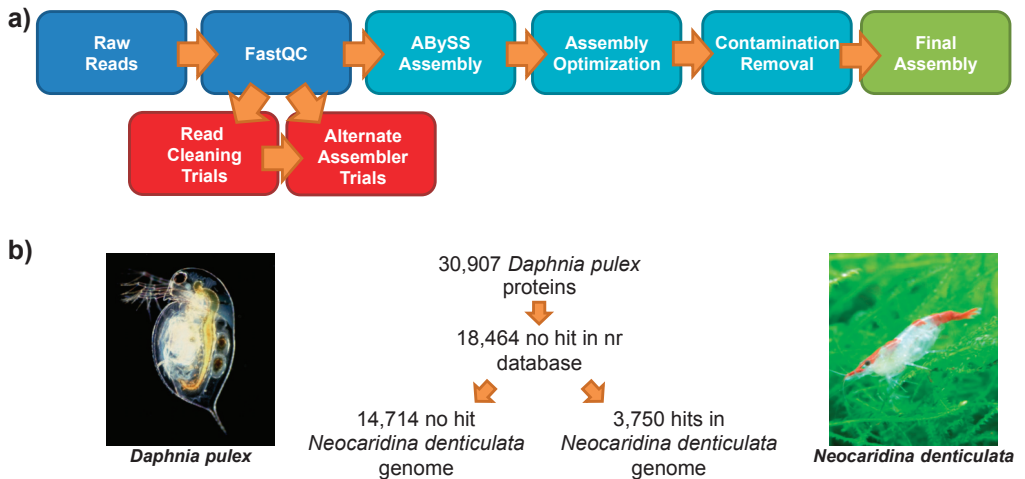
**Table 1.** Basic metrics relating to raw reads.

Platform	Illumina HiSeq2000
Number of Reads	364,013,140
Read Length (bp)	100
Average GC %	36
Fragment Size	167.22
Fragment Size SD (bp)	12.01

### 2.3. Genomic Assembly

Genomic assembly procedures are summarized in Figure 3a. After initial trials using a range of assembly software, including Velvet [25] and SOAPdenovo [26], raw reads were assembled using the abyss-pe script in ABySS [27] with a  $k$ -mer size of 51. Read cleaning using Sickle [28] and Musket [29] was assayed, but found to impair assembly by conventional metrics. Results of the empirically-determined “best” assembly are shown in Table 2. This assembly can be downloaded from [30] or can be supplied by the authors upon request.

**Figure 3.** (a) Schematic diagram of the genomic assembly of shrimp *N. denticulata*. (b) The summary statistics relating to the comparison of *D. pulex* and *N. denticulata* genomes, compared to the non-redundant (nr) database. *D. pulex* image is courtesy of Paul Hebert [32].



While the genome size of *N. denticulata* has not been measured, a closely related species in the same family, Atyidae, *Antecaridina* sp., has been determined to have a  $C$ -value of 3.30 pg, or approximately 3.2 Gbp [31]. Such large genomes are known to be difficult to assemble and traditionally exhibit a large amount of repetitive sequences. Our efforts have recovered sequences totalling 1.2 Gbp. If the genome size of *N. denticulata* is close to 3 Gb, one possibility could be that the short fragment length used for library construction constrains the contiguity of our sequences across repetitive regions and, thus, also accounts for the relatively short N50 (Table 2). Assuming a

3 Gb genome, our sequence data provide approximately 12x coverage. A small amount of contamination with bacterial DNA (three large contigs greater than 30 kb in length, similar to the *Novosphingobium* sp. bacterial DNA sequence) without high similarity to the known *Wolbachia* sequences was removed manually after BLASTN detection. The availability of funding for additional long mate pair data for scaffolding in the future would greatly enhance contiguity and allow the exploration of the content of non-coding regions, which we suspect are poorly recovered in this assembly.

**Table 2.** Metrics relating to final assembly.

Criteria	Value (base pairs)
Min. contig length	200
Max. contig length	124,746
Mean contig length	383.84
Standard deviation of contig length	285.33
Median contig length	302
N50 contig length	400
Number of contigs	3,346,358
Number of contigs $\geq 1$ kb	97,432
Number of contigs in N50	987,201
Number of bases in all contigs	1,284,468,468
Number of bases in contigs $\geq 1$ kb	132,397,543
GC Content of contigs (%)	35.21

#### 2.4. Comparison of Core Eukaryotic Genes

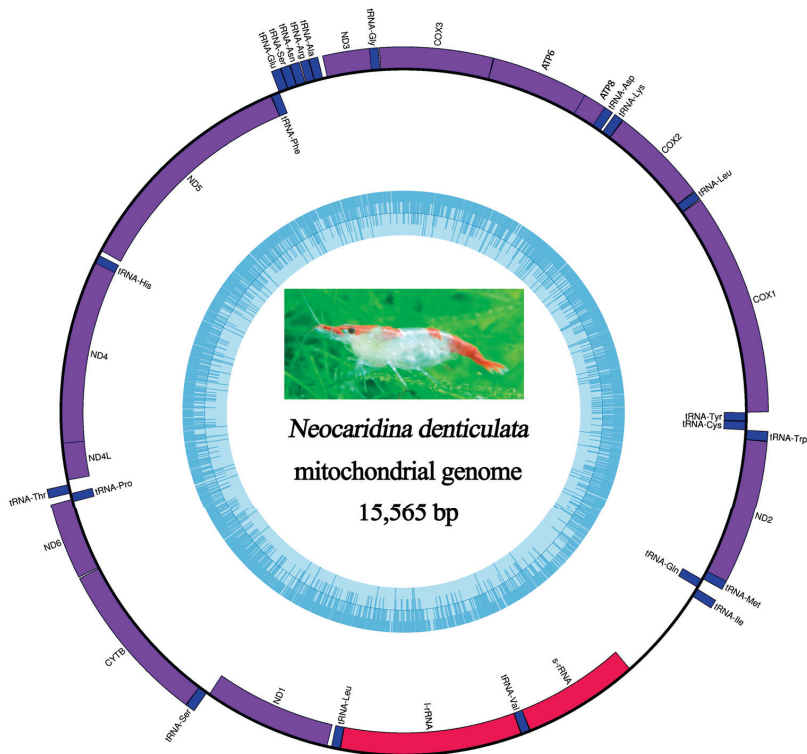
Despite the scaffold size being relatively short, our data contain a great deal of useful information concerning the coding regions of this genome. We used the Core Eukaryotic Gene Mapping Approach (CEGMA) dataset [33], which consists of 458 single-copy genes found in almost every eukaryote genome, as an assay of the completeness of the coding sequence coverage contained in our sequence data. Using TBLASTN [34] with a cut-off of  $10^{-3}$ , of the 458 genes, only three (ribosome biogenesis protein RLP24, ribosomal 60S subunit protein L24A and the HSP binding protein, YER156C) did not possess a recognizable hit in our sequence. This *E*-value cut-off was selected empirically after several trials and, at this stringency, represents 455 genes or 99.3% recovery of the expected coding sequences, which suggests that our dataset is excellent as a starting point for assaying the presence of genes in decapod crustaceans. Of these contigs annotated with CEGMA, the mean size of the contigs identified is 2500.01 bp and the median is 534 bp, which are longer than our N50 and mean/median contig sizes.

#### 2.5. Mitochondrial Genomic Characteristics

Retrieval of the *N. denticulata denticulata* (Crustacea: Caridea) mitochondrial genome from our dataset in a single, well-assembled contig revealed a circular molecule of 15,565 bp that encodes the typical set of 37 metazoan genes (13 protein-coding genes, 22 transfer RNA genes and two ribosomal RNA genes). The majority-strand ( $\alpha$ ) and minority-strand ( $\beta$ ) encode 23 and 14 genes, respectively

(Figure 4 and Supplementary Information: Table S1 in mtDNA). The result is comparable to the mitogenome of a related subspecies, *N. denticulata sinensis*, which differs by 4 bp in length and has slight differences in amino acid and codon usage [35]. Due to the compactness of the mitochondrial genome, ten instances of gene overlaps were found. A total of 841 bp non-coding nucleotides were found, with 153 bp in 13 intergenic regions and a 688 bp-long non-coding region between the *srRNA* and *trnIle* (Supplementary Information: Table S1 in mtDNA).

**Figure 4.** The *N. denticulata denticulata* mitochondrial genome. The orientation of genes is represented by the position on outside circle (transcription clockwise or anticlockwise is represented outside or inside the form, respectively). Local nucleotide identity (GC, dark blue) is represented on the inner ring as implemented by OrganellarGenomeDRAW (OGDRAW) [36].



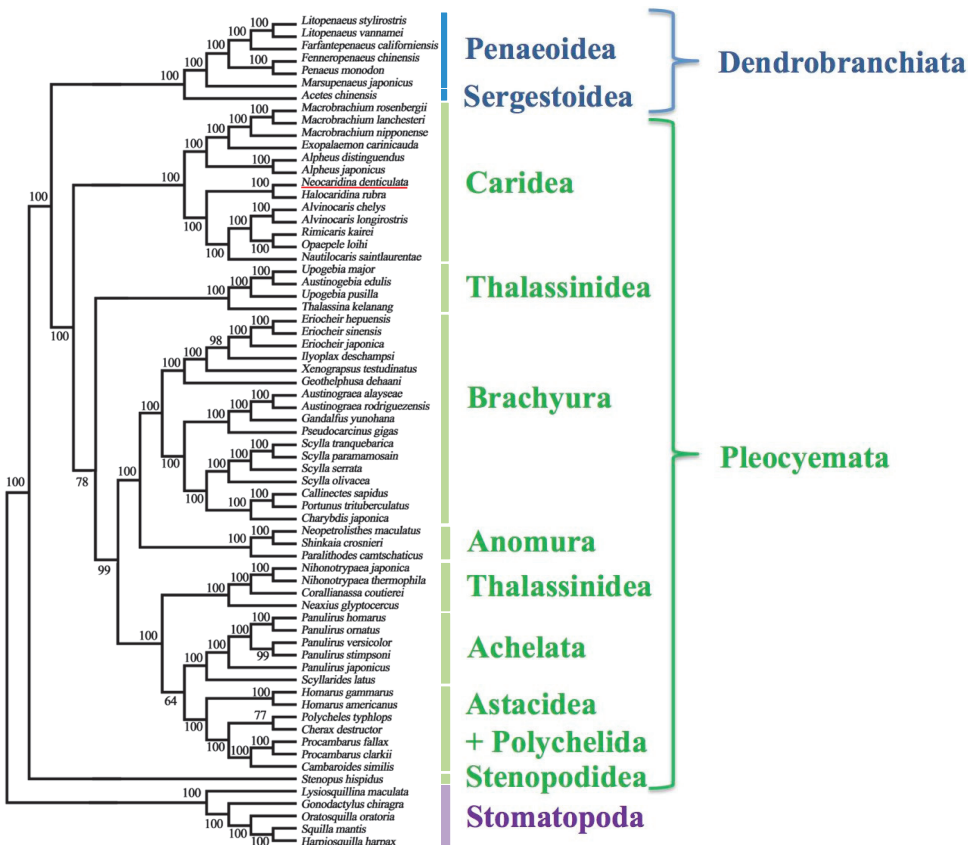
The typical metazoan initiation codon for transcription “ATN” is used by 12 out of 13 protein-coding genes, whereas *cox1* employs “AAG” as the start codon, which is similar to other caridean mitochondrial genomes (Supplementary Information: Table S2 in mtDNA). The open-reading frames of 11 protein-coding genes are terminated by the typical stop codon (TAA or TAG), while the remaining two genes (*cox2* and *nad4*) have an incomplete stop codon “T-”. All protein-coding genes and both rRNAs have skewed T vs. A (AT skew ranging from  $-0.041$  to  $-0.293$ ). The majority of protein-coding genes have a skew of C vs. G, but both rRNAs have a skew of G vs. C (the GC skews are 0.316 and 0.273 for *srRNA* and *lrRNA*, respectively)



(Supplementary Information: Table S3 in mtDNA). In total, there are 3696 codons in all 13 mitochondrial protein-coding genes, excluding incomplete termination codons, and the most frequently used amino acids are Leu (15.58%), followed by Ser (9.60%), Ile (8.39%), Phe (8.12%) and Val (7.06%) (Supplementary Information: Table S4 in mtDNA).

Using the nucleotide sequences of the mitogenome of *N. denticulata denticulata* presented here, a Bayesian phylogenetic reconstruction of malacostracan inter-relationships was performed and summarized in Figure 5, which reinforces our knowledge of the inter-relationships of the Caridea.

**Figure 5.** The Bayesian phylogenetic tree showing inter-relationships of a variety of malacostracan crustacean species, including the position of *N. denticulata* (underlined in red), based on concatenated nucleotide sequences from mitochondrial genomes. Numbers at nodes represent the posterior probability expressed out of 100.



Further in our analysis, the arrangement of the *N. denticulata* mitochondrial genes is found to be identical to the hypothetical pancrustacean ground pattern (Figure 6), whereas some other members of infraorder Caridea, such as *Exopalaemon carinicauda* (Palaemonidae), *Alpheus japonicus* and *A. distinguendus* (Alpheidae), all have their mitochondrial gene orders rearranged ([37]; Figure 6).

**Figure 6.** *N. denticulata* mitochondrial genome organisation compared to that of other crustaceans. *N. denticulata* possesses the stereotypical pancrustacean mitochondrial gene order as described first in *Limulus polyphemus* [38]; the orders of closely related species are provided for ease of comparison.

*Neocaridina denticulata* and *Halocaridina rubra* (Atyidae)

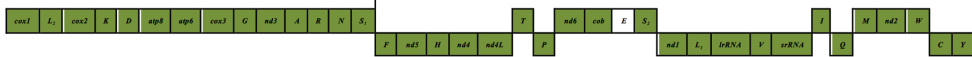
*Macrobrachium lanchesteri*, *M. nipponense* and *M. rosenbergii* (Palaemonidae)

*Rimicaris kairei*, *Nautilocaris saintlaurentae*, *Alvinocaris longirostris*, *A. chelys* and *Opaepele loihi* (Alvinocarididae)

Pancrustacean ground pattern



*Alpheus japonicus* and *A. distinguendus* (Alpheidae)



*Exopalaemon carinicauda* (Palaemonidae)



## 2.6. Recovery of Hox Genes and Other Families

To confirm the coverage of the coding regions of this genome, several well-annotated and catalogued developmental gene families were assayed. Our searches suggest that most, if not all, of the coding regions of the genome were recovered in our assembly. For example, Hox genes pattern the developing anteroposterior axis of animals, and 12 families of Hox genes are commonly described in pancrustaceans [39]. In our analysis, nine of the 12 Hox gene members could be identified (Figure 7). Of the three missing families, *zen2* and *bcd* have not been identified in any crustaceans outside the Insecta to date [39], so their absence in our dataset very probably indicates that these genes are insect novelties. Only one Hox gene absent from our dataset, *pb*, could be a consequence of the poor recovery of this genomic locus or the first loss of this gene reported in the Crustacea *sensu stricto*. The identification of Hox gene *zen1* in *N. denticulata* provides the first identification of this gene in the decapods (Figure 7). Unfortunately, these sequences are predominantly found on short contigs (see Supplementary Information: HoxL tab), and therefore, no syntenic relationship information can be gleaned from the data as it stands.

Similarly, our recovery of other families of well-catalogued genes is equally impressive (Table 3). The Fox genes, which are helix-turn-helix genes with an 80 to 100 amino acid “Forkhead Box” motif, are separated into 23 classes, which perform a variety of roles in metabolism and embryonic development [40,41]. We find 21 homologues of these genes in our dataset, from 16 families, with almost all those missing probably restricted to clades to which *N. denticulata* does not belong and, hence, was not expected to be found in the genome sequence data. The one exception to this is *Fox L1*, which appears to be absent from our dataset, while being described in other protostomes.

T-box genes are also well-catalogued and perform a similarly wide range of vital evolutionarily conserved roles [42]. Of these genes, we recovered 10 sequences corresponding to five families. The

families missing, *T-Brain*, *Tbx4/5* and *Tbx 15/18/22*, are genes limited to other Superphyla [42–44] within the Metazoa and, hence, are not expected to be found in *N. denticulata*.

Another gene repertoire examined to show the conservation of key pathways was the core microRNA/miRNA processing cassette [45]. Sequences (such as *Ago*, *Dicer*, *Exportin-5*) from the totality of the expected pathway were recovered. These findings further suggest that the coding sequences of the *N. denticulata* genome are well-recovered in our genomic build.

**Figure 7.** Hox cluster gene recovery in *N. denticulata*, compared to a number of other pancrustacean species (diagram after [39]). Sequences provided in Supplementary Information, HoxL tab.

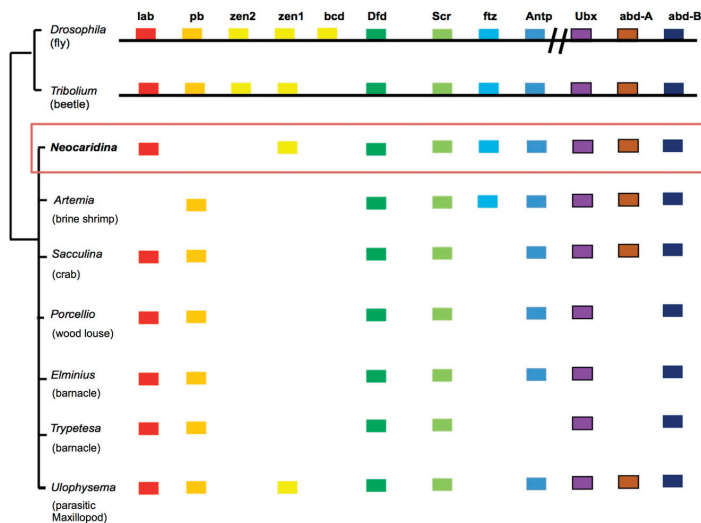


**Table 3.** Recovery of developmentally important gene families. Details and sequences provided in Supplementary Information. Missing genes are generally absent ancestrally, rather than in our assembly, as discussed in the main text.

Gene Classes	Homologues Recovered	Missing
Homeobox Genes (HoxL)	20	Pb
Fox Genes	21	Fox E, H, I, J2/3, L1, M, Q1
T-box Genes	10	T-Brain, Tbx 4/5, Tbx 15/18/22
miRNA processing genes	8	-

### 2.7. Comparison to the Lineage-Specifically Gained Genes of *Daphnia Pulex*

To gain an understanding of crustacean genome evolution, we compared the genome composition of *N. denticulata* with that of the branchiopod, *D. pulex*, the only publicly available crustacean genome sequence to date. The genome of *D. pulex* is noted for its large number of gene duplications and a rapid rate of genomic evolution, and a previous study has suggested 17,424 new and 1079 lost genes in the branch leading to *D. pulex* [7].

To determine whether the genes gained in *D. pulex* represent a Crustacea-wide gain or are truly limited to *D. pulex* alone, we used BLASTX to compare the *D. pulex* proteome to the *N. denticulata* genome (Figure 3b). As significant numbers of sequences have been added to the non redundant (nr) database since the publication of the *D. pulex* genome in 2011, the 30,907-sequence proteome of *D. pulex* was blasted against the nr database using Blast2GO (database as of October, 2013, BLASTP, cut-off  $e^{-6}$ , crustacean genes (excluding the Insecta) excluded from blast hits). At this threshold, 18,464 *D. pulex* genes were found to have no hits in nr.

The *D. pulex* proteome was then compared to our genomic build using BLASTX. As *E*-values cannot be directly compared between datasets, as they depend on the size of the database and the search used, and a number of *E*-values were trialled for the initial comparison of the *D. pulex* proteome and *N. denticulata* genome. By way of example, 16,640 *D. pulex* genes were found to have no hits in *N. denticulata* at an *E*-value of  $10^{-3}$ , whereas 18,739 *D. pulex* genes have no hits at an *E*-value of  $10^{-6}$ . As this latter figure represented a similar number to the unannotatable gene complement of *D. pulex*, this was taken as our cut-off for further comparison.

Of the 18,464 *D. pulex* genes with no hit in the nr database, 14,714 had no identifiable homologue in shrimp either. However, 3750 *D. pulex* genes, unidentifiable previously, were found to have hits in *N. denticulata* above the cut-off threshold of an *E*-value of  $10^{-6}$  (Figure 3b). These 3750 genes may represent novelties gained in the maxillopod, branchiopod and malacostracan lineages or pancrustacean genes lost in sequenced insects. These genes will be key targets for future work on crustacean novelties and are likely of interest to a range of researchers. The list of 3750 *D. pulex* genes, along with the lists of all other genes and appropriate sequences, are summarized in Supplementary Information, under the Details of Hits and Sequences tabs.

Additionally, 1927 of the 12,443 *D. pulex* genes identifiable in the nr database have no hit in the shrimp, which either represents genes not assembled in our dataset or losses on the malacostracan lineage leading to *N. denticulata*.

## 2.8. MS-222 Treatment

In addition to describing the culture and sequencing of the draft genome of *N. denticulata*, we have also established an anaesthesia technique using tricaine methanesulfonate (MS-222) for future genetic manipulation requiring microinjection of eggs or adults.

The average induction time for the adult shrimp in 1500, 2000, 2500 and 3000 mg L<sup>-1</sup> baths of MS-222 were 27 min 5 s (Standard error (SE) = 3 min 41 s), 12 min 42 s (SE = 1 min 15 s), 10 min 58 s (SE = 53 s) and 6 min 27 s (SE = 47 s), respectively (Figure 8). As only two out of ten individuals entered anaesthesia in 1000 mg L<sup>-1</sup> bath of MS-222 after 40 min, we concluded this concentration is too low to induce anaesthesia in *N. denticulata*, and no further analysis was performed at this or a lower concentration. Both the anaesthetic concentration and bath duration clearly affect the recovery time of *N. denticulata* (Figure 8a,b). At higher MS-222 concentrations, shrimp took a longer time for their first movement (Figure 8a; General Linear Model (GLM):  $F_{3,30} = 26.1, p < 0.001$ ) and complete recovery (Figure 8b; GLM:  $F_{3,24} = 21.4, p < 0.001$ ) was observed. Similarly, a longer bath duration also led to a longer time to their first movement (Figure 8a; GLM:  $F_{3,30} = 11.0, p < 0.001$ ) and complete recovery (Figure 8b; GLM:  $F_{3,24} = 16.8, p < 0.001$ ). The effect of bath duration was more

obvious in higher rather than in lower MS-222 concentrations (the interactive effect of concentration and duration on time until first movement:  $F_{3,30} = 3.2, p < 0.05$ ). At a concentration of  $3000 \text{ mg L}^{-1}$  MS-222, one/four individuals of five sampled were dead after 10 and 20 min of anaesthetic bath, respectively. Therefore, a  $3000 \text{ mg L}^{-1}$  concentration is too high for safe anaesthesia in *N. denticulata*. Following the treatment of animals with  $2000 \text{ mg L}^{-1}$  for 30 min, one individual of the three sampled died, suggesting that a long bath duration could be lethal to more susceptible individuals, even at a lower anaesthetic concentration. In our experiments, all other individuals treated with MS-222 at less than  $3000 \text{ mg L}^{-1}$  could recover completely, and none died in the following three days.

**Figure 8.** Boxplot of recovery time when (a) the first movement and (b) complete recovery was observed in *N. denticulata* individuals after anaesthesia in different MS-222 concentrations and bath durations. The horizontal line shows the median, boxes the first and third quartiles, whiskers the highest and lowest values that are within the 1.5 inter-quartile range, black dots the outliers and numbers above boxes the sample size. <sup>a</sup> A ten-minute bath duration is insufficient to induce anaesthesia at a concentration of  $1500 \text{ mg L}^{-1}$ . <sup>b</sup> A thirty-minute bath duration is lethal to some individuals at a concentration of  $2000 \text{ mg L}^{-1}$  and was not performed for higher concentrations. <sup>c</sup> The forty minute bath duration was not performed for concentrations higher than  $1500 \text{ mg L}^{-1}$ . <sup>d</sup> Some individuals that showed signs of movement were not fully recovered at the end of the assayed period.

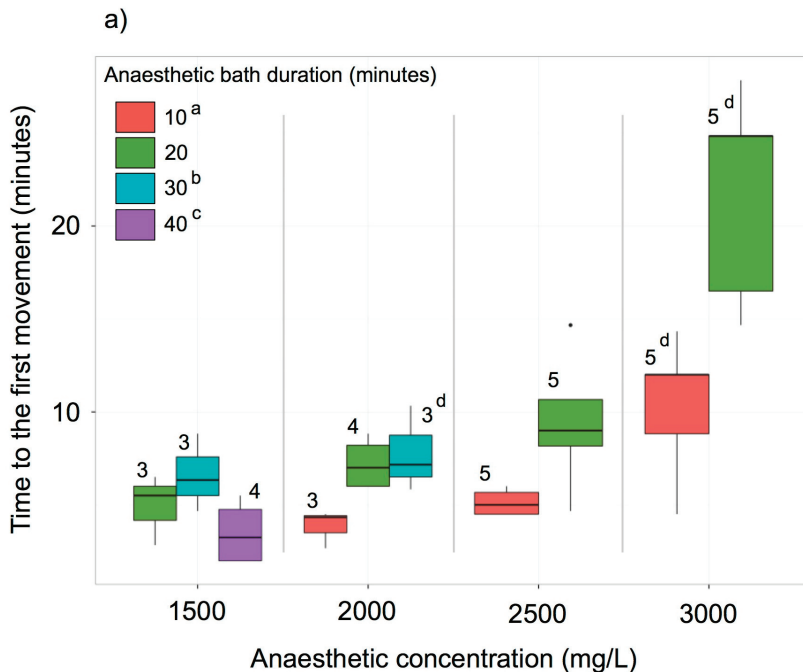
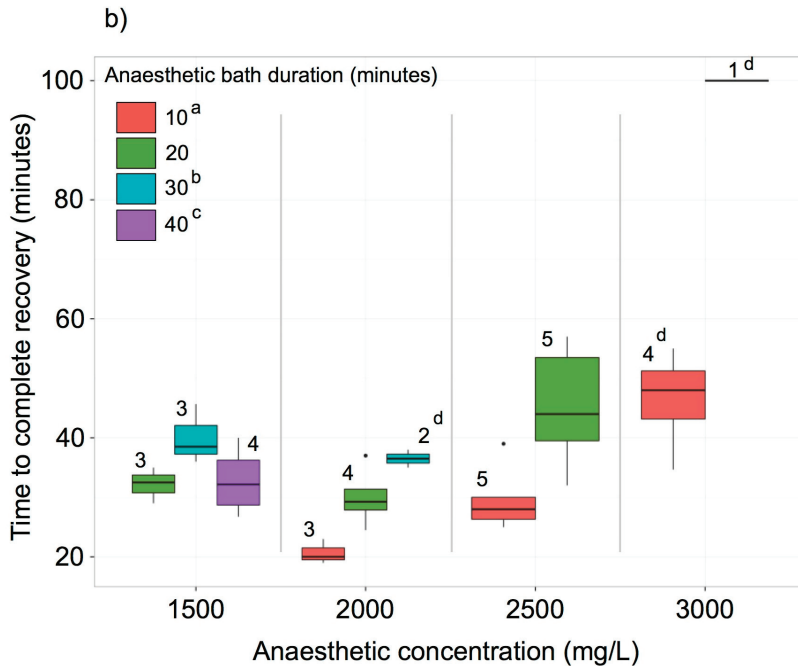


Figure 8. Cont.



To allow sufficient time for experimental manipulation, we have determined that bathing *N. denticulata* for 20 min in 2500 mg L<sup>-1</sup> MS-222 is optimal for longest non-lethal dose and duration. Under these conditions, the recovery time until first movement is 9 min 26 s (SE = 1 min 38 s). Compared to other aquatic animals, the MS-222 concentration we suggest is higher than those for fish anaesthesia in general, which vary from 50–400 mg L<sup>-1</sup> [46]. However, the effective MS-222 concentration for crustacean anaesthesia is generally found to be high, for example, 500 mg/L on the microcrustacean *Eucypris virens* [47], and could vary among different crustaceans with 100 mg L<sup>-1</sup> and 1000 mg L<sup>-1</sup> MS-222 being found ineffective on the shrimp, *Macrobrachium rosenbergii* [48], Chinese mitten crab, *Eriocheir sinensis* [49], and crayfish, *Orconectes virilis* [50].

### 3. Experimental Section

#### 3.1. Animal Husbandry and Genomic DNA Extraction

*N. denticulata denticulata* (red patched strain) were sourced from local suppliers and kept in a recirculating freshwater aquarium at room temperature, at approximately 25 °C. A single adult was starved for 2 days prior to gut dissection, and whole animal genomic DNA was extracted using DNeasy Blood & Tissue Kit (Qiagen, Hilden, Germany), according to the manufacturer's protocol.

### 3.2. Illumina Hi-Seq and Assembly

The *N. denticulata* genomic DNA sample was sequenced on a single lane on the Illumina HiSeq2000 platform. DNA was prepared for sequencing using a TruSeq DNA Sample Preparation Kit by BGI Hong Kong. Reads were first filtered by BGI according to their internal protocol, including the removal of the adaptor sequence, contamination and low-quality reads. Raw sequence data were uploaded to NCBI's SRA (Bioproject PRJNA224755, Biosample SAMN02384679, experiment SRX375172, reads SRR1027643). ABySS 1.3.3 [27] was used to assemble the genome at a *k*-mer length of 51 and all default settings. A minimum scaffold length of 200 bp was imposed after the assembly was complete.

### 3.3. mtDNA/Nuclear Gene Retrieval

Gene sequences were identified using TBLASTN [34] searches using known gene sequences of confirmed homology downloaded from the NCBI nr database as queries. Genes thus putatively identified were then reciprocally blasted against the NCBI nr database using BLASTX to further confirm their identity. Characteristic domains and trees constructed in MrBayes 3.1 [51] using genes of known homology downloaded from the nr database and aligned using MAFFT [52] were used to further confirm the homology for developmental gene families (data not shown).

### 3.4. Gene Comparison

For the comparison of *D. pulex* and *N. denticulata* sequences, the *D. pulex* proteome (FilteredModelsv1.1.aa) was downloaded from the Joint Genome Institute (JGI) website [53]. Standalone ncbi-blast-2.2.23+ [34] and Blast2GO [54] were used to perform blasts locally, as described in the text, with the latter used only for the comparison of the *D. pulex* dataset with the nr database.

### 3.5. mtDNA Annotation and Display

The locations of the 13 protein-coding genes (PCGs) and 2 rRNAs were determined with Dual Organellar GenoMe Annotator (DOGMA) [55] and subsequent alignments with caridean mitochondrial genes. All tRNA genes were identified by tRNAscan-SE 1.21 [56]. The gene map of the mitochondrial genome was drawn by OrganellarGenomeDRAW (OGDRAW) [36]. Codon usage in 13 PCGs of the mitochondrial genome was estimated with DnaSP 5.10.1 [57]. The nucleic acid sequences of 13 PCGs were aligned using Clustal W [58]. To determine the best fitting model of sequence evolution for the nucleic acid dataset, a nested likelihood ratio test was performed using jModelTest 2 [59]. After the evolutionary model (GTR + G + I) was determined, the phylogenetic relationship was inferred by MrBayes 3.1 [51]. The Markov Chain Monte Carlo analyses were run for 1,000,000 generations (sampling every 1000 generations) to allow adequate time for convergence. After omitting the first 250 sampled trees as “burn-in”, the remaining 750 sampled trees were used to estimate the Bayesian posterior probabilities.

### 3.6. MS222 Anaesthesia

Anaesthesia was performed by dissolving MS-222 salt (Sigma, St. Louis, MO, USA) in culture tank water. Sodium bicarbonate was added to neutralize the pH to the original culture tank water pH (*i.e.*, 7.2). Ten individual adult shrimp were tested for each of the five MS-222 concentrations (1000, 1500, 2000, 2500 and 3000 mg/L). Shrimp were kept in an aerated anaesthetic bath for durations as stated (10, 20, 30 or 40 min). The induction time (the time from immersion in the anaesthetic bath until the shrimp showed no movement and no reaction to touch stimuli) was recorded. After the anaesthetic bath, the shrimps were immediately put in aerated water from the original tank for recovery. The recovery time for each individual was also recorded, including: (a) the time until the first movement of pleopods and/or pereopods; and (b) the time until complete recovery at which the individual resumed balanced movements and normal feeding behaviour. A general linear model (GLM) was used to test the recovery time difference between different anaesthetic conditions, with the recovery time being used as the dependent variable and anaesthetic concentration and duration as independent factors.

## 4. Conclusions

To date, genomic sampling in Crustacea remains depauperate, but resources such as the one presented here will aid in the further study of this neglected taxon. As suggested by the recovery of the majority of core eukaryotic genes, the complete and un-rearranged mitogenome and considerable fractions of several developmental gene cassettes, the *N. denticulata* sequences presented here represent an excellent crustacean model for comparison to other arthropods. Our analysis also allows the identification of 3750 putatively crustacean-specific genes that could shed light on the understanding of the crustacean genome evolution. A non-lethal anaesthesia protocol has also been established for use in future genetic manipulation of this species. Given the lack of an easily-cultivable decapod laboratory model, we propose the shrimp, *N. denticulata*, as an experimentally tractable, easily grown species for a wide variety of future investigations in aquacultural, developmental, ecotoxicological, evolution, food safety, genetic, hormonal, physiological and reproductive research of decapod crustaceans.

## Conflicts of Interest

The authors declare no conflict of interest.

## Author Contributions

Jerome H.L. Hui conceived and supervised the project. Nathan J. Kenny assembled the next-generation sequencing reads, and identified genes. Nathan J. Kenny, Xin Shen, Sebastian M. Shimeld and Jerome H.L. Hui analysed and compared the genes. Yung Wa Sin, Qu Zhe, Jerome H.L. Hui maintained animal culture. Qu Zhe and Wei Wang prepared the genomic DNA for sequencing. Yung Wa Sin carried out the MS-222 anaesthesia. Nathan J. Kenny, Yung Wa Sin, Xin Shen, Qu



Zhe, Wei Wang, Ting Fung Chan, Stephen S. Tobe , Sebastian M. Shimeld , Ka Hou Chu and Jerome H.L. Hui wrote the manuscript. All authors read and approved the final manuscript.

### Acknowledgements

The authors would like to thank members of the CUHK Laboratory of Evolution and Development, whose discussions contributed to this manuscript, and BGI Hong Kong for the help with the sequencing. We thank two anonymous reviewers for their time in commenting on and improving this work. NJ Kenny's work on this manuscript was carried out under the Global Scholarship Programme for Research Excellence, CUHK. This study was supported by a direct grant (4053034) of the Chinese University of Hong Kong (JHL Hui).

### References

1. Stillman, J.H.; Colbourne, J.K.; Lee, C.E.; Patel, N.H.; Phillips, M.R.; Towle, D.W.; Eads, B.D.; Gelembuik, G.W.; Henry, R.P.; Johnson, E.A.; *et al.* Recent advances in crustacean genomics. *Integr. Comp. Biol.* **2008**, *48*, 852–868.
2. Kenny, N.J.; Quah, S.; Holland, P.W.H.; Tobe, S.S.; Hui, J.H.L. How are comparative genomics and the study of microRNAs changing our views on arthropod endocrinology and adaptations to the environment? *Gen. Comp. Endocrinol.* **2013**, *188*, 16–22.
3. Martin, J.W.; Davis, G.E. An updated classification of the recent Crustacea. *Sci. Ser.* **2001**, *39*, 1–124.
4. Zhang, Z.Q. Phylum Arthropoda von Siebold, 1848. *Zootaxa* **2011**, *3148*, 99–103.
5. Regier, J.C.; Shultz, J.W.; Zwick, A.; Hussey, A.; Ball, B.; Wetzer, R.; Martin, J.W.; Cunningham, C.W. Arthropod relationships revealed by phylogenomic analysis of nuclear protein-coding sequences. *Nature* **2010**, *463*, 1079–1083.
6. Rota-Stabelli, O.; Campbell, L.; Brinkmann, H.; Edgecombe, G.D.; Longhorn, S.J.; Peterson, K.J.; Pisani, D.; Philippe, H.; Telford, M.J. A congruent solution to arthropod phylogeny: Phylogenomics, microRNAs and morphology support monophyletic Mandibulata. *Proc. Biol. Sci.* **2011**, *278*, 298–306.
7. Colbourne, J.K.; Pfrender, M.E.; Gilbert, D.; Thomas, W.K.; Tucker, A.; Oakley, T.H.; Tokishita, S.; Aerts, A.; Arnold, G.J.; Basu, M.K.; *et al.* The ecoresponsive genome of *Daphnia pulex*. *Science* **2011**, *331*, 555–561.
8. Rehm, E.J.; Hannibal, R.L.; Chaw, R.C.; Vargas-Vila, M.A.; Patel, N.H. The crustacean *Parhyale hawaiiensis*: A new model for arthropod development. *Cold Spring Harb. Protoc.* **2009**, *1*, 373–404.
9. Sloof, W.; de Kruijf, H.; Hopkin, S.P.; Jones, D.T.; Dietrich, D. The isopod *Porcellio scaber* as a monitor of the bioavailability of metals in terrestrial ecosystems: Towards a global “woodlouse watch” scheme. *Sci. Total Environ.* **1993**, *134*, 357–365.
10. Hart, R.C. Population dynamics and production of the tropical freshwater shrimp *Caridina nilotica* (Decapoda: Atyidae) in the littoral of Lake Sibaya. *Freshw. Biol.* **1981**, *11*, 531–547.

11. De Silva, P.K.; de Silva, K.H.G.M. Aspects of the population ecology of a tropical freshwater atyid shrimp *Caridina fernandoi* Arud. & Costa, 1962 (Crustacea: Decapoda: Caridea). *Arch. Hydrobiol.* **1962**, *117*, 237–253.
12. De Grave, S.; Pentcheff, N.D.; Ahyong, S.T.; Chan, T.Y.; Crandall, K.A.; Dworschak, P.C.; Felder, D.L.; Feldmann, R.M.; Franssen, C.H.J.M.; Goulding, L.Y.D.; *et al.* A classification of living and fossil genera of decapod crustaceans. *Raffles Bull. Zool.* **2009**, *21*, 1–109.
13. Huang, D.; Chen, H. Effects of chlordane and lindane on testosterone and vitellogenin levels in green neon shrimp (*Neocaridina denticulata*). *Int. J. Toxicol.* **2004**, *23*, 91–95.
14. Huang, D.-J.; Chen, H.-C.; Wu, J.-P.; Wang, S.-Y. Reproduction obstacles for the female green neon shrimp (*Neocaridina denticulata*) after exposure to chlordane and lindane. *Chemosphere* **2006**, *64*, 11–16.
15. Mizue, K.; Iwamoto, Y. On the development and growth of *Neocaridina denticulata* de Haan. *Bull. Fac. Fish. Nagasaki Univ.* **1961**, *10*, 15–24.
16. Liang, X. Crustacea: Decapoda: Atyidae. In *Fauna Sinica: Invertebrata*; Science Press: Beijing, China, 2004; Volume 36.
17. Bracken, H.; de Grave, S.; Felder, D. Phylogeny of the infraorder Caridea based on mitochondrial and nuclear genes (Crustacea: Decapoda). *Decapod Crustac.* **2009**, *18*, 281–305.
18. Englund, R.; Cai, Y. Occurrence and description of *Neocaridina denticulata sinensis* (Kemp, 1918) (Crustacea: Decapoda: Atyidae), a new introduction to the Hawaiian Islands. *Bish. Museum Occas. Pap.* **1999**, *58*, 58–65.
19. Oh, C.-W.; Ma, C.-W.; Hartnoll, R.G.; Suh, H.-L. Reproduction and population dynamics of the temperate freshwater shrimp, *Neocaridina denticulata denticulata* (De Haan, 1844), in a Korean stream. *Crustaceana* **2003**, *76*, 993–1015.
20. Dudgeon, D. The population dynamics of some freshwater carideans (Crustacea: Decapoda) in Hong Kong, with special reference to *Neocaridina serrata* (Atyidae). *Hydrobiologia* **1985**, *120*, 141–149.
21. Marshall, S.; Warburton, K.; Paterson, B.; Mann, D. Cannibalism in juvenile blue-swimmer crabs *Portunus pelagicus* (Linnaeus, 1766): Effects of body size, moult stage and refuge availability. *Appl. Anim. Behav.* **2005**, *90*, 65–82.
22. Hung, M.; Chan, T.; Yu, H. Atyid shrimps (Decapoda: Caridea) of Taiwan, with descriptions of three new species. *J. Crustac. Biol.* **1993**, *13*, 481–503.
23. Shy, J.; Ho, P.; Yu, H. Complete larval development of *Neocaridina denticulata* (De Haan, 1884) (Crustacean, Decapoda, Caridea) reared in the laboratory. *Ann. Taiwan Mus.* **1992**, *35*, 75–89.
24. Langmead, B.; Trapnell, C.; Pop, M.; Salzberg, S.L. Ultrafast and memory-efficient alignment of short DNA sequences to the human genome. *Genome Biol.* **2009**, *10*, R25.
25. Zerbino, D.R.; Birney, E. Velvet: Algorithms for *de novo* short read assembly using de Bruijn graphs. *Genome Res.* **2008**, *18*, 821–829.
26. Luo, R.; Liu, B.; Xie, Y.; Li, Z.; Huang, W.; Yuan, J.; He, G.; Chen, Y.; Pan, Q.; Liu, Y.; *et al.* SOAPdenovo2: An empirically improved memory-efficient short-read *de novo* assembler. *Gigascience* **2012**, *1*, 18.

27. Simpson, J.T.; Wong, K.; Jackman, S.D.; Schein, J.E.; Jones, S.J.; Birol, I. ABySS: A parallel assembler for short read sequence data. *Genome Res.* **2009**, *19*, 1117–1123.
28. Sickel Github Repository. Available online: <https://github.com/najoshi/sickle> (accessed on 21 April 2013).
29. Liu, Y.; Schröder, J.; Schmidt, B. Musket: A multistage k-mer spectrum-based error corrector for Illumina sequence data. *Bioinformatics* **2013**, *29*, 308–315.
30. *Neocaridina denticulata* Genome Website. Available online: <http://tiny.cc/shrimpgenome/> (accessed on 18 July 2013).
31. Bachmann, K.; Rheinsmith, E.L. Nuclear DNA amounts in Pacific Crustacea. *Chromosoma* **1973**, *43*, 225–236.
32. Gewin, V. Functional genomics thickens the biological plot. *PLoS Biol.* **2005**, *3*, e219.
33. Parra, G.; Bradnam, K.; Korf, I. CEGMA: A pipeline to accurately annotate core genes in eukaryotic genomes. *Bioinformatics* **2007**, *23*, 1061–1067.
34. Altschul, S.F.; Gish, W.; Miller, W.; Myers, E.W.; Lipman, D.J. Basic local alignment search tool. *J. Mol. Biol.* **1990**, *215*, 403–410.
35. Yu, Y.-Q.; Yang, W.-J.; Yang, J.-S. The complete mitogenome of the Chinese swamp shrimp *Neocaridina denticulata sinensis* Kemp 1918 (Crustacea: Decapoda: Atyidae). *Mitochondrial DNA* **2013**, doi:10.3109/19401736.2013.796465.
36. Lohse, M.; Drechsel, O.; Bock, R. OrganellarGenomeDRAW (OGDRAW): A tool for the easy generation of high-quality custom graphical maps of plastid and mitochondrial genomes. *Curr. Genet.* **2007**, *52*, 267–274.
37. Shen, X.; Li, X.; Sha, Z.; Yan, B.; Xu, Q. Complete mitochondrial genome of the Japanese snapping shrimp *Alpheus japonicus* (Crustacea: Decapoda: Caridea): Gene rearrangement and phylogeny within Caridea. *Sci. China Life Sci.* **2012**, *55*, 591–598.
38. Lavrov, D.V.; Boore, J.L.; Brown, W.M. The complete mitochondrial DNA sequence of the horseshoe crab *Limulus polyphemus*. *Mol. Biol. Evol.* **2000**, *17*, 813–824.
39. Cook, C.E.; Smith, M.L.; Telford, M.J.; Bastianello, A.; Akam, M. Hox genes and the phylogeny of the arthropods. *Curr. Biol.* **2001**, *11*, 759–763.
40. Kaestner, K.H.; Knoechel, W.; Martinez, D.E. Unified nomenclature for the winged helix/forkhead transcription factors. *Genes Dev.* **2000**, *14*, 142–146.
41. Shimeld, S.M.; Degan, B.; Luke, G.N. Evolutionary genomics of the Fox genes: Origin of gene families and the ancestry of gene clusters. *Genomics* **2010**, *95*, 256–260.
42. Papaioannou, V.E.; Silver, L.M. The T-box gene family. *Bioessays* **1998**, *20*, 9–19.
43. Tagawa, K.; Humphreys, T.; Satoh, N. *T-brain* expression in the apical organ of hemichordate tornaria larvae suggests its evolutionary link to the vertebrate forebrain. *J. Exp. Zool.* **2000**, *288*, 23–31.
44. Kenny, N.J.; Shimeld, S.M. Additive multiple k-mer transcriptome of the keelworm *Pomatoceros lamarckii* (Annelida; Serpulidae) reveals annelid trochophore transcription factor cassette. *Dev. Genes Evol.* **2012**, *222*, 325–339.
45. Winter, J.; Jung, S.; Keller, S.; Gregory, R.I.; Diederichs, S. Many roads to maturity: microRNA biogenesis pathways and their regulation. *Nat. Cell Biol.* **2009**, *11*, 228–34.

46. Sneddon, L.U. Clinical anesthesia and analgesia in fish. *J. Exot. Pet. Med.* **2012**, *21*, 32–43.
47. Schmit, O.; Mezquita, F. Experimental test on the use of MS-222 for ostracod anaesthesia: concentration, immersion period and recovery time. *J. Limnol.* **2010**, *69*, 350–352.
48. Coyle, S.D.; Dasgupta, S.; Tidwell, J.H.; Beavers, T.; Bright, L.A.; Yasharian, D.K. Comparative efficacy of anesthetics for the freshwater prawn *Macrobrachium rosenbergii*. *J. World Aquac. Soc.* **2007**, *36*, 282–290.
49. Hajek, G.; Choczewski, M.; Dziaman, R.; Klyszejko, B. Evaluation of immobilizing methods for the Chinese mitten crab, *Eriocheir sinensis*. *Electron. J. Pol. Agric. Univ.* **2009**, *12*, 1.
50. Brown, P.; White, M. Evaluation of three anesthetic agents for crayfish (*Orconectes virilis*). *J. Shellfish Res.* **1996**, *15*, 433–436.
51. Ronquist, F.; Huelsenbeck, J.P. MrBayes 3: Bayesian phylogenetic inference under mixed models. *Bioinformatics* **2003**, *19*, 1572–1574.
52. Katoh, K.; Standley, D.M. MAFFT multiple sequence alignment software version 7: Improvements in performance and usability. *Mol. Biol. Evol.* **2013**, *30*, 772–780.
53. JGI *Daphnia pulex* Genome Resources. Available online: <http://genome.jgi-psf.org/Dappu1/Dappu1.home.html> (accessed on 25 September 2013).
54. Conesa, A.; Gotz, S.; Garcia-Gomez, J.M.; Terol, J.; Talon, M.; Robles, M. Blast2GO: A universal tool for annotation, visualization and analysis in functional genomics research. *Bioinformatics* **2005**, *21*, 3674–3676.
55. Wyman, S.K.; Jansen, R.K.; Boore, J.L. Automatic annotation of organellar genomes with DOGMA. *Bioinformatics* **2004**, *20*, 3252–3255.
56. Lowe, T.M.; Eddy, S.R. tRNAscan-SE: A program for improved detection of transfer RNA genes in genomic sequence. *Nucleic Acids Res.* **1997**, *25*, 955–964.
57. Librado, P.; Rozas, J. DnaSP v5: A software for comprehensive analysis of DNA polymorphism data. *Bioinformatics* **2009**, *25*, 1451–1452.
58. Thompson, J.D.; Higgins, D.G.; Gibson, T.J. Clustal-W: Improving the sensitivity of progressive multiple sequence alignment through sequence weighting, position-specific gap penalties and weight matrix choice. *Nucleic Acids Res.* **1994**, *22*, 4673–4680.
59. Darriba, D.; Taboada, G.L.; Doallo, R.; Posada, D. jModelTest 2: More models, new heuristics and parallel computing. *Nat. Methods* **2012**, *9*, 772.

# CS5931, a Novel Polypeptide in *Ciona savignyi*, Represses Angiogenesis via Inhibiting Vascular Endothelial Growth Factor (VEGF) and Matrix Metalloproteinases (MMPs)

Ge Liu, Ming Liu, Jianteng Wei, Haijuan Huang, Yuyan Zhang, Jin Zhao, Lin Xiao, Ning Wu, Lanhong Zheng and Xiukun Lin

**Abstract:** CS5931 is a novel polypeptide from *Ciona savignyi* with anticancer activities. Previous study in our laboratory has shown that CS5931 can induce cell death via mitochondrial apoptotic pathway. In the present study, we found that the polypeptide could inhibit angiogenesis both *in vitro* and *in vivo*. CS5931 inhibited the proliferation, migration and formation of capillary-like structures of HUVECs (Human Umbilical Vein Endothelial Cell) in a dose-dependent manner. Additionally, CS5931 repressed spontaneous angiogenesis of the zebrafish vessels. Further studies showed that CS5931 also blocked vascular endothelial growth factor (VEGF) production but without any effect on its mRNA expression. Moreover, CS5931 reduced the expression of matrix metalloproteinases (MMP-2 and MMP-9) both on protein and mRNA levels in HUVEC cells. We demonstrated that CS5931 possessed strong anti-angiogenic activity both *in vitro* and *in vivo*, possible via VEGF and MMPs. This study indicates that CS5931 has the potential to be developed as a novel therapeutic agent as an inhibitor of angiogenesis for the treatment of cancer.

Reprinted from *Mar. Drugs*. Cite as: Liu, G.; Liu, M.; Wei, J.; Huang, H.; Zhang, Y.; Zhao, J.; Xiao, L.; Wu, N.; Zheng, L.; Lin, X. CS5931, a Novel Polypeptide in *Ciona savignyi*, Represses Angiogenesis via Inhibiting Vascular Endothelial Growth Factor (VEGF) and Matrix Metalloproteinases (MMPs). *Mar. Drugs* **2014**, *12*, 153061544.

## 1. Introduction

Angiogenesis, the sprouting or intussusception of pre-existing blood vessels to form new vessels, involves many coordinated endothelial cell activities, including proliferation, migration, alignment, and cord formation [1,2]. It is well documented that angiogenesis is a prerequisite of solid tumor growth, since the tumor progression and metastasis depend on the existence of a functional blood supply system [3–6]. The angiogenesis process was regulated by many angiogenic factors; VEGF (vascular endothelial growth factor) is one of the major regulators of angiogenesis and can stimulate the growth of blood vessels directly; MMPs (matrix metalloproteinases), particularly MMP-2 and MMP-9, involved in extracellular matrix degradation [7], are crucial for the endothelial cell migration, organization and hence, angiogenesis [8,9]. Therefore, VEGF and MMPs are closely related to the angiogenesis, and targeting these factors has become a promising anticancer strategy [6,10]. In recent years, a number of anti-angiogenic agents have progressed to clinical studies [7,11]. However, most of the anti-angiogenic candidates do not target tumor cells specifically and can cause endothelial dysfunction and vessel pruning in healthy tissues, and what is more, can induce drug

resistance of cancer and stromal cells [12,13]. To overcome these defects, the continuous effort in searching for novel anti-angiogenic agents remains pressing.

The ocean is an important source of biologically active substances and numerous novel peptides with anticancer activity have been isolated from marine organisms [14–16]. Many of them have been reported to display anti-angiogenic activity. For example, Somocystinamide A (ScA), a lipopeptide derived from *L.majuscula*, could inhibit angiogenesis by inducing apoptosis in angiogenic endothelial cells [17]. Aplidine, a cyclic depsipeptide isolated from the Mediterranean tunicate *Aplidium albicans*, also displayed anti-angiogenic activity both *in vitro* and *in vivo* [5].

In our previous study, a novel polypeptide, CS5931, with potent antitumor activity, was purified from *Ciona savignyi*. We found that CS5931 polypeptide displayed significant cytotoxicity against several cancer cells and induced apoptosis in HCT-8 cells via mitochondrial-mediated pathway [18]. Sequence analysis reveals that there is high homology between CS5931 and human granulins A in their primary and 3D structure [19]. However, little is known about its mode of action. Our primary study shows that CS5931 also inhibits the proliferation of HUVEC cells, suggesting the possibility of its anti-angiogenic activity. In the present study, we evaluated the effects of recombinant CS5931 polypeptide on proliferation, migration and cord formation of HUVECs, and the effect of the polypeptide on the formation of new vessels in zebrafish embryos was also examined.

## 2. Results and Discussion

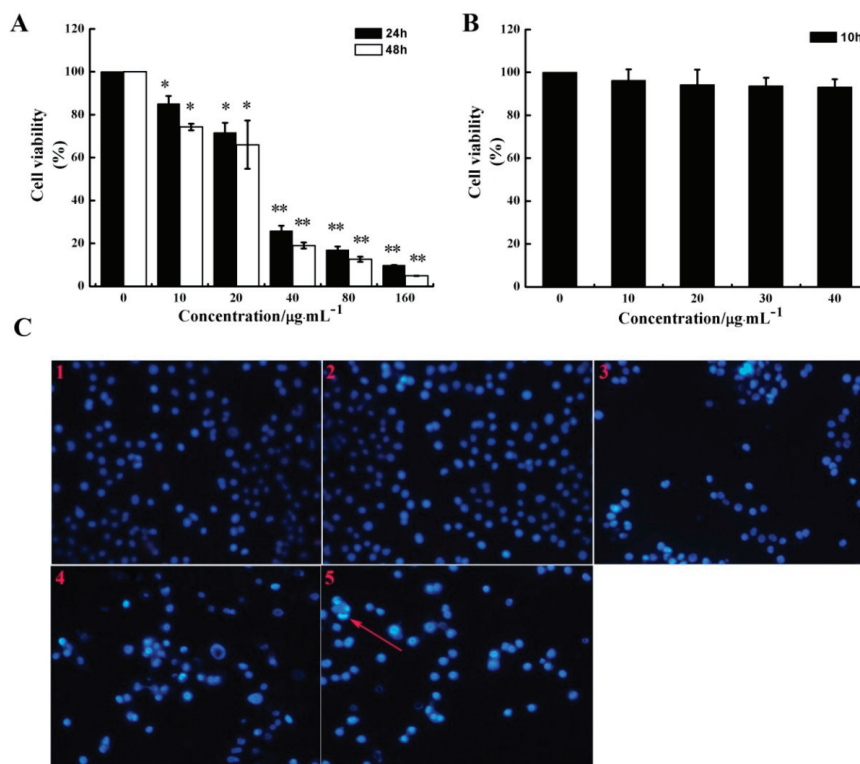
### 2.1. CS5931 Inhibits the Proliferation of HUVECs

MTT assay was performed to determine if CS5931 could inhibit the proliferation of HUVECs. As shown in Figure 1A, the polypeptide caused a significant growth-inhibiting effect on HUVECs compared with the untreated HUVECs; the proliferation rate decreased by 74.3, 83.1 and 90.2% after incubation for 24 h, while it decreased by 81.0, 87.4 and 95.1% after incubation for 48 h, when treating the cells with CS5931 at a concentration of 40, 80 and 160  $\mu\text{g}/\text{mL}$ , respectively.

A previous study has shown that CS5931 induced cell death via mitochondrial-mediated pathway in human colon cancer HCT116 cells. In order to determine if the polypeptide can induce apoptosis in HUVEC, PI/Hoechst 33258 staining assay was performed. Our results showed that treatment with higher concentration of CS5931 for 24 h could induce endothelial cell apoptosis to some extent (Figure 1C). These results revealed that the repression of HUVEC growth induced by CS5931 is in a dose and time dependent manner (Figure 1A,B) and the polypeptide could inhibit the proliferation of HUVEC cells via apoptosis pathway when treating the cells for more than 24 h.

It is reported that some cytotoxic antitumor drugs can affect endothelial cell functions and angiogenesis [20,21]. However, not all of them are true anti-angiogenic agents because they need a higher drug concentration to achieve inhibitory effect in endothelial cells than that in tumor cells [22,23]. CS5931 inhibits endothelial cell proliferation, with an  $\text{IC}_{50}$  similar to that observed for tumor cells [19], indicating that the anti-angiogenic effect might indeed occur in tumors and contribute to the final anticancer activity.

**Figure 1.** Effect of CS5931 on HUVEC proliferation. The cells were incubated in the absence or presence of certain concentrations of CS5931 at 37 °C for 24 h, 48 h (A) and 10 h (B) and cell viability was determined by MTT assay as described in the Materials and Methods section. (C) Cells were stained by PI/Hoechst 33258 after they were treated with 0 (1), 10 (2), 20 (3), 30 (4), 40  $\mu\text{g}/\text{mL}$  (5) CS5931 for 24 h and pictures were taken using a fluorescence microscopy. The apoptotic cell with bright blue fluorescence was indicated by an arrow. Results are normalized to untreated cells. All experiments were repeated more than three times. Values represent the means  $\pm$  SD of triplicate measurements. \*  $P < 0.05$ , \*\*  $P < 0.01$  versus medium control.

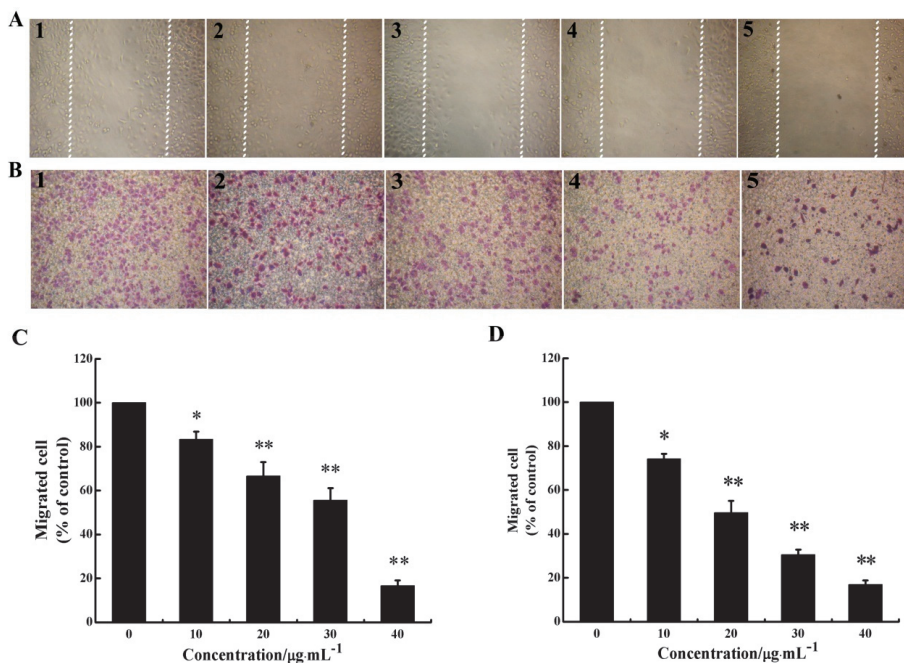


## 2.2. CS5931 Represses the Migration of HUVECs

As migration of endothelial cell is necessary for angiogenesis, we investigated the effect of CS5931 on directional cell motility using a scratch-wound assay and Transwell assay. The results of scratch-wound assay showed that the wound healing was gradually reduced as the concentration of the polypeptide increased in a dose-dependent relationship (Figure 2A,C). The results of Transwell assay revealed that treatment with CS5931 resulted in a concentration-dependent suppression of cell migration; the inhibition rate of the cells was 25.8, 50.3, 69.4 and 83.1%, when treating the cells with CS5931 at a concentration of 10, 20, 30 and 40  $\mu\text{g}/\text{mL}$ , respectively (Figure 2B,D). Both the findings indicated that CS5931 could prevent HUVECs migration significantly. Since the inhibition of cell migration by CS5931 occurred at exposure times at which cell proliferation was not obviously

affected (Figure 1B) and cell apoptosis did not happen, the results suggested that CS5931 might indeed exert its anti-angiogenic effect by affecting HUVEC migration.

**Figure 2.** CS5931 inhibits the migration of HUVECs. Cells were treated without (1) or with 10 (2), 20 (3), 30 (4) and 40  $\mu\text{g}/\text{mL}$  (5) of CS5931. After incubation for 8 h, cell migration was analyzed using scratch-wound assay (A) as well as Transwell assay (B). (C) Quantitative evaluations of HUVECs migration induced by CS5931 in the scratch-wound assay and Transwell assay (D). Results are normalized to untreated cells. All experiments were repeated more than three times. Values represent the means  $\pm$  SD of triplicate measurements. \*  $P < 0.05$ , \*\*  $P < 0.01$  versus medium control.

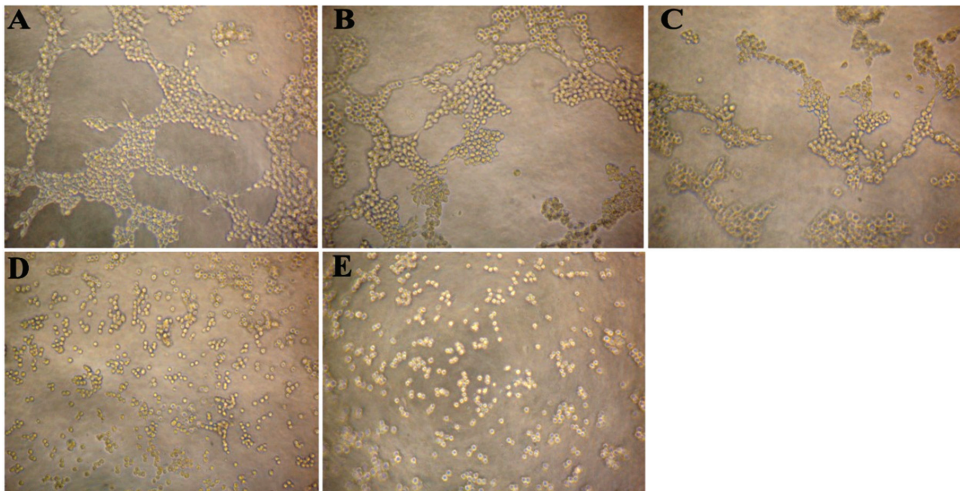


### 2.3. CS5931 Disrupts the Cord Formation of HUVECs

Since tube formation is an important process in angiogenesis, we then explored the effects of CS5931 on capillary-like tube structure formation ability. Three-dimensional layer of Matrigel experiment was performed and the results showed that the capillary-like tube formation was inhibited significantly when treating the cells with CS5931 (Figure 3B–E); higher concentration of CS5931 abrogated the cord formation completely (Figure 3E). In contrast, the capillary-like tube structure network could be clearly found in cells untreated with the polypeptide (Figure 3A). These findings demonstrated that CS5931 could suppress endothelial cell cord formation.



**Figure 3.** Effect of CS5931 on the formation of capillary-like structures of HUVECs. HUVECs were seeded on the surface of the Matrigel in a 96-well plate and treated without (A) or with 10 (B), 20 (C), 30 (D) and 40  $\mu\text{g}/\text{mL}$  (E) of CS5931. After incubation for 6 h, capillary tube formation was examined using an inverted microscope.



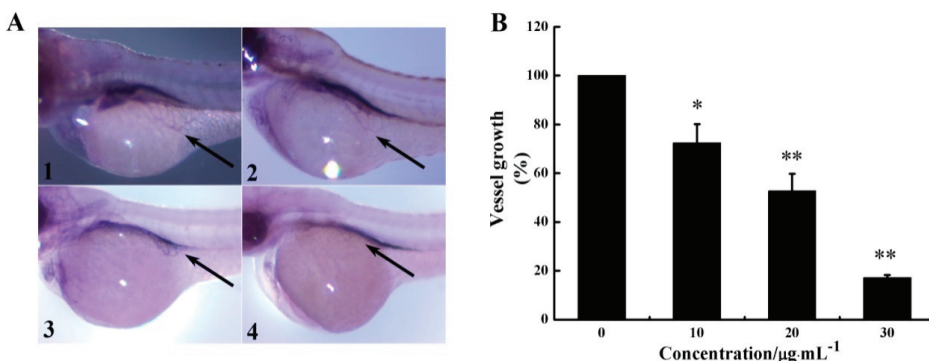
The antimotility activity of CS5931 was apparently sufficient to confer true anti-angiogenic activity. This was further supported by the finding that CS5931 prevented cord formation *in vitro*, an assay that mimics the final events during angiogenesis, when endothelial cells become aligned and organized in a capillary-like structure. Once again, the inhibitory effect occurred before endothelial cell proliferation was dramatically affected and apoptosis has not happened, suggesting that CS5931 might indeed prevent the process of angiogenesis.

#### 2.4. CS5931 Blocks Vessel Formation in Zebrafish Embryos *in Vivo*

Zebrafish has been used as an ideal model to evaluate the angiogenic activity of anticancer agents. In the present study, SIV (subintestinal vessel) formation of zebrafish embryos was measured to assess the anti-angiogenic activity of CS5931 *in vivo*.

As seen in Figure 4A, CS5931 prevented SIV formation in zebrafish embryos significantly; treatment with 10, 20, 30  $\mu\text{g}/\text{mL}$  CS5931 reduced SIVs growth by 27.6, 47.2 and 82.8%, respectively (Figure 4B). Our results confirmed that CS5931 significantly inhibited angiogenesis both *in vitro* and *in vivo*. Cisplatin, a cytotoxic antineoplastic drug, can inhibit endothelial cell proliferation *in vitro* but not affect angiogenesis *in vivo* [24–27], implying that drugs affecting endothelial cell proliferation are not necessarily anti-angiogenic. Our study revealed that the polypeptide also affected the growth of SIVs in zebrafish embryos. The results suggest that CS5931, unlike cisplatin, not only affects angiogenesis of HUVECs *in vitro*, but also impairs the development of angiogenesis *in vivo*.

**Figure 4.** CS5931 affects subintestinal vessel (SIV) formation in zebrafish embryos. (A) Lateral view of stained zebrafish embryos at 72 hpf. Embryos were treated without (1), or with 10 (2), 20 (3), and 30  $\mu\text{g}/\text{mL}$  (4) of CS5931. Vessels of zebrafish embryos were observed using a dissecting stereomicroscope. SIVs were indicated by an arrow. (B) Quantification of growth repression of SIVs induced by CS5931. Results are normalized to untreated embryos. All experiments were repeated more than three times. Values represent the means  $\pm$  SD of triplicate measurements. \*  $P < 0.05$ , \*\*  $P < 0.01$  versus medium control.

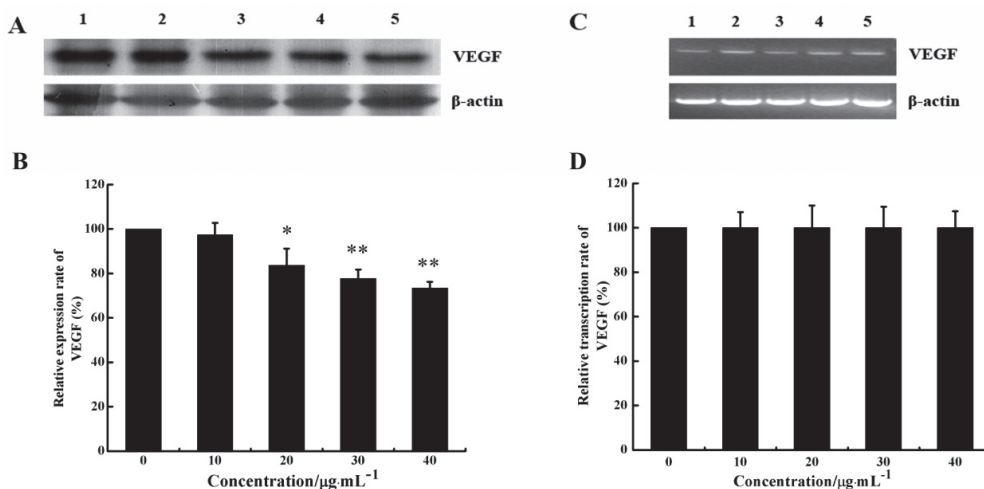


### 2.5. CS5931 Reduces VEGF Expression in HUVECs

Since VEGF is one of the foremost regulators of angiogenesis, we investigated whether CS5931 could decrease VEGF expression of HUVECs both at mRNA and protein levels using RT-PCR and Western Blotting. As shown in Figure 5A,B, the VEGF protein level decreased significantly in cells treated with CS5931. To further investigate if CS5931 affected the expression of VEGF mRNA, we also assessed the VEGF mRNA expression in HUVECs. The results showed that after treatment of the cells with CS5931 for 24 h, the mRNA expression of VEGF remained basically unchanged (Figure 5C,D). These results suggested that the effect of CS5931 on VEGF expression occurs at the translational level. However, the exact mechanism of action still remains unknown; whether the polypeptide affects the translational efficiency of VEGF mRNA or increases its degradation still needs to be addressed.

Several peptides from marine organisms have been identified with anti-angiogenic activity. Aplidine, a peptide isolated from the Mediterranean tunicate *Aplidium albicans*, displays potent anti-angiogenic activity [5] with an obvious inhibitory effect on VEGF production [28]. A polypeptide, PG155, isolated from Shark Cartilage in our laboratory possesses strong anti-angiogenic activity both *in vitro* and *in vivo* [29]; PG155 also suppresses the expression of VEGF in HUVECs. This study also reveals that CS5931 displays its anti-angiogenic activity via the repression of VEGF expression.

**Figure 5.** Effect of CS5931 on the expression of VEGF protein and mRNA. Cells were treated without (1) or with 10 (2), 20 (3), 30 (4) and 40  $\mu\text{g}/\text{mL}$  (5) of CS5931, respectively. After incubation for 24 h, the VEGF expression was analyzed by Western Blotting (A) and RT-PCR analysis (C). (B) and (D) represent the quantitative evaluation of the expression of VEGF. Results are normalized to untreated cells. All experiments were repeated more than three times. Values represent the means  $\pm$  SD of triplicate measurements. \*  $P < 0.05$ , \*\*  $P < 0.01$  versus medium control.

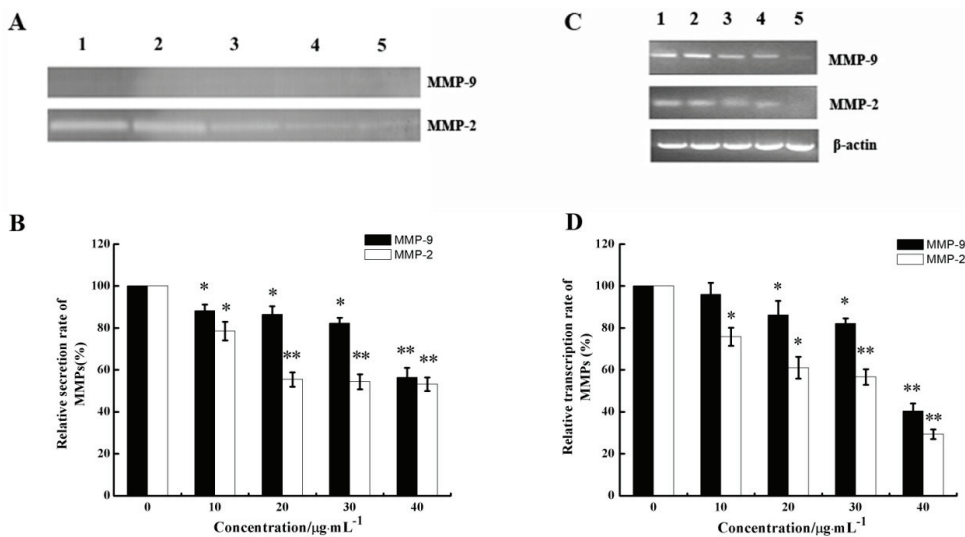


## 2.6. CS5931 Down-Regulates the Secretion and mRNA Expression of MMPs

Given that the process of cell invasion requires enzymatic digestion of the matrix, we investigated whether CS5931 affected the production of matrix-degrading metalloproteinases in endothelial cells. Gelatin zymography was carried out to investigate whether CS5931 affects the gelatinolytic activity of MMP-2 and MMP-9 secreted from endothelial cells. As shown in Figure 6A, CS5931 suppressed MMP-2 and MMP-9 secretion in a dose-response pattern. The quantitative analysis of the gelatinolytic activity indicated that, when cells were treated with 10, 20, 30, and 40  $\mu\text{g}/\text{mL}$  CS5931, MMP-2 activity was reduced by 21.6, 44.6, 45.6 and 46.8%, while MMP-9 activity was reduced by 11.9, 13.5, 17.8 and 43.6%, respectively (Figure 6B). These results indicated that CS5931 inhibited the secretion of MMP-2/9 in endothelial cells.

The mRNA levels of MMP-2/9 were further examined by semi-quantitative RT-PCR after HUVECs were treated with certain concentrations of CS5931 for 24 h. As shown in Figure 6C, CS5931 could inhibit the gene expression of MMP-2/9 in a concentration-dependent manner. The inhibition rate of MMP-2 and MMP-9 was about 70.7% and 59.7%, respectively, when treating the cells with CS5931 at a concentration of 40  $\mu\text{g}/\text{mL}$  for 24 h (Figure 6D). These results revealed that CS5931 not only inhibited the expression of MMP-2/9 mRNA, but also eliminated the secretion of MMP-2/9 and MMPs, which are also involved in the anti-angiogenic activity induced by CS5931.

**Figure 6.** Effect of CS5931 on the secretion of matrix metalloproteinases (MMPs) protein and mRNA expression. HUVECs were treated without (1) or with 10 (2), 20 (3), 30 (4) and 40  $\mu\text{g}/\text{mL}$  (5) of CS5931, respectively. After incubation for 24 h, the secretion of MMPs protein was analyzed by gelatin zymography (A) and MMPs mRNA expression was analyzed by RT-PCR (C). (B) and (D) represent the quantitative analysis of MMPs secretion and mRNA expression. Results are normalized to untreated cells. All experiments were repeated more than three times. Values represent the means  $\pm$  SD of triplicate measurements. \*  $P < 0.05$ , \*\*  $P < 0.01$  versus medium control.



### 3. Experimental Section

#### 3.1. Materials and Reagents

The recombinant CS5931 polypeptide was prepared in our laboratory according to the method described by Zhao *et al.* [19]. Transwell inserts with 8  $\mu\text{m}$  pores polycarbonate filters was purchased from Corning company (Corning Costar, Cambridge, MA, USA). Matrigel was provided by BD company (Becton Dickinson, Bedford, MA, USA). All other reagents used in the experiment were analytical grade.

#### 3.2. Cells and Cell Culture

HUVECs were purchased from American Type Culture Collection and cultured at 37  $^{\circ}\text{C}$  in a humidified atmosphere of 5%  $\text{CO}_2$  and 95% air in RPMI-1640 (GIBCO, Invitrogen, Grand Island, NY, USA) supplemented with 10% fetal bovine serum (FBS; GIBCO, Invitrogen, Grand Island, NY, USA). All experiments were carried out with the same batch of HUVECs.

### 3.3. HUVEC Proliferation Assay

The anti-proliferative effects of CS5931 on the growth of HUVECs were examined *in vitro* using MTT assay [30]. In brief, cells ( $3.5 \times 10^3$ /well) were plated in the 96-well plate in RPMI-1640 medium containing 10% FBS and cultured at 37 °C for 24 h. Then, CS5931 with certain concentrations were added to the medium. After incubation for 48 h, MTT solution (5 mg/mL, 20  $\mu$ L) was added into each well and incubated for another 4 h. Then, 150  $\mu$ L DMSO was added, and the plate was gently agitated until the color reaction was uniform and the OD490 was determined by a microplate reader with subtracted background absorbance. The inhibition ratio was calculated as follows:

$$\text{Inhibition ratio (\%)} = (\text{OD}_{\text{control group}} - \text{OD}_{\text{experimental value}}) / \text{OD}_{\text{control group}} \times 100\%$$

The IC<sub>50</sub> value was expressed as the concentration of drugs causing 50% inhibition.

### 3.4. PI/Hoechst 33258 Staining Assay

HUVECs were counted and plated in 24-well plates and cultured at 37 °C for 24 h. CS5931 with certain concentrations (0, 10, 20, 30 and 40  $\mu$ g/mL) were added to the medium. After incubation for another 24 h, cells were stained with propidium iodide (PI) and Hoechst 33258 and then examined by fluorescence microscopy.

### 3.5. Scratch-Wound Cell Migration Assay

HUVECs were counted and plated in 96-well plates. After growth to 90% confluence, “scratch” wounds were created by scraping cell monolayers with sterile disposable yellow tips [31–33]. After washing the scratched cell monolayers with PBS twice, RPMI-1640 medium supplemented with 2% FBS containing certain concentrations of CS5931 was added. After incubation for 10 h, 3 fields of each wound were selected and photographed with an inverted phase-contrast microscope. The number of HUVECs migrated from the edge of the injured monolayer was quantified by measuring the distance between the wound edges before and after injury. The migration rate at the start of the experiment was measured and arbitrarily defined as 100%. After incubation for 10 h, the width of the remaining wound was measured and the migration inhibition rate was calculated using the following formula:

$$\text{Inhibition rate (\%)} = [1 - (\text{average size in drug treated group} / \text{average size in control group})] \times 100\%$$

### 3.6. Transwell Migration Assay

Migration of HUVECs was determined in a Transwell Boyden chamber (Corning Costar, Cambridge, MA, USA) containing a polycarbonate filter with a pore size of 8  $\mu$ m as described previously [29]. In brief, cell suspension ( $5 \times 10^5$  cell/mL, 100  $\mu$ L) containing certain concentrations of CS5931 (0, 10, 20, 30 and 40  $\mu$ g/mL) was added to the upper compartment of each well. The lower compartment contained 0.6 mL of RPMI-1640 medium supplemented with 20% FBS. After incubation for 8 h at 37 °C, the filter was removed and fixed with 95% ethanol and stained with 0.1%

crystal violet. HUVECs remained on the upper side of the filter were removed with the cotton swabs. Cells on the lower surface of the filter (migrated) were counted manually with a digital camera in five random fields and the average number of total fields was calculated. The inhibition rate of migration was calculated as using the following formula:

$$\text{Inhibition rate} = [1 - (\text{migrated cells treated}/\text{migrated cells control})] \times 100\%$$

### 3.7. HUVEC Tube Formation Assay

The ability of HUVEC to form capillary-like structures on a 3D layer of basement membrane (Matrigel) was tested as described previously [26]. In brief, ice-cold Matrigel (BD, Bedford, MA, USA) diluted with serum-free RPMI-1640 medium was layered in a 96-well plate and incubated at 37 °C for 30 min to allow polymerisation. HUVECs ( $3 \times 10^4$  cell/well) were plated onto the Matrigel layer in the culture medium containing certain concentrations of CS5931 (10, 20, 30 and 40 µg/mL) for 6 h. Photographs from randomly chosen fields were taken using a digital camera when cords were formed.

### 3.8. Alkaline Phosphatase Staining for Visual Inspection in Zebrafish Embryos

Zebrafish embryos were generated by natural pairwise mating as described in the zebrafish handbook [34]. Embryos at 24 h post-fertilization (hpf) were manually dechorionated with 1 mg/mL trypsin for 10 min at room temperature immediately prior to drug treatment. Embryos treated with CS5931 were maintained in 24-well plates (20 embryos/well) for an additional 48 h.

Vessel staining was performed as described previously [29,35,36]. Briefly, at 72 hpf, embryos were fixed with 4% paraformaldehyde for 2 h at room temperature, then washed three times in PBS and dehydrated by immersing in 25, 50, 75 and 100% methanol in PBT buffer and rehydrated stepwise to 100% PBT. The embryos were then equilibrated in NTMT buffer (0.1 M Tris-HCl at pH 9.5, 50 mM MgCl<sub>2</sub>, 0.1 M NaCl, and 0.1% Tween-20) at room temperature for 45 min. The staining reaction was started by incubating embryos with NBT/BCIP solution for about 45 min and the reaction was stopped by adding PBST. Embryos were then immersed in a solution of 5% formamide and 10% hydrogen peroxide in PBS for 30 min to remove endogenous melanin in the pigment cells and allow full visualization of the stained vessels. Embryos were then examined on a dissecting stereomicroscope (Zeiss, Jena, Germany). Images were collected and stored using digital camera and total SIV vessel length was determined by point-to-point measurement using Image J software.

### 3.9. Western Blotting Analysis

To determine the effect of CS5931 on VEGF protein, Western Blotting was performed as previously described [37]. Briefly, HUVECs were placed in a 6-well plate for 24 h, and CS5931 with certain concentrations (0, 10, 20, 30 and 40 µg/mL) was added and incubated for another 24 h. Cells were collected by trypsin digestion method and then lysed in the ice-cold RIPA lysis buffer supplemented with a protease inhibitor cocktail. The protein concentration of the lysates was quantified using the BCA protein assay (Pierce, Thermo Scientific, Waltham, MA, USA). Cell

lysates (50 µg per lane) were resolved by 15% SDS-PAGE and transferred to nitrocellulose membranes. After incubation in blocking solution (7.5% non-fat milk) for 2 h, nitrocellulose membranes were incubated with 1:1000 dilution primary antibodies to human VEGF and  $\beta$ -actin proteins overnight at 4 °C. Membranes were incubated with 1:2000 dilution of HRP-conjugated second antibody for 1 h at room temperature and then the signal was detected with the enhanced chemiluminescence system and the relative intensity was analyzed using Image J software.

### 3.10. Production of Matrix Metalloproteinases (MMPs)

HUVEC cells were seeded in a 6-well plate for 24 h. CS5931 with certain concentrations were added. After incubation for another 24 h, the MMPs were analyzed using gelatin zymography assay as described previously [5,9,38]. Briefly, the presence of MMP-2/9 in the serum-free supernatants was analyzed by electrophoresis on an 8% non-denaturing SDS-PAGE containing 0.1% gelatin. After electrophoresis, the gel was washed with 2.5% Triton-X100 four times for 15 min to remove SDS and incubated in 50 mM Tris-HCl buffer, pH 7.6, containing 0.15 M NaCl, 10 mM CaCl<sub>2</sub>, and 0.02% (w/v) Brij-35 for 42 h at 37 °C. Gels were then stained with 0.5% Coomassie brilliant blue R250 in 25% methanol and 10% acetic acid, and destained in the same solution without Coomassie blue. Gelatinolytic activity was visualized by negative staining and the results were analyzed using gel documentation system and Image J software.

### 3.11. Semi-Quantitative Reverse Transcription and Polymerase Chain Reaction (RT-PCR)

Total cellular RNA was isolated from HUVEC cells and RT-PCR was performed using PrimeScript RT reagent kit with gDNA Eraser (TaKaRa Bio Group, Otsu, Japan), according to manufacturer's protocol. Briefly, cDNA was synthesized using total RNA (2 µg), Oligo dT Primer, and dNTP Mixture. The sequences of the primers used are shown in Table 1.

### 3.12. Statistical Analysis

Data was expressed as mean  $\pm$  standard deviation (SD). Statistics was analyzed using Student's *t*-test. *P* values less than 0.05 were considered statistically significant.

**Table 1.** Primers.

	Primers	Sequences	Base pairs
P1	$\beta$ -actin primer forward	5'-ACACTGTGCCCATCTAGGAGG -3'	21
P2	$\beta$ -actin primer reverse	5'-AGGGGCCGGACTCGTCATACT-3'	21
P3	VEGF primer forward	5'-TTGCTGCTCTACCTCCAC-3'	18
P4	VEGF primer reverse	5'-AATGCTTTCTCCGCTCTG-3'	18
P5	MMP-2 primer forward	5'-GGCCCTGTCACTCCTGAGAT-3'	20
P6	MMP-2 primer reverse	5'-GGCATCCAGGTTATCGGGGA-3'	20
P7	MMP-9 primer forward	5'-CGGAGCACGGAGACGGGTAT-3'	20
P8	MMP-9 primer reverse	5'-TGAAGGGGAAGACGCACAGC-3'	20

PCR reactions were carried out in 50  $\mu\text{L}$  of reaction mixture containing 25  $\mu\text{L}$  Premix Taq DNA polymerase buffer, 0.5  $\mu\text{L}$  of each primer (20  $\mu\text{M}$ ), and 2  $\mu\text{L}$  cDNA. PCR was performed under the following conditions: an initial denaturation step at 94  $^{\circ}\text{C}$  for 5 min, followed by 35 cycles at 94  $^{\circ}\text{C}$  for 30 s, 60  $^{\circ}\text{C}$  for 30 s, 72  $^{\circ}\text{C}$  for 1 min, and a final extension step at 72  $^{\circ}\text{C}$  for 10 min. PCR fragments were separated on a 2% agarose gel. After ethidium bromide staining, the gels were illuminated at UV transilluminator and photographed and the relative intensity was analyzed using Image J software.

#### 4. Conclusions

Taken together, our study confirmed that the marine polypeptide CS5931 inhibits angiogenesis both *in vitro* and *in vivo*. VEGF and MMPs play an important role in the anti-angiogenic activity of the polypeptide. Considering its low molecular weight as well as its high production in genetic preparation, CS5931 possesses the potential to be developed as a novel anticancer agent. Further study is in progress in our laboratory to address if the polypeptide can inhibit tumor growth in xenograft nude mice model.

#### Acknowledgments

This work was supported by National Innovative Drugs Development program of China (No. 2014ZX-091022043-0001) and 863 High Technology Project (No. 2014AA093503). This work was also supported by the National Natural Science Foundation of China (No. 81001396, No. 81273550 and No. 41306157) and International Cooperation project of China-Israel (2013DFG33000). The authors are grateful to all members of the laboratory for their continuous technical advice and helpful discussion.

#### Author Contributions

X.L. and M.L. contributed to the study concept and design, and the manuscript preparation. G.L. performed the experimental studies *in vitro* and *in vivo*, and analyzed the data. W.J., H.H., Y.Z. and J.Z. helped acquire data and statistical analysis. L.X., N.W. and L.Z. revised the article critically for intellectual content.

#### Conflicts of Interest

The authors declare no conflict of interest.

#### References

1. Wang, Z.; Zheng, L.; Yang, S.; Niu, R.; Chu, E.; Lin, X. *N*-acetylchitoooligosaccharide is a potent angiogenic inhibitor both *in vivo* and *in vitro*. *Biochem. Biophys. Res. Commun.* **2007**, *357*, 26–31.



2. Ellis, L.M.; Liu, W.; Ahmad, S.A.; Fan, F.; Jung, Y.D.; Shaheen, R.M.; Reinmuth, N. Overview of angiogenesis: biologic implications for antiangiogenic therapy. *Semin. Oncol.* **2001**, *28*, 94–104.
3. Carmeliet, P.; Jain, R.K. Angiogenesis in cancer and other diseases. *Nature* **2000**, *407*, 249–257.
4. Folkman, J. Angiogenesis in cancer, vascular, rheumatoid and other disease. *Nature Med.* **1995**, *1*, 27–30.
5. Taraboletti, G.; Poli, M.; Dossi, R.; Manenti, L.; Borsotti, P.; Faircloth, G.T.; Brogгинi, M.; D'Incalci, M.; Ribatti, D.; Giavazzi, R. Antiangiogenic activity of aplidine, a new agent of marine origin. *Br. J. Cancer* **2004**, *90*, 2418–2424.
6. Jubb, A.M.; Oates, A.J.; Holden, S.; Koeppen, H. Predicting benefit from anti-angiogenic agents in malignancy. *Nature Rev. Cancer* **2006**, *6*, 626–635.
7. Taraboletti, G.; Margosio, B. Antiangiogenic and antivascular therapy for cancer. *Curr. Opin. Pharmacol.* **2001**, *1*, 378–384.
8. Fidler, I.J.; Singh, R.K.; Yoneda, J.; Kumar, R.; Xu, L.; Dong, Z.; Bielenberg, D.R.; McCarty, M.; Ellis, L.M. Critical determinants of neoplastic angiogenesis. *Cancer J.* **2000**, *6*, S225–S236.
9. Li, A.; Varney, M.L.; Valasek, J.; Godfrey, M.; Dave, B.J.; Singh, R.K. Autocrine role of interleukin-8 in induction of endothelial cell proliferation, survival, migration and MMP-2 production and angiogenesis. *Angiogenesis* **2005**, *8*, 63–71.
10. Folkman, J. What is the evidence that tumors are angiogenesis dependent? *J. Natl. Cancer Inst.* **1990**, *82*, 4–7.
11. Brower, V. Tumor angiogenesis-new drugs on the block. *Nat. Biotechnol.* **1999**, *17*, 963–968.
12. Loges, S.; Schmidt, T.; Carmeliet, P. Mechanisms of resistance to anti-angiogenic therapy and development of third-generation anti-angiogenic drug candidates. *Genes Cancer* **2010**, *1*, 12–25.
13. Deplanque, G.; Harris, A. Anti-angiogenic agents: Clinical trial design and therapies in development. *Eur. Cancer* **2000**, *36*, 1713–1724.
14. Suarez-Jimenez, G.-M.; Burgos-Hernandez, A.; Ezquerro-Brauer, J.-M. Bioactive peptides and depsipeptides with anticancer potential: Sources from marine animals. *Mar. Drugs* **2012**, *10*, 963–986.
15. Jha, R.K.; Zi-rong, X. Biomedical compounds from marine organisms. *Mar. Drugs* **2004**, *2*, 123–146.
16. Zheng, L.; Lin, X.; Wu, N.; Liu, M.; Zheng, Y.; Sheng, J.; Ji, X.; Sun, M. Targeting cellular apoptotic pathway with peptides from marine organisms. *Biochim. Biophys. Acta* **2013**, *1836*, 42–48.
17. Wrasidlo, W.; Mielgo, A.; Torres, V.A.; Barbero, S.; Stoletov, K.; Suyama, T.L.; Klemke, R.L.; Gerwick, W.H.; Carson, D.A.; Stupack, D.G. The marine lipopeptide somocystinamide A triggers apoptosis via caspase 8. *Proc. Natl. Acad. Sci. USA* **2008**, *105*, 2313–2318.
18. Cheng, L.; Wang, C.; Liu, H.; Wang, F.; Zheng, L.; Zhao, J.; Chu, E.; Lin, X. A Novel Polypeptide Extracted From *Ciona savignyi* Induces Apoptosis Through a Mitochondrial-Mediated Pathway in Human Colorectal Carcinoma Cells. *Clin. Colorectal Cancer* **2012**, *11*, 207–214.

19. Zhao, J.; Wei, J.; Liu, M.; Xiao, L.; Wu, N.; Liu, G.; Huang, H.; Zhang, Y.; Zheng, L.; Lin, X. Cloning, characterization and expression of a cDNA encoding a granulatin-like polypeptide in *Ciona savignyi*. *Biochimie* **2013**, *95*, 1611–1619.
20. Hanahan, D.; Bergers, G.; Bergsland, E. Less is more, regularly: metronomic dosing of cytotoxic drugs can target tumor angiogenesis in mice. *J. Clin. Investig.* **2000**, *105*, 1045–1047.
21. Kerbel, R.; Folkman, J. Clinical translation of angiogenesis inhibitors. *Nature Rev. Cancer* **2002**, *2*, 727–739.
22. Schirner, M. Antiangiogenic chemotherapeutic agents. *Cancer Metastasis Rev.* **2000**, *19*, 67–73.
23. Miller, K.D.; Sweeney, C.J.; Sledge, G.W. Redefining the target: chemotherapeutics as antiangiogenics. *J. Clin. Oncol.* **2001**, *19*, 1195–1206.
24. Nicoletti, M.; Lucchini, V.; Massazza, G.; Abbott, B.; D’Incalci, M.; Giavazzi, R. Antitumor activity of taxol (NSC-125973) in human ovarian carcinomas growing in the peritoneal cavity of nude mice. *Ann. Oncol.* **1993**, *4*, 151–155.
25. Yamamoto, T.; Sudo, K.; Fujita, T. Significant inhibition of endothelial cell growth in tumor vasculature by an angiogenesis inhibitor, TNP-470 (AGM-1470). *Anticancer Res.* **1994**, *14*, 1–3.
26. Belotti, D.; Vergani, V.; Drudis, T.; Borsotti, P.; Pitelli, M.R.; Viale, G.; Giavazzi, R.; Taraboletti, G. The microtubule-affecting drug paclitaxel has antiangiogenic activity. *Clin. Cancer Res.* **1996**, *2*, 1843–1849.
27. Prestayko, A.; D’Aoust, J.; Issell, B.; Crooke, S. Cisplatin (*cis*-diamminedichloroplatinum II). *Cancer Treat. Rev.* **1979**, *6*, 17–39.
28. Brogini, M.; Marchini, S.; Galliera, E.; Borsotti, P.; Taraboletti, G.; Erba, E.; Sironi, M.; Jimeno, J.; Faircloth, G.; Giavazzi, R. Aplidine, a new anticancer agent of marine origin, inhibits vascular endothelial growth factor (VEGF) secretion and blocks VEGF-VEGFR-1 (flt-1) autocrine loop in human leukemia cells MOLT-4. *Leukemia* **2003**, *17*, 52–59.
29. Zheng, L.; Ling, P.; Wang, Z.; Niu, R.; Hu, C.; Zhang, T.; Lin, X. A novel polypeptide from shark cartilage with potent anti-angiogenic activity. *Cancer Biol. Ther.* **2007**, *6*, 775–780.
30. Taraboletti, G.; Micheletti, G.; Rieppi, M.; Poli, M.; Turatto, M.; Rossi, C.; Borsotti, P.; Roccabianca, P.; Scanziani, E.; Nicoletti, M.I. Antiangiogenic and antitumor activity of IDN 5390, a new taxane derivative. *Clin. Cancer Res.* **2002**, *8*, 1182–1188.
31. Mottet, D.; Bellahcène, A.; Pirotte, S.; Waltregny, D.; Deroanne, C.; Lamour, V.; Lidereau, R.; Castronovo, V. Histone deacetylase 7 silencing alters endothelial cell migration, a key step in angiogenesis. *Circ. Res.* **2007**, *101*, 1237–1246.
32. van Mil, A.; Grundmann, S.; Goumans, M.-J.; Lei, Z.; Oerlemans, M.I.; Jaksani, S.; Doevendans, P.A.; Sluijter, J.P. MicroRNA-214 inhibits angiogenesis by targeting Quaking and reducing angiogenic growth factor release. *Cardiovasc. Res.* **2012**, *93*, 655–665.
33. Dimmeler, S.; Dernbach, E.; Zeiher, A.M. Phosphorylation of the endothelial nitric oxide synthase at Ser-1177 is required for VEGF-induced endothelial cell migration. *FEBS Lett.* **2000**, *477*, 258–262.

34. Westerfield, M. *The Zebrafish Book: A Guide for the Laboratory Use of Zebrafish* (Brachydanio rerio); Institution of Neuro Science: Eugene, OR, USA, 1993; pp. 231–236.
35. He, Z.-H.; He, M.-F.; Ma, S.-C.; But, P.P.-H. Anti-angiogenic effects of rhubarb and its anthraquinone derivatives. *J. Ethnopharmacol.* **2009**, *121*, 313–317.
36. Serbedzija, G.N.; Flynn, E.; Willett, C.E. Zebrafish angiogenesis: A new model for drug screening. *Angiogenesis* **1999**, *3*, 353–359.
37. Wei, J.; Liu, M.; Liu, H.; Wang, H.; Wang, F.; Zhang, Y.; Han, L.; Lin, X. Oleanolic acid arrests cell cycle and induces apoptosis via ROS-mediated mitochondrial depolarization and lysosomal membrane permeabilization in human pancreatic cancer cells. *J. Appl. Toxicol.* **2013**, *33*, 756–765.
38. Wang, H.; Wei, J.; Wu, N.; Liu, M.; Wang, C.; Zhang, Y.; Wang, F.; Liu, H.; Lin, X. Mere15, a novel polypeptide from *Meretrix meretrix*, inhibits adhesion, migration and invasion of human lung cancer A549 cells via down-regulating MMPs. *Pharm. Biol.* **2013**, *51*, 145–151.

# Antifouling Activity of Synthetic Alkylpyridinium Polymers Using the Barnacle Model

Veronica Piazza, Ivanka Dragić, Kristina Sepčić, Marco Faimali, Francesca Garaventa, Tom Turk and Sabina Berne

**Abstract:** Polymeric alkylpyridinium salts (poly-APS) isolated from the Mediterranean marine sponge, *Haliclona (Rhizoniera) sarai*, effectively inhibit barnacle larva settlement and natural marine biofilm formation through a non-toxic and reversible mechanism. Potential use of poly-APS-like compounds as antifouling agents led to the chemical synthesis of monomeric and oligomeric 3-alkylpyridinium analogues. However, these are less efficient in settlement assays and have greater toxicity than the natural polymers. Recently, a new chemical synthesis method enabled the production of poly-APS analogues with antibacterial, antifungal and anti-acetylcholinesterase activities. The present study examines the antifouling properties and toxicity of six of these synthetic poly-APS using the barnacle (*Amphibalanus amphitrite*) as a model (cyprids and II stage nauplii larvae) in settlement, acute and sub-acute toxicity assays. Two compounds, APS8 and APS12-3, show antifouling effects very similar to natural poly-APS, with an anti-settlement effective concentration that inhibits 50% of the cyprid population settlement (EC<sub>50</sub>) after 24 h of 0.32 mg/L and 0.89 mg/L, respectively. The toxicity of APS8 is negligible, while APS12-3 is three-fold more toxic (24-h LC<sub>50</sub>: nauplii, 11.60 mg/L; cyprids, 61.13 mg/L) than natural poly-APS. This toxicity of APS12-3 towards nauplii is, however, 60-fold and 1200-fold lower than that of the common co-biocides, Zn- and Cu-pyrithione, respectively. Additionally, exposure to APS12-3 for 24 and 48 h inhibits the naupliar swimming ability with respective IC<sub>50</sub> of 4.83 and 1.86 mg/L.

Reprinted from *Mar. Drugs*. Cite as: Piazza, V.; Dragić, I.; Sepčić, K.; Faimali, M.; Garaventa, F.; Turk, T.; Berne, S. Antifouling Activity of Synthetic Alkylpyridinium Polymers Using the Barnacle Model. *Mar. Drugs* **2014**, *12*, 195961976.

## 1. Introduction

Marine biofouling is a dynamic natural process that occurs on ocean-submerged surfaces and leads to the undesired accumulation of organic polymers and of microbial, plant and animal communities and their by-products [1]. Although there is a wide diversity of fouling organisms and a variety of contributing environmental factors, a general sequence of fouling events is frequently observed [2]. The initial conditioning of the submerged surfaces by the adsorption of organic macromolecules is followed by the attachment of marine bacteria, which form a complex multi-species biofilm [3,4]. The complexity of “microfoulers” is further increased when fungi, diatoms and protozoa colonize this microbial slime layer [5]. Within hours to days, “soft macrofouling” is observed, as algal spores and various invertebrate larvae begin to attach and develop [6,7]. Shelled invertebrates, like barnacles, mussels and tubeworms, represent the “hard macrofouling” phase, which results in the formation of a mature fouling community [8].

The settlement and accumulation of marine organisms is a severe problem on engineered structures that are submerged in the sea, and it incurs substantial economic costs in the shipping [9,10], desalination [11] and offshore oil and gas [12] industries and in marine aquaculture [13]. Traditionally, the most effective strategy for controlling biofouling has been achieved using paints and antifouling coatings that contain toxic constituents (e.g., Cu, Zn) or biocides (e.g., tributyltin, bis(tributyltin) oxide) [14,15]. However, the accumulation of these compounds in harbors and ports led to massive pollution problems [14] and had detrimental effects on non-target marine organisms [16]. Consequently, the use of organotin-based antifouling coatings was prohibited by the Antifouling System Convention of the International Maritime Organization (effective from 17 September 2008).

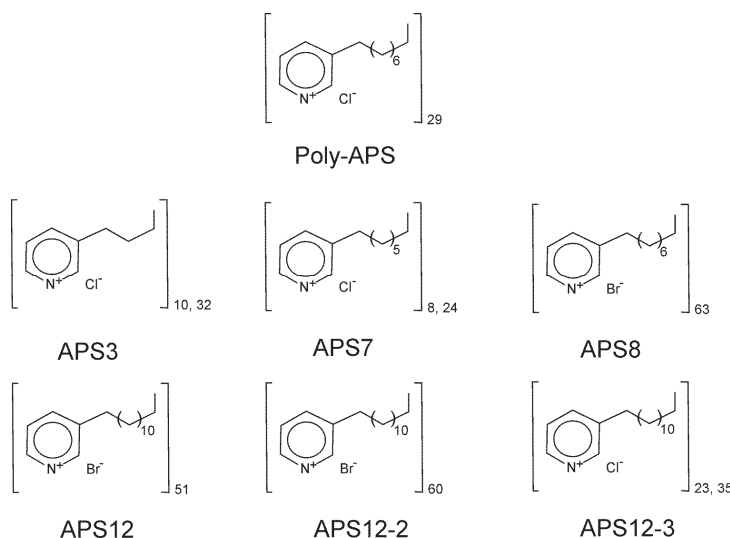
Modern antifouling approaches are investigating behavioral, chemical and physical defense mechanisms that have evolved in living organisms, to translate these into novel antifouling applications [17]. The creation of self-polishing and foul-release coatings has been inspired by the skin of marine mammals and fish, which respond to environmental stimuli, like temperature and pH [1]. Bio-inspired physical antifouling strategies have exploited the physical properties for fouling prevention, such as the surface energy and microtopography [1,15,18–20]. Antifoulants based on natural products have been proposed as one of the best ecologically relevant antifouling solutions [21,22], due to their lower toxicity, reversible effects at lower effective concentrations and biodegradability, compared with conventional biocides [23]. Natural antifouling compounds are produced as secondary metabolites by a wide range of organisms, and they include terpenoids, steroids, carotenoids, phenolics, furanones, alkaloids, peptides and lactones [24–26].

To date, over 80 different bioactive 3-alkylpyridinium and 3-alkylpyridine compounds have been identified in marine sponges of the order Haplosclerida [27,28]. One of the most studied of these compounds are water-soluble polymeric 3-alkylpyridinium salts (poly-APS), secondary metabolites produced by the Mediterranean marine sponge, *Haliclona (Rhizoniera) sarai* [29]. Poly-APS (5.52 kDa; [30]) have been chemically defined as polymers that are composed of 29 monomeric *N*-butyl-3-butyl pyridinium units, with 3-octyl chains linked to the nitrogen of the adjacent unit in a head-to-tail organization (see Figure 1). In aqueous solutions, poly-APS behave as cationic detergents at concentrations >0.23 g/L and form large supramolecular structures of a 23 nm mean hydrodynamic radius [31]. At concentrations >1 g/L, poly-APS have toxic and lethal effects in rodents upon intravenous administration [23].

Among the numerous biological activities of poly-APS that were detailed by [27], their antifouling activity is of particular interest for the current study. In a static laboratory bioassay [2] using the most common hard macrofouler species, the barnacle, *Amphibalanus amphitrite*, poly-APS effectively deterred the settlement of cyprids (effective concentration that inhibits 50% of the cyprid population settlement ( $EC_{50}$ ), 0.27 mg/L), with low toxicity towards nauplii (lethal concentration that kills 50% of the cyprid population ( $LC_{50}$ ), 30.01 mg/L) and the non-target organisms, the alga, *Tetraselmis suecica*, and the mussel, *Mytilus galloprovincialis* [32]. Additionally, in a laboratory anti-microfouling activity assay and in the range of 0.1 mg/L to 1.0 mg/L, poly-APS prevented the formation of the natural marine biofilm, through inhibition of the growth of certain marine bacteria [33]. The molecular mechanisms behind poly-APS antifouling activity presumably involve

neurotransmission blockade/modulation [34] through acetylcholinesterase inhibition, combined with their surfactant-like properties that decrease the surface tension [28].

**Figure 1.** Chemical structures of natural polymeric 3-alkylpyridinium salts (poly-APS) and the synthetic poly-APS investigated. Molecular weights: natural poly-APS, 5.52 kDa; APS3, 1.46 kDa; APS7, 2.33 kDa; APS8, 11.9 kDa; APS12, 12.5 kDa; APS12-2, 14.7 kDa; APS12-3, 6.08 kDa.



Despite extensive studies of such natural antifoulants over the past 20 years, their incorporation into antifouling paints has been hampered by their limited supply [24]. Sufficient amounts of target poly-APS for broad biological screening and of poly-APS analogues for structure-activity relationship studies can be supplied through synthetic organic chemistry [35]. Using such an approach, dimers and tetramers of linear 3-alkylpyridinium salts have been produced that have high antibacterial and moderate anti-acetylcholinesterase activities [36]. In the barnacle anti-settlement assay, these oligomeric compounds did not reach the antifouling potential of natural poly-APS and were considerably more toxic [37]. In contrast, screening for novel antimicrobial agents has revealed that some of these APS analogues have considerable antibacterial activity towards biofilm-forming marine bacteria and has indicated that their charged pyridinium moiety and bromine atom, and the length of their alkyl chain, are decisive factors in this bioactivity [38]. Recently, new microwave-assisted polymerization has allowed the production of high-molecular-weight analogues of poly-APS [39,40]. Certain poly-APS analogues have been seen to behave similarly to natural poly-APS when their antifungal, antibacterial, anti-acetylcholinesterase, antitumoral and membrane-damaging activities have been assessed [39–41].

In the present study, we investigated the antifouling activity of six synthetic poly-APS analogues using *A. amphitrite* cyprids as the macrofouling model in a static laboratory settlement assay. In parallel, we examined the toxicity towards *A. amphitrite* cyprids after 24 h, 48 h and 72 h of exposure to these synthetic poly-APS and calculated their therapeutic ratios. We monitored the acute and

sub-acute toxicity towards II stage *A. amphitrite* nauplii after 24 h and 48 h exposure to these poly-APS analogues. Finally, the behavior of II stage nauplii was studied for one of the most promising analogues, APS12-3, using swimming speed alteration assay as a measure of sub-lethal toxicity.

## 2. Results and Discussion

Marine biofouling is a complex and dynamic natural process that is very difficult to reproduce under laboratory conditions. As direct evaluation of antifouling coatings *in situ* is expensive and time-consuming, several bioassays have been developed to estimate the antifouling potential of novel natural products [2]. Due to the large diversity of organisms implicated in the marine biofouling process, it has been recommended that as many target species are used as possible, taken from both the microfouling and macrofouling communities [25]. Generally, bacteria, diatoms and fungi isolated from marine biofilms are studied in microfouling bioassays, while sessile hard-foulers (e.g., barnacles, tube worms, mussels) and soft-foulers (e.g., the bryozoan, *Bugula neritina*, the polychaete, *Hydroides elegans*) or seaweed (e.g., *Ulva*) are frequently used as representative macrofouling organisms. In our previous studies [32,33,42], we demonstrated that natural poly-APS can effectively inhibit the settlement and/or growth of different target fouling organisms. Using synthetic monomeric and oligomeric analogues of natural poly-APS, we also demonstrated their considerable antimicrobial activity [38]. However, in the anti-settlement assay against *A. amphitrite* cyprids, we identified only one synthetic poly-APS analogue (1,8-di(3-pyridyl)octane) that showed similar efficacy to natural poly-APS, although with a noticeably different toxic mechanism of action [37].

In the present study, we focused on the antifouling activities of synthetic poly-APS using *A. amphitrite* as the primary invertebrate model for biofouling [43]. The structures of the synthetic poly-APS evaluated in this study are illustrated in Figure 1.

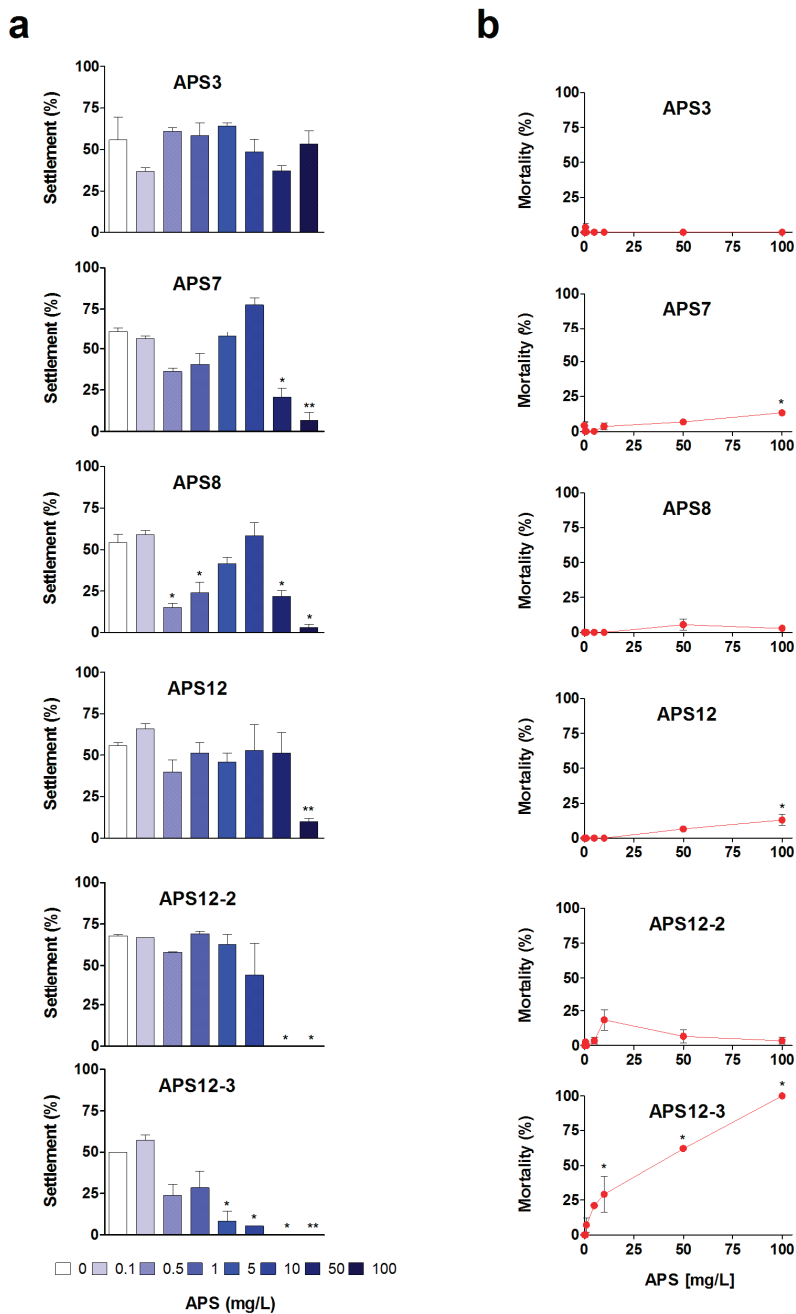
### 2.1. Anti-Settlement Assay

We investigated the settlement of laboratory-reared cyprids of *A. amphitrite* after 24 h, 48 h and 72 h of exposure to these synthetic poly-APS in 24-well plates (see the Experimental section). The results of the 72 h anti-settlement assays are shown in Figure 2a.

APS8 was the most effective of the synthetic poly-APS for the inhibition of the settlement of cyprids ( $p < 0.01$ ; Figure 2a). With an  $EC_{50}$  of 0.32 mg/L after 24 h (Table 1), APS8 matches the anti-settlement activity of natural poly-APS ( $EC_{50}$ , 0.27 mg/L). Moreover, when these are expressed as molar concentrations, APS8 is almost two-fold more effective than natural poly-APS (Table 1). The biphasic dose response seen for APS8 (Figure 2a) is characterized by a significant inhibition of settlement at 0.5 and 1 mg/L, followed by the loss of anti-settlement activity at concentrations from 5 to 10 mg/L and then by the return of inhibition at 50 and 100 mg/L, thus suggesting the phenomenon of hormesis [44]. The underlying mechanism of such adaptive responses might be mediated via specific receptor and/or cell-signaling pathways [45,46]. For natural poly-APS, one of the possible molecular mechanisms of this anti-settlement activity is interference with the cyprid cholinergic system [28]. A recent novel hypothesis proposed that the cellular quality control systems that are

involved in the recognition, repair and prevention of cell stress represent the underlying molecular mechanisms that account for the benefits of hormesis [47].

**Figure 2.** Anti-settlement activity (a) and toxicity (b) of synthetic poly-APS on *A. amphitrite* cyprids after 72-h exposure to the different poly-APS concentrations (as indicated). Data are expressed as the means  $\pm$  standard error. \*  $p < 0.05$ ; \*\*  $p < 0.001$ .





We observed a hormetic-like response also for APS7, even though this is not supported by *a posteriori* comparison of the means and less clearly for APS12. However, for both analogues, 50% inhibition of the cyprid settlement occurred at concentrations that are an order of magnitude higher than APS8 (Table 1). For all of these tested synthetic poly-APS, the settlement inhibition decreased with the time of exposure. This effect is particularly evident for polymer APS3, which shows no significant effect on the cyprid settlement ( $p = 0.45$ ;  $F = 1.08$ ) and is thus less interesting for further antifouling research.

**Table 1.** Antifouling activities of natural poly-APS, Zn and Cu pyrithiones, and the synthetic poly-APS, assessed as the settlement ( $EC_{50}$ ) and mortality ( $LC_{50}$ ) of *A. amphitrite* cyprids.

Compound	Treatment (h)	$EC_{50}$ (mg/L)	$LC_{50}$ (mg/L)	$EC_{50}$ ( $\mu$ M)	$LC_{50}$ ( $\mu$ M)
Poly-APS <sup>1</sup>	24	0.27 (0.15–0.47)		0.049	
Zn pyrithione <sup>1</sup>	24	0.02		0.063	
Cu pyrithione <sup>1</sup>	24	<0.01		<0.032	
APS3	24	5.72 (4.24–7.72)	>100	3.9	
	48	>100	>100		
	72	>100	>100		
APS7	24	10.50 (8.47–13.01)	>100	4.5	
	48	25.86 (23.29–28.71)	>100	11.1	
	72	29.38 (26.17–32.99)	>100	12.6	
APS8 <sup>2</sup>	24	0.32 (0.26–0.39)	>100	0.026	
	48	0.50 (0.36–0.70)	>100	0.042	
	72	2.33 (1.78–3.04)	>100	0.195	
APS12	24	<i>nc</i>	>100		
	48	<i>nc</i>	>100		
	72	49.82 (37.18–66.76)	>100	4.0	
APS12-2	24	8.78 (8.37–9.20)	>100	0.597	
	48	9.38 (8.76–10.05)	>100	0.638	
	72	11.13 (10.38–11.94)	>100	0.757	
APS12-3 <sup>2</sup>	24	0.89 (0.48–1.65)	61.13 (51.65–72.36)	0.146	10.0
	48	4.03 (3.49–4.65)	24.24 (20.09–29.24)	0.661	4.0
	72	4.76 (4.44–5.11)	17.97 (14.88–21.70)	0.781	2.9

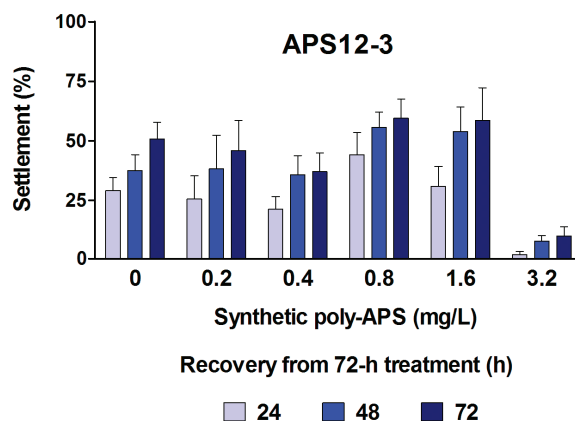
Data are expressed as  $EC_{50}$  or  $LC_{50}$  (95% confidence interval);  $EC_{50}$ , effective concentration that inhibits 50% of the cyprid population settlement;  $LC_{50}$ , lethal concentration that kills 50% of the cyprid population; *nc*, not calculable;

<sup>1</sup> data measured after a 24 h-treatment with poly-APS or commercial co-biocide [32]; <sup>2</sup>  $EC_{50}$  calculated from an additional experiment (see the Experimental Section).

The synthetic polymers, APS12-2 and APS12-3, inhibit the settlement of cyprids in a concentration-dependent manner, with the respective  $EC_{50}$  of 8.78 and 0.89 mg/L at 24 h (Table 1). As reported by Zovko *et al.* [40], APS12-3 has the highest antibacterial and antifungal activity among all of these synthetic poly-APS. By comparing the data for the inhibition of cyprid settlement with those for the toxicity of APS12-3 (Figure 2b), for the longer incubation times of 48 h and 72 h, it can be concluded that the inhibitory effects probably occur due to the toxic action of APS12-3.

Interestingly, however, the potent inhibition of cyprid settlement by APS12-3 is reversible at concentrations up to 1.6 mg/L (Figure 3). The other synthetic poly-APS tested here did not show any significant toxic effects against these barnacle cyprids at concentrations of up to 100 mg/L (Figure 2b).

**Figure 3.** Recovery of *A. amphitrite* cyprid settlement in fresh filtered natural seawater after 72-h treatment with different concentrations of APS12-3 monitored for three consecutive days. Data are the means  $\pm$  standard error.



## 2.2. Naupliar Mortality, Immobility and Swimming Speed Alteration Assays

*Amphibalanus amphitrite* nauplii normally swim continuously, and their inability to move is evidence of toxicity [48]. On this basis, we measured the acute (mortality) and sub-acute (immobility) toxicity end-points of II stage nauplii exposed to the different solutions of the synthetic poly-APS for 24 h and 48 h. These immobility and naupliar mortality results are shown in Figure 4.

In ecotoxicological studies, the behavioral changes are more sensitive, short-term indicators of chemical toxicity than the assessment of lethal effects. Therefore, we investigated the sub-lethal toxicity of one of the synthetic analogues with the highest anti-settlement activity, APS12-3, using a swimming speed alteration test (Figure 5). Due to a lack of compound, the same evaluation has not been performed also for APS8. The synthetic poly-APS APS12-3 inhibited the mobility of nauplii in a concentration-dependent manner. The  $EC_{50}$  for immobility was 9.43 mg/L (after 24 h), and the ability of the nauplii to swim was completely lost at 50 mg/L APS12-3, and above. Thus, APS12-3 is moderately toxic to these nauplii, and indeed, the mortality ( $LC_{50}$  of 11.60 mg/L after 24 h) is three-fold greater compared to that for natural poly-APS (24-h  $LC_{50}$  of 30.01 mg/L; Table 2). The greater toxicity of APS12-3 towards this model organism, compared to natural poly-APS, is evidenced also by their 24-h swimming speed inhibition  $IC_{50}$  of 4.83 and >10 mg/L, respectively.

Increasing concentrations of APS12-2 also progressively inhibited the naupliar mobility and resulted in increased mortality. Prolonging the time of exposure to APS12-2 increased this immobility of nauplii ( $EC_{50}$ , 36.92 mg/L at 24 h; 2.28 mg/L at 48 h). The toxicity of APS12-2 towards these nauplii is comparable to that of APS12-3.

**Table 2.** Lethal (mortality) and sub-lethal (immobility) toxicity of natural poly-APS, Zn and Cu pyrithiones and the synthetic poly-APS, as assessed with *A. amphitrite* II stage nauplii.

Compound	Treatment (h)	EC <sub>50</sub> (mg/L)	LC <sub>50</sub> (mg/L)	EC <sub>50</sub> (μM)	LC <sub>50</sub> (μM)
Poly-APS <sup>1</sup>	24	>10	30.01 (21.71–41.49)	>1.81	5.43
Zn pyrithione <sup>1</sup>	24	0.23 (0.16–0.33)	0.19 (0.13–0.30)	0.725	0.6
Cu pyrithione <sup>1</sup>	24	0.03 (0.03–0.04)	<0.01	0.095	<0.032
APS3	24	>100	>100		
	48	>100	>100		
APS7	24	>100	>100		
	48	30.64 (25.43–36.9)	94.02 (81.73–108.17)	13.1	40.3
APS8	24	>100	>100		
	48	>100	79.37 (68.29–92.25)		6.7
APS12	24	>100	>100		
	48	>100	>100		
APS12-2	24	36.92 (29.33–46.46)	>100	2.5	
	48	2.28 (1.95–2.67)	4.80 (4.21–5.46)	0.15	0.32
APS12-3	24	9.43 (8.10–10.97)	11.60 (10.06–13.38)	1.5	1.9
	48	3.61 (3.14–4.16)	5.44 (4.64–6.37)	0.59	0.89

Data are expressed as EC<sub>50</sub> or LC<sub>50</sub> (95% confidence interval); EC<sub>50</sub>, effective concentration that inhibits mobility of 50% naupliar population; LC<sub>50</sub>, lethal concentration that kills 50% of the naupliar population; <sup>1</sup> data measured after a 24 h-treatment with poly-APS or commercial co-biocide [32].

At concentrations above 10 mg/L, APS7 and APS8 inhibited the naupliar mobility. This effect was more prominent after 48-h exposure at the higher doses of 50 mg/L and 100 mg/L APS7 and APS8. Both APS7 and APS8 showed a low toxicity towards these nauplii, with 48-h LC<sub>50</sub> values of 94.02 mg/L and 79.37 mg/L, respectively.

The naupliar immobility was only minor upon exposure to APS3 and APS12.

A therapeutic ratio (TR; lethal concentration for 50% mortality (LC<sub>50</sub>) divided by the effective concentration for 50% inhibition of settlement (EC<sub>50</sub>)) is commonly used to evaluate compounds' potential [2,26]. Generally, compounds with a TR > 50 and EC<sub>50</sub> < 5 mg/L are considered to be promising non-toxic antifouling candidates [25]. We calculated TR values both for naupliar (TR<sub>N</sub>) and cyprids (TR<sub>C</sub>) toxicity (Table 3). TR<sub>C</sub> denotes an antifouling mechanism (toxic or non-toxic), whereas TR<sub>N</sub> indicates an environmental impact of a compound, since it is calculated by using LC<sub>50</sub> towards non-target organisms (e.g., nauplii as representatives of the plankton) [49].

After a 24-h treatment of cyprids with synthetic analogue APS12-3, this analogue has a very promising antifouling activity (EC<sub>50</sub> = 0.89 mg/L), and it seems to act through a non-toxic mechanism with a TR<sub>C</sub> of 68.68. However, it is potentially hazardous for the environment (TR<sub>N</sub> = 13.3). After 72 h, the antifouling activity of APS12-3 is less significant, and the compound displays a high toxicity towards target and non-target organisms (TR<sub>C</sub> = 3.77 and TR<sub>N</sub> = 1.35, respectively).

Another synthetic analogue, APS8, shows an anti-settlement activity (EC<sub>50</sub>, 0.32 mg/L) similar to natural poly-APS (EC<sub>50</sub>, 0.27 mg/L). Its TR<sub>N</sub> is higher than that of the natural compound (158.74

and 111.15, respectively) suggesting an even lower environmental risk. Based on this, we propose its use as one of the pharmacophores in the prospective studies of non-toxic antifouling compounds.

**Figure 4.** Immobility (white bars) and mortality (blue bars) of the synthetic poly-APS for *A. amphitrite* II stage nauplii after 24 h and 48 h exposure. Data are the means  $\pm$  standard error. \*  $p < 0.05$ ; \*\*  $p < 0.001$ .

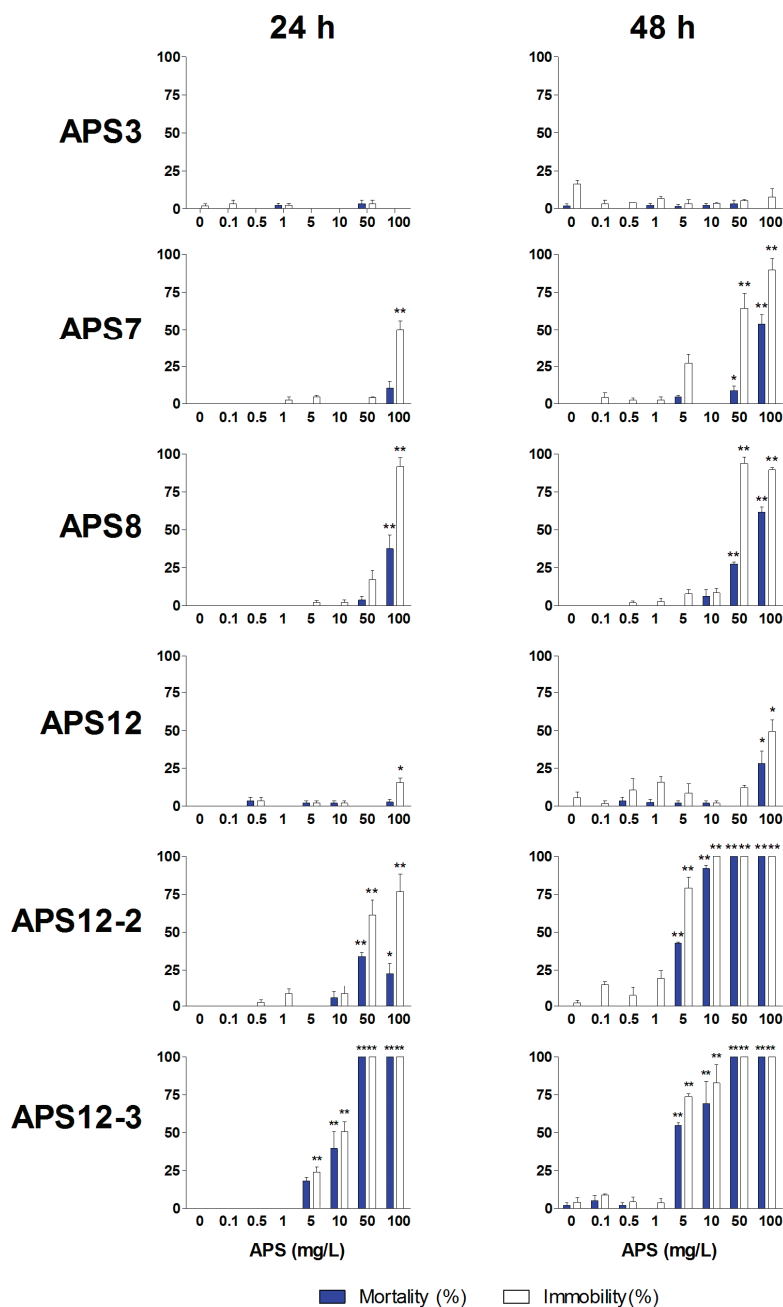
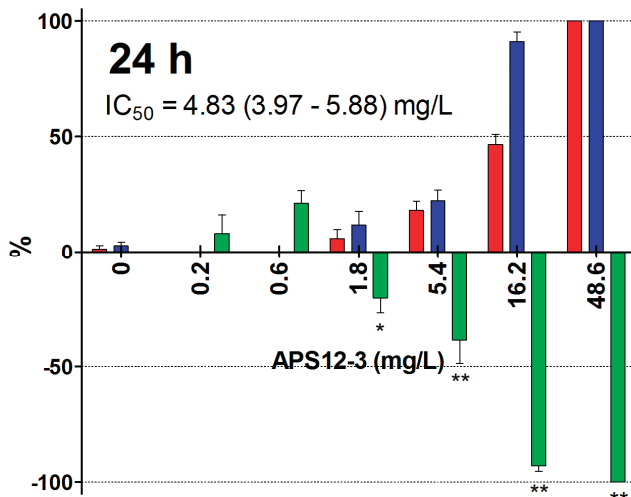


**Figure 5.** Swimming speed alteration (green bars), immobility (blue bars) and mortality (red bars) of the APS12-3 for *A. amphitrite* II stage nauplii after 24-h (a) and 48-h (b) incubations. Data are the means  $\pm$  standard error. \*  $p < 0.05$ ; \*\*  $p < 0.001$ .

**a**



**b**

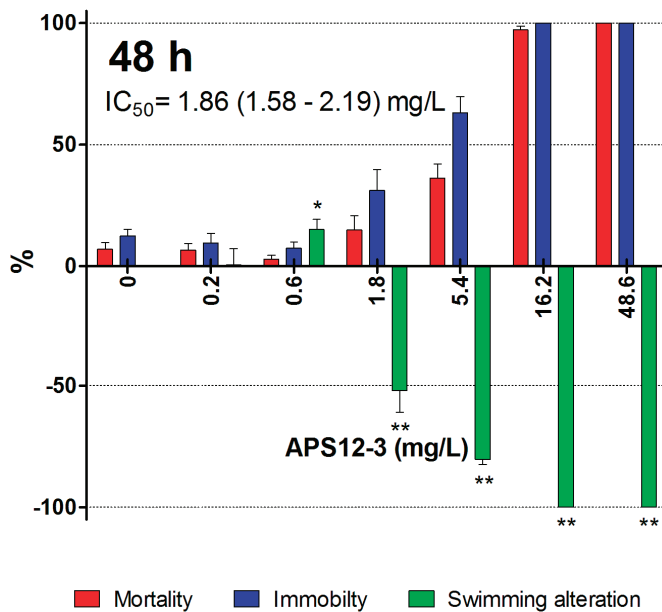


**Table 3.** Therapeutic ratio values calculated using both data of naupliar (TR<sub>N</sub>) and cyprids (TR<sub>C</sub>) toxicity.

Compounds	Treatment (h)	EC <sub>50</sub> (mg/L)	LC <sub>50(N)</sub> (mg/L)	LC <sub>50(C)</sub> (mg/L)	TR <sub>C</sub>	TR <sub>N</sub>
Poly-APS <sup>1</sup>	24	0.27	30.01	/	/	111.15
Zn pyriithione <sup>1</sup>	24	0.02	0.19	/	/	9.50
Cu pyriithione <sup>1</sup>	24	<0.01	<0.01	/	/	/
APS3	24	5.72	>100	>100	nc	nc
	48	nc	>100	>100	nc	nc
	72	nc	/	>100	nc	/
APS7	24	10.50	>100	>100	nc	nc
	48	25.86	94.02	>100	nc	3.64
	72	29.38	/	>100	nc	/
APS8	24	0.32	>100	>100	nc	
	48	0.50	79.37	>100	nc	158.74
	72	2.33	/	>100	nc	/
APS12	24	nc	>100	>100	nc	nc
	48	nc	>100	>100	nc	nc
	72	49.82	/	>100	nc	/
APS12-2	24	8.78	>100	>100	nc	11.39
	48	9.38	4.8	>100	nc	0.51
	72	11.13	/	>100	nc	/
APS12-3	24	0.89	11.6	61.13	68.68	13.3
	48	4.03	5.44	24.24	6.01	1.35
	72	4.76	/	17.97	3.77	/

<sup>1</sup> Data measured after a 24 h-treatment with poly-APS or commercial co-biocide [32]; nc, not calculable.

### 3. Experimental Section

#### 3.1. Chemicals

Stock solutions (100 mg/L) of each synthetic poly-APS were prepared by dissolving them in filtered (0.22 µm) natural seawater. The information on the synthesis and NMR analyses of APS8, APS12 and APS12-2 is available in [39] and of APS3, APS7 and APS12-3 in [40]. The chemical structures of the synthetic poly-APS are illustrated in Figure 1. The Zn pyriithione (Zinc Omadine<sup>®</sup>) and Cu pyriithione (Copper Omadine<sup>®</sup>) were from Arch Chemicals Incorporated, Atlanta, USA.

#### 3.2. Rearing of *Amphibalanus amphitrite* Larvae

Adult barnacles were maintained in aerated, filtered (0.45 µm) natural seawater at 20 °C, on a 16-h:8-h light-dark cycle. They were fed every two days with *Artemia salina* (50 to 100 mL; 200 larvae/mL) and *Tetraselmis suecica* (100 to 200 mL; 2 × 10<sup>6</sup> cells/mL). The seawater was changed three times per week, and the barnacles were periodically rinsed with fresh water to remove epibionts or debris.

To obtain the nauplii for cyprid cultures, the adults were left to dry for 30 min to 40 min and then immersed in fresh seawater. The hatched nauplii were attracted to a light source and collected using

a Pasteur pipette. They were reared to the cyprid stage as described in [50], by keeping them at 28 °C in natural filtered (0.22 µm) seawater and feeding them three times a week with *Tetraselmis suecica* ( $2 \times 10^6$  cells/mL). In these conditions nauplii reach the cyprids stage in 5–6 days. The cyprids were harvested by filtration and aged for 4 days prior to use, in filtered (0.45 µm) natural seawater at 4 °C in the dark [48].

### 3.3. Settlement Assay

The effects of poly-APS on the barnacle cyprids settlement were tested using these *A. amphitrite* cyprids. In the preliminary settlement assays, all poly-APS-like compounds were tested within a wide range of concentrations (from 0 to 100 mg/L). The settlement assays were conducted in 24-well microplates (Greiner Bio-One International AG, Austria) by adding 20 to 25 cyprids per well, with each well containing 2 mL of the relevant poly-APS solution (*i.e.*, 0.1, 0.5, 1, 5, 10, 50, 100 mg/L), or control seawater (*i.e.*, 0 mg/L poly-APS). For each compound, the experiment was performed in duplicate (two wells per concentration).

The test plates were sealed to prevent evaporation and incubated at 28 °C in the dark. The settlement was evaluated after 24 h, 48 h and 72 h of incubation. The larvae were examined under a dissecting microscope, to record the number of dead and permanently attached and metamorphosed individuals. The experiments were terminated by the addition of three droplets of 40% formaldehyde into each test well and the counting of the settled and non-settled larvae. The results were expressed as the percentages ( $\pm$ standard error) of the settlement of the total number of larvae incubated (20–25). The EC<sub>50</sub> was determined as the concentration of poly-APS causing 50% inhibition of the cyprids' population settlement.

The settlement assay was repeated only for those synthetic poly-APS-like compounds that showed the best antifouling activities: APS8 and APS12-3. To better define the EC<sub>50</sub>, the assays were slightly modified in terms of the range of concentrations of these poly-APS solutions (0, 0.3, 0.6, 1.2, 2.4, 4.8, 9.6, 19.2 mg/L for APS8; 0, 0.2, 0.4, 0.8, 1.6, 3.2, 6.4, 12.8 mg/L for APS12-3), and the experiments were performed with three replicates (three wells per concentration). The data for the inhibition of cyprid settlement are not illustrated, but EC<sub>50</sub> values are reported in Table 1.

As APS12-3 caused significant mortality of these cyprids at the higher concentrations, another experiment was designed to study the recovery of the settlement ability of these cyprid larvae. Briefly, after the 72 h treatment with APS12-3, the unsettled cyprids were collected from the wells, rinsed with filtered seawater and transferred into new microplates with clean fresh filtered (0.45 µm) natural seawater. The percentages of settled cyprids were then determined after 24 h, 48 h and 72 h at 28 °C.

### 3.4. Toxicity Assay

Acute (mortality) and sub-acute (immobility) toxicities of the synthetic poly-APS were assessed using II stage nauplii or cyprids of *A. amphitrite*. All of these tests were performed in duplicate (two wells per concentration) in 24-well microplates (Greiner Bio-One International AG, Kremsmünster, Austria), each well containing 2 mL of the relevant poly-APS solution (*i.e.*, 0.1, 0.5,

1, 5, 10, 50 and 100 mg/L), or filtered seawater as control (*i.e.*, 0 mg/L poly-APS), with 20 to 25 larvae per well.

The naupliar mortality and immobility were evaluated after 24 h and 48 h of incubation at 20 °C in the dark, while the cyprids' mortality was evaluated after 24 h, 48 h and 72 h of incubation at 28 °C. After the exposure to the relevant poly-APS or control filtered seawater, the larvae were examined under a dissecting microscope, and the number of dead larvae was recorded. The data are presented as the percentage of mortality  $\pm$  standard error, and the LC<sub>50</sub> is expressed as the concentration of the poly-APS that induced death in 50% of the tested organisms. When assessing naupliar immobility, the number of immobile larvae is expressed as the sum of dead larvae (not swimming and moving appendages for 10 s of observation) and non-swimming larvae (not shifting their barycenter, but moving their appendages). The EC<sub>50</sub> was calculated as the concentration of the toxicant that caused 50% immobility of the exposed organisms after 24 and 48 h.

### 3.5. Naupliar Swimming Speed Test

A swimming speed assay [51,52] was used to measure the behavioral effects of the synthetic analogue APS12-3 on the *A. amphitrite* larvae. Briefly, II stage nauplii (15–20 per well) were exposed to the APS12-3 test solutions in 24-well microplates for 48 h, at 20 °C in the dark, without aeration and feeding. All of these experiments were performed in duplicate (two wells per concentration).

A Swimming Behavioral Recorder System (e-magine IT, Genova, Italy) was used to track the paths of the swimming nauplii. Prior to the video recording under infrared light, the nauplii were adapted to the dark for 2 min, to gain their steady swimming speeds and to reach a uniform spatial distribution. The swimming behavior was monitored in the dark at 20 °C, for about three seconds, at 25 frames/s. The resulting digital images were analyzed using advanced image processing software to reconstruct the individual naupliar swimming paths and to measure the average swimming speed (mm/s) for each of the nauplii (15–20 nauplii). Finally, the data are expressed as percentages in terms of the swimming alteration, after normalization to the mean swimming speed ( $v$ ) of the control (filtered natural seawater), as follows (Equation 1):

$$\text{Swimming alteration (\%)} = \frac{v_{\text{treated}} - v_{\text{control}}}{v_{\text{control}}} \times 100\% \quad (1)$$

The IC<sub>50</sub> value was determined as the concentration of APS12-3 that caused changes in swimming behavior in 50% of the test nauplii.

### 3.6. Statistical Analyses

The EC<sub>50</sub> for the cyprid settlement inhibition after 24, 48 and 72 h, the EC<sub>50</sub> for the naupliar immobility after 24 and 48 h, the LC<sub>50</sub> for the larval mortality after 24, 48 and 72 h and the IC<sub>50</sub> for naupliar swimming speed alteration were calculated using a trimmed Spearman–Kärber analysis [53]. One-way analysis of variance (ANOVA) was performed, with the level of significance set at  $p < 0.05$  or  $p < 0.001$ , followed by Student–Newman–Keuls (SNK) tests to compare the treatment means [54].



#### 4. Conclusions

The present study was designed to determine the antifouling potential of six synthetic poly-APS that differ in the lengths of their alkyl chains (3–12 carbon atoms), their degree of polymerization (eight to 63 monomeric subunits) and the nature of their counter ions (chloride or bromide). Although several studies have reported that these structural features influence the biological activities of amphiphilic compounds, particularly in terms of their membrane-damaging potential and antimicrobial activities [55–59], we were not able to observe such a relationship.

The antifouling activity of natural poly-APS is believed to derive from its surfactant-like properties, or is potentially due to the inhibition of the cholinergic system, which is involved in cyprid settlement [28]. The underlying antifouling mechanism of these synthetic poly-APS remains unsolved; however, the hormetic responses observed imply the involvement of receptor system(s). Recently, a strong interaction between the synthetic poly-APS APS8 and human  $\alpha 7$  nicotinic acetylcholine receptors was reported [60]. Acetylcholine serves as a neurotransmitter/neuromodulator during the settlement of *A. amphitrite* larvae [50], and therefore, the antifouling activity of APS8 and possibly also of these other synthetic poly-APS might derive from the binding of these synthetic poly-APS to these receptors and the subsequent competition with acetylcholine.

Although numerous natural products with anti-settlement activities have been reported to date, only a few have shown potential for commercialization [24]. Among these, natural poly-APS has been suggested as a non-toxic natural antifoulant [22,26]. With the recent chemical synthesis of various poly-APS [39,40] now ensuring an adequate supply of these compounds, we focused our current research on the finding of synthetic poly-APS with comparable or improved antifouling activities to natural poly-APS. Among the polymers tested, APS8 prevented the settlement of *A. amphitrite* cyprids via a non-toxic mechanism and with similar potency to natural poly-APS. On the other hand, APS12-3 showed an anti-settlement efficacy similar to the natural poly-APS, but with higher toxicity.

#### Acknowledgments

Financial support from the Slovenian Research Agency through grant J1-4044 (Tom Turk), from the Italian National Research Council (CNR)—Institute of Marine Science and from the Erasmus Programme (Ivanka Dragić) is gratefully acknowledged. We sincerely thank Christopher Berrie for critical reading and editing of the manuscript.

#### Author Contributions

Veronica Piazza, Francesca Garaventa, Marco Faimali, Kristina Sepčić, Tom Turk and Sabina Berne contributed to conception and design of the study. Veronica Piazza and Ivanka Dragić performed the experiments. Veronica Piazza, Francesca Garaventa, Sabina Berne and Kristina Sepčić analyzed and interpreted the data. All authors participated in drafting the article and critically revising it.

## Conflicts of Interest

The authors declare no conflict of interest.

## References

1. Kirschner, C.M.; Brennan, A.B. Bio-Inspired Antifouling Strategies. *Annu. Rev. Mater. Res.* **2012**, *42*, 211–229.
2. Briand, J.-F. Marine antifouling laboratory bioassays: An overview of their diversity. *Biofouling* **2009**, *25*, 297–311.
3. Jain, A.; Bhosle, N.B. Biochemical composition of the marine conditioning film: Implications for bacterial adhesion. *Biofouling* **2009**, *25*, 13–19.
4. Dobretsov, S. Marine Biofilms. In *Biofouling*; Dürr, S., Thomason, J.C., Eds.; Wiley-Blackwell: Oxford, UK, 2009; pp. 123–136.
5. Railkin, A.I.; Ganf, T.A.; Manylov, O.G. Biofouling as a Process. In *Marine Biofouling: Colonization Processes and Defenses*; CRC Press: Boca Raton, FL, USA, 2003; pp. 25–39.
6. Joint, I.; Tait, K.; Callow, M.E.; Callow, J.A.; Milton, D.; Williams, P.; Cámara, M. Cell-to-cell communication across the prokaryote-eukaryote boundary. *Science* **2002**, *298*, 1207.
7. Hadfield, M.G.; Paul, V.J. Natural chemical cues for settlement and metamorphosis of marine-invertebrate larvae. In *Marine Chemical Ecology*; McClintock, J.B., Baker, B.J., Eds.; CRC Press: Boca Raton, FL, USA, 2001; pp. 431–461.
8. Hadfield, M.G. Biofilms and marine invertebrate larvae: What bacteria produce that larvae use to choose settlement sites. *Ann. Rev. Mar. Sci.* **2011**, *3*, 453–470.
9. Schultz, M.P. Effects of coating roughness and biofouling on ship resistance and powering. *Biofouling* **2007**, *23*, 331–341.
10. Schultz, M.P.; Bendick, J.A.; Holm, E.R.; Hertel, W.M. Economic impact of biofouling on a naval surface ship. *Biofouling* **2011**, *27*, 87–98.
11. Elimelech, M.; Phillip, W.A. The future of seawater desalination: Energy, technology, and the environment. *Science* **2011**, *333*, 712–717.
12. Page, H.M.; Dugan, J.E.; Piltz, F. Fouling and antifouling in oil and other offshore industries. In *Biofouling*; Dürr, S., Thomason, J.C., Eds.; Wiley-Blackwell: Oxford, UK, 2009; pp. 252–266.
13. Fitridge, I.; Dempster, T.; Guenther, J.; de Nys, R. The impact and control of biofouling in marine aquaculture: A review. *Biofouling* **2012**, *28*, 649–669.
14. Dafforn, K.A.; Lewis, J.A.; Johnston, E.L. Antifouling strategies: History and regulation, ecological impacts and mitigation. *Mar. Pollut. Bull.* **2011**, *62*, 453–465.
15. Rosenhahn, A.; Schilp, S.; Kreuzer, H.J.; Grunze, M. The role of “inert” surface chemistry in marine biofouling prevention. *Phys. Chem. Chem. Phys.* **2010**, *12*, 4275–4286.
16. Sonak, S.; Pangam, P.; Giriyan, A.; Hawaldar, K. Implications of the ban on organotinols for protection of global coastal and marine ecology. *J. Environ. Manag.* **2009**, *90*, S96–S108.
17. Ralston, E.; Swain, G. Bioinspiration—The solution for biofouling control? *Bioinspir. Biomim.* **2009**, *4*, 015007.

18. Salta, M.; Wharton, J.A.; Stoodley, P.; Dennington, S.P.; Goodes, L.R.; Werwinski, S.; Mart, U.; Wood, R.J.K.; Stokes, K.R. Designing biomimetic antifouling surfaces. *Philos. Trans. A Math. Phys. Eng. Sci.* **2010**, *368*, 4729–4754.
19. Scardino, A.J.; de Nys, R. Mini review: Biomimetic models and bioinspired surfaces for fouling control. *Biofouling* **2011**, *27*, 73–86.
20. Banerjee, I.; Pangule, R.C.; Kane, R.S. Antifouling coatings: Recent developments in the design of surfaces that prevent fouling by proteins, bacteria, and marine organisms. *Adv. Mater.* **2011**, *23*, 690–718.
21. Rittschof, D. Natural product antifoulants: One perspective on the challenges related to coatings development. *Biofouling* **2000**, *15*, 119–127.
22. Fusetani, N. Biofouling and antifouling. *Nat. Prod. Rep.* **2004**, *21*, 94–104.
23. Turk, T.; Frangež, R.; Sepčić, K. Mechanisms of toxicity of 3-alkylpyridinium polymers from marine sponge *Reneira sarai*. *Mar. Drugs* **2007**, *5*, 157–167.
24. Raveendran, T.V.; Limna Mol, V.P. Natural product antifoulants. *Curr. Sci.* **2009**, *97*, 508–520.
25. Qian, P.-Y.; Xu, Y.; Fusetani, N. Natural products as antifouling compounds: Recent progress and future perspectives. *Biofouling* **2010**, *26*, 223–234.
26. Fusetani, N. Antifouling marine natural products. *Nat. Prod. Rep.* **2011**, *28*, 400–410.
27. Turk, T.; Sepčić, K.; Mancini, I.; Guella, G. 3-Akylpyridinium and 3-alkylpyridine compounds from marine sponges, their synthesis, biological activities and potential use. In *Studies in Natural Products Chemistry*; Elsevier: Amsterdam, The Netherlands, 2008; Volume 35, pp. 355–397.
28. Sepčić, K.; Turk, T. 3-Alkylpyridinium compounds as potential non-toxic antifouling agents. In *Antifouling Compounds SE-4*; Fusetani, N., Clare, A., Eds.; Springer: Berlin/Heidelberg, Germany, 2006; Volume 42, pp. 105–124.
29. Sepčić, K.; Guella, G.; Mancini, I.; Pietra, F.; Serra, M.D.; Menestrina, G.; Tubbs, K.; Maček, P.; Turk, T. Characterization of anticholinesterase-active 3-alkylpyridinium polymers from the marine sponge *Reniera sarai* in aqueous solutions. *J. Nat. Prod.* **1997**, *60*, 991–996.
30. Grandič, M.; Sepčić, K.; Turk, T.; Juntas, P.; Frangež, R. *In vivo* toxic and lethal cardiovascular effects of a synthetic polymeric 1,3-dodecylpyridinium salt in rodents. *Toxicol. Appl. Pharmacol.* **2011**, *255*, 86–93.
31. Malovrh, P.; Sepčić, K.; Turk, T.; Maček, P. Characterization of hemolytic activity of 3-alkylpyridinium polymers from the marine sponge *Reniera sarai*. *Comp. Biochem. Physiol. Part C Pharmacol. Toxicol. Endocrinol.* **1999**, *124*, 221–226.
32. Faimali, M.; Sepčić, K.; Turk, T.; Geraci, S. Non-toxic antifouling activity of polymeric 3-alkylpyridinium salts from the Mediterranean sponge *Reniera sarai* (Pulitzer-Finali). *Biofouling* **2003**, *19*, 47–56.
33. Garaventa, F.; Faimali, M.; Sepčić, K.; Geraci, S. Laboratory analysis of antimicrofouling activity of Poly-APS extracted from *Reniera sarai* (Porifera: Demospongiae). *Biol. Mar. Mediterr.* **2003**, *10*, 565–567.
34. Qian, P.-Y.; Chen, L.; Xu, Y. Mini-review: Molecular mechanisms of antifouling compounds. *Biofouling* **2013**, *29*, 381–400.

35. Mancini, I.; Defant, A.; Guella, G. Recent synthesis of marine natural products with antibacterial activities. *Anti-Infect. Agents Med. Chem.* **2007**, *6*, 17–48.
36. Mancini, I.; Sicurelli, A.; Guella, G.; Turk, T.; Maček, P.; Sepčić, K. Synthesis and bioactivity of linear oligomers related to polymeric alkyipyridinium metabolites from the Mediterranean sponge *Reniera sarai*. *Org. Biomol. Chem.* **2004**, *2*, 1368–1375.
37. Faimali, M.; Garaventa, F.; Mancini, I.; Sicurelli, A.; Guella, G.; Piazza, V.; Greco, G. Antisettlement activity of synthetic analogues of polymeric 3-alkylpyridinium salts isolated from the sponge *Reniera sarai*. *Biofouling* **2005**, *21*, 49–57.
38. Chelossi, E.; Mancini, I.; Sepčić, K.; Turk, T.; Faimali, M. Comparative antibacterial activity of polymeric 3-alkylpyridinium salts isolated from the Mediterranean sponge *Reniera sarai* and their synthetic analogues. *Biomol. Eng.* **2006**, *23*, 317–323.
39. Houssen, W.E.; Lu, Z.; Edrada-Ebel, R.; Chatzi, C.; Tucker, S.J.; Sepčić, K.; Turk, T.; Zovko, A.; Shen, S.; Mancini, I.; *et al.* Chemical synthesis and biological activities of 3-alkyl pyridinium polymeric analogues of marine toxins. *J. Chem. Biol.* **2010**, *3*, 113–125.
40. Zovko, A.; Vaukner Gabrič, M.; Sepčić, K.; Pohleven, F.; Jaklič, D.; Gunde-Cimerman, N.; Lu, Z.; Edrada-Ebel, R.; Houssen, W.E.; Mancini, I.; *et al.* Antifungal and antibacterial activity of 3-alkylpyridinium polymeric analogs of marine toxins. *Int. Biodeterior. Biodegrad.* **2012**, *68*, 71–77.
41. Grandič, M.; Aráoz, R.; Molgó, J.; Turk, T.; Sepčić, K.; Benoit, E.; Frangež, R. Toxicity of the synthetic polymeric 3-alkylpyridinium salt (APS3) is due to specific block of nicotinic acetylcholine receptors. *Toxicology* **2013**, *303*, 25–33.
42. Eleršek, T.; Kosi, G.; Turk, T.; Pohleven, F.; Sepčić, K. Influence of polymeric 3-alkylpyridinium salts from the marine sponge *Reniera sarai* on the growth of algae and wood decay fungi. *Biofouling* **2008**, *24*, 137–143.
43. Holm, E.R. Barnacles and biofouling. *Integr. Comp. Biol.* **2012**, *52*, 348–355.
44. Calabrese, E.J. Biphasic dose responses in biology, toxicology and medicine: Accounting for their generalizability and quantitative features. *Environ. Pollut.* **2013**, *182*, 452–460.
45. Calabrese, E.J.; Mattson, M.P. Hormesis provides a generalized quantitative estimate of biological plasticity. *J. Cell Commun. Signal.* **2011**, *5*, 25–38.
46. Calabrese, E.J. Hormetic mechanisms. *Crit. Rev. Toxicol.* **2013**, *43*, 580–606.
47. Wiegant, F.A.C.; de Poot, S.A.H.; Boers-Trilles, V.E.; Schreij, A.M.A. Hormesis and cellular quality control: A possible explanation for the molecular mechanisms that underlie the benefits of mild stress. *Dose-Response* **2012**, *11*, 413–430.
48. Rittschof, D.; Clare, A.S.; Gerhart, D.J.; Mary, S.A.; Bonaventura, J. Barnacle *in vitro* assays for biologically active substances: Toxicity and settlement inhibition assays using mass cultured *Balanus amphitrite amphitrite* Darwin. *Biofouling* **1992**, *6*, 115–122.
49. Piazza, V.; Roussis, V.; Garaventa, F.; Greco, G.; Smyrniotopoulos, V.; Vagias, C.; Faimali, M. Terpenes from the red alga *Sphaerococcus coronopifolius* inhibit the settlement of barnacles. *Mar. Biotechnol.* **2011**, *13*, 764–772.
50. Faimali, M.; Falugi, C.; Gallus, L.; Piazza, V.; Tagliafierro, G. Involvement of acetyl choline in settlement of *Balanus amphitrite*. *Biofouling* **2003**, *S19*, 213–220.

51. Faimali, M.; Garaventa, F.; Piazza, V.; Greco, G.; Corrà, C.; Magillo, F.; Pittore, M.; Giacco, E.; Gallus, L.; Falugi, C.; *et al.* Swimming speed alteration of larvae of *Balanus amphitrite* as a behavioural end-point for laboratory toxicological bioassays. *Mar. Biol.* **2006**, *149*, 87–96.
52. Garaventa, F.; Gambardella, C.; di Fino, A.; Pittore, M.; Faimali, M. Swimming speed alteration of *Artemia* sp. and *Brachionus plicatilis* as a sub-lethal behavioural end-point for ecotoxicological surveys. *Ecotoxicology* **2010**, *19*, 512–519.
53. Hamilton, M.A.; Russo, R.C.; Thurston, R.V. Trimmed Spearman-Kärber method for estimating median lethal concentrations in toxicity bioassays. *Environ. Sci. Technol.* **1977**, *11*, 714–719.
54. De Muth, J.E. *Basic Statistics and Pharmaceutical Statistical Applications*, 2nd ed.; Chapman and Hall/CRC: Boca Raton, FL, USA, 2006; p. 744.
55. Kleszczyńska, H.; Bielecki, K.; Sarapuk, J.; Bonarska-Kujawa, D.; Pruchnik, H.; Trela, Z.; Łuczyński, J. Biological activity of new *N*-oxides of tertiary amines. *Z. Naturforsch. C J. Biosci.* **2009**, *61*, 715–720.
56. Zarif, L.; Riess, J.G.; Pucci, B.; Pavia, A.A. Biocompatibility of alkyl and perfluoroalkyl telomeric surfactants derived from THAM. *Biomater. Artif. Cells Immobil. Biotechnol.* **1993**, *21*, 597–608.
57. Kuroda, K.; DeGrado, W.F. Amphiphilic polymethacrylate derivatives as antimicrobial agents. *J. Am. Chem. Soc.* **2005**, *127*, 4128–4129.
58. Sarapuk, J.; Kleszczyńska, H.; Pernak, J.; Kalewska, J.; Rózycka-Roszak, B. Influence of counterions on the interaction of pyridinium salts with model membranes. *Z. Naturforsch. C* **1999**, *54*, 952–955.
59. Kleszczyńska, H.; Sarapuk, J.; Rózycka-Roszak, B. The role of counterions in the interaction of some cationic surfactants with model membranes. *Pol. J. Environ. Stud.* **1998**, *7*, 327–329.
60. Zovko, A.; Viktorsson, K.; Lewensohn, R.; Kološa, K.; Filipič, M.; Xing, H.; Kem, W.R.; Paleari, L.; Turk, T. APS8, a polymeric alkylpyridinium salt blocks  $\alpha 7$  nAChR and induces apoptosis in non-small cell lung carcinoma. *Mar. Drugs* **2013**, *11*, 2574–2594.

# Molecular Response to Toxic Diatom-Derived Aldehydes in the Sea Urchin *Paracentrotus lividus*

Stefano Varrella, Giovanna Romano, Adrianna Ianora, Matt G. Bentley, Nadia Ruocco and Maria Costantini

**Abstract:** Diatoms are dominant photosynthetic organisms in the world's oceans and represent a major food source for zooplankton and benthic filter-feeders. However, their beneficial role in sustaining marine food webs has been challenged after the discovery that they produce secondary metabolites, such as polyunsaturated aldehydes (PUAs), which negatively affect the reproductive success of many invertebrates. Here, we report the effects of two common diatom PUAs, heptadienal and octadienal, which have never been tested before at the molecular level, using the sea urchin, *Paracentrotus lividus*, as a model organism. We show that both PUAs are able to induce teratogenesis (*i.e.*, malformations), as already reported for decadienal, the better-studied PUA of this group. Moreover, post-recovery experiments show that embryos can recover after treatment with all three PUAs, indicating that negative effects depend both on PUA concentrations and the exposure time of the embryos to these metabolites. We also identify the time range during which PUAs exert the greatest effect on sea urchin embryogenesis. Finally, we report the expression levels of thirty one genes (having a key role in a broad range of functional responses, such as stress, development, differentiation, skeletogenesis and detoxification processes) in order to identify the common targets affected by PUAs and their correlation with morphological abnormalities. This study opens new perspectives for understanding how marine organisms afford protection from environmental toxicants through an integrated network of genes.

Reprinted from *Mar. Drugs*. Cite as: Varrella, S.; Romano, G.; Ianora, A.; Bentley, M.G.; Ruocco, N.; Costantini, M. Molecular Response to Toxic Diatom-Derived Aldehydes in the Sea Urchin *Paracentrotus lividus*. *Mar. Drugs* **2014**, *12*, 208962113.

## Abbreviations

FSW, filtered sea water; hpf, hours post fertilization;  $\mu\text{L}$ , microliter;  $\mu\text{M}$ , micromolar; min, minutes; mM, millimolar; nm, nanometer.

## 1. Introduction

Diatoms are a highly productive class of microalgae, widespread in both marine and freshwater habitats, that are widely fed upon by both planktonic and benthic invertebrates. However, while diatoms may provide a source of energy for larval growth, they often reduce fecundity and/or hatching success or cause malformations (teratogenesis) during growth, due to the production of secondary metabolites, such as polyunsaturated aldehydes (PUAs) and other products deriving from the oxidation of polyunsaturated fatty acids (PUFAs), collectively termed oxylipins (reviewed by [1] and [2]). This biological model is new and has no other equivalent in marine plant-herbivore

systems, since most of the known negative plant-animal interactions are generally related to repellent or poisoning processes, but never to reproductive failure.

Oxylipins, and PUAs in particular, have important biological and biochemical properties, including the disruption of gametogenesis, gamete functionality, fertilization, embryonic mitosis and larval fitness and competence [1]. The dominant bioactive PUAs released by diatoms are C<sub>10</sub> 2-*trans*-4-*trans*-decadienal, 2-*trans*-4-*cis*-7-*cis*-decatrienal and 2-*trans*-4-*trans*-7-*cis*-decatrienal [3], but also C<sub>8</sub> 2-*trans*-4-*cis*-7-octatrienal, 2-*trans*-4-*trans*-7-octatrienal, 2-*trans*-4-*cis*-7-octadienal, 2-*trans*-4-*trans*-7-octadienal, C<sub>7</sub> 2-*trans*-4-*cis*-7-heptadienal and 2-*trans*-4-*trans*-7-heptadienal [4,5]. The first two PUAs were isolated from the freshwater diatom, *Melosira varians*, by Wendel and Jüttner [6], but the biological activity of these molecules was not known at the time. Miralto *et al.* [3] showed, for the first time, that they arrested the embryonic development of copepod and sea urchin embryos in a dose-dependent manner and also had anti-proliferative and apoptotic effects on human carcinoma cells. Successive studies have shown that sea urchin gametes incubated with decadienal have impaired fertilization success, due to the inhibition of sperm motility [7,8]. At concentrations higher than the dose required to arrest cell cleavage progression, decadienal induced apoptotic events in *Paracentrotus lividus* embryos by inducing caspase-3-like protease activity [9].

Hansen *et al.* [10] studied the effects of decadienal on the sea urchin, *Sphaerechinus granularis*, and showed that this PUA inhibited cyclin B/Cdk1 kinase activity, DNA replication and tubulin polymerization, leading to arrest of the cell cycle. Romano *et al.* [11] showed that PUAs compromised embryonic and larval development of sea urchins even at low doses and that the most deleterious of the PUAs tested were the longer chain aldehydes, such as decadienal.

The first molecular studies on the effects of PUAs on the sea urchin, *P. lividus*, were reported very recently [12,13]. In particular, newly fertilized sea urchin eggs were exposed to low concentrations of decadienal, and the expression levels of seventeen genes, implicated in a broad range of functional responses, were followed by real-time qPCR. At low decadienal concentrations, the sea urchin, *P. lividus*, activated different classes of genes to defend itself against this toxic aldehyde, ranging from canonical stress genes to developmental and skeletogenic genes [13]. The authors suggested that this orchestrated defence system against decadienal represents part of the chemical defensible of *P. lividus*, affording protection from environmental toxicants.

Since information on the molecular effects of PUAs are scant and mostly related to the effects induced by decadienal, the aim of the present study was to explore the effects of two other ecologically important aldehydes, heptadienal and octadienal, which have never been tested before on *P. lividus* embryos from the molecular point of view, and to compare these effects with those induced by decadienal. The sea urchin, *P. lividus*, is considered a good model system to study the ecotoxicological response of marine invertebrates to environmental pollutants for several reasons: its ecological relevance, benthic and relatively sedentary lifestyle, rapid response and high sensitivity to many types of contaminants, transparent embryos that grow rapidly in the laboratory and its long reproductive period. For these reasons, we decided to adopt it for our study and treated sea urchin embryos with increasing concentrations of heptadienal and octadienal to analyse morphological changes induced by exposure to these natural products and to define their

mechanism of action and possible teratogenic activity. We also followed, by real-time qPCR, thirty one genes to identify potential target genes. Fourteen of these genes, having a key role in a broad range of functional responses, such as development, differentiation and detoxification processes, are now compared to those investigated in our previous study on the effects of decadienal on *P. lividus* development [13].

## 2. Results

### 2.1. Determination of Teratogenic Effects and PUA Dose-Dependent Concentrations

As reported in previous studies [11,12], decadienal induced teratogenesis at low concentrations, with an increase in the number of abnormal plutei in the sea urchin, *P. lividus*. Marrone *et al.* [13] also reported a dose-dependent effect of this PUA in *P. lividus*, with severe malformations in plutei, such as asymmetrical arms and spicules and reduced arm length and shortening of the apex. Romano *et al.* [12] showed that a decadienal concentration of 1.6  $\mu\text{M}$  (0.25  $\mu\text{g/mL}$ ) was ideal to study morphogenetic changes in embryo development and gene expression levels in *P. lividus*, with the production of about 35% abnormal plutei.

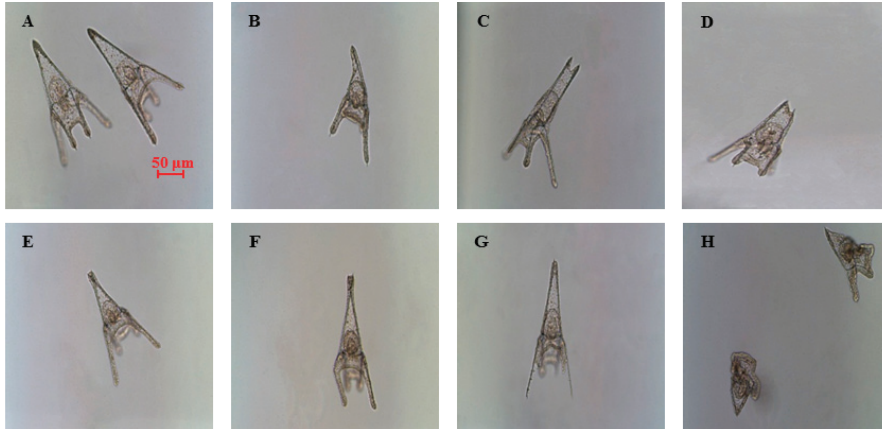
The present study explores further the effects of decadienal at the molecular level and compares these effects with those induced by two other PUAs, heptadienal and octadienal, which have never been tested before on *P. lividus* embryo development. Treatment with the three PUAs induced similar malformations in the plutei (see Figure 1), with effects on the arms, spicules and apex. Such plutei had a poorly-formed apex (Figure 1B) because of the spicules that appeared either parallel or disjoined at the tip (Figure 1C,D) or crossed at the apex (Figure 1E), with arms that appeared longer and broader or crooked and asymmetrical (Figure 1F) or completely degenerated (Figure 1G), compared to controls (Figure 1A). At times, the entire body plan of the plutei was strongly compromised and malformed (Figure 1H). For a more detailed overview of the abnormal plutei produced by PUAs, see Supplementary Figure S1.

The percentage of abnormal plutei was calculated at the different concentrations tested (Figure 2; see also the Experimental Section for more details).

The effect was dose-dependent for the three PUAs tested, even if the range of concentrations inducing teratogenesis differed (from 0.5 to 2.5  $\mu\text{M}$  for decadienal, from 1.0 to 6.0  $\mu\text{M}$  for heptadienal and from 2.0 to 9.0  $\mu\text{M}$  for octadienal). Decadienal was the strongest of the three, because of the very narrow range (2.0  $\mu\text{M}$ ) that affected embryonic development; heptadienal and octadienal required higher ranges of concentrations to reach the same effects as decadienal. Therefore, we chose as teratogenic concentrations 3.0  $\mu\text{M}$  for heptadienal and 4.5  $\mu\text{M}$  for octadienal, in order to obtain the same percentage of abnormal plutei (about 35%), as in the case of decadienal. Controls were also performed in filtered sea water (FSW) and in FSW plus methanol, and we found that methanol had no interference with the embryo development. In fact, the percentage of abnormal plutei was the same for embryos in FSW, as well as in FSW plus methanol.



**Figure 1.** Examples of malformations induced in *Paracentrotus lividus* plutei at 48 hours post fertilization (hpf) after incubation with the three polyunsaturated aldehydes (PUAs), heptadienal, octadienal and decadienal (**B–H**) in comparison with (**A**), the control; embryos are in sea water without aldehydes.



## 2.2. Post-Recovery Experiments

Post-recovery experiments were performed in order to investigate if sea urchin embryos were able to recover after exposure to these PUAs. Eggs were incubated with three different concentrations of PUAs and then fertilized. The lowest concentrations represented the concentration inducing teratogenesis for each PUA (decadienal 1.6  $\mu\text{M}$ , heptadienal 3.0  $\mu\text{M}$ , octadienal 4.5  $\mu\text{M}$ ) and were also used to study the gene stress response (see below); the other concentrations (decadienal two and 2.5  $\mu\text{M}$ ; heptadienal five and 6  $\mu\text{M}$ ; octadienal six and 8  $\mu\text{M}$ ) were chosen to have comparable percentages of abnormal plutei (about 60% and 75%). Embryos were washed at different times after fertilization, 40 min, two, five, nine and 24 hours post fertilization (hpf), corresponding to two-cell, eight-cell, early blastula, swimming blastula and prism, respectively. After washing, embryos were grown to the pluteus stage to calculate the number of abnormal embryos. The results indicate that embryos were able to recover at all concentrations tested and at all times after fertilization (Figure 3), with the exception of the highest concentrations at 24 hpf. Moreover, the results suggest that octadienal could have a different mechanism of action compared to decadienal and heptadienal, because embryos were less able to recover at all times after fertilization at the highest concentrations. According to these results, we conclude that the post-recovery effects depend both on PUA concentrations and the exposure time of embryos to these metabolites, with the exception of octadienal at the highest concentration.

**Figure 2.** Percentage of abnormal plutei (%) produced when *Paracentrotus lividus* newly-fertilized eggs are exposed to different concentrations (in  $\mu\text{M}$ ) of heptadienal, octadienal and decadienal for 48 h post fertilization (\*\*\*) with a  $p$ -value  $<0.001$ , Student's  $t$ -test, GraphPad Software Inc., San Diego, CA, USA).

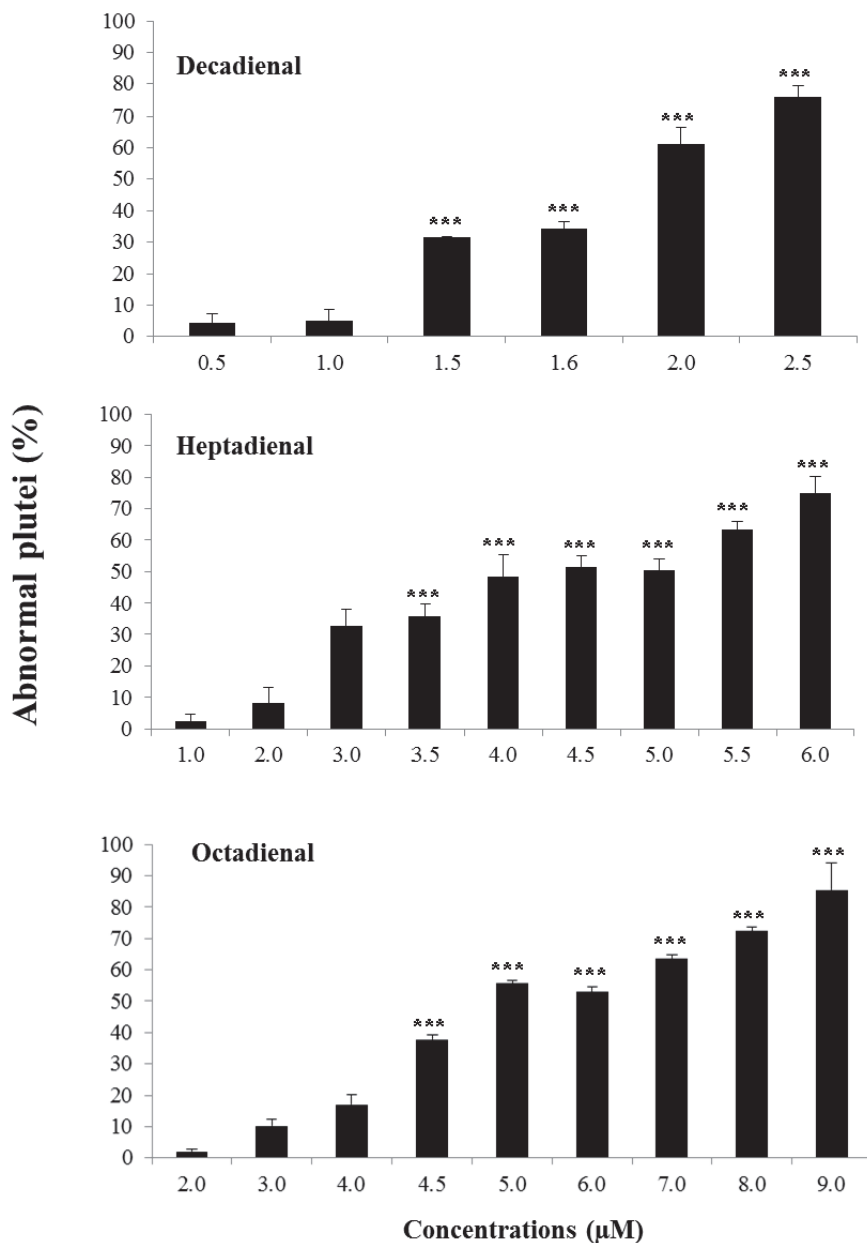
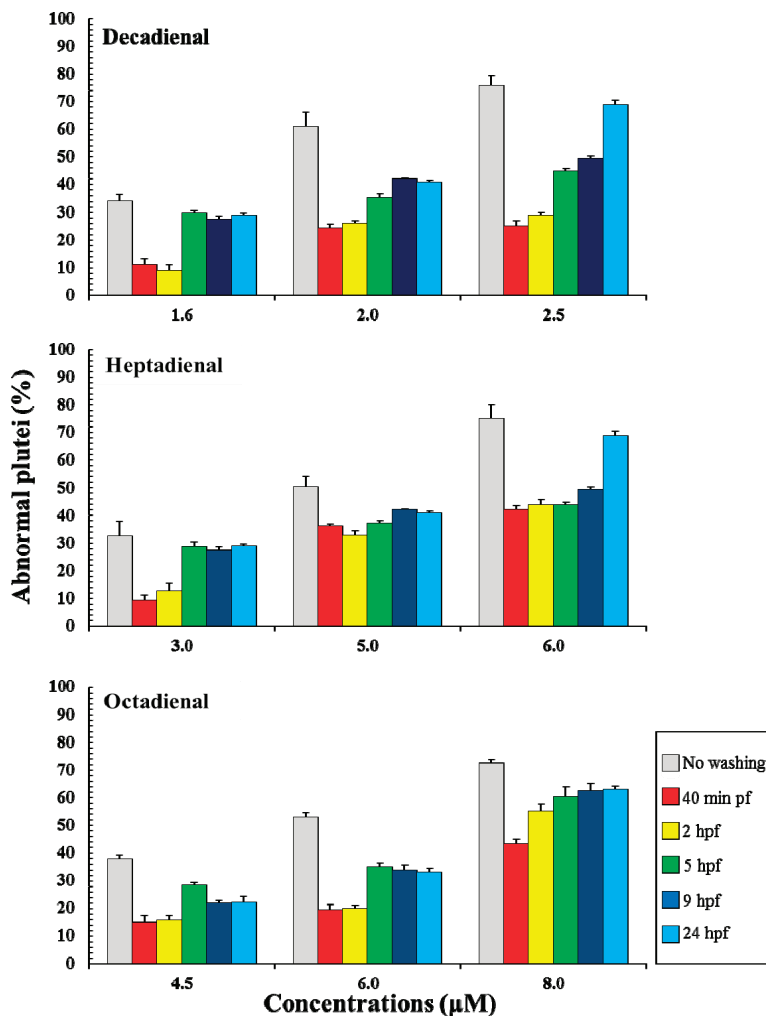


**Figure 3.** Percentage of abnormal *Paracentrotus lividus* plutei (%) produced after exposure to different concentrations of heptadienal, octadienal and decadienal and at different development times after fertilization. The percentages of abnormal plutei without washing are also reported.

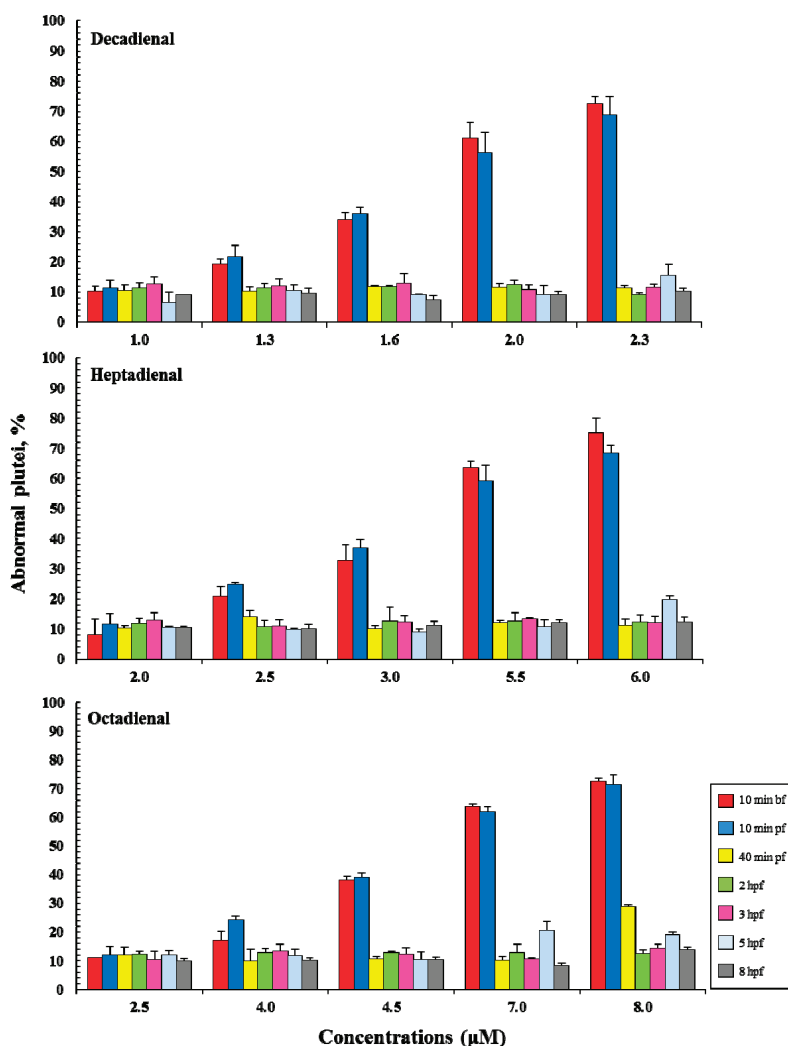


### 2.3. Addition of PUAs at Different Developmental Stages

To define the stage at which PUAs affect embryo development, aldehydes were added: 10 min before fertilization (bf), 10 min pf, 40 min pf, 2, 3, 5 and 8 hpf. These stages represented key stages during sea urchin embryogenesis. In fact, 40 min pf corresponds to the two-cell stage; from this stage until 5 hpf, only mitotic cell division occurs; at 5 hpf (corresponding to early blastula stage) the differentiation of blastomeres begins, and cell fates in specific embryonic territories are defined; at 8 hpf, the embryo envelope starts to be digested, so the embryos comes into direct

contact with the external environment for the first time. The results show that the addition of PUAs affect embryonic development in the same way, whether they are added 10 min before fertilization (bf) and/or 10 min pf, resulting in the same percentage of abnormal plutei (Figure 4). The addition of PUAs in later developmental stages does not seem to affect the embryonic development of *P. lividus*. In fact, the percentage of abnormal plutei remains very low (about 10%–20%) for each concentration tested.

**Figure 4.** The percentage of abnormal *Paracentrotus lividus* plutei (%) produced after the exposure of newly fertilized eggs to different concentrations of heptadienal, octadienal and decadienal and examined at different developmental stages: 10 min before fertilization (bf), 10 min and 40 min post fertilization (pf) and two, three, five and 8 hpf.



#### 2.4. Gene Stress Response to PUAs

To better understand the morphological effects at the molecular level, *P. lividus* embryos were allowed to develop in the presence of PUAs at concentrations inducing teratogenesis (1.6  $\mu$ M for decadienal, 3.0  $\mu$ M for heptadienal and 4.5  $\mu$ M for octadienal), and embryos were collected at different development times after fertilization, corresponding to the stages of early blastula (5 hpf), swimming blastula (9 hpf), prism (24 hpf) and pluteus (48 hpf). The expression levels of thirty one genes (see the Experimental Section for more details) were followed by real-time qPCR to identify potential gene targets. These genes are implicated in a broad range of functional responses, such as stress, development, differentiation, skeletogenesis and detoxification processes (see Table 1).

**Table 1.** The function for the genes analysed in the present study.

Gene Name	Acronym	Function	Reference
<i>Pl-p19</i>	<i>p19</i>	small acidic proteins, involved in the formation of the biomineralised skeleton of sea urchin embryos and adults	[14]
<i>Pl-p16</i>	<i>p16</i>		
<b><i>ALG-2 interacting protein X/1</i></b>	<i>Alix</i>	protein involved in endocytic membrane trafficking, filamentous (F)-actin remodelling and cytokinesis	[15]
<b><i>Blimp</i></b>	<i>Blimp</i>	zinc finger transcription factor, which plays a central role in both early and late endomesoderm specification	[16]
<b><i>Wnt 5</i></b>	<i>Wnt5</i>	initiates the specification of the sea urchin posterior ectoderm	[17]
<b><i>Wnt 6</i></b>	<i>Wnt6</i>	activates endoderm in the sea urchin gene regulatory network	[18]
<b><i>Wnt 8</i></b>	<i>Wnt8</i>	endomesodermal specification, embryo patterning, early primary mesenchyme cells-gene regulatory network regulator	[19]
<b><i>Multi drug resistance protein 1</i></b>	<i>MDR1</i>	ATP-binding cassette protein	[20]
<b><i>Metallothionein 4</i></b>	<i>MT4</i>	proteins capable of binding to heavy metals, involved in the transport of heavy metals and cellular detoxification	[21]
<b><i>Metallothionein 5</i></b>	<i>MT5</i>		
<b><i>Metallothionein 6</i></b>	<i>MT6</i>		
<b><i>Metallothionein 7</i></b>	<i>MT7</i>		
<b><i>Metallothionein 8</i></b>	<i>MT8</i>		
<b><i>Catalase</i></b>	<i>Cat</i>	antioxidant defensive protein	

The control gene for real-time qPCR was ubiquitin, the expression of which remained constant in all sea urchin developmental stages. The histograms reported in Figures 5–8 show the relative expression ratios of the analysed genes with respect to control embryos in sea water without PUAs. Only expression values greater than a two-fold difference with respect to the controls were considered significant.

**Figure 5.** The histograms show the differences in the expression levels of thirty one genes followed by real-time qPCR. *Paracentrotus lividus* embryos were grown in the presence of decadienal, heptadienal and octadienal at teratogenic concentrations (1.6, 3.0 and 4.5  $\mu$ M, respectively) and collected at 5 hpf. Data are reported as a fold difference (mean  $\pm$  SD), compared to the control embryos in sea water without aldehydes. Fold differences greater than  $\pm 2$  (see the dotted horizontal guide lines at the values of +2 and -2) were considered significant.

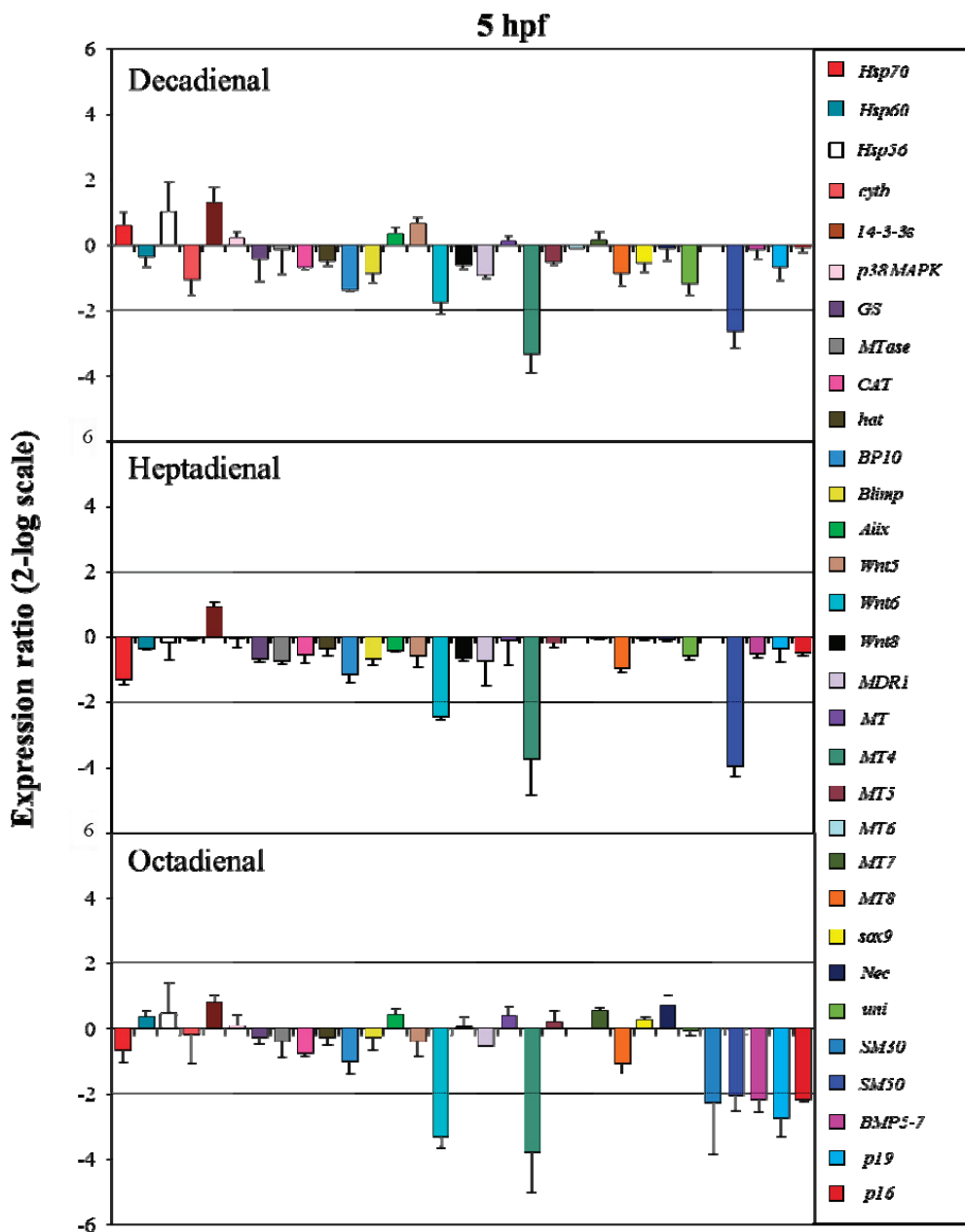


**Figure 6.** The histograms show the differences in the expression levels of thirty one genes followed by real-time qPCR. *Paracentrotus lividus* embryos were grown in the presence of decadienal, heptadienal and octadienal at teratogenic concentrations (1.6, 3.0 and 4.5  $\mu$ M, respectively) and collected at 9 hpf. For more details, see also the legend to Figure 5.

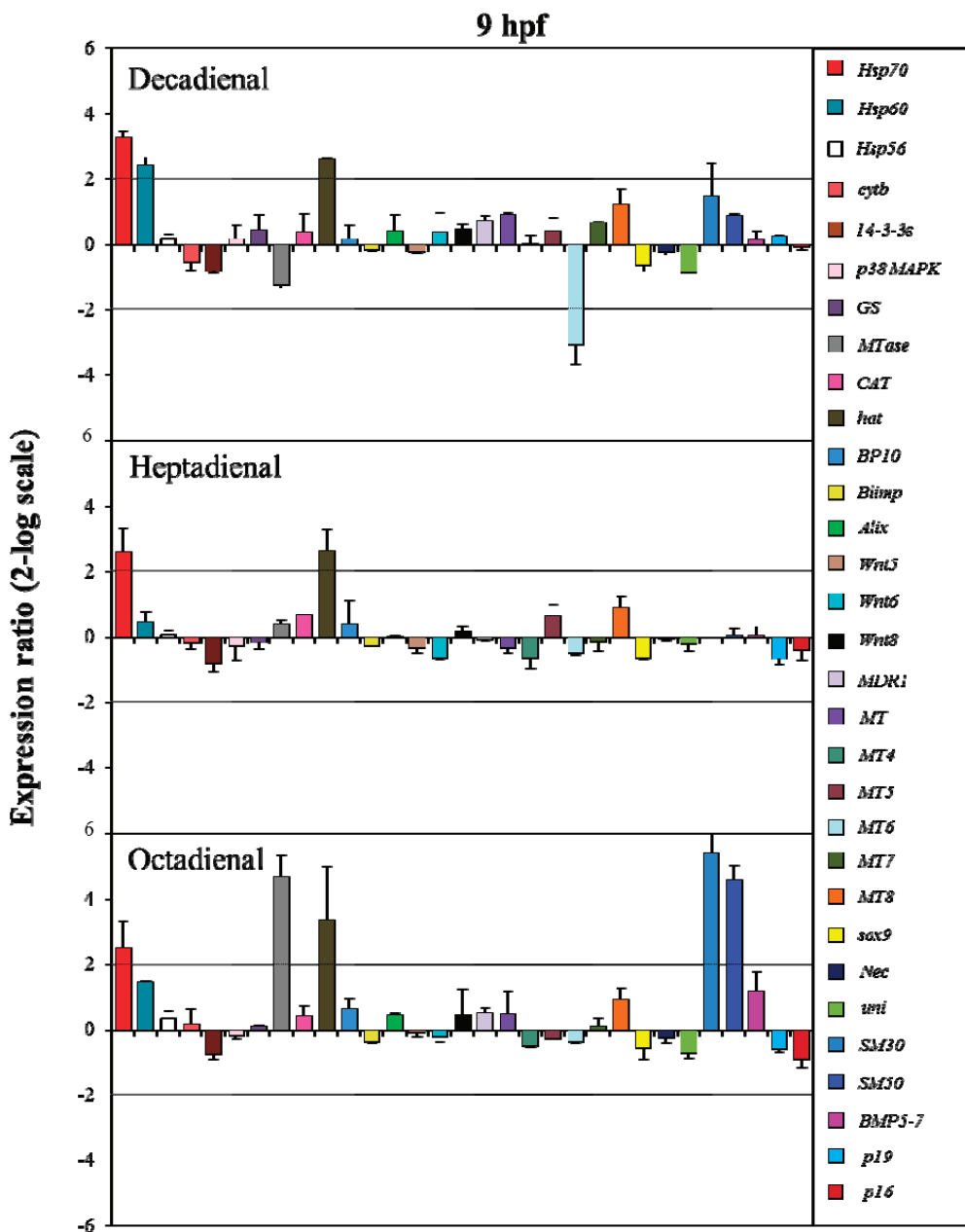


**Figure 7.** The histograms show the differences in the expression levels of thirty one genes followed by real-time qPCR. *Paracentrotus lividus* embryos were grown in the presence of decadienal, heptadienal and octadienal at teratogenic concentrations (1.6, 3.0 and 4.5  $\mu$ M, respectively) and collected at 24 hpf. For more details, see also the legend to Figure 5.

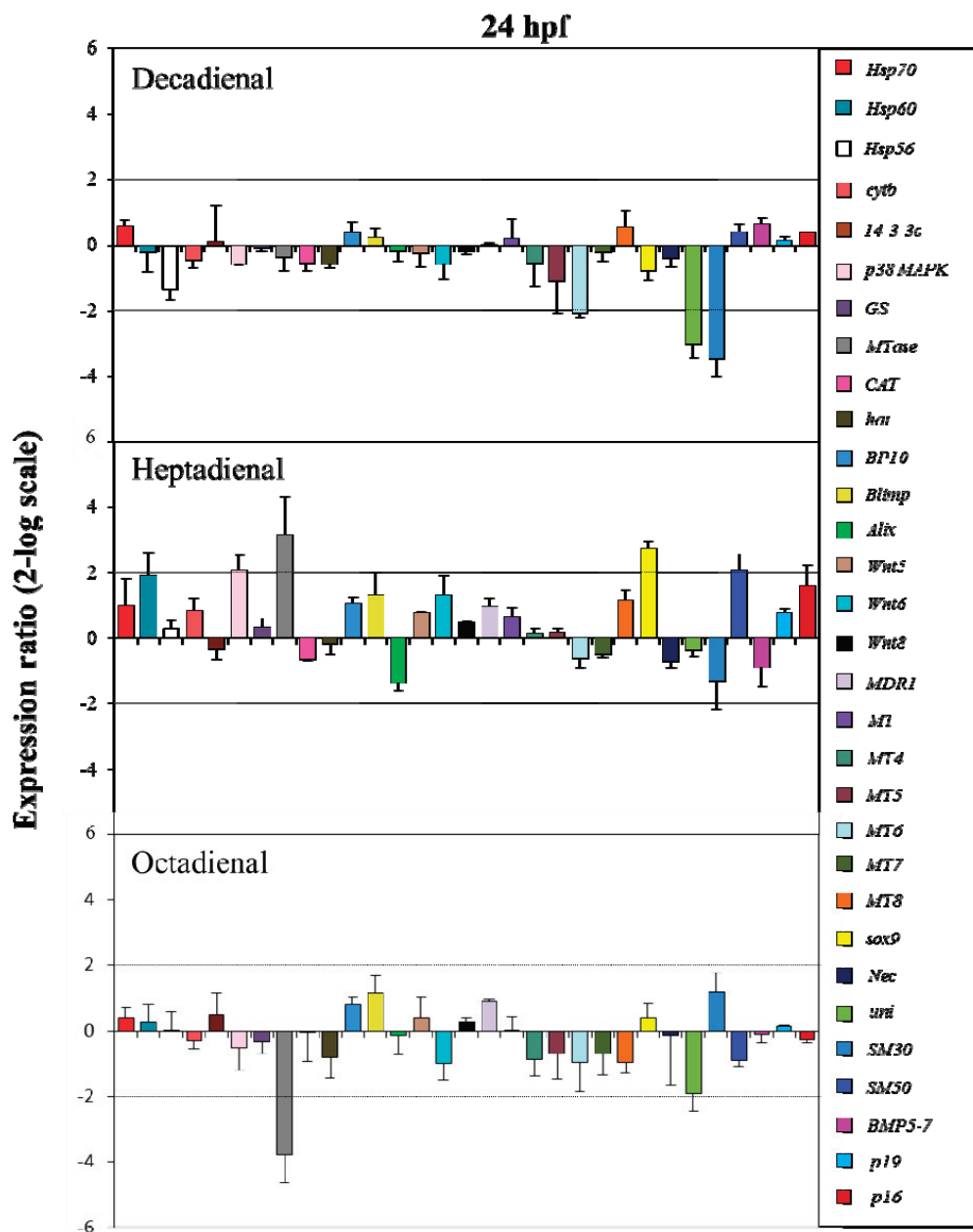
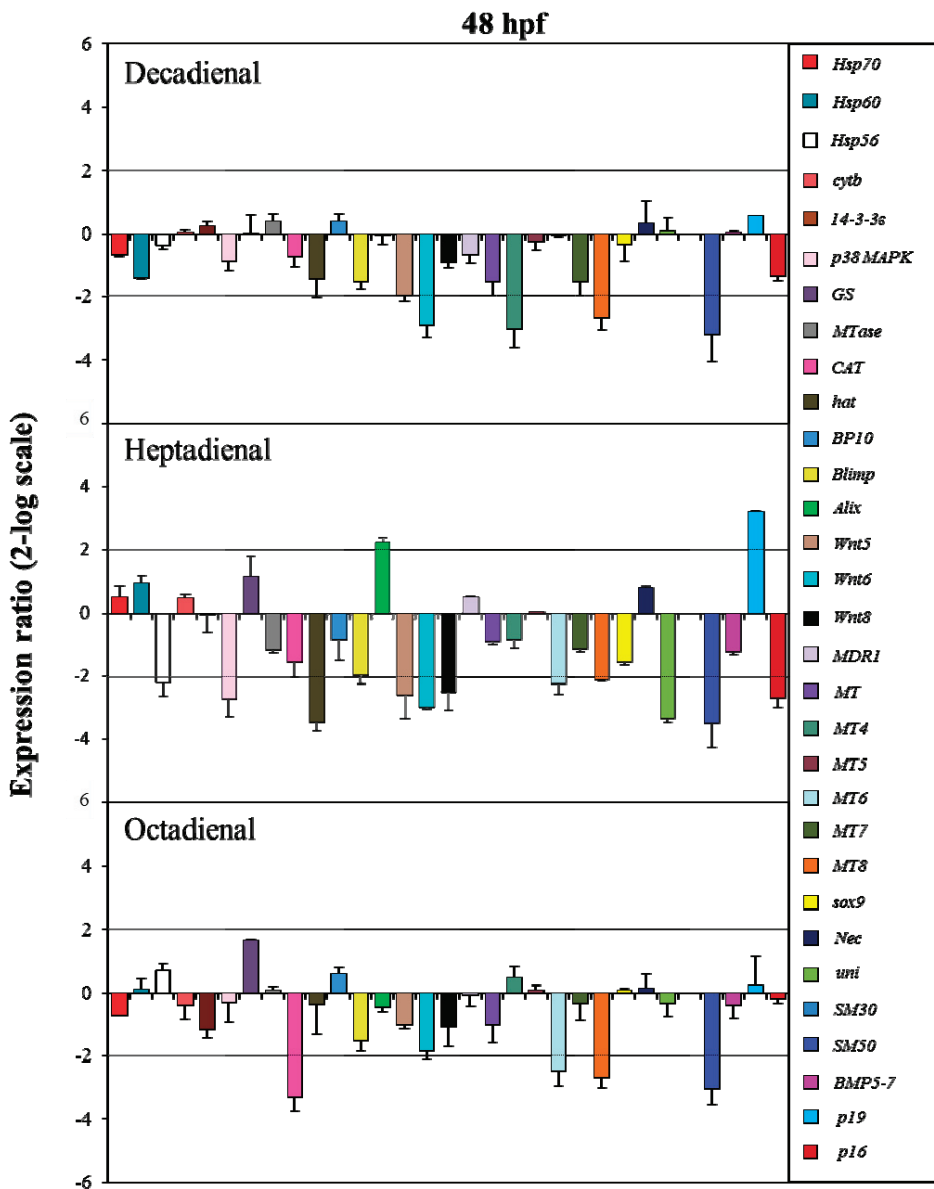




**Figure 8.** The histograms show the differences in the expression levels of thirty one genes followed by real-time qPCR. *Paracentrotus lividus* embryos were grown in the presence of decadienal, heptadienal and octadienal at teratogenic concentrations (1.6, 3.0 and 4.5  $\mu$ M, respectively) and collected at 48 hpf. For more details, see also the legend to Figure 5.



At the early blastula stage (5 hpf; see Figure 5), one metallothionein and one skeletogenic gene, *MT4* and *SM50*, were targeted by all three PUAs, showing a 2.6-, 4.0- and 2.1-fold decrease in expression levels with respect to the control, respectively. The expression level of *Wnt6*, a gene

implicated in the developmental and differentiation processes, was significantly reduced by heptadienal (2.4-fold) and octadienal (3.3-fold) compared to the control. Moreover, at this stage, only octadienal affected the expression levels of four skeletogenic genes, which were downregulated: *SM30*, *Bmp5-7*, *p19* and *p16*, showing a 2.2-, 2.2-, 2.7- and 2.2-fold decrease with respect to the control, respectively.

At the swimming blastula stage (9 hpf; see Figure 6), two genes were upregulated: the stress gene *hsp70* (3.2- for decadienal, 2.6- for heptadienal and 2.5-fold for octadienal) and the protease *hat* (2.6-fold for decadienal and heptadienal; 3.5-fold for octadienal). Moreover, treatment with decadienal showed a 2.4-fold increase in the expression level of the stress gene, *hsp60*, and a three-fold decrease for metallothionein *MT6*. At this stage, octadienal activated one stress gene and two skeletogenic genes: *MTase*, *SM30* and *SM50*, with a 4.7-, 5.4- and 4.6-fold increase with respect to the control.

At the prism stage (24 hpf; see Figure 7), heptadienal and octadienal differentially affected the expression levels of the stress gene, *MTase*. Whereas heptadienal upregulated this gene with a 3.2-fold increase, octadienal downregulated with a 3.8-decrease in expression levels. At this developmental stage, the genes targeted by heptadienal were the stress gene, *p38 MAPK*, and the skeletogenic gene, *SM50*, both of which showed a 2.1-fold increase in expression levels with respect to the control, and the developmental gene, *sox9*, with a 2.7-fold increase. Decadienal affected the expression levels of the metallothionein, *MT6*, and the two skeletogenic genes, *uni* and *SM30*, with a 2.1-, 3- and 3.5-fold downregulation, respectively.

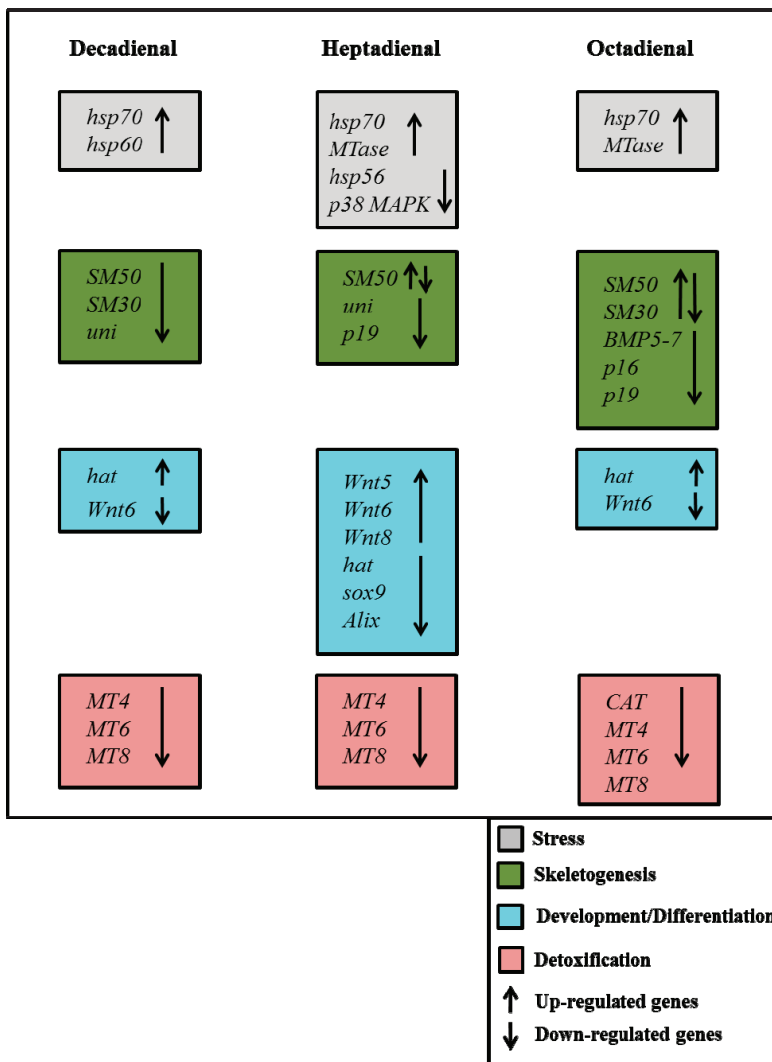
At the pluteus stage (48 hpf; see Figure 8), all three PUAs targeted the metallothionein, *MT8*, and the skeletogenic *SM50* genes. In particular, the expression levels of these genes were all downregulated: *MT8* had a 2.7-fold decrease for decadienal and octadienal and a 2.1-fold decrease for heptadienal; *SM50* a 3.2-, 3.5- and 3.1-fold decrease for decadienal, heptadienal and octadienal, respectively. The metallothionein *MT6* gene was targeted by both heptadienal and octadienal, with a 2.2- and 2.5-fold downregulation of their expression levels, respectively. Decadienal and heptadienal induced a 2.9-fold downregulation of *Wnt6*. Moreover, decadienal also affected the expression level of the metallothionein *MT4* gene, causing a 3-fold decrease with respect to the control. Heptadienal upregulated the expression level of two genes, the developmental gene, *Alix* (2.2-fold), and the skeletogenic gene, *p19* (3.2-fold), and downregulated several genes: two stress genes, *hsp56* and *p38 MAPK* (2.2- and 2.7-fold decrease, respectively); three developmental genes, *hat*, *Wnt5* and *Wnt 8* (3.5, 2.6- and 2.5-fold decrease, respectively); and two skeletogenic genes, *uni* and *p16* (3.4 and 2.7-fold decrease, respectively). Octadienal was the only PUA that downregulated the *CAT* gene (3.3-fold decrease) implicated in detoxification processes.

### 3. Discussion

Our results greatly expand on previous investigations on the stress response to the toxic PUA, decadienal, during sea urchin development [12,13]. Here, we probe more deeply into the effects induced by two ecologically important, but relatively unknown, PUAs, heptadienal and octadienal, which have never been tested before on *P. lividus* embryos from the molecular point of view, in comparison with the better-known PUA, decadienal. Since mainly heptadienal and octadienal are

released when diatom cells are wounded during grazing [5,22,23] or lysed from senescent cells during bloom periods [24], it should be interesting to determine the direct effects of these pure molecules. Until now, very few studies have tested the effects of pure PUAs on copepods [25–27] or reported their effects at the molecular level in copepods [28,29] or the sea urchin, *P. lividus* [12,13]. Sea urchins have been widely used as a sensible bioindicator of biochemical, morphological and physiological changes related to environmental stressors, such as pesticides, essential and heavy metals, ionizing radiations, ocean warming and acidification, metal nanoparticles and natural toxins [30–39].

**Figure 9.** Synopsis of the patterns of up- and down-regulation of different classes of genes in the sea urchin, *Paracentrotus lividus*, in the presence of the PUAs decadienal, heptadienal and octadienal.



An important outcome of this study was the finding that the expression levels of a great number of genes in the sea urchin, *P. lividus*, appears to be modulated by the PUAs, decadienal, heptadienal and octadienal. A synopsis showing the patterns of up- and down-regulation of different classes of genes is shown in Figure 9. These three aldehydes have very few common targets, but specifically affect different classes of genes and at different times of development.

Of the stress genes, the canonical stress gene, *hsp70*, was affected by the three aldehydes at the same development time (at the swimming blastula stage), confirming that embryos were subjected to stress, resulting in the activation of this gene as a first defence system [12]. The other two heat shock proteins, *hsp60* and *hsp56*, were also targeted by PUAs; these genes are reported as a part of a protection system against different stressors enhancing cell survival and normal cellular homeostasis [12,28,40–42].

The possible role of DNA methylation as a molecular marker in response to stress [43] was confirmed by the increase in the expression level of *MTase* after treatment with heptadienal at the prism stage and octadienal at the swimming blastula and prism stages. The expression level of *p38 MAPK*, participating in a signalling cascade in response to different stimuli [33], was affected by heptadienal at the prism and pluteus stages. Very recently, Pinsino *et al.* [44] emphasized the role of p38 MAPK in the regulation of sea urchin embryonic development after exposure to manganese.

Of the genes involved in development and differentiation processes, PUAs affected the expression levels of *hat*, *sox9*, *alix* and *Wnt*. We found an increase in the expression level of *hat*, an early embryonic messenger transiently expressed during the blastula stage [45,46] with all three PUAs. The *sox9* gene was upregulated by heptadienal at the prism stage, suggesting an effect on left-right asymmetry processes [47]. *Alix*, a multifunctional protein involved in different cellular processes, including endocytic membrane trafficking, filamentous-actin remodelling and cytokinesis [15], was upregulated only by heptadienal at the pluteus stage. In sea urchins, this transcript encodes for a maternal protein involved in determination/differentiation events that is expressed from fertilization to the two-cell embryo stage. In sea urchin eggs, the gene is localized throughout the cytoplasm with a punctuated pattern, and soon after fertilization, it accumulates in the cytosol and in microvilli-like protrusions.

Of the genes belonging to the canonical Wnt pathway, *Wnt6* was targeted by all three PUAs that induced a decrease in the expression levels of this gene. This represents a very interesting result, supporting the essential role of *Wnt6* to in triggering endoderm specification [18]. In fact, heptadienal and octadienal affected the expression level of this gene at 5 hpf, when the differentiation of blastomeres occurs and cell fates in specific embryonic territories are defined. Heptadienal was also able to determine a decrease in the expression levels of two other genes of the Wnt pathway: *Wnt5*, which acts as a short-range inter-blastomere signal, activating cells in the ectoderm, integrating different types of positional information from both the primary and secondary embryonic axes in order to correctly locate the production site of signals needed for skeleton formation to take place [17]; and *Wnt8* is associated with cell fate determination through canonical signalling pathways and is important for the morphogenetic movement of primary mesenchyme cells [19].

All genes involved in skeletogenesis were downregulated by PUAs, except for the *Nec* gene. *SM30*, *SM50* and *Uni* were previously found to be target genes for decadienal [13]. Octadienal downregulated the expression level of *BMP5-7*, a gene family that is reported as being positive regulators of oral and aboral ectoderm specification [17]. *P19* was upregulated by heptadienal, but was downregulated by octadienal together with *p16*; these are two small acidic proteins involved in the formation of the biomineralised skeleton of sea urchin embryos and adults [14].

We also analysed eight genes involved in detoxification processes. In particular, of six metallothioneins that were analysed in this work, only the expression levels of three genes appeared to be perturbed by PUAs. Ragusa *et al.* [21] reported that two metallothionein genes (*MT7* and *MT8*) appeared to be constitutively expressed and upregulated upon cadmium treatment, whereas other genes (*MT4*, *MT5* and *MT6*) were not transcribed in control embryos and were specifically activated in response to cadmium treatment. Our results show the down-expression of the induced metallothioneins, *MT4* and *MT6*, and the constitutive one, *MT8*, at a later stage of development (48 hpf). The induction of other metallothioneins may require exposure to higher concentrations of PUAs or may depend on the nature of the stress agent, considering that metallothioneins seem to respond very specifically to heavy metal exposure. The gene, *MDR1*, belongs to ATP-binding cassette transporters, which are activated by sub-lethal doses of specific contaminants (such as oxybenzone, mercuric chloride and tributyltin) during embryonic development (from the zygote to the blastula stage) of sea urchins [20]. Moreover, sea urchin embryos utilize it in cell signalling and lysosomal and mainly mitochondrial homeostasis [48]. The expression level of this gene was not affected by PUA exposure, probably due to the low levels of exposure. In fact, we demonstrated the loss of mitochondrial functionality only at higher concentrations of decadienal in a previous study [12]. The down-expression of the *CAT* gene only in the case of octadienal suggests that a specific detoxification system could be activated in sea urchins after exposure to this PUA.

These molecular results are in accordance with our morphological results that revealed that the majority of malformations affected the skeleton and the plan of the development and differentiation of sea urchin embryos, as reported in Figure 1. In fact, several genes belonging to the skeletogenic, developmental and differentiation classes were affected by PUAs. Even if, according to our morphological analyses, octadienal seems to be the weakest of the three aldehydes, our study on gene expression levels reveals that this aldehyde affects a very early stage of embryonic development. In fact, octadienal differentially affected the expression levels of five skeletogenic genes at the early blastula stage compared to the other aldehydes. These data are also in accordance with our post-recovery experiments, in which we hypothesized that octadienal could have a different mechanism of action, because embryos cannot recover in the presence of this aldehyde at the highest concentration. This different behaviour could be correlated with the downregulation of skeletogenic genes at an early stage of embryo development, which does not give embryos the chance to recover. The strongest molecular effects seem to occur after treatment with heptadienal, but at a later stage of development. In fact, at 48 hpf (pluteus stage), heptadienal affected the expression levels of thirteen genes. Taken together, these results suggest that although treatment

with the three aldehydes did not induce any visible differences at the morphological level, they affected different physiological processes.

The genes identified in this work as targets for PUAs may represent possible biomarkers to detect exposure to pollutants that may include microbial products, heavy metals and phytotoxins. More generally, the new genes analysed in this work can be considered as an additional part of the stress surveillance system or chemical defense of the sea urchin, as proposed in Marrone *et al.* [13], affording protection from environmental xenobiotics.

## 4. Experimental Section

### 4.1. Ethics Statement

*Paracentrotus lividus* (Lamarck) sea urchins were collected from a location that is not privately-owned or protected in any way, according to Italian legislation of the Marina Mercantile (Decreto del Presidente della Repubblica DPR 1639/68, 09/19/1980 confirmed on 01/10/2000). The field studies did not involve endangered or protected species. All animal procedures were in compliance with the guidelines of the European Union (Directive 609/86).

### 4.2. Gamete Collection, Embryo Culture, Exposure to Aldehydes and Morphological Analysis

Adult sea urchins of the species, *P. lividus*, were collected during the breeding season by scuba-diving in the Gulf of Naples, transported in an insulated box to the laboratory within 1 h after collection and maintained in tanks with circulating sea water until testing. Sea urchins were injected with 2 M KCl through the peribuccal membrane to obtain the emission of gametes. Eggs were washed with filtered sea water (FSW) and kept in FSW until use. Concentrated sperm was collected, dried and kept undiluted at +4 °C until use.

Before fertilization, eggs were incubated at room temperature for 10 min in the presence of different concentrations of the three PUAs: *2-trans,4-trans*-decadienal at 1.0, 1.3, 1.6, 2.0, 2.3 µM (similar to the concentrations tested in reference [13]); *2-trans,4-trans*-heptadienal at 1.0, 2.0, 3.0, 3.5, 4.0, 4.5, 5.0, 5.5, 6.0 µM; *2-trans,4-trans*-octadienal (Sigma-Aldrich, Milan, Italy) at 2.0, 3.0, 4.0, 4.5, 5.0, 6.0, 7.0, 8.0, 9.0 µM; and the controls were in FSW without PUAs.

Eggs were fertilized utilising sperm-to-egg ratios of 100:1 for both controls and treated embryos. Fertilized eggs were kept at 20 °C in a controlled temperature chamber on a 12 h:12 h light:dark cycle. PUAs were diluted in methanol, considering a methanol to FSW ratio of 10 µL:1 mL, so as to avoid interference with embryo development. Controls were also performed in FSW and in FSW in the presence of methanol.

Experiments were conducted in triplicate using three egg groups collected from three different females. After 48 h of incubation, morphological malformations were determined for at least 200 plutei using a light microscope (Zeiss Axiovert 135TV, Carl Zeiss, Jena, Germany) in comparison to control embryos in FSW without PUAs.

#### 4.3. Post-Recovery Experiments

The procedure for the treatments with the three PUAs was the same as reported above. For each PUA, three concentrations were tested according to the percentage of abnormal plutei recorded during previous tests. The lowest concentrations were those inducing teratogenesis: 1.6  $\mu\text{M}$  for decadienal, 3.0  $\mu\text{M}$  for heptadienal and 4.5  $\mu\text{M}$  for octadienal, all three of which induced the production of about 35% abnormal plutei that were also used for molecular experiments (see below). We then tested the concentrations that induced the production of about 60% and 75% of abnormal plutei, so as to have comparable results with the three PUAs. Embryos were washed twice at different development times: 40 min and 2, 5, 9 and 24 h post-fertilization (hpf). Embryos were grown to the pluteus stage. The number of abnormal embryos was evaluated by fixing embryos in formaldehyde (4% in FSW) and counting under the light microscope.

One-way ANOVA with Tukey's post-hoc test was performed using GraphPad Prism version 4.00 for Windows (GraphPad Software, San Diego, CA, USA).

#### 4.4. Addition of PUAs after Fertilization

Eggs were fertilized without PUAs, according to the procedure reported above. The development of embryos was followed by microscopic examination for different development times after fertilization (10 min pf, 40 min pf, 2, 3, 5 and 8 hpf). PUAs were then added at the same concentrations used for post-recovery experiments. As controls, PUAs were also added 10 min before fertilization. The number of abnormal plutei was evaluated from fixed embryos. One-way ANOVA with Tukey's post-hoc test was performed using GraphPad Prism version 4.00 for Windows (GraphPad Software, San Diego, CA, USA).

#### 4.5. RNA Extraction and cDNA Synthesis

About 30,000 eggs in 200 mL of FSW were treated for 10 min with the three PUAs at the following concentrations: 1.6  $\mu\text{M}$  for decadienal (as in [13]); 3.0  $\mu\text{M}$  for heptadienal; and 4.5  $\mu\text{M}$  for octadienal. Eggs were then fertilized and collected at different developmental times. Samples were collected at 5, 9, 24 and 48 hpf by centrifugation at 1800 relative centrifugal force for 10 min in a swing out rotor at 4 °C. The pellet was washed with phosphate buffered saline and then frozen in liquid nitrogen and kept at -80 °C.

Total RNA was extracted from each developmental stage using TRIzol (Invitrogen, Life Technologies, Carlsbad, CA, USA) according to the manufacturer's instructions. Extraction with chloroform/isoamyl alcohol (24:1) was performed following RNA precipitation by addition of glycogen and isopropyl alcohol. Contaminating DNA was degraded by treating each sample with a DNase RNase-free kit (Roche, Milan, Italy) according to the manufacturer's instructions. The amount of total RNA extracted was estimated by the absorbance at 260 nm and the purity by 260/280 and 260/230 nm ratios, by a NanoDrop spectrophotometer (ND-1000 UV-Vis Spectrophotometer; NanoDrop Technologies, Wilmington, DE, USA). The integrity of RNA was evaluated by agarose gel electrophoresis. Intact rRNA subunits (28S and 18S) were observed on the gel indicating minimal degradation of the RNA. For each sample, 600 ng of total RNA

extracted was retrotranscribed with an iScript™ cDNA Synthesis kit (Bio-Rad, Milan, Italy), following the manufacturer's instructions. Synthetized cDNA was used in real-time qPCR experiments without dilution.

To evaluate the efficiency of cDNA synthesis, a PCR was performed with primers of the reference gene, ubiquitin. The reaction was carried out on the C1000 Touch Thermal Cycler GeneAmp PCR System 9700 (Applied Biosystem, Monza, Italy) in a 30  $\mu$ L final volume with 3  $\mu$ L 10 $\times$  PCR reaction buffer (Roche, Milan, Italy), 3  $\mu$ L 10 $\times$  2 mM dNTP, 1  $\mu$ L 5 U/ $\mu$ L Taq (Roche, Milan, Italy), 100 ng/ $\mu$ L of each oligo, template cDNA and nuclease free water to 30  $\mu$ L. The PCR program consisted of a denaturation step at 95 °C for 5 min, 35 cycles at 95 °C for 45 s, 60 °C for 1 min and 72 °C for 30 s and a final extension step at 72 °C for 10 min.

#### 4.6. Gene Expression by Real-Time qPCR

For all real-time qPCR experiments, the data from each cDNA sample were normalized using ubiquitin mRNA as the endogenous control level, the level of which remained relatively constant in all developmental stages examined according to Nemer *et al.* ([49]; for more details, see Romano *et al.* [12]). The expression level of seventeen genes, previously analysed by real-time qPCR in Marrone *et al.* [13], were analysed together with fourteen new genes (see Table 1): Pl-p19 (*p19*), Pl-p16 (*p16*; [14]), metallothionein 4 (*MT4*; [21]), metallothionein 5 (*MT5*; [21]), metallothionein 6 (*MT6*; [21]), metallothionein 7 (*MT7*; [21]), metallothionein 8 (*MT8*; [21]), blimp (*Blimp*; [16]), ALG-2 interacting protein X/1 (*Alix*; [15]), multi-drug resistance protein 1 (*MDR 1*), Wnt5 (*Wnt5*), Wnt6 (*Wnt6*) and Wnt8 (*Wnt8*). We also analysed the catalase gene (*CAT*); since the *CAT* sequence of *P. lividus* is not available, a 156-bp fragment was amplified using specific primers for this gene from *Strongylocentrotus purpuratus*. The amplified fragment using a Taq High Fidelity PCR System (Roche, Milan, Italy) was purified from agarose gel using the QIAquick Gel Extraction kit (Qiagen, Milan, Italy), and the specificity of the PCR product for catalase was checked by DNA sequencing.

Gene sequences were retrieved from NCBI [50]. For each gene, specific primers were designed on the basis of nucleotide sequences of *P. lividus* (see Table 2); primers reported in the indicated references were used for six genes. The same procedure for the amplified fragments used for *CAT* was applied for these genes to check for the specificity of the amplified products.

The specificity of amplification reactions was verified by melting curve analysis. The efficiency of each primer pair was calculated according to standard method curves using the equation  $E=10^{-1/\text{slope}}$ . Five serial dilutions were set up to determine Ct values and reaction efficiencies for all primer pairs. Standard curves were generated for each oligonucleotide pair using Ct values *versus* the logarithm of each dilution factor. PCR efficiencies were calculated for control and target genes and were found to be 2. Diluted cDNA was used as a template in a reaction containing a final concentration of 0.3 mM for each primer and 1 $\times$  FastStart SYBR Green master mix (total volume of 10  $\mu$ L) (Applied Biosystems, Monza, Italy). PCR amplifications were performed in a ViiATM7 Real Time PCR System (Applied Biosystems, Monza, Italy) thermal cycler using the following thermal profile: 95 °C for 10 min, one cycle for cDNA denaturation; 95 °C for 15 s and 60 °C for 1 min, 40 cycles for amplification; 72 °C for 5 min, one cycle for final elongation; one cycle for



melting curve analysis (from 60 °C to 95 °C) to verify the presence of a single product. Each assay included a no-template control for each primer pair. To capture intra-assay variability, all real-time qPCR reactions were carried out in triplicate. Fluorescence was measured using ViiATM7 software (Applied Biosystems, Monza, Italy). The expression of each gene was analysed and internally normalized against ubiquitin using REST software (Relative Expression Software Tool, Weihenstephan, Germany) based on the Pfaffl method [51,52]. Relative expression ratios above two cycles were considered significant. Experiments were repeated at least twice. Statistical analysis was performed using GraphPad Prism version 4.00 for Windows (GraphPad Software, San Diego, CA, USA).

**Table 2.** Gene name, acronym, accession numbers, primer sequences and lengths of PCR amplified fragments are reported for the genes analysed. For the genes that have a reference, the lengths of PCR fragments were not reported.

Gene Name	Acronym	Accession Number	Primer	Sequence (5'→3')	PCR Fragment (bp)
<i>Pl-p19</i>	<i>p19</i>	FR693764	Pl_P19_F1 Pl_P19_R1	GACAAGCTCGACATCAACAAG CTGGAGTCGATGCTGCATCATG	205
<i>Pl-p16</i> [14]	<i>p16</i>	FR693763	Pl-p16 For Pl-p16 Rev	CGGGCAGCGATGACTCA AAATGCCATACCGCTCTTCTGT	104
<i>Metallothionein 4</i> [21]	<i>MT4</i>		MT4 For MT4 Rev	GCTCAAAATCTTCAACATGGCTAATGA AGCACTTTCCAGTTTCACAACAAGC	
<i>Metallothionein 5</i> [21]	<i>MT5</i>		MT5 For MT5 Rev	CGACTTTAGCTCAAATTCATCACCATG TCCACAGCATTACCATCCTTGC	
<i>Metallothionein 6</i> [21]	<i>MT6</i>		MT6 For MT6 Rev	CACGATTGTGCTCAATCCTTCAT TTTGTGCATGATGTCCACAGC	
<i>Metallothionein 7</i> [21]	<i>MT7</i>		MT7 For MT7 Rev	CGTCAAGAGATCAAAATCATCAACCA ACAGCACTCGCCAGTAATACAGCAC	

Table 2. Cont.

<i>Metallothionein 8</i> [21]	<i>MT8</i>		MT8 For MT8 Rev	GATGGTTGTCGTCGCTCCTAACA TCAAGAAAGGCTGGTATCAAATCTGAC	
<i>Blimp</i>	<i>Blimp</i>	HQ322503	PI_Blimp1_For PI_Blimp1_Rev	CTGTCTACTCCATGCCGTCC GCCTCCTGCTTCAGATCAGC	161
<i>ALG-2 interacting protein X/1</i> [15]	<i>Alix</i>	HE646599	AL1500for AL1610rev	TACCAGACCATTCTCAACAAT TGCTATTCCGCTTCGCTTTT	110
<i>Multi drug resistance protein 1</i>	<i>MDR1</i>	JQ793791	PI_MDR1_F2 PI_MDR1_Rev	GTCAAGTACTCAATGGGGTC CGGATGTCAATGCCATCAATC	158
<i>Wnt 5</i>	<i>Wnt5</i>	HM449806	PI_Wnt5_F2 PI_Wnt5_Rev	CACCCAGCCCCTGTGCAGTG CTGCAGTCCACCTCCTATTC	135
<i>Wnt 6</i>	<i>Wnt6</i>	HQ322504	PI_Wnt6_For PI_Wnt6_For	CGAATCTGCCGACGATCACG GCATTGTCGTACAGTTCACC	164
<i>Wnt 8</i>	<i>Wnt8</i>	HM449816	PI_Wnt8_For PI_Wnt8_For	CTGTAAGTGTTCATGGCGTCTC GAGCGAATCGGAGATGACGG	197
<i>Catalase</i>	<i>CAT</i>	SPU_000281.1	Sp-CAT_F1 Sp-CAT_R1	GACTTCGTCTTCACCGACGAG GACTCAAAGGGTGCAGCCTTG	156

## 5. Conclusions

In conclusion, our findings provide molecular evidence for the toxic effects of diatom-derived PUAs and propose novel tools for understanding the cellular mechanisms of the response to aldehyde exposure in benthic organisms. Sea urchins may come in contact with diatom PUAs in the field at the end of a bloom, with the mass sinking of diatoms to the sediment, which represents a major source of organic matter for benthic systems [53]. This is of considerable ecological relevance given the importance of diatom blooms in nutrient-rich aquatic environments. Moreover, our results may be useful in understanding how changes in gene expression levels may be used as an early indicator of stressful conditions in the marine environment. Generally, these studies are fundamental to our understanding of how marine organisms attempt to defend themselves from environmental toxicants, benefitting from the protection provided by an integrated network of genes.

## Acknowledgments

We thank the Molecular Biology Service for providing primers for PCR experiments and for PCR product sequencing. We also thank the Fishing Service of our institute for providing sea urchins. Many thanks are also due to Davide Caramiello of the Marine Resources for Research

Service for his technical support in sea urchin maintenance and gamete collection. Stefano Varrella has been supported by a Stazione Zoologica Anton Dohrn PhD fellowship.

### Author Contributions

M.C., G.R., A.I. conceived and designed the experiments. S.V., N.R., M.C., G.R. performed the experiments. M.C., G.R., A.I., M.B., S.V. analyzed the data. M.C., G.R., A.I. contributed reagents/materials/analysis tools. M.C., G.R., A.I., M.B., S.V. wrote the paper.

### Conflicts of Interest

The authors declare no conflict of interest.

### References

1. Caldwell, G.S. The Influence of Bioactive Oxylipins from Marine Diatoms on Invertebrate Reproduction and Development. *Mar. Drugs* **2009**, *7*, 367–400.
2. Ianora, A.; Miralto, A. Toxicogenic effects of diatoms on grazers, phytoplankton and other microbes: A review. *Ecotoxicology* **2010**, *19*, 493–511.
3. Miralto, A.; Barone, G.; Romano, G.; Poulet, S.A.; Ianora, A.; Russo, G.L.; Buttino, I.; Mazzarella, G.; Laabir, M.; Cabrini, M.; *et al.* The insidious effect of diatoms on copepod reproduction. *Nature* **1999**, *402*, 173–176.
4. D'Ippolito, G.; Iadicicco, I.; Romano, G.; Fontana, A.; Iadicicco, O. Detection of short-chain aldehydes in marine organisms: The diatom *Thalassiosira rotula*. *Tetrahedron Lett.* **2002**, *43*, 6137–6140.
5. Wichard, T.; Poulet, S.A.; Halsband-Lenk, C.; Albaina, A.; Harris, R.; Liu, D.; Pohnert, G. Survey of the chemical defence potential of diatoms: Screening of fifty species for  $\alpha,\beta,\gamma,\delta$ -unsaturated aldehydes. *J. Chem. Ecol.* **2005**, *31*, 949–958.
6. Wendel, T.; Juttner, F. Lipxygenase-mediated formation of hydrocarbons and unsaturated aldehydes in freshwater diatoms. *Phytochemistry* **1996**, *41*, 1445–1449.
7. Caldwell, G.S.; Olive, P.J.W.; Bentley, M.G. Inhibition of embryonic development and fertilization in broadcast spawning marine invertebrates by water soluble diatom extracts and the diatom toxin 2-*trans*,4-*trans* decadienal. *Aquat. Toxicol.* **2002**, *60*, 123–137.
8. Caldwell, G.S.; Bentley, M.G.; Olive, P.J.W. First evidence of sperm motility inhibition by the diatom aldehyde 2*E*,4*E*-decadienal. *Mar. Ecol. Prog. Ser.* **2004**, *273*, 97–108.
9. Romano, G.; Russo, G.L.; Buttino, I.; Ianora, A.; Miralto, A. A marine diatom-derived aldehyde induces apoptosis in copepod and sea urchin embryos. *J. Exp. Biol.* **2003**, *206*, 3487–3494.
10. Hansen, E.; Even, Y.; Genevieve, A.M. The alpha,beta,gamma,delta-unsaturated aldehyde 2-*trans*-4-*trans*-decadienal disturbs DNA replication and mitotic events in early sea urchin embryos. *Toxicol. Sci.* **2004**, *81*, 190–197.
11. Romano, G.; Miralto, A.; Ianora, A. Teratogenic Effects of diatom metabolites on sea urchin *Paracentrotus lividus* embryos. *Mar. Drugs* **2010**, *8*, 950–967.

12. Romano, G.; Costantini, M.; Buttino, I.; Ianora, A.; Palumbo, A. Nitric oxide mediates the stress response induced by diatom aldehydes in the sea urchin *Paracentrotus lividus*. *PLoS One* **2011**, *6*, e25980.
13. Marrone, V.; Piscopo, M.; Romano, G.; Ianora, A.; Palumbo, A.; Costantini, M. Defensome against toxic diatom aldehydes in the sea urchin *Paracentrotus lividus*. *PLoS One* **2012**, *7*, e31750.
14. Costa, C.; Karakostis, K.; Zito, F.; Matranga, V. Phylogenetic analysis and expression patterns of p16 and p19 in *Paracentrotus lividus* embryos. *Dev. Genes Evol.* **2012**, *222*, 245–251.
15. Romancino, D.P.; Anello, L.; Morici, G.; d’Azzo, A.; Bongiovanni, A.; Di Bernardo, M. Identification and characterization of PIAlix, the Alix homologue from the Mediterranean sea urchin *Paracentrotus lividus*. *Dev. Growth Differ.* **2013**, *55*, 237–246.
16. Lhomond, G.; McClay, D.R.; Gache, C.; Croce, J.C. Frizzled 1/2/7 signaling directs  $\beta$ -catenin nuclearisation and initiates andoderm specification in macromeres during sea urchin embryogenesis. *Development* **2012**, *139*, 816–825.
17. McIntyre, D.C.; Seay, N.W.; Croce, J.C.; McClay, D.R. Short-range Wnt5 signaling initiates specification of sea urchin posterior ectoderm. *Development* **2013**, *140*, 4881–4889.
18. Croce, J.; Range, R.; Wu, S.Y.; Miranda, E.; Lhomond, G.; Peng, J.C.; Lepage, T.; McClay, D.R. Wnt6 activates endoderm in the sea urchin gene regulatory network. *Development* **2011**, *138*, 3297–3306.
19. Hammond, L.M.; Hofmann, G.E. Early developmental gene regulation in *Strongylocentrotus purpuratus* embryos in response to elevated CO<sub>2</sub> seawater conditions. *J. Exp. Biol.* **2012**, *215*, 2445–2454.
20. Bošnjak, I.; Zaja, R.; Klobučar, R.S.; Sver, L.; Franekić, J.; Smital, T. Identification of ABC transporter genes in gonad tissue of two mediterranean sea urchin species: Black, *Arbacia lixula* L., and rocky, *Paracentrotus lividus* L. *Bull. Environ. Contam. Toxicol.* **2013**, *91*, 415–419.
21. Ragusa, M.A.; Costa, S.; Gianguzza, M.; Roccheri, M.C.; Gianguzza, F. Effects of cadmium exposure on sea urchin development assessed by SSH and RT-qPCR: Metallothionein genes and their differential induction. *Mol. Biol. Rep.* **2013**, *40*, 2157–2167.
22. Pohnert, G. Wound-activated chemical defense in unicellular planktonic algae. *Angew. Chem. Int. Ed.* **2000**, *39*, 4352–4354.
23. Wichard, T.; Gerecht, A.; Boersma, M.; Poulet, S.A.; Wiltshire, K.; Pohnert, G. Lipid and fatty acid composition of diatoms revisited: Rapid wound-activated change of food quality parameters influences herbivorous copepod reproductive success. *Chembiochem* **2007**, *8*, 1146–1153.
24. Vidoudez, C.; Nejstgaard, J.C.; Jakobsen, H.H.; Pohnert, G. Dynamics of dissolved and particulate polyunsaturated aldehydes in mesocosms inoculated with different densities of the diatom *Skeletonema marinoi*. *Mar. Drugs* **2011**, *9*, 345–358.
25. Buttino, I.; De Rosa, G.; Carotenuto, Y.; Mazzella, M.; Ianora, A.; Esposito, F.; Vitiello, V.; Quaglia, F.; La Rotonda, M.I.; Miralto, A. Aldehyde-encapsulating liposomes impair marine grazer survivorship. *J. Exp. Biol.* **2008**, *211*, 1426–1433.

26. Ceballos, S.; Ianora, A. Different diatoms induce contrasting effects on the reproductive success of the copepod *Temora stylifera*. *J. Exp. Mar. Biol. Ecol.* **2003**, *294*, 189–202.
27. Taylor, R.L.; Caldwell, G.S.; Dunstan, H.J.; Bentley, M.G. Short-term impacts of polyunsaturated aldehyde-producing diatoms on the harpacticoid copepod, *Tisbe holothuriae*. *J. Exp. Mar. Biol. Ecol.* **2007**, *341*, 60–69.
28. Lauritano, C.; Borra, M.; Carotenuto, Y.; Biffali, E.; Miralto, A.; Procaccini, G.; Ianora, A. First molecular evidence of diatom effects in the copepod *Calanus helgolandicus*. *J. Exp. Mar. Biol. Ecol.* **2011**, *404*, 79–86.
29. Lauritano, C.; Carotenuto, Y.; Miralto, A.; Procaccini, G.; Ianora, A. Copepod population-specific response to a toxic diatom diet. *PLoS One* **2012**, *7*, e47262.
30. Aluigi, M.G.; Angelini, C.; Corte, G.; Falugi, C. The sea urchin, *Paracentrotus lividus*, embryo as a “bioethical” model for neurodevelopmental toxicity testing: Effects of diazinon on the intracellular distribution of OTX2-like proteins. *Cell Biol. Toxicol.* **2008**, *24*, 587–601.
31. Pinsino, A.; Matranga, V.; Trinchella, F.; Roccheri, M.C. Sea urchin embryos as an *in vivo* model for the assessment of manganese toxicity: Developmental and stress response effects. *Ecotoxicology* **2010**, *19*, 555–562.
32. Russo, R.; Bonaventura, R.; Zito, F.; Schroder, H.C.; Muller, I.; Muller, W.E.G.; Matranga, V. Stress to cadmium monitored by metallothionein gene induction in *Paracentrotus lividus* embryos. *Cell Stress Chaperones* **2003**, *8*, 232–241.
33. Bonaventura, R.; Poma, V.; Costa, C.; Matranga, V. UVB radiation prevents skeleton growth and stimulates the expression of stress markers in sea urchin embryos. *Biochem. Biophys. Res. Commun.* **2005**, *328*, 150–157.
34. Bonaventura, R.; Zito, F.; Costa, C.; Giarrusso, S.; Celi, F.; Matranga, V. Stress response gene activation protects sea urchin embryos exposed to X-rays. *Cell Stress Chaperones* **2011**, *16*, 681–687.
35. Lister, K.N.; Lamare, M.D.; Burrirt, D.J. Sea ice protects the embryos of the Antarctic sea urchin *Sterechinus neumayeri* from oxidative damage due to naturally enhanced levels of UV-B radiation. *J. Exp. Biol.* **2010**, *213*, 1967–1975.
36. Lister, K.N.; Lamare, M.D.; Burrirt, D.J. Oxidative damage in response to natural levels of UV-B radiation in larvae of the tropical sea urchin *Tripneustes gratilla*. *Photochem. Photobiol.* **2010**, *86*, 1091–1098.
37. Adams, N.L.; Campanale, J.P.; Foltz, K.R. Proteomic responses of sea urchin embryos to stressful ultraviolet radiation. *Integr. Comp. Biol.* **2012**, *52*, 665–680.
38. Byrne, M. Global change ecotoxicology: Identification of early life history bottlenecks in marine invertebrates, variable species responses and variable experimental approaches. *Mar. Environ. Res.* **2012**, *76*, 3–15.
39. Falugi, C.; Aluigi, M.G.; Chiantore, M.C.; Privitera, D.; Ramoino, P.; Gatti, M.A.; Fabrizi, A.; Pinsino, A.; Matranga, V. Toxicity of metal oxide nanoparticles in immune cells of the sea urchin. *Mar. Environ. Res.* **2012**, *76*, 114–121.

40. Roccheri, M.C.; Agnello, M.; Bonaventura, R.; Matranga, V. Cadmium induces the expression of specific stress proteins in sea urchin embryos. *Biochem. Biophys. Res. Commun.* **2004**, *321*, 80–87.
41. Diller, K.R. Stress protein expression kinetics. *Annu. Rev. Biomed. Eng.* **2006**, *8*, 403–424.
42. Rhee, J.-S.; Raisuddin, S.; Lee, K.-W.; Seo, J.S.; Ki, J.-S.; Kim, I.-C.; Park, H.G.; Lee, J.-S. Heat shock protein (Hsp) gene responses of the intertidal copepod *Tigriopus japonicus* to environmental toxicants. *Comp. Biochem. Physiol. C Toxicol. Pharmacol.* **2009**, *149*, 104–112.
43. Campos, A.C.E.; Molognoni, F.; Melo, F.H.M.; Galdieri, L.C.; Carneiro, C.R.W.; D’Almeida, V.; Correa, M.; Jasiulionis, M.G. Oxidative stress modulates DNA methylation during melanocyte anchorage blockade associated with malignant transformation. *Neoplasia* **2007**, *9*, 1111–1121.
44. Pinsino, A.; Roccheri, M.C.; Matranga, V. Manganese overload affects p38 MAPK phosphorylation and metalloproteinase activity during sea urchin embryonic development. *Mar. Environ. Res.* **2014**, *93*, 64–69.
45. Lepage, T.; Sardet, C.; Gache, C. Spatial expression of the hatching enzyme gene in the sea urchin embryo. *Dev. Biol.* **1992**, *150*, 23–32.
46. Ghiglione, C.; Lhomond, G.; Lepage, T.; Gache, C. Structure of the sea urchin hatching enzyme gene. *Eur. J. Biochem.* **1994**, *219*, 845–854.
47. Duboc, V.; Röttinger, E.; Lapraz, F.; Besnardeau, L.; Lepage, T. Left-right asymmetry in the sea urchin embryo is regulated by nodal signaling on the right side. *Dev. Cell* **2005**, *9*, 147–158.
48. Shipp, L.E.; Hamdoun, A. ATP-binding cassette (ABC) transporter expression and localization in sea urchin development. *Dev. Dyn.* **2012**, *241*, 1111–1124.
49. Nemer, M.; Rondinelli, E.; Infante, D.; Infante, A.A. Polyubiquitin RNA characteristics and conditional induction in sea urchin embryos. *Dev. Biol.* **1991**, *145*, 255–265.
50. National Center for Biotechnology Information. Available online: <http://www.ncbi.nlm.nih.gov> (accessed on 20 January 2013).
51. Pfaffl, M.W. A new mathematical model for relative quantification in real-time RT-PCR. *Nucleic Acids Res.* **2001**, *29*, e45.
52. Pfaffl, M.W.; Horgan, G.W.; Dempfle, L. Relative expression software tool (REST) for group-wise comparison and statistical analysis of relative expression results in real-time PCR. *Nucleic Acids Res.* **2002**, *30*, e36.
53. Vanaverbeke, J.; Franco, M.A.; van Oevelen, D.; Moodley, L.; Provoost, P.; Steyaert, M.; Soetaert, K.; Vincx, M. Benthic responses to sedimentation of phytoplankton on the Belgian Continental Shelf. In *Current Status of Eutrophication in the Belgian Coastal Zone*; Presses Universitaires de Bruxelles: Bruxelles, Belgium, 2006; pp. 73–90.

# **Omega-3 Polyunsaturated Fatty Acids Protect Neural Progenitor Cells against Oxidative Injury**

**Qiang Liu, Di Wu, Na Ni, Huixia Ren, Chuanming Luo, Chengwei He, Jing-Xuan Kang, Jian-Bo Wan and Huanxing Su**

**Abstract:** The omega-3 polyunsaturated fatty acids ( $\omega$ -3 PUFAs), eicosapentaenoic acid (EPA) and docosahexaenoic acid (DHA), derived mainly from fish oil, play important roles in brain development and neuroplasticity. Here, we reported that application of  $\omega$ -3 PUFAs significantly protected mouse neural progenitor cells (NPCs) against H<sub>2</sub>O<sub>2</sub>-induced oxidative injury. We also isolated NPCs from transgenic mice expressing the *Caenorhabditis elegans fat-1* gene. The *fat-1* gene, which is absent in mammals, can add a double bond into an unsaturated fatty acid hydrocarbon chain and convert  $\omega$ -6 to  $\omega$ -3 fatty acids. Terminal deoxynucleotidyl transferase dUTP nick end labeling (TUNEL) staining showed that a marked decrease in apoptotic cells was found in *fat-1* NPCs after oxidative injury with H<sub>2</sub>O<sub>2</sub> as compared with wild-type NPCs. Quantitative RT-PCR and Western blot analysis demonstrated a much higher expression of nuclear factor erythroid 2-related factor 2 (Nrf2), a master transcriptional factor for antioxidant genes, in *fat-1* NPCs. The results of the study provide evidence that  $\omega$ -3 PUFAs resist oxidative injury to NPCs.

Reprinted from *Mar. Drugs*. Cite as: Liu, Q.; Wu, D.; Ni, N.; Ren, H.; Luo, C.; He, C.; Kang, J.-X.; Wan, J.-B.; Su, H. Omega-3 Polyunsaturated Fatty Acids Protect Neural Progenitor Cells against Oxidative Injury. *Mar. Drugs* **2014**, *12*, 234162356.

## **1. Introduction**

Oxidative stress-induced neuronal apoptosis plays a critical role in the pathogenesis of stroke and neurodegenerative diseases [1,2]. Oxidants, such as hydrogen peroxide and free radicals, produce cell damage by inducing production of reactive oxygen species (ROS) and activate an inflammatory response [3]. Several studies confirmed the transcription factor nuclear factor erythroid 2-related factor 2 (Nrf2) represents an important cellular protective mechanism against oxidative stress over the Nrf2-ARE pathway [4,5]. Activation of Nrf2 signaling induces the transcriptional regulation of ARE-dependent expression of various antioxidant and phase II detoxification enzymes, which include hemeoxygenase-1 (HO-1), NAD(P)H quinine oxidoreductase 1 (NQO-1), glutamate-cysteine ligase modifier subunit (GCLM), and glutamate-cysteine ligase catalytic subunit (GCLC) [6].

The long-chain omega-3 polyunsaturated fatty acids ( $\omega$ -3 PUFAs) from fish oil, for example, Docosahexaenoic acid (DHA), are highly enriched in the brain and play a key role in brain development and repair under many conditions [7,8]. Dietary DHA has been suggested to improve neuronal development [9], restore and enhance cognitive functions [10–12], and protect against beta-amyloid production, accumulation, and potential downstream toxicity in an aged Alzheimer mouse model [13]. DHA have also been shown to exert a beneficial effect on ROS related cellular

damage [14]. These studies indicate that omega-3, such as DHA, can increase neural resistance to various types of insults.

Mammals are unable to synthesize  $\omega$ -3 PUFAs de novo and must rely on a dietary source of these essential fatty acids. The *C. elegans fat-1* gene encodes an *n*-3 fatty acid desaturase that converts  $\omega$ -6 to  $\omega$ -3 PUFA, which could significantly reduce the omega-6/omega-3 fatty acid ratio [15]. The *fat-1* transgenic mice are rich in endogenous  $\omega$ -3 PUFAs, specifically in the brain, with a reduction in  $\omega$ -6 fatty acids, which provides an optimal model to evaluate the actions of  $\omega$ -3 PUFAs [16,17].

In the present study, we investigated whether  $\omega$ -3 PUFAs could protect neural progenitor cells (NPCs) against oxidative injury. NPCs are multipotent with a broad self-renewing potential and with the capacity to generate neurons, astrocytes and oligodendrocytes. Their inherent biological properties of NPCs provide multiple potentials to treat various neurological dysfunctions. Our results provide evidence that both exogenous and endogenous  $\omega$ -3 PUFAs can resist oxidative injury to NPCs.

## 2. Results

### 2.1. In Vitro Characterization of $NPCs^{WT}$ and $NPCs^{fat-1}$

Neural progenitor cells (NPCs) are self-renewing, multipotent cells that could be effectively differentiated into neurons, astrocytes, and oligodendrocytes [18]. With bFGF-supplemented culture medium, both  $NPCs^{WT}$  and  $NPCs^{fat-1}$  cells showed bipolar or multipolar morphology with small cell bodies. Nestin is an intermediate filament protein and widely used as a specific marker for NPCs. Immunostaining showed that more than 95% cells in both  $NPCs^{WT}$  and  $NPCs^{fat-1}$  culture were nestin-positive, confirming that the majority of  $NPCs^{WT}$  and  $NPCs^{fat-1}$  were immature (Figure 1A). PCR analysis demonstrated the high expression of *fat-1* in  $NPCs^{fat-1}$  (lanes 3 and 4) while no expression in  $NPCs^{WT}$  (lanes 1 and 2) (Figure 1B). To study differentiation potential of  $NPCs^{WT}$  and  $NPCs^{fat-1}$  *in vitro*, bFGF was replaced with 1% FBS in the cell culture medium and NPCs began to differentiate. At the 5th day, cultures with this differentiating medium, both  $NPCs^{WT}$  and  $NPCs^{fat-1}$  were successfully differentiated into Tuj1-positive neurons, GFAP-positive astrocytes and Rip-positive oligodendrocytes with similar differentiation capacities ( $NPCs^{WT}$ : 14.7% neurons, 61.3% astrocytes, and 11.5% oligodendrocytes;  $NPCs^{fat-1}$ : 15.4% neurons, 65.6% astrocytes, and 12.1% oligodendrocytes) (Figure 1C,D).

### 2.2. DHA Protected NPCs against $H_2O_2$ -Mediated Apoptosis

To evaluate the effect of  $H_2O_2$  on cell viability, we first incubated NPCs with 200  $\mu$ M  $H_2O_2$  and investigated cell viability at different time points. Cell viability was measured using the WST-8 assay. A 200  $\mu$ M concentration of  $H_2O_2$  in culture was used to establish the oxidative injury model according to a previous study reporting that cultured NPCs exposed to  $H_2O_2$  at this concentration was sufficiently induced to undergo apoptosis [19]. As shown in Figure 2A, cell viability was significantly reduced in a time-dependent manner. Incubation of 200  $\mu$ M  $H_2O_2$  for 6 h caused an approximate 50% cell loss, which was considered to be an optimal oxidative injury model for investigating drug effects.



**Figure 1.** Characterization on NPCs<sup>WT</sup> and NPCs<sup>fat-1</sup>. **(A)** The purity of neural progenitor cells (NPCs) was identified by Nestin staining and nuclei were counter-stained with DAPI. More than 95% of NPCs<sup>WT</sup> or NPCs<sup>fat-1</sup> were nestin-positive cells; **(B)** Gel electrophoresis of PCR products using primers for *fat-1* gene. Wild-type controls (lanes 1 and 2) and positive *fat-1* specimens (lanes 3 and 4); **(C)** Both NPCs<sup>WT</sup> and NPCs<sup>fat-1</sup> were shown to successfully differentiate into Tuj1-positive neurons, GFAP-positive astrocytes, and Rip-positive oligodendrocytes; **(D)** The bar graph showing the percentage of neural cells differentiated from NPCs at the 5th day in the differentiating medium. Scale bar: 250  $\mu$ m in (A) and 100  $\mu$ m in (C).

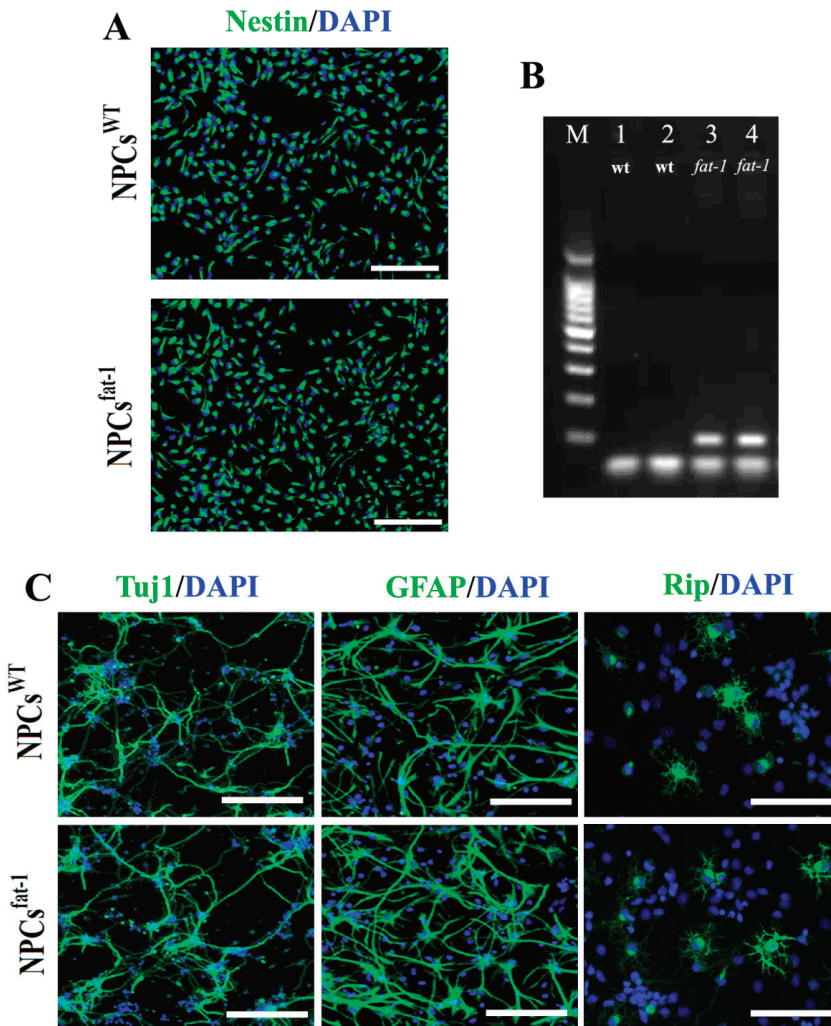
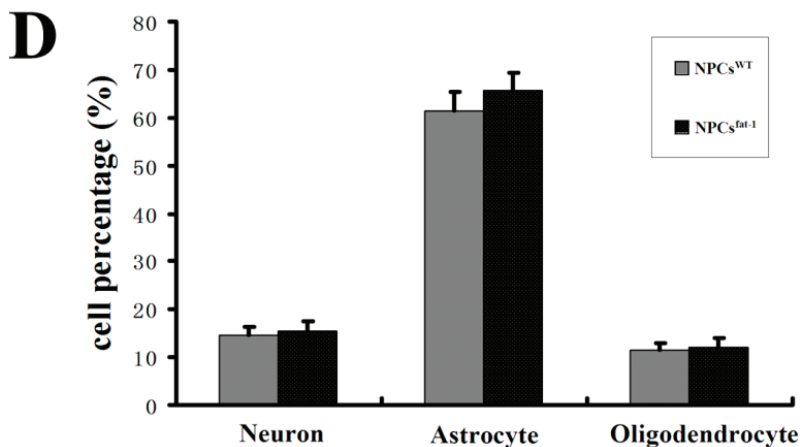
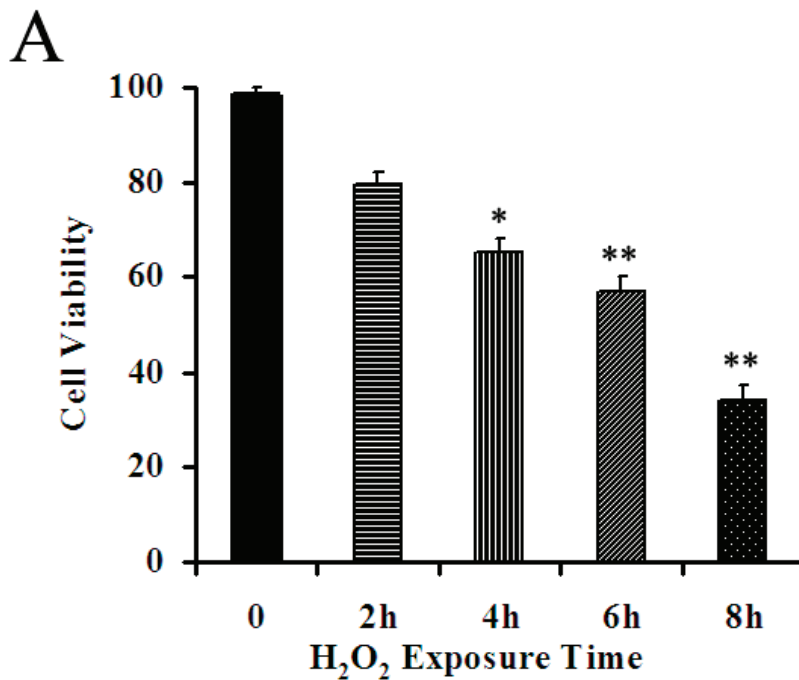


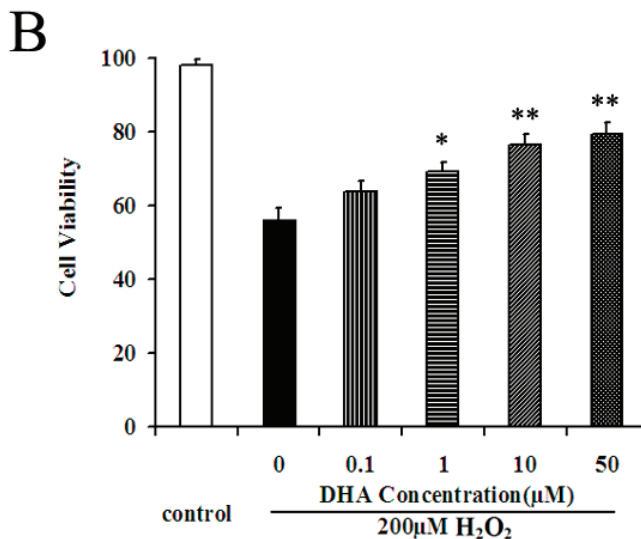
Figure 1. *Cont.*



**Figure 2.** DHA pretreatment reduced oxidative stress on cultured NPCs. (A) WST-8 assays revealed that incubation of 200  $\mu M$   $H_2O_2$  has caused a significant cytotoxicity in a time-dependent manner. (B) DHA prevented  $H_2O_2$ -induced cell death in a concentration-dependent manner. Cell viability was presented as a percentage of control, and each value represents the mean  $\pm$  SD of three independent experiments; \*  $p < 0.05$  and \*\*  $p < 0.001$  versus control.



**Figure 2. Cont.**

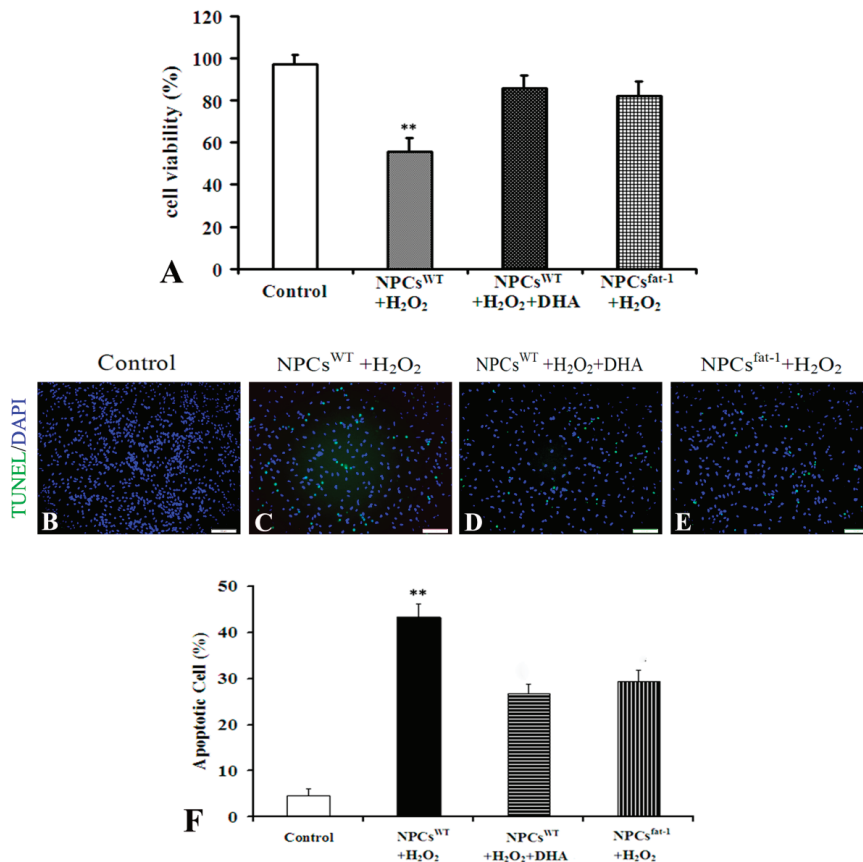


We then investigated the neuroprotective effects of exogenous DHA on H<sub>2</sub>O<sub>2</sub>-mediated apoptosis. NPCs<sup>WT</sup> at the confluence of 80% was pretreated with DHA (0, 0.1, 1, 10, and 50 µM) for 2 h and then suffered an oxidative injury induced by incubation of 200 µM H<sub>2</sub>O<sub>2</sub> for 6 h. WST-8 assay revealed that the cell viability increased in a concentration-dependent manner: The pretreatment of 1 µM DHA increased the cell viability by 22.1% as compared to vehicle control ( $p < 0.05$ , Figure 2B), while the pretreatment of 10 µM and 50 µM increased the cell viability by 35.6% and 36.2%, respectively, as compared to the vehicle control ( $p < 0.001$ , Figure 2B).

### 2.3. NPCs<sup>fat-1</sup> Prevented H<sub>2</sub>O<sub>2</sub>-Mediated Apoptosis

We further investigated anti-oxidative effects of endogenous ω-3 PUFAs in NPCs. NPCs<sup>fat-1</sup> were isolated from *fat-1* mice, which are rich in endogenous ω-3 PUFAs, specifically in the brain [16,17]. WST-8 assay showed that NPCs<sup>fat-1</sup> exhibited a potent anti-oxidative effect similar to that found in the DHA-treated NPCs<sup>WT</sup> group when exposed to H<sub>2</sub>O<sub>2</sub> for 6 h. The cell viability of these two groups was significantly increased as compared to the vehicle control (Figure 3A). Terminal deoxynucleotidyl transferase-mediated UTP end-labeling (TUNEL) staining was also performed to detect H<sub>2</sub>O<sub>2</sub>-mediated apoptosis. Only a very small proportion of intrinsic apoptosis were detected in cultured NPCs<sup>WT</sup> (Figure 3B,F). Incubation with 200 µM H<sub>2</sub>O<sub>2</sub> for 6 h induced approximately 40% NPCs<sup>WT</sup> to undergo apoptosis (Figure 3C,F), while pretreatment of NPCs<sup>WT</sup> with 10 µM DHA significantly attenuated H<sub>2</sub>O<sub>2</sub>-mediated apoptosis to less than 30% (Figure 3D,F). NPCs<sup>fat-1</sup> exhibited potent anti-oxidative properties, as shown by a significant decrease in apoptosis compared to NPCs<sup>WT</sup> when exposed to H<sub>2</sub>O<sub>2</sub> for 6 h (Figure 3E,F). These findings indicated that both exogenous and endogenous ω-3 PUFAs could protect NPCs against H<sub>2</sub>O<sub>2</sub>-mediated oxidative injury.

**Figure 3.** NPCS<sup>fat-1</sup> attenuated H<sub>2</sub>O<sub>2</sub>-mediated apoptosis. (A) The cell viability of NPCS was assessed after exposure to H<sub>2</sub>O<sub>2</sub> for 6 h by WST-8 analysis. Each value represents the mean ± SD of three independent experiments ( $n = 3$ , \*\*  $p < 0.01$  versus other groups); (B–E) Representative photomicrographs of TUNEL assay; (F) Quantitative analysis was carried out by measuring TUNEL-positive cells in each group. Figures were selected as representative data from three independent experiments. Cell apoptosis was significantly reduced in DHA-pretreated NPCS<sup>WT</sup> and NPCS<sup>fat-1</sup>. Each value represents the mean ± SD of three independent experiments ( $n = 3$ , \*\*  $p < 0.01$  versus other groups). Scale bar: 75 μm.

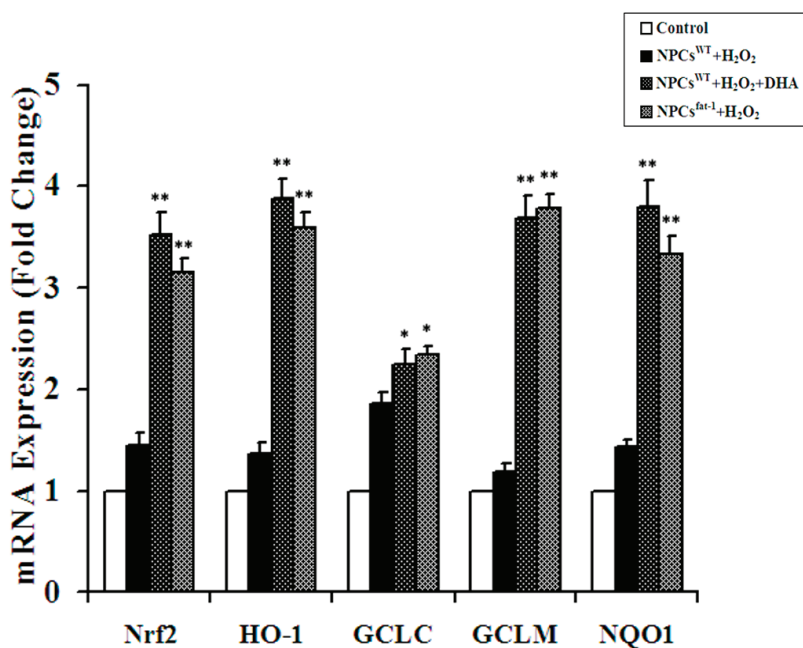


#### 2.4. Expression Analyses of Nrf2-ARE Pathway Genes

To study the anti-oxidative mechanisms of  $\omega$ -3 PUFAs against H<sub>2</sub>O<sub>2</sub>-induced apoptosis in NPCS, we first investigated whether Nrf2, the principal transcription factor that regulates the basal and inducible expression of a battery of antioxidant genes, was up-regulated after pretreatment with DHA and in NPCS<sup>fat-1</sup>. Real-time RT-PCR assays showed that both DHA pretreatment and NPCS<sup>fat-1</sup> induced a nearly 2.5-fold increase in the transcript level of Nrf2 when compared with the controls (Figure 4). Furthermore, significant increases in the expression level of the downstream gene and

phase II detoxification gene transcripts (HO-1, NQO-1, GCLC, GCLM) were found in NPCS<sup>fat-1</sup> and DHA-pretreated NPCS<sup>WT</sup> (Figure 4).

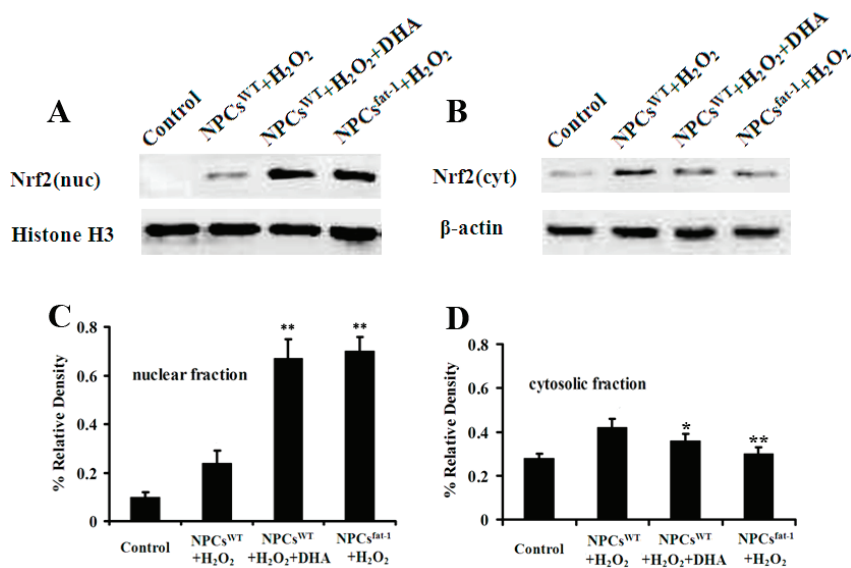
**Figure 4.** Expression analyses of Nrf2-ARE pathway genes in DHA-pretreated NPCS<sup>WT</sup> and NPCS<sup>fat-1</sup>. Real-time RT-PCR assays showed that both DHA pretreatment and NPCS<sup>fat-1</sup> induced significant increases in the transcript level of Nrf2 and its downstream gene and phase II detoxification gene transcripts HO-1, NQO-1, GCLC, GCLM when compared with the controls. Data are shown as mean  $\pm$  SD ( $n = 3$ ); \*  $p < 0.05$  versus control; \*\*  $p < 0.01$  versus control.



### 2.5. Expression Profiles of Nuclear and Cytosolic Nrf2 by Western Blot Analysis

Real-time RT-PCR assays demonstrated that both DHA pretreatment and NPCS<sup>fat-1</sup> induced significant increases in the transcript level of Nrf2. As nuclear translocation of protein Nrf-2 is very critical in inducing gene expression of anti-oxidant genes, we then investigated the expression profiles of cytosolic and nuclear fraction Nrf2 by Western blot analysis. Consistent with real-time RT-PCR results, Western blot analysis demonstrated that both DHA pretreatment and NPCS<sup>fat-1</sup> significantly increased the protein expression of nuclear Nrf2 when compared with the controls (Figure 5A,C). However, the expression of cytosolic Nrf2 in DHA pretreatment and NPCS<sup>fat-1</sup> was significantly decreased when compared with the control (Figure 5B,D). These results demonstrated an obvious translocation of Nrf2 from the cytoplasm to the nucleus in DHA pretreatment and NPCS<sup>fat-1</sup>.

**Figure 5.** DHA pretreatment and NPCs<sup>fat-1</sup> induced a significant increase in nuclear Nrf2 expression and a significant decrease in cytosolic Nrf2 expression. DHA-pretreated NPCs<sup>WT</sup> and NPCs<sup>fat-1</sup> were treated with 200  $\mu$ M H<sub>2</sub>O<sub>2</sub> for the indicated time points. Cells were lysed and fractionated to isolate nuclear and cytosolic fractions as indicated. Fractions were confirmed using Western blot with histone H3 for nuclear fractions (A) and  $\beta$ -actin as a marker for cytosolic fractions (B); Densitometry analysis showed that DHA pretreatment and NPCs<sup>fat-1</sup> induced a significant increase in nuclear Nrf2 expression (C) and a significant decrease in cytosolic Nrf2 expression (D). Data are shown as mean  $\pm$  SD ( $n = 3$ ); \*  $p < 0.05$  versus control; \*\*  $p < 0.01$  versus control.



### 3. Discussion

Neurodegenerative diseases are characterized by the progressive loss of neurons and usually influence the cognitive function, movement control or muscle strength [1,2]. Neurodegenerative diseases are commonly late-onset disorders, including Alzheimer's disease (AD), Parkinson's disease (PD), Huntington's disease (HD), and Amyotrophic lateral sclerosis (ALS). Oxidative stress has a significant role in the pathogenesis and/or progression of several neurodegenerative diseases and aging diseases, which are closely associated with disease-specific proteins aggregation, inflammation, mitochondrial dysfunction, and neurotoxicity [1,2,18]. Effective antioxidants have promising potential for therapeutic application. A prospective strategy in disease control has been focused on development of antioxidants as preventive and therapeutic medicine.

NPCs are largely undifferentiated cells originating in the central nervous system. They have the potential to give rise to offspring cells and efficiently differentiate into neurons, astrocytes and oligodendrocytes [19,20]. The inherent biological properties of NPCs may provide multiple strategies to treat CNS dysfunction and enable them to be an optimal model to screen antioxidants, which have therapeutic potentials for the treatment of neurological diseases.

DHA is an *n*-3 long chain PUFA, highly enriched in the central nervous system, and is critical for brain development and function. DHA is reported to play a neuroprotective role against oxidative stress in astrocytes [14], oligodendroglia cells [21], retinal ganglion cells [22], and human lymphocytes [23]. The animal with DHA diet or transgenic *fat-1* mice rich in endogenous *n*-3 PUFA showed a better behavior performance [11–13,24]. H<sub>2</sub>O<sub>2</sub> is a common oxidant to cause oxidative damage to cells and widely used in establishment of oxidative injury models [25]. Our present study reported that both exogenous and endogenous  $\omega$ -3 PUFAs significantly protected NPCs against H<sub>2</sub>O<sub>2</sub>-induced oxidative injury, suggesting that  $\omega$ -3 PUFAs might be an effective supplement for the prevention of neurodegenerative diseases which are associated with oxidative stress. DHA has been reported to scavenge the intracellular radical productions induced by hydrogen peroxide (H<sub>2</sub>O<sub>2</sub>), superoxide anion (O<sub>2</sub><sup>-</sup>), and hydroxyl radical ( $\bullet$ OH) [22]. Many previous studies reported that DHA treatment could significantly reduce ROS production, which is a possible mechanism underlying DHA's protective effects [14]. However, no significant differences in intracellular ROS levels were found between treatments in our study using 2',7'-dichlorofluorescein diacetate (DCFH-DA) to measure intracellular ROS levels. A previous study reported that DHA at some certain concentrations showed no effects on the fluorescence change by use of ROS probe [26]. It could be a reason why we were unable to detect the differences in intracellular ROS levels between the DHA treatment and control group. Another possible reason may be the cell type used in our study. Our study investigated whether DHA could protect NPCs against oxidative injury. NPCs are capable of self-renewal and they grow and proliferate rapidly in the culture, which may make it difficult to accumulate ROS to sufficient levels for measurement inside cells. To detect ROS changes in NPCs may require more sensitive methods or probes. Regarding protective effects of DHA on attenuating oxidative stress/damage induced by H<sub>2</sub>O<sub>2</sub>, our study suggests that DHA exert its antioxidative effects possibly via initiating a translocation of Nrf2 from the cytoplasm to the nucleus and subsequently stimulating the expression of a battery of antioxidant and phase II detoxification molecules as a response to oxidative injury.

The nuclear factor erythroid 2-related factor 2 (Nrf2) is an emerging regulator of cellular resistance to oxidants [4–6]. Nrf2 is localized mainly in the cytoplasm bound to its specific repressor Keap1. Oxidative stress will cause the liberation of Nrf2 and allow it to translocate into the nucleus. Nrf2 will induce transcriptional upregulation of numerous antioxidant and phase II detoxification genes to provide efficient cytoprotection [27]. The activated Nrf2 has shown protective effects in animal models of many neurodegenerative disorders [28–30]. In the present investigation, we demonstrated that both exogenous and endogenous DHA enhanced Nrf2 translocation from the cytoplasm to the nucleus of cultured NPCs when exposed to the oxidative stress and subsequently stimulated the mRNA levels of Nrf2, GCLC, GCLM, NQO-1, and HO-1. These results confirm previous findings that treatment of DHA can induce antioxidant and detoxifying genes [31,32].

Although our study demonstrated a similar antioxidative effect between exogenous and endogenous DHA on cultured NPCs, a difference in mechanisms underlying protective effects of exogenous and endogenous DHA may exist. The *fat-1* gene, which is absent in mammals, encodes  $\omega$ -3 polyunsaturated fatty acids ( $\omega$ -3 PUFAs) that convert  $\omega$ -6 to  $\omega$ -3 PUFAs, leading to an elevated amount of  $\omega$ -3 PUFAs such as DHA and higher  $\omega$ -3 PUFAs/ $\omega$ -6 PUFAs ratio in cells and

tissues from *fat-1* mice. PUFAs are essential components of membrane phospholipids and have a specific influence on membrane properties. Membranes enriched in  $\omega$ -3 PUFAs show increased membrane fluidity [33] and can directly or indirectly affect the function of a number of membrane proteins such as receptors since receptors and their affinity to their respective hormones/growth factors/proteins depend on the fluidity of the cell membrane [34,35]. The increased membrane fluidity can be involved in antioxidative effects of endogenous DHA in addition to its direct action on initiating Nrf2 translocation from the cytoplasm to the nucleus, while exogenous DHA is considered to exert its antioxidative effects possibly via a direct action on initiating a translocation of Nrf2 from the cytoplasm to the nucleus and subsequently stimulating the expression of a battery of antioxidant and phase II detoxification molecules as a response to oxidative injury.

## 4. Experimental Section

### 4.1. Animals

We obtained *fat-1* breeders on a C57BL/6 background from Dr. Jing X. Kang (Harvard Medical School, Boston, MA, USA) and arose in the Laboratory Animal Center, University of Macau (Macau, China). Mice were housed in a temperature-controlled, 12:12 light/dark room and were allowed free access to water and food. The F1 progeny were obtained by mating C57BL/6  $\times$  C3H *fat-1* breeders with C57BL/6 WT mice. Generations of heterozygous *fat-1* mice were then mated with WT littermates to obtain WT and heterozygous *fat-1* mice. All animals were treated in accordance with prevailing laws on animal experiments that were approved by the ethical committee of the University of Macau (Macau, China).

### 4.2. Genomic DNA Extractions and PCR Amplification

The *fat-1* C57BL6 mice (*fat-1*) and *fat-1* negative C57BL6 mice (WT) were identified by genotyping using PCR. Genomic DNA was prepared from 1 to 2 mm sections of tail tip using DNA Isolation Kit for Cells and Tissues (Roche, Mannheim, Germany). The DNA was used running polymerase chain reactions (PCR) using oligonucleotide primers that are specific for the transgene. Primer pair sets for the *fat-1* gene were constructed from Invitrogen (Carlsbad, CA, USA) and were as follows: *Fat-1* forward: 5'-TGTTTCATGCCTTCTT-CTTTTCC-3'; reverse: 5'-GCGACCATACCTCAAACCTTGGA-3'. PCR was carried out using rTaq (Takara, Otsu, Japa) with the following conditions: 95 °C 60 s (1 cycle); 95 °C 20 s, 58 °C 30 s, 72 °C 40 s (34 cycles). Amplified fragments were separated by 1.5% agarose gel electrophoresis.

### 4.3. Cell Isolation and Culture

Under sterile conditions, cerebral cortex from E13.5 *fat-1* mice and WT littermates were dissected out and prepared for NPCs culture following procedures described previously with minor modifications [25]. Briefly, the cortex was separated from surrounding tissues. After peeling off the meninges, the cortex was transferred into a 15 mL centrifuge tube containing culture medium (described below) and dissociated to a single-cell suspension by gentle mechanical trituration



through a fire polished Pasteur pipette. The dissociated cells were filtered through a cell strainer (BD Falcon, Franklin Lakes, NJ, USA) and then cultured in T25 flask in suspension. The culture medium consisted of DMEM-F12, BSA (1 mg/mL), B27 (20 IU/mL), N2 (10 IU/mL), EGF (20 ng/mL), and bFGF (20 ng/mL). Cells were maintained in an incubator with a humidified atmosphere containing 5% CO<sub>2</sub> at 37 °C. NPCs isolated from fat-1 mice and their WT littermates were confirmed by genomic DNA analyses and designated as NPCs<sup>fat-1</sup> and NPCs<sup>WT</sup> respectively. The medium was changed every two days. After five to six days, cells grew in neurospheres with the diameter of approximately 150 µm. Cells in the neurospheres were passaged at the ratio of 1:6 after initial plating. These subcultured cells were designated as “first passage” (P1). The third passage (P3) cells were used for all the following experiments. For differentiation studies, growth factors were removed from the culture medium and 1% fetal bovine serum (FBS, Gibco, Life Technologies Inc., Grand Island, NY, USA) was added. The cultures were allowed to differentiate for up to five days.

#### 4.4. Exposure to H<sub>2</sub>O<sub>2</sub> and Pretreatment with DHA

Dilutions of H<sub>2</sub>O<sub>2</sub> (Sigma-Aldrich, St. Louis., MO, USA) were made fresh from a 30% stock solution into cell culture medium to the different terminal concentrations. The NPCs<sup>WT</sup> were seeded at a density of  $1 \times 10^4$  cells per well into 96-well plates, then incubated in a humidified atmosphere of 95% air and 5% CO<sub>2</sub> at 37 °C. A 200 µM H<sub>2</sub>O<sub>2</sub> concentration in NPCs was determined to be optimal for this study (data not shown).

DHA (Sigma-Aldrich, St. Louis., MO, USA) was dissolved in 100% ethanol and kept at -20 °C in the dark as described in a previous study [24]. Immediately before use, the DHA stock solution was diluted in the bath solution and adjusted to the final concentrations needed. To examine the protective effects of DHA on H<sub>2</sub>O<sub>2</sub>-mediated apoptosis, NPCs<sup>WT</sup> at a confluence of around 75% was pretreated with DHA (0, 0.1, 1, 10, and 50 µM) for 2 h and followed by oxidative injury induced by H<sub>2</sub>O<sub>2</sub> treatment. NPCs<sup>fat-1</sup> were exposed to H<sub>2</sub>O<sub>2</sub> directly to investigate the protective effects of endogenous ω-3 PUFAs against oxidative injury. These cultures were then proceeded to cell viability analysis and TUNEL staining.

#### 4.5. Analysis of Cell Viability and TUNEL

Cell viability was assessed using the WST-8 dye (Beyotime Inst Biotech, Haimen, China) according to the manufacturer's instructions. After 10 µL WST-8 dye was add to each well, cells were incubated at 37 °C for 2 h and the absorbance was finally determined at 450 nm using a microplate reader (Molecular Devices, Sunnyvale, CA, USA). The results were expressed as relative cell viability (%). The apoptotic cell death of NPCs was estimated using TUNEL staining (Roche Applied Science, Indianapolis, IN, USA) according to the manufacturer's protocol. Cell cultures were counterstained with DAPI (5 µg/mL), which stained the nuclei of all cells.

#### 4.6. Real-Time RT-PCR

Total RNA was extracted from NPCs<sup>WT</sup>, NPCs<sup>fat-1</sup> and pretreated NPCs<sup>WT</sup> with 10 µM DHA after exposed to 200 µM H<sub>2</sub>O<sub>2</sub> for 6 h using TRIzol reagent (Invitrogen, Carlsbad, CA, USA) according to

the manufacturer's instructions. cDNAs were amplified and quantified in ABI Prism 7500 Sequence Detection System (Applied Biosystems, Foster City, CA, USA) using dye SYBR Green I (Takara, Otsu, Japan). The fold change in the levels of Nrf2, HO-1, GCLC, GCLM, and NQO-1 between the NPCs<sup>WT</sup> and NPCs<sup>fat-1</sup>, normalized by the level of  $\beta$ -actin, was determined using the following equation: Fold change =  $2^{-\Delta(\Delta Ct)}$ , where  $\Delta Ct = Ct(\text{target}) - Ct(\beta\text{-actin})$  and  $\Delta(\Delta Ct) = \Delta Ct(\text{treated}) - \Delta Ct(\text{untreated})$ . The primer sequences are listed in Table 1.

**Table 1.** Primers for real-time PCR assay.

Gene	Primer (5'-3')
Nrf2	F: TTCTTTCAGCAGCATCCTCTCCAC
	R: ACAGCCTTCAATAGTCCCCTCCAG
NQO1	F: GCGAGAAGAGCCCTGATTGTACTG
	R: TCTCAAACCAGCCTTTCAGAAATGG
HO-1	F: CAAGCCGAGAATGCTGAGTTCATG
	R: GCAAGGGATGATTTCTGCCAG
GCLM	F: GCCACCAGATTTGACTGCCTTTG
	R: TGCTCTTACGATGACCGAGTACC
GCLC	F: ACATCTACCACGCAGTCAAGGACC
	R: CTCAAGAACATCGCCTCCATTCAG
$\beta$ -actin	F: TCGTGCGTGACATTAAGGAGAAG
	R: GTTGAAGGTAGTTTCGTGGATGC

#### 4.7. Immunofluorescence

Immunocytochemistry was performed to characterize NPCs<sup>WT</sup> and NPCs<sup>fat-1</sup>. Briefly, cells were fixed with 4% paraformaldehyde, blocked with 5% goat serum, and then incubated with primary antibodies overnight at 4 °C, including rabbit anti-nestin (1:1000, Millipore, Billerica, MA, USA), mouse anti-Rip (1:50, kindly gift from Dr. XM Xu, University of Louisville, Louisville, KY, USA), rabbit anti-GFAP (1:1000, Sigma-Aldrich, St. Louis., MO, USA), mouse anti-Tuj1 (1:1000, Sigma-Aldrich, St. Louis., MO, USA). The cells were then rinsed three times with PBS and incubated for 30 min with species-specific secondary antibody conjugated to the fluorescent labels Alexa 568 or 488 (1:400, Invitrogen, Carlsbad, CA, USA). Cell cultures were counterstained with DAPI (5  $\mu$ g/mL) to stained the nuclei of all cells. Finally, the cells were visualized under a fluorescent laser microscope (IX73, Olympus Corp., Tokyo, Japan).

#### 4.8. Western Blotting Analysis

Cells were washed twice with ice-cold PBS and lysed using a Nuclear and Cytoplasmic Protein Extraction Kit (Beyotime, Haimen, China) according to the protocol described by the manufacturer. The protein concentrations were determined using Bradford method. The protein extracts were separated in sodium dodecylsulfate polyacrylamide gel electrophoresis (SDS-PAGE) gel and then transferred to a poly-vinylidene difluoride (PVDF) membrane. They were then incubated overnight at 4 °C with primary monoclonal antibodies against Nrf2 (1:1000; R & D Systems, Minneapolis, MN, USA). Histone H3 (1:1000; Cell Signaling Technology, Beverly, MA, USA) and  $\beta$ -actin

(1:1000; Cell Signaling Technology, Beverly, MA, USA) used as controls were detected in the nuclear fraction and cytosolic fraction, respectively. The blots were washed thoroughly in TBST buffer and incubated for 1 h with appropriate HRP-linked secondary antibodies (1:1000; Cell Signaling Technology, Beverly, MA, USA). Immunoreactive proteins were visualized with the ECL Western blotting detection reagent (Amersham Biosciences, GE Healthcare, Piscataway, NJ, USA). Relative band intensities were determined by Quality-one 1-D analysis software (Bio-Rad, Hercules, CA, USA).

#### 4.9. Statistical Analysis

The results were expressed as the mean  $\pm$  S.D. of triplicate measurements representative of three independent experiments. The one-way analysis of variance and Tukey test were used for the multiple comparisons. Statistical significance was defined as  $P < 0.05$ .

### 5. Conclusions

Both exogenous and endogenous DHA showed protective effects on NPCs against oxidative injury possibly via Nrf-ARE pathway, suggesting that DHA might be an effective supplement for the prevention of neurodegenerative diseases which are associated with oxidative stress.

### Acknowledgments

This study was supported by Macao Science and Technology Development Fund (003/2012/A and 018/2013/A1) and multi-year research grant, university of Macau, MYRG122 (Y1-L3)-ICMS12-SHX and MYRG110 (Y1-L2)-ICMS13-SHX.

### Author Contributions

Conceived and designed the experiments: HS, JK, JW; Performed the experiments: QL, DW, NN; Analyzed the data: CH, HR, CL; Wrote the paper: HS, QL.

### Conflicts of Interest

The authors declare no conflict of interest.

### References

1. Barnham, K.J.; Masters, C.L.; Bush, A.I. Neurodegenerative diseases and oxidative stress. *Nat. Rev. Drug Discov.* **2004**, *3*, 205–214.
2. Xu, J.; Kao, S.Y.; Lee, F.J.; Song, W.; Jin, L.W.; Yankner, B.A. Dopamine-dependent neurotoxicity of alpha-synuclein: A mechanism for selective neurodegeneration in Parkinson disease. *Nat. Med.* **2002**, *8*, 600–606.
3. Zahler, S.; Kupatt, C.; Becker, B.F. Endothelial preconditioning by transient oxidative stress reduces inflammatory responses of cultured endothelial cells to TNF-alpha. *FASEB J.* **2000**, *14*, 555–564.

4. Johnson, J.A.; Johnson, D.A.; Kraft, A.D.; Calkins, M.J.; Jakel, R.J.; Vargas, M.R.; Chen, P.C. The Nrf2-ARE pathway: An indicator and modulator of oxidative stress in neurodegeneration. *Ann. N. Y. Acad. Sci.* **2008**, *1147*, 61–69.
5. Kraft, A.D.; Johnson, D.A.; Johnson, J.A. Nuclear factor E2-related factor 2-dependent antioxidant response element activation by tert-butylhydroquinone and sulforaphane occurring preferentially in astrocytes conditions neurons against oxidative insult. *J. Neurosci.* **2004**, *24*, 1101–1112.
6. Ma, Q. Role of nrf2 in oxidative stress and toxicity. *Annu. Rev. Pharmacol. Toxicol.* **2013**, *53*, 401–426.
7. Chang, Y.L.; Chen, S.J.; Kao, C.L.; Hung, S.C.; Ding, D.C.; Yu, C.C.; Chen, Y.J.; Ku, H.H.; Lin, C.P.; Lee, K.H.; *et al.* Docosahexaenoic acid promotes dopaminergic differentiation in induced pluripotent stem cells and inhibits teratoma formation in rats with Parkinson-like pathology. *Cell Transplant.* **2012**, *21*, 313–332.
8. Russell, F.D.; Bürgin-Maunders, C.S. Distinguishing health benefits of eicosapentaenoic and docosahexaenoic acids. *Mar. Drugs.* **2012**, *10*, 2535–2559.
9. Tixier-Vidal, A.; Picart, R.; Loudes, C.; Bauman, A.F. Effects of polyunsaturated fatty acids and hormones on synaptogenesis in serum-free medium cultures of mouse fetal hypothalamic cells. *Neuroscience* **1986**, *17*, 115–132.
10. Greiner, R.S.; Moriguchi, T.; Hutton, A.; Slotnick, B.M.; Salem, N., Jr. Rats with low levels of brain docosahexaenoic acid show impaired performance in olfactory-based and spatial learning tasks. *Lipids* **1999**, *34*, S239–S243.
11. Gamoh, S.; Hashimoto, M.; Sugioka, K.; Hossain, M.S.; Hata, N.; Misawa, Y.; Masumura, S. Chronic administration of docosahexaenoic acid improves reference memory-related learning ability in young rats. *Neuroscience* **1999**, *93*, 237–241.
12. Gamoh, S.; Hashimoto, M.; Hossain, S.; Masumura, S. Chronic administration of docosahexaenoic acid improves the performance of radial arm maze task in aged rats. *Clin. Exp. Pharmacol. Physiol.* **2001**, *28*, 266–270.
13. Lim, G.P.; Calon, F.; Morihara, T.; Yang, F.; Teter, B.; Ubeda, O.; Salem, N., Jr.; Frautschy, S.A.; Cole, G.M. A diet enriched with the omega-3 fatty acid docosahexaenoic acid reduces amyloid burden in an aged Alzheimer mouse model. *J. Neurosci.* **2005**, *25*, 3032–3040.
14. Kim, E.J.; Park, Y.G.; Baik, E.J.; Jung, S.J.; Won, R.; Nahm, T.S.; Lee, B.H. Dehydroascorbic acid prevents oxidative cell death through a glutathione pathway in primary astrocytes. *J. Neurosci. Res.* **2005**, *79*, 670–679.
15. Kang, Z.B.; Ge, Y.; Chen, Z.; Cluette-Brown, J.; Laposata, M.; Leaf, A.; Kang, J.X. Adenoviral gene transfer of *Caenorhabditis elegans* n-3 fatty acid desaturase optimizes fatty acid composition in mammalian cells. *Proc. Natl. Acad. Sci. USA* **2001**, *98*, 4050–4054.
16. Kang, J.X.; Wang, J.; Wu, L.; Kang, Z.B. Transgenic mice: Fat-1 mice convert n-6 to n-3 fatty acids. *Nature* **2004**, *427*, doi:10.1038/427504a.
17. Xia, S.; Lu, Y.; Wang, J.; He, C.; Hong, S.; Serhan, C.N.; Kang, J.X. Melanoma growth is reduced in fat-1 transgenic mice: Impact of omega-6/omega-3 essential fatty acids. *Proc. Natl. Acad. Sci. USA* **2006**, *103*, 12499–12504.

18. Agar, J.; Durham, H. Relevance of oxidative injury in the pathogenesis of motor neuron diseases. *Amyotroph. Lateral Scler. Other Motor Neuron Disord.* **2003**, *4*, 232–242.
19. Reynolds, B.A.; Weiss, S. Generation of neurons and astrocytes from isolated cells of the adult mammalian central nervous system. *Science* **1992**, *255*, 1707–1710.
20. Lin, H.J.; Wang, X.; Shaffer, K.M.; Sasaki, C.Y.; Ma, W. Characterization of H<sub>2</sub>O<sub>2</sub>-induced acute apoptosis in cultured neural stem/progenitor cells. *FEBS Lett.* **2004**, *570*, 102–106.
21. Brand, A.; Schonfeld, E.; Isharel, I.; Yavin, E. Docosahexaenoic acid-dependent iron accumulation in oligodendroglia cells protects from hydrogen peroxide-induced damage. *J. Neurochem.* **2008**, *105*, 1325–1335.
22. Shimazawa, M.; Nakajima, Y.; Mashima, Y.; Hara, H. Docosahexaenoic acid (DHA) has neuroprotective effects against oxidative stress in retinal ganglion cells. *Brain Res.* **2009**, *1251*, 269–275.
23. Bechoua, S.; Dubois, M.; Dominguez, Z.; Goncalves, A.; Némoz, G.; Lagarde, M.; Prigent, A.F. Protective effect of docosahexaenoic acid against hydrogen peroxide-induced oxidative stress in human lymphocytes. *Biochem. Pharmacol.* **1999**, *57*, 1021–1030.
24. He, C.; Qu, X.; Cui, L.; Wang, J.; Kang, J.X. Improved spatial learning performance of fat-1 mice is associated with enhanced neurogenesis and neuritogenesis by docosahexaenoic acid. *Proc. Natl. Acad. Sci. USA* **2009**, *106*, 11370–11375.
25. Su, H.X.; Zhang, W.M.; Guo, J.S.; Guo, A.C.; Yuan, Q.J.; Wu, W.T. Neural Progenitor Cells Enhance the Survival and Axonal Regeneration of Injured Motoneurons after Transplantation into the Avulsed Ventral Horn of Adult Rats. *J. Neurotrauma* **2009**, *26*, 67–80.
26. Zhao, Z.; Wen, H.; Fefelova, N.; Allen, C.; Guillaume, N.; Xiao, D.; Huang, C.; Zang, W.; Gwathmey, J.K.; Xie, L.H. Docosahexaenoic Acid reduces the incidence of early afterdepolarizations caused by oxidative stress in rabbit ventricular myocytes. *Front. Physiol.* **2012**, *3*, doi:10.3389/fphys.2012.00252.
27. Lee, J.M.; Johnson, J.A. An important role of Nrf2-ARE pathway in the cellular defense mechanism. *J. Biochem. Mol. Biol.* **2004**, *37*, 139–143.
28. Ryu, J.; Zhang, R.; Hong, B.H.; Yang, E.J.; Kang, K.A.; Choi, M.; Kim, K.C.; Noh, S.J.; Kim, H.S.; Lee, N.H.; *et al.* Phloroglucinol attenuates motor functional deficits in an animal model of Parkinson's disease by enhancing Nrf2 activity. *PLoS One* **2013**, *8*, e71178.
29. Kanninen, K.; Heikkinen, R.; Malm, T.; Rolova, T.; Kuhmonen, S.; Leinonen, H.; Ylä-Herttua, S.; Tanila, H.; Levonen, A.L.; Koistinaho, M.; *et al.* Intrahippocampal injection of a lentiviral vector expressing Nrf2 improves spatial learning in a mouse model of Alzheimer's disease. *Proc. Natl. Acad. Sci. USA* **2009**, *106*, 16505–16510.
30. Nanou, A.; Higginbottom, A.; Valori, C.F.; Wyles, M.; Ning, K.; Shaw, P.; Azzouz, M. Viral delivery of antioxidant genes as a therapeutic strategy in experimental models of amyotrophic lateral sclerosis. *Mol. Ther.* **2013**, *21*, 1486–1496.
31. Yang, Y.C.; Lii, C.K.; Wei, Y.L.; Li, C.C.; Lu, C.Y.; Liu, K.L.; Chen, H.W. Docosahexaenoic acid inhibition of inflammation is partially via cross-talk between Nrf2/heme oxygenase 1 and IKK/NF- $\kappa$ B pathways. *J. Nutr. Biochem.* **2013**, *24*, 204–212.

32. Stulnig, G.; Frisch, M.T.; Crnkovic, S.; Stiegler, P.; Sereinigg, M.; Stacher, E.; Olschewski, H.; Olschewski, A.; Frank, S. Docosahexaenoic acid (DHA)-induced heme oxygenase-1 attenuates cytotoxic effects of DHA in vascular smooth muscle cells. *Atherosclerosis* **2013**, *230*, 406–413.
33. Stillwell, W.; Wassall, S.R. Docosahexaenoic acid: Membrane properties of a unique fatty acid. *Chem. Phys. Lipids* **2003**, *126*, 1–27.
34. Yamashima, T. A putative link of PUFA, GPR40 and adult-born hippocampal neurons for memory. *Prog. Neurobiol.* **2008**, *84*, 105–115.
35. Lafourcade, M.; Larrieu, T.; Mato, S.; Duffaud, A.; Sepers, M.; Matias, I.; De Smedt-Peyrusse, V.; Labrousse, V.F.; Bretillon, L.; Matute, C.; *et al.* Nutritional omega-3 deficiency abolishes endocannabinoid-mediated neuronal functions. *Nat. Neurosci.* **2011**, *14*, 345–350.

# Extraction of Fucoxanthin from Raw Macroalgae excluding Drying and Cell Wall Disruption by Liquefied Dimethyl Ether

Hideki Kanda, Yuichi Kamo, Siti Machmudah, Wahyudiono and Motonobu Goto

**Abstract:** Macroalgae are one of potential sources for carotenoids, such as fucoxanthin, which are consumed by humans and animals. This carotenoid has been applied in both the pharmaceutical and food industries. In this study, extraction of fucoxanthin from wet brown seaweed *Undaria pinnatifida* (water content was 93.2%) was carried out with a simple method using liquefied dimethyl ether (DME) as an extractant in semi-continuous flow-type system. The extraction temperature and absolute pressure were 25 °C and 0.59 MPa, respectively. The liquefied DME was passed through the extractor that filled by *U. pinnatifida* at different time intervals. The time of experiment was only 43 min. The amount of fucoxanthin could approach to 390 µg/g dry of wet *U. pinnatifida* when the amount of DME used was 286 g. Compared with ethanol Soxhlet and supercritical CO<sub>2</sub> extraction, which includes drying and cell disruption, the result was quite high. Thus, DME extraction process appears to be a good method for fucoxanthin recovery from *U. pinnatifida* with improved yields.

Reprinted from *Mar. Drugs*. Cite as: Kanda, H.; Kamo, Y.; Machmudah, S.; Wahyudiono; Goto, M. Extraction of Fucoxanthin from Raw Macroalgae excluding Drying and Cell Wall Disruption by Liquefied Dimethyl Ether. *Mar. Drugs* **2014**, *12*, 238362396.

## 1. Introduction

*Undaria pinnatifida* is consumed as one of the most popular, traditional seaweeds, particularly in East Asian countries such as Japan and Korea. In the current food industry, *U. pinnatifida* is mainly manufactured in the form of dry particles by using coarse grinder. Dry *U. pinnatifida* particles swell in hot water, and are used as an ingredient in popular foods such as bean paste soup in Japan. The main functional constituent of *U. pinnatifida* is fucoxanthin [1,2], which is a xanthophylls pigment contained in the chloroplasts of brown macroalgae. Fucoxanthin also had ability to exert effects in humans, such as antidiabetic effect [3,4], cholesterol metabolism [5,6], anti-obesity effect [1], anti-oxidant properties [2,7,8], anti-proliferative effect on cancer cells [9,10], and anti-inflammatory [11]. Extraction of bioactive compounds from macroalgae has great potential and its applications will continue to grow in the following years [12]. Pressurized solvent extraction has been used, for example, to isolate carotenoids from brown macroalgae, such as *Eisenia bicyclis* [13], *Cystoseira abies-marina*, and *Himanthalia elongata* [14]. The results showed that ethanol at high temperatures provide high recoveries of fucoxanthin and other oxygenated carotenoids. Moreover, many studies of biomaterials production have reported that cell disruption is a significant important factor to extract organic components contained in cells. For example, microwave assisted extraction of fucoxanthin from *U. pinnatifida* cells [15–18]. However, fucoxanthin exhibited sensitivity towards some factors such as light and pH, the least stable in

acidic pH condition and higher concentration of ascorbic acid supplementation exerted stabilization role on fucoxanthin [19], and carotenoids are thermally decomposed in hot-drying.

Liquefied DME was used as an extractant to enhance extraction of fucoxanthin from *U. pinnatifida*. DME is the simplest form of ether [20], with the following characteristics. (i) DME has a low normal boiling point ( $-24.8\text{ }^{\circ}\text{C}$ ) [21], therefore, DME is not present in the final products at normal temperatures; (ii) Relative permittivity of DME is 1.08 and 5.34 at  $30.5\text{ }^{\circ}\text{C}$ , in gaseous and liquid states, respectively. Liquefied DME has high affinity to oily substances [22] and partial miscibility with water [23]; (iii) DME has been approved as a safe extraction solvent for the production of foodstuff and food ingredients by the European Food Safety Authority (EFSA) [24], by the Food Standards Australia New Zealand, and by the United States [25]. The panels of EFSA consider the intended use of dimethyl ether as an extraction solvent to remove fat from animal protein raw materials. Considering (a) that the defatted animal protein is submitted to vacuum which assures that most of the volatile dimethyl ether is eliminated from final animal protein products (b) that the maximum residual limit of dimethyl ether is of  $9\text{ }\mu\text{g/kg}$  of extracted animal proteins and (c) that these proteins are used at a level of up to 2% in the final food, the Panel considered that there is no safety concern [24]; (iv) DME exhibits resistance to autoxidation, unlike other alkyl ethers [26]. Owing to these characteristics, the authors successfully extracted lipids and water from wet vegetal biomasses by liquefied DME. In the DME-based extraction technique, drying, cell disruption, and heating of solvent were not needed to improve extraction yields [27].

In this work, the effect of pressure, temperature, and ethanol as co-solvent on the recovery of fucoxanthin from *U. pinnatifida* using supercritical  $\text{CO}_2$  would be also presented. However, the lipids content in the extract is not presented, although supercritical  $\text{CO}_2$  is well known as an effective technique to extract lipids. Several experimental studies of extraction by supercritical  $\text{CO}_2$  have reported that supercritical  $\text{CO}_2$  extraction is an environmentally-friendly for lipids and carotenoids extraction from micro- and macroalgae. Mendes *et al.* carried out supercritical  $\text{CO}_2$  extraction of carotenoids and other lipids on whole and crushed *Chlorella vulgaris* [28]. Machmudah *et al.* and Kitada *et al.* also extracted carotenoids and astaxanthin from microalgae *Haematococcus pluvialis* [29] and *C. vulgaris* [30] with supercritical  $\text{CO}_2$ . The results showed that supercritical  $\text{CO}_2$  is more selective for carotenes than the usual organic liquid extraction and it is preferred for handling temperature-sensitive molecules. Extraction using supercritical  $\text{CO}_2$  with ethanol as the co-solvent has also been performed with brown seaweed at 0.8 to 30 MPa and 303 to 333 K [31]. The significant amount of oil from brown seaweed was extracted within 50 min. Roh *et al.* reported that the oil extraction yield of brown seaweed was high at higher pressure, and the amounts of fucoxanthin extracted at 20 MPa of  $\text{CO}_2$  pressure and 323 K of extraction temperature showed much higher than other extraction conditions [31]. As a comparison, the extraction yield from *U. pinnatifida* was also tested by using the conventional solvent ethanol with a Soxhlet extractor. As explained before that fucoxanthin has been implicated as important dietary nutrients having antioxidant potential. It is one of the reasons why some researchers had evaluated the *in vitro* antioxidant activity of fucoxanthin extracted from algae. For example, Roh *et al.* suggested that fucoxanthin content should be considered as an important feature of brown seaweed, as some of its nutritive and pharmacological effects could be attributed to their presence in plant material [31]. Billakanti *et al.*



also reported that the yield of fucoxanthin from *U. pinnatifida* could be improved by using an enzyme-assisted extraction process followed by DME extraction. The results showed that extraction of fucoxanthin from *U. pinnatifida* using supercritical CO<sub>2</sub> with ethanol as a co-solvent and enzymatic pre-treatment followed by DME extraction have no effect on the fucoxanthin properties [20]. Therefore, in this study the antioxidant activity of fucoxanthin was not conducted. Isolation and purification of fucoxanthin from extraction products were also not carried out.

## 2. Results and Discussion

### 2.1. Ethanol Soxhlet Extraction

It was well known that the extraction of organic compounds using a range of organic solvents from matrices (soils, sewage sludges, vegetables, and plants) has historically been carried out by using Soxhlet extraction. The apparatus for Soxhlet extraction consisted of a solvent reservoir, extractor body, an electric heat source and a water-cooled reflux condenser. Since the temperature plays a significant role for extraction, increased temperatures can disrupt the strong solute-matrix interactions caused by van der Waals forces, hydrogen bonding, and dipole attractions of the solute molecules and active sites on the matrix [32]. Therefore, the use of ethanol as an extract solvent at elevated temperature is enhanced solubility and mass transfer effects, and disruption of surface equilibria. Kim *et al.* reported that ethanol provided the best fucoxanthin extraction yield from *Phaeodactylum tricornutum* (15.71 mg/g freeze-dried sample weight) [33]. They explained that fucoxanthin content in the extracts produced by the different methods was quite constant (15.42–16.51 mg/g freeze-dried sample weight) but increased steeply based on the percentage of ethanol in water, emphasizing the importance of ethanol in the extraction. Kanazawa *et al.* also reported that 191 µg/g wet sample weight was extracted from *Laminalia japonica* with ethanol at 40 °C [34].

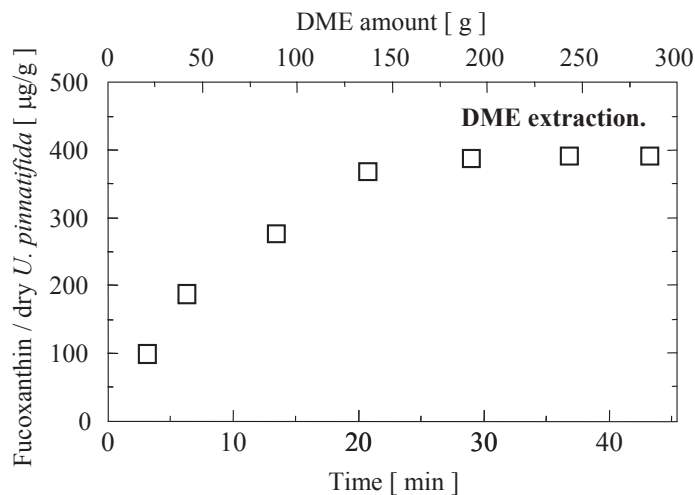
In this work, by using ethanol solvent, 50 µg of fucoxanthin has been extracted from *U. pinnatifida* 6 g. This result might be due to some contribution from the physical properties of *U. pinnatifida*. The size of *U. pinnatifida* was 0.5–3 cm directly fed without pre-treatment. The particle size is other factors that high influence the mass transfer during Soxhlet process. Bigger particles present lower ratios of surface area to volume. Conversely, smaller particles present higher ratios of surface area to volume, which enhance the contact between solvent and solid matrix and diminish the diffusion path of the particle to reach the surface, resulting in a high extraction yield. In addition, there was possibility that the degradation of fucoxanthin in ethanol solution might have occurred during Soxhlet extraction process (12 h).

### 2.2. Liquefied DME Extraction

As shown in Figure 1, fucoxanthin has been extracted from *U. pinnatifida* with small amount of DME (24 g). It should be noted that the lipids content in the extract is not determined. The increasing amount of DME used was followed by increasing the amount of fucoxanthin extracted. When the amount of DME used was 286 g (at the last time point of extraction process), the residue of the *U. pinnatifida* was almost perfectly dewatered as like as such kind of dry paper. The color of

*U. pinnatifida* was also changed to light green color. The amount of fucoxanthin could approach up to 390  $\mu\text{g/g}$  dry of *U. pinnatifida* at this point.

**Figure 1.** Yield of fucoxanthin in the extract obtained from wet *U. pinnatifida* by liquefied dimethyl ether (DME).



Compared with other, ethanol soxhlet, the fucoxanthin amount by liquefied DME was quite high. It is well known that liquefied DME could dissolve a wide range of polar and non-polar substances. They are also good solvents for many hydrogen-bonded substances. To dissolve hydrogen bonded substances, high solvation energy was needed to break the hydrogen bonds. In this case, DME has ability to act hydrogen bond acceptors, forming hydrogen bonds with hydrogen-bonding solutes. Therefore, liquefied DME can enter into *U. pinnatifida* cells and goes out together with *U. pinnatifida* components include fucoxanthin. In addition, the cumulative fucoxanthin extracted looks like complete after 191 g of DME consumption, however, the cumulative fucoxanthin extracted seemed clearly to be enhanced with increasing the DME consumption. As mentioned before, despite liquefied DME had high dissolving ability, liquefied DME could also generate a lower viscosity of the analytes in the matrix and, accordingly, a better diffusion rate of the solute from the solid phase to the solvent. Consequently, the fucoxanthin in *U. pinnatifida* might be extracted easily.

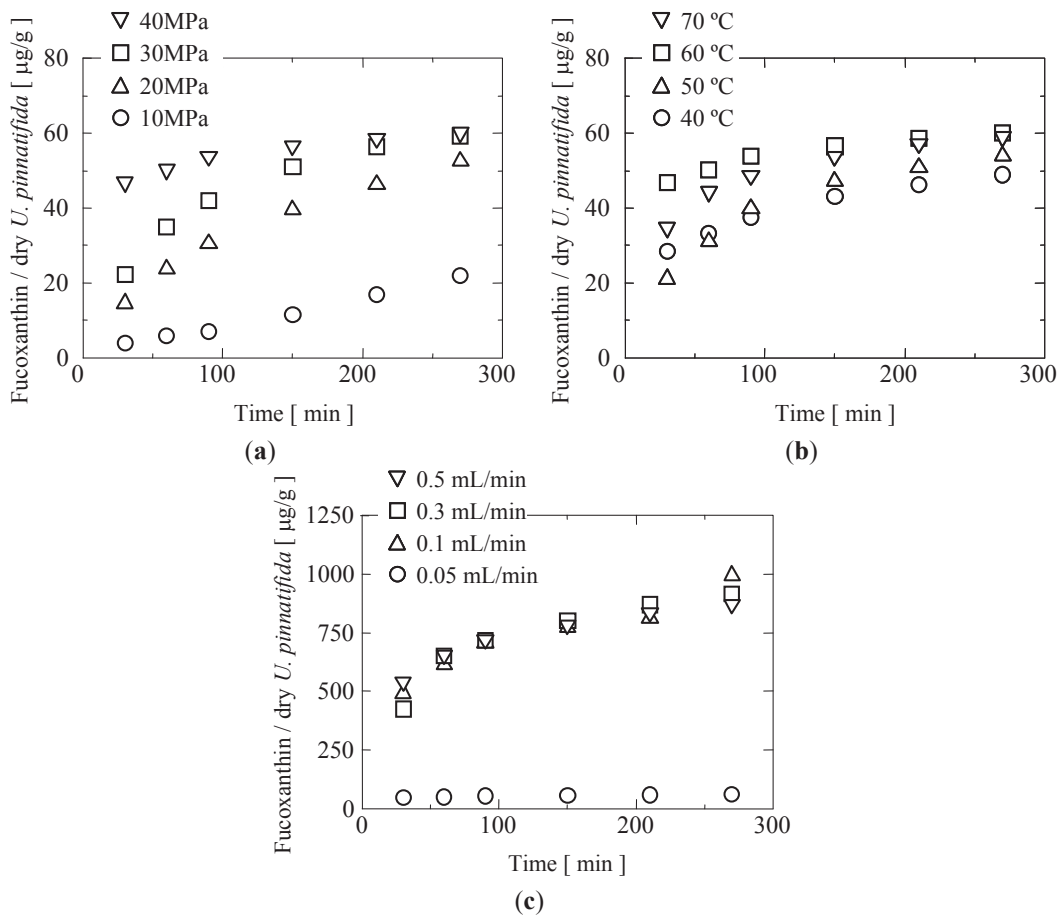
### 2.3. Supercritical $\text{CO}_2$ Extraction

For supercritical  $\text{CO}_2$  extraction system, the extraction of fucoxanthin was performed in a semi-continuous flow-type. Physically, the appearance of the extracts was oily. In general, they increased with the increase of pressure at constant temperature. This tendency happened due to direct increase of density and hence solvating power of supercritical  $\text{CO}_2$  [35,36]. Figure 2a,b showed the extraction curves of fucoxanthin from *U. pinnatifida* for different extraction times and under different conditions in terms of pressure (10–40 MPa; 60  $^\circ\text{C}$ ) and temperatures (40–70  $^\circ\text{C}$ ;

40 MPa). Initially, the yield of fucoxanthin increased significantly up to 150 min extraction time. For example, the yield of fucoxanthin is about 47  $\mu\text{g/g}$  dry weight of *U. pinnatifida* dried after 30 min at 40 MPa and 60 °C. Then, it increased gradually to 58  $\mu\text{g/g}$  dry weight of *U. pinnatifida* at 150 min extraction time. Over 150 min extraction time, the yield of fucoxanthin was not increase significantly. At the same extraction temperature, the same trend was found at 10, 20, and 30 MPa. As previously mentioned, the effect of pressure can be attributed to the increase in solvent power and by the strengthening of intermolecular physical interactions. It is also evident that an increase in pressure had effect on the solubility of fucoxanthin in supercritical CO<sub>2</sub>. This result is in agreement with similar trends reported by other authors [29,37]. Machmudah *et al.* reported that the total extract and the astaxanthin extracted were not significantly affected by the increasing pressure at 30–50 MPa, and after which the dramatic increase was observed at the pressure of 55 MPa. They explained that the dependency on the pressure was expected as the CO<sub>2</sub> density increases at higher pressure, and therefore the solvent power to dissolve the substances increases [29]. At constant pressure (40 MPa), the yield of fucoxanthin also increased with increasing extraction temperature. It increased rapidly till 150 min extraction time then remained constant after 200 min extraction time in each extraction temperature. The highest extraction rate of fucoxanthin was reached when the extraction temperature is 60 °C. The maximum fucoxanthin content obtained was 60  $\mu\text{g/g}$  dry weight of *U. pinnatifida* after 270 min extraction time. As shown in the Figure 2b, the amount of fucoxanthin increased with an increase in temperature. These results indicated that the fucoxanthin extractions are dependent on solute vapor pressure which increased with an increase in temperature. Instead of that, the increasing temperature contributed to the decomposition of cell walls, and as a result fucoxanthin and extractable compounds availability for extraction was increased [29]. In addition, due to the fast extraction rate of fucoxanthin from *U. pinnatifida*, this figure also showed that an increase in temperature likely had a stronger effect on the solubility than an increase in pressure. At 70 °C, the yield of fucoxanthin is lower than at 60 °C. In this case, degradation of fucoxanthin might also take place, considering that carotenoids in general are considered to be heat-sensitive [33].

In this work, the amounts of fucoxanthin extracted by supercritical CO<sub>2</sub> extraction with and without ethanol as entrainer were compared. The experiments were conducted under 60 °C and 40 MPa with various entrainer concentrations (1.64%–14.29% in volume). This condition was selected because at that condition the extraction rate of fucoxanthin was high. When the concentration of 1.67% ethanol was employed, there was no significant effect on the amount of fucoxanthin extracted. As shown in Figure 2c, the enhancement of ethanol concentration had high effect on the amount of fucoxanthin extracted. The recovery of fucoxanthin could reach 10-fold. This considerable increase in extraction efficiency was because the ethanol added could enhance the solvent power of supercritical CO<sub>2</sub> and caused swelling of the matrix, thus increasing the internal volume and the surface area for the contact with supercritical CO<sub>2</sub> [29]. Machmudah *et al.* explained that the addition of ethanol in supercritical CO<sub>2</sub> also could cause decomposition of the *H. pluvialis* cellular wall, with the result that the astaxanthin availability for extraction increased [29].

**Figure 2.** (a) Effect of pressures on the amount of fucoxanthin as a function of time at 60 °C of extraction temperature; (b) Effect of temperatures on the amount of fucoxanthin as a function of time at 40 MPa of extraction pressure; (c) Effect of entrainer flow rate on the amount of fucoxanthin as a function of time at 60 °C and 40 MPa.



#### 2.4. Comparison of the Results of Three Extraction Techniques

As shown in Table 1, different extraction techniques, such as soxhlet, DME, and supercritical CO<sub>2</sub> extraction have been used to isolate fucoxanthin from the *U. pinnatifida* plant, however none of them can be considered as an optimal method for this purpose. Except DME extraction technique, pre-treatment of *U. pinnatifida*, such as drying, was needed. The main disadvantages of soxhlet extraction are the long time required and the large amount of solvent wasted, which is costly and cause environmental problems. Due to the long extraction time at the boiling point of the ethanol solvent, the possible degradations of fucoxanthin due to local overheating effects might occur. This process was performed to disrupt the cell membrane in *U. pinnatifida*, thus extraction efficiency of fucoxanthin increases. Supercritical CO<sub>2</sub> as known is attractive extraction method for food industries because the solvent is safe, nontoxic and easily removable, the method is fast and

extraction parameters can be changed in a wide range of pressure and temperature. However, CO<sub>2</sub> is non-polar fluid and it is the main disadvantage in its use for the isolation of antioxidants. As explained before, to improve the fucoxanthin yield, ethanol was introduced to increase the polarity of CO<sub>2</sub>. However, respecting to separation process, it is not only expensive but also difficult. On the contrary, the cell disruption of *U. pinnatifida* is not required when the DME was employed as extractant due to the properties of DME (see “Introduction”). That is why this technique of fucoxanthin extraction is very simple and versatile.

**Table 1.** Best recoveries of fucoxanthin obtained using different extraction techniques.

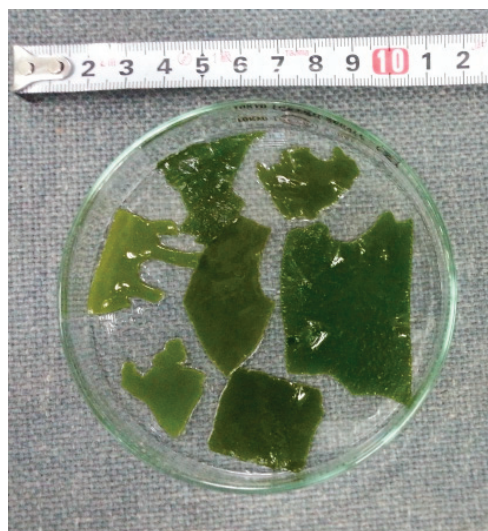
Extraction Techniques	Time (h)	Temperature (°C)	Pressure (MPa)	Yield of Fucoxanthin (µg/g)
Ethanol soxhlet	12	78	*	50
Liquefied DME	0.72	25	*	390
Supercritical CO <sub>2</sub>	3	60	40	60.12
	3	70	40	59.51
Supercritical CO <sub>2</sub> with entrainer (3.23%)	3	60	40	994.53

\* not determined.

### 3. Experimental Section

#### 3.1. Materials

*U. pinnatifida* was obtained from Fukui Prefecture, Japan and used as a starting material. Most of *U. pinnatifida* that did not meet strict quality standards are usually discarded as wastes, a situation, which is becoming an environmental concern. The appearance of *U. pinnatifida* is shown in Figure 3. The elemental composition of *U. pinnatifida* is given in Table 2. The apparatus of elemental analysis was conducted by a CHN analyzer (MT-6 Elemental analyzer, Yanaco New Science Inc., Kyoto, Japan) based on flash combustion, which converts all organic substances into combustion gases (H<sub>2</sub>O, CO<sub>2</sub>, N<sub>2</sub>). DME and CO<sub>2</sub> were purchased from Tamiya, Inc. Japan and Sogo Kariya Sanso, Inc. Japan, respectively. Fucoxanthin (94.0%) purchased from Wako Pure Chemicals Industries Ltd. (Osaka, Japan) was used as standard. It was stored at -60 °C in freezer (NF-75SF3, Nihon Freezer Co. Ltd., Tokyo, Japan). The analytical reagents used were acetonitrile, chloroform, and ethanol (HPLC-grade) from Wako Pure Chemicals Industries Ltd. (Osaka, Japan). All chemicals were used as received.

**Figure 3.** Wet *U. pinnatifida* sample.**Table 2.** Elemental analysis of *U. pinnatifida* by CHN analyzer, on average.

Materials	Ultimate Analysis (wet weight%, DAF)			
	C ( $\pm 0.2$ )	H ( $\pm 0.1$ )	N ( $\pm 0.1$ )	O * ( $\pm 0.3$ )
Original algae	33.0	5.5	3.5	58.0
Residue	36.1	5.9	4.7	53.3
Extract	55.6	8.6	1.4	34.4

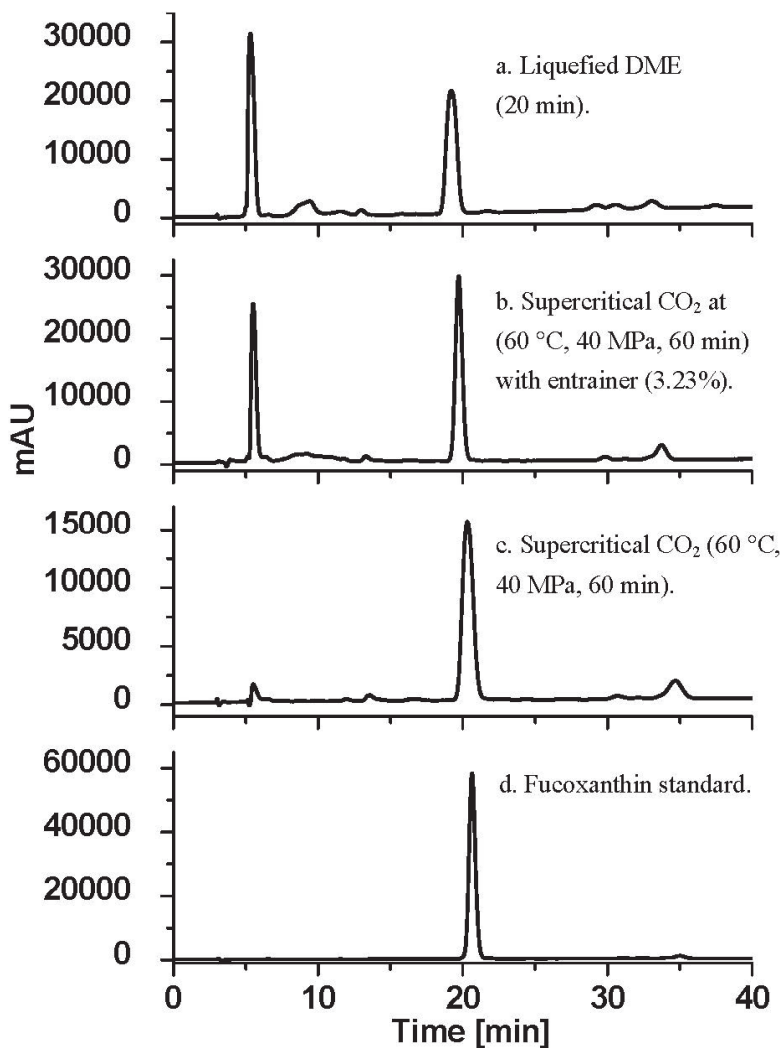
\* Oxygen content was determined by difference.

### 3.2. Analytical Methods

There are many carotenoids could be extracted from plant material. However, in this work, fucoxanthin was subjected as the target of carotenoid compounds recovery from *U. pinnatifida*, and determined quantitatively by using HPLC (high-performance liquid chromatography). The organic components in extracts were recovered with 2 mL of chloroform, and all the solutions were filtered using a disposable filter of 0.45  $\mu\text{m}$  pore size prior to HPLC analysis. The separation of fucoxanthin was carried out according to a previous published method [30] with modification. Initially, the pure compound of fucoxanthin dissolved in chloroform as a standard was injected in the HPLC system to construct calibration curve in 5 point. After separation process in the HPLC column, the amount of fucoxanthin leaving the column will determine the intensity of the signal produced in the detector. By comparing the time it takes for the peak to show up (the retention time) with the retention times for fucoxanthin, the amount of fucoxanthin in the extract can be identified (Figure 4). This analysis can be performed with good precision; therefore, other techniques analysis was not conducted. The HPLC instrument used was an ultraviolet-visible spectroscopy detector (UV-970; JASCO, Tokyo, Japan) equipped with an ODS-3 column (GL Sciences, Tokyo, Japan; 5  $\mu\text{m}$ ; 250 mm  $\times$  4.6 mm) and operated at 40  $^{\circ}\text{C}$ . The mobile phase

contained acetonitrile and water (80/20, v/v) with flow rate of 1.0 mL/min. Preparation of standard curve and detection were accomplished at wavelength of 445 nm.

**Figure 4.** HPLC chromatogram of fucoxanthin extract from *U. pinnatifida*.



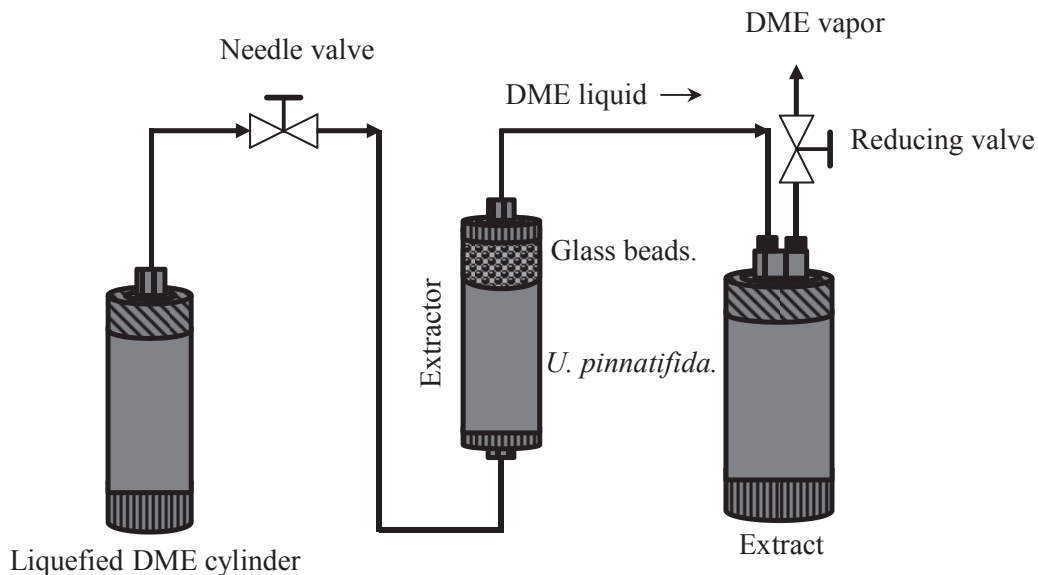
### 3.3. Ethanol Soxhlet Extraction

In this extraction, the heating mantle temperature was set at 78 °C for 12 h. The amount of dried *U. pinnatifida* and ethanol used in flask were 6 g and 200 mL, respectively. The flask was then removed from the mantle, and the liquid extracts were transferred to bottle that covered with aluminium foil and refrigerated until analysis. In this work (DME extraction, supercritical CO<sub>2</sub> extraction and ethanol soxhlet extraction), the *U. pinnatifida* was fed without any pre-treatments such as microparticulation.

### 3.4. DME Extraction

Figure 5 depicted the apparatus scheme that used to evaluate the extraction efficiency of the DME extraction. The main apparatus consisted of extractor (HPG-10-5; Taiatsu Techno Corp., Saitama, Japan; volume: 10 cm<sup>3</sup>), needle valve to control the DME flow rate, and extract storage tank (HPG-96-3; Taiatsu Techno Corp., Saitama, Japan; volume: 96 cm<sup>3</sup>). Briefly, they were connected in series included feed materials. The extractor and DME storage tank were made of pressure-resistant glass coated with polycarbonate. 4.40 g of the raw *U. pinnatifida* (water content: 93.2%) was loaded into the lower half of the extractor, and the upper half was loaded with colorless glass beads. The DME flow rate was  $10 \pm 2$  cm<sup>3</sup> min<sup>-1</sup>. The extraction temperature and absolute pressure were  $25 \pm 1$  °C and  $0.59 \pm 0.02$  MPa, respectively. After passing liquefied DME through the extractor at different time intervals, the DME was evaporated by opening the reducing valve of the storage vessel. Next, liquefied DME pass through the lower half of extractor, color of glass beads in the upper half was changed to olive-green color. Because the glass beads and liquefied DME were colorless, the olive-green color indicated the probable presence of fucoxanthin. The extraction test was finished when the color of glass beads was changed again to colorless. The total time needed was less than 43 min.

**Figure 5.** Schematic diagram of DME extraction.



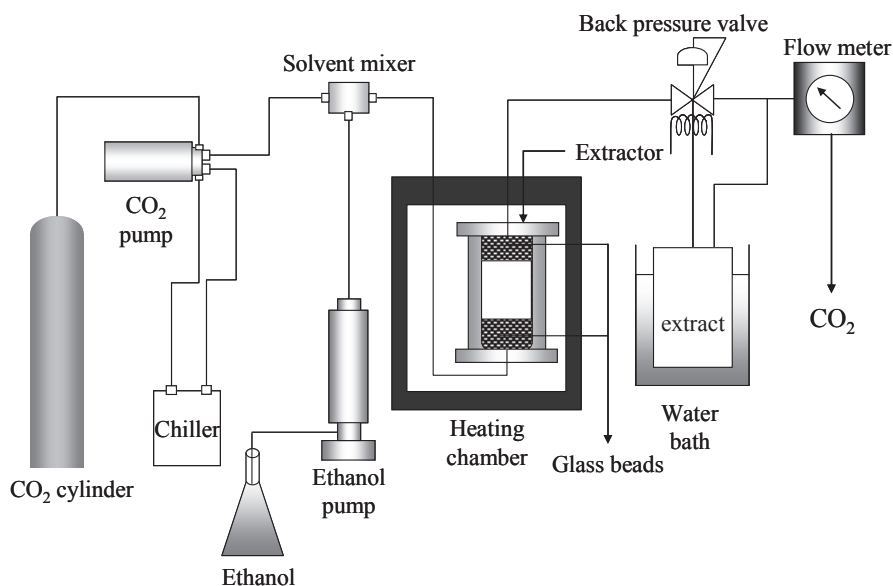
### 3.5. Supercritical CO<sub>2</sub> Extraction

The supercritical CO<sub>2</sub> extraction was carried out in an apparatus with schematic diagram as shown in Figure 6. The apparatus includes a high-pressure pump for CO<sub>2</sub> (PU-2086; Jasco, Hachioji, Japan), a heating chamber (WFO-400; EYELA, Tokyo, Japan), a 25 mL extraction cell (Thar Technologies, Inc., Pittsburgh, PA, USA) and back pressure regulator (AKICO, Tokyo,



Japan). In this work, the extraction of fucoxanthin from *U. pinnatifida* by supercritical CO<sub>2</sub> was conducted at temperatures of 40–70 °C and pressures of 20–40 MPa using a semi-continuous flow-type system with CO<sub>2</sub> flow rate of 3 mL min<sup>-1</sup>. In each experiment, 3.0 g of dry *U. pinnatifida* sample was loaded into the extraction vessel, filled with glass beads at the bottom and top of the extraction vessel. The extraction vessel was placed in the heating chamber to maintain the operating temperature. The extracts were collected every 1 h for 5 h, weighed and analyzed immediately after collection. In all experiments, including ethanol soxhlet extraction and DME extraction, the extraction products were directly stored in the refrigerator at -60 °C. The bottles used for the collection of extracts were wrapped in aluminum foil. These processes were maintained until analysis. Co-solvent effect of ethanol on the supercritical CO<sub>2</sub> extraction was also examined. Ethanol flow rates that supplied by using high-pressure pump (PU-2080; Jasco, Hachioji, Japan) were between 0.05 and 0.5 mL min<sup>-1</sup>. In the case of co-solvent used, the pressure and temperature selected were 40 MPa and 60 °C, respectively.

**Figure 6.** Schematic diagram of supercritical CO<sub>2</sub> extraction.



#### 4. Conclusions

Liquefied DME extraction of fucoxanthin from *U. pinnatifida* was studied at temperature of 25 °C and pressure of 0.59 MPa using a semi-continuous flow-type system, a simple and environmentally friendly extraction method. Under these conditions, DME has ability to act hydrogen bond acceptors, forming hydrogen bonds with hydrogen-bonding solutes. Therefore, liquefied DME can enter into *U. pinnatifida* cells and goes out together with *U. pinnatifida* components include fucoxanthin. The amount of fucoxanthin could approach to 390 µg/g dry *U. pinnatifida* when the amount of DME used was 286 g. Compared with supercritical CO<sub>2</sub> and ethanol Soxhlet extraction, the result was quite high. Thus, DME extraction process appears to be

a good method for fucoxanthin recovery from *U. pinnatifida* with improved yields. On the basis of these results, it is proposed that DME extraction is applicable to isolate carotenoids from other types of biomass.

### Acknowledgments

A part of this research was supported by a grant from the Precursory Research for Embryonic Science and Technology Program of Japan Science and Technology Agency.

### Author Contributions

Kanda, H.: responsible to research publication, Kamo, Y.: carried out the experiment, Machmudah, S. and Wahyudiono: conducted all data analyses, Goto, M.: supervised this work and provided all experimental and analytical equipment. All authors read and approved the final manuscript.

### Conflicts of Interest

The authors declare no conflict of interest.

### References

1. Maeda, H.; Hosokawa, M.; Sashima, T.; Funayama, K.; Miyashita, K. Fucoxanthin from edible seaweed, *Undaria pinnatifida*, shows antiobesity effect through UCP1 expression in white adipose tissues. *Biochem. Biophys. Res. Commun.* **2005**, *332*, 392–397.
2. Yan, X.; Chuda, Y.; Suzuki, M.; Nagata, T. Fucoxanthin as the major antioxidant in *Hijikia fusiformis*, a common edible seaweed. *Biosci. Biotechnol. Biochem.* **1999**, *63*, 605–607.
3. Jung, H.A.; Islam, M.N.; Lee, C.M.; Jeong, H.O.; Chung, H.Y.; Woo, H.C.; Choi, J.S. Promising antidiabetic potential of fucoxanthin isolated from the edible brown algae *Eisenia bicyclis* and *Undaria pinnatifida*. *Fish. Sci.* **2012**, *78*, 1321–1329.
4. Maeda, H.; Hosokawa, M.; Sashima, T.; Miyashita, K. Dietary combination of fucoxanthin and fish oil attenuates the weight gain of white adipose tissue and decreases blood glucose in obese/diabetic KK-A<sup>y</sup> mice. *J. Agric. Food Chem.* **2007**, *55*, 7701–7706.
5. Beppu, F.; Hosokawa, M.; Niwano, Y.; Miyashita, K. Effects of dietary fucoxanthin on cholesterol metabolism in diabetic/obese KK-A<sup>y</sup> mice. *Lipids Health Dis.* **2012**, *11*, 112–119.
6. Hu, X.; Li, Y.; Li, C.; Fu, Y.; Cai, F.; Chen, Q.; Li, D. Combination of fucoxanthin and conjugated linoleic acid attenuates body weight gain and improves lipid metabolism in high-fat diet-induced obese rats. *Arch. Biochem. Biophys.* **2012**, *519*, 59–65.
7. Fung, A.; Hamid, N.; Lu, J. Fucoxanthin content and antioxidant properties of *Undaria pinnatifida*. *Food Chem.* **2013**, *136*, 1055–1062.
8. Sachindra, N.M.; Sato, E.; Maeda, H.; Hosokawa, M.; Niwano, Y.; Kohno, M.; Miyashita, K. Radical scavenging and singlet oxygen quenching activity of marine carotenoid fucoxanthin and its metabolites. *J. Agric. Food Chem.* **2007**, *55*, 8516–8522.

9. Hosokawa, M.; Kudo, M.; Maeda, H.; Kohno, H.; Tanaka, T.; Miyashita, K. Fucoxanthin induces apoptosis and enhances the antiproliferative effect of the PPAR $\gamma$  ligand, troglitazone, on colon cancer cells. *Biochim. Biophys. Acta* **2004**, *1675*, 113–119.
10. Kotake-Nara, E.; Kushiro, M.; Zhang, H.; Sugawara, T.; Miyashita, K.; Nagao, A. Carotenoids affect proliferation of human prostate cancer cells. *J. Nutr.* **2002**, *131*, 3303–3306.
11. Shiratori, K.; Ohgami, K.; Ilieva, I.; Jin, X.-H.; Koyama, Y.; Miyashita, K.; Yoshida, K.; Kase, S.; Ohno, S. Effects of fucoxanthin on lipopolysaccharide-induced inflammation *in vitro* and *in vivo*. *Exp. Eye Res.* **2005**, *81*, 422–428.
12. Plaza, M.; Cifuentes, A.; Ibanez, E. In the search of new functional food ingredients from algae. *Trends Food Sci. Technol.* **2008**, *19*, 31–39.
13. Shang, Y.F.; Kim, S.M.; Lee, W.J.; Um, B.-H. Pressurized liquid method for fucoxanthin extraction from *Eisenia bicyclis* (Kjellman) Setchell. *J. Biosci. Bioeng.* **2011**, *111*, 237–241.
14. Plaza, M.; Santoyo, S.; Jaime, L.; Garcia-Blairsy, R.G.; Herrero, M.; Senorans, F.J.; Ibanez, E. Screening for bioactive compounds from algae. *J. Pharm. Biomed. Anal.* **2010**, *51*, 450–455.
15. Xiao, X.; Si, X.; Yuan, Z.; Xu, X.; Li, G. Isolation of fucoxanthin from edible brown algae by microwave-assisted extraction coupled with high-speed countercurrent chromatography. *J. Sep. Sci.* **2012**, *35*, 2313–2317.
16. Halim, R.; Harun, R.; Danquah, M.K.; Webley, P.A. Microalgal cell disruption for biofuel development. *Appl. Energy* **2012**, *91*, 116–121.
17. Halim, R.; Danquah, M.K.; Webley, P.A. Extraction of oil from microalgae for biodiesel production: A review. *Biotechnol. Adv.* **2012**, *30*, 709–732.
18. Halim, R.; Rupasinghe, T.W.T.; Tull, D.L.; Webley, P.A. Mechanical cell disruption for lipid extraction from microalgal biomass. *Bioresour. Technol.* **2013**, *140*, 53–63.
19. Hii, S.-L.; Choong, P.-Y.; Woo, K.-K.; Wong, C.-L. Stability studies of fucoxanthin from *Sargassum Bunderi*. *Aust. J. Basic Appl. Sci.* **2010**, *4*, 4580–4584.
20. Billakanti, J.M.; Catchpole, O.; Fenton, T.; Mitchell, K. Extraction of fucoxanthin from *Undaria pinnatifida* using enzymatic pre-treatment followed by DME and EtOH co-solvent extraction. In Proceedings of the 10th International Symposium on Supercritical Fluids, San Fransisco, CA, USA, 13–16 May 2012; King, J., Ed.; CASSS: Emeryville, CA, USA, 2012.
21. Wu, J.; Zhou, Y.; Lemmon, E.W. An equation of state for the thermodynamic properties of dimethyl ether. *J. Phys. Chem. Ref. Data* **2011**, *40*, 023104.
22. Eltringham, W.; Catchpole, O.J. Relative permittivity measurements of gaseous, liquid, and supercritical dimethyl ether. *J. Chem. Eng. Data* **2007**, *52*, 363–367.
23. Holldorff, H.; Knapp, H. Binary vapor-liquid-liquid equilibrium of dimethyl ether-water and mutual solubilities of methyl chloride and water: Experimental results and data reduction. *Fluid Phase Equilibria* **1988**, *44*, 195–209.
24. European Food Safety Authority. Scientific opinion of the panel on food contact materials, enzymes, flavourings and processing aids (CEF) on dimethyl ether as an extraction solvent. *EFSA J.* **2009**, *984*, 1–13.
25. Varlet, V.; Smith, F.; Augsburger, M. New trends in the kitchen: Propellants assessment of edible food aerosol sprays used on food. *Food Chem.* **2014**, *142*, 311–317.

26. Naito, M.; Radcliffe, C.; Wada, Y.; Hoshino, T.; Liu, X.; Arai, M.; Tamura, M. A comparative study on the autoxidation of dimethyl ether (DME) comparison with diethyl ether (DEE) and diisopropyl ether (DIPE). *J Loss Prev. Process Ind.* **2005**, *18*, 469–473.
27. Li, P.; Kanda, H.; Makino, H. Simultaneous production of bio-solid fuel and bio-crude from vegetal biomass using liquefied dimethyl ether. *Fuel* **2014**, *116*, 370–376.
28. Mendes, R.L.; Fernandes, H.L.; Coelho, J.P.; Reis, E.C.; Cabral, J.M.S.; Novais, J.M.; Palavra, A.F. Supercritical CO<sub>2</sub> extraction of carotenoids and other lipids from *Chlorella vulgaris*. *Food Chem.* **1995**, *53*, 99–103.
29. Machmudah, S.; Shotipruk, A.; Goto, M.; Sasaki, M.; Hirose, T. Extraction of Astaxanthin from *Haematococcus pluvialis* using supercritical CO<sub>2</sub> and ethanol as entrainer. *Ind. Eng. Chem. Res.* **2006**, *45*, 3652–3657.
30. Kitada, K.; Machmudah, S.; Sasaki, M.; Goto, M.; Nakashima, Y.; Kumamoto, S.; Hasegawa, T. Supercritical CO<sub>2</sub> extraction of pigment components with pharmaceutical importance from *Chlorella vulgaris*. *J. Chem. Technol. Biotechnol.* **2009**, *84*, 657–661.
31. Roh, M.K.; Uddin, M.S.; Chun, B.S. Extraction of fucoxanthin and polyphenol from *Undaria pinnatifida* using supercritical carbon dioxide with co-solvent. *Biotechnol. Bioprocess Eng.* **2008**, *13*, 724–729.
32. Richter, B.E.; Jones, B.A.; Ezell, J.L.; Avdalovic, N.; Pohl, C. Accelerated solvent extraction: A technique for sample preparation. *Anal. Chem.* **1996**, *68*, 1033–1039.
33. Kim, S.M.; Jung, Y.J.; Kwon, O.N.; Cha, K.H.; Um, B.H.; Chung, D.; Pan, C.H. A potential commercial source of fucoxanthin extracted from the microalgae *Phaeodactylum tricornutum*. *Appl. Biochem. Biotechnol.* **2012**, *166*, 1843–1855.
34. Kanazawa, K.; Ozaki, Y.; Hashimoto, T.; Das, S.K.; Matsushita, S.; Hirano, M.; Okada, T.; Komoto, A.; Mori, N.; Nakatsuka, M. Commercial-scale preparation of biofunctional fucoxanthin from waste parts of brown sea algae *Laminaria japonica*. *Food Sci. Technol. Res.* **2008**, *14*, 573–582.
35. Bai, S.; Craig, M.V.; Liu, L.F.; Mayne, C.L.; Pugmire, R.J.; Grant, D.M. CO<sub>2</sub> clustering of 1-decanol and methanol in supercritical fluids by <sup>13</sup>C nuclear spin-lattice relaxation. *J. Phys. Chem.* **1997**, *101*, 2923–2928.
36. Bulgarevic, D.S.; Sako, T.; Sujeta, T.; Otake, K.; Takebayashi, Y.; Kamizawa, C.; Horikawa, Y.; Kato, M. The role of general hydrogen-bonding interaction in the solvation process of organic compounds by supercritical CO<sub>2</sub>/n-alcohol mixtures. *Ind. Eng. Chem. Res.* **2002**, *41*, 2074–2081.
37. Nehari, A.A.; Kim, S.B.; Lee, Y.B.; Lee, H.T.; Chun, B.S. Characterization of oil including astaxanthin extracted from krill (*Euphausia superba*) using supercritical carbon dioxide and organic solvent as comparative method. *Korean J. Chem. Eng.* **2012**, *29*, 329–336.

# Development of Pedigree Classification Using Microsatellite and Mitochondrial Markers for Giant Grouper Broodstock (*Epinephelus lanceolatus*) Management in Taiwan

Hsiao-Che Kuo, Hao-Hsuan Hsu, Chee Shin Chua, Ting-Yu Wang, Young-Mao Chen and Tzong-Yueh Chen

**Abstract:** Most giant groupers in the market are derived from inbred stock. Inbreeding can cause trait depression, compromising the animals' fitness and disease resistance, obligating farmers to apply increased amounts of drugs. In order to solve this problem, a pedigree classification method is needed. Here, microsatellite and mitochondrial DNA were used as genetic markers to analyze the genetic relationships among giant grouper broodstocks. The 776-bp fragment of high polymorphic mitochondrial D-loop sequence was selected for measuring sibling relatedness. In a sample of 118 giant groupers, 42 haplotypes were categorized, with nucleotide diversity ( $\pi$ ) of 0.00773 and haplotype diversity (HD) of 0.983. Furthermore, microsatellites were used for investigation of parentage. Six out of 33 microsatellite loci were selected as markers based on having a high number of alleles and compliance with Hardy-Weinberg equilibrium. Microsatellite profiles based on these loci provide high variability with low combined non-exclusion probability, permitting practical use in aquaculture. The method described here could be used to improve grouper broodstock management and lower the chances of inbreeding. This approach is expected to lead to production of higher quality groupers with higher disease resistance, thereby reducing the need for drug application.

Reprinted from *Mar. Drugs*. Cite as: Kuo, H.-C.; Hsu, H.-H.; Chua, C.S.; Wang, T.-Y.; Chen, Y.M.; Chen, T.-Y. Development of Pedigree Classification Using Microsatellite and Mitochondrial Markers for Giant Grouper Broodstock (*Epinephelus lanceolatus*) Management in Taiwan. *Mar. Drugs* **2014**, *12*, 239762407.

## 1. Introduction

The numbers of domesticated and farmed fish are increasing to facilitate feeding of the burgeoning human population [1]. More than 50 different species of grouper inhabit the tropical waters around Taiwan and some have been farmed since 1979. Among them, giant grouper is the most valuable grouper species in Taiwan. Although key aquaculture techniques on an industrial scale have been well established, outbreaks of various diseases remain a major unsolved problem [2–4]. However, most grouper broodstocks are second generation from wild-caught parent fish [5]. The larvae (third generation) cultivated in the fish farm for sale are derived from those broodstocks, and some of these larvae may be kept and used as broodstocks. The mixture of second- and third-generation broodstocks in the same pond means that the larvae (fourth generation) will be derived by inbreeding. Inbreeding is expected to lead to the appearance of defective recessive alleles that will reduce the trait quality and survival rate, resulting in growth depression and sensitive to environmental stress [6–9]. To solve this problem, a systematic broodstock management platform

that can track the family tree by using genetic markers must be established [10]. An ideal genetic marker would be one that incorporates aspects of variability, heritability, stability, and accessibility during identification [11]. Microsatellite DNA is commonly used as a genetic identification tool due to its high polymorphism, co-dominant features and neutral mutation [12,13]. Microsatellite markers can reveal the genetic inheritance of an individual within a population [14,15], given that there is a low probability of different and non-related individuals exhibiting the same microsatellite pattern [16]. Besides, the use of the mitochondrial D-loop has been proposed as a genetic marker as well; this segment of the mitochondrion, a maternally inherited genetic material, exhibits high variability and can be used to identify sibling relationship within a population [17].

Microsatellite and mitochondria markers have been used previously for tracking the genetic history of groupers [18–22]. Although there are many successful applications of both microsatellites and mitochondrial D-loop as genetic markers for identification of individual groupers, the management of giant grouper broodstocks in Taiwan still lacks a practical methodology. In this study, we used both microsatellite markers and mitochondrial D-loop sequences to develop a system for identification of parentage and sibling relationships. Establishment of these genetic markers is expected to ensure trait quality of broodstocks while not only preventing inbreeding depression like physical and health defects but also reducing drug and therapeutant use in aquaculture.

## 2. Results and Discussion

### 2.1. Analysis of Mitochondrial D-Loop Region

Within the 776-nt D-loop fragment examined here, 56 nucleotides exhibited variations, including insertion and deletion, among the 118 giant grouper broodstocks (Table 1). Among those 56 nucleotide variations, 42 haplotypes can be identified (a single mutation site correspond to a single genotype). The nucleotide diversity ( $\pi$ ) was 0.00773, and the haplotype diversity (HD) was 0.983 (Table 1). The genetic distance of haplotypes ranged between 0.215 and 0.0013, with an average of 0.0079 (Table 1). From 118 samples, the variation of nucleotides ranged between 16.684 and 1.0088 (average = 6.1304). These values indicate that the D-loop region used in this study is reliable for biogeographic analysis and sibling relationship determination.

In other developed systems, either of two distinct genetic markers (the mitochondrial D-loop and multiallelic microsatellites) has been used to assess variation within populations and to identify individuals. Low variation in D-loop nucleotide sequences of this fish species from our investigation suggested that the broodstock inbreeding level in Taiwan is high.

### 2.2. Analysis of Giant Grouper Microsatellite Loci

Examination of the results for microsatellite loci in giant grouper (Table 2) revealed that there were only 21 amplifiable sequences. Those loci were analyzed for allele number, allele distribution, expected heterozygosity (EH), and observed heterozygosity (OH) (Table 2). Among those loci, six were shortlisted based on their high heterozygosity and variability, properties that were expected to permit reliable parentage relationship determinations with high distinguishability and low error

probability. These six shortlisted loci included Efu19 (EH, 0.746063; OH, 0.8125), ELMS009 (EH, 0.77842; OH, 0.875), ELMS015 (EH, 0.83157; OH, 0.640625), RH\_CA\_2 (EH, 0.822466; OH, 0.890625) and RH\_GATA\_3 (EH, 0.845349; OH, 0.828125) (Table 2) are all carry a high number of alleles and comply with Hardy-Weinberg Equilibrium.

**Table 1.** Mitochondrial D-loop-based genetic diversity of giant groupers in Taiwan aquaculture industry.

<b>Parameter to the Genetic Diversity</b>	
Farms	3
Samples	118
Haplotypes	42
Length (base pair)	776
Nucleotide variations	56
Haplotype diversity(Hd)	0.983
Nucleotide diversity( $\pi$ )	0.00773
Maximum distance between each two haplotypes	0.0215
Minimum distance between each two haplotypes	0.0013
Mean distance between each two haplotypes	0.0079

By applying these six loci to a subset of 64 fish, the first parent non-exclusion probability is 0.01138738 (or 98.86% accurate) which we can identify the parentage relationship without knowing the genotypes of both parent fish. The non-exclusion probability (second parent) will lower (0.00089627 or 99.91% accurate) when one of the parent fish genotype is known (Table 3). It is important to obtain low combined non-exclusion probability (first and second parent) which means the combination of all six loci is predicted to determine parentage with low chance of misjudgment.

Knowing the origin of the broodstock can help to preclude collection of genetically closely related fish. We collected the samples from farms known to constantly replenish the broodstock from wild-caught fish or by purchasing small numbers of giant groupers from each of multiple different fish farms. This approach is recommended, since it can increase genetic variation within the fish population.

Table 2. Primers used for characterization of microsatellite loci in giant grouper.

Locus *	Accession Number	Repeat Motif	Primer Sequences (5'→3')	Allele Size	Allele Number	Expected Heterozygosity (EH)	Observed Heterozygosity (OH)
Efu02 <sup>a</sup>	EU016533	(CA) <i>n</i>	F: CTGTCAGCTGATTTATGG R: TTTACAGTCTCGTGGTTTCA	345–371	10	0.667815	0.484375
Efu06 <sup>a</sup>	EU016535	(GACA) <i>n</i>	F: CATTGTCATTGTGCTGTTTCTGTGC R: CCCTTTGGCCAATTGATGTGAT	308	1	0	0
Efu08 <sup>a</sup>	EU016537	(CA) <i>n</i>	F: TGGAGAAGCCTGTAGATTATTGTG R: AAGCAGGAGAGGAGTTGAAGGAGT	292–330	9	0.783465	0.796875
Efu18 <sup>a</sup>	EU016543	(CA) <i>n</i>	F: ACTGGCTCCCTTCTGTTC R: ATTGCCACCATCGCTACC	370–384	2	0.361713	0.4375
Efu19 <sup>a</sup>	EU016544	(CA) <i>n</i>	F: GGGGGTAACTCTCCAG R: AGCAGCAACACCTTCTTCTCA	93–115	7	0.746063	0.8125
Efu41 <sup>a</sup>	EU016545	(CA) <i>n</i>	F: CAGCAGCAGTTTAATTTACCAG R: CAGACCCGAGCTTCAGAA	243–249	2	0.353223	0.390625
ELMS009 <sup>b</sup>	EF607131	(CA) <i>n</i>	F: TTCCACAGCAATTAGCAGCA R: TTTCTCCACACAGTCCAAAG	260–278	8	0.77842	0.875
ELMS015 <sup>b</sup>	EF607136	(TG) <i>n</i>	F: AAGCTGAGCCGAAATTTTCA R: GCTCCTCGTGTTCGGATTA	335–369	12	0.83157	0.640625
Epaw3 <sup>c</sup>	EU684479	(GT) <i>n</i>	F: GTCGTGCTGTGACCCATGAG R: TAAGGAGGGGGCTAAAATGAT	72–76	2	0.503445	0
Epaw6 <sup>c</sup>	EU684482	(GT) <i>n</i>	F: ATGGTGTGGGAAAAGAGAGT R: TTGTTTCAGGACAAGTGAGC	146–233	5	0.619218	0.453125
Epaw19 <sup>c</sup>	EU684495	(GT) <i>n</i>	F: AGGTGGCTTGTGTGTATT R: GCTTCTTGACTGCTATGAC	243–247	3	0.215428	0.234375
Epaw34 <sup>c</sup>	EU684510	(TG) <i>n</i>	F: ACAGCACCTCTACCATGAAC R: CGTCCCCGTATATATCTCTG	224–248	3	0.212968	0.078125



Table 2. Cont.

CA-2 <sup>d</sup>	AF539606	(CA) <i>n</i>	F: GACTTGATTCAGCAAAAATAAAGATG R: AGAGACGGTGCCAGTAAATGAA	150–262	6	0.350271	0.0625
CA-3 <sup>d</sup>	AF539605	(CA) <i>n</i>	F: ATGTGACACGTTGACAGGCAAGT R: GACCTTGATATTTTCATTTGCTTG	300	1	0	0
CA-6 <sup>d</sup>	AF539608	(CA) <i>n</i>	F: GTGTGCTGGGGTTACTAATGAAG R: TTAGACACATTTGCACGATGGTCC	266–290	4	0.495325	0.5
RH_CA_1 <sup>e</sup>	DQ223785	(CA) <i>n</i>	F: CGAGATAAGCCCTGGTGAAG R: AGTCCCGATGTGGTAAACGAG	376–388	3	0.452879	0.46875
RH_GATA_2 <sup>e</sup>	DQ223791	(GATA) <i>n</i>	F: CTCGACAGTGGACAAGGTCA R: AAGGGCATGATGGGAAAATG	132	1	0	0
RH_CA_2 <sup>e</sup>	DQ223785	(CA) <i>n</i>	F: CTCGTTACCCACATCGGGACT R: AACACTGGCTGGTTTGCAC	135–175	13	0.822466	0.890625
RH_GATA_3 <sup>e</sup>	DQ223790	(GATA) <i>n</i>	F: GGGCAAATTTGGTTCTTCACA R: TGTCAATGCCACAGGATACA	225–273	10	0.845349	0.828125
RH_CA_7 <sup>e</sup>	DQ223786	(CA) <i>n</i>	F: CAGAAACATCTCCCCAAAA R: CTGGCAGAGCAATTAGAGGC	259–335	12	0.639887	0.34375
RH_CA_8 <sup>e</sup>	DQ223787	(CA) <i>n</i>	F: AGTTGCCCAAGTTACACGAG R: TTGGGTCTGGCATTAGAG	219–227	4	0.554995	0.515625

\* The loci listed here represent 21 microsatellite loci selected from previous studies of various species: (i) Tiger group: Efu02, Efu06, Efu08, Efu18, Efu19, Efu41; (ii) Giant group: ELMS009, ELMS015; (iii) Banded group: Epaw3, Epaw6, Epaw19, Epaw34; (iv) Hawaiian group: CA-2, CA-3, CA-6; (v) Red-spotted group: RH\_CA\_1, RH\_CA\_2, RH\_CA\_7, RH\_CA\_8, RH\_GATA\_2, RH\_GATA\_3; The references used for microsatellite loci primer design are <sup>a</sup> Lo and Yue, 2008

<sup>b</sup> Zeng *et al.*, 2008 [24]; <sup>c</sup> Zhao *et al.*, 2009 [25]; <sup>d</sup> Rivera *et al.*, 2003 [21]; <sup>e</sup> Ramirez *et al.*, 2006 [26], respectively.

**Table 3.** Paternity exclusion probabilities based on six selected microsatellite loci.

<b>Paternity Exclusion Probabilities</b>	
Combined non-exclusion probability (first parent)	0.01138738
Combined non-exclusion probability (second parent)	0.00089627

The observed large numbers of haplotypes (from the mitochondrial D-loop sequence) and high allele numbers (among the six multiallelic microsatellite loci) indicate that our samples were derived from different genetic pools. Nevertheless, the present study analyzed only a small number of giant groupers; the sample sizes of future studies will affect the determination of the number of D-loop haplotypes, number of microsatellite loci alleles, and their combined non-exclusive probabilities. Analysis of mitochondrial D-loop alone may have limitations. Offspring from a single female are expected to share a single mitochondrial haplotype [27]. However, in practical giant grouper breeding, the occurrence of transsexuality is expected to confuse the derivation of mitochondrial haplotypes. Such transsexual fish represents a problem, since these events may cause misidentification of the parent. However, the inclusion of the six selected microsatellite loci is expected to resolve this shortcoming. To determine sibling relationships between any two individuals, microsatellite loci of one parent must be known. However, there is no microsatellite loci database for grouper broodstock.

### 3. Experimental Section

#### 3.1. Fish Samples

The fin tissue samples from 118 individual broodstock animals were collected in three different locations (Linbian (44 fish), Jiadong (64 fish), and Fangliao (10 fish); Figure 1). Each fish in the same fishing pond was implanted and tagged with radio frequency identification (RFID) chips.

#### 3.2. DNA Extraction

A piece of fin tissue (100 mg) sampled from each grouper was subjected to the following DNA extraction procedure. The fin tissue was homogenized in 1 mL of extraction buffer (10 mM Tris-HCl, pH = 8.0, 2 mM EDTA, 10 mM NaCl, 10 M DTT, 1% SDS) with 100  $\mu\text{g mL}^{-1}$  of proteinase K, then incubated at 55 °C in a water bath until the tissue was completely dissolved. After lysis was completed, 20  $\mu\text{L}$  of RNAses A (10  $\mu\text{g/mL}$ ) was added to the tube, and then incubated at 37 °C for 1 h. DNA extraction was performed using the phenol-chloroform (phenol:chloroform:isoamyl alcohol = 25:24:1) method. Following precipitation in 99% ethanol, air dry and resuspension in TE buffer (10 mM Tris-HCl, pH = 8.0, 2 mM EDTA).

**Figure 1.** Giant grouper samples collected from farms in Pingtung region, Taiwan. Map (Modified from a map [28] under a Creative Commons Attribution-ShareAlike 1.0 License) inset shows locations of three different farms used for sampling: Linbian ( $n = 44$ ), Jiadong ( $n = 64$ ), and Fangliao ( $n = 10$ ), for a total of 118 fish.



### 3.3. Establishment of Haplotype Database

Full-length (16,642 bp) giant grouper mitochondrial DNA, as sequenced by our laboratory (accession number: KJ451389), was used for primer design. The forward (ATCATCGGCCA AATCGCATC) and reverse (GAACTGTAGGGCATTCTCAC) primers were designed to amplify a 1259-bp fragment. We then focused on the 776-bp D-loop sequence. Genetic analysis, including nucleotide composition, mutation rate, nucleotide diversity ( $\pi$ ) [29], haplotype diversity ( $H_d$ ) [30] and genetic distance (Kimura's two-parameter model), were performed using MEGA 5.1 [31] software. DAMBE 5.3.10 [24] software was used to analyze the transition/transversion ratio of D-loop mutations.

### 3.4. PCR and Analysis of Microsatellite Loci

The selection of the potential microsatellite loci as genetic markers in our species was based on previous studies. Primer design focused on several loci described in previous studies for various species (Table 2), including *Epinephelus lanceolatus* [26], *E. guttatus* [23], *E. fuscoguttatus* [25], *E. coioides* [20], *E. quernus* [21] and *E. awoara* [32]. The PCR reaction consisted of an initial round at 94 °C for 5 min, followed by 30 cycles of 94 °C for 1 min, 55 °C for 1 min, and 72 °C for 1 min, with a final extension at 72 °C for 10 min. In order to get a better resolution, ten microliters

of the PCR product then was analyzed by electrophoresis on a 12% polyacrylamide gel at 100 volts for 75 min and visualized by ethidium bromide. Following clean-up, the PCR products were sequenced using an ABI PRISM 3730 DNA analyzer (Life Technologies Co., Carlsbad, CA, USA).

The number of alleles for each locus, distribution of alleles, observed heterozygosity (OH), expected heterozygosity (EH), and agreement with Hardy-Weinberg equilibrium was measured using MSA 4.05 [33] software. Cervus 3.0.3 [34] software was used to calculate the combination of non-exclusion probability of the loci as parentage identification. The primers used in this study are listed in Table 2.

#### **4. Conclusions**

So far, there are about 300 male giant grouper broodstocks in Taiwan. Collection the genetic information from microsatellite to develop markers for each broodstock will be crucial for addressing the problem of inbreeding. For the techniques described in the present work, the mitochondrial D-loop should be used first to determine the potential sibling relationships among fish; biogeographic analysis then can be used to identify the individual broodstock to reduce inbreeding. Furthermore, the marker can be used to preclude the offspring from parent fish which shared the same microsatellite pattern but different in mitochondrial DNA sequence. In fact, the numbers of male broodstock typically are much lower than those of female broodstock, so maintenance of a separate male broodstock (along with genetic screening) may constitute an effective way to manage the genetic variation of farmed giant grouper.

#### **Acknowledgments**

We thank Chien-Hsien Kuo for his assistance with data analysis. We also thank the fish farmers for providing samples for this study. This study was supported by a grant from the Council of Agriculture, Taiwan (100AS-1.1.2-FA-F1, 101AS-11.3.1-FA-F5, 102AS-11.3.3-FA-F3) and National Science Council, Taiwan (NSC 101-2321-B-006-015, NSC 102-2321-B-006-016, NSC 103-2321-B-006-013).

#### **Author Contributions**

Conceived and designed the experiments: TYC. Performed the experiments: HCK, HHH, CSC, YMC, TYW. Analyzed the data: HCK, HHH, YMC, TYW, TYC. Wrote the paper: HCK, HHH, TYW, TYC. Assisted in drafting of text and figures of manuscript: HCK, HHH. Revised manuscript critically for important intellectual content: HCK, HHH, TYC.

#### **Conflicts of Interest**

The authors declare no conflict of interest.

## References

1. Duarte, C.M.; Marbá, N.; Holmer, M. Rapid domestication of marine species. *Science* **2007**, *316*, 382–383.
2. Kuo, H.C.; Wang, T.Y.; Chen, P.P.; Chen, Y.M.; Chuang, H.C.; Chen, T.Y. Real-time quantitative PCR assay for monitoring of nervous necrosis virus infection in grouper aquaculture. *J. Clin. Microbiol.* **2011**, *49*, 1090–1096.
3. Kuo, H.C.; Wang, T.Y.; Hsu, H.H.; Lee, S.H.; Chen, Y.M.; Tsai, T.J. Ou, M.C.; Ku, H.T.; Lee, G.B.; Chen, T.Y. An automated microfluidic chip system for detection of piscine nodavirus and characterization of its potential carrier in grouper farms. *PLoS One* **2012**, *7*, e42203.
4. Kuo, H.C.; Wang, T.Y.; Hsu, H.H.; Chen, P.P.; Lee, S.H.; Chen, Y.M.; Tsai, T.J.; Wang, C.K.; Ku, H.T.; Lee, G.B.; *et al.* Nervous necrosis virus replicates following the embryo development and dual infection with iridovirus at juvenile stage in grouper. *PLoS One* **2012**, *7*, e36183.
5. Pierre, S.; Gaillard, S.; Prevot-D'Alvise, N.; Aubert, J.; Rostaing-Capaillon, O.; Leung-Tack, D.; Grillasca, J.P. Grouper aquaculture: Asian success and Mediterranean trials. *Aquat. Conserv. Mar. Freshw. Ecosyst.* **2008**, *18*, 297–308.
6. Gjerde, B.; Gunnes, K.; Gjedrem, T. Effect of inbreeding on survival and growth in rainbow trout. *Aquaculture* **1983**, *34*, 327–332.
7. Pante, M.J.R.; Gjerde, B.; McMillan, I. Effect of inbreeding on body weight at harvest in rainbow trout, *Oncorhynchus mykiss*. *Aquaculture* **2001**, *192*, 201–211.
8. Chiang, T.Y.; Lee, T.W.; Hsu, K.C.; Kuo, C.H.; Lin, D.Y.; Lin, H.D. Population structure in the endangered cyprinid fish *Pararasbora moltrechti* in Taiwan, based on mitochondrial and microsatellite DNAs. *Zool. Sci.* **2011**, *28*, 642–651.
9. Jackson, T.R.; Martin-Robichaud, D.J.; Reith, M.E. Application of DNA markers to the management of Atlantic halibut (*Hippoglossus hippoglossus*) broodstock. *Aquaculture* **2003**, *220*, 245–259.
10. Jonsson, B.; Jonsson, N. Cultured Atlantic salmon in nature: A review of their ecology and interaction with wild fish. *ICES J. Mar. Sci.* **2006**, *63*, 1162–1181.
11. Sunnucks, P. Efficient genetic markers for population biology. *Trends Ecol. Evol.* **2000**, *15*, 199–203.
12. Sekino, M.; Takagi, N.; Hara, M.; Takahashi, H. Analysis of microsatellite DNA polymorphisms in rockfish *Sebastes thompsoni* and application to population genetics studies. *Mar. Biotechnol.* **2001**, *3*, 45–52.
13. Powell, W.; Morgante, M.; Andre, C.; McNicol, J.W.; Machray, G.C.; Doyle, J.J.; Tingey, S.V.; Rafalski, J.A. Hypervariable microsatellites provide a general source of polymorphic DNA markers for the chloroplast genome. *Curr. Biol.* **1995**, *5*, 1023–1029.
14. Beacham, T.D.; Pollard, S.; Le, K.D. Microsatellite DNA population structure and stock identification of steelhead trout (*Oncorhynchus mykiss*) in the Nass and Skeena Rivers in northern British Columbia. *Mar. Biotechnol.* **2000**, *2*, 587–600.

15. Olsen, J.B.; Bentzen, P.; Banks, M.A.; Shaklee, J.B.; Young, S. Microsatellites reveal population identity of individual pink salmon to allow supportive breeding of a population at risk of extinction. *Trans. Am. Fish. Soc.* **2000**, *129*, 232–242.
16. Bierne, N.; Beuzart, I.; Vonau, V.; Bonhomme, F.; Bédier, E.A. Microsatellite-associated heterosis in hatchery-propagated stocks of the shrimp *Penaeus stylirostris*. *Aquaculture* **2000**, *184*, 203–219.
17. Sang, T.K.; Chang, H.Y.; Chen, C.T.; Hui, C.F. Population structure of the Japanese eel, *Anguilla japonica*. *Mol. Biol. Evol.* **1994**, *11*, 250–260.
18. Zhu, Z.Y.; Lo, L.C.; Lin, G.; Xu, Y.X.; Yue, G.H. Isolation and characterization of polymorphic microsatellites from red coral grouper (*Plectropomus maculatus*). *Mol. Ecol. Notes* **2005**, *5*, 579–581.
19. An, H.S.; Kim, J.W.; Lee, J.W.; Kim, S.K.; Lee, B.I.; Kim, D.J.; Kim, Y.C. Development and characterization of microsatellite markers for an endangered species, *Epinephelus bruneus*, to establish a conservation program. *Anim. Cell Syst.* **2012**, *16*, 50–56.
20. Wang, L.; Meng, Z.; Liu, X.; Zhang, Y.; Lin, H. Genetic diversity and differentiation of the orange-spotted grouper (*Epinephelus coioides*) between and within cultured stocks and wild populations inferred from microsatellite DNA analysis. *Int. J. Mol. Sci.* **2011**, *12*, 4378–4394.
21. Rivera, M.A.; Graham, G.C.; Roderick, G.K. Isolation and characterization of nine microsatellite loci from the Hawaiian grouper *Epinephelus quernus* (Serranidae) for population genetic analyses. *Mar. Biotechnol.* **2003**, *5*, 126–129.
22. Han, J.; Lv, F.; Cai, H. Detection of species-specific long VNTRs in mitochondrial control region and their application to identifying sympatric Hong Kong grouper (*Epinephelus akaara*) and yellow grouper (*Epinephelus awoara*). *Mol. Ecol. Resour.* **2011**, *11*, 215–218.
23. Ramírez, M.A.; Patricia-Acevedo, J.; Planas, S.; Carlin, J.L.; Funk, S.M.; McMillan, W.O. New microsatellite resources for groupers (Serranidae). *Mol. Ecol. Notes* **2006**, *6*, 813–817.
24. Xia, X.; Xie, Z. DAMBE: Software package for data analysis in molecular biology and evolution. *J. Heredity* **2001**, *92*, 371–373.
25. Lo, L.C.; Yue, G.H. Microsatellites for broodstock management of the Tiger grouper, *Epinephelus fuscoguttatus*. *Anim. Genet.* **2008**, *39*, 90–91.
26. Zeng, H.S.; Ding, S.X.; Wang, J.; Su, Y.Q. Characterization of eight polymorphic microsatellite loci for the giant grouper (*Epinephelus lanceolatus* Bloch). *Mol. Ecol. Resour.* **2008**, *8*, 805–807.
27. Lin, L.Y.; Cheng, I.P.; Tzeng, C.S.; Huang, P.C. Maternal transmission of mitochondrial DNA in ducks. *Biochem. Biophys. Res. Comm.* **1990**, *168*, 188–193.
28. Mapsof.net. Available online: <http://mapsof.net> (accessed on 15 February 2013).
29. Nei, M.; Gojobori, T. Simple methods for estimating the numbers of synonymous and nonsynonymous nucleotide substitutions. *Mol. Biol. Evol.* **1986**, *3*, 418–426.
30. Nei, M.; Tajima, F. DNA polymorphism detectable by restriction endonucleases. *Genetics* **1981**, *97*, 145–163.
31. Tamura, K.; Dudley, J.; Nei, M.; Kumar, S. MEGA4: Molecular Evolutionary Genetics Analysis (MEGA) software version 4.0. *Mol. Biol. Evol.* **2007**, *24*, 1596–1599.

32. Zhao, L.; Shao, C.; Liao, X.; Ma, H.; Zhu, X.; Chen, S. Twelve novel polymorphic microsatellite loci for the Yellow grouper (*Epinephelus awoara*) and cross-species amplifications. *Conserv. Genet.* **2009**, *10*, 743–745.
33. Dieringer, D.; Schlotterer, C. MICROSATELLITE ANALYSER (MSA): A platform independent analysis tool for large microsatellite data sets. *Mol. Ecol. Notes* **2003**, *3*, 167–169.
34. Kalinowski, S.T.; Taper, M.L.; Marshall, T.C. Revising how the computer program CERVUS accommodates genotyping error increases success in paternity assignment. *Mol. Ecol.* **2007**, *16*, 1099–1106.

# Identification of Plakortide E from the Caribbean Sponge *Plakortis halichondroides* as a Trypanocidal Protease Inhibitor using Bioactivity-Guided Fractionation

Swarna Oli, Usama Ramadan Abdelmohsen, Ute Hentschel and Tanja Schirmeister

**Abstract:** In this paper, we report new protease inhibitory activity of plakortide E towards cathepsins and cathepsin-like parasitic proteases. We further report on its anti-parasitic activity against *Trypanosoma brucei* with an IC<sub>50</sub> value of 5 μM and without cytotoxic effects against J774.1 macrophages at 100 μM concentration. Plakortide E was isolated from the sponge *Plakortis halichondroides* using enzyme assay-guided fractionation and identified by NMR spectroscopy and mass spectrometry. Furthermore, enzyme kinetic studies confirmed plakortide E as a non-competitive, slowly-binding, reversible inhibitor of rhodesain.

Reprinted from *Mar. Drugs*. Cite as: Oli, S.; Abdelmohsen, U.R.; Hentschel, U.; Schirmeister, T. Identification of Plakortide E from the Caribbean Sponge *Plakortis halichondroides* as a Trypanocidal Protease Inhibitor using Bioactivity-Guided Fractionation. *Mar. Drugs* **2014**, *12*, 261462622.

## 1. Introduction

Proteases enable breakdown of proteins via catalytic hydrolysis of peptide bonds [1]. Malfunction in the control of protease activity leads to undesired and unregulated proteolysis which causes many diseases. Therefore, inhibitors of proteases have the potential to provide successful therapeutics for a wide range of diseases [2,3].

Marine sponges of the family Plakinidae are known to be rich sources of structurally unique and biologically active metabolites [4]. Bioactivity-guided fractionation of the crude cyclohexane extract from the sponge *Plakortis halichondroides* yielded a pure endoperoxide metabolite, named plakortide E (Figure 1), which was previously isolated from the same sponge species [5,6]. Plakortide E was previously shown to stimulate sarcoplasmic reticulum (SR) Ca<sup>2+</sup> ATPase activity [5]. Other endoperoxides from the plakortin family, e.g., six-membered plakortin [7], dihydroplakortin, 3-epiplakortin, plakortide Q [8] and plakortide M [9], are known to be active against Plasmodia, while the five-membered endoperoxide plakortide E was reported to be inactive [10]. In this work, we highlight its new anti-protease and anti-parasitic activities.

## 2. Results and Discussion

The lyophilized material of the sponge *Plakortis halichondroides* was sequentially extracted with three different solvents and the crude extracts were tested for protease inhibitory activity against the following proteases: Human cysteine proteases cathepsin B [11] and L [12], the related parasite enzyme rhodesain [13] from *Trypanosoma brucei rhodesiense*, and the two cysteine proteases expressed by the SARS coronavirus, namely SARS main protease [14] and SARS



papain-like protease [15]. The active crude cyclohexane extract (CY) was further fractionated using column chromatography and finally purified with HPLC to yield the active pure metabolite plakortide E (Figure 1). The purification process was based upon the bioactivity results, *i.e.*, only fractions which showed activity against the enzymes were purified further. The activity of the fractions gradually enhanced with every step of purification process, with the exception of the first cyclohexane extract which showed very high inhibition of cathepsins B and L (Figure 2) probably being due to presence of other non polar active compounds.

**Figure 1.** Structure of plakortide E.

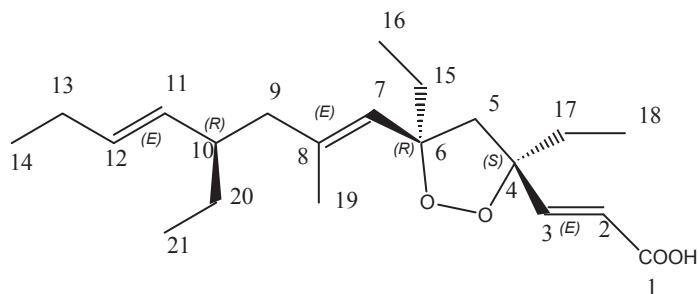
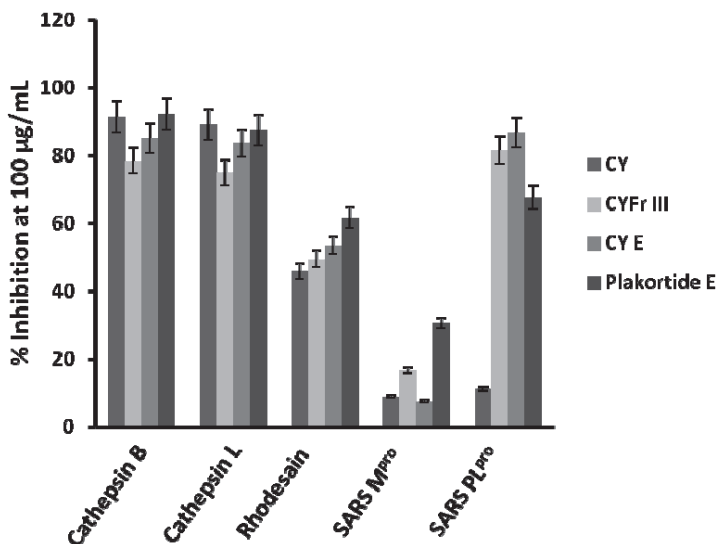
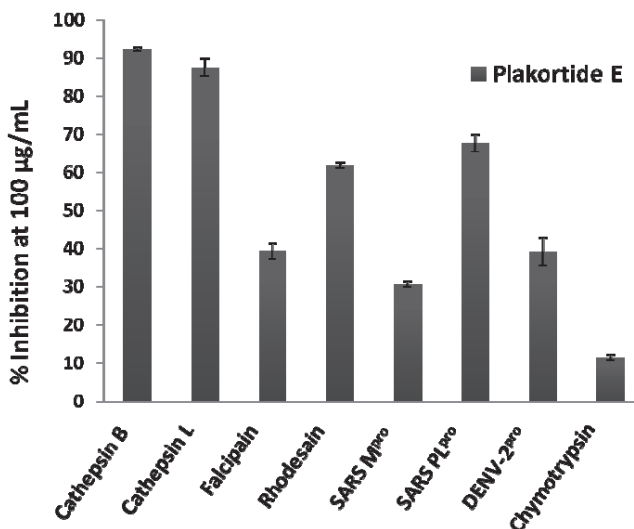


**Figure 2.** Protease inhibitory activity of the crude cyclohexane extract (CY), the subfractions CYFr III and CY E as well as plakortide E.



The pure metabolite plakortide E was further tested against the parasite cathepsin-L like protease falcipain-2 [16] from *Plasmodium falciparum*, as well as against the mammalian serine proteases chymotrypsin and the serine protease from Dengue virus (NS2B/NS3 protease) [17]. Inhibition at 100 µg/mL (285.71 µM) was only found with the cathepsins and the cathepsin-like proteases (Figure 3), especially with cathepsin B, L, rhodesain and SARS PL<sup>pro</sup>.

**Figure 3.** Percent inhibition of proteases by plakortide E at 100  $\mu\text{g}/\text{mL}$  (285  $\mu\text{M}$ ), tests were performed in triplicates.



In order to study the inhibition mechanism of plakortide E, enzyme assays [18] with various inhibitor and substrate concentrations were performed with cathepsin B to determine whether the inhibition is competitive with respect to the substrate. The  $\text{IC}_{50}$  values for cathepsin B were determined at three different substrate concentrations (50, 100, 200  $\mu\text{M}$ ). The values (29, 26, 36  $\mu\text{g}/\text{mL}$ , 82, 73, 103  $\mu\text{M}$ ) were almost similar indicating non-competitive inhibition. For cathepsin L, an  $\text{IC}_{50}$  of 37  $\mu\text{g}/\text{mL}$  (105  $\mu\text{M}$ ) at a substrate concentration of  $[\text{S}] = 6.25 \mu\text{M}$  and for rhodesain an  $\text{IC}_{50}$  of 44  $\mu\text{g}/\text{mL}$  (124  $\mu\text{M}$ ) at a substrate concentration of  $[\text{S}] = 30.0 \mu\text{M}$  was determined. With rhodesain, non-linear progress curves for the substrate hydrolysis were observed in the presence of inhibitor. Therefore, we determined the time-dependency of inhibition by measuring  $\text{IC}_{50}$  values in correlation to incubation time of enzyme with the inhibitor added, prior to substrate addition. The  $\text{IC}_{50}$  values decrease with longer incubation times (5 min  $\rightarrow$  90  $\mu\text{g}/\text{mL}$  (257  $\mu\text{M}$ ); 30 min  $\rightarrow$  72  $\mu\text{g}/\text{mL}$  (205  $\mu\text{M}$ ); 60 min  $\rightarrow$  27  $\mu\text{g}/\text{mL}$  (77  $\mu\text{M}$ )) indicating covalent inhibition or other mechanisms leading to slow binding. To address whether the inhibition is reversible or irreversible, further kinetic studies were performed as described by Copeland [19]. Dilution assays were performed and compared with K11777 [20], an irreversible vinylsulfone-based inhibitor of rhodesain. The enzyme rhodesain (100 fold concentration as used in the normal enzyme assays) was preincubated with the 10 fold  $\text{IC}_{50}$  concentration of the compound for one hour, which allows the formation of enzyme-inhibitor complexes and leads to total block of enzyme activity. The above complex was then diluted 100 fold by adding assay buffer and substrate. Thus, the enzyme concentration was reduced to the one used in the normal assays and the inhibitor concentration was reduced to 1/10 of the  $\text{IC}_{50}$ . If reversible, the inhibitor will dissociate from the complex and enzyme activity is recovered. In case of irreversible inhibition, dissociation of the complex cannot occur and no enzyme activity will be detected. These assays showed reactivation of the enzyme in the case of plakortide E to about 50% activity, while in contrast no enzyme activity was detected with K11777.

This indicates a reversible inhibition by plakortide E. In summary, plakortide E was determined to be a non-competitive, reversible, inhibitor of cysteine proteases, in case of rhodesain slow-binding was observed.

Furthermore, plakortide E was tested against the parasites *Leishmania major* promastigotes and the trypomastigote forms of *Trypanosoma brucei*, *Candida albicans*, and was also tested for its cytotoxicity against J774.1 macrophages. The compound exhibited trypanocidal activity with an IC<sub>50</sub> value of 5 µM (after 48 h and also after 72 h). This may at least in parts be due to the protease inhibiting properties of plakortide E. It did not show activity against *Leishmania* which also express a variety of cathepsin-like proteases [21]. No activity against *Candida*, and no cytotoxic effects against macrophages at 100 µM were observed. Since *Leishmania* promastigote forms express less cysteine proteases than the amastigote forms, the cysteine-protease inhibiting properties of the compound may not be sufficient for detectable leishmanicidal activity.

### 3. Experimental Section

The sponge *Plakortis halichondroides* was collected by SCUBA diving at depths of 30 m in Bahamas in July 2008 (GPS: 26°27'3.25"N, 77°54'14.59"W). Sponge tissues were cut into small pieces and preserved at -80 °C until extraction. The frozen material was then dried by lyophilization. The lyophilized material (640 g) was subsequently macerated and sequentially extracted with cyclohexane (CY), methylene dichloride (DCM), and finally methanol (MeOH). After filtration, the crude extracts were concentrated under reduced pressure. The crude cyclohexane extract (15.27 g) was chromatographed on a silica gel (200 g) column and eluted with an isocratic solvent (cyclohexane/methylene dichloride/methanol/formic acid (2:1:1:0.05)). The eluted fractions were combined based upon TLC results to yield five fractions (CYFr I–V). Further fractionation of the fraction CYFr III by silica gel column chromatography using the solvent system (cyclohexane/methylene dichloride (90:10) with increasing polarity (chloroform/methanol (10:90))) afforded seven subfractions (CY A–G). The subfraction CY E was subjected to preparative HPLC using a RP 18 column (eluent methanol/water with 0.1% formic acid 70:30, flow 8 mL/min) affording 3 fractions (CY M, N and P). The fraction CY N was further purified using preparative HPLC using RP 18 column (methanol/water amended with 0.1% formic acid 70:30, flow 8 mL/min, and the retention time of the peak was observed at 40 min) to yield the pure bioactive compound **1**. The compound **1** was identified as plakortide E, by means of MS and NMR spectral data (Table 1) and comparison to previously published NMR data [5,6,22]. Enzyme assays [18,21,23–25] and parasite growth assays [21,23–26] were performed as described previously.

NMR spectra (Table 1) were obtained with a BRUKER (Bruker Biospin GmbH, Rheinstetten Germany), Typ Advance 400 spectrometer. Mass spectra were measured using a Bruker micrOTOF 88 mass spectrometer. Column chromatography was performed using silica gel (0.063–0.200 mm mesh, Merck, Darmstadt, Germany). TLC was conducted on pre-coated silica gel 60 F254 plates (0.20 mm, Merck, Darmstadt, Germany); spots were detected using vanillin spray reagent, UV 254 nm and iodine vapours. Reagents were purchased from Sigma-Aldrich (Munich, Germany) or Fluka (Munich, Germany). Solvents were purchased from Roth (Karlsruhe, Germany) or Merck (Darmstadt, Germany). High performance liquid chromatography was performed on a Varian

ProStar (Rheinfelden, Schweiz), consisting of an analytical/preparative HPLC Upscale Linear system (0.05–50 mL/min at 275 bar pressure with scale-mast), a preparative autosampler and a 2-channel UV detector. The detection wavelengths were 254 nm and 230 nm.

**Table 1.** NMR-spectroscopic data of plakortide E (**1**) in CDCl<sub>3</sub> (<sup>1</sup>H: 400 MHz; <sup>13</sup>C: 100 MHz,  $\delta$  in ppm).

Position	$\delta_C$	Multiplicity	$\delta_H$	Multiplicity	$J$ (Hz)
1	171.76	C			
2	119.75	CH	6.09	d	15.8
3	152.31	CH	6.96	d	15.8
4	87.31	C			
5	56.11	CH <sub>2</sub>	2.55 2.45	d d	12.0 12.0
6	89.39	C			
7	126.71	CH	5.12	s	
8	136.82	C			
9	46.67	CH <sub>2</sub>	2.00 1.85	m m	
10	42.68	CH	1.99	m	
11	132.91	CH	5.05	ddt	15.2, 8.3
12	132.10	CH	5.34	dt	15.2, 6.3, 6.3
13	25.73	CH <sub>2</sub>	1.96	m	
14	14.19	CH <sub>3</sub>	0.94	t	7.4
15	32.36	CH <sub>2</sub>	1.88 1.64	m m	
16	9.01	CH <sub>3</sub>	0.89	t	7.4
17	30.88	CH <sub>2</sub>	1.76	m	
18	8.95	CH <sub>3</sub>	0.92	t	7.5
19	17.92	CH <sub>3</sub>	1.62	d	1.2
20	27.79	CH <sub>2</sub>	1.34 1.10	m m	
21	11.72	CH <sub>3</sub>	0.81	t	7.4

Plakortide E: The product was obtained as colourless viscous oil (0.018 g). CDCl<sub>3</sub> was used as solvent for measuring NMR spectra. ESI-MS found: 373.23404 [M + Na]<sup>+</sup>, calcd. for C<sub>21</sub>H<sub>34</sub>O<sub>4</sub>, 350.49. The specific rotation of plakortide E was  $[\alpha]_{D22}^{25} = +60.7^\circ$ ,  $c = 0.00313$  in CHCl<sub>3</sub>.

Enzyme assays and *in vitro* tests for antiparasitic activity were performed as published previously: for cathepsin-like cysteine proteases see [18,23–26], for SARS M<sup>PRO</sup> see [27], for SARS PL<sup>PRO</sup> see [15], for Dengue virus protease see [28], for assays against *T. brucei* see [24,29–32], for assays on macrophages see [33], for assays on *L. major* promastigotes see [21], for assays on *C. albicans* see [34,35].

#### 4. Conclusions

Plakortide E, obtained from the marine sponge *Plakortis halichondroides*, was identified as a new protease inhibitor. Plakortide E showed selectivity towards the cathepsin-like cysteine proteases, with a non-competitive, reversible, and, in the case of rhodesain, a slow-binding inhibitory mode of action. The anti-protease activity of the compound may contribute to its anti-parasitic activity against *Trypanosoma brucei*, as rhodesain and also the cathepsin B like protease TbCatB [13] are known to be essential for the parasite's growth and pathogenicity.

#### Acknowledgments

We would like to thank Cornelia Heindl and Anna Kucharski from University of Wuerzburg, Germany and Ulrike Nowe, Sabine Maehrlein, Nicole Heindl from University of Mainz for performing the enzyme assays. We gratefully acknowledge Antje Fuss and Svetlana Sologub (SFB 630 TP Z1, University of Wuerzburg) for performing the parasite and toxicity tests. We thank Joe Pawlik (UNC Wilmington, USA) for excellent organisation of the Bahamas 2008 expedition, during which the material was collected. Financial support is provided by the Deutsche Forschungsgemeinschaft, SFB 630 (TPs A4, A5).

#### Author Contributions

Swarna Oli, isolation and characterization of plakortide E, manuscript preparation, structure elucidation; Usama Ramadan Abdelmohsen, compound purification; Ute Hentschel, manuscript preparation; Tanja Schirmeister, manuscript preparation, analysis of assay results.

#### Conflicts of Interest

The authors declare no conflict of interest.

#### References

1. Turk, B. Targeting proteases: Successes, failures and future prospects. *Nat. Rev. Drug Discov.* **2006**, *5*, 785–799.
2. Powers, J.C.; Asgian, J.L.; Ekici, Ö.D.; James, K.E. Irreversible inhibitors of serine, cysteine and threonine proteases. *Chem. Rev.* **2002**, *102*, 4639–4750.
3. Rawlings, N.D.; Morton, F.R. The MEROPS batch BLAST: A tool to detect peptidases and their non-peptidase homologues in a genome. *Biochimie* **2008**, *90*, 243–259.
4. Sata, N.; Abinsay, H.; Yoshida, W.Y.; Horgen, F.D.; Sitachitta, N.; Kelly, M.; Scheuer, P.J. Lehaulides A–D, metabolites from a Hawaiian sponge of the genus *Plakortis*. *J. Nat. Prod.* **2005**, *68*, 1400–1403.
5. Patil, A.D.; Freyer, A.J.; Bean, M.F.; Carte, B.K.; Westley, J.W.; Johnson, R.K.; Lahouratate, P. The plakortones, novel bicyclic lactones from the sponge *Plakortis halichondroides*: Activators of cardiac SR-Ca<sup>2+</sup> pumping ATPase. *Tetrahedron* **1996**, *52*, 377–394.

6. Chen, Y.; McCarthy, P.J.; Harmody, D.K.; Schimoler-O'Rourke, R.; Chilson, K.; Selitrennikoff, C.; Pomponi, S.A.; Wright, A.E. New bioactive peroxides from marine sponges of the family plakiniidae. *J. Nat. Prod.* **2002**, *65*, 1509–1512.
7. Fattorusso, C.; Campiani, G.; Catalanotti, B.; Persico, M.; Basilico, N.; Parapini, S.; Taramelli, D.; Campagnuolo, C.; Fattorusso, E.; Romano, A.; *et al.* Endoperoxide derivatives from marine organisms: 1,2-Dioxanes of the plakortin family as novel antimalarial agents. *J. Med. Chem.* **2006**, *49*, 7088–7094.
8. Campagnuolo, C.; Fattorusso, E.; Romano, A.; Tagliatela-Scafati, O.; Basilico, N.; Parapini, S.; Taramelli, D. Antimalarial polyketide cycloperoxides from the marine sponge *Plakortis simplex*. *Eur. J. Org. Chem.* **2005**, *23*, 5077–5083.
9. Hu, J.-F.; Gao, H.-F.; Kelly, M.; Hamann, M.T. Plakortides I–L, four new cyclic peroxides from an undescribed Jamaican sponge *Plakortis* sp. (Homosclerophorida, Plakinidae). *Tetrahedron* **2001**, *57*, 9379–9383.
10. Fattorusso, E.; Parapini, S.; Campagnuolo, C.; Basilico, N.; Tagliatela-Scafati, O.; Taramelli, D. Activity against *Plasmodium falciparum* of cycloperoxide compounds obtained from the sponge *Plakortis simplex*. *J. Antimicrob. Chemother.* **2002**, *50*, 883–888.
11. Palermo, C.; Joyce, J.A. Cysteine cathepsin proteases as pharmacological targets in cancer. *Trends Pharm. Sci.* **2008**, *29*, 22–28.
12. Lankelma, J.M.; Voorend, D.M.; Barwari, T.; Koetsveld, J.; Van der Spek, A.H.; de Porto, A.P.N.A.; Van Rooijen, G.; Van Noorden, C.J.F. Cathepsin L target in cancer treatment? *Life Sci.* **2010**, *86*, 225–233.
13. Kerr, I.D.; Wu, P.; Marion-Tsukamaki, R.; Mackey, Z.B.; Brinen, L.S. Crystal structures of TbCatB and rhodesain, potential chemotherapeutic targets and major cysteine proteases of *Trypanosoma brucei*. *PLoS Negl. Trop. Dis.* **2010**, *4*, doi:10.1371/journal.pntd.0000701.
14. Anand, K.; Ziebuhr, J.; Wadhwani, P.; Mesters, J.R.; Hilgenfeld, R. Coronavirus main proteinase (3CLpro) structure: Basis for design of anti-SARS drugs. *Science* **2003**, *300*, 1763–1767.
15. Han, Y.-S.; Chang, G.-G.; Juo, C.-G.; Lee, H.-J.; Yeh, S.-H.; Hsu, J.T.-A.; Chen, X. Papain-like protease 2 (PLP2) from Severe Acute Respiratory Syndrome Coronavirus (SARS-CoV): Expression, purification, characterization, and inhibition. *Biochemistry* **2005**, *44*, 10349–10359.
16. Rosenthal, P. Falcipains and other cysteine proteases of malaria parasites. In *Cysteine Proteases of Pathogenic Organisms*; Robinson, M., Dalton, J., Eds.; Springer: San Francisco, California, USA, 2011; Volume 712, pp. 30–48.
17. Bessaud, M.; Pastorino, B.A.M.; Peyrefitte, C.N.; Rolland, D.; Grandadam, M.; Tolou, H.J. Functional characterization of the NS2B/NS3 protease complex from seven viruses belonging to different groups inside the genus *Flavivirus*. *Virus Res.* **2006**, *120*, 79–90.
18. Breuning, A.; Degel, B.; Schulz, F.; Buchold, C.; Stempka, M.; Machon, U.; Heppner, S.; Gelhaus, C.; Leippe, M.; Leyh, M.; *et al.* Michael acceptor based antiplasmodial and antitrypanosomal cysteine protease inhibitors with unusual amino acids. *J. Med. Chem.* **2010**, *53*, 1951–1963.

19. Copeland, R.A. A Guide for Medicinal Chemists and Pharmacologists. In *Evaluation of Enzyme Inhibitors in Drug Discovery*; John Wiley & Sons, Inc.: Hoboken, NJ, USA, 2005.
20. Yang, P.-Y.; Wang, M.; He, C.Y.; Yao, S.Q. Proteomic profiling and potential cellular target identification of K11777, a clinical cysteine protease inhibitor, in *Trypanosoma brucei*. *Chem. Commun.* **2012**, *48*, 835–837.
21. Ponte-Sucre, A.; Vicik, R.; Schultheis, M.; Schirmeister, T.; Moll, H. Aziridine-2,3-dicarboxylates, peptidomimetic cysteine protease inhibitors with antileishmanial activity. *Antimicrob. Agents Chemother.* **2006**, *50*, 2439–2447.
22. Sun, X.Y.; Tian, X.Y.; Li, Z.W.; Peng, X.S.; Wong, H.N. Total synthesis of plakortide E and biomimetic synthesis of plakortone B. *Chemistry* **2011**, *17*, 5874–5880.
23. Vicik, R.; Busemann, M.; Gelhaus, C.; Stiefl, N.; Scheiber, J.; Schmitz, W.; Schulz, F.; Mladenovic, M.; Engels, B.; Leippe, M.; *et al.* Aziridide-based inhibitors of cathepsin L: synthesis, inhibition activity, and docking studies. *ChemMedChem* **2006**, *1*, 1126–1141.
24. Vicik, R.; Hoerr, V.; Glaser, M.; Schultheis, M.; Hansell, E.; McKerrow, J.H.; Holzgrabe, U.; Caffrey, C.R.; Ponte-Sucre, A.; Moll, H.; Stich, A.; *et al.* Aziridine-2,3-dicarboxylate inhibitors targeting the major cysteine protease of *Trypanosoma brucei* as lead trypanocidal agents. *Bioorg. Med. Chem. Lett.* **2006**, *16*, 2753–2757.
25. Ehmke, V.; Heindl, C.; Rottmann, M.; Freymond, C.; Schweizer, W.B.; Brun, R.; Stich, A.; Schirmeister, T.; Diederich, F. Potent and selective inhibition of cysteine proteases from *Plasmodium falciparum* and *Trypanosoma brucei*. *ChemMedChem* **2011**, *6*, 273–278.
26. Ettari, R.; Zappala, M.; Micale, N.; Giofre, S.; Schirmeister, T.; Grasso, S. Peptidomimetics containing a vinyl ketone warhead as falcipain-2 inhibitor. *Eur. J. Med. Chem.* **2011**, *46*, 2058–2065.
27. K appler, U.; Stiefl, N.; Schiller, M.; Vicik, R.; Breuning, A.; Schmitz, W.; Rupprecht, D.; Schmuck, C.; Baumann, K.; Ziebuhr, J.; *et al.* A new lead for non-peptidic active-site-directed inhibitors of the SARS coronavirus main protease discovered by a combination of screening and docking methods. *J. Med. Chem.* **2005**, *48*, 6832–6842.
28. Steuer, C.; Heinonen, K.H.; Kattner, L.; Klein, C.D. Optimization of assay conditions for dengue virus protease: Effect of various polyols and nonionic detergents. *J. Biomol. Screen.* **2009**, *14*, 1102–1108.
29. Baltz, T.; Baltz, D.; Giroud, C.; Crocket, J. Cultivation in a semi-defined medium of animal infective forms of *Trypanosoma brucei*, *T. equiperdum*, *T. evansi*, *T. rhodesiense* and *T. gambiense*. *EMBO J.* **1985**, *4*, 1273–1277.
30. R az, B.; Iten, M.; Grether-B uhler, Y.; Kaminsky, R.; Brun, R. The Alamar Blue assay to determine drug sensitivity of African trypanosomes (*T.b. rhodesiense* and *T.b. gambiense*) *in vitro*. *Acta Trop.* **1997**, *68*, 139–147.
31. Merschjohann, K.; Sporer, F.; Steverding, D.; Wink, M. *In vitro* effect of alkaloids on bloodstream forms of *Trypanosoma brucei* and *T. congolense*. *Planta Med.* **2001**, *67*, 623–627.
32. Huber, W.; Koella, J.C. A comparison of three methods of estimating EC<sub>50</sub> in studies of drug resistance of malaria parasites. *Acta Trop.* **1993**, *55*, 257–261.

33. Ahmed, S.A.; Gogal, R.M.; Walsh, J.E. A new rapid and simple non-radioactive assay to monitor and determine the proliferation of lymphocytes: An alternative to [<sup>3</sup>H] thymidine incorporation assay. *J. Immunol. Methods* **1994**, *170*, 211–224.
34. Degel, B.; Staib, P.; Rohrer, S.; Scheiber, J.; Martina, E.; Büchold, C.; Baumann, K.; Morschhäuser, J.; Schirmeister, T. *Cis*-configured aziridines are new pseudo-irreversible dual-mode inhibitors of *Candida albicans* secreted aspartic protease 2. *ChemMedChem* **2008**, *3*, 302–315.
35. Büchold, C.; Hemberger, Y.; Heindl, C.; Welker, A.; Degel, B.; Pfeuffer, T.; Staib, P.; Schneider, S.; Rosenthal, P.J.; Gut, J.; *et al.* New *cis*-configured aziridine-2-carboxylates as aspartic acid protease inhibitors. *ChemMedChem* **2011**, *6*, 141–152.



## Discovery of Novel Saponins from the Viscera of the Sea Cucumber *Holothuria lessoni*

Yadollah Bahrami, Wei Zhang and Chris Franco

**Abstract:** Sea cucumbers, sometimes referred to as marine ginseng, produce numerous compounds with diverse functions and are potential sources of active ingredients for agricultural, nutraceutical, pharmaceutical and cosmeceutical products. We examined the viscera of an Australian sea cucumber *Holothuria lessoni* Massin *et al.* 2009, for novel bioactive compounds, with an emphasis on the triterpene glycosides, saponins. The viscera were extracted with 70% ethanol, and this extract was purified by a liquid-liquid partition process and column chromatography, followed by isobutanol extraction. The isobutanol saponin-enriched mixture was further purified by high performance centrifugal partition chromatography (HPCPC) with high purity and recovery. The resultant purified polar samples were analyzed using matrix-assisted laser desorption/ionization mass spectrometry (MALDI-MS)/MS and electrospray ionization mass spectrometry (ESI-MS)/MS to identify saponins and characterize their molecular structures. As a result, at least 39 new saponins were identified in the viscera of *H. lessoni* with a high structural diversity, and another 36 reported triterpene glycosides, containing different aglycones and sugar moieties. Viscera samples have provided a higher diversity and yield of compounds than observed from the body wall. The high structural diversity and novelty of saponins from *H. lessoni* with potential functional activities presents a great opportunity to exploit their applications for industrial, agricultural and pharmaceutical use.

Reprinted from *Mar. Drugs*. Cite as: Bahrami, Y.; Zhang, W.; Franco, C. Discovery of Novel Saponins from the Viscera of the Sea Cucumber *Holothuria lessoni*. *Mar. Drugs* **2014**, *12*, 263362667.

### 1. Introduction

Holothurians are sedentary marine invertebrates, commonly known as sea cucumbers, trepang, bêche-de-mer, or gamat [1,2], belonging to the class Holothuroidea of the *Echinodermata* phylum. Sea cucumbers produce numerous compounds with diverse functions and are potential sources of agricultural or agrochemical, nutraceutical, pharmaceutical and cosmeceutical products [3–5]. It is for this reason they are called “marine ginseng” in Mandarin.

Even though sea cucumbers contain different types of natural compounds, saponins are their most important and abundant secondary metabolites [6–12]. Saponins are reported as the major bioactive compound in many effective traditional Chinese and Indian herbal medicines.

Sea cucumber saponins are known to have a wide range of medicinal properties due to their cardiovascular, immunomodulator, cytotoxic, anti-asthma, anti-eczema, anti-inflammatory, anti-arthritis, anti-oxidant, anti-diabetics, anti-bacterial, anti-viral, anti-cancer, anti-angiogenesis, anti-fungal, hemolytic, cytostatic, cholesterol-lowering, hypoglycemia and anti-dementia activities [4,7,13–24].

Saponins are amphipathic compounds that generally possess a triterpene or steroid backbone or aglycone. Triterpenoid saponins have aglycones that consist of 30 carbons, whereas steroidal saponins possess aglycones with 27 carbons, which are rare in nature [4].

Triterpene saponins belong to one of the most numerous and diverse groups of natural occurring products, which are produced in relatively high abundance. They are reported primarily as typical metabolites of terrestrial plants [25]. A few marine species belonging to the phylum *Echinodermata* [26] namely holothuroids (sea cucumbers) [7,10,13,27–33] and asteroids, and sponges from the phylum *Porifera* [13,34,35] produce saponins.

The majority of sea cucumber saponins, generally known as Holothurins, are usually triterpene glycosides, belonging to the holostane type group rather than nonholostane [36,37], which is comprised of a lanostane-3 $\beta$ -ol type aglycone containing a  $\gamma$ -18 (20)-lactone in the D-ring of tetracyclic triterpene (3 $\beta$ ,20*S*-dihydroxy-5 $\alpha$ -lanostano-18,20-lactone) [25] sometimes containing shortened side chains, and a carbohydrate moiety consisting of up to six monosaccharide units covalently connected to C-3 of the aglycone [7,8,13,37–42].

The sugar moiety of the sea cucumber saponins consists mainly of D-xylose, D-quinovose, 3-*O*-methyl-D-glucose, 3-*O*-methyl-D-xylose and D-glucose and sometimes 3-*O*-methyl-D-quinovose, 3-*O*-methyl-D-glucuronic acid and 6-*O*-acetyl-D-glucose [40,41,43–48]. In the oligosaccharide chain, the first monosaccharide unit is always a xylose, whereas either 3-*O*-methylglucose or 3-*O*-methylxylose is always the terminal sugar.

Although some identical saponins have been given different names by independent research groups [6] as they could be isomeric compounds, our comprehensive literature review showed that more than 250 triterpene glycosides have been reported from various species of sea cucumbers [7,13,18,25,29,41,44,49,50]. They are classified into four main structural categories based on their aglycone moieties; three holostane type glycoside group saponins containing a (1) 3 $\beta$ -hydroxyholost-9 (11)-ene aglycone skeleton; (2) saponins with a 3 $\beta$ -hydroxyholost-7-ene skeleton and (3) saponins with an aglycone moiety different to the other two holostane type aglycones (other holostane type aglycones); and (4) a nonholostane aglycone [25,38,46,51,52].

One of the most noteworthy characteristics of many of the saponins from marine organisms is the sulfation of aglycones or sugar moieties [4]. In sea cucumber saponins, sulfation of the oligosaccharide chain in the Xyl, Glc and MeGlc residues has been reported [38,40,46,53,54]. Most of them are mono-sulfated glycosides with few occurrences of di- and tri-sulfated glycosides. Saponin diversity can be further enhanced by the position of double bonds and lateral groups in the aglycone.

Triterpene glycosides have been considered a defense mechanism, as they are deleterious for most organisms [6–10,12,55–57]. In contrast, a recent study has shown that these repellent chemicals are also kairomones that attract the symbionts and are used as chemical “signals” [58]. However, in the sea cucumber, it has been suggested that saponins may also have two regulatory roles during reproduction: (1) to prevent oocyte maturation and (2) to act as a mediator of gametogenesis [18,59].

The wide range of biological properties and various physiological functions of sea cucumber extracts with high chemical structural diversity and the abundance of their metabolites have spurred

researchers to study the ability of sea cucumbers to be used as an effective alternative source for potential future drugs. However, the large number of very similar saponin glycosides structures has led to difficulties in purification, and the complete structure elucidation of these molecules (especially isomers), has made it difficult to conduct tests to determine structure-activity relationships, which can lead to the development of new compounds with commercial applications [16]. Therefore, in order to overcome this problem, we employed High Performance Centrifugal Partition Chromatography (HPCPC) to successfully purify saponins in this study. HPCPC is more efficient in purifying large amounts of a given sample and also lower solvent consumption with high yields compared to other conventional chromatography methods.

This project aims to identify and characterize the novel bioactive compounds from the viscera (all internal organs other than the body wall) of an Australian sea cucumber *Holothuria lessoni* Massin *et al.* 2009 (golden sandfish) with an emphasis on saponins. *H. lessoni* was selected because it is a newly-identified Holothurian species, which is abundant in Australian waters. While only a few studies have compared the saponin contents of the body wall with that of the cuvierian tubules in other species [50,60–62], to our knowledge, no study has investigated the contribution of saponins of the body wall or the viscera of *Holothuria lessoni*. Sea cucumbers expel their internal organs as a defense mechanism called evisceration, a reaction that includes release of the respiratory tree, intestine, cuvierian tubules and gonads through the anal opening [50,58,61,63–68]. We hypothesize that the reason for this ingenious form of defense is because these organs contain high levels of compounds that repel predators [60,61,69,70]. Furthermore, the results of this project may identify the potential economic benefits of transforming viscera of the sea cucumber into high value co-products important to human health and industry.

Matrix-assisted laser desorption/ionization time-of-flight mass spectrometry (MALDI-ToF/MS) and electrospray ionization mass spectrometry (ESI-MS) techniques allow the “soft” ionization of large biomolecules, which has been a big challenge until recently [71]. Therefore, MALDI and ESI-MS, and MS/MS were performed to detect saponins and to elucidate their structures.

## 2. Results and Discussion

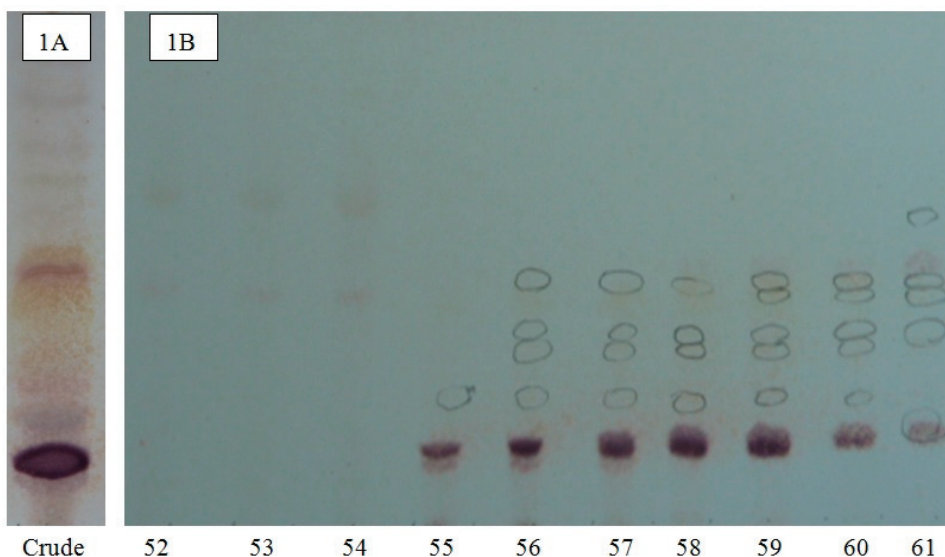
An effective method for the purification of saponins has been developed, and several saponins were isolated and purified from the viscera of *H. lessoni*. The enriched saponin mixtures of the viscera extract were successfully purified further by HPCPC, which is very efficient in purifying compounds with low polarity as well as in processing large amounts of sample. This method yielded saponins with higher than a 98% recovery of sample with high purities [72]. Purifying saponins from mixtures of saponins also helps to overcome the problem associated with identifying multiple saponins with liquid chromatography-tandem mass spectrometry (LC-MS) and ESI-MS. Mass spectrometry has been applied for the structure elucidation of saponins in both negative and positive ion modes [73–79]. In this study, identification of the saponin compounds was attempted by soft ionization MS techniques including MALDI and ESI in the positive mode. Previous studies have reported that the fragment ions of alkali metal adducts of saponins provide valuable structural information about the feature of the aglycone and the sequence and linkage site of the sugar residues [80]. Therefore, the MS analyses were conducted by introducing sodium ions to the

samples. However, saponin spectra can also be detected without adding a sodium salt. Because of the high affinity of alkali cations for triterpene glycosides, all saponins detected in the positive ion mode spectra were predominantly singly charged sodium adducts of the molecules  $[M + Na]^+$  [19,81]. The main fragmentation of saponins generated by cleavage of the glycosidic bond yielded oligosaccharide and monosaccharide fragments [19]. Other visible peaks and fragments were generated by the loss of other neutral moieties such as  $CO_2$ ,  $H_2O$  or  $CO_2$  coupled with  $H_2O$ .

The saponins obtained from the viscera of this tropical holothurian were profiled using MALDI-MS and ESI-MS. MALDI is referred to as a “soft” ionization technique, because the spectrum shows mostly intact, singly charged ions for the analyte molecules. However, in some cases, MALDI causes minimal fragmentation of analytes [71].

The chromatographic purification of isobutanol-soluble saponin-enriched fractions of *H. lessoni* viscera was monitored on pre-coated thin-layer chromatography (TLC) plates (Figure 1A) showing the presence of several bands. As a typical example, the TLC profile of HPCPC Fractions 52–61 of the isobutanol-saponin enriched fraction from the viscera of the *H. lessoni* sea cucumber is shown in Figure 1B. The centrifugal partition chromatography (CPC) technique not only allowed for the purification of saponins, but in some cases it could separate isomeric saponins e.g., separation of the isomers detected in the ion peak at  $m/z$  1303.6, which will be discussed later.

**Figure 1.** The thin-layer chromatography (TLC) pattern of a saponin mixture (A) and the high performance centrifugal partition chromatography (HCPCP) fractions (B) from the purified extracts of the viscera of the *Holothuria lessoni* sea cucumber using the lower phase of  $CHCl_3$ -MeOH- $H_2O$  (7:13:8) system. The numbers under each lane indicate the fraction number of fractions in the fraction collector. Here, only the fractions 52 to 61 of one analysis (of 110 fractions) are shown as a representative.



Mass spectrometry has been used extensively for the characterization of saponins and their structural confirmation. One of the powerful methods, which are widely used for the analysis of high molecular weight, non-volatile molecules is MALDI [82]. The appropriate HPCPC fractions were consequently pooled based on their TLC profiles and concentrated to dryness and analyzed by MALDI MS and MS/MS, and ESI MS/MS. In the positive ion mode, all detected ions were sodium-coordinated species such as  $[M + Na]^+$  corresponding to sulfated and non-sulfated saponins [64]. The prominence of the parent ions  $[M + Na]^+$  in MS spectra also enables the analysis of saponins in mixtures or fractions. The MALDI results indicate that the saponin fractions are quite pure, which is consistent with the TLC data. As a representative example, the full-scan MALDI mass spectrum of the saponin extract obtained from HPCPC Fraction 55 of the *H. lessoni* viscera is shown in Figure 2.

This spectrum displays the major intense peak detected at  $m/z$  1243.4, which corresponds to Holothurin A, with an elemental composition of  $C_{54}H_{85}NaO_{27}S$   $[M + Na]^+$ . Other visible peaks seem to correspond to the sugar moieties and aglycone ions generated by the losses of sugars and/or losses of water and/or carbon dioxide from cationized saponins upon MALDI ionization. These analyses show that this fraction contains one main saponin. Therefore, even though the HPCPC fractionation separated the saponin mixture, some saponin congeners, due to the similarity in their TLC migration, were detected in some of the pooled fractions. It was found that the total separation of the saponins was difficult within a single HPCPC run. However, this technique allowed the separation of a number of saponins, including some isomers (Figure 3).

**Figure 2.** The full-scan matrix-assisted laser desorption/ionization mass spectrometry (MALDI) mass spectrum of HPCPC Fraction 55 in the (+) ion mode.

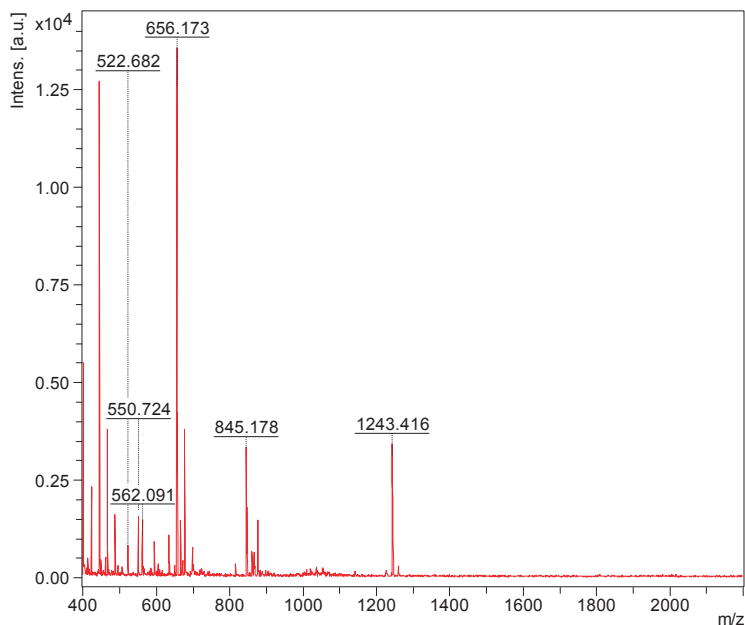
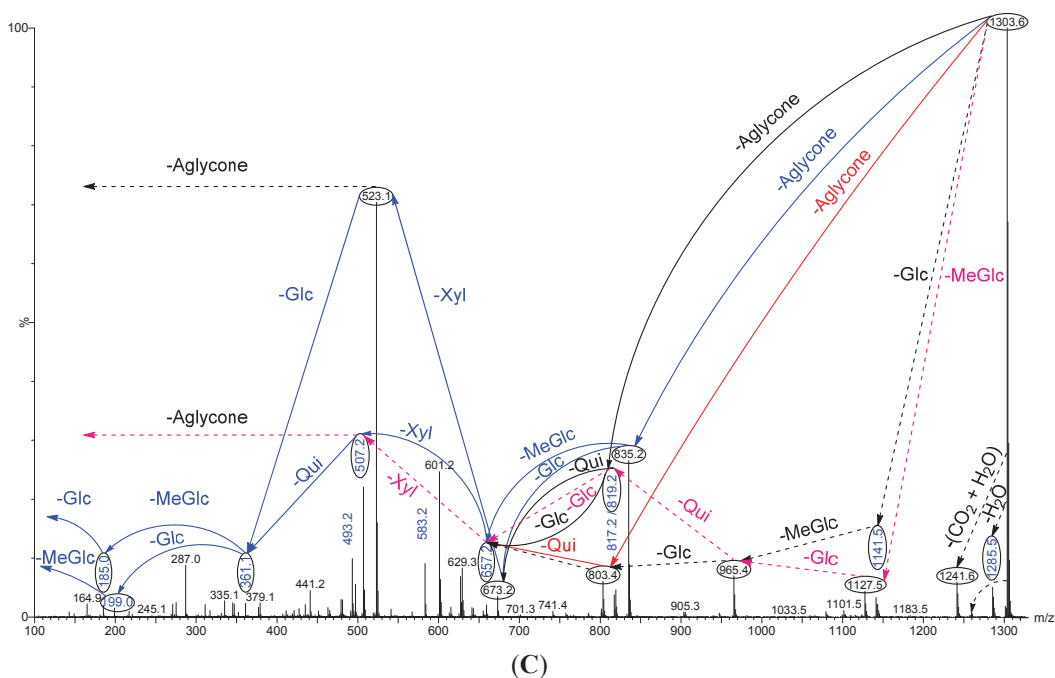




Figure 3. Cont



The full-scan MALDI mass spectrum of the isobutanol-enriched saponin extract obtained from the viscera of the *H. lessoni* is shown in Figure 4. A diverse range of saponins with various intensities was identified. This spectrum displays 13 intense peaks that could each correspond to at least one saponin congener. The most abundant ions observed under positive ion conditions were detected at  $m/z$  1335, 1303, 1289, 1287, 1259, 1245, 1243, 1229, 1227, 1149, 1141, 1123 and 845. Further analysis revealed that some of these MS peaks represented more than one compound. For instance the peaks at  $m/z$  1303 and 1287 were shown to contain at least six and five different congeners, respectively (Figures 3 and 5–7).

The accurate mass measurements acquired by MALDI-MS detected the saponin peaks, and molecular formulae and elemental compositions were assigned by ESI-MS/MS as summarized in Table 1. Our results revealed that at least 75 saponins were detected in *H. lessoni*, including 39 new sulfated, non-sulfated and acetylated triterpene glycosides, containing a wide range of aglycone and sugar moieties.

**Figure 4.** The full-scan MALDI mass spectrum of the isobutanol-enriched saponin extract from the viscera of the *H. lessoni*. A mass range of 600 to 1500 Da is shown here. It is noted that this spectrum is unique for this species.

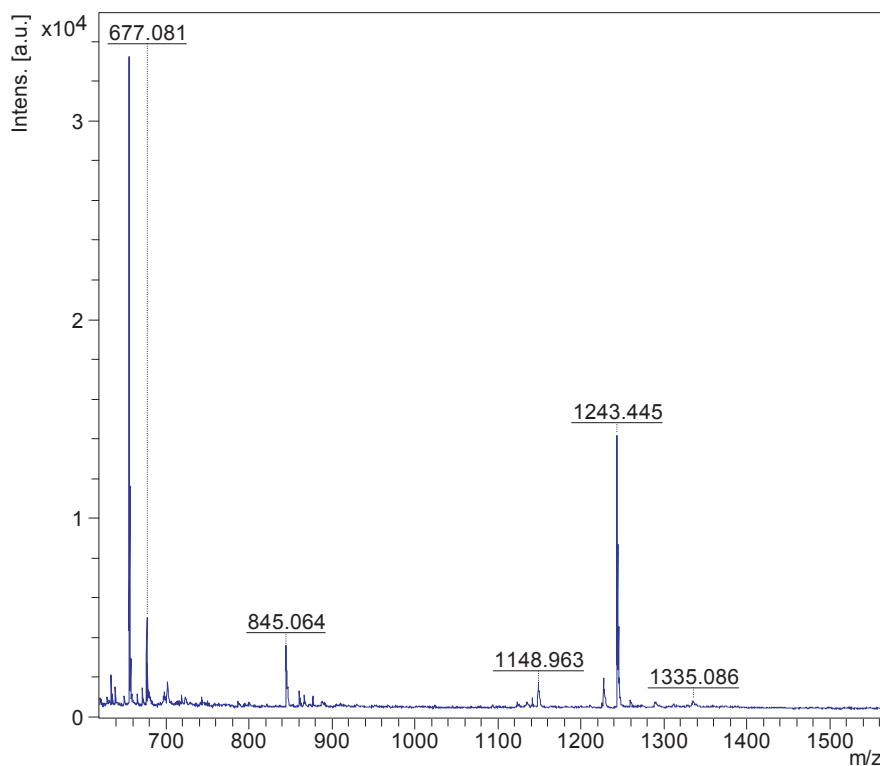


**Figure 5.** The schematic diagram of the proposed isomeric structures of ion at  $m/z$  1303.6.

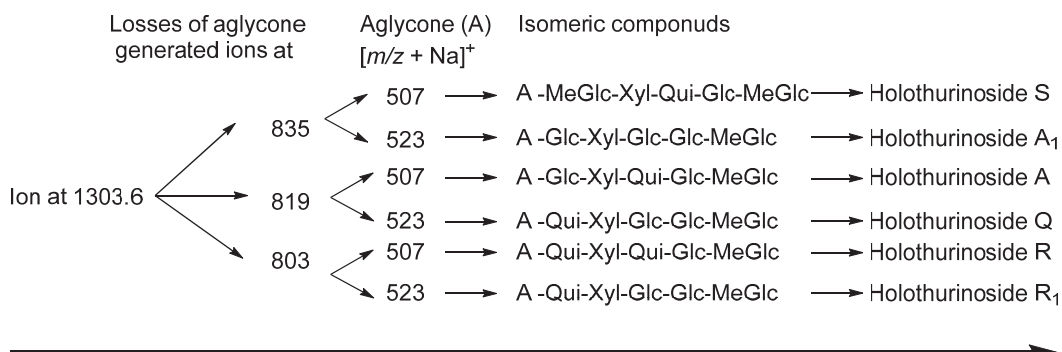




**Figure 6.** (+) ion mode ESI-MS/MS spectrum of saponins detected at  $m/z$  1287.6. This spectrum shows the presence of two different aglycones, which led to the isomeric saponins. Full and dotted arrows illustrate the two main possible fragmentation pathways.

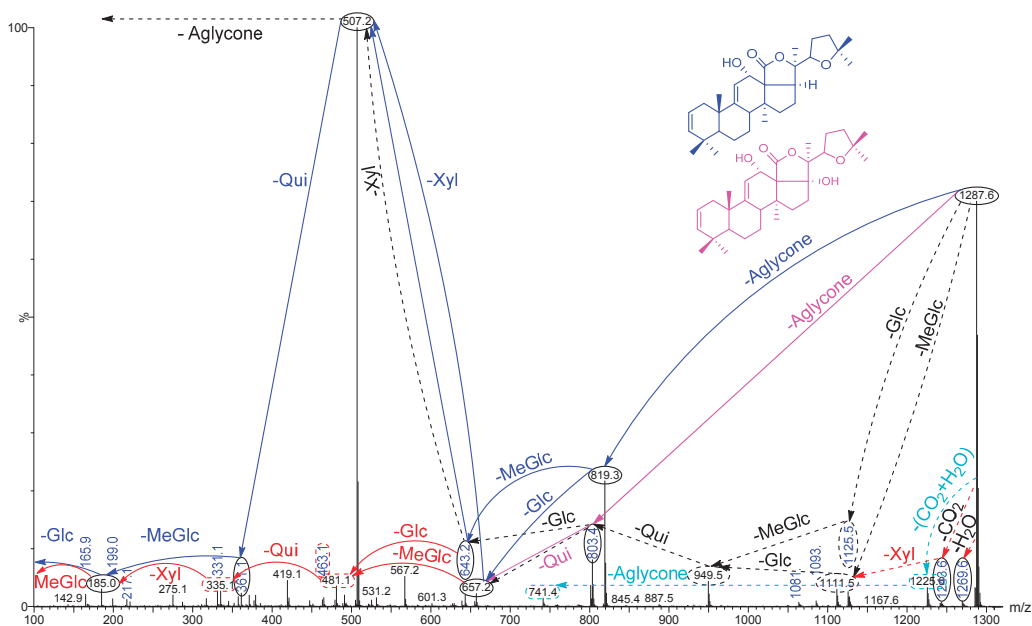


**Figure 7.** A schematic diagram of the proposed isomeric structures of ion at  $m/z$  1287.6.

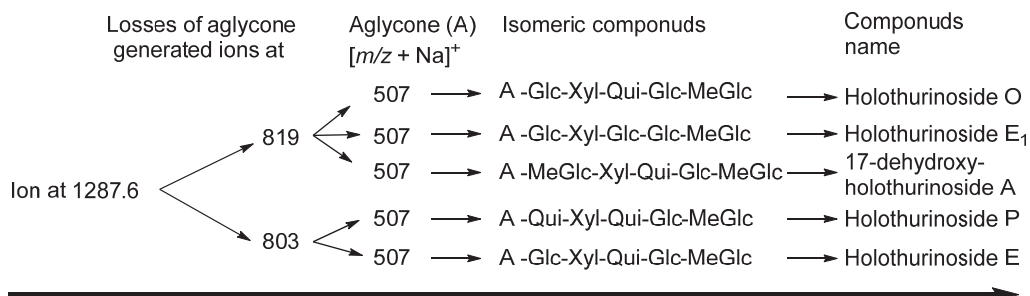


**Table 1.** Summary of saponins identified from the viscera of *H. lessoni* by matrix-assisted laser desorption/ionization time-of-flight mass spectrometry (MALDI-ToF-MS) and electrospray-ionization mass spectrometry (ESI-MS). This table illustrates the 39 novel identified compounds (N) along with the 36 known compounds (P). This table also shows some identical saponins, which have been given different names by different researchers in which they might be isomeric congeners.

[M + Na] <sup>+</sup> <i>m/z</i>	MW	Formula	Compound's Name	Novel (N)/ Published (P)	References
889.4	866	C <sub>41</sub> H <sub>63</sub> NaO <sub>16</sub> S	Holothurin B <sub>3</sub>	P	[83]
		C <sub>42</sub> H <sub>67</sub> NaO <sub>15</sub> S	Unidentified	N	–
905.4	882	C <sub>41</sub> H <sub>63</sub> NaO <sub>17</sub> S	Holothurin B <sub>4</sub>	P	[83]
			Holothurin B	P	[61,84–86]
			Nobiliside B	P	[87]
907.4	884	C <sub>41</sub> H <sub>65</sub> NaO <sub>17</sub> S	Holothurin B <sub>2</sub>	P	[83]
			Leucospilotaside B	P	[8]
911.6	888	C <sub>45</sub> H <sub>92</sub> O <sub>16</sub>	Unidentified	N	–
917.4	994	C <sub>44</sub> H <sub>71</sub> NaO <sub>15</sub> S	Unidentified	N	–
921.4	898	C <sub>41</sub> H <sub>63</sub> NaO <sub>18</sub> S	Leucospilotaside A	P	[84]
1034.1	1011	a*	Unidentified	N	–
1065.5	1042	C <sub>48</sub> H <sub>82</sub> O <sub>24</sub>	Unidentified	N	–
1071.5	1048	C <sub>47</sub> H <sub>93</sub> NaO <sub>21</sub> S	Unidentified	N	–
1078.5	1055	a *	Unidentified	N	–
1083.3	1060	C <sub>58</sub> H <sub>64</sub> O <sub>25</sub>	Unidentified	N	–
1087.6	1064	C <sub>47</sub> H <sub>93</sub> NaO <sub>22</sub> S	Unidentified	N	–
1123.5	1100	C <sub>54</sub> H <sub>84</sub> O <sub>23</sub>	Unidentified	N	–
1125.5	1102	C <sub>54</sub> H <sub>86</sub> O <sub>23</sub>	Holothurinoside C	P	[62,69,88,89]
			Holothurinoside C <sub>1</sub>		
1127.6	1104	C <sub>54</sub> H <sub>88</sub> O <sub>23</sub>	Unidentified	N	–
			Unidentified	N	–
1141.6	1118	C <sub>54</sub> H <sub>86</sub> O <sub>24</sub>	Desholothurin A (Nobiliside 2a), Desholothurin A <sub>1</sub> (Arguside E)	P	[5,62,69,88–90]
1149.2	1126	a *	Unidentified	N	–
1157.5	1134	C <sub>54</sub> H <sub>109</sub> O <sub>25</sub>	Holothurinoside J <sub>1</sub>	P	[50]
		C <sub>49</sub> H <sub>91</sub> NaO <sub>25</sub> S	Unidentified	N	–
1193.5	1170	C <sub>55</sub> H <sub>87</sub> NaO <sub>23</sub> S	Unidentified	N	–
1199.4	1176	C <sub>54</sub> H <sub>64</sub> O <sub>29</sub>	Unidentified	N	–
1221.5 **	1198	C <sub>56</sub> H <sub>78</sub> O <sub>28</sub>	Unidentified	N	–
1225.5	1202	C <sub>54</sub> H <sub>83</sub> NaO <sub>26</sub> S	Unidentified	N	–
1227.5	1204	C <sub>54</sub> H <sub>85</sub> NaO <sub>26</sub> S	Fuscocineroside B/C, Scabraside A or 24-Dehydroechinoside A	P	[29,56,89,91,92]
1229.5	1206	C <sub>54</sub> H <sub>87</sub> NaO <sub>26</sub> S	Holothurin A <sub>2</sub> , Echinoside A	P	[7,61,91,93–95]

**Table 1. Cont.**

1243.5	1220	C <sub>54</sub> H <sub>85</sub> NaO <sub>27</sub> S	Holothurin A Scabraside B 17-Hydroxy fuscocineroside B 25-Hydroxy fuscocinerosiden B	P	[29,58,61,95–97]
1245.5	1222	C <sub>54</sub> H <sub>87</sub> NaO <sub>27</sub> S	Holothurin A <sub>1</sub> Holothurin A <sub>4</sub> Scabraside D	P	[91] [36] [92]
1259.5	1236	C <sub>54</sub> H <sub>85</sub> NaO <sub>28</sub> S	Holothurin A <sub>3</sub> Unidentified	P N	[36] –
1265.5	1242	C <sub>56</sub> H <sub>83</sub> NaO <sub>27</sub> S	Unidentified	N	–
1271.6	1248	C <sub>60</sub> H <sub>96</sub> O <sub>27</sub>	Impatienside B	P	[5,98]
1287.6	1264	C <sub>60</sub> H <sub>96</sub> O <sub>28</sub>	Holothurinoside E, Holothurinoside E <sub>1</sub> Unidentified Unidentified	P N N	[62,69] – –
			17-Dehydroxyholothurinoside A	P	[5,99]
1289.6	1266	C <sub>60</sub> H <sub>98</sub> O <sub>28</sub>	Griseaside A	P	[99]
1301.6	1278	C <sub>61</sub> H <sub>98</sub> O <sub>28</sub> C <sub>60</sub> H <sub>94</sub> O <sub>29</sub>	Holothurinoside M Unidentified	P N	[65] –
1303.6	1280	C <sub>60</sub> H <sub>96</sub> O <sub>29</sub>	Holothurinoside A Holothurinoside A <sub>1</sub> Unidentified Unidentified Unidentified Unidentified	P N N N N	[5,62,69,88] – – – –
1305.6	1282	a *	Unidentified	N	–
1317.6	1294	C <sub>61</sub> H <sub>98</sub> O <sub>29</sub>	Unidentified	N	–
1335.3	1312	a *	Unidentified	N	–
1356.4	1333	a *	Unidentified	N	–
1409.4	1386	C <sub>61</sub> H <sub>78</sub> O <sub>36</sub>	Unidentified	N	–
1411.7	1388	C <sub>62</sub> H <sub>116</sub> O <sub>33</sub>	Unidentified	N	–
1419.7	1396	C <sub>66</sub> H <sub>108</sub> O <sub>31</sub>	Unidentified	N	–
1435.7	1412	C <sub>66</sub> H <sub>108</sub> O <sub>32</sub>	Unidentified	N	–
1465.7	1442	C <sub>67</sub> H <sub>110</sub> O <sub>33</sub>	Arguside B Arguside C	P	[5,32]
1475.6	1452	C <sub>65</sub> H <sub>96</sub> O <sub>36</sub>	Unidentified	N	–
1477.7 **	1454	C <sub>61</sub> H <sub>114</sub> O <sub>38</sub>	Unidentified	N	–
1481.7	1458	C <sub>66</sub> H <sub>106</sub> O <sub>35</sub>	Unidentified	N	–
1493.7	1470	C <sub>65</sub> H <sub>114</sub> O <sub>36</sub>	Unidentified	N	–
1495.7	1472	C <sub>61</sub> H <sub>116</sub> O <sub>39</sub> C <sub>72</sub> H <sub>112</sub> O <sub>31</sub>	Holothurinoside K <sub>1</sub> Unidentified	P N	[50] –
1591.7	1568	C <sub>66</sub> H <sub>120</sub> O <sub>41</sub>	Unidentified	N	–

a\* The composition was not measured through the ESI analysis; \*\* acetylated compounds.

A number of studies have reported the presence of multiple saponins. Elbandy *et al.* [5] described the structures of 21 non-sulfated saponins from the body wall of *Bohadschia cousteaui*. These authors reported 10 new compounds together with 11 known triterpene glycosides including Holothurinoside I, Holothurinoside H, Holothurinoside A, Desholothurin A, 17-dehydroxyholothurinoside A, Arguside C, Arguside F, Impatienside B, Impatienside A, Marmoratoside A and Bivittoside. Bondoc *et al.* [64] investigated saponin congeners in three species from Holothuriidae (*H. scabra* Jaeger 1833, *H. fuscocinerea* Jaeger 1833, and *H. impatiens* Forskal 1775). This group reported 20 saponin ion peaks, with an even number of sulfated and non-sulfated types, in *H. scabra*, which contained the highest saponin diversity among the examined species, followed by *H. fuscocinerea* and *H. impatiens* with 17 and 16 saponin peaks, respectively. These authors also described a total of 32 compounds in *H. scabra* and *H. impatiens* and 33 compounds in *H. fuscocinerea*. The saponin content of five tropical sea cucumbers including *H. atra*, *H. leucospilota*, *P. graeffei*, *A. echinites* and *B. subrubra* was also studied by Van Dyck *et al.* [50]. These authors reported the presence of four, six, eight, ten and nineteen saponin congeners in these species, respectively. In addition, this group [69] also detected a higher number of saponins (26) in the cuvierian tubules of *H. forskali* compared to the body wall (12 saponins). These results further support the evidence, suggested by the present study, of greater saponin congeners in viscera.

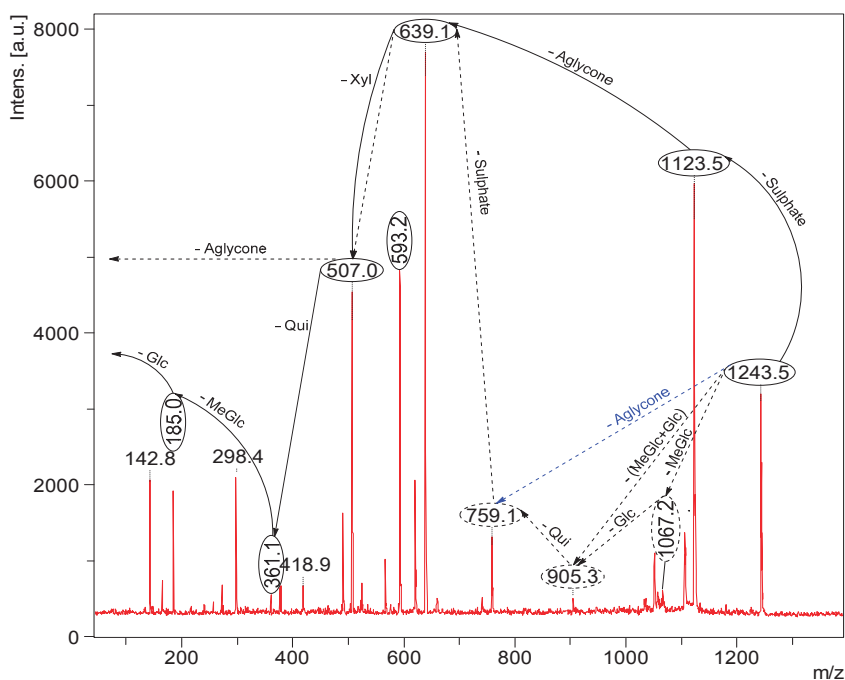
### 2.1. MALDI-MS/MS Data of Compound Holothurin A in the Positive Ion Mode

The conventional procedures to differentiate between isomeric saponins, including chemical derivatization and stereoscopic analysis, are tedious and time-consuming [100]. Tandem mass spectrometry was conducted to obtain more structural information about the saccharide moiety and elucidate their structural features. In order to ascertain that ions (signals) detected in the full-scan MALDI MS spectrum indeed correspond to saponin ions, tandem mass spectrometry analyses were performed for each ion, and saponin ion peaks were further analyzed using MS/MS fingerprints generated with the aid of collision-induced dissociation (CID) from their respective glycan structures. CID can provide a wealth of structural information about the nature of the carbohydrate components, as it preferentially cleaves glycosides at glycosidic linkages, allowing a straightforward interpretation of data. Almost all of observed daughter ions originated from the cleavage of glycosidic bonds (Figure 8). Therefore, the reconstruction of their fingerprints (fragmentation patterns) created by the glycosidic bond cleavages was utilized to deduce the structure of sugar moieties. This technique was also able to distinguish the structural differences between the isomers following HPCPC separation. However, in some cases, the MS/MS spectra obtained from the CID could be essentially identical for isomeric precursor ions. As a typical example, the MALDI-MS/MS mass spectrum for the ion detected at  $m/z$  1243.5 is shown in Figure 8. The fragmentation pattern of the sodiated compound at  $m/z$  1243.5  $[M + Na]^+$  in successive MS experiments is discussed in detail below for stepwise elucidation of the molecular structure of these compounds.

Collisional induced-dissociation activates two feasible fragmentation pathways of cationized parent ions shown in full and dotted arrows. First, the loss of the sugar unit; the successive losses of

3-*O*-methylglucose (-MeGlc), glucose (-Glc), quinovose (-Qui), sulfate and xylose (-Xyl) units generate ion products detected at  $m/z$  1067, 905, 759, 639 and 507, respectively. As this figure illustrates, the consecutive losses of the (MeGlc + Glc) simultaneously generated the ion at  $m/z$  905.3, and Qui (-146 Da) resulted in the peak at  $m/z$  759.1 which corresponds to [Aglycone + sulXyl-H + 2Na]<sup>+</sup>.

**Figure 8.** Positive tandem MALDI spectrum analysis of the precursor ion (saponin) detected at  $m/z$  1243.5. The figure shows the collision-induced fragmentation of parent ions at  $m/z$  1243.5. The consecutive losses of sulfate group, aglycone, xylose (Xyl), quinovose (Qui) and 3-*O*-methylglucose (MeGlc) residues affords product ions detected at  $m/z$  1123, 639, 507, 361 and 185, respectively.



Secondly the decomposition of the precursor ions can also be triggered by the loss of the aglycone residue, creating peaks at  $m/z$  759 (Figure 8) corresponding to the sugar moieties of 1243.5. The losses of the NaHSO<sub>4</sub> (ion generated at  $m/z$  1123.5), aglycone residue (ion generated at  $m/z$  639.1), and xylose (ion generated at  $m/z$  507.0), respectively, were produced by glycone and aglycone fingerprint peaks from the precursor ion. Therefore, the consecutive losses of the sodium monohydrogen sulfate (NaHSO<sub>4</sub>) from 1243.5 and aglycone unit produced signals observed at  $m/z$  1123 and 639 (Figure 8); the latter peak corresponding to the total desulfated sugar moiety. Furthermore, the consecutive losses of Xyl, Qui and MeGlc presenting signals observed at  $m/z$  507, 361 and 185, respectively, additionally proved that the decomposing ions were definitely generated from sodiated Holothurin A ( $m/z$  1243.5). The implementations of these molecular techniques on all ions detected in the MALDI spectra allow us to identify the molecular structures of the

saponins. All spectra were analyzed and fragmented, and some of them shared common fragmentation patterns. Key fragments from the tandem MS spectra of the positive ion mode of MALDI and ESI were reconstructed according to the example illustrated in order to propose the saponin structures. On the bases of these fragment signatures, 39 new saponins can be postulated. Some of these compounds, which share the common  $m/z$  507 or/and  $m/z$  523 key signals as a signature of the sodiated MeGlc-Glc-Qui and the sodiated MeGlc-Glc-Glc oligosaccharide residues, respectively, were easily identified. The identified saponins possess different aglycone structural elements.

The loss of 18 Da from the sodiated molecular ion, suggested the elimination of a neutral molecule ( $H_2O$ ) from the sugar group [19]. The simultaneous loss of two sugar units indicated characteristics of a branched sugar chain. Other visible peaks correspond to saponin product ions produced by the losses of water and/or carbon dioxide from sodiated saponins upon MALDI ionization. Hereby the sugar sequence of saponins can be determined by applying CID. The MALDI MS/MS data for this  $m/z$  value were in complete agreement with those reported in a previous study [50,64]. The predominant fragment signal at  $m/z$  593.2 results from  $\alpha$   $^{1,5}A_4$  cross-ring cleavage of the sulXyl residue, which was consistent with previous findings for the MS/MS analyses of sea cucumber saponins [64]. However, this peak was only detected as an intense signal in the sulfated saponins such as Holothurin A, whereas it was not observed in the non-sulfated saponins such as Holothurinoside A. Therefore, this cross-ring cleavage seems to occur only with the sulfated Xyl. Analysis by MALDI resulted in an information rich tandem mass spectrum containing glycosidic bond and cross-ring cleavages that provided more structural information than previous studies on the same precursor ion. The sugar moiety of saponins developed from non-sulfated hexaosides to sulfated tetraosides [64]. The assignment of the sulfate group was determined by the mass difference between the parent ion at  $m/z$  1243 and daughter ion  $m/z$  1123 peaks based on knowing the molecular weight of the sulfate unit (120 Da). Complete glycosidic bond cleavage was observed, which enabled us to determine the locations of the sulfate ( $m/z$  1123), the entire sugar moieties ( $m/z$  639), and each component of sugar residue.

The losses of the aglycone and sugar residues are largely observed from glycosidic bond cleavages. Even though one cross-ring cleavage is assigned, the generation of glycosidic bond cleavages in combination with accurate mass is sufficient to assign the position of the sulfate group along the tetrasaccharide sequence for Holothurin A. The ion detected at  $m/z$  1105 (Figure 8) is the water-loss ion derived from the ion at  $m/z$  1123, whereas the ion observed at  $m/z$  1061 corresponds to the neutral loss of  $CO_2$  (44 Da).

As described by Song *et al.* [100], the cross-ring cleavages that occurred in the CID spectra of saccharides with  $\alpha$  1–2 linkage, such as the sugar residue for Holothurin A, are X and A types, whereas the glycoside bond cleavages are C and B types. The major peak at  $m/z$  593.2 was attributed to cross-ring cleavage of the sugar unit.

This MS/MS spectrum allows us to reconstruct the collision-induced fragmentation pattern of the parent ion (Figure 4) and consequently to confirm that ions monitored at  $m/z$  1243.5 correspond to the Holothurin A elucidated by Van Dyck *et al.* [50], Kitagawa *et al.* [96] and Rodriguez *et al.* [88].

The occurrence of a sulfate group (NaHSO<sub>4</sub>) in saponin compounds, such as in the case of Holothurin A, was assigned by a loss of 120 Da during the MS/MS. By the combination of accurate mass and MS/MS information, saponins were categorized into seven distinct carbohydrate structural types: (A) MeGlc-Glc-Qui-Xyl-Aglycone; (B) MeGlc-Glc-Glc-Xyl-Aglycone; (C) (MeGlc-Glc)-Qui-sulXyl-Aglycone; (D) MeGlc-Glc-Qui-(Qui-Glc)-Xyl-Aglycone; (E) MeGlc-Glc-Qui-(MeGlc-Glc)-Xyl-Aglycone; (F) MeGlc-Glc-Glc- (MeGlc-Glc)-Xyl-Aglycone; and (G) MeGlc-Glc-Glc-(Qui-Glc)-Xyl-Aglycone. Non-sulfated saponins had one to six monosaccharide units and six distinct structural types. All sulfated saponins ranging from  $m/z$  889 to 1259 had a structure (C), in which Xyl was sulfated. However, in some cases, the sulfation of Xyl, MeGlc and Glc was reported [13]. The MS analyses also indicated that this sea cucumber species produced a mixture of common and unique saponin types. Unique saponin types were also identified when the mass spectra of this species were compared with others. Saponin peaks with the ion signatures at  $m/z$  values of 1477, 1335, 1221, 1149 and 1123 were unique in *H. lessoni*. In the tandem MS, in general, the most abundant ions were attributed to the losses of aglycones and/or both key diagnostic sugar moieties (507 and 523). For 1243.5, the most abundant ions observed under positive ion conditions were at  $m/z$  1123, 639 and 507, corresponding to the losses of sulfate, aglycone and Xyl moieties. The major ion at  $m/z$  621.2 corresponded to the loss of water from ion at  $m/z$  639. Some saponins were commonly found among species (e.g., Holothurins A and B), whereas others were unique to each species (e.g., 1221 in *H. lessoni*), as Bondoc *et al.* [64] and Caulier *et al.* [6] have also indicated. The saponin profile (peaks) of sea cucumbers indicated the different relative intensities of saponins in the viscera. The peaks observed (Figure 4) at  $m/z$  1149.0, 1227.5, 1229.5, 1243.5, and 1259.5 in the positive ion mode corresponded to an unidentified saponin, Scabraside A or Fuscocinerosides B/C (isomers), Holothurin A<sub>2</sub> (Echinoside A), Holothurin A, and Holothurin A<sub>3</sub>, respectively [36,56,61,89,93,94]. Most of these sulfated saponins were also reported by Kitagawa *et al.* [89] and Bondoc *et al.* [64]. The ion peaks of the non-sulfated saponins at  $m/z$  1125, 1141, 1287, 1289, 1301 and 1303 corresponded to Holothurinosides C/C<sub>1</sub> (isomers), Desholothurin A (synonymous with Nobilicide 2A) or Desholothurin A<sub>1</sub>, Holothurinosides E/E<sub>1</sub>, Griseaside A, Holothurinosides M and A, respectively [69]. *H. scabra*, *H. impatiens* and *H. fuscocinerea* were also reported to contain Holothurin A, Scabraside B and Holothurinoside C [64]. This group also detected 24-dehydroechinoside A and Scabraside A in *H. scabra*. The presence of Holothurinosides C/C<sub>1</sub> (isomers), Holothurinosides A/A<sub>1</sub> (isomers), Desholothurin A (synonymous with Nobilicide 2A), Desholothurin A<sub>1</sub> and Holothurinosides E/E<sub>1</sub> were also described in *H. forskali* by several groups [65,69,88]. We were not able to identify all the saponin congeners detected in the semi-pure extract in the HPCPC-fractionated samples. Bondoc *et al.* [64] experienced a similar issue in that they observed some peaks in MALDI MS, which were not seen in the isomeric separation done in LC-ESI MS. For instance, we could not find ions at  $m/z$  1149 and 1335 in the spectra of HPCPC fractions by ESI-MS. The MALDI mass spectra of the semi-pure and HPCPC fractionated samples of the *H. lessoni* revealed 75 ions (29 sulfated and 46 non-sulfated) in which a total of 13 isomers was found (Table 1), of which 36 congeners had previously been identified in other holothurians. It is the first time that the presence of these identified saponins has been reported in *H. lessoni*, apart from the saponins

reported by Caulier *et al.* [58] that were found in the seawater surrounding *H. lessoni*. They reported saponins with  $m/z$  values of 1141, 1229, 1243 and 1463 namely Desholothurin A, Holothurin A<sub>2</sub>, Scabraside B (synonymous with Holothurin A) and Holothurinoside H, respectively [58]. However, we could not detect the ion at  $m/z$  1463 in our sample.

Most of the sulfated saponins that had previously been reported were detected in this species, including Holothurin B<sub>3</sub> ( $m/z$  889), Holothurin B/B<sub>4</sub> ( $m/z$  905), Holothurin B<sub>2</sub> ( $m/z$  907), Fuscocinerosides B or C, which are functional group isomers ( $m/z$  1227), Holothurin A<sub>2</sub> ( $m/z$  1229), Holothurin A ( $m/z$  1243), Holothurin A<sub>1</sub>/A<sub>4</sub> ( $m/z$  1245), and Holothurin A<sub>3</sub> ( $m/z$  1259). The common sulfated congeners among this species and other sea cucumbers are Holothurin B ( $m/z$  905) and Holothurin A ( $m/z$  1243). Among these saponins, Holothurin A is the reported to be the major congener with the highest relative abundance in this species.

To illustrate the identification of a novel compound at  $m/z$  1149.0, the parent ion at  $m/z$  1149.0 was subjected to MS/MS fragmentation. The MALDI fingerprints revealed that the compound contained a novel aglycone at  $m/z$  493 and a tetrasaccharide moiety with  $m/z$  value of 656 Da including -Xyl, -Qui, -Glc and -MeGlc in the ratio of 1:1:1:1. This saponin possessed the common  $m/z$  507 key signal as a fingerprint of MeGlc-Glc-Qui + Na<sup>+</sup>. We propose to name Holothurinoside T.

The isomers within one sample showed different MS<sup>n</sup> spectra [101] allowing their structures to be elucidated based on the ion fingerprints. Here we indicate that the occurrence of many product ions in the spectrum of viscera extract is due to the presence of a mixture of saponins and isomeric saponins (Figures 3 and 5–7). This observation is consistent with the findings proposed by Van Dyck and associates [69] for the Cuvierian tubules of *H. forskali*. Mass spectrometry alone, however, is not powerful enough to obtain more structural information about the isomeric congeners. Nonetheless, it provides a quick and straightforward characterization of the element components and saponin distributions by the presence of ions at  $m/z$  507 and 523 in the tandem spectra of the viscera extracts.

## 2.2. Key Fragments and Structure Elucidation of Novel Saponins

The common key fragments facilitated the structure elucidation of novel saponins. Tandem mass spectrometry analyses of saponins led to identification of several diagnostic key fragments corresponding to certain common structural element of saponins as summarized in Table 2.

**Table 2.** Key diagnostic ions in the MS/MS of the holothurians saponins.

Diagnostic ions in CID Spectra of [M + Na] <sup>+</sup>			
$m/z$ Signals (Da)			
	507	523	639
Chemical signatures	MeGlc-Glc-Qui + Na	MeGlc-Glc-Glc + Na	MeGlc-Glc-Qui-Xyl + Na

The structures of saponins were deduced by the identification and implementation of the key fragment ions generated by tandem mass spectrometry. The presence of these oligosaccharide residues ( $m/z$  507 and/or 523) facilitated the determination of the saponin structure. However, some



compounds with a  $m/z$  value of less than 1100 Da including 921, 907, 905 and 889 did not yield the peak  $m/z$  523, which reflected the lack of this oligosaccharide unit in their structures. Unlike other compounds, the MS/MS spectrum of the ion at  $m/z$  1477.7 illustrated the unique fingerprint profile, which contained ions at  $m/z$  511 and 493 instead of an ion at  $m/z$  507. The structure of compound was further confirmed by MS/MS analyses.

The MALDI analysis revealed that the ion with  $m/z$  1243.5 was the prominent peak in the spectrum, which corresponded to Holothurin A, which was found in several species of sea cucumbers [6,29,50,58,61,64,89,95–97]. The MALDI data were confirmed by ESI-MS.

Table 1 summarizes data of all analyses performed on the saponin-enriched sample and HPCPC fractionated samples using MALDI and ESI on compounds from the viscera of *H. lessoni*. The identified saponin mixture contains a diverse range of molecular weights and structures. The chemical structures of the identified compounds are illustrated in Figure 9. The isobutanol and HPCPC fractionated samples indicated 29 sulfated and 46 non-sulfated saponin ions. The number of MS ion peaks was lower than the number of isomers identified by MS/MS following HPCPC separation (Figure 3).

**Figure 9.** The structure of identified saponins in the viscera of *H. lessoni*.

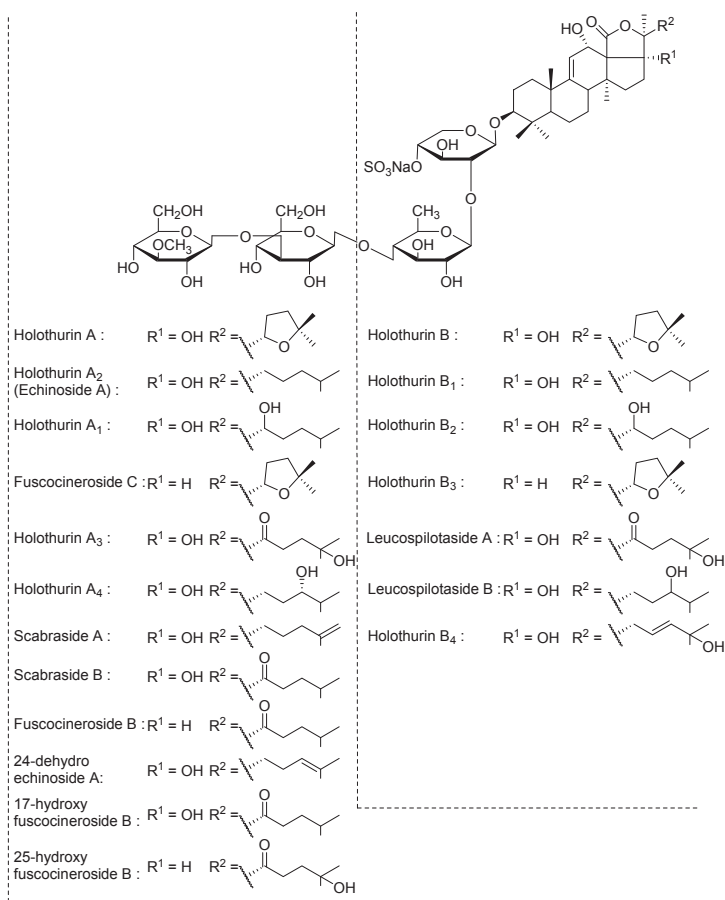
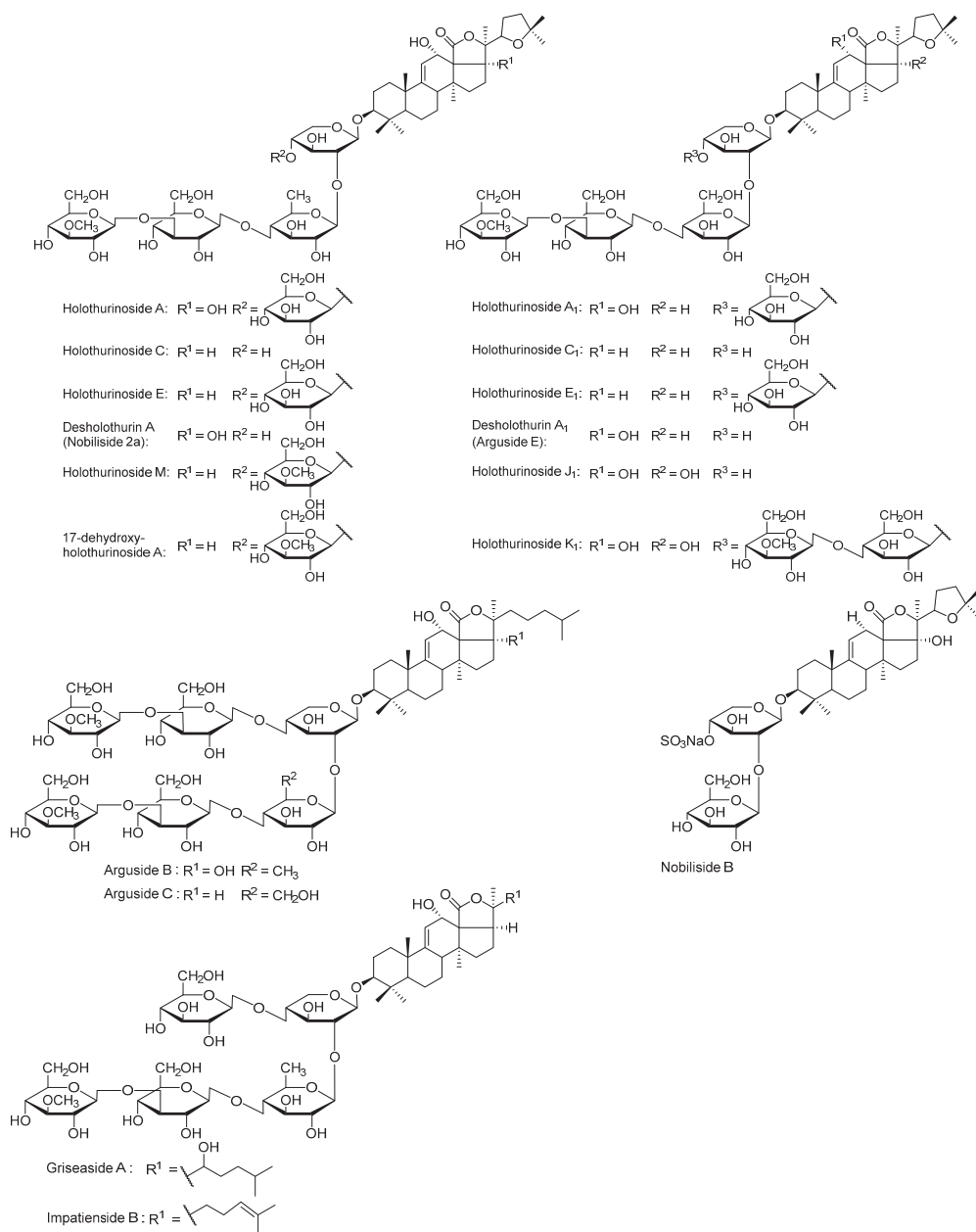


Figure 9. Cont.



### 2.3. Analyses of Saponins by ESI-MS

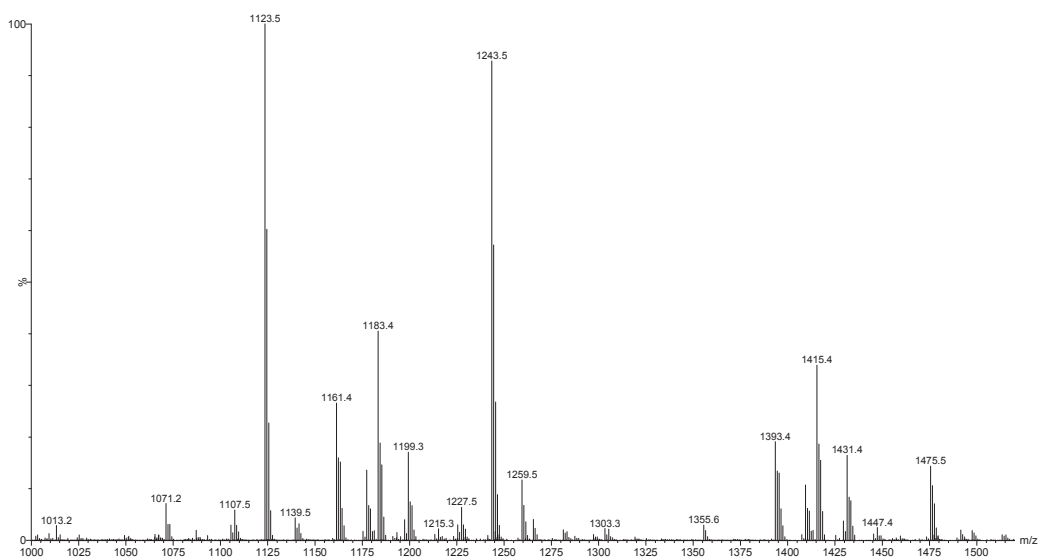
The positive ion mode ESI-MS analyses were also conducted on the samples. ESI mass spectra of the saponins are dominated by  $[M + Na]^+$ . There were some instances where peaks observed in the MALDI-MS spectra were not monitored from the isomer separation done in the ESI-MS, such

as the peak detected at  $m/z$  1149 in the MALDI spectra. Other researchers had experienced the same issue [50,64].

ESI-MS<sup>n</sup> is a very effective and powerful technique to differentiate isomeric saponins [100]. Tandem MS analyses on  $[M + Na]^+$  ions provided abundant structural information about saponins. The positive ion mode ESI-MS/MS analyses were also performed on all compound ions detected in the ESI-MS spectrum of HPCPC fractions. This technique also confirmed the existence of saponins reported in the literature and allowed the discovery of new saponin congeners in the species examined. The molecular masses of the identified compounds are summarized in Table 1. The ESI-MS spectrum of the saponin extract from the viscera of *H. lessoni* is shown in the Figure 10.

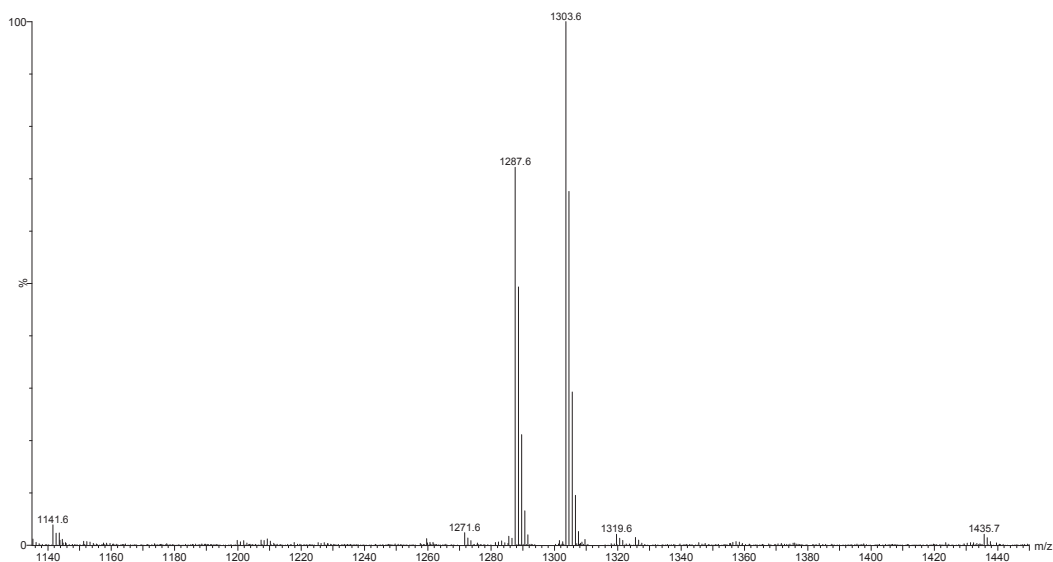
Several major peaks were detected. The peaks at  $m/z$  1123 and 1243 correspond to a novel compound and Holothurin A with the elemental compositions of  $C_{54}H_{84}O_{23}$  and  $C_{54}H_{85}NaO_{27}S$ , respectively. The ESI-MS analyses were also carried out on all HPCPC fractions. As a typical example, Figure 11 shows the ESI-MS spectrum of Fraction 14.

**Figure 10.** (+) ESI-MS spectrum of saponins extract from the viscera of *H. lessoni*.



As can be seen in Figure 11, there are two major peaks at  $m/z$  1287.6 and 1303.6, which correspond to Holothurinosides E/E<sub>1</sub> and Holothurinosides A/A<sub>1</sub>, respectively. These two peaks, as the MS/MS analyses show which will be discussed later, were found to correspond to at least five and six isomers, respectively (Figures 3, 6 and Supplementary Figure S2). A comparison of the molecular weights of both saponins revealed some mass differences between them, such as a 16 Da (O) mass differences between Holothurinosides E/E<sub>1</sub> and Holothurinosides A/A<sub>1</sub>, reflecting the small structural alterations and the intrinsic connections between them. Their MS/MS analyses indicated, as will be discussed later, the presence of some identical aglycones in both ions.

**Figure 11.** (+) ion mode ESI-MS spectrum of saponins extract from Fraction 14.



### 2.3.1. Molecular Mass of Saponins by ESI

ESI/MS provide considerable structural information with very high sensitivity for saponins [60,63]. Peaks corresponding to the sodium adduct of the complete sugar side chains were often quite intense in the product ion spectra of the sodiated saponin precursor. Tandem mass spectra of saponins reflected the different fingerprints with different relative intensities.

### 2.3.2. Structure Elucidation of the Saponins by ESI-MS/MS

Seventy-five different triterpene saponins purified from sea cucumber were investigated by MALDI and electrospray ionization tandem mass spectrometry (ESI-MS/MS) in the positive ion modes. All spectra were analyzed and fragmented, and some of them shared common fragmentation patterns. Key fragments from the positive ion mode MS/MS spectra of MALDI and ESI were reconstructed with an example illustrated that proposes the saponin structures. Peak intensities of fragment ions in MS/MS spectra were also correlated with structural features and fragmentation preferences of the investigated saponins. In general, the formation of fragments occurred predominantly by cleavages of glycosidic bonds in the positive mode (Figure 12), which was applied to identify the structure of saponins. Interpretation of fragment ions of MS/MS spectra provided the key information for the structural elucidation of saponins as exemplified in Figure 12.

Fragmentation of the ion at  $m/z$  1243.5 (sulfated saponin) under collisionally activated dissociation (CAD) conditions is shown in Figure 12. Full and dotted arrows show the two main fragmentation pathways in this saponin. The peak at  $m/z$  507 corresponds to both the aglycone and the key diagnostic fragment of sugar moiety.

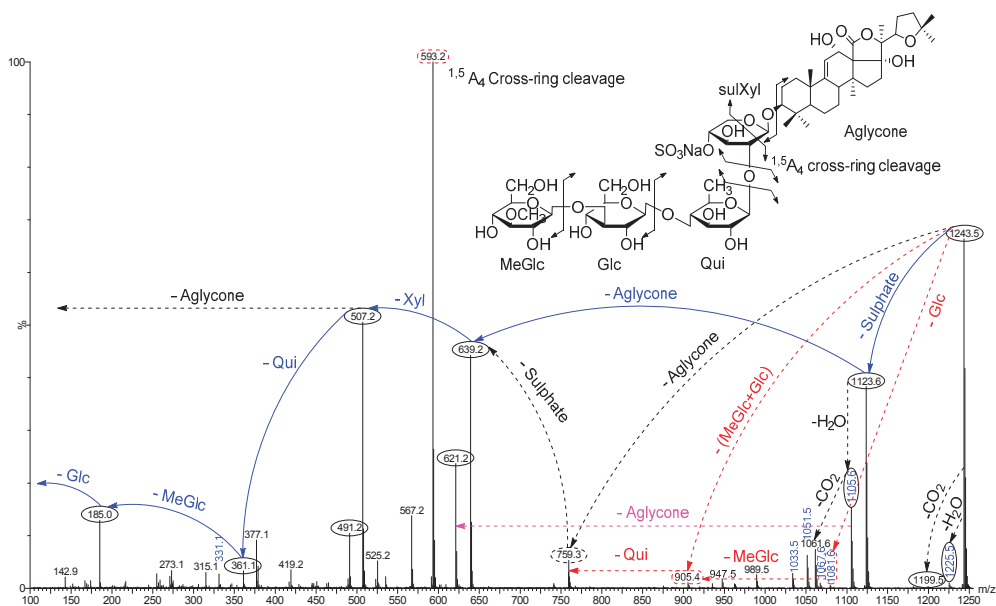
The most abundant peaks were detected at  $m/z$  1123  $[M + Na - 120 (\text{sulfate})]^+$ , 639  $[M + Na - 120 - 484 (\text{aglycone})]^+$  and 507  $[M + Na - 120 - 484 - 132]^+$ . In addition, the peaks

observed at  $m/z$  1225.5 and 1199.5 were generated by the losses of  $H_2O$  and  $CO_2$  from their respective parent ion.

The most intensive peak was observed at  $m/z$  593 stemming from a cross-ring cleavage. The observed fragments are consistent with the structure of the Holothurin A proposed by Van Dyck *et al.* [50]. This ESI-MS/MS analysis confirmed the MALDI data on the ion at  $m/z$  1243.5. The full analysis can be seen in Supplementary Figure S1.

ESI-MS was applied to distinguish the isomeric saponins by Song *et al.* [100]. Isomers of saponins were also identified using tandem mass spectrometry combined with electrospray ionization (ESI-MS/MS) following HPCPC separation. MS/MS spectra of these ions gave detailed structural information and enabled differentiation of the isomeric saponins. The results are exemplified in the following figures. The analyses applied on the ion at  $m/z$  1303.6 (non-sulfated saponins), which was obtained from Fractions 15, 14 and 12, are shown in Figure 3A–C. The main fragmentation patterns observed for this isomeric compound are shown with full and dotted arrows.

**Figure 12.** (+) Ion mode ESI-MS/MS spectrum of saponin detected at 1243.5 (Holothurin A). Full and dotted arrows show the two main feasible fragmentation pathways. The structure of saponin was elucidated on the base of tandem mass spectrometry.



The structures of six isomeric saponins were ascribed to the ions detected at  $m/z$  1303.6 (Figure 3A–C). These isomers have at least three different aglycone structures with  $m/z$  468, 484 and 500 and contain five different monosaccharaide residues. These figures illustrate different isomers of ions detected at  $m/z$  1303. For instance, Figure 3A (Fraction 15) shows the stepwise structure elucidation of Holothurinoside A. The consecutive losses of MeGlc, Glc, Qui, Glc, and Xyl units generate signals detected at  $m/z$  1127.5, 965.5, 819.3, 657.2 and 507.2, respectively,

which correspond to Holothurinoside A [5,62,69,88]. As can be seen in Figure 3A, this saponin fraction is quite pure.

In one of these isomers (Figure 3B), the consecutive losses of aglycone, Glc, Xyl, Qui and Glc units provided signals detected at  $m/z$  819, 657, 507, 361 and 199, respectively, further confirming that the fragment ions unambiguously originate from sodium-cationized Holothurinoside A. In addition ( $m/z$  1303.6), the precursor ion sequentially lost MeGlc ( $m/z$  1127.5), Glc ( $m/z$  965.5), Glc ( $m/z$  803.4), Qui ( $m/z$  657.2) and Xyl ( $m/z$  507.2) (Figure 3B) thereby indicating the structure of another isomer of this molecule. The characteristic peak observed at  $m/z$  507.2 generated by tandem MS was identified either as a sodiated MeGlc-Glc-Who residue or sodiated aglycone residue. The ion at  $m/z$  803 resulted from the loss of aglycone from the parent ion at  $m/z$  1303.6, which is the fragment ion corresponding to the complete saccharide chain, which subsequently (Figure 3B) produces the ions at  $m/z$  657 and ion at  $m/z$  507 by the losses of Qui and Xyl residues. Moreover, the ions ( $m/z$  507) further fragmented to form ions of the same  $m/z$  value at  $m/z$  361 and  $m/z$  199 or 185. The observation of ions at  $m/z$  507 and 657 further supports the above conclusion. The ions detected at  $m/z$  1285.5 and 1241.6 correspond to the losses of H<sub>2</sub>O and H<sub>2</sub>O + CO<sub>2</sub>, respectively. These two fragments correspond to the sequential losses of water and carbon dioxide. It is notable that the configurations of all the sugars in all previously known sea cucumber triterpene glycosides are D-configurations.

A similar analysis was carried out (Figure 3C) on the ion at  $m/z$  1303.6 of Fraction 12. As can be seen in the figure, the spectrum has a different fragmentation pattern compared to the spectra in Figure 3A,B even though they have the same  $m/z$  value. In one of the isomers, the consecutive losses of aglycone, Glc, Xyl, Glc and MeGlc units generated signals detected at  $m/z$  835.2, 673.2, 523.1, 361.1 and 185, respectively, further confirming the structure of one of the isomeric compounds (Figures 3C and 5). The full analysis can be seen in the Supplementary Figure S2 (Fraction 12).

Further, the cleavage of the C<sub>2</sub> ion at  $m/z$  673, 643, 629, 601, 583, 541 and 523 (Figure 3C) produced the ion at  $m/z$  613, 583, 569, 541, 523, 481 and 463, respectively, through the loss of C<sub>2</sub>H<sub>4</sub>O<sub>2</sub> (60 Da) which indicates an  $\alpha$  1–4-linked glycosidic bond in the  $\alpha$ -chain, which is in agreement with a previous study [100]. This observation is consistent with the fragmentation rules for ions of 1–4-linked disaccharides.

The MS/MS spectra show the presence of three different aglycone structures, namely ions detected at  $m/z$  835.2, 819.2 and 803.4 by the losses of aglycone moieties. This analysis reveals the presence of at least six different isomers with different aglycones and sugar moieties, as the MS/MS spectra generate both key diagnostic fragments at  $m/z$  507 and 523. These isomers are composed of five monosaccharides including MeGlc-Glc-Who (Glc)-Xyl-MeGlc (Glc or Who). The proposed structures are shown in Figure 5 and correspond to Holothurinoside A<sub>1</sub> and Holothurinoside A, and four novel saponins [5,69,88]. We propose to call these molecules Holothurinosides S, Q, R and R<sub>1</sub>, respectively.

It should be noted that both major fragment ions (507 and 523) can correspond to partial glycoside compositions or aglycone moieties, further supporting the presence of isomeric saponins. The predominant fragment ion at  $m/z$  507 results from the sodium adduct ion

of the [MeGlc-Glc-Qui + Na] side chain or the aglycone. Similarly, the abundant fragment ion at  $m/z$  523 arises from the sodium adduct ion of the [MeGlc-Glc-Glc + Na]<sup>+</sup> side chain or the aglycone. Since the masses of sodiated aglycones are identical with their relative partial sugar residues, namely [MeGlc-Glc-Qui + Na]<sup>+</sup> and [MeGlc-Glc-Glc + Na]<sup>+</sup>, the ions at  $m/z$  507.2 and 523.2, respectively, correspond to both sugar residues and their aglycones. When the decomposition of the parent ion ( $m/z$  1303.6) is triggered by the losses of sugar residues, as exemplified by the black and pink dotted arrows in Figure 3A–C, the ions at  $m/z$  507.2 and 523.2 correspond to the aglycone moieties. Alternatively, the fragmentation of the parent ion can proceed by the losses of all five sugar residues, which generates ions at  $m/z$  507.2 and 523.2, which correspond to the aglycone moieties. Similar conclusions were drawn by Van Dyck *et al.* (2009) [69] for triterpene glycosides. Losses of H<sub>2</sub>O and CO<sub>2</sub> or their combination result from cleavage at the glycosidic linkages as noted by Waller and Yamasaki [3].

Different fractions of the HPCPC separation were compared to show the presence of one aglycone (Figure 3A), the presence of two different aglycones (Figure 3B) and the presence of three different aglycones (Figure 3C) indicating that the HPCPC allowed the separation of the isomers.

On comparison of the MS/MS spectra of 1303.6 and 1243.5 (Figures 3 and 12), it is notable that the  $m/z$  523 fragment (aglycone loss) of the [M + Na]<sup>+</sup> ions was only observed with 1303.6, which corresponds to the presence of a new aglycone unit at  $m/z$  500 (sodiated 523). Individual patterns were detected from sulfated and non-sulfated saponins as indicated in Holothurin A and Holothurinoside A as representative examples. This sequential decomposition confirms the proposed Holothurin A and Holothurinoside A structures.

Another typical chemical structure elucidation of isomeric saponins by tandem MS is exemplified in Figure 6. This spectrum shows the ion signature of the sample under tandem MS from the ion detected at  $m/z$  1287.6. Tandem MS analyses revealed the presence of two different aglycones with  $m/z$  values of 484 and 468, confirming the presence of chemical isomeric structures. The same fragmentation behaviors have been observed from the positive ESI-MS/MS spectra of saponins with  $m/z$  1303. The structures of aglycones are identical with those reported for the ion at  $m/z$  1303. The possible fragmentation pathways were shown using full and dotted arrows. The losses of aglycone moieties (Figure 6) generated ions at  $m/z$  819.3 and 803.4, which correspond to the complete sugar components. The successive losses of aglycone, Glc or MeGlc, Xyl, Qui and MeGlc yielded to ion fragments at  $m/z$  819, 657 or 643, 507, 361 and 185, respectively.

The decomposition of the parent ion can also be triggered by the loss of a sugar moiety, namely MeGlc, Glc, Qui, Qui or Glc and Xyl, followed by the aglycone, which generates daughter ions at  $m/z$  1111.5, 949.5, 803.4, 657.2 or 643.2 and 507.2. It is clear that the ion at  $m/z$  507 is the most abundant fragment ion and is the signature of the sodiated aglycone and/or the key sugar component. The losses of water (−18 Da) and/or carbon dioxide (−44 Da) are observed from the spectrum, and some of the peaks are also designated to those molecules.

This analysis revealed the presence of at least five different isomers with different aglycones and sugar moieties. These isomers contain some identical aglycone structures with those identified in the ion at 1303 (Figure 5). These isomers are also pentaglycosidic saponins. The proposed structures are

shown in Figure 7, which correspond to Holothurinoside E<sub>1</sub>, Holothurinoside E, 17-dehydroxy-holothurinoside A and two novel saponins (the first and fourth compounds). We propose to name these molecules Holothurinosides O and P, respectively.

The data indicate that the terminal sugar is preferentially lost first in glycosidic bond cleavages. Since Holothurinosides A and E contain the same terminal sugar units in their sugar residue, they yield the ions with the same  $m/z$  value ( $m/z$  507).

### 3. Experimental Section

#### 3.1. Sea Cucumber Sample

Twenty sea cucumber samples of *Holothuria lessona* Massin *et al.* 2009, commonly known as Golden sandfish were collected off Lizard Island (latitude 14°41'29.46" S; longitude 145°26'23.33" E), Queensland, Australia in September 2010. The viscera (all internal organs) were separated from the body wall and kept separately in zip-lock plastic bags which were snap-frozen, then transferred to the laboratory and kept at -20 °C until use.

#### 3.2. Extraction Protocol

The debris and sand particles were separated from the viscera (all internal organs) manually and the visceral mass was freeze-dried (VirTis, BenchTop K, New York, NY, USA). The dried specimens were then pulverized to a fine powder using liquid nitrogen and a mortar and pestle.

All aqueous solutions were prepared with ultrapure water generated by a Milli-Q systems (18.2 MΩ, Millipore, Bedford, MA, USA). All organic solvents were purchased from Merck (Darmstadt, Germany) except when the supplier was mentioned, and were either of HPLC grade or the highest degree of purity.

#### Extraction of Saponins

The extraction and purification procedures were adapted from Campagnuolo *et al.* [34], Van Dyck *et al.* [69], Garneau *et al.* [102] and Grassia *et al.* [103]. The pulverized viscera sample (40 g) was extracted four times with 70% ethanol (EtOH) (400 mL) followed by filtration through Whatman filter paper (No.1, Millipore, Bedford, MA, USA) at room temperature. The extract was concentrated under reduced pressure at 30 °C using a rotary evaporator (Büchi AG, Flawil, Switzerland) to remove the ethanol, and the residual sample was freeze-dried to remove water (VirTis, BenchTop K, New York, NY, USA). The dried residue was successively extracted using a modified Kupchan partition procedure [104]: The dried extract (15 g) was dissolved in 90% aqueous methanol (MeOH) (any remaining solid residue was removed by filtration), and partitioned against 400 mL of *n*-hexane (v/v) twice. The water content of the hydromethanolic phase was then adjusted to 20% (v/v) and then to 40% (v/v) and the solutions partitioned against CH<sub>2</sub>Cl<sub>2</sub> (450 mL) and CHCl<sub>3</sub> (350 mL), respectively. In the next step, the hydromethanolic phase was concentrated to dryness using a rotary evaporator and freeze-drier. The dry powder



was solubilized in 10 mL of MilliQ water (the aqueous extract) in order to undergo chromatographic purification.

### 3.3. Purification of the Extract

A solution of the aqueous extract was then subjected to a prewashed Amberlite® XAD-4 column (250 g XAD-4 resin 20–60 mesh; Sigma-Aldrich, MO, USA; 4 × 30 cm column) chromatography. After washing the column extensively with water (1 L), the saponins were eluted sequentially with MeOH (450 mL) and acetone (350 mL) and water (250 mL). The eluates (methanolic, acetone and water fractions) were then concentrated, dried, and redissolved in 5 mL of MilliQ water. Finally, the aqueous extract was partitioned with 5 mL isobutanol (v/v). The isobutanolic saponin-enriched fraction was either stored for subsequent mass spectrometry analyses or concentrated to dryness and the components of the extract were further examined by HPCPC and RP-HPLC. The profile of fractions was also monitored by Thin Layer Chromatography (TLC) using the lower phase of CHCl<sub>3</sub>/MeOH/H<sub>2</sub>O (7:13:8 v/v/v) solvent system.

### 3.4. Thin Layer Chromatography (TLC)

Samples were dissolved in 90% or 50% aqueous MeOH and 10 microliters were loaded onto silica gel 60 F<sub>254</sub> aluminum sheets (Merck #1.05554.0001) and developed with the lower phase of CHCl<sub>3</sub>/MeOH/H<sub>2</sub>O (7:13:8) biphasic solvent system. The profile of separated compounds on the TLC plate was visualized by UV light and by spraying with a 15% sulfuric acid in EtOH solution and heating for 15 min at 110 °C until maroon-dark purple spots developed.

### 3.5. High Performance Centrifugal Partition Chromatography (HPCPC or CPC)

The solvent system containing CHCl<sub>3</sub>/MeOH/H<sub>2</sub>O–0.1% HCO<sub>2</sub>H (7:13:8) was mixed vigorously using a separating funnel and allowed to reach hydrostatic equilibration. Following the separation of the two-immiscible phase solvent systems, both phases were degassed using a sonicator-degasser (Soniclean Pty Ltd., Adelaide, SA, Australia). Then the rotor column of HPCPC™, CPC240 (Ever Seiko Corporation, Tokyo, Japan) was filled with the liquid stationary phase at a flow rate of 5 mL/min by Dual Pump model 214 (Tokyo, Japan).

The CPC was loaded with the aqueous upper phase of the solvent system in the descending mode at a flow rate of 5 mL/min with a revolution speed of 300 rpm. The lower mobile phase was pumped in the descending mode at a flow rate of 1.2 mL/min with a rotation speed of 900 rpm within 2 h. One hundred and twenty milligrams of isobutanol-enriched saponin mixture was dissolved in 10 mL of the upper phase and lower phase in a ratio of 1:1 and injected to the machine from the head-end direction (descending mode) following hydrostatic equilibration of the two phases indicated by a clear mobile phase eluting at the tail outlet. This indicated that elution of the stationary phase had stopped and the back pressure was constant. The chromatogram was developed at 254 nm for 3.0 h at 1.2 mL/min and 900 rpm using the Variable Wavelength UV-VIS Detector S-3702 (Soma optics Ltd., Tokyo, Japan) and chart recorder (Ross Recorders, Model 202, Topac Inc., Cohasset, MA, USA). The fractions were collected in 3 mL/tubes using a Fraction collector. The

elution of the sample with the lower organic phase proceeded to remove the compounds with low polarity from the sample, within 200 mL of which several peaks were eluted. At this point (Fraction 54), the elution mode was switched to ascending mode and the aqueous upper phase was pumped at the same flow rate for 3.0 h. Recovery of saponins was achieved by changing the elution mode to the aqueous phase which allowed the elution of the remaining compounds with high polarity in the stationary phase. A few minor peaks were also monitored. Fractions were analyzed by TLC using the lower phase of  $\text{CHCl}_3/\text{MeOH}/\text{H}_2\text{O}$  (7:13:8) as the developing system. The monitoring of the fractions is necessary, as most of the saponins were not detected by UV due to the lack of a chromophore structure. Fractions were concentrated with nitrogen gas.

### 3.6. Mass Spectrometry

The isobutanol saponin-enriched fractions and the resultant HPCPC purified polar samples were further analyzed by MALDI and ESI MS to elucidate and characterize the molecular structures of compounds.

#### 3.6.1. MALDI-MS

MALDI analysis was performed on a Bruker Autoflex III Smartbeam (Bruker Daltonik, Bremen, Germany). All MALDI MS equipment, software and consumables were from Bruker Daltonics (Bremen, Germany). The laser (355 nm) had a repetition rate of 200 Hz and operated in the positive reflectron ion mode for MS data over the mass range of 400 to 2200 Da under the control of the FlexControl and FlexAnalysis software (V 3.3 build 108, Bruker Daltonik, Bremen, Germany). External calibration was performed using PEG. MS spectra were processed in FlexAnalysis (version 3.3, Bruker Daltonik, Bremen, Germany). MALDI MS/MS spectra were obtained using the LIFT mode of the Bruker Autoflex III with the aid of CID. The isolated ions were submitted to collision against argon in the collision cell to collisionally activate and fragment, and afford intense product ion signals. For MALDI, a laser energy was used that provided both good signal levels and mass resolution, the laser energy for MS/MS analysis was generally 25% higher than for MS analysis.

The samples were placed onto a MALDI stainless steel MPT AnchorChip TM 600/384 target plate. Alpha-cyano-4-hydroxycinnamic acid (CHCA) in acetone/ iso-propanol in ratio of 2:1 (15 mg/mL) was used as a matrix to produce gas-phase ions. The matrix solution (1  $\mu\text{L}$ ) was spotted onto the MALDI target plate and air-dried. Subsequently 1  $\mu\text{L}$  of sample was added to the matrix crystals and air-dried. Finally, 1  $\mu\text{L}$  of NaI (Sigma-Aldrich #383112, St Louis, MO, USA) solution (2 mg/mL in acetonitrile) was applied onto the sample spots. The samples were mixed on the probe surface and dried prior to analysis.

#### 3.6.2. ESI-MS

The ESI mass spectra were obtained with a Waters Synapt HDMS (Waters, Manchester, UK). Mass spectra were obtained in the positive ion mode with a capillary voltage of 3.0 kV and a sampling cone voltage of 100 V.

The other conditions were as follows: extraction cone voltage, 4.0 V; ion source temperature, 80 °C; desolvation temperature, 350 °C; desolvation gas flow rate, 500 L/h. Data acquisition was carried out using Waters MassLynx (V4.1, Waters Corporation, Milford, CT, USA). Positive ion mass spectra were acquired in the V resolution mode over a mass range of 100–2000  $m/z$  using continuum mode acquisition. Mass calibration was performed by infusing sodium iodide solution (2  $\mu\text{g}/\mu\text{L}$ , 1:1 (v/v) water/isopropanol). For accurate mass analysis a lock mass signal from the sodium attached molecular ion of Raffinose ( $m/z$  527.1588) was used.

MS/MS spectra were obtained by mass selection of the ion of interest using the quadrupole, fragmentation in the trap cell where argon was used as collision gas. Typical collision energy (Trap) was 50.0 V. Samples were infused at a flow rate of 5  $\mu\text{L}/\text{min}$ , if dilution of the sample was required then acetonitrile was used [100]. Chemical structures were determined from fragmentation schemes calculated on tandem mass spectra and from the literature.

#### 4. Conclusions

The extract of the viscera of sea cucumber *H. lessoni* was processed by applying HPCPC to purify the saponin mixture and to isolate saponin congeners and isomeric saponins. The tandem MS approach enabled us to determine the structure of a range of saponins. The purity of HPCPC fractions allowed mass spectrometry analyses to reveal the structure of isomeric compounds containing different aglycones and/or sugar residues. Several novel saponins, along with known compounds, were identified from the viscera of sea cucumber.

This study is the first on saponins from the viscera of sea cucumbers. Our results to date highlight that there are a larger number of novel saponins in the viscera compared to the body wall (data not shown) indicating the viscera as a major source of these compounds. This paper is the first not only to report the presence of several novel saponins in the viscera of *H. lessoni* but also to indicate the highest number of saponin congeners detected in the viscera of any sea cucumber species. The mass of reported saponins for this species ranged from 460 Da to 1600 Da. So far we have identified more than ten aglycone structures in this species. Evidence from MALDI-MS suggested that the most intensive saponin ion was  $m/z$  1243.5, a major component which seemed to correspond to Holothurin A. However, in the tandem MS, the most abundant ions are generally attributed to the loss of aglycones and/or both key diagnostic sugar moieties (507 and 523). Our results also showed that the incidence of the cross-ring cleavages was higher in the sulfated compounds compared to non-sulfated glycosides. It can be concluded that the presence of a sulfate group in the sugar moiety of saponins made them more vulnerable to cross-ring cleavages.

At the moment, MS is one of the most sensitive techniques of molecular analysis to determine saponin structures. This methodology of molecular structure identification using fragmentation patterns acquired from MS/MS measurements helps to propose and identify the structure of saponins. It was found that under CID some of the identified saponins had the same ion fingerprints for their aglycone units, yielding the same  $m/z$  daughter ions. Some of these saponins were easily characterized based on MS/MS measurement since their CID spectra contained the key diagnostic signals at  $m/z$  507 and 523, corresponding to the oligosaccharide chains [MeGlc-Glc-Qui + Na<sup>+</sup>] and [MeGlc-Glc-Glc + Na<sup>+</sup>], respectively. The simultaneous loss of two sugar units indicated

characteristics of a branched sugar chain. This methodology also permitted the structural elucidation of isomers.

Sea cucumbers have developed a chemical defense against potential predators based upon saponins. Our finding indicates that the viscera are rich in saponins, in both diversity and quantity, and that these saponins are apparently more localized in the viscera than in the body wall.

The chromatography techniques used in this study were able to for the first time, separate high purity saponins from sea cucumber, highlight the diversity of saponin congeners, and stress the unique profile of saponins for this species. MALDI and ESI-MS proved to be sensitive, ultra-high-throughput methodologies to identify these secondary metabolites in a complex mixture. Therefore, mass spectrometry has become the preferred techniques for analysis of saponins, as both ESI-MS and the MALDI-MS spectra provide remarkable structural information. However, the MALDI data is simpler to interpret compared to ESI-MS data due to the singly charged ions. This ancient creature with a long evolutionary history is a unique source of high-value novel compounds.

This manuscript describes the structure elucidation of seven novel compounds; Holothurinoside O, Holothurinoside P, Holothurinoside Q, Holothurinoside R, Holothurinoside R<sub>1</sub>, Holothurinoside S and Holothurinoside T in addition to six known compounds, including Holothurin A, Holothurinoside A, Holothurinoside A<sub>1</sub>, Holothurinoside E, Holothurinoside E<sub>1</sub> and 17-dehydroxy-holothurinoside A.

In conclusion, our findings show that the viscera of *H. lessoni* contain numerous unique and novel saponins with a high range of structural diversity, including both sulfated and non-sulfated congeners, and with different aglycone and sugar moieties. Furthermore, the tremendous range of structural biodiversity of this class of natural metabolites, which enables them to present in a remarkable functional diversity, is potentially an important source for the discovery of high-value compounds for biotechnological applications.

## Acknowledgments

We would like to express our gratitude to the Australian SeaFood CRC for financially supporting this project, Ben Leahy for supplying the sea cucumber samples. The authors gratefully acknowledge the technical assistance provided by Daniel Jardine at Flinders Analytical Laboratory and Tim Chataway at Flinders Proteomics Facility.

## Author Contributions

Y.B., C.F. and W.Z. designed the experiments. Y.B. carried out the experiments with guidance of C.F. and W.Z., who assisted in setting up the HCPCP analysis. Y.B., C.F. and W.Z. worked together on chemical structure elucidation, and all three authors contributed in writing the manuscript.

## Conflicts of Interest

The authors declare no conflict of interest.

## References

1. Lovatelli, A.; Conand, C. *Advances in Sea Cucumber Aquaculture and Management*; FAO: Rome, Italy, 2004.
2. Purcell, S.W.; Samyn, Y.; Conand, C. *Commercially Important Sea Cucumbers of the World*; FAO Species Catalogue for Fishery Purposes No. 6; FAO: Rome, Italy, 2012; p. 150.
3. Waller, G.R.; Yamasaki, K. *Saponins Used in Food and Agriculture*; Plenum Press: New York, NY, USA, 1996; Volume 405.
4. Hostettmann, K.; Marston, A. *Saponins*; Cambridge University Press: Cambridge, MA, USA, 1995.
5. Elbandy, M.; Rho, J.; Afifi, R. Analysis of saponins as bioactive zoochemicals from the marine functional food sea cucumber *Bohadschia cousteaui*. *Eur. Food Res. Technol.* **2014**, doi:10.1007/s00217-014-2171-6.
6. Caulier, G.; van Dyck, S.; Gerbaux, P.; Eeckhaut, I.; Flammang, P. Review of saponin diversity in sea cucumbers belonging to the family Holothuriidae. *SPC Beche-de-mer Inf. Bull.* **2011**, *31*, 48–54.
7. Dong, P.; Xue, C.; Du, Q. Separation of two main triterpene glycosides from sea cucumber *Pearsonothuria graeffei* by high-speed countercurrent chromatography. *Acta Chromatogr.* **2008**, *20*, 269–276.
8. Han, H.; Zhang, W.; Yi, Y.H.; Liu, B.S.; Pan, M.X.; Wang, X.H. A novel sulfated holostane glycoside from sea cucumber *Holothuria leucospilota*. *Chem. Biodivers.* **2010**, *7*, 1764–1769.
9. Naidu, A.S. *Natural Food Antimicrobial Systems*; CRC Press: New York, NY, USA, 2000.
10. Zhang, S.L.; Li, L.; Yi, Y.H.; Sun, P. Philinopsides E and F, two new sulfated triterpene glycosides from the sea cucumber *Pentacta quadrangularis*. *Nat. Prod. Res.* **2006**, *20*, 399–407.
11. Zhang, S.L.; Li, L.; Yi, Y.H.; Zou, Z.R.; Sun, P. Philinopgenin A, B, and C, three new triterpenoid aglycones from the sea cucumber *Pentacta quadrangulasis*. *Mar. Drugs* **2004**, *2*, 185–191.
12. Zhang, S.Y.; Yi, Y.H.; Tang, H.F.; Li, L.; Sun, P.; Wu, J. Two new bioactive triterpene glycosides from the sea cucumber *Pseudocolochirus violaceus*. *J. Asian Nat. Prod. Res.* **2006**, *8*, 1–8.
13. Chludil, H.D.; Muniain, C.C.; Seldes, A.M.; Maier, M.S. Cytotoxic and antifungal triterpene glycosides from the Patagonian sea cucumber *Hemoiedema spectabilis*. *J. Nat. Prod.* **2002**, *65*, 860–865.
14. Francis, G.; Kerem, Z.; Makkar, H.P.; Becker, K. The biological action of saponins in animal systems: A review. *Br. J. Nutr.* **2002**, *88*, 587–605.
15. Maier, M.S.; Roccatagliata, A.J.; Kuriss, A.; Chludil, H.; Seldes, A.M.; Pujol, C.A.; Damonte, E.B. Two new cytotoxic and virucidal trisulfated triterpene glycosides from the Antarctic sea cucumber *Staurocucumis liouvillei*. *J. Nat. Prod.* **2001**, *64*, 732–736.
16. Osbourn, A.; Goss, R.J.M.; Field, R.A. The saponins-polar isoprenoids with important and diverse biological activities. *Nat. Prod. Rep.* **2011**, *28*, 1261–1268.

17. Jha, R.K.; Zi-rong, X. Biomedical Compounds from Marine organisms. *Mar. Drugs* **2004**, *2*, 123–146.
18. Kalinin, V.I.; Aminin, D.L.; Avilov, S.A.; Silchenko, A.S.; Stonik, V.A. Triterpene glycosides from sea cucumbers (Holothurioidea, Echinodermata). Biological activities and functions. In *Studies in Natural Products Chemistry*; Atta-ur, R., Ed.; Elsevier: Amsterdam, The Netherlands, 2008; Volume 35, pp. 135–196.
19. Liu, J.; Yang, X.; He, J.; Xia, M.; Xu, L.; Yang, S. Structure analysis of triterpene saponins in *Polygala tenuifolia* by electrospray ionization ion trap multiple-stage mass spectrometry. *J. Mass Spectrom.* **2007**, *42*, 861–873.
20. Kim, S.K.; Himaya, S.W.; Kang, K.H. Sea Cucumber Saponins Realization of Their Anticancer Effects. In *Marine Pharmacognosy: Trends and Applications*; Kim, S.K., Ed.; CRC Press: New York, NY, USA, 2012; pp. 119–128.
21. Mohammadzadeh, F.; Ehsanpor, M.; Afkhami, M.; Mokhlesi, A.; Khazaali, A.; Montazeri, S. Antibacterial, antifungal and cytotoxic effects of a sea cucumber *Holothuria leucospilota*, from the north coast of the Persian Gulf. *J. Mar. Biol. Assoc. UK* **2013**, *93*, 1401–1405.
22. Mohammadzadeh, F.; Ehsanpor, M.; Afkhami, M.; Mokhlesi, A.; Khazaali, A.; Montazeri, S. Evaluation of antibacterial, antifungal and cytotoxic effects of *Holothuria scabra* from the north coast of the Persian Gulf. *J. Med. Mycol.* **2013**, *23*, 225–229.
23. Mokhlesi, A.; Saeidnia, S.; Gohari, A.R.; Shahverdi, A.R.; Nasrolahi, A.; Farahani, F.; Khoshnood, R.; Es' haggi, N. Biological activities of the sea cucumber *Holothuria leucospilota*. *Asian J. Anim. Vet. Adv.* **2012**, *7*, 243–249.
24. Sarhadzadeh, N.; Afkhami, M.; Ehsanpour, M. Evaluation bioactivity of a sea cucumber, *Stichopus hermanni* from Persian Gulf. *Eur. J. Exp. Biol.* **2014**, *4*, 254–258.
25. Kim, S.K.; Himaya, S.W. Triterpene glycosides from sea cucumbers and their biological activities. *Adv. Food Nutr. Res.* **2012**, *65*, 297–319.
26. Yamanouchi, T. On the poisonous substance contained in holothurians. *Publ. Seto Mar. Biol. Lab.* **1955**, *4*, 183–203.
27. Avilov, S.A.; Drozdova, O.A.; Kalinin, V.I.; Kalinovskiy, A.I.; Stonik, V.A.; Gudimova, E.N.; Riguera, R.; Jimenez, C. Frondoside C, a new nonholostane triterpene glycoside from the sea cucumber *Cucumaria frondosa*: Structure and cytotoxicity of its desulfated derivative. *Can. J. Chem.* **1998**, *76*, 137–141.
28. Girard, M.; Bélanger, J.; ApSimon, J.W.; Garneau, F.X.; Harvey, C.; Brisson, J.R.; Frondoside, A. A novel triterpene glycoside from the holothurian *Cucumaria frondosa*. *Can. J. Chem.* **1990**, *68*, 11–18.
29. Han, H.; Yi, Y.; Xu, Q.; La, M.; Zhang, H. Two new cytotoxic triterpene glycosides from the sea cucumber *Holothuria scabra*. *Planta Med.* **2009**, *75*, 1608–1612.
30. Kalinin, V.I.; Avilov, S.A.; Kalinina, E.Y.; Korolkova, O.G.; Kalinovskiy, A.I.; Stonik, V.A.; Riguera, R.; Jimenez, C. Structure of eximiside A, a novel triterpene glycoside from the Far-Eastern sea cucumber *Psolus eximius*. *J. Nat. Prod.* **1997**, *60*, 817–819.

31. Kitagawa, I.; Yamanaka, H.; Kobayashi, M.; Nishino, T.; Yosioka, I.; Sugawara, T. Saponin and saponenol. XXVII. Revised structures of holotoxin A and holotoxin B, two antifungal oligoglycosides from the sea cucumber *Stichopus japonicus* Selenka. *Chem. Pharm. Bull. (Tokyo)* **1978**, *26*, 3722–3731.
32. Liu, B.S.; Yi, Y.H.; Li, L.; Sun, P.; Yuan, W.H.; Sun, G.Q.; Han, H.; Xue, M. Argusides B and C, two new cytotoxic triterpene glycosides from the sea cucumber *Bohadschia argus* Jaeger. *Chem. Biodivers.* **2008**, *5*, 1288–1297.
33. Miyamoto, T.; Togawa, K.; Higuchi, R.; Komori, T.; Sasaki, T. Structures of four new triterpenoid oligoglycosides: DS-penaustrosides A, B, C, and D from the sea cucumber *Pentacta australis*. *J. Nat. Prod.* **1992**, *55*, 940–946.
34. Campagnuolo, C.; Fattorusso, E.; Tagliatalata-Scafati, O. Feroxosides A–B, two norlanostane tetraglycosides from the Caribbean sponge *Ectyoplasia ferox*. *Tetrahedron* **2001**, *57*, 4049–4055.
35. Thompson, J.; Walker, R.; Faulkner, D. Screening and bioassays for biologically-active substances from forty marine sponge species from San Diego, California, USA. *Mar. Biol.* **1985**, *88*, 11–21.
36. Dang, N.H.; Thanh, N.V.; Kiem, P.V.; Huong le, M.; Minh, C.V.; Kim, Y.H. Two new triterpene glycosides from the Vietnamese sea cucumber *Holothuria scabra*. *Arch. Pharm. Res.* **2007**, *30*, 1387–1391.
37. Kerr, R.G.; Chen, Z. *In vivo* and *in vitro* biosynthesis of saponins in sea cucumbers. *J. Nat. Prod.* **1995**, *58*, 172–176.
38. Chludil, H.D.; Murray, A.P.; Seldes, A.M.; Maier, M.S. Biologically active triterpene Glycosides from sea cucumbers (Holothuroidea, Echinodermata). In *Studies in Natural Products Chemistry*; Atta-ur, R., Ed.; Elsevier: Amsterdam, The Netherlands, 2003; Volume 28, Part I, pp. 587–615.
39. Habermehl, G.; Volkwein, G. Aglycones of the toxins from the Cuvierian organs of *Holothuria forskali* and a new nomenclature for the aglycones from Holothurioidea. *Toxicon* **1971**, *9*, 319–326.
40. Kalinin, V.I.; Silchenko, A.S.; Avilov, S.A.; Stonik, V.A.; Smirnov, A.V. Sea cucumbers triterpene glycosides, the recent progress in structural elucidation and chemotaxonomy. *Phytochem. Rev.* **2005**, *4*, 221–236.
41. Stonik, V.A.; Kalinin, V.I.; Avilov, S.A. Toxins from sea cucumbers (holothuroids): Chemical structures, properties, taxonomic distribution, biosynthesis and evolution. *J. Nat. Toxins* **1999**, *8*, 235–248.
42. Zhang, S.Y.; Tang, H.F.; Yi, Y.H. Cytotoxic triterpene glycosides from the sea cucumber *Pseudocolochirus violaceus*. *Fitoterapia* **2007**, *78*, 283–287.
43. Aminin, D.L.; Chaykina, E.L.; Agafonova, I.G.; Avilov, S.A.; Kalinin, V.I.; Stonik, V.A. Antitumor activity of the immunomodulatory lead Cumaside. *Int. Immunopharmacol.* **2010**, *10*, 648–654.

44. Antonov, A.S.; Avilov, S.A.; Kalinovsky, A.I.; Anastyuk, S.D.; Dmitrenok, P.S.; Evtushenko, E.V.; Kalinin, V.I.; Smirnov, A.V.; Taboada, S.; Ballesteros, M.; *et al.* Triterpene glycosides from antarctic sea cucumbers. 1. Structure of liouvillosides A<sub>1</sub>, A<sub>2</sub>, A<sub>3</sub>, B<sub>1</sub>, and B<sub>2</sub> from the sea cucumber *Staurocucumis liouvillei*: New procedure for separation of highly polar glycoside fractions and taxonomic revision. *J. Nat. Prod.* **2008**, *71*, 1677–1685.
45. Antonov, A.S.; Avilov, S.A.; Kalinovsky, A.I.; Dmitrenok, P.S.; Kalinin, V.I.; Taboada, S.; Ballesteros, M.; Avila, C. Triterpene glycosides from Antarctic sea cucumbers III. Structures of liouvillosides A<sub>4</sub> and A<sub>5</sub>, two minor disulphated tetraosides containing 3-*O*-methylquinovose as terminal monosaccharide units from the sea cucumber *Staurocucumis liouvillei* (Vaney). *Nat. Prod. Res.* **2011**, *25*, 1324–1333.
46. Avilov, S.A.; Silchenko, A.S.; Antonov, A.S.; Kalinin, V.I.; Kalinovsky, A.I.; Smirnov, A.V.; Dmitrenok, P.S.; Evtushenko, E.V.; Fedorov, S.N.; Savina, A.S.; *et al.* Synaptosides A and A<sub>1</sub>, triterpene glycosides from the sea cucumber *Synapta maculata* containing 3-*O*-methylglucuronic acid and their cytotoxic activity against tumor cells. *J. Nat. Prod.* **2008**, *71*, 525–531.
47. Iniguez-Martinez, A.M.D.M.; Guerra-Rivas, G.; Rios, T.; Quijano, L. Triterpenoid oligoglycosides from the sea cucumber *Stichopus parvimensis*. *J. Nat. Prod.* **2005**, *68*, 1669–1673.
48. Stonik, V.A.; Elyakov, G.B. Secondary metabolites from echinoderms as chemotaxonomic markers. *Bioorg. Mar. Chem.* **1988**, *2*, 43–86.
49. Bordbar, S.; Anwar, F.; Saari, N. High-value components and bioactives from sea cucumbers for functional foods—A review. *Mar. Drugs* **2011**, *9*, 1761–1805.
50. Van Dyck, S.; Gerbaux, P.; Flammang, P. Qualitative and quantitative saponin contents in five sea cucumbers from the Indian ocean. *Mar. Drugs* **2010**, *8*, 173–189.
51. Avilov, S.A.; Antonov, A.S.; Drozdova, O.A.; Kalinin, V.I.; Kalinovsky, A.I.; Stonik, V.A.; Riguera, R.; Lenis, L.A.; Jiménez, C. Triterpene glycosides from the far-eastern sea cucumber *Pentamera calcigera*. 1. Monosulfated glycosides and cytotoxicity of their unsulfated derivatives. *J. Nat. Prod.* **2000**, *63*, 65–71.
52. Avilov, S.A.; Kalinovsky, A.I.; Kalinin, V.I.; Stonik, V.A.; Riguera, R.; Jiménez, C.; Koreoside A, a new nonholostane triterpene glycoside from the sea cucumber *Cucumaria koraiensis*. *J. Nat. Prod.* **1997**, *60*, 808–810.
53. Avilov, S.A.; Antonov, A.S.; Drozdova, O.A.; Kalinin, V.I.; Kalinovsky, A.I.; Riguera, R.; Lenis, L.A.; Jimenez, C. Triterpene glycosides from the far eastern sea cucumber *Pentamera calcigera* II: Disulfated glycosides. *J. Nat. Prod.* **2000**, *63*, 1349–1355.
54. Avilov, S.A.; Antonov, A.S.; Silchenko, A.S.; Kalinin, V.I.; Kalinovsky, A.I.; Dmitrenok, P.S.; Stonik, V.A.; Riguera, R.; Jimenez, C. Triterpene glycosides from the far eastern sea cucumber *Cucumaria conicospermium*. *J. Nat. Prod.* **2003**, *66*, 910–916.
55. Jia, L.; Qian, K. An Evidence-Based Perspective of *Panax Ginseng* (Asian Ginseng) and *Panax Quinquefolius* (American Ginseng) as a Preventing or Supplementary Therapy for Cancer Patients. In *Evidence-Based Anticancer Materia Medica*; Springer Verlag: New York, NY, USA, 2011; pp. 85–96.



56. Zhang, S.Y.; Yi, Y.H.; Tang, H.F. Bioactive triterpene glycosides from the sea cucumber *Holothuria fuscocinerea*. *J. Nat. Prod.* **2006**, *69*, 1492–1495.
57. Zhang, S.Y.; Yi, Y.H.; Tang, H.F. Cytotoxic sulfated triterpene glycosides from the sea cucumber *Pseudocolochirus violaceus*. *Chem. Biodivers.* **2006**, *3*, 807–817.
58. Caulier, G.; Flammang, P.; Gerbaux, P.; Eeckhaut, I. When a repellent becomes an attractant: Harmful saponins are kairomones attracting the symbiotic *Harlequin crab*. *Sci. Rep.* **2013**, *3*, doi:10.1038/srep02639.
59. Mercier, A.; Sims, D.W.; Hamel, J.F. *Advances in Marine Biology: Endogenous and Exogenous Control of Gametogenesis and Spawning in Echinoderms*; Academic Press: New York, NY, USA, 2009; Volume 55.
60. Matsuno, T.; Ishida, T. Distribution and seasonal variation of toxic principles of sea-cucumber (*Holothuria leucospilota*; Brandt). *Cell. Mol. Life Sci.* **1969**, *25*, doi:10.1007/BF01897485.
61. Kobayashi, M.; Hori, M.; Kan, K.; Yasuzawa, T.; Matsui, M.; Suzuki, S.; Kitagawa, I. Marine natural products. XXVII: Distribution of lanostane-type triterpene oligoglycosides in ten kinds of Okinawan Sea cucumbers. *Chem. Pharm. Bull. (Tokyo)* **1991**, *39*, 2282–2287.
62. Van Dyck, S.; Flammang, P.; Meriaux, C.; Bonnel, D.; Salzet, M.; Fournier, I.; Wisztorski, M. Localization of secondary metabolites in marine invertebrates: contribution of MALDI MSI for the study of saponins in Cuvierian tubules of *H. forskali*. *PLoS One* **2010**, *5*, e13923.
63. Bakus, G.J. Defensive mechanisms and ecology of some tropical holothurians. *Mar. Biol.* **1968**, *2*, 23–32.
64. Bondoc, K.G.V.; Lee, H.; Cruz, L.J.; Lebrilla, C.B.; Juinio-Meñez, M.A. Chemical fingerprinting and phylogenetic mapping of saponin congeners from three tropical holothurian sea cucumbers. *Comp. Biochem. Physiol. B Biochem. Mol. Biol.* **2013**, *166*, 182–193.
65. Van Dyck, S.; Caulier, G.; Todesco, M.; Gerbaux, P.; Fournier, I.; Wisztorski, M.; Flammang, P. The triterpene glycosides of *Holothuria forskali*: Usefulness and efficiency as a chemical defense mechanism against predatory fish. *J. Exp. Biol.* **2011**, *214*, 1347–1356.
66. Kalyani, G.A.; Kakrani, H.K.N.; Hukkeri, V.I. Holothurin—A Review. *Indian J. Nat. Prod.* **1988**, *4*, 3–8.
67. Kalinin, V.; Anisimov, M.; Prokofieva, N.; Avilov, S.; Afiyatullo, S.S.; Stonik, V. Biological activities and biological role of triterpene glycosides from holothuroids (Echinodermata). *Echinoderm Stud.* **1996**, *5*, 139–181.
68. Kalinin, V.I.; Prokofieva, N.G.; Likhatskaya, G.N.; Schentsova, E.B.; Agafonova, I.G.; Avilov, S.A.; Drozdova, O.A. Hemolytic activities of triterpene glycosides from the holothurian order Dendrochirotida: Some trends in the evolution of this group of toxins. *Toxicon* **1996**, *34*, 475–483.
69. Van Dyck, S.; Gerbaux, P.; Flammang, P. Elucidation of molecular diversity and body distribution of saponins in the sea cucumber *Holothuria forskali* (Echinodermata) by mass spectrometry. *Comp. Biochem. Physiol. B Biochem. Mol. Biol.* **2009**, *152*, 124–134.

70. Elyakov, G.B.; Stonik, V.A.; Levina, E.V.; Slanke, V.P.; Kuznetsova, T.A.; Levin, V.S. Glycosides of marine invertebrates—I. A comparative study of the glycoside fractions of pacific sea cucumbers. *Comp. Biochem. Physiol. B Comp. Biochem.* **1973**, *44*, 325–336.
71. Cai, Z.; Liu, S.; Asakawa, D. *Applications of MALDI-TOF Spectroscopy*; Springer: Berlin, Germany, 2013.
72. Du, Q.; Jerz, G.; Waibel, R.; Winterhalter, P. Isolation of dammarane saponins from *Panax notoginseng* by high-speed counter-current chromatography. *J. Chromatogr.* **2003**, *1008*, 173–180.
73. Cui, M.; Song, F.; Zhou, Y.; Liu, Z.; Liu, S. Rapid identification of saponins in plant extracts by electrospray ionization multi-stage tandem mass spectrometry and liquid chromatography/tandem mass spectrometry. *Rapid Commun. Mass Spectrom.* **2000**, *14*, 1280–1286.
74. Schöpke, T.; Thiele, H.; Wray, V.; Nimtz, M.; Hiller, K. Structure elucidation of a glycoside of 2 $\beta$ , 3 $\beta$ , t23-trihydroxy-16-oxoolean-12-en-28-oic acid from *Bellis bernardii* using mass spectrometry for the sugar sequence determination. *J. Nat. Prod.* **1995**, *58*, 152–155.
75. Bankefors, J.; Broberg, S.; Nord, L.I.; Kenne, L. Electrospray ionization ion-trap multiple-stage mass spectrometry of Quillaja saponins. *J. Mass Spectrom.* **2011**, *46*, 658–665.
76. Liu, S.; Cui, M.; Liu, Z.; Song, F.; Mo, W. Structural analysis of saponins from medicinal herbs using electrospray ionization tandem mass spectrometry. *J. Am. Soc. Mass Spectrom.* **2004**, *15*, 133–141.
77. Wang, X.; Sakuma, T.; Asafu-Adjaye, E.; Shiu, G.K. Determination of ginsenosides in plant extracts from *Panax ginseng* and *Panax quinquefolius* L. by LC/MS/MS. *Anal. Chem.* **1999**, *71*, 1579–1584.
78. Wolfender, J.L.; Rodriguez, S.; Hostettmann, K. Liquid chromatography coupled to mass spectrometry and nuclear magnetic resonance spectroscopy for the screening of plant constituents. *J. Chromatogr.* **1998**, *794*, 299–316.
79. Zheng, Z.; Zhang, W.; Kong, L.; Liang, M.; Li, H.; Lin, M.; Liu, R.; Zhang, C. Rapid identification of C<sub>21</sub> steroidal saponins in *Cynanchum versicolor* Bunge by electrospray ionization multi-stage tandem mass spectrometry and liquid chromatography/tandem mass spectrometry. *Rapid Commun. Mass Spectrom.* **2007**, *21*, 279–285.
80. Cui, M.; Song, F.; Liu, Z.; Liu, S. Metal ion adducts in the structural analysis of ginsenosides by electrospray ionization with multi-stage mass spectrometry. *Rapid Commun. Mass Spectrom.* **2001**, *15*, 586–595.
81. Fang, S.; Hao, C.; Sun, W.; Liu, Z.; Liu, S. Rapid analysis of steroidal saponin mixture using electrospray ionization mass spectrometry combined with sequential tandem mass spectrometry. *Rapid Commun. Mass Spectrom.* **1998**, *12*, 589–594.
82. Li, L. *MALDI Mass Spectrometry for Synthetic Polymer Analysis*; Wiley & Sons: Hoboken, NJ, USA, 2009; Volume 175.
83. Silchenko, A.S.; Stonik, V.A.; Avilov, S.A.; Kalinin, V.I.; Kalinovskiy, A.I.; Zaharenko, A.M.; Smirnov, A.V.; Mollo, E.; Cimino, G. Holothurins B<sub>2</sub>, B<sub>3</sub>, and B<sub>4</sub>, new triterpene glycosides from mediterranean sea cucumbers of the genus *holothuria*. *J. Nat. Prod.* **2005**, *68*, 564–567.

84. Han, H.; Yi, Y.H.; Li, L.; Wang, X.H.; Liu, B.S.; Sun, P.; Pan, M.X. A new triterpene glycoside from sea cucumber *Holothuria leucospilota*. *Chin. Chem. Lett.* **2007**, *18*, 161–164.
85. Kitagawa, I.; Nishino, T.; Matsuno, T.; Akutsu, H.; Kyogoku, Y. Structure of holothurin B a pharmacologically active triterpene-oligoglycoside from the sea cucumber *Holothuria leucospilota* Brandt. *Tetrahedron Lett.* **1978**, *19*, 985–988.
86. Han, H.; Yi, Y.H.; Liu, B.S.; Wang, X.H.; Pan, M.X. Leucospilataside C, a new sulfated triterpene glycoside from sea cucumber *Holothuria leucospilota*. *Chin. Chem. Lett.* **2008**, *19*, 1462–1464.
87. Wu, J.; Yi, Y.H.; Tang, H.F.; Wu, H.M.; Zou, Z.R.; Lin, H.W. Nobilisides A–C, three new triterpene glycosides from the sea cucumber *Holothuria nobilis*. *Planta Med.* **2006**, *72*, 932–935.
88. Rodriguez, J.; Castro, R.; Riguera, R. Holothurinosides: New antitumour non sulphated triterpenoid glycosides from the sea cucumber *Holothuria forskalii*. *Tetrahedron* **1991**, *47*, 4753–4762.
89. Kitagawa, I.; Kobayashi, M.; Kyogoku, Y. Marine natural products. IX. Structural elucidation of triterpenoidal oligoglycosides from the Bahamean sea cucumber *Actinopyga agassizi* Selenka. *Chem. Pharm. Bull. (Tokyo)* **1982**, *30*, 2045–2050.
90. Liu, B.S.; Yi, Y.H.; Li, L.; Sun, P.; Han, H.; Sun, G.Q.; Wang, X.H.; Wang, Z.L. Argusides D and E, two new cytotoxic triterpene glycosides from the sea cucumber *Bohadschia argus* Jaeger. *Chem. Biodivers.* **2008**, *5*, 1425–1433.
91. Han, H.; Yi, Y.H.; Li, L.; Liu, B.S.; La, M.P.; Zhang, H.W. Antifungal active triterpene glycosides from sea cucumber *Holothuria scabra*. *Acta Pharm. Sin.* **2009**, *44*, 620–624.
92. Han, H.; Li, L.; Yi, Y.-H.; Wang, X.-H.; Pan, M.-X. Triterpene glycosides from sea cucumber *Holothuria scabra* with cytotoxic activity. *Chin. Herbal Med.* **2012**, *4*, 183–188.
93. Kalinin, V.; Stonik, V. Glycosides of marine invertebrates. Structure of Holothurin A<sub>2</sub> from the holothurian *Holothuria edulis*. *Chem. Nat. Compd.* **1982**, *18*, 196–200.
94. Kitagawa, I.; Kobayashi, M.; Inamoto, T.; Fuchida, M.; Kyogoku, Y. Marine natural products. XIV. Structures of echinosides A and B, antifungal lanostane-oligosides from the sea cucumber *Actinopyga echinites* (Jaeger). *Chem. Pharm. Bull. (Tokyo)* **1985**, *33*, 5214–5224.
95. Thanh, N.V.; Dang, N.H.; Kiem, P.V.; Cuong, N.X.; Huong, H.T.; Minh, C.V. A new triterpene glycoside from the sea cucumber *Holothuria scabra* collected in Vietnam. *ASEAN J. Sci. Technol. Dev.* **2006**, *23*, 253–259.
96. Kitagawa, I.; Nishino, T.; Kyogoku, Y. Structure of holothurin A a biologically active triterpene-oligoglycoside from the sea cucumber *Holothuria leucospilota* Brandt. *Tetrahedron Lett.* **1979**, *20*, 1419–1422.
97. Yuan, W.; Yi, Y.; Tang, H.; Xue, M.; Wang, Z.; Sun, G.; Zhang, W.; Liu, B.; Li, L.; Sun, P. Two new holostan-type triterpene glycosides from the sea cucumber *Bohadschia marmorata* JAEGER. *Chem. Pharm. Bull. (Tokyo)* **2008**, *56*, 1207–1211.

98. Yuan, W.H.; Yi, Y.H.; Tan, R.X.; Wang, Z.L.; Sun, G.Q.; Xue, M.; Zhang, H.W.; Tang, H.F. Antifungal triterpene glycosides from the sea cucumber *Holothuria (Microthele) axiloga*. *Planta Med.* **2009**, *75*, 647–653.
99. Sun, G.Q.; Li, L.; Yi, Y.H.; Yuan, W.H.; Liu, B.S.; Weng, Y.Y.; Zhang, S.L.; Sun, P.; Wang, Z.L. Two new cytotoxic nonsulfated pentasaccharide holostane (=20-hydroxy lanostan-18-oic acid  $\gamma$ -lactone) glycosides from the sea cucumber *Holothuria grisea*. *Helv. Chim. Acta* **2008**, *91*, 1453–1460.
100. Song, F.; Cui, M.; Liu, Z.; Yu, B.; Liu, S. Multiple-stage tandem mass spectrometry for differentiation of isomeric saponins. *Rapid Commun. Mass Spectrom.* **2004**, *18*, 2241–2248.
101. Van Setten, D.C.; Jan ten Hove, G.; Wiertz, E.J.H.J.; Kamerling, J.P.; van de Werken, G. Multiple-stage tandem mass spectrometry for structural characterization of saponins. *Anal. Chem.* **1998**, *70*, 4401–4409.
102. Garneau, F.X.; Simard, J.; Harvey, O.; ApSimon, J.; Girard, M. The structure of psoluthurin A, the major triterpene glycoside of the sea cucumber *Psolus fabricii*. *Can. J. Chem.* **1983**, *61*, 1465–1471.
103. Grassia, A.; Bruno, I.; Debitus, C.; Marzocco, S.; Pinto, A.; Gomez-Paloma, L.; Riccio, R. Spongidepsin, a new cytotoxic macrolide from *Spongia* sp. *Tetrahedron* **2001**, *57*, 6257–6260.
104. Kupchan, S.M.; Britton, R.W.; Ziegler, M.F.; Sigel, C.W. Bruceantin, a new potent antileukemic simaroubolide from *Brucea antidysenterica*. *J. Org. Chem.* **1973**, *38*, 178–179.

# Identification of Marine Neuroactive Molecules in Behaviour-Based Screens in the Larval Zebrafish

Si-Mei Long, Feng-Yin Liang, Qi Wu, Xi-Lin Lu, Xiao-Li Yao, Shi-Chang Li, Jing Li, Huanxing Su, Ji-Yan Pang and Zhong Pei

**Abstract:** High-throughput behavior-based screen in zebrafish is a powerful approach for the discovery of novel neuroactive small molecules for treatment of nervous system diseases such as epilepsy. To identify neuroactive small molecules, we first screened 36 compounds (**1–36**) derived from marine natural products xyloketal and marine isoprenyl phenyl ether obtained from the mangrove fungus. Compound **1** demonstrated the most potent inhibition on the locomotor activity in larval zebrafish. Compounds **37–42** were further synthesized and their potential anti-epilepsy action was then examined in a PTZ-induced epilepsy model in zebrafish. Compound **1** and compounds **39**, **40** and **41** could significantly attenuate PTZ-induced locomotor hyperactivity and elevation of *c-fos* mRNA in larval zebrafish. Compound **40** showed the most potent inhibitory action against PTZ-induced hyperactivity. The structure-activity analysis showed that the OH group at 12-position played a critical role and the substituents at the 13-position were well tolerated in the inhibitory activity of xyloketal derivatives. Thus, these derivatives may provide some novel drug candidates for the treatment of epilepsy.

Reprinted from *Mar. Drugs*. Cite as: Long, S.-M.; Liang, F.-Y.; Wu, Q.; Lu, X.-L.; Yao, X.-L.; Li, S.-C.; Li, J.; Su, H.; Pang, J.-Y.; Pei, Z. Identification of Marine Neuroactive Molecules in Behaviour-Based Screens in the Larval Zebrafish. *Mar. Drugs* **2014**, *12*, 330763322.

## Abbreviations

HT, high-throughput; PTZ, pentylenetetrazol; GABA,  $\gamma$ -Aminobutyric acid; 5-HT, 5-hydroxy-tryptamine; NMDA, *N*-Methyl-D-aspartic acid; CBZ, carbamazepine; DMSO, dimethyl sulfoxide; dpf, days post-fertilization; hpf, hours post fertilization; CNS, central nervous system; IEGs, immediate early genes; EEG, electroencephalography.

## 1. Introduction

Disorders of the central nervous system (CNS) are very common and devastating. However, CNS diseases are usually poorly treated due to of the limited availability of selective neuroactive drugs. Thus, the development of novel neuroactive drugs is of high priority. It has been very difficult to discover novel neuroactive drugs in the past years [1]. Many current behavior-altering drugs were discovered by chance in the 1940s and 1950s. A major obstacle to the discovery of novel neuroactive drugs is the lack of available relevant model systems for screening large numbers of active compounds. Modeling the brain activity *in vitro* is problematic because of the complex networks of the brain. In addition, the screens in mice and rats are low-throughput due to the expense and ethical issues [2]. Recently, zebrafish has become a powerful model system for whole organism small molecule screening. Zebrafish are small, cheap to keep, fast to develop, and easy to

breed. Similar to mammals, zebrafish larvae can display diverse behaviors including the optokinetic response [3], the optomotor response [4], prepulse inhibition [5] and sleep [6,7]. Combined with the video track system, several high-throughput behavior-based assays have been successfully applied to identify novel neuroactive small molecules in the zebrafish [8,9].

The marine habitat is a rich resource for the discovery of new drugs because of its vast chemical and biological diversity. However, most marine-derived lead compounds are stereochemically complex or have low activity. Thus, the appropriate structural modifications of lead compounds are important to develop chemically simple and active drug candidates [10]. In this paper, we conducted a behavior-based screen for neuroactive small molecules on 12 benzopyran compounds derived from natural xyloketals from marine mangrove fungus (NO. 2508) [11] and 24 isoprenyl phenyl ether derivatives modified from marine isoprenyl phenyl ether from Mangrove fungus (NO. B60) [12] (Chart 1). We further modified compound **1** (Chart 2) to study structure-activity relationships and optimize the biological activity of compound **1** derived compounds. Finally, we explored the potential of compound **40** as a new antiepileptic candidate in pentylenetetrazol (PTZ)-induced epilepsy model in zebrafish.

**Chart 1.** Structures selected for neuroactive screening.

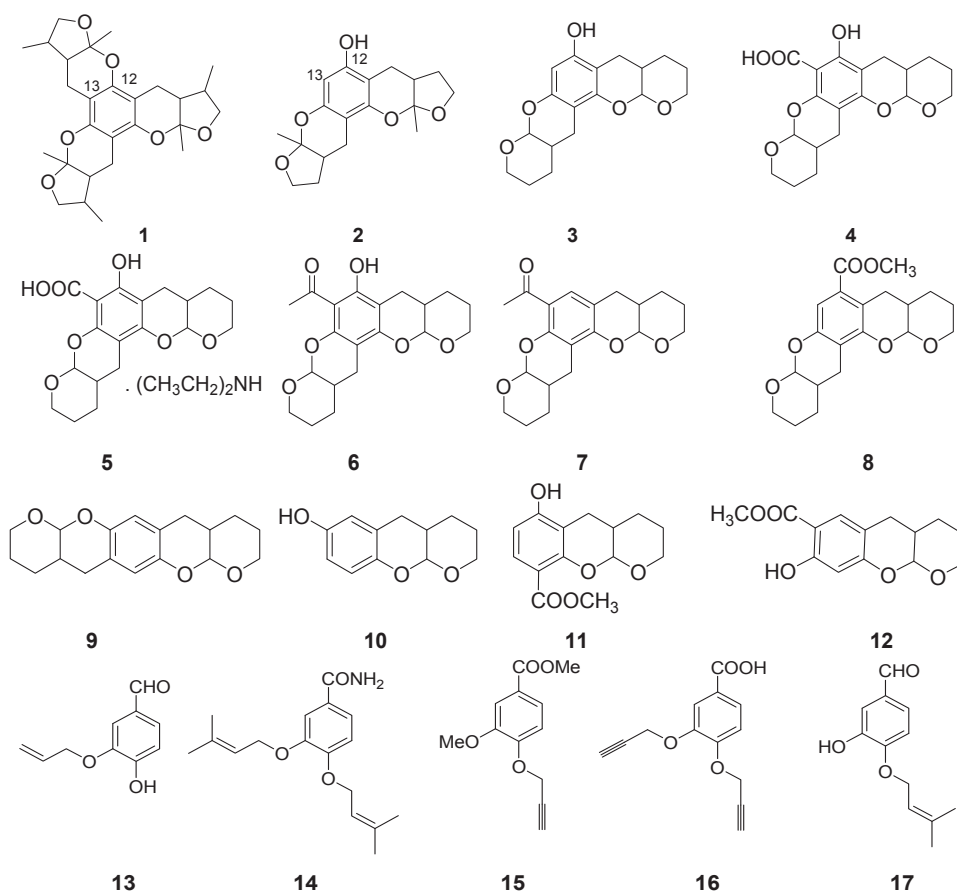


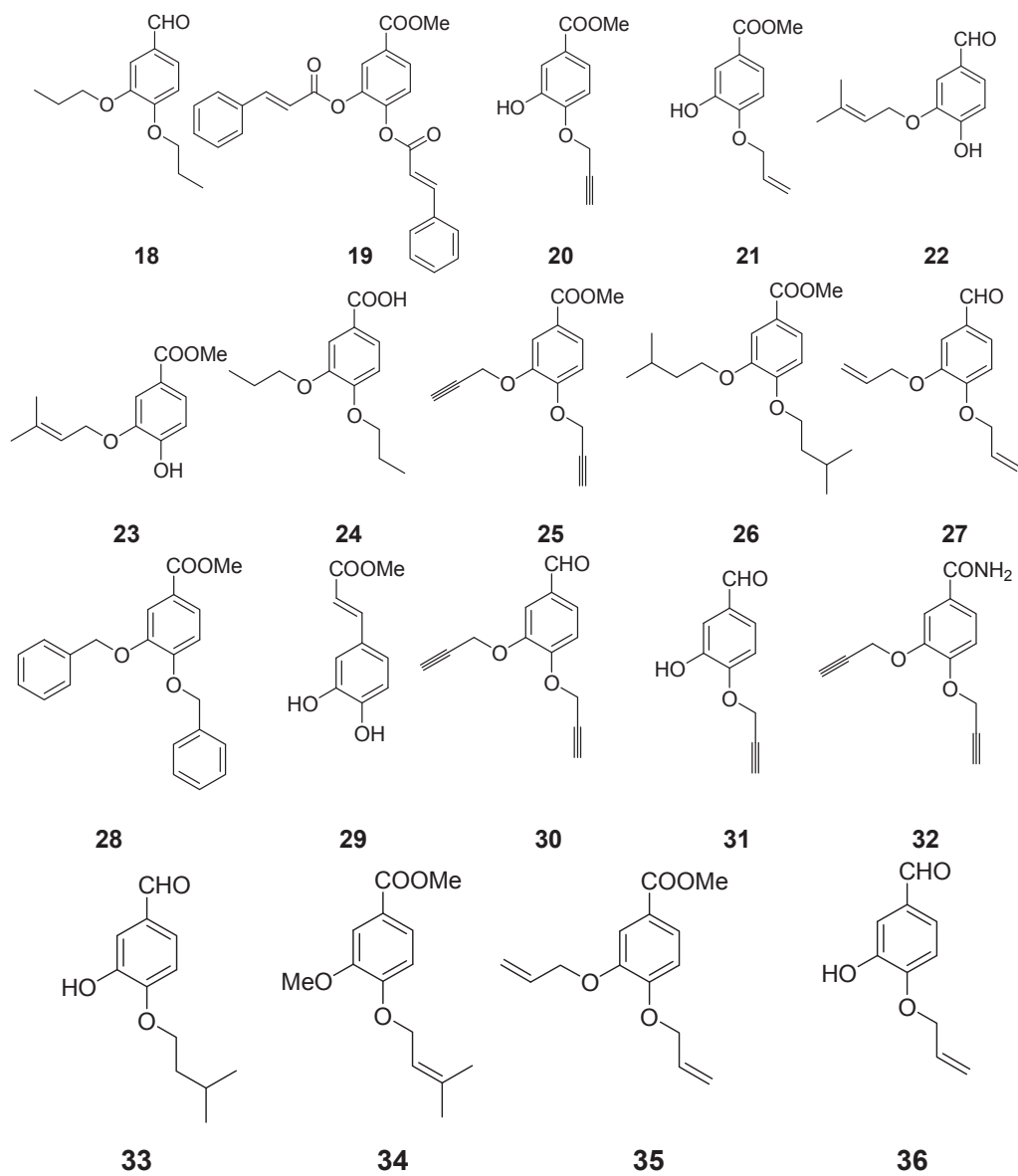
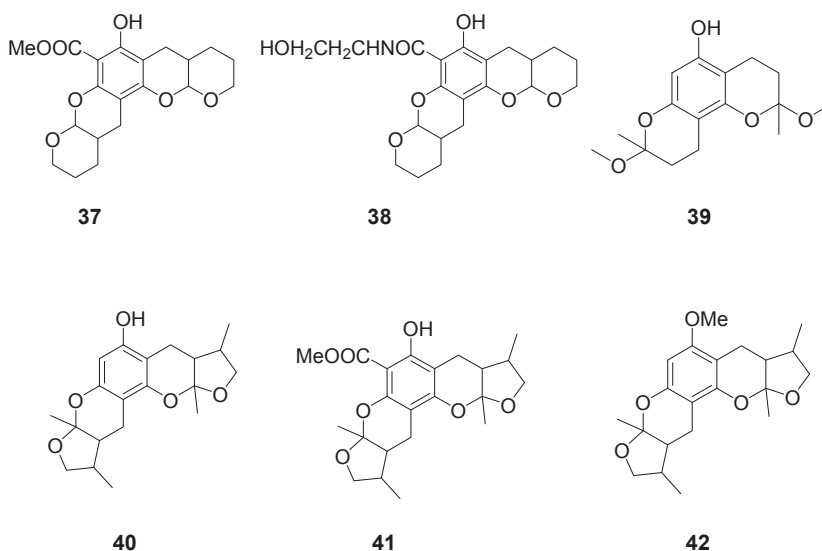
Chart 1. *Cont.*

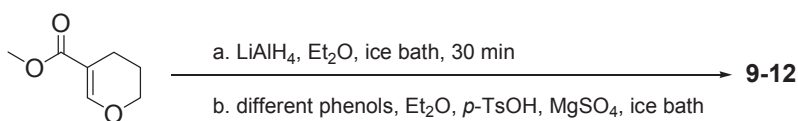
Chart 2. Modification of compound 1.



## 2. Results and Discussion

### 2.1. Chemistry

Forty-two analogues of the natural xyloketal and isoprenyl phenyl ether were obtained, and the general synthetic routes of compounds **1–42** have been described previously [10,12–14]. Compounds **9–12** were new compounds synthesized by reduction and electrophilic aromatic substitution reactions of 3,4-dihydro-2*H*-pyran-5-carboxylate with different phenols with 29%–52% yield (Scheme 1). The reduction product of 3,4-dihydro-2*H*-pyran-5-carboxylate was unstable and was immediately used for the subsequent experiment. The title compounds were isolated as their bis- and mono- adducts in different phenol proportions. Different substituted compounds of methyl 2,4-dihydroxybenzoate **11** and **12** could be obtained in one pot reaction and detected using TLC, followed by purifying, easily done by flash chromatography. However, the final products were obtained in low yields and further optimizations were required. Compounds **9–12** were fully characterized by HRMS and NMR.

Scheme 1. Synthesis of compounds **9–12**.

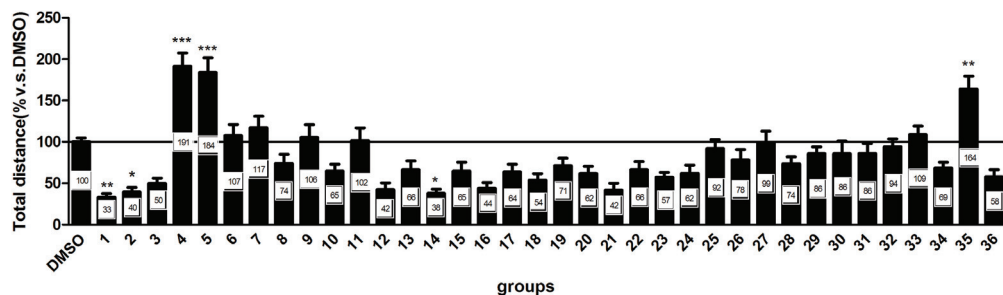
### 2.2. Neuroactive Activity of 36 Compounds were Evaluated in Zebrafish Behavioral Assay

Zebrafish have neural networks similar to mammals and their locomotor activity is a measurable complex behavior. Similar to higher vertebrates, locomotor activity of zebrafish is also regulated



by light. In zebrafish behavioral assays, the total swimming distance traveled is often measured to determine the changes in the locomotor activity. Therefore, we examine the effect of different compounds on the total distance during the initial screen. All marine-derived compounds (1–36) were dissolved in DMSO and diluted with E3 buffer (5 mM NaCl, 0.17 mM KCL, 0.33 mM CaCl<sub>2</sub>·2H<sub>2</sub>O, 0.33 mM MgSO<sub>4</sub>) to a final concentration of 20 μM. The results (Figure 1) showed that three compounds including compounds 1, 2 and 14 significantly inhibited locomotor activity ( $p < 0.01$  vs. DMSO) to 33%, 40% and 38%, respectively. Meanwhile, several compounds exhibited a hyperactive effect on locomotor activity ( $p < 0.01$  vs. DMSO). For example, compounds 4, 5 and 35 could significantly increase locomotor activity by 91%, 84% and 64%, respectively.

**Figure 1.** The larval zebrafish behavioral assay was performed on 120-hpf zebrafish dosed with compounds at 20 μM concentrations in DMSO. Each group had 24 replicates and three independent experiments were performed. The data of total distance are normalized as the percentage of control and representative of three independent experiments. Data was analyzed using One-way ANOVA followed by Post Hoc test (Bonferroni's Multiple Comparison Test). \*  $p < 0.05$  vs. DMSO, \*\*  $p < 0.01$  vs. DMSO, \*\*\*  $p < 0.001$  vs. DMSO.



### 2.3. Neuroactive Compounds Exhibited Different Behavioral Patterns

The behavioral assay used here has been well-characterized. During this assay, zebrafish typically exhibited robust but transient behavioral activity in response to sudden transitions from light to dark [15]. In the present study, we used a modified version of this test consisting of a single transition from light to dark. The basal swimming activity was recorded during 10 min with lights on. Immediately following the basal activity recording, the lights were suddenly turned off for 10 min. Consistent with previous reports, the control animals displayed a normal pattern of locomotor activity, *i.e.*, the activity of zebrafish decreased when the visible light was on (light) whereas the activity of zebrafish rapidly and markedly increased when the light was off (dark). We further analyzed these six neuroactive (compounds 1, 2, 4, 5, 14, 35) compounds obtained from the initial screen. We found that neuroactive compounds exhibited distinct patterns and some neuroactive compounds altered the orderly normal activity pattern (Figure 2). Based on the behavior assay, marine-derived compounds tested could be simply categorized as two major types: hyperactive and hypoactive compounds. The behaviors also varied among different compounds within the same types. For example, among these hyperactive compounds, compounds 4 and 5 showed hyperactive

activities which were more prevalent in darkness than in light (Figure 2A,E) whereas compound **35** induced a constant hyperactivity all the time regardless of dark or light conditions (Figure 2B,F). Among hypoactive compounds, compound **2** decreased activities during the first dark and light cycle and activities were then returned to normal in the subsequent cycles whereas compound **14** decreased activity during all the periods (Figure 2C,G). In addition, animals treated with compound **1** decreased activity in every dark and light period (Figure 2D,H).

**Figure 2.** The behavioral assay of neuroactive compounds. The larvae were placed into the compound solutions (final concentration is 20  $\mu$ M) and recording began 20 min later in alternating periods of darkness and light for a total duration of 70 min. (A–D) Total activity (distance moved, cm) in two-minute intervals for total duration of 70 min. (E–H) Total activity (distance moved, cm) in each 10-minute light and dark period. Values are reported as mean ( $n = 21\text{--}24$  larvae/concentration/plate, for 2 plates)  $\pm$ SEM. \*  $p < 0.05$  vs. DMSO, \*\*  $p < 0.01$  vs. DMSO.

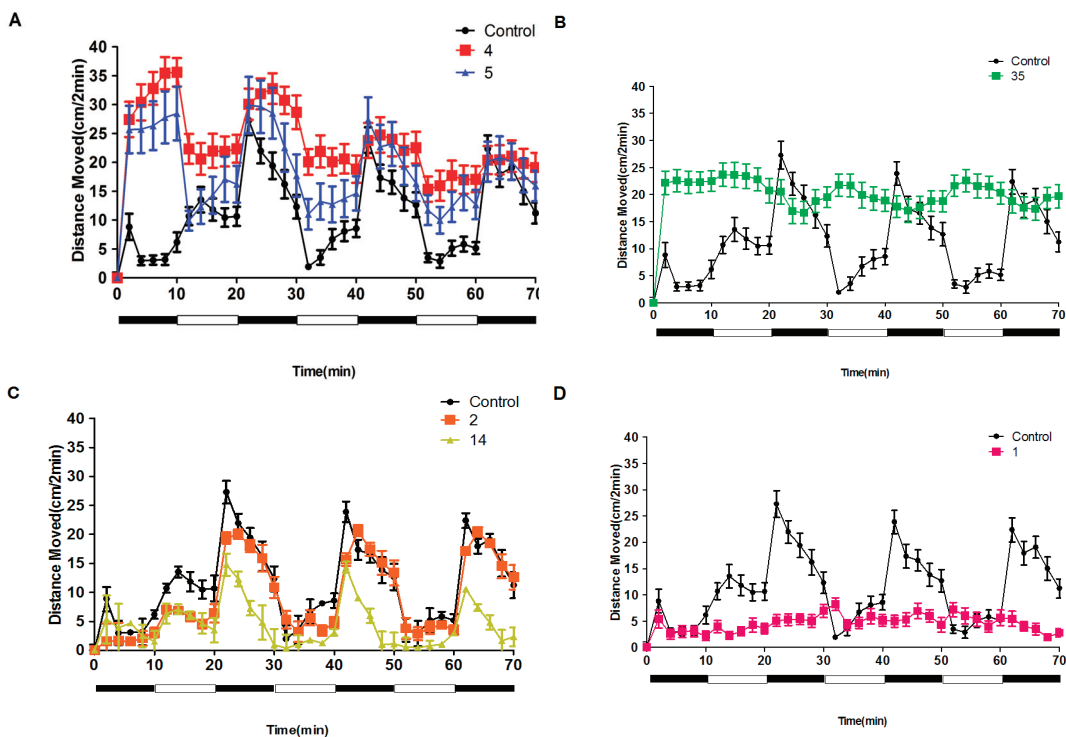
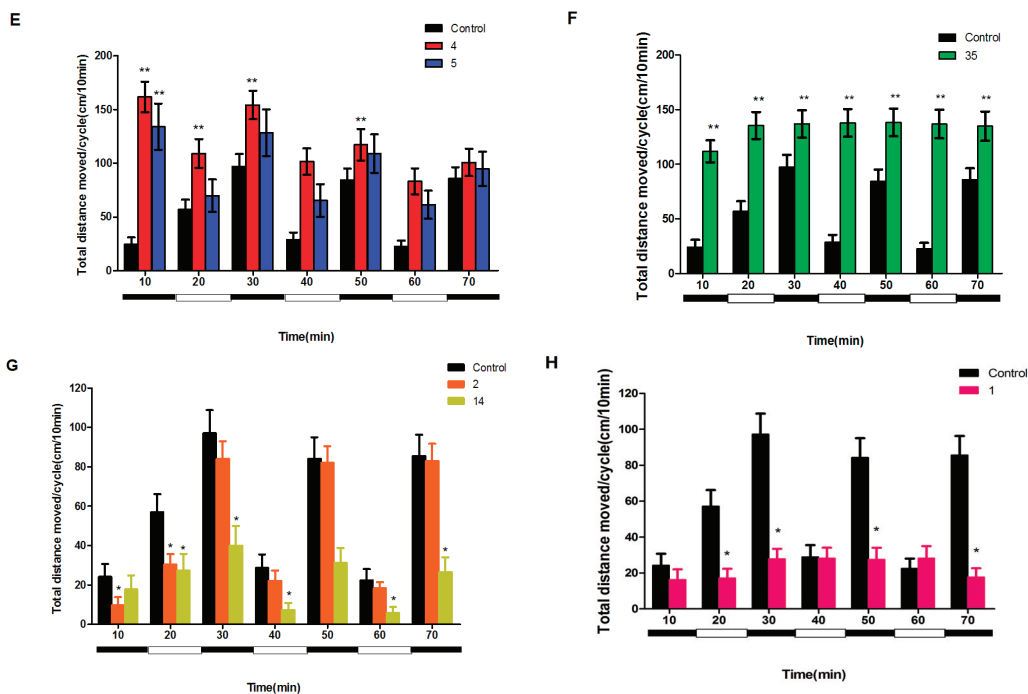


Figure 2. Cont.



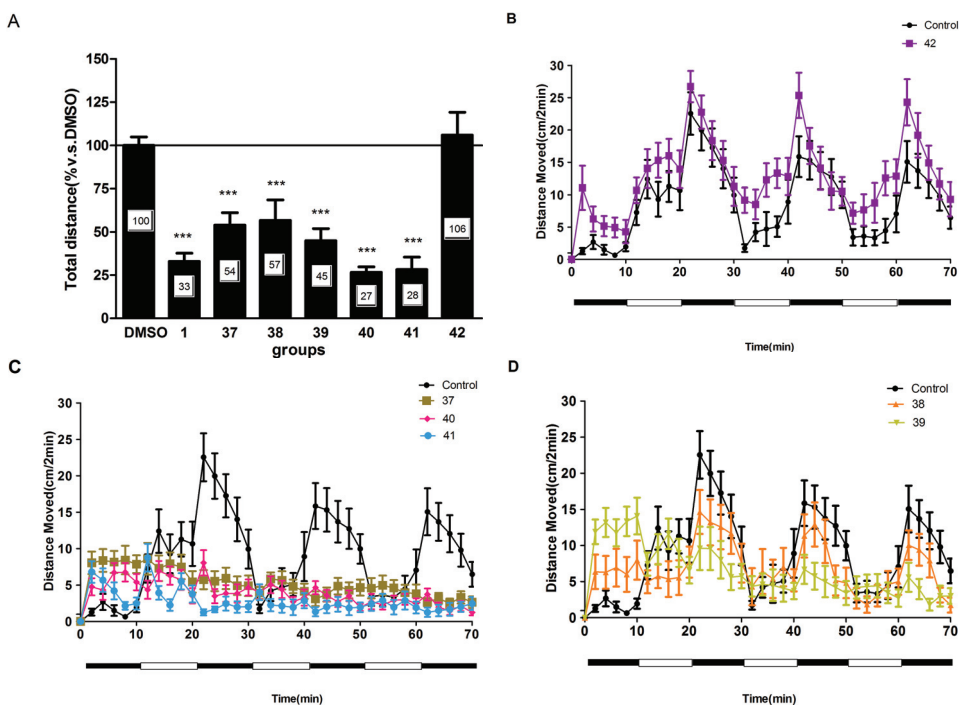
#### 2.4. Compounds **1** and **37–41** Suppressed Locomotor Activity in Larval Zebrafish

To further study the structure-activity relationships and optimize biological activity of compound **1**, three compounds (**40–42**) derived from **1** and three more compounds (**37–39**) were synthesized (Scheme 1). The results (Figure 3A) showed that the majority of compounds inhibited the locomotor activity (total distance) at the concentration of 20  $\mu\text{M}$  ( $p < 0.05$  vs. DMSO). Among them, compounds **37–41** could significantly reduce total distance by up to 57%. Moreover, compounds **40** and **41** displayed more potent inhibition compared to the lead compound **1** (reduced activity level to 27% and 28%, respectively). Six derivatives displayed different patterns of locomotor activity (Figure 3B–D). Compound **42** displayed a reverse effect with a higher activity during all of the dark and light cycles. Similar to compound **1**, compounds **37**, **40** and **41** induced a constant inhibition on locomotor activity throughout every dark and light period. Furthermore, compounds **40** and **41** displayed much lower activity compare to compound **1**. Although compounds **38** and **39** suppressed the locomotor activity, they did not disturb the normal orderly pattern of activity. Altogether, we found that compound **40** showed the most potent inhibitory action on locomotor activity.

Structure-activity investigation was conducted to identify the active components within xyloketal derivatives. We found that xyloketal derivatives possessing the benzopyrano furan skeleton exhibited more potent inhibitory action compared to that possessing benzopyrano pyran. However, methyl ether derivative **42** did not show any suppression of activity compared to controls. Thus, an unsubstituted hydroxyl group or easily cleaved hydroxyl prodrug, such as a phenolic ester at

12-position of the benzopyran scaffold, may be important for the inhibitory action. Furthermore, the substituents at the 13-position may be tolerated but not necessary for the inhibitory activity. However, compound **1** does not possess an OH group at this position perhaps hinting at different binding modes between **1** and **40/41**.

**Figure 3.** Compounds **1** and **37–41** suppressed larval zebrafish locomotor activity. (A) The behavior assay was performed with compounds **37–42**. The relative distance of DMSO group was set as control and other groups were shown relative to DMSO group. (B–D) Different activity patterns of compound **1** and compounds **37–42**. \*  $p < 0.05$  vs. DMSO, \*\*\*  $p < 0.001$  vs. DMSO.



### 2.5. The Potential of Selected Compounds for New Antiepileptic Drug Development in PTZ-Induced Seizure Model

Epilepsy is one of the most common CNS disorders and affects about 50 million people worldwide [16]. A variety of pharmacological and genetic models of epilepsy have been developed to study seizure mechanisms and to identify new anti-epileptic drugs. PTZ is a noncompetitive antagonist of the GABA receptor complex and its epileptogenic properties have been widely used for anti-epileptic drug discovery. Similarly, PTZ can induce measurable seizure-related behaviors in zebrafish. These behaviors can be reversed by known anti-epileptic drugs. Thus, zebrafish are emerging as a useful model system for anti-epileptic drug discovery.

The potential of compounds **1** and **39–41** as anti-epileptic drugs was further explored in a PTZ-induced epilepsy model in zebrafish. Consistent with previous reports [17], PTZ at 10 mM

induced a robust locomotor activity (hyperactivity) in zebrafish larvae (Figure 4A). In contrast, all three compounds (**39–41**) demonstrated significant inhibitory action (hypoactivity) in this PTZ model. Among compounds tested, compound **40** showed the most potent inhibitory activity (Figure 4B).

PTZ induced changes not only in activity but also in gene expression. The expression levels of IEGs are well correlated with seizure activity. The expression of *c-fos* has been used as an indicator of neuronal activity in zebrafish which is often measured by using the electroencephalography (EEG) [18], To investigate whether compounds **1** and **39–41** affects PTZ-induced expression of the gene *c-fos*, quantitative real time PCR of *c-fos* was performed on larval zebrafish (Figure 4C). The results indicated that the PTZ treatment (10 mM for 60 min) induced about 43-fold expression of *c-fos* mRNA in five dpf larval zebrafish whereas compounds **1** and **39–41** significantly attenuated the PTZ-induced increase in *c-fos* expression. The inhibitory action on *c-fos* expression by compounds tested corresponded to their suppression of PTZ-induced movement in the larval zebrafish. Consistent with the behavior assay, compound **40** exhibited one of the most potent inhibitory actions. Given that PTZ induces *c-fos* expression exclusively in central nervous system in zebrafish, our data also suggests that the compounds are able to cross the blood brain barrier [19].

**Figure 4.** The effect of compounds **1** and **39–41** on PTZ-induced hyperactivity in zebrafish. (A) The effect of PTZ on larval activity was initially tested across a broad concentration range (0–40 mM). \*\*\*  $p < 0.001$  vs. DMSO. (B) The total distances in larval zebrafish exposure to 10 mM PTZ with or without compound **1** and compounds **39–41**. \*\*\*  $p < 0.001$  vs. PTZ. (C) The expression levels of *c-fos* mRNA in larval zebrafish exposure to PTZ (10 mM for 60 min) with or without tested compounds (\*\*  $p < 0.01$  vs. PTZ, \*\*\*  $p < 0.0001$ ).

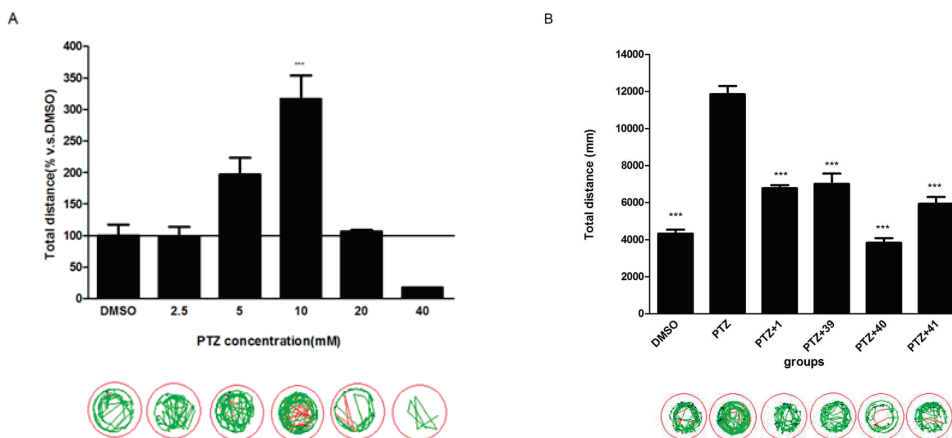
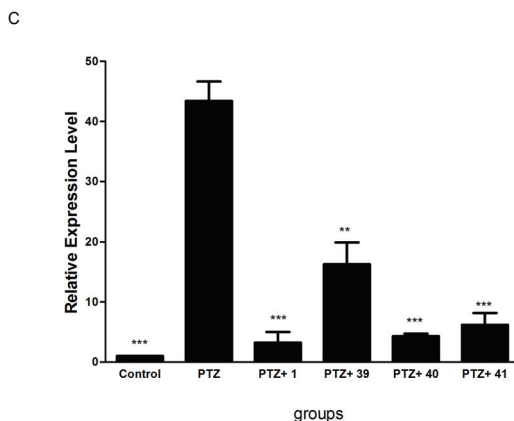


Figure 4. Cont.



### 2.6. The Dose-Response Study of Compound 40 in PTZ Model

We then conducted a dose-response study on compound **40**, the most potent inhibitory compound tested, to explore its efficacy and toxicity. We found that compound **40** at doses between 10  $\mu\text{M}$  and 1 mM significantly reduced PTZ-induced hyperactivity in larval zebrafish (Figure 5F). To investigate whether compound **40** causes potential toxicity to zebrafish, we examined the morphology of compound **40**-treated larval zebrafish. The results (Figure 5A–E) showed normal morphology in larval zebrafish receiving different doses of **40**, indicating that compound **40** alone at doses between 1  $\mu\text{M}$  and 1 mM did not cause toxic effects on larval zebrafish. Images of larval zebrafish were taken using an OLYMPUS IX71 inverted microscope at 4 $\times$  magnification.

**Figure 5.** The effect of compound **40** on PTZ-induced morphological changes. (A) The morphology of larval zebrafish at five dpf. (B–E) The morphology of five dpf larval zebrafish exposed to compound **40** at different concentrations (100 nM, 1, 10, 100  $\mu\text{M}$  and 1 mM). Scale bar represents 100  $\mu\text{m}$ . (F) The total distances in larval zebrafish exposure to PTZ with or without different concentrations of compound **40**. \*  $p < 0.05$  vs. PTZ, \*\*  $p < 0.01$  vs. PTZ.

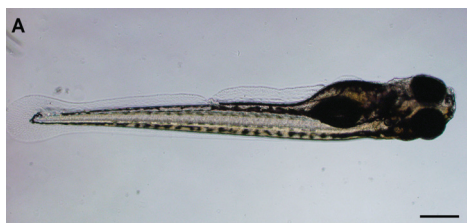
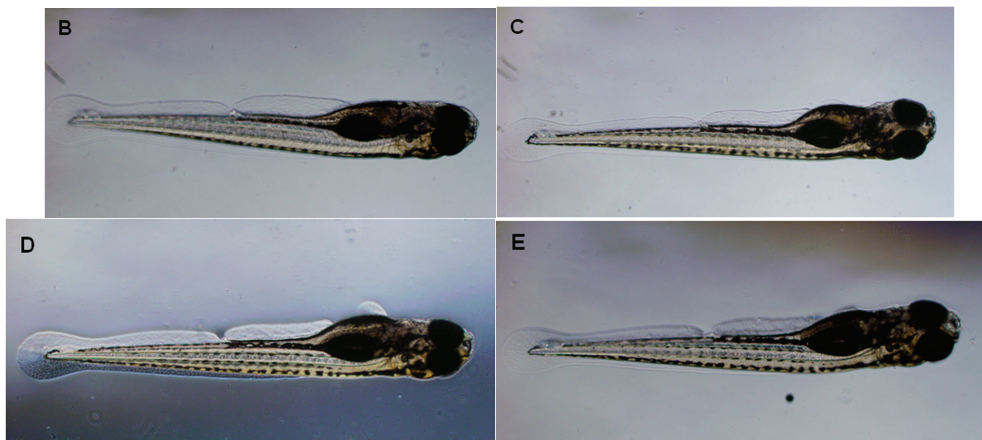
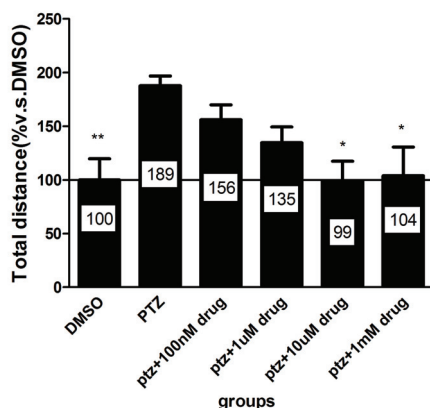


Figure 5. Cont.



F



Calcium has been implicated in the pathophysiology of seizure. It has been reported that calcium influx mediates seizure induction whereas blockage of calcium channels reduces epileptic activity [20–22]. Xyloketal derivatives have multiple-properties and their inhibitory action on L-calcium channel activity has been reported [23]. Therefore, xyloketal derivatives may exert their anti-convulsive effect by inhibiting the activity of calcium channels. In addition to the direct anti-convulsive action, calcium channel antagonists can potentiate the anticonvulsant action of other anti-epileptics such as diazepam. Xyloketal derivatives deserve further investigation as a potential anticonvulsant drug candidate.

### 3. Experimental Section

#### 3.1. Chemistry

All commercial available reagents and solvents were used directly without further purification unless otherwise stated.  $^1\text{H}$  and  $^{13}\text{C}$  NMR data were recorded on a 300 MB NMR spectrometer

operating at 400 MHz and 100 MHz for  $^1\text{H}$  and  $^{13}\text{C}$ , respectively. Tetramethylsilane (TMS) as internal standard and all chemical shifts are in ppm ( $\delta$ ). Mass spectra were detected on DSQ (Low Resolution Mass Spectrometer) and MAT95XP (High Resolution Mass Spectrometer).

### 3.2. General Procedure of Synthesizing Compounds 9–12; Take 9 for Example

#### 3.2.1. Compound 9

To a suspension of lithium aluminum hydride (0.76 g, 20 mmol) in ether (30 mL) with an ice water bath was added a solution of 3,4-dihydro-2*H*-pyran-5-carboxylate (1.88 g, 13.2 mmol, 3.2 molar equivalent to the subsequent reagent hydroquinone) in ether (20 mL) dropwise. The resultant mixture was allowed to warm to room temperature and stirred for additional 1 hour. Then, aqueous solution of 2 M sodium hydroxide (1.2 g) was added at 0 °C. The resultant mixture was filtered, washed with ether ( $3 \times 50$  mL), and the combined filtrates were concentrated in vacuo below 10 °C to afford the reduction product as a colorless liquid. This material was immediately diluted with ether (20 mL) and used for the subsequent experiment without storage because of its instability.

To a suspension of hydroquinone (0.52 g, 4.1 mmol) and anhydrous magnesium sulfate (2 g) in 40 mL ether at 0 °C was added the prepared above ether solution as soon as possible. After stirring for 1 min, *p*-toluene sulfonic acid (0.1 g) was added. The resultant mixture was allowed to warm to room temperature and stirred for 30 min. The reaction mixture was then filtered and the filter-cake was washed with ether ( $3 \times 50$  mL). The combined filtrates were washed with water (100 mL) and saturated brine (100 mL) followed by drying over anhydrous magnesium sulfate and concentrated in vacuo. Purification by flash chromatography using ether: dichloromethane (2:25) afforded 0.71 g title compound **9** as a colorless crystal in 50% yield.  $^1\text{H}$  NMR (400 MHz,  $\text{CDCl}_3$ )  $\delta$  6.68 (s, 1H), 6.52 (s, 1H), 5.28–5.14 (m, 2H), 4.06–3.93 (m, 2H), 3.72–3.63 (m, 2H), 2.93–2.39 (m, 4H), 2.25–2.05 (m, 2H), 1.71–1.59 (m, 8H). EI-MS  $m/z$  302 (M). EI-HR-MS  $m/z$  Found: 302.1510, Calcd. for  $\text{C}_{18}\text{H}_{22}\text{O}_4$ : 302.1513.

#### 3.2.2. Compound 10

The title compound **10** was obtained 0.48 g from hydroquinone as a colorless crystal in 52% yield.  $^1\text{H}$  NMR (400 MHz,  $\text{CDCl}_3$ )  $\delta$  6.69 (d,  $J = 8.7$  Hz, 1H), 6.58 (dd,  $J = 8.7, 3.0$  Hz, 1H), 6.49 (d,  $J = 2.9$  Hz, 1H), 6.13 (s, 1H), 5.25 (d,  $J = 2.6$  Hz, 1H), 4.05–3.96 (m, 1H), 3.73–3.66 (m, 1H), 2.81 (dd,  $J = 16.7, 6.1$  Hz, 1H), 2.57 (dd,  $J = 16.7, 5.3$  Hz, 1H), 2.17–2.06 (m, 1H), 1.69–1.59 (m, 4H).  $^{13}\text{C}$  NMR (100 MHz,  $\text{CDCl}_3$ )  $\delta$  149.73, 146.07, 120.57, 116.82, 115.35, 114.46, 96.45, 62.76, 31.51, 28.50, 24.11, 23.12. EI-MS  $m/z$  206 (M). EI-HR-MS  $m/z$  Found: 206.0940, Calcd. for  $\text{C}_{12}\text{H}_{14}\text{O}_3$ : 206.0937.

#### 3.2.3. Compound 11

The title compound was obtained 0.18 g from methyl 2,4-dihydroxybenzoate as a colorless crystal in 29% yield.  $^1\text{H}$  NMR (400 MHz,  $\text{CDCl}_3$ )  $\delta$  11.18 (s, 1H), 7.62 (d,  $J = 8.9$  Hz, 1H),



6.43 (d,  $J = 8.9$  Hz, 1H), 5.34 (d,  $J = 2.5$  Hz, 1H), 4.06–3.96 (m, 1H), 3.90 (s, 3H), 3.79–3.68 (m, 1H), 2.85–2.61 (m, 2H), 2.29–2.12 (m, 1H), 1.76–1.58 (m, 4H).  $^{13}\text{C}$  NMR (100 MHz,  $\text{CDCl}_3$ )  $\delta$  170.77, 161.21, 158.86, 128.67, 108.42, 107.88, 105.09, 96.96, 62.57, 51.87, 30.92, 24.09, 23.63, 23.02. EI-MS  $m/z$  264 (M). EI-HR-MS  $m/z$  Found: 264.0998, Calcd. for  $\text{C}_{14}\text{H}_{16}\text{O}_5$ : 264.0992.

### 3.2.4. Compound **12**

The title compound **12** was obtained 0.21 g from methyl 2,4-dihydroxybenzoate as a colorless crystal in 34% yield.  $^1\text{H}$  NMR (400 MHz,  $\text{CDCl}_3$ )  $\delta$  10.61 (s, 1H), 7.52 (s, 1H), 6.45 (s, 1H), 5.38 (s, 1H), 4.04–3.93 (m, 1H), 3.90 (s, 3H), 3.79–3.63 (m, 1H), 2.97–2.74 (m, 1H), 2.65–2.49 (m, 1H), 2.27–2.07 (m, 1H), 1.73–1.53 (m, 4H).  $^{13}\text{C}$  NMR (100 MHz,  $\text{CDCl}_3$ )  $\delta$  170.16, 161.81, 159.56, 130.88, 111.86, 106.15, 103.82, 97.13, 62.22, 51.84, 31.77, 28.41, 23.63, 23.57. EI-MS  $m/z$  264 (M).

## 3.3. Zebrafish Behavior-Based Activity Screen

### 3.3.1. Zebrafish Maintenance

Zebrafish (*Danio rerio*) were maintained according to standard animal care protocols [24]. AB strain zebrafish were bred to yield embryos. Embryos and larvae were maintained on a re-circulating Tecniplast aquatic system at  $28 \pm 1$  °C and between pH 7.0 and 7.5 on a 14/10 h light/dark (L/D) cycle. Embryos were collected from multiple AB/Tubingen breeding. Embryos were collected, rinsed in E3 buffer (5 mM NaCl, 0.17 mM KCl, 0.33 mM  $\text{CaCl}_2 \cdot 2\text{H}_2\text{O}$ , 0.33 mM  $\text{MgSO}_4$ ), washed three times, transferred to Petri dishes and incubated at 28 °C until 4 dpf. They were washed twice every day to remove dead or unfertilized embryos.

### 3.3.2. Zebrafish Behavioral Assay

AB strain zebrafish were bred to yield embryos. At 4 dpf, larval zebrafish were transferred to 96-well microplates and acclimated at 28 °C overnight. Twenty-four h later, compounds were added and incubated with zebrafish for 30 min at 28 °C. The 96-well microplates were then put into the zebrafish tracking box (Viewpoint Life Sciences Inc., Montreal, Canada) and the activity of zebrafish was monitored using automated video-tracking (the Viewpoint video tracking system and software).

After zebrafish acclimated at the tracking box for 20 min, their behaviors were recorded in infrared light (which will hereafter be referred to as “dark”), and the infrared light remained on throughout the recording session. In the behavior assay, the visible light (or “light”) was switched on for 10 min and then switched off for 10 min (dark period). This light/dark transition was continued for a total duration of 70 min. Each drug challenge was conducted on at least two separate plates with  $n = 12$  larvae/plate in the compounds challenges, and 24 larvae/plate in the PTZ challenge (for controls,  $n = 12$  larvae/plate in the compounds challenge and 24 larvae/plate in the PTZ challenge). All experiments consisted of 20 min of acclimation in the dark followed by seven 10 min-cycles containing a darkness and light phase (90 min total). To capture the different types

of activity, a threshold was set at 25 mm/s in order to separate the fast/darting activity and 4 mm/s to separate the slow activity.

### 3.3.3. Morphology Assay

Briefly, 5 dpf zebrafish with or without compounds were anaesthetized by treatment with 0.4% tricaine and mounted onto glass slide. The morphology was visualized at 4× magnification under an OLYMPUS IX71 inverted microscope.

### 3.3.4. Quantitative RT Real Time PCR

Total RNA from zebrafish was extracted using E.Z.N.A. total RNA extraction kit (OMEGA biotek, Inc., Norcross, GA, USA). Intact RNA was checked by running a 1.0% agarose/formaldehyde gel and quantified spectrometrically (Beckman Coulter DU 800) before proceeding to subsequent steps. Five hundred ng of total RNA was reverse-transcribed using PrimeScript™ RT Master Mix (Perfect Real Time) Kit (Takara Inc., Otsu, Japan) according to manufacturer's instructions. Real-Time PCR was performed on an Opticon MONITOR™ Software (MJ Research Inc., Quebec, Canada) using SYBR® Premix Ex Taq™ II (Tli RNaseH Plus) (Takara Inc.). Expression levels for each target gene were calculated by the 2<sup>-DDCT</sup> method [25]. All analyses were performed in triplicates. Primers used for the RT real-time PCR are as follow:

*c-fos* Forward primer: 5'-GCTCCATCTCAGTCCCAGAG-3'

*c-fos* Reverse primer: 5'-AGAGTGGGCTCCAGATCAGA-3'

*β-actin* Forward primer: 5'-CCGTTGCCCGAGGCTCTCT-3'

*β-actin* Reverse primer: 5'-CGCATCCTGAGTCAATGCGCCA-3'

### 3.3.5. Data Analysis

Dead larvae or larvae with physical abnormalities were not included in any data analyses or figures. Any observed death or abnormalities were not due to drug exposures, and the total amount of dead and abnormal animals on each plate represented less than 5% of the total population. Data were analyzed using Graph Pad Prism software. Replicate experiments were run on two separate days ( $n = 12/\text{day}$ ) for both the therapeutic dilution series test and the PTZ dilution series test, with a carrier control group in each plate. The data for each drug were first assessed using a repeated measures analysis of variance (ANOVA) with time and dose as the independent variables and locomotor activity (distance moved/time) as the dependent variable. All data are presented as mean ± standard error of the mean (SEM).

## 4. Conclusions

In the present study, we have evaluated the neuroactive activity of 36 natural compounds and six designed novel derivatives in zebrafish model. Compound **1** and compounds **39**, **40** and **41** could significantly attenuate PTZ-induced locomotor hyperactivity and elevation of *c-fos* mRNA in larval zebrafish. Compound **40** showed the most potent inhibitory action against PTZ-induced changes.

The structure-activity analysis showed that the OH group at the 12-position had a critical role and the substituents at the 13-position had a favorable role in the inhibitory activity of xyloketal derivatives. Thus, these derivatives may provide some novel drug candidates for the treatment of epilepsy.

### Acknowledgments

This study was supported by grants from the National Key Clinical Department, National Key Discipline, Guangdong Key Laboratory For Diagnosis and Treatment of Major Neurological Diseases, the National Natural Science Foundation of China (No. 81371255, 81100936, 21172271), Doctoral Program of Higher Education of China (No. 20110171110058), Guangdong Technological grant (No. 2010B050700024, 2011B050400031, 2012B031800107), and the Natural Science Foundation of Guangdong Province (No. S2011010004860). This study was also supported by the multi-year research grant, university of Macau, MYRG122 (Y1-L3)-ICMS12-SHX.

### Author Contributions

Conceived and designed the experiments: S.-M. Long, F.-Y. Liang, J.-Y. Pang, Z. Pei; Performed the experiments: S.-M. Long, F.-Y. Liang, Q. Wu, X.-L. Liu, X.-L. Yao, S.-C. Li, J. Li; Analyzed the data: S.-M. Long, H. Su, J.-Y. Pang; Wrote the paper: S.-M. Long, J.-Y. Pang, Z. Pei.

### Conflicts of Interest

The authors declare no conflict of interest.

### References

1. Pangalos, M.N.; Schechter, L.E.; Hurko, O. Drug development for CNS disorders: Strategies for balancing risk and reducing attrition. *Nat. Rev. Drug Discov.* **2007**, *6*, 521–532.
2. Kokel, D.; Peterson, R.T. Chemobehavioural phenomics and behaviour-based psychiatric drug discovery in the zebrafish. *Brief. Funct. Genomics Proteomics* **2008**, *7*, 483–490.
3. Brockerhoff, S.E.; Hurley, J.B.; Janssen-Bienhold, U.; Neuhauss, S.C.; Driever, W.; Dowling, J.E. A behavioral screen for isolating zebrafish mutants with visual system defects. *Proc. Natl. Acad. Sci. USA* **1995**, *92*, 10545–10549.
4. Neuhauss, S.C.; Biehlmaier, O.; Seeliger, M.W.; Das, T.; Kohler, K.; Harris, W.A.; Baier, H. Genetic disorders of vision revealed by a behavioral screen of 400 essential loci in zebrafish. *J. Neurosci.* **1999**, *19*, 8603–8615.
5. Burgess, H.A.; Granato, M. Sensorimotor gating in larval zebrafish. *J. Neurosci.* **2007**, *27*, 4984–4894.
6. Prober, D.A.; Rihel, J.; Onah, A.A.; Sung, R.J.; Schier, A.F. Hypocretin/orexin overexpression induces an insomnia-like phenotype in zebrafish. *J. Neurosci.* **2006**, *26*, 13400–13410.
7. Zhdanova, I.V.; Wang, S.Y.; Leclair, O.U.; Danilova, N.P. Melatonin promotes sleep-like state in zebrafish. *Brain Res.* **2001**, *903*, 263–268.

8. Kokel, D.; Bryan, J.; Laggner, C.; White, R.; Cheung, C.Y.; Mateus, R.; Healey, D.; Kim, S.; Werdich, A.A.; Haggarty, S.J.; *et al.* Rapid behavior-based identification of neuroactive small molecules in the zebrafish. *Nat. Chem. Biol.* **2010**, *6*, 231–237.
9. Rihel, J.; Prober, D.A.; Arvanites, A.; Lam, K.; Zimmerman, S.; Jang, S.; Haggarty, S.J.; Kokel, D.; Rubin, L.L.; Peterson, R.T.; *et al.* Zebrafish behavioral profiling links drugs to biological targets and rest/wake regulation. *Science* **2010**, *327*, 348–351.
10. Li, S.; Shen, C.; Guo, W.; Zhang, X.; Liu, S.; Liang, F.; Xu, Z.; Pei, Z.; Song, H.; Qiu, L.; Lin, Y.; Pang, J. Synthesis and neuroprotective action of xyloketal derivatives in Parkinson's disease models. *Mar. Drugs* **2013**, *11*, 5159–5189.
11. Liu, R.; Zhou, Z.Y.; Jiang, M.Y.; Wang, F.; Liu, J.K. A new isoprenyl phenyl ether riboside from the culture of basidiomycete *Laccaria amethystea*. *J. Asian Nat. Prod. Res.* **2010**, *12*, 723–726.
12. Li, J.; Zhang, D.; Zhu, X.; He, Z.; Liu, S.; Li, M.; Pang, J.; Lin, Y. Studies on synthesis and structure-activity relationship (SAR) of derivatives of a new natural product from marine fungi as inhibitors of influenza virus neuraminidase. *Mar. Drugs* **2011**, *9*, 1887–1901.
13. Pettigrew, J.D.; Wilson, P.D. Synthesis of xyloketal A, B, C, D, and G analogues. *J. Organ. Chem.* **2006**, *71*, 1620–1625.
14. Xu, Z.; Li, Y.; Xiang, Q.; Pei, Z.; Liu, X.; Lu, B.; Chen, L.; Wang, G.; Pang, J.; Lin, Y. Design and synthesis of novel xyloketal derivatives and their vasorelaxing activities in rat thoracic aorta and angiogenic activities in zebrafish angiogenesis screen. *J. Med. Chem.* **2010**, *53*, 4642–4653.
15. Guo, S. Linking genes to brain, behavior and neurological diseases: What can we learn from zebrafish? *Genes Brain Behav.* **2004**, *3*, 63–74.
16. Epilepsy Fact Sheet, World Health Organization. October 2012. Available online: <http://www.who.int/mediacentre/factsheets/fs999/en/> (accessed on 10 May 2014).
17. Mussulini, B.H.; Leite, C.E.; Zenki, K.C.; Moro, L.; Baggio, S.; Rico, E.P.; Rosemberg, D.B.; Dias, R.D.; Souza, T.M.; Calcagnotto, M.E.; *et al.* Seizures induced by pentylene tetrazole in the adult zebrafish: a detailed behavioral characterization. *PLoS One* **2013**, *8*, e54515.
18. Scallet, A.C.; Kowalke, P.K.; Rountree, R.L.; Thom, B.T.; Binienda, Z.K. Electroencephalographic, behavioral, and *c-fos* responses to acute domoic acid exposure. *Neurotoxicol. Teratol.* **2004**, *26*, 331–342.
19. Fleming, A.; Diekmann, H.; Goldsmith, P. Functional characterisation of the maturation of the blood-brain barrier in larval zebrafish. *PLoS One* **2013**, *8*, e77548.
20. Ghasemi, M.; Shafaroodi, H.; Nazarbeiki, S.; Meskar, H.; Heydarpour, P.; Ghasemi, A.; Talab, S.S.; Ziai, P.; Bahreman, A.; Dehpour, A.R. Voltage-dependent calcium channel and NMDA receptor antagonists augment anticonvulsant effects of lithium chloride on pentylene tetrazole-induced clonic seizures in mice. *Epilepsy Behav.* **2010**, *18*, 171–178.
21. Meyer, F.B.; Anderson, R.E.; Sundt, T.M., Jr.; Yaksh, T.L.; Sharbrough, F.W. Suppression of pentylene tetrazole seizures by oral administration of a dihydropyridine Ca<sup>2+</sup> antagonist. *Epilepsia* **1987**, *28*, 409–414.

22. Moron, M.A.; Stevens, C.W.; Yaksh, T.L. The antiseizure activity of dihydropyridine calcium channel antagonists in the conscious rat. *J. Pharmacol. Exp. Ther.* **1990**, *252*, 1150–1155.
23. Wu, X.Y.; Liu, X.H.; Lin, Y.C.; Luo, J.H.; She, Z.G.; Jin, L.H.; Chan, W.L.; Antus, S.; Kurtan, T.; Elsässer, B.; *et al.* Xyloketal F: A strong L-calcium channel blocker from the mangrove fungus *xylaria* sp. (#2508) from the South China Sea Coast. *Eur. J. Org. Chem.* **2005**, *2005*, 4061–4064.
24. Westerfield, M. *The Zebrafish Book: A Guide for Laboratory Use of Zebrafish (Danio rerio)*; University of Oregon Press: Eugene, OR, USA, 1995.
25. Livak, K.J.; Schmittgen, T.D. Analysis of relative gene expression data using real-time quantitative PCR and the  $2^{-\Delta\Delta C(T)}$  method. *Methods* **2001**, *25*, 402–408.

# Characterization of a Novel *Conus bandanus* Conopeptide Belonging to the M-Superfamily Containing Bromotryptophan

Bao Nguyen, Jean-Pierre Le Caer, Gilles Mourier, Robert Thai, Hung Lamthanh, Denis Servent, Evelyne Benoit and Jordi Molgó

**Abstract:** A novel conotoxin (conopeptide) was biochemically characterized from the crude venom of the molluscivorous marine snail, *Conus bandanus* (Hwass in Bruguière, 1792), collected in the south-central coast of Vietnam. The peptide was identified by screening bromotryptophan from chromatographic fractions of the crude venom. Tandem mass spectrometry techniques were used to detect and localize different post-translational modifications (PTMs) present in the BnIIID conopeptide. The sequence was confirmed by Edman's degradation and mass spectrometry revealing that the purified BnIIID conopeptide had 15 amino acid residues, with six cysteines at positions 1, 2, 7, 11, 13, and 14, and three PTMs: bromotryptophan,  $\gamma$ -carboxy glutamate, and amidated aspartic acid, at positions "4", "5", and "15", respectively. The BnIIID peptide was synthesized for comparison with the native peptide. Homology comparison with conopeptides having the III-cysteine framework ( $-CCX_1X_2X_3X_4CX_1X_2X_3CX_1CC-$ ) revealed that BnIIID belongs to the M-1 family of conotoxins. This is the first report of a member of the M-superfamily containing bromotryptophan as PTM.

Reprinted from *Mar. Drugs*. Cite as: Nguyen, B.; le Caer, J.-P.; Mourier, G.; Thai, R.; Lamthanh, H.; Servent, D.; Benoit, E.; Molgó, J. Characterization of a Novel *Conus bandanus* Conopeptide Belonging to the M-Superfamily Containing Bromotryptophan. *Mar. Drugs* **2014**, *12*, 344963465.

## 1. Introduction

The peptides from the venom of cone snails (conotoxins or conopeptides) constitute a rich source of useful pharmacological tools and peptide probes for ion channels, transporters, and neurotransmitter receptors with a high degree of diversity, specificity, and potency [1–3]. Each *Conus* species is estimated to have a large number of species-specific conotoxins comprising cysteine poor-/rich-peptides [4–6]. Most mature peptides range between 8 and 40 amino acid residues with various cysteine-framework, and inter-cysteine variations in the number and kind of amino acids. Moreover, they have a high degree of post-translational modifications (PTMs) [7], whereby the modifications serve to create efficiently new conotoxin structures and pharmacological properties [4]. In addition to extensive disulphide linkages, which are a common feature of conotoxins, common PTMs include C-terminal amidation, proline hydroxylation,  $\gamma$ -carboxylation of glutamic acid, pyroglutamic acid, tyrosine sulfation, tryptophan bromination, and glycosylations [8–11]. Thus, there is an important role to entirely characterize the complement of mature peptides from cone snails.

In the search of new conopeptides from the venom of *Conus bandanus*, collected from the coast of Vietnam, we have found an unusual peptide containing bromine. We used tandem mass spectrometry to characterize the primary peptide sequence and localize the positions of tryptophan

bromination, and  $\gamma$ -carboxylation of glutamic acid. The amidation of aspartic acid of the C-terminus was confirmed by the combination of theoretical mass calculation, Edman degradation, and homology comparison. We compared also the peptide sequence similarity of BnIIID to that of other conopeptides from *Conus marmoreus*, considered a close-relative interspecies with the molluscivorous *Conus bandanus* [12,13]. In addition, the BnIIID peptide was synthesized for comparison with the native peptide. This is the first report of an M-superfamily conopeptide containing a bromotryptophan.

## 2. Results and Discussion

### 2.1. Venom Fractionation and Purification

*C. bandanus* dissected crude venom was fractionated, sub-fractionated, and purified by reversed-phase chromatography on Vydac semi-preparative and analytical columns (Figure 1). Each HPLC fraction containing conopeptides (Figure 1A) was analyzed by Matrix-Assisted Laser Desorption/Ionization Time-Of-Flight (MALDI-TOF) mass spectrometry. The fraction 3.2 highlighted in black (Figure 1B) shows several different molecules with major intensity (Figure S1 in the Supplementary Information) containing an unusual monoisotopic ion. Figure 1C,D show further purifications from the previous fraction 3.2. An asterisk tags the subfraction that exhibited an unusual isotopic distribution for a peptide. This fraction was purified to near homogeneity on the same reversed-phase analytical column, by optimizing the elution gradient slope, hence, avoiding the use of a two dimensional chromatography (Figure 1D) and was named BnIIID.

### 2.2. Determination of the Number of Disulphide Bonds

Analysis of the native BnIIID by MALDI-TOF/TOF MS showed two single-charged ion distributions (Figure 2A), which yielded two monoisotopic ion signals at  $m/z$  1819.129 and  $m/z$  1863.159. The BnIIID isotopic distributions indicated the possible presence of one bromine atom [14,15]. The abundance of these peaks “doublet” at  $m/z$  (1819.129; 1821.21) and  $m/z$  (1863.159; 1865.159) is typical of a molecule containing the equally abundant bromine isotopes (50.69%  $^{79}\text{Br}$  and 49.31%  $^{81}\text{Br}$ , respectively). Following reduction with TCEP, BnIIID signals were shifted by 6 u indicating the presence of three disulfide bonds (Figure 2B).

### 2.3. Presence of Gamma-Carboxylate Glutamate Residue

To elucidate the two different major masses of the pure fraction, we reduced and alkylated the cysteines to avoid disulfide reformation and to improve fragmentation yield during ESI-MSMS measurements (Figure 3). The CID fragmentation of the major compound in the fraction, 2214.55 Da, produce the decarboxylated fragment. In order to elucidate the sequence, the decarboxylated fragment was submitted to MS<sup>3</sup> CID fragmentation. Figure 3C illustrate the *b* and *y* series obtained, confirming again the presence of a bromotryptophan. Thus, we could predict BnIIID having one  $\gamma$ -carboxylated glutamate residue and a bromotryptophan.

**Figure 1.** HPLC purification profile of dissected *C. bandanus* venom, extract, and BnIIID purification. **(A)** Fractionation was carried out with a Vydac semi-preparative C<sub>18</sub> column (300 Å, 5 μm, 10 mm i.d. × 250 mm) and eluted at 3 mL min<sup>-1</sup> with gradient 0%–56% of B buffer/50 min; **(B)** Fractionation from zone 3 with a Vydac analytical C<sub>18</sub> column (300 Å, 5 μm, 4.6 mm i.d. × 250 mm) and eluted at 1 mL min<sup>-1</sup> with gradient (0%–0.5% B/5 min, 0.5%–15% B/1 min and 15%–40% of B/40 min); **(C)** Further purification of fraction 3.2, from the previous step, was further purified with gradient (10%–15% B/7.5 min, 15%–20% B/42.5 min and 20%–35% B/45 min); **(D)** The asterisk indicates BnIIID. The purity of BnIIID peak was checked by MALDI-TOF-MS.

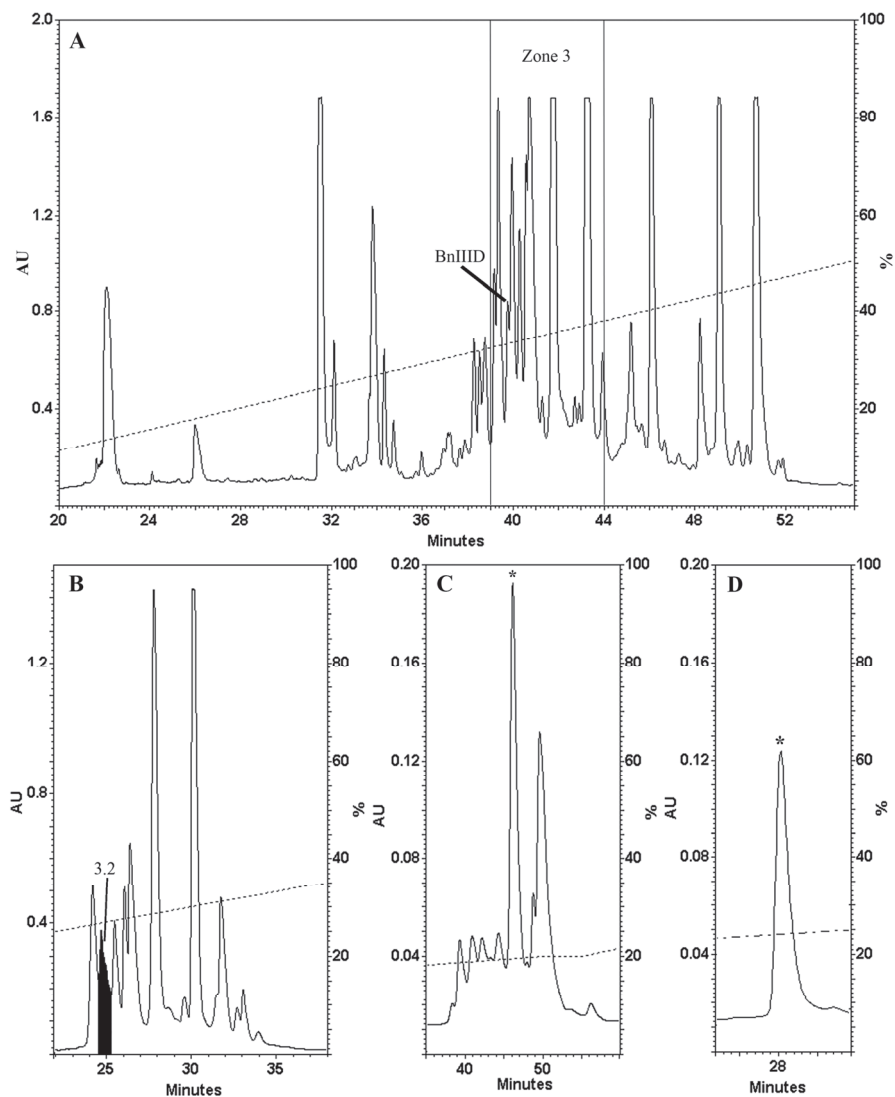
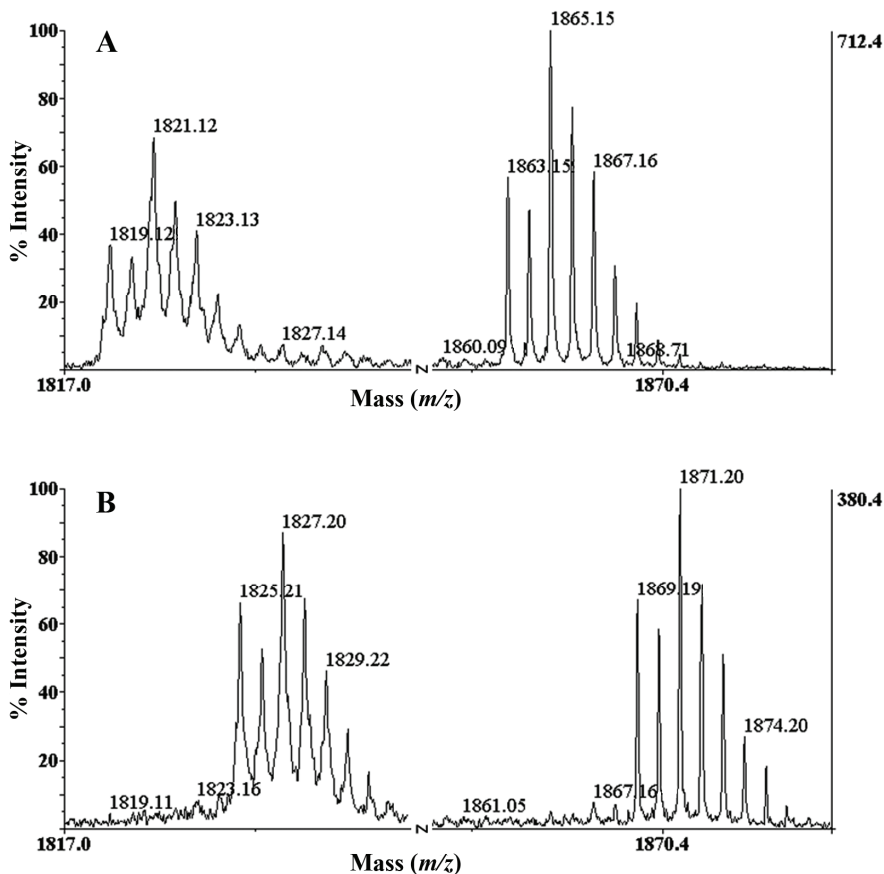




**Figure 2.** Identification of bromination using isotopic distributions of native BnIIID (A); and reduced BnIIID form (B); from off-line LC/MALDI-TOF MS. A shift of 6 u is observed characterizing the reduction of three S-S bonds.



#### 2.4. Peptide Sequencing

To determine the amino acid sequence of BnIIID, we also employed the CID fragmentation technique using a MALDI TOF/TOF mass spectrometer that generated predominantly *b* and *y*-type product ions. Figure 4 shows two CID mass spectra of IAA-labeled BnIIID, with and without-carboxylation. Moreover, the product ions that contained a bromotryptophan residue showed unusual isotope patterns. The MS/MS spectrum of the parent ion at  $m/z$  2167.245, without carboxylation (Figure 4A), showed complete series of *b* and *y*-type ions from position 1 to 15. We clearly observed a shift corresponding to the bromotryptophan residue (+260/262 u) between  $b_3$  and  $b_4$  ions or  $y_{11}$  and  $y_{12}$  ions. The glutamic acid residue is also identified after the bromotryptophan residue using the  $b_4/b_5$  and  $y_{10}/y_{11}$  ions. Furthermore, the  $m/z$  increment of 160 u between ( $b_1/b_2$ ;  $b_6/b_7$ ;  $b_{10}/b_{11}$ ;  $b_{12}/b_{13}$ ;  $b_{13}/b_{14}$ ) ions confirmed the presence of an IAA-modified cysteine. Therefore, the mass of an IAA-modified cysteine at first position is inferred from  $m/z$  161  $b_1$  ion and t corresponding  $m/z$  2007  $y_{14}$  ion. Thus, BnIIID linear sequence exhibits a cysteine

framework III, with the following pattern CC–C–C–CC. There are limits in distinguishing leucine/isoleucine residue (mass 113 Da) at position “10”, and amidated aspartic acid/asparagine residue (mass of 114 Da) at the C-terminus (C-terminal amidation is a common PTM due to 1 Da reduction in mass). Therefore, the initial sequence assignment of  $m/z$  2167.245 parent ion was CCDWENCDH(L/I)CSCC(D\*/N), as shown in Figure 4A.

**Figure 3.** Analysis of reduced and alkylated BnIIID by high resolution MS and MSMS mass spectrometry: (A) Deconvoluted spectrum of the fraction shown in Figure 1D after reduction and alkylation with IAA; (B) Deconvoluted spectrum of the CID fragmentation of the 2214.55 Da ion; (C) MS<sup>3</sup> product (2168.55 Da) corresponding to the decarboxylation of the precursor ion. Note: C<sub>1</sub>: carbamidomethyl-cysteine; alkylated cystein by IAA; W: bromotryptophan.

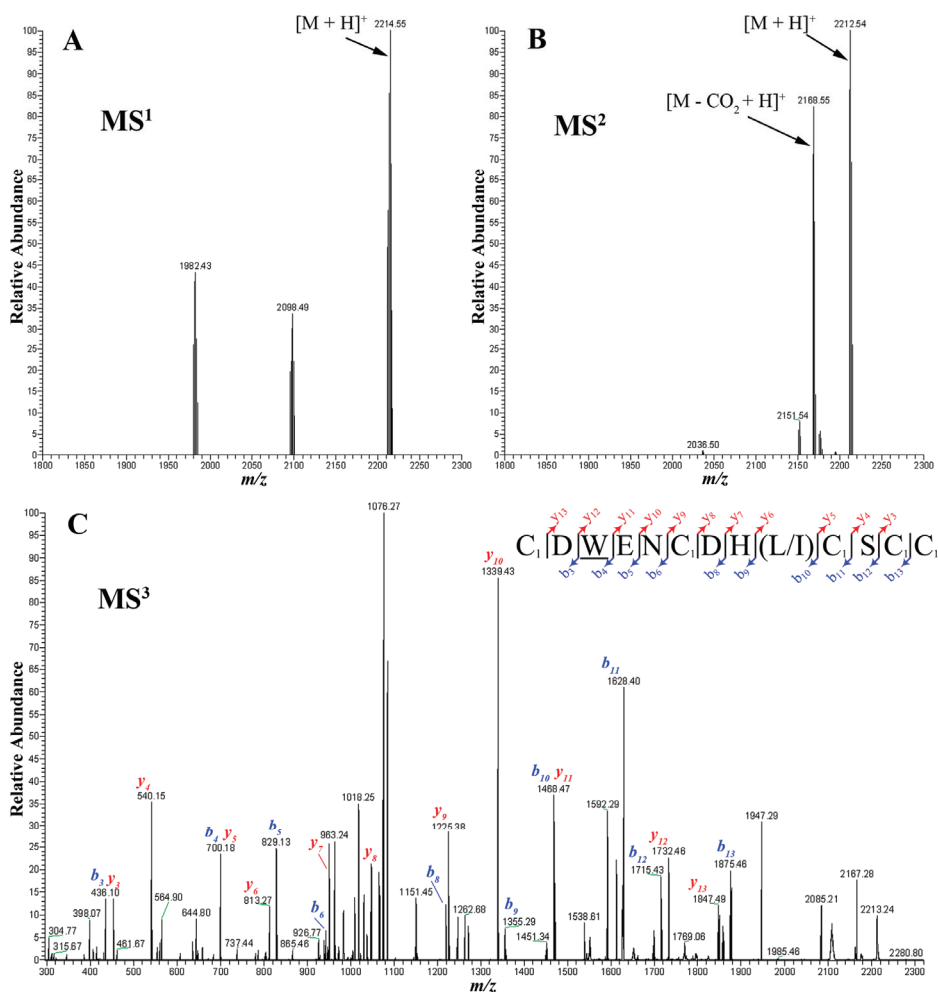


**Figure 4.** CID MS/MS spectrum of TCEP-reduced and IAA-labeled BnIIID, recorded with the MALDI-TOF/TOF 4800 mass spectrometer. MS/MS fragmentation of BnIIID without (A), and with carboxylation of E (B). Insets show the sequences derived from these MS/MS spectra. Note: C<sub>1</sub>: carbamidomethyl-cysteine; alkylated cystein by IAA; W: bromotryptophan; E:  $\gamma$ -carboxylic glutamic acid; \*: C-terminal amidation.

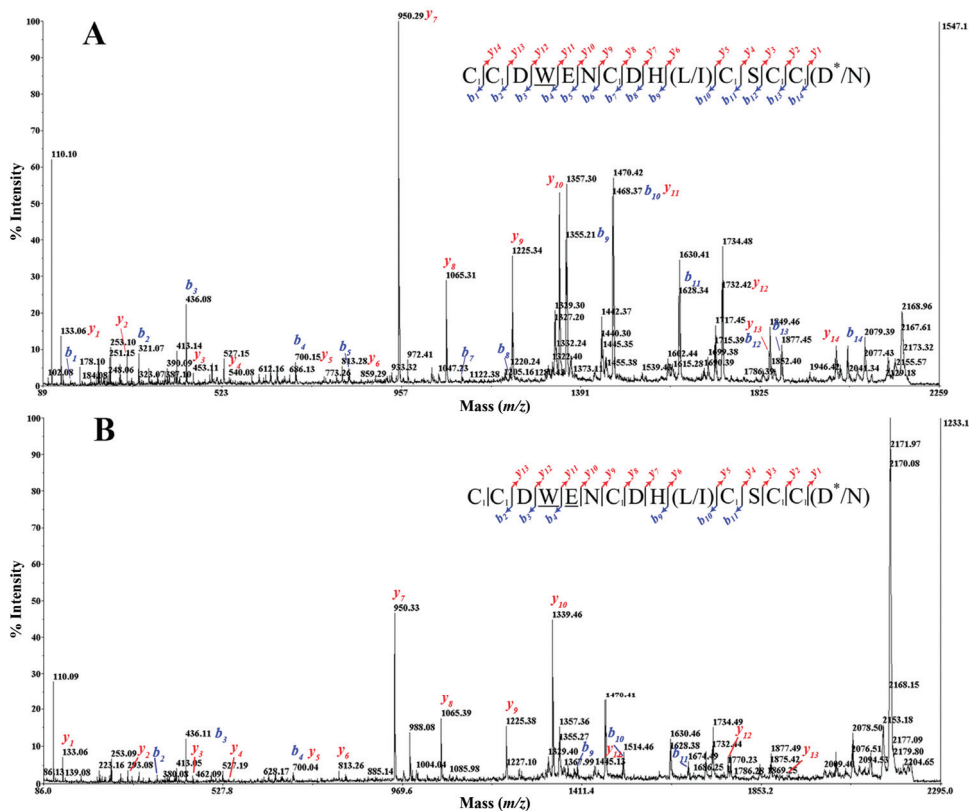
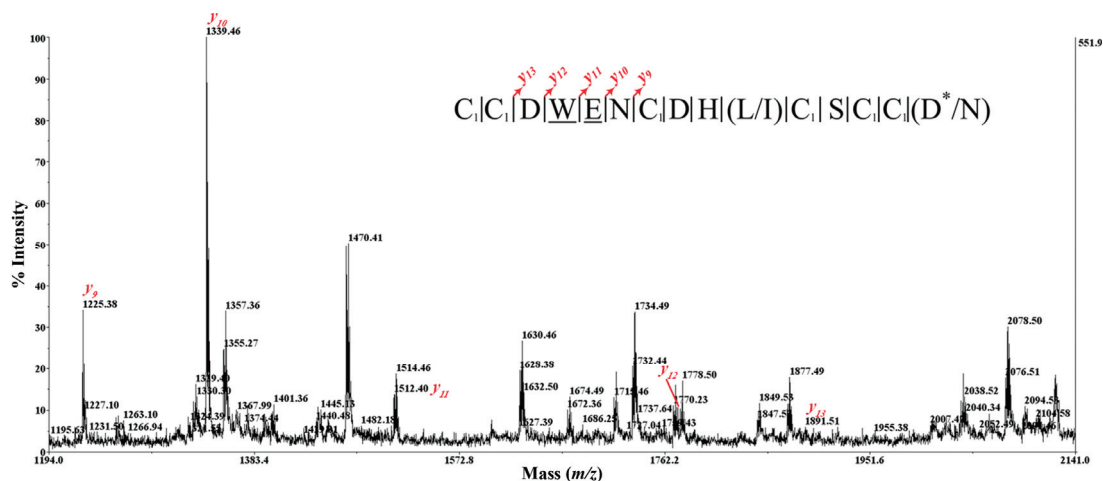


Figure 4B shows the spectrum of the parent ion at  $m/z$  2211.198 with predicted carboxylation. Here we focused on the identification of the  $\gamma$ -carboxylic glutamic acid residue. The  $m/z$  2211.198-CID MS/MS spectrum is not so informative than the  $m/z$  2167.245-spectrum due to the preferential loss of the carboxylic group of the  $\gamma$ -carboxylic glutamic acid residue during the fragmenting process. Though, we determined a  $\gamma$ -carboxy glutamate (E) according to the difference of 173 u at the same position “5”, *i.e.*, between  $y_{10}$  and  $y_{11}$  ions (Figure 5). We also found a perfect agreement with ESI-MS/MS data using the series of  $y$ -type ions. Thus, the initial BnIIID sequence is CCDWENC<sub>1</sub>D[H](L/I)CSCC(D\*/N) with two confirmed PTMs: bromotryptophan (W) and  $\gamma$ -carboxy glutamate (E). Nair *et al.* have used the Fourier transform ion cyclotron resonance MS/MS technique of electron capture dissociation, infrared multiphoton dissociation and CID to detect, and localize the bromotryptophan of a conopeptide, named Mo 1274, from *Conus monile* venom [16]. There was difficulty in the initial sequence assignment of CID mass spectrum of the Mo 1274

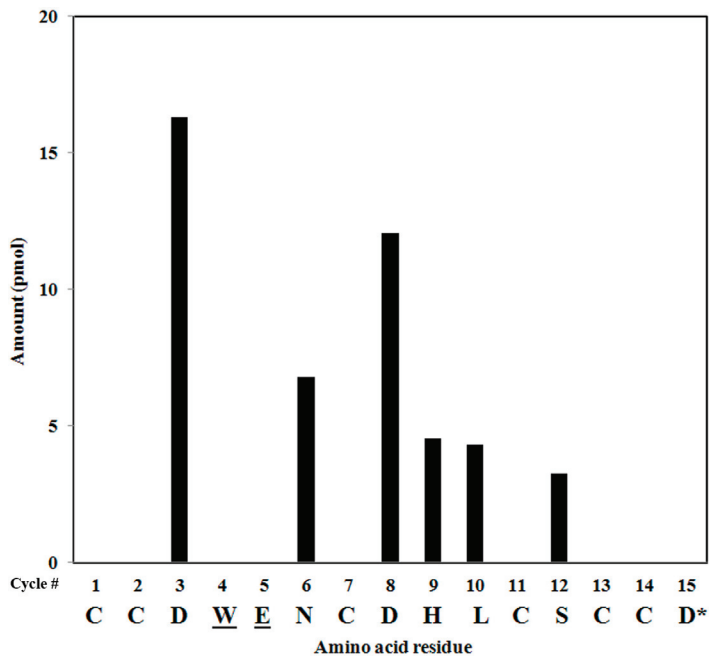
peptide. In our case, the MALDI-TOF CID MS/MS was used to characterize simply the initial sequence, and also positions of bromotryptophan and  $\gamma$ -carboxy glutamate.

**Figure 5.** A zoom of CID MS/MS mass spectrum profile of IAA-labeled BnIIID with carboxylation of E (Figure 4B). Insets show the sequences derived from these MS/MS spectra. Note: C<sub>1</sub>: carbamidomethyl-cysteine; alkylated cystein by IAA; W: bromotryptophan; E:  $\gamma$ -carboxylic glutamic acid; \*: C-terminal amidation.



To confirm the complete amino acid sequence of BnIIID, this native conopeptide was submitted to Edman's degradation. Figure 6 presents the release of BnIIID PTH-amino acid residues for each cycle. BnIIID sequence has totally 15 amino acid residues with six cysteines at positions "1; 2; 7; 11; 13; 14" which supports well the CID MS/MS obtained data. Additionally, there are no amounts of PTH-amino acid residues at cycle "4" and "5", and it explains clearly that PTH-amino acid residue of bromotryptophan and  $\gamma$ -carboxy glutamate are not noted in Edman's degradation profile of the standard program. At position "10", we can confirm the leucine residue having an amount of 4.3 pmol in place of isoleucine. No data are observed at the last cycle, which may propose that there is a PTM in the amino acid residue. The MS/MS spectrum data and theoretical calculation offered previously two possibilities: an amidated aspartic acid (D\*) or an asparagine (N) residue. Therefore, it may be inferred an aspartic acid amidation at the C-terminus. Thus, the complete linear BnIIID sequence is CCDWENCDHLCSCCD\* with three PTMs: bromotryptophan,  $\gamma$ -carboxy glutamate, and amidated aspartic acid, at positions "4", "5", and "15", respectively. This sequence is also in agreement with the experimental mass obtained in Figure 3B for BnIIID; theoretical mass of BnIIID (C<sub>78</sub> H<sub>111</sub> N<sub>26</sub> O<sub>33</sub> S<sub>6</sub> Br) = 2210.5309 Da, experimental mass: 2210.5293 Da ( $\Delta = 1.6$  ppm).

**Figure 6.** Solid-phase Edman degradation of native BnIIID. Note: W: bromotryptophan; E:  $\gamma$ -carboxylic glutamic acid; \*: C-terminal amidation.



### 2.5. Peptide Synthesis

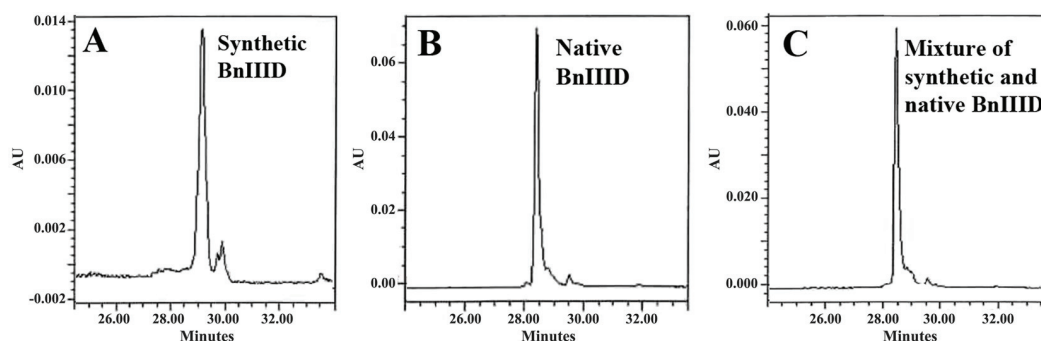
To confirm the refolding of the peptide like the native product, a synthetic BnIIID peptide was prepared (containing 6-D/L-6 bromotryptophan,  $\gamma$ -carboxy glutamate and amidated aspartic acid at positions “4”, “5”, and “15”, respectively). Figure 7 demonstrates the near identity of RP-HPLC chromatogram profiles from the same retention time, co-elution of refolded synthetic and native peptides. It is worth noting that the synthetic BnIIID was purified from the racemic mixture containing both D and L forms of 6-bromotryptophan. We deduced that the isomer position occurring in BnIIID is 6-bromotryptophan, following the earlier study by Craig *et al.* [14]. Remarkably, 6-bromotryptophan has also been found, mostly in other marine animals. The peptide component that co-eluted with the native peptide was less hydrophobic (data do not shown). This phenomenon is similar in the synthetic bromoheptapeptide purification of *Conus imperialis*, which demonstrated L-6-bromotryptophan from digestion with  $\alpha$ -chymotrypsin [14]. Thus, it could be deduced that the native BnIIID contains L-6-bromotryptophan.

### 2.6. Sequence Similarity Analysis

As shown in Table 1, the BnIIID sequence was compared to other conopeptide sequences having the same “4/3/1”, III-cysteine framework (like  $-CCX_1X_2X_3X_4CX_1X_2X_3CX_1CC-$ ) in three different *Conus* species (piscivorous, vermivorous, and molluscivorous) on the ConoServer [17]. The BnIIID peptide shares some homology with two conopeptides (S3-S01, S3-S02) of the

piscivorous *Conus striatus*, and two other peptides (Ts3.6, LtIIID) of the vermivorous *Conus tessulatus* and *Conus litteratus*, respectively. Interestingly, BnIIID exhibits high homology with five *C. marmoreus* conopeptide sequences (e.g., Mr3.16, MrIIIIE, MrIIIF, Mr3.18, and Mr3.8). The MrIIIIE peptide of *C. marmoreus* has been shown to have (C1–C5, C2–C4, C3–C6) disulfide linkage arrangement using Edman analysis of the partially reduced peptide [18]. We suggest that the BnIIID conopeptide could share the same disulfide connectivity as the MrIIIIE peptide. However, further work will be necessary to definitively attribute the disulfide linkage of BnIIID. All compared conopeptides presented in Table 1 belong to M-1 family of the M-superfamily. Thus, it can be inferred that BnIIID also belongs to the same family. Moreover, the bomotryptophan residue in BnIIID is found as a PTM for the first time, not only in a conopeptide having the cysteine framework III, but also in the M superfamily sequences.

**Figure 7.** Verification of the synthetic peptide folding. The HPLC chromatograms of the synthetic BnIIID (A); the native peptide (B); and the co-elution of the mixture of synthetic and native BnIIID (C). The experiments were carried out with a X-Bridge analytical C<sub>18</sub> column and eluted at 1 mL·min<sup>-1</sup> with a gradient 0%–45% of acetonitrile in 40 min.



Craig *et al.* (1997) [14] were the first to report the bromination of tryptophan residues in *Conus venom* components. The initial work was focused on two conopeptides: the bromosleeper conopeptide isolated from the piscivorous *Conus radiatus*, and a heptapeptide isolated from the vermivorous *Conus imperialis*. A mechanism for tryptophan bromination in cone snails has been proposed, such as the bromination of tryptophan to L-6-bromotryptophan by a bromoperoxidase [10,19,20]. The relative importance and the role of bromination in conopeptides are currently unknown.

*Conus* are well-known for using many different strategies to capture their own preys through the use of a variety of conotoxins. The capacity to generate conopeptides, in which the number and nature of amino-acid residues can vary within putative inter-cysteines, is one of their most important and efficient strategies. To these characteristics it should be added that conopeptides may become still more diverse and complex considering the reported PTMs in *Conus venoms* [7,17]. Here, BnIIID was analyzed as belonging to the M-superfamily of conotoxins [18,21,24,25], which shares the same cysteine framework (–CC–C–C–CC–) pattern (Table 2). The conopeptide

framework-III, according to available data, can be represented by  $\mu$ -,  $\iota$ -,  $\psi$ -, and  $\kappa$ -conotoxins, with pharmacological properties, such as blockage of voltage-gated sodium channels ( $\mu$ -conotoxins), activation of voltage-gated sodium channels, without delaying channel inactivation ( $\iota$ -conotoxins), modulation or blockage of nicotinic acetylcholine receptors ( $\psi$ -conotoxins), and blockage of voltage-gated potassium channels ( $\kappa$ -conotoxins). Studies are in progress to determine the molecular target(s) of BnIIID.

**Table 1.** BnIIID sequence similarity with other conopeptides, from piscivorous (p), vermivorous (v), and molluscivorous (m) cone snails, belonging to the M superfamily.

Note: W: bromotryptophan; E:  $\gamma$ -carboxylic glutamic acid; \*: C-terminal amidation.

Name	Cone snail	Diet	Sequence											Reference					
S3-S01	<i>C. striatus</i>	p -	C	C	P	K	E	W	C	N	R	D	C	S	C	C	T	-	[17,21]
S3-S02	<i>C. striatus</i>	p -	C	C	P	A	R	M	C	M	A	A	C	S	C	C	D	-	[17,21]
Ts3.6	<i>C. tessulatus</i>	v Q	C	C	D	W	Q	W	C	D	G	A	C	D	C	C	A	-	[22]
LtIIID	<i>C. litteratus</i>	v -	C	C	D	W	E	W	C	D	E	L	C	S	C	C	W	-	[23]
Mr3.16	<i>C. marmoreus</i>	m V	C	C	S	F	G	S	C	D	S	L	C	Q	C	C	D*	-	[5]
MrIIIE	<i>C. marmoreus</i>	m V	C	C	P	F	G	G	C	H	E	L	C	Y	C	C	D*	-	[18]
MrIIIF	<i>C. marmoreus</i>	m V	C	C	P	F	G	G	C	H	E	L	C	L	C	C	D*	-	[18]
Mr3.18	<i>C. marmoreus</i>	m -	C	C	H	R	N	W	C	D	H	L	C	S	C	C	G	S	[5]
Mr3.8	<i>C. marmoreus</i>	m -	C	C	H	W	N	W	C	D	H	L	C	S	C	C	G	S	[18]
BnIIID	<i>C. bandanus</i>	m -	C	C	D	<u>W</u>	<u>E</u>	N	C	D	H	L	C	S	C	C	D*	-	This work

The  $-CCX_1X_2X_3X_4CX_1X_2X_3CX_1CC-$  conopeptides have been poorly explored for their specific pharmacological targets. The conopeptide LtIIIA from *C. litteratus*, among ~63 other peptides, was evaluated as belonging to the  $\iota$ -conotoxin class [26]. Remarkably, this pattern exists mostly in mollusk- and worm-hunting cone snails (e.g., eight conopeptides in *C. marmoreus*). The synthesis of BnIIID conopeptide will enable us to investigate in detail its pharmacological properties, and, what is more important, the eventual role of the PTMs, since three other peptides (BnIIIA, BnIIIB, and BnIIIC) have been just isolated by us, and such peptides lack some of the PTMs (bromotryptophan and  $\gamma$ -carboxylglutamate) here reported.

**Table 2.** Inter-cysteine variation of “framework III” conopeptides vs. their pharmacological properties. Note: W: bromotryptophan; E:  $\gamma$ -carboxylic glutamic acid; \* : C-terminal amidation; p: piscivorous; m: molluscivorous; v: vermivorous.

Name	Organism	Diet	Sequence										Pharmacology			Reference																			
BullIA	<i>C. bullatus</i>	p	V	T	D	R	C	C	K	G	K	R	E	-	C	R	D	H	S	R	C	C	*	-	-	-	$\mu$ -conotoxin	[27]							
BullIB	<i>C. bullatus</i>	p	V	G	E	R	C	C	K	N	G	K	R	G	-	C	R	D	H	S	R	C	C	*	-	-	-	$\mu$ -conotoxin	[27]						
CIII A	<i>C. catus</i>	p	-	-	G	R	C	C	E	G	P	N	G	-	C	S	S	R	W	-	C	K	D	H	A	R	C	C	*	-	-	-	$\mu$ -conotoxin	[28]	
CnIII A	<i>C. consors</i>	p	-	-	G	R	C	C	D	V	P	N	A	-	C	S	G	R	W	-	C	R	D	H	A	Q	C	C	*	-	-	-	$\mu$ -conotoxin	[28]	
CnIII B	<i>C. consors</i>	p	-	-	Z	G	C	C	G	E	P	N	L	-	C	F	T	R	W	-	C	R	N	N	A	R	C	C	R	Q	Q	-	-	$\mu$ -conotoxin	[28]
GIII A	<i>C. geographus</i>	p	-	-	R	D	C	C	T	O	O	K	K	-	C	K	D	R	Q	-	C	K	O	Q	R	-	C	C	A	*	-	-	$\mu$ -conotoxin	[29]	
GIII B	<i>C. geographus</i>	p	-	-	R	D	C	C	T	O	O	R	K	-	C	K	D	R	R	-	C	K	O	M	K	-	C	C	A	*	-	-	$\mu$ -conotoxin	[30]	
GIII C	<i>C. geographus</i>	p	-	-	R	D	C	C	T	O	O	K	K	-	C	K	D	R	R	-	C	K	O	L	K	-	C	C	A	*	-	-	$\mu$ -conotoxin	[31]	
KIII A	<i>C. kinoshitai</i>	p	-	-	-	-	C	C	N	-	-	-	-	-	C	S	S	K	W	-	C	R	D	H	S	R	C	C	*	-	-	-	$\mu$ -conotoxin	[32]	
LtIII A	<i>C. litteratus</i>	v	-	-	D	E	C	C	E	O	Q	W	-	-	C	D	G	A	-	-	C	D	-	-	-	-	C	C	S	-	-	-	t-conotoxin	[26]	
MIII A	<i>C. magus</i>	p	-	-	Z	G	C	C	N	V	P	N	G	-	C	S	G	R	W	-	C	R	D	H	A	Q	C	C	*	-	-	-	$\mu$ -conotoxin	[33]	
PIII A	<i>C. purpurascens</i>	p	-	Z	R	L	C	C	G	F	O	K	S	-	C	R	S	R	Q	-	C	K	O	H	R	-	C	C	*	-	-	-	$\mu$ -conotoxin	[34]	
PIII E	<i>C. purpurascens</i>	p	-	H	O	O	C	C	L	Y	G	K	-	-	C	R	R	Y	O	G	-	C	S	S	A	S	-	C	C	Q	R	*	-	$\psi$ -conotoxin	[35]
PIII F	<i>C. purpurascens</i>	p	-	G	O	O	C	C	L	Y	G	S	-	-	C	R	O	F	O	G	-	C	Y	N	A	L	-	C	C	R	K	*	-	$\psi$ -conotoxin	[36]
Pr-III E	<i>C. parius</i>	p	-	A	A	R	C	C	T	Y	H	G	S	-	C	L	K	E	K	-	C	R	R	K	Y	-	C	C	*	-	-	-	$\psi$ -conotoxin	[37]	
RIII J	<i>C. radiatus</i>	p	-	L	O	O	C	C	T	O	O	K	K	H	-	C	O	A	O	A	-	C	K	Y	K	O	-	C	C	K	S	-	-	k-conotoxin	[38]
RIII K	<i>C. radiatus</i>	p	-	L	O	S	C	C	S	L	N	L	R	L	-	C	O	V	O	A	-	C	K	R	N	O	-	C	C	T	*	-	-	k-conotoxin	[39]
SIII A	<i>C. striatus</i>	p	-	-	Z	N	C	C	N	G	-	-	-	-	C	S	S	K	W	-	C	R	D	H	A	R	C	C	*	-	-	-	$\mu$ -conotoxin	[32]	
SIII B	<i>C. striatus</i>	p	-	-	Z	N	C	C	N	G	G	-	-	-	C	S	S	K	W	-	C	K	G	H	A	R	C	C	*	-	-	-	$\mu$ -conotoxin	[40]	
SmlIII A	<i>C. stercoriscarum</i>	p	-	-	Z	R	C	C	N	G	R	R	G	-	C	S	S	R	W	-	C	R	D	H	S	R	C	C	-	-	-	-	$\mu$ -conotoxin	[41]	
SxIII A	<i>C. striolatus</i>	p	-	-	-	R	C	C	T	G	K	K	G	S	-	C	K	N	L	K	-	C	K	N	L	K	-	C	C	A	*	-	-	$\mu$ -conotoxin	[42]
SxIII B	<i>C. striolatus</i>	p	-	-	Z	K	C	C	T	G	K	K	G	S	-	C	K	N	L	R	-	C	K	N	L	R	-	C	C	A	*	-	-	$\mu$ -conotoxin	[42]
TIII A	<i>C. tulipa</i>	p	-	R	H	G	C	C	K	G	O	K	G	-	C	S	S	R	E	-	C	R	O	Q	H	-	C	C	*	-	-	-	$\mu$ -conotoxin	[43]	
BnIII D	<i>C. bandanus</i>	m	-	-	-	-	C	C	D	<u>W</u>	<u>E</u>	N	-	-	C	D	H	L	-	-	C	S	-	-	-	-	-	C	C	D	*	-	-	unknown	This work



### 3. Experimental Section

#### 3.1. Isolation and Purification of Native Conopeptides

Twelve adult specimens ( $\geq 72$  mm shell length) of *C. bandanus* were collected in the Nha Trang bay in the South central coast of Vietnam. We have used the same methods for venom extraction as previously described [13]. The extract was lyophilized and stored at  $-80$  °C for later fractionation. All subfractions, purifications, and analyses were performed on a HPLC (System Gold with programmable solvent module 126 pumps using 32 Karat software; Beckman Coulter, Fullerton, CA, USA) at room temperature. Fractions were collected based on absorbance at 220 nm (System Gold 166 detector; Beckman Coulter, Fullerton, CA, USA). The elution buffers used for all HPLC were the following: A buffer (1000 mL H<sub>2</sub>O/1 mL trifluoroacetic acid (TFA; Merck, Darmstadt, Germany); B buffer (900 mL CH<sub>3</sub>CN/100 mL H<sub>2</sub>O/1 mL TFA). The lyophilized *C. bandanus* venom (~300 mg) was dissolved in A buffer, and the extract was loaded in batches of ~10 mg on a Vydac semi-preparative C<sub>18</sub> column (300 Å, 5 µm, 10 mm i.d. × 250 mm). The gradient program for the semi-preparative column was 0% of B buffer/10 min, then 0%–56% of B buffer/50 min with the flow rate 3 mL/min. Further purification steps were carried out using a Vydac analytical C<sub>18</sub> column (300 Å, 5 µm, 4.6 mm i.d. × 250 mm) at flow rate 1 mL/min.

#### 3.2. Reduction-Alkylation Procedures

The purified fraction was reduced by incubation for 10 min at 65 °C in a solution of 20 mM tris-2-carboxyethyl-phosphine (TCEP) in 0.5 M HEPES. Alkylation was then performed by addition of iodoacetamide (IAA) 0.05 M and incubation for 20 min at room temperature in darkness. The mixture was finally desalted by solid phase extraction on a Zip Tip C<sub>18</sub> column (Millipore, Billerica, MA, USA).

#### 3.3. Mass Spectrometry Analysis

MALDI analysis—all bioactive fractions were analyzed with a 5800 MALDI-TOF/TOF mass spectrometer (AB Sciex, Les Ulis, France). The instrument was equipped with an Nd:YAG laser operating at 355 nm wavelength. Aliquots of 0.5 µL of a purified fraction were mixed with 0.5 µL of a solution of 4 mg/mL of cyano-4-hydroxycinnamic acid. Acquisitions were performed on positive reflection mode. Instrument calibration was done using a peptide mixt (peptide calibration 1 and 2 from ABSciex between 700 and 3700 Da). For MS/MS experiments, precursor ions were accelerated at 8 keV and the MS/MS spectra were acquired using 2 keV collision energy, with CID gas (air) at a pressure of  $3.5 \times 10^{-6}$  Torr. MS and MS/MS data were processed using DataExplorer 4.9 (AB Sciex).

Nano ESI orbitrap analysis—some important fractions were verified on their accurate mass on a LTQ Orbitrap mass spectrometer equipped with a nano-electrospray source (Thermo Scientific, Bremen, Germany). Few microliters of chromatographic fraction were loaded onto metal-coated borosilicate emitters (Thermo Scientific). The 1.2 KV were applied to the emitter and the acquisition was monitored on the orbitrap set with a theoretical resolution of 30,000 at  $m/z$  400. For

MS2 and MS3, normalized collision energy of 36 eV was applied. Spectra were treated with Xcalibur 2.1, the multiplied-charged species were recalculated into its singly-charged form using the Xtract software (Thermo Scientific, San Jose, CA, USA).

### 3.4. Automatic Amino Acid Sequencing

Pure peptide fractions were dissolved in buffer A and their concentration were measured by scan mode “Absorbance” (range 240–350 nm wavelength) in a DU 800 Spectrophotometer (Beckman-Coulter, Brea, CA, USA). The 2  $\mu$ L native peptide (~190  $\mu$ M) was sequenced using an automated Edman degradation using a Procise protein sequencer (Applied Biosystem model 492, Applied Biosystem, Foster City, CA, USA).

### 3.5. Chemical Synthesis

Materials—Fmoc-amino acids and 2-(6-Chloro-1-H-benzotriazole-1-yl)-1,1,3,3-tetramethylammonium hexafluorophosphate (HCTU) were obtained from Activotec (Cambridge, UK), Fmoc-Gla(OtBu)<sub>2</sub>-OH from Iris Biotech (Marktredwitz, Germany) and Fmoc-DL-6-Bromotryptophan from AnaSpec (Fremont, CA, USA). The Chemmatrix resin and all the peptide synthesis grade reagents (*N*-methylpyrrolidone (NMP), *N*-methylmorpholine (NMM), piperidine, trifluoroacetic acid (TFA), anisole, thioanisole and triisopropylsilane (TPS) were purchased from Sigma Aldrich (Saint-Quentin Fallavier, France).

Synthesis—peptide synthesis was performed on a Protein Technologies, Inc Prelude synthesizer at a 50  $\mu$ mole scale using fivefold excess of Fmoc-amino acid relative to the rink amide chemmatrix resin (0.4–0.6 mmol/g). All the amino acids were coupled twice 5 min using 1:1:2 amino acid/HCTU/NMM in *N*-methylpyrrolidone (NMP) with the exception of Fmoc-DL-6-bromotryptophane and Fmoc-Gla(OtBu)<sub>2</sub>-OH where a single 30 min coupling was used. Fmoc deprotection was performed using 20% piperidine in NMP, and NMP top washes were performed between deprotection and coupling steps. All cysteines were protected with S-trityl groups. Following chain assembly, the peptidyl-resin was treated with a mixture of TFA/thioanisole/anisole/TPS/water (82:5:5:2.5:5) for 2 h. The crude peptide was obtained after precipitation and washes in cold ethyl ether followed by dissolution in 10% acetic acid and lyophilisation.

Folding and characterization—refolding of the peptide was performed by stirring the crude reduced toxin in aqueous 0.1 M Tris buffer, pH 8.2 containing reduced and oxidized glutathione at 2 mM and 1 mM respectively for 24 and 3 h, respectively. The solution was then acidified using TFA 20% followed by purification by semi-preparative RP-HPLC using a X-Bridge (Waters, Milford, MA, USA) C<sub>18</sub> column with a linear gradient from 0% to 60% buffer B in A at 4mL/min during 40 min, (buffer A, 0.1% TFA in water; Buffer B, acetonitrile, 0.1% TFA). The main fraction was collected and lyophilized. The homogeneity of the peptide was confirmed by MALDI-TOF mass spectrometry (AB SCIEX 4800, Les Ulis, France). The co-elution of the synthetic and native peptides was checked by analytical RP-HPLC.

#### 4. Conclusions

In this work, we describe the characterization of a novel conopeptide named BnIIID, isolated from the venom of the molluscivorous snail species *C. bandanus* collected from the south central coast of Vietnam. The determination of the primary conopeptide structure on the basis of CID MS/MS mass-spectra analysis and Edman degradation revealed that BnIIID contained PTMs, such as bromotryptophan,  $\gamma$ -carboxy glutamate, and amidated aspartic acid at positions “4”, “5”, and “15”, respectively. The complete amino acid sequence of the conopeptide (CCDWENCDHLCCSD\*) and its III-cysteine framework allowed to categorize BnIIID in the M-1 family of conotoxins, belonging to the M-superfamily.

#### Acknowledgments

We are grateful to the Institute of Biotechnology and Environment (Nha Trang University, Vietnam) for the specimen preparation. Bao NGUYEN was supported in part by a pre-doctoral fellowship from the French government (Embassy of France in Vietnam), and in part by the National Center for Scientific Research. We are grateful to P. Villeneuve for technical assistance. We thank David Touboul from the Natural Product Chemistry Institute of CNRS for helpful comments and suggestions.

#### Author Contributions

J.M., J.P.L.C., G.M., and D.S. designed research; B.N., J.P.L.C., G.M., and R.T. performed research; B.N., J.P.L.C., G.M., H.L., and E.B. analyzed data; J.M., B.N., J.P.L.C., and G.M. wrote the manuscript. All authors discussed the results and commented on the manuscript.

#### Conflicts of Interest

The authors declare no conflict of interest.

#### References

1. Olivera, B.M. *Conus* peptides: Biodiversity-based discovery and exogenomics. *J. Biol. Chem.* **2006**, *281*, 31173–31177.
2. Lewis, R.J.; Dutertre, S.; Vetter, I.; Christie, M.J. *Conus* venom peptide pharmacology. *Pharmacol. Rev.* **2012**, *64*, 259–298.
3. Favreau, P.; Stocklin, R. Marine snail venoms: Use and trends in receptor and channel neuropharmacology. *Curr. Opin. Pharmacol.* **2009**, *9*, 594–601.
4. Olivera, B.M.E.E. Just Lecture, 1996. *Conus* venom peptides, receptor and ion channel targets, and drug design: 50 million years of neuropharmacology. *Mol. Biol. Cell* **1997**, *8*, 2101–2109.
5. Dutertre, S.; Jin, A.H.; Kaas, Q.; Jones, A.; Alewood, P.F.; Lewis, R.J. Deep venomics reveals the mechanism for expanded peptide diversity in cone snail venom. *Mol. Cell. Proteomics* **2013**, *12*, 312–329.

6. Terlau, H.; Olivera, B.M. Conus venoms: A rich source of novel ion channel-targeted peptides. *Physiol. Rev.* **2004**, *84*, 41–68.
7. Craig, A.G.; Bandyopadhyay, P.; Olivera, B.M. Post-translationally modified neuropeptides from *Conus* venoms. *Eur. J. Biochem.* **1999**, *264*, 271–275.
8. Jakubowski, J.A.; Kelley, W.P.; Sweedler, J.V. Screening for post-translational modifications in conotoxins using liquid chromatography/mass spectrometry: An important component of conotoxin discovery. *Toxicon* **2006**, *47*, 688–699.
9. Gerwig, G.J.; Hocking, H.G.; Stocklin, R.; Kamerling, J.P.; Boelens, R. Glycosylation of conotoxins. *Mar. Drugs* **2013**, *11*, 623–642.
10. Buczek, O.; Bulaj, G.; Olivera, B.M. Conotoxins and the posttranslational modification of secreted gene products. *Cell. Mol. Life Sci.* **2005**, *62*, 3067–3079.
11. Yates, J.R., III. Mass spectrometry. From genomics to proteomics. *Trends Genet.* **2000**, *16*, 5–8.
12. Nam, H.H.; Corneli, P.S.; Watkins, M.; Olivera, B.; Bandyopadhyay, P. Multiple genes elucidate the evolution of venomous snail-hunting *Conus* species. *Mol. Phylogenet. Evol.* **2009**, *53*, 645–652.
13. Nguyen, B.; Molgó, J.; Lamthanh, H.; Benoit, E.; Khuc, T.A.; Ngo, D.N.; Nguyen, N.T.; Millares, P.; le Caer, J.P. High accuracy mass spectrometry comparison of *Conus bandanus* and *Conus marmoreus* venoms from the South Central Coast of Vietnam. *Toxicon* **2013**, *75*, 148–159.
14. Craig, A.G.; Jimenez, E.C.; Dykert, J.; Nielsen, D.B.; Gulyas, J.; Abogadie, F.C.; Porter, J.; Rivier, J.E.; Cruz, L.J.; Olivera, B.M.; *et al.* A novel post-translational modification involving bromination of tryptophan. Identification of the residue, L-6-bromotryptophan, in peptides from *Conus imperialis* and *Conus radiatus* venom. *J. Biol. Chem.* **1997**, *272*, 4689–4698.
15. England, L.J.; Imperial, J.; Jacobsen, R.; Craig, A.G.; Gulyas, J.; Akhtar, M.; Rivier, J.; Julius, D.; Olivera, B.M. Inactivation of a serotonin-gated ion channel by a polypeptide toxin from marine snails. *Science* **1998**, *281*, 575–578.
16. Nair, S.S.; Nilsson, C.L.; Emmett, M.R.; Schaub, T.M.; Gowd, K.H.; Thakur, S.S.; Krishnan, K.S.; Balaram, P.; Marshall, A.G. *De novo* sequencing and disulfide mapping of a bromotryptophan-containing conotoxin by Fourier transform ion cyclotron resonance mass spectrometry. *Anal. Chem.* **2006**, *78*, 8082–8088.
17. Kaas, Q.; Yu, R.; Jin, A.H.; Dutertre, S.; Craik, D.J. ConoServer: updated content, knowledge, and discovery tools in the conopeptide database. *Nucleic Acids Res.* **2012**, *40*, D325–D330.
18. Han, Y.H.; Wang, Q.; Jiang, H.; Liu, L.; Xiao, C.; Yuan, D.D.; Shao, X.X.; Dai, Q.Y.; Cheng, J.S.; Chi, C.W. Characterization of novel M-superfamily conotoxins with new disulfide linkage. *FEBS J.* **2006**, *273*, 4972–4982.
19. Jimenez, E.C.; Craig, A.G.; Watkins, M.; Hillyard, D.R.; Gray, W.R.; Gulyas, J.; Rivier, J.E.; Cruz, L.J.; Olivera, B.M. Bromocontryphan: Post-translational bromination of tryptophan. *Biochemistry* **1997**, *36*, 989–994.
20. Jimenez, E.C.; Watkins, M.; Olivera, B.M. Multiple 6-bromotryptophan residues in a sleep-inducing peptide. *Biochemistry* **2004**, *43*, 12343–12348.

21. Zhou, M.; Wang, L.; Wu, Y.; Zhu, X.; Feng, Y.; Chen, Z.; Li, Y.; Sun, D.; Ren, Z.; Xu, A. Characterizing the evolution and functions of the M-superfamily conotoxins. *Toxicon* **2013**, *76*, 150–159.
22. Conticello, S.G.; Gilad, Y.; Avidan, N.; Ben-Asher, E.; Levy, Z.; Fainzilber, M. Mechanisms for evolving hypervariability: The case of conopeptides. *Mol. Biol. Evol.* **2001**, *18*, 120–131.
23. Pi, C.; Liu, J.; Peng, C.; Liu, Y.; Jiang, X.; Zhao, Y.; Tang, S.; Wang, L.; Dong, M.; Chen, S.; Xu, A. Diversity and evolution of conotoxins based on gene expression profiling of *Conus litteratus*. *Genomics* **2006**, *88*, 809–819.
24. Corpuz, G.P.; Jacobsen, R.B.; Jimenez, E.C.; Watkins, M.; Walker, C.; Colledge, C.; Garrett, J.E.; McDougal, O.; Li, W.; Gray, W.R.; *et al.* Definition of the M-conotoxin superfamily: Characterization of novel peptides from molluscivorous *Conus* venoms. *Biochemistry* **2005**, *44*, 8176–8186.
25. Jacob, R.B.; McDougal, O.M. The M-superfamily of conotoxins: A review. *Cell. Mol. Life Sci.* **2010**, *67*, 17–27.
26. Wang, L.; Liu, J.; Pi, C.; Zeng, X.; Zhou, M.; Jiang, X.; Chen, S.; Ren, Z.; Xu, A. Identification of a novel M-superfamily conotoxin with the ability to enhance tetrodotoxin sensitive sodium currents. *Arch. Toxicol.* **2009**, *83*, 925–932.
27. Holford, M.; Zhang, M.M.; Gowd, K.H.; Azam, L.; Green, B.R.; Watkins, M.; Ownby, J.P.; Yoshikami, D.; Bulaj, G.; Olivera, B.M. Pruning nature: Biodiversity-derived discovery of novel sodium channel blocking conotoxins from *Conus bullatus*. *Toxicon* **2009**, *53*, 90–98.
28. Zhang, M.M.; Fiedler, B.; Green, B.R.; Catlin, P.; Watkins, M.; Garrett, J.E.; Smith, B.J.; Yoshikami, D.; Olivera, B.M.; Bulaj, G. Structural and functional diversities among mu-conotoxins targeting TTX-resistant sodium channels. *Biochemistry* **2006**, *45*, 3723–3732.
29. Wakamatsu, K.; Kohda, D.; Hatanaka, H.; Lancelin, J.M.; Ishida, Y.; Oya, M.; Nakamura, H.; Inagaki, F.; Sato, K. Structure-activity relationships of mu-conotoxin GIIIA: Structure determination of active and inactive sodium channel blocker peptides by NMR and simulated annealing calculations. *Biochemistry* **1992**, *31*, 12577–12584.
30. Hill, J.M.; Alewood, P.F.; Craik, D.J. Three-dimensional solution structure of mu-conotoxin GIIIB, a specific blocker of skeletal muscle sodium channels. *Biochemistry* **1996**, *35*, 8824–8835.
31. Cruz, L.J.; Gray, W.R.; Olivera, B.M.; Zeikus, R.D.; Kerr, L.; Yoshikami, D.; Moczydlowski, E. *Conus geographus* toxins that discriminate between neuronal and muscle sodium channels. *J. Biol. Chem.* **1985**, *260*, 9280–9288.
32. Bulaj, G.; West, P.J.; Garrett, J.E.; Watkins, M.; Zhang, M.M.; Norton, R.S.; Smith, B.J.; Yoshikami, D.; Olivera, B.M. Novel conotoxins from *Conus striatus* and *Conus kinoshitai* selectively block TTX-resistant sodium channels. *Biochemistry* **2005**, *44*, 7259–7265.
33. Wilson, M.J.; Yoshikami, D.; Azam, L.; Gajewiak, J.; Olivera, B.M.; Bulaj, G.; Zhang, M.M. mu-Conotoxins that differentially block sodium channels NaV1.1 through 1.8 identify those responsible for action potentials in sciatic nerve. *Proc. Natl. Acad. Sci. USA* **2011**, *108*, 10302–10307.

34. Shon, K.J.; Olivera, B.M.; Watkins, M.; Jacobsen, R.B.; Gray, W.R.; Floresca, C.Z.; Cruz, L.J.; Hillyard, D.R.; Brink, A.; Terlau, H.; *et al.* mu-Conotoxin PIIIA, a new peptide for discriminating among tetrodotoxin-sensitive Na channel subtypes. *J. Neurosci.* **1998**, *18*, 4473–4481.
35. Shon, K.J.; Grilley, M.; Jacobsen, R.; Cartier, G.E.; Hopkins, C.; Gray, W.R.; Watkins, M.; Hillyard, D.R.; Rivier, J.; Torres, J.; *et al.* A noncompetitive peptide inhibitor of the nicotinic acetylcholine receptor from *Conus purpurascens* venom. *Biochemistry* **1997**, *36*, 9581–9587.
36. Van Wagoner, R.M.; Jacobsen, R.B.; Olivera, B.M.; Ireland, C.M. Characterization and three-dimensional structure determination of psi-conotoxin Piiif, a novel noncompetitive antagonist of nicotinic acetylcholine receptors. *Biochemistry* **2003**, *42*, 6353–6362.
37. Lluisma, A.O.; Lopez-Vera, E.; Bulaj, G.; Watkins, M.; Olivera, B.M. Characterization of a novel psi-conotoxin from *Conus parius* Reeve. *Toxicon* **2008**, *51*, 174–180.
38. Chen, P.; Dendorfer, A.; Finol-Urdaneta, R.K.; Terlau, H.; Olivera, B.M. Biochemical characterization of kappaM-RIIIIJ, a Kv1.2 channel blocker: evaluation of cardioprotective effects of kappaM-conotoxins. *J. Biol. Chem.* **2010**, *285*, 14882–14889.
39. Ferber, M.; Sporning, A.; Jeserich, G.; DeLaCruz, R.; Watkins, M.; Olivera, B.M.; Terlau, H. A novel *Conus* peptide ligand for K<sup>+</sup> channels. *J. Biol. Chem.* **2003**, *278*, 2177–2183.
40. Schroeder, C.I.; Ekberg, J.; Nielsen, K.J.; Adams, D.; Loughnan, M.L.; Thomas, L.; Adams, D.J.; Alewood, P.F.; Lewis, R.J. Neuronally micro-conotoxins from *Conus striatus* utilize an alpha-helical motif to target mammalian sodium channels. *J. Biol. Chem.* **2008**, *283*, 21621–21628.
41. West, P.J.; Bulaj, G.; Garrett, J.E.; Olivera, B.M.; Yoshikami, D. Mu-conotoxin SmIIIA, a potent inhibitor of tetrodotoxin-resistant sodium channels in amphibian sympathetic and sensory neurons. *Biochemistry* **2002**, *41*, 15388–15393.
42. Walewska, A.; Skalicky, J.J.; Davis, D.R.; Zhang, M.M.; Lopez-Vera, E.; Watkins, M.; Han, T.S.; Yoshikami, D.; Olivera, B.M.; Bulaj, G. NMR-based mapping of disulfide bridges in cysteine-rich peptides: Application to the mu-conotoxin SxIIIA. *J. Am. Chem. Soc.* **2008**, *130*, 14280–14286.
43. Lewis, R.J.; Schroeder, C.I.; Ekberg, J.; Nielsen, K.J.; Loughnan, M.; Thomas, L.; Adams, D.A.; Drinkwater, R.; Adams, D.J.; Alewood, P.F. Isolation and structure-activity of mu-conotoxin TIIIA, a potent inhibitor of tetrodotoxin-sensitive voltage-gated sodium channels. *Mol. Pharmacol.* **2007**, *71*, 676–685.

## Analysis of the Biomass Composition of the Demosponge *Amphimedon queenslandica* on Heron Island Reef, Australia

Jabin R. Watson, Timothy C. R. Brennan, Bernard M. Degnan, Sandie M. Degnan and Jens O. Krömer

**Abstract:** Marine sponges are a potential source of important pharmaceutical drugs, the commercialisation of which is restricted by the difficulties of obtaining a sufficient and regular supply of biomass. One way to optimize commercial cell lines for production is the in-depth characterization and target identification through genome scale metabolic modeling and flux analysis. By applying these tools to a sponge, we hope to gain insights into how biomass is formed. We chose *Amphimedon queenslandica* as it has an assembled and annotated genome, a prerequisite for genome scale modeling. The first stepping stone on the way to metabolic flux analysis in a sponge holobiont, is the characterization of its biomass composition. In this study we quantified the macromolecular composition and investigated the variation between and within sponges of a single population. We found lipids and protein to be the most abundant macromolecules, while carbohydrates were the most variable. We also analysed the composition and abundance of the fatty acids and amino acids, the important building blocks required to synthesise the abundant macromolecule types, lipids, and protein. These data complement the extensive genomic information available for *A. queenslandica* and lay the basis for genome scale modelling and flux analysis.

Reprinted from *Mar. Drugs*. Cite as: Watson, J.R.; Brennan, T.C.R.; Degnan, B.M.; Degnan, S.M.; Krömer, J.O. Analysis of the Biomass Composition of the Demosponge *Amphimedon queenslandica* on Heron Island Reef, Australia. *Mar. Drugs* **2014**, *12*, 373363753.

### 1. Introduction

Marine sponges and their associated bacteria are prolific producers of secondary metabolites that are an important source of bioactive compounds with pharmacological potential. More than 5000 compounds have been identified to date, including 355 new compounds reported in 2012 alone [1]. However, despite this enormous potential, approval for use as a therapeutic compound is scarce [2]. The lack of commercial development of sponge-derived compounds is attributed to both a biomass supply problem—no reliable method to culture either whole sponges or cells exists—and a lack of understanding of sponge-bacterial interactions. Together, these constraints limit the applicability of metabolic engineering approaches to microbial isolates or sponge cells for over-production of secondary metabolites. To move forward in the development of sponge-derived drugs requires extending the research activities beyond the current major focus on identifying secondary compounds and, to a limited extent, characterizing the biosynthetic pathways that produce these secondary metabolites [3]. We need to understand how the sponge holobiont (the animal and its resident microbes) is able to grow; understanding how the central metabolic pathways contribute to biomass production is crucial to overcoming the biomass supply problem.

The metabolic processes underlying sponge growth can be comprehensively investigated by the application of genome scale modeling and flux analyses [4]. An essential step of such analyses is characterization of the biochemical composition of the sponge holobiont, with a focus on the components that contribute significantly to overall biomass production [5]. Characterizing the biochemical composition allows the formation of a biomass equation, essential for genome scale modeling and flux analysis as it constrains hundreds of fluxes through the system [6]. The focus on secondary metabolic compounds has left the products of central metabolism comparatively overlooked, including analysis of the major cellular macromolecules—protein, lipid, carbohydrate, DNA, and RNA—and their constituent building blocks—amino acids, fatty acids, sugars and nucleotides. Although protein, lipid, and carbohydrate content has been quantitated in a number of marine sponges [7–12], a complete analysis of the main biomass components has not been reported.

In addition to quantifying the components that contribute to biomass formation, information about how variable the composition is across the population and within an individual sponge is important for guiding the design of experiments associated with flux analysis. Although sponges appear to be morphologically simple and homogenous, it has been shown that production of secondary metabolites can be controlled and restricted to specific areas of an individual [13]. This apparent heterogeneity may be related to physiological differences in the sponge itself or in the associated microbial community. Marine sponges typically host large and diverse communities of microbes [14], often in a symbiotic relationship [15]. These microbes have been shown to be the source of certain secondary metabolites [16], and also to interact with central metabolic pathways in the host sponge [17]. Thus the distribution of particular bacterial species and communities within an individual sponge has the potential to influence local metabolic activity. Nonetheless, subsampling the main biomass components within an individual sponge typically has not been performed, as most biochemical analyses performed in sponges have been restricted to a single sample from an individual or small number of individuals within a population [7–12]. Analysing multiple samples within individuals will give insights into the variation in the macromolecule composition within an individual sponge.

We report here the first analysis of the products of central metabolism of the marine demosponge, *Amphimedon queenslandica* from the Southern Great Barrier Reef. We have quantified the protein, lipid, carbohydrate, DNA and RNA content of this sponge. These analyses are supplemented with a detailed analysis of amino acid and fatty acid composition. By analysing multiple areas within multiple individuals within one *A. queenslandica* population we reveal marked variation within and between sponges for most of these macromolecular classes. These results, along with the extensive genomic resources available for this demosponge [18], provide a strong foundation for future detailed understanding of the metabolic pathways that contribute to biomass production.

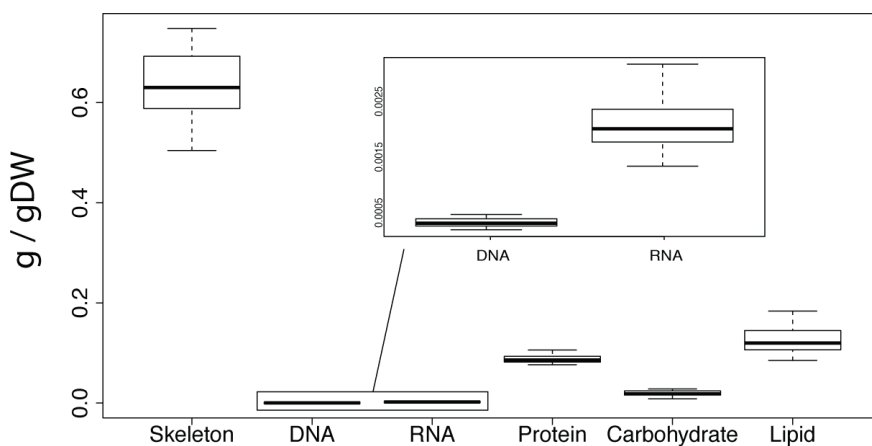


## 2. Results

### 2.1. Displacement to Dry Weight Composition Conversion Factor

Metabolic flux analysis requires the ability to quantify the biomass involved in the turn-over of the substrate. In order to relate the amount of live sponge to the dry weight composition, we established a correlation between displacement volume of a sponge piece and its dry weight. The displacement volume and dry weight from 97 samples were used to estimate a conversion factor of 0.091 (std. dev. = 0.012) grams of dry sponge weight (gDW) per mL of displacement.

**Figure 1.** Mean skeleton and macromolecular composition of *A. queenslandica* calculated from all biomass samples summarised in Table 1. The box represents the upper and lower quartile, split by the mean value. The upper and lower whiskers denote the minimum and maximum values. Units are grams per gram of dry weight.



### 2.2. Overall Macromolecular Composition

For each biochemical analysis, we analysed five biopsies from several parts of four *A. queenslandica* individuals, all of which were collected from a single wild population in Shark Bay on Heron Island Reef, Australia (for detailed methods see Section 4). This sampling regime allowed us to document biochemical differences both within and between individual sponges. Analysis of mean values of the macro-components shows the skeleton (0.6342 g/gDW) to be the dominant component of the dry weight of *A. queenslandica* (Figure 1 and Table 1). The most abundant macromolecule type was lipid with 0.1251 g/gDW, followed by protein (0.0881 g/gDW), carbohydrate (0.0197 g/gDW), RNA (0.0021 g/gDW) and DNA (0.0003 g/gDW). The coefficient of variation revealed that carbohydrates were the most variable, followed by DNA, RNA, and lipids (Table 1). Protein and skeleton had the least overall variability (Table 1).

**Table 1.** Mean skeletal and macromolecular composition of *A. queenslandica* calculated from all biomass samples.

Macro-Component	Mean (g/gDW)	Standard Deviation	Standard Error	Coefficient of Variation (%)	<i>n</i>
Skeleton	0.6343	0.0647	0.0152	9.81	18
Lipid	0.1252	0.0251	0.0058	20.09	19
Protein	0.0881	0.0082	0.0018	9.31	20
Carbohydrate	0.0197	0.0055	0.0012	27.53	20
RNA	0.0021	0.0005	0.0001	22.24	20
DNA	0.0003	0.0001	0.00002	25.78	19

### 2.3. The Source of Variation in the Overall Composition

We used a linear mixed effects model to investigate how much of the variation observed in the mean values (Table 1, Coefficient of variation column) was attributable to the between-individual variation. Over half of the variation seen in the skeleton (58%) and lipids (54%) was due to differences between individuals. The significance of this relationship was tested using a  $\chi^2$  test. The variation of skeleton ( $p = 0.009$ ) and lipids ( $p = 0.016$ ) between individuals had significant effects on the overall variation of both macromolecule types (Table 2). Figure 2 shows the variation seen within each individual for the respective macro-components.

**Table 2.** The source and degree of variation.

Macro-Component	Percentage of Overall Variation Caused by between Individual Variation (%)	$\chi^2$	<i>P</i> -value
Skeleton	58	6.691	0.009
Lipid	54	5.763	0.016
Protein	24	1.393	0.237
Carbohydrate	15	0.597	0.439
RNA	1	2.309	0.128
DNA	32	$3.53 \times 10^{-8}$	0.999

### 2.4. Fatty Acid and Sterol Analysis

The lipid extractions were analysed using a fatty acid methyl ester (FAME) analysis using gas chromatography-mass spectrometry (GC-MS). We were interested in the main components that contribute to forming sponge lipids. Compounds were considered essential if they were found in most of the 23 replicate pieces of sponge. Eleven fatty acid (FA) compounds were identified and confirmed with standards. Palmitic acid was the most abundant FA, contributing 98.14  $\mu\text{mol/gDW}$ . Octadecanoic acid (62.21  $\mu\text{mol/gDW}$ ) and an unknown FA (UU4-FA, 71.749 in Table 3) were other significant FAs. Three additional compounds matched compounds in the NIST database but were not confirmed with a standard (Table 3), this included cholesterol. Based on the fragmentation patterns, eleven compounds were classified as unknown FAs and one as an unknown sterol, highlighting the diversity and complexity of the lipid metabolism in *A. queenslandica*. If the total

area under all peaks in the chromatogram is assumed to represent the total lipid fraction, then the main FA and sterols reported here cover 82.5% of the lipid fraction.

**Figure 2.** Variation of the composition of macro-components within and between individuals of *A. queenslandica*. Four individual sponges were sampled for each macromolecule. Each box and whisker plot represents samples collected from an individual sponge. The box represents the upper and lower quartile, split by the mean value. The upper and lower whiskers denote the minimum and maximum values. All of the components apart from DNA showed marked variation between and within individual sponges.

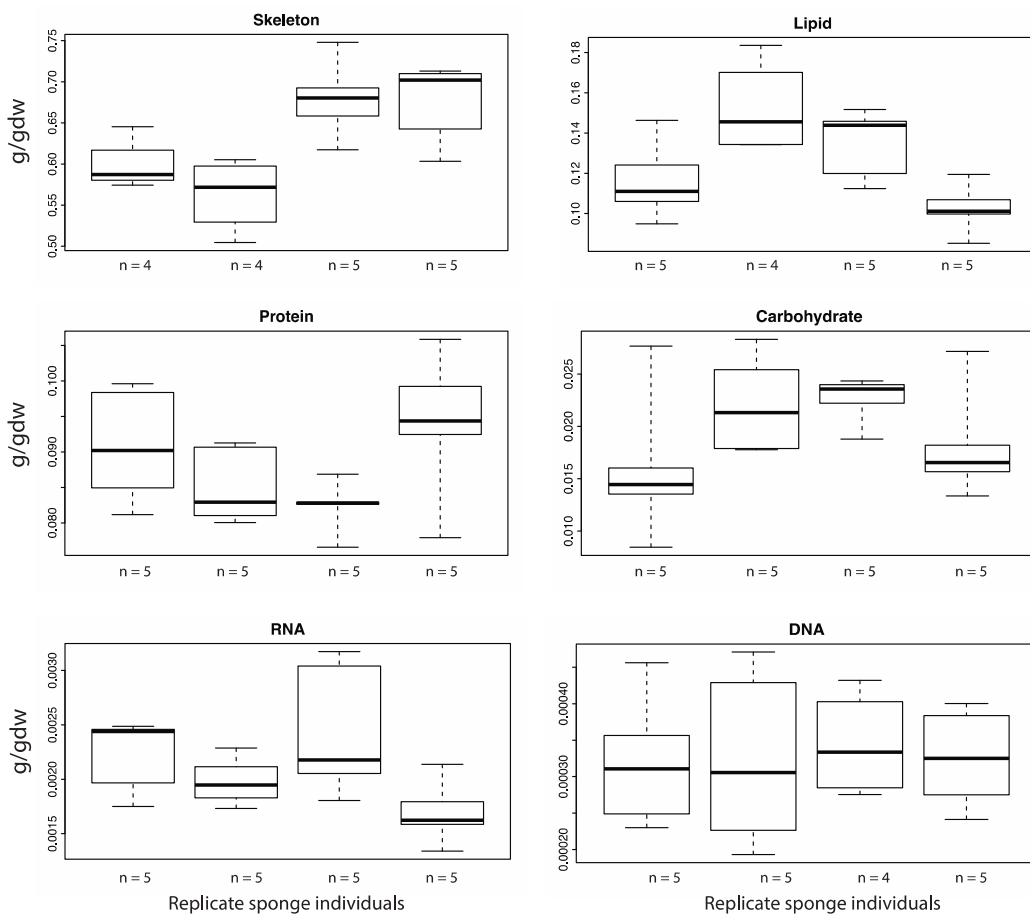


**Table 3.** Main compounds that contribute to the lipid biomass.

Compound	Lipid Number	$\mu\text{mol/gDW}$	Standard Deviation
<b>Fatty Acids</b>			
Docosanoic acid FAME	C22:0	9.769	4.299
Eicosanoic acid FAME	C20:1	1.947	0.579
Erucic acid FAME	C22:1 $\omega$ 9	1.721	0.668
Heptadecanoic acid FAME	C17:0	0.922	0.234
Myristic acid FAME	C14:0	3.957	1.455
Nervonic acid FAME	C24:1 $\omega$ 9	10.090	3.451
Octadecanoic acid FAME	C18:0	62.210	19.095
Palmitic acid FAME	C16:0	98.140	22.426
Pentadecanoic acid FAME	C15:0	7.065	2.468
Tetracosanoic acid FAME	C24:0	6.769	3.546
Tricosanoic acid FAME	C23:0	1.147	0.323
11-Eicosenoic acid FAME *	C20:1 $\omega$ 9	5.342	1.737
U6-FA **		1.005	0.580
U7-FA **		5.973	3.845
U8-FA **		2.279	0.722
U10-FA **		3.288	3.014
UU2-FA **		7.732	2.805
UU3-FA **		5.669	1.897
UU4-FA **		71.749	17.820
UU7-FA **		0.690	0.604
UU8-FA **		4.215	2.155
UU9-FA **		29.843	10.551
UU11-FA **		4.460	1.846
UU1 ***		1.728	1.766
UU6 ***		9.617	4.268
<b>Sterols</b>			
Cholesterol *		4.706	2.477
Brassicasterol *		7.581	4.806
UU13-sterol **		6.264	3.375

\* Compounds that did not match a compound in the standard mix but matched a compound in a database;

\*\* interpreted from the fragmentation pattern; \*\*\* compounds that are neither FA nor sterols.

### 2.5. Amino Acid Analysis

We analysed the amino acid composition of 20 samples of complete sponge biomass (Table 4). Samples of biomass were lyophilized and the hydrolysis incubation time was optimized before quantifying the amino acids with high performance liquid chromatography (HPLC). We found glycine to be the most abundant amino acid with 4.582 mmol/gDW, followed by alanine (1.538 mmol/gDW). Due to the oxidation of asparagine and glutamine to aspartate and glutamate respectively during acid hydrolysis, a 50:50 abundance ratio was assumed between asparagine:aspartate and glutamine:glutamate. Tryptophan (0.089 mmol/gDW), tyrosine (0.157 mmol/gDW), and histidine (0.110 mmol/gDW) were the least abundant amino acids. Tryptophan

and methionine are known to be degraded during the hydrolysis. While methionine was not detected tryptophan was measurable but *in vivo* concentrations may be higher than what was observed. Neither cysteine, nor cystine was measured with the methods used and thus not reported.

**Table 4.** Mean amino acid composition of complete sponge biomass.

Amino Acid	mmol/gDW	Standard Deviation (mmol/gDW)	Amino Acid Contribution (mol/mol)
ALA	1.538	0.565	0.097
ARG	0.694	0.258	0.044
ASP	0.841	0.312	0.053
ASN	0.841	0.312	0.053
GLN	0.767	0.287	0.048
GLU	0.767	0.287	0.048
GLY	4.582	1.702	0.289
HIS	0.110	0.042	0.007
ILE	0.402	0.149	0.025
LEU	0.597	0.222	0.038
LYS	0.688	0.268	0.043
PHE	0.369	0.137	0.023
PRO	1.050	0.387	0.066
SER	0.806	0.318	0.051
THR	0.826	0.304	0.052
TRP *	0.089	0.053	0.006
TYR	0.157	0.060	0.010
VAL	0.753	0.281	0.047

\* Tryptophan is largely destroyed during the hydrolysis, so concentrations *in vivo* may be higher than observed.

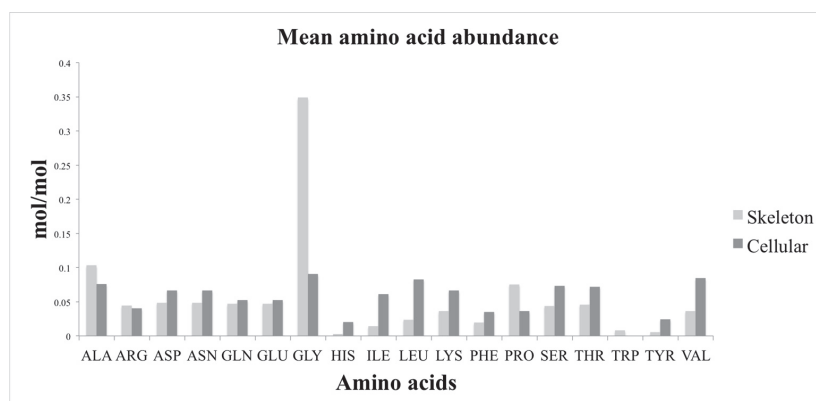
The skeleton is the most abundant component in *A. queenslandica* and is comprised of inorganic silica spicules and a collagen based extracellular matrix. Sponges produce a specific collagen, called spongin [19]. As the skeleton contributes significantly to the overall sponge composition, we analysed the amino acid composition of the skeleton (Table 5). The hydrolysis incubation time was optimized before the analysis was performed on 20 samples. As above, a 50:50 ratio between aspartate and asparagine and between glutamine and glutamate was assumed. The most abundant amino acids in the skeleton were glycine with 4.248 mmol/gDW and alanine with 1.257 mmol/gDW. The least abundant amino acids were tyrosine (0.066 mmol/gDW) and histidine (0.034 mmol/gDW).

A comparison of the relative amino acid composition of the skeleton and the cellular component revealed that glycine was the most abundant amino acid for both components (Figure 3). The skeleton had relatively more glycine, proline, and alanine than the cellular fraction. The cellular fraction had a higher relative abundance of isoleucine, leucine, and valine than the skeleton. Histidine and tyrosine were the least abundant of the amino acids measured for both the skeleton and cellular components.

**Table 5.** Mean amino acid composition of the skeleton.

Amino Acid	mmol/gDW	Standard Deviation (mmol/gDW)	Amino Acid Contribution (mol/mol)
ALA	1.257	0.537	0.103
ARG	0.545	0.226	0.045
ASP	0.594	0.250	0.049
ASN	0.594	0.250	0.049
GLN	0.573	0.243	0.047
GLU	0.573	0.243	0.047
GLY	4.248	1.807	0.349
HIS	0.034	0.016	0.003
ILE	0.176	0.080	0.014
LEU	0.290	0.121	0.024
LYS	0.442	0.173	0.036
PHE	0.239	0.102	0.020
PRO	0.916	0.351	0.075
SER	0.534	0.211	0.044
THR	0.559	0.226	0.046
TRP	0.100	0.041	0.008
TYR	0.066	0.028	0.005
VAL	0.440	0.177	0.036

**Figure 3.** A comparison of the relative amino acid composition of the cellular biomass and the skeleton. The amino acid composition of the cellular components was calculated by subtracting the quantified amino acid values of the skeleton (Table 5) from the values for the complete sponge biomass (Table 4). The skeletal and estimated cellular amino acid values were then normalized by converting to percentages.



## 2.6. Nucleotide Composition

The molar contribution of nucleotides to the DNA and RNA composition was estimated using available genome and transcriptome data. The genomic GC content was estimated to be 31.14% using the publicly available genome [18]. The RNA GC content was estimated to be 39.76%, using

an adult transcriptome [20]. These percentages were then converted into micromoles per gram of dry weight, using the molecular weight of a polymerized nucleotide (Tables 6 and 7).

**Table 6.** Deoxyribonucleotide composition.

	MW (g/mol)	mol/ mol DNA	μmol/gDW
dAMP	313	0.3443	0.37
dCMP	289	0.1557	0.17
dGMP	329	0.1557	0.17
dTMP	304	0.3443	0.37

**Table 7.** Ribonucleotide composition.

	MW (g/mol)	mol/ mol DNA	μmol/gDW
AMP	313	0.3012	2.03
CMP	289	0.1988	1.34
GMP	329	0.1988	1.34
UMP	308	0.3012	2.03

### 3. Discussion

#### 3.1. Macromolecule Composition

To gain insights into how sponges produce biomass, the complex metabolic processes must be investigated as a complete functioning system. The systems biology approach of genome scale metabolic modeling requires the biochemical composition of the organism to be known. The biochemical composition identifies the products of central metabolism that contribute to growth. With the products of central metabolism known, the synthesis pathways can be identified and the fluxes of metabolites modeled. As a first step towards genome scale modeling, we analysed the macromolecular abundance and composition of the marine sponge *A. queenslandica* and investigated the variation seen across the population and within individuals.

The skeleton was the dominant component of the biomass, contributing 63% of the dry weight. Lipids and protein were the most abundant macromolecules, while carbohydrates were the most variable (Table 1). Variation in the amount of skeleton and lipids between individual sponges had significant effects on the overall variability of the respective macro-components (Table 2). The apparent variation in the abundance of macromolecules within an individual (Figure 2) was not significant and had limited effect on the overall population variability. This implies that not only do the central metabolic pathways have an overall response to the individual's microenvironment, but localised stimulus could also cause compositional differences across an individual. This highlights the need for compositional and metabolic studies to sample appropriately to ensure accurate representation.

Overall, the macromolecular composition of *A. queenslandica* in the current study fits within the ranges reported for protein, lipids, and carbohydrates for 71 tropical marine sponge species [7]. *A. queenslandica* notably contained more lipids than protein (Table 1), a characteristic that has been reported previously for two marine demosponges, *Aplysinia archeri* and *Plaktortis*

*halichondroides* [7]. The high lipid content in *A. queenslandica* could indicate the accumulation of energy storage products in response to increased food availability and, thus, variably depending on food abundance. Alternatively, Elvin [8] found that, for *Haliclona permollis*, an increase in lipid content was associated with oogenesis and the formation of mesenchymal amoebocytes. Although *A. queenslandica* is reproductively active year round, larval production peaks in the warmer months [21]. It is not clear if oogenesis is the reason for the high lipid content as the sampling time of this study corresponds with the end of summer when reproductive output is starting to decline. In addition, *A. queenslandica* concentrates its oocytes and embryos in localised brood chambers [21], unlike many sponges, suggesting that these levels should vary markedly within an individual sponge.

In *A. queenslandica*, the cellular biomass accounts for less than half of the dry weight. We defined the skeleton as the solid, inorganic spicules and the flexible, organic collagen. The skeleton, being a product of cellular metabolism, is a considerable sink of metabolic resources, accounting for 64% of the total dry weight (Table 1). The amount of skeleton in *A. queenslandica* is within the ranges of both Antarctic [12] and tropical [7] sponges. The high skeletal requirement by all sponges, greater than 50% dry weight, is likely due to the lack of defined tissues, including connective tissues, that are required to support complex body plans. Without the significant support and framework that the skeleton provides, sponges would not be able to achieve the sizes observed across the phylum [22].

Although sponges do not have defined tissues, the distribution of cells in *A. queenslandica* does not appear to be even if DNA is used as a proxy for cell number. This could be in part due to the large size range of sponge cells, as smaller cells are able to occupy less space yet all cells contain the same amount of DNA. Cells typically contain more RNA than DNA [23], and this is also the case for *A. queenslandica*, in which RNA was more abundant than DNA.

### 3.2. The Variation in Macromolecule Composition

Metabolic networks are dynamic, plastic, and redundant [23]. These characteristics have evolved to give organisms the flexibility to rapidly adapt to variations in environment or external stimulus [23]. As the aim of this study is to gather baseline data for use in metabolic modeling, we sampled different individuals and took sub-samples within each individual to investigate the source of potential variation. This is important information that will help guide future work. There was marked variation both between and within individual sponges in the abundance of macromolecules (Figure 2).

The skeleton was the most abundant component, and the variation in between-individual abundance was shown to have a significant effect on the overall population variation. The skeleton is the structural support for the cellular biomass and it guides the irregular canal network through which water is pumped to supply food and oxygen [14]. The variability seen in the amount of skeleton is likely a result of *A. queenslandica*'s encrusting-lobate growth form [24], combined with the irregular substrate and different structural requirements of specific internal features, such as canals and brood chambers.

It was previously mentioned that the high lipid content could be due to the reproductive state of the population. The reproductive state would also explain the variability in the lipid content within



an individual. *A. queenslandica* forms localised brood chambers where embryos are matured before release [25] and not all of the biopsies would have contained brood chambers.

The variation in macromolecule composition may underlie the metabolic responses of the sponge to an unpredictable and competitive environment. Thus, at the scale of within an individual, differences in microhabitat such as food abundance, predatory pressures and conflicts for space can influence the macromolecular composition. This is potentially exacerbated by the nature of the biochemical assays and the error associated with correcting for salt content. Our results reveal significant effects of between-individual variation and a lesser effect of within-individual variation. This indicates that future work on the composition or metabolic processes of *A. queenslandica* should maintain a minimum of four representative individuals, supplemented with at least some subsampling within each individual. Care should still be taken with experimental design as this dataset is representative of a single metabolic state, and assumptions relating these results to different seasonal or ontogenetic stages should be made with caution. These results highlight the importance of biomass composition analysis, rather than the use of literature values.

### 3.2. Fatty Acid and Sterol Composition

The lipidome consists of a mixture of fatty acids and sterols, of which sponges are renowned for their diversity and often unique compounds [26–29]. Despite this diversity among FA structures in sponges, there are no clear or reliable taxonomic trends [26,28]; this can in part be attributed to the microbial communities associated with sponges [28]. We did not want to focus on identifying each compound in the lipid fraction as this is not necessary for modeling the sponge holobiont and performing flux balance analysis. As the precursor molecule for all lipid synthesis is acetyl coenzyme A, flux balance analysis may be performed if the contribution of lipids towards the overall biomass is known. We identified what compounds matched our databases as their inclusion will increase the models accuracy. Unidentified compounds were classified as FAs, sterols or neither based on their fragmentation pattern.

The two most abundant FAs in *A. queenslandica* were palmitic acid and octadecanoic acid. Both of these FAs are common in nature and have been reported in sponges previously [30–34]. Palmitic acid is a precursor with chain elongation, desaturation and addition of side chain modifications possible [35]. Apart from pentadecanoic acid (15:0) and heptadecanoic acid (17:0), the remaining identified FAs are long chain FA. FA with carbon chain length 20 (eicosanoic acid), 22 (docosanoic acid) and 24 (tetracosanoic acid), along with desaturated FAs of the same length (11-eicosanoic acid, erucic acid and nervonic acid, respectively) were identified as contributing to biomass formation. All of these FAs have been reported in sponges previously (see references above). Eleven out of twenty-three FAs considered important for biomass production were unknown. Sponges, and their associated bacteria, have been shown to produce extensive modifications including methylation [28] and hydroxylation [33] that would prevent the matching of novel compounds to commercial FA databases. This diversity and high number of unknown compounds highlights the complexity of the *A. queenslandica* lipidome and the potential for novel compound discovery.

The FAME analysis also identified the sterol fraction of the extracted lipids. The three sterols that fit our criteria of contributing to the overall biomass were brassicasterol, cholesterol, and an unknown sterol (UU13). Surprisingly, the most abundant of these was the brassicasterol, a plant steroid hormone [35] that is synthesized by terrestrial and marine plants, including macro and unicellular algae. Brassicasterol has been previously reported in a range of filter feeding and grazing marine invertebrates including sponges [36], gorgonian corals (Cnidaria; Anthozoa; Octocorallia; Gorgonacea) [37] and sea urchins (Echinodermata; Echinozoa; Echinoidea) [38]. In these other classes of animals, brassicasterol is a minor sterol and its presence could be a result of dietary uptake. This is likely the case for the *A. queenslandica* holobiont, as neither animals nor bacteria have been shown to synthesize brassicasterol [36–38]. Nevertheless, the high abundance implies an important biological function that this study is unable to discern. While brassicasterol is an unusual, dominant sterol for an animal, cholesterol is considered an important component of all cellular membranes in animals [23]. The concentration of cholesterol in a membrane performs two important functions. The overall fluidity of a membrane is regulated by the amount of cholesterol. Increases in cholesterol content reduce the fluidity of the membrane and permeability of neutral ions [39]. Membrane bound cholesterol can also act as a promoter or inhibitor of membrane bound protein reactions [40]. Additionally, cholesterol functions as an important substrate molecule for bioactive compounds and other sterols, including brassicasterol [35]. Without identifying the second most abundant sterol, UU13, we are unable to infer its biological role, or synthesis pathway.

### 3.3. Amino Acid Composition

Analysing the amino acid composition identifies the relative amounts of precursor molecules that are required to synthesis the protein component of the biomass. When complemented with information from genome scale modeling of the synthetic pathways that are present in an organism, these data allow for the identification of essential amino acids that cannot be produced by the organism [5]. Subsequent flux analysis can identify bottlenecks where the high requirement of a compound for biomass synthesis slows overall growth. The protein component of *A. queenslandica* comprises of two distinct products of metabolism. The overall sponge biomass consists of soluble, cellular derived protein, and an insoluble, extracellular protein matrix. This extracellular matrix is dominated by a sponge specific collagen called spongin [19], which is the main component of the sponge skeleton.

We defined the skeleton of *A. queenslandica* as the inorganic silica spicules, together with the organic collagen matrix. Collagen is an important structural component of metazoans. We found that the spongin in *A. queenslandica* contained 34.9% glycine (Table 6). This is close to the values reported for *Chondria reniformis* (30.5%) ([41], *Scypha graminea* (31.5%–32.3%) [42] and *Ircinia* sp. (32.3%) [43]. Alanine (10.3%) and proline (7.5%) were the next two most abundant amino acids (Table 6) and are very close in abundance to the values of these other sponges. Although the amino acid composition of sponge collagens is well documented [41–43], the amino acid composition of the complete sponge biomass has not been reported.

The complete amino acid composition may give insights into the many primary cell culture attempts that so far have had limited success [44]. Many studies have utilised mammalian cell

culture media, with and without serum [44]. A comparison of the amino acid composition of the complete *A. queenslandica* biomass (Table 4) with a hybridoma cell line [45] revealed nine amino acids that are at least twice as abundant in *A. queenslandica*. Proline and glycine stand out at 3.3 and 8.5 times more abundant in *A. queenslandica* than the hybridoma line. If we use DMEM F12 medium as an example of mammalian cell culture media, both proline and glycine are minor contributors to the amino acid fraction [46] and could present significant bottlenecks for the production of biomass. In addition, due to the different amino acid bias in serum compared to sponge biomass, in the serum experiments excess waste amino acids could lead to growth limitations and may point to necessary changes in the approach to sponge cell culture.

We analysed the amino acid composition of the complete sponge biomass. From this we were able to estimate the average amino acid composition of the cellular fraction by subtracting the average composition of the skeleton. Values were then normalized for comparison by converting to a percentage. This showed that the cellular composition was distinct from the skeleton. The skeleton proportionally contained more glycine, alanine and proline than the cellular biomass. These three amino acids are key in giving collagen its triple helix shape and physical properties [23]. Amino acids that are essential in higher animals—in particular isoleucine, leucine, and valine [23]—were proportionally higher in abundance in the cellular biomass than in the skeleton. Whether these are also essential amino acids for *A. queenslandica* is yet to be shown.

## 4. Experimental Section

### 4.1. Sample Collection and Preparation

*A. queenslandica* were collected from Shark Bay, Heron Island, Australia (23°26'37.92" S, 151°55'8.81" E). Individual sponges and their coral rubble substrate were collected with a hammer and chisel [25] and transported submerged to the Heron Island Research Station. Sponges were held in a flow through aquaria system and processed within 8 h of collection. Biopsy samples were collected from a total of 29 sponges. The samples were cut with a sterile scalpel and contained a representative cross section of sponge biomass that consistently included the pinacoderm layer through to biomass just above the substratum. A thin layer of biomass was removed from the bottom of the sponge to avoid contamination by the substrata. Pieces of sponge biomass that had foreign material incorporated were avoided. To investigate the variation in composition within individual sponges, biopsies were collected from each sponge in multiples of 5. This resulted in 20 sponge samples per analysis, comprising 5 biopsy samples each of 4 individual adult sponges. Samples were snap frozen in liquid nitrogen then stored at  $-80^{\circ}\text{C}$  and transported at on dry ice. Lyophilisation was performed overnight. Dry weights were recorded on an analytical balance and corrected for salt content by multiplying the amount of water lost through lyophilisation by the specific gravity of seawater. We assumed that the salt content of the cells was the same as the seawater. Throughout the study, the weight of each reagent in each reaction was recorded. The specific gravity of each reagent was then used to ensure that accurate calculations were made.

#### 4.2. Skeleton Dry Weight

Cellular material was removed from the *A. queenslandica* biopsies by re-hydrating with a 2% SDS solution made with MilliQ water and incubating for 2 h at room temperature on a shaker table. The biopsies were then washed thoroughly for 5 min with running RO water. The SDS incubation and washing times were optimized by inspecting with a Nikon Eclipse Ti-E inverted microscope (Nikon, Tokyo, Japan) to ensure all cellular material was removed. The pieces were then lyophilised overnight and dry weights recorded. These samples were stored at  $-80^{\circ}\text{C}$ .

#### 4.3. Nucleic Acids

DNA was quantified by Hoechst fluorescence assay. The lyophilised samples from 4.1 were re-hydrated with 3.0 mL of TE buffer (pH 8.0) with 0.01 g/mL lysozyme and incubated at  $37^{\circ}\text{C}$  for 1 h on a shaker table set to 100 rpm. Re-hydrating the lyophilised biopsies caused complete lysis of the *A. queenslandica* cells, but not the bacterial fraction. Lysozyme was added to ensure lysis of the bacterial fraction. After incubation, sterile tweezers were used to remove the sponge skeleton from the tube. The piece of skeleton was squeezed and rolled against the inside wall to ensure that the lysis buffer was retained. Samples were then vortexed and centrifuged for 5 min at 4000 g to pellet cellular debris. Aliquots of the supernatant were used in the Hoechst fluorescence assay. Calf thymus DNA was used to generate a standard curve [47]. All samples and standards were measured in triplicate.

RNA content was quantified by digesting the lyophilised samples from 4.1 with 3.0 mL of 0.3 M KOH for 1 h at  $37^{\circ}\text{C}$  [48]. The reaction was then acidified with the addition of 1.0 mL of 3 M perchloric acid. [49]. Following centrifugation to remove DNA and protein, the RNA-containing supernatant was quantified in triplicate by UV absorbance at 260 nm [48].

The nucleotide composition of both the DNA and RNA was calculated using the GC content of the genome and an adult transcriptome. The calculations assumed that the DNA and RNA is all sponge derived as the bacterial genomic and transcriptomic sequence data, in addition to bacterial diversity and abundance data is not yet available. The GC content of the *A. queenslandica* genome and adult transcriptome are 31.14% [18] and 39.76% [20], respectively. The percentage contribution of each nucleotide was calculated, assuming an even guanine-cytosine and thymine-adenine/thymine-uracil ratios. Next the average molecular weight of one nucleotide was calculated. This was done by multiplying the abundance of each nucleotide by its molecular weight. These values were then added together to give the average molecular weight. This was multiplied by the mean total amount of DNA or RNA (g/gDW) to give the number of mols of average nucleotide per gram of dry weight. The amount of each nucleotide (mols) was then calculated using this value and the guanine-cytosine to thymine-adenine/thymine-uracil ratios. Values were converted to micromoles for reporting.

#### 4.4. Protein

Sponge biopsies from 4.1 were digested with 3.0 mL of 1.0 M NaOH incubated at  $95^{\circ}\text{C}$  for 5 min. The reaction was cooled in iced water and then centrifuged at  $4000\times g$  for 5 min to pellet

suspended skeleton solids. The supernatant was assayed in triplicate using the Coomassie Plus™ (Bradford) Assay Kit (Thermo Scientific, Rockford, MI, USA). Bovine serum albumin was used as the standard [50].

#### 4.5. Carbohydrate

Carbohydrate content was quantified using the phenol-sulfuric acid method [51]. The sponge biopsies from 4.1 were rehydrated with 1.0 mL of MilliQ water. 5.0 mL of concentrated sulfuric acid was added and the reaction let proceed for 10 min. The reaction was rapidly cooled by placing the tube in iced water for 1 min. [52]. 50  $\mu$ L of phenol was added and incubated for 30 min in a water bath set to 25 °C. The reaction was diluted 1:50 using concentrated sulfuric acid and the absorbance read at 488 nm. All measurements were taken in triplicate and glucose was used as the standard [52].

#### 4.6. Lipid

Biopsy samples from 4.1 were rehydrated with 1.0 mL MilliQ water and extracted overnight with 3:2 hexane:isopropanol [53]. 5.0 mL of 0.47 M NaSO<sub>4</sub> was added, mixed and then separated by centrifugation at 4000 $\times$  g for 5 min. The hydrophobic upper hexane phase contains the lipid fraction and was transferred to a clean glass tube. The initial solution was washed with 7:2 hexane:isopropanol to ensure that all of the lipids were recovered [53]. This second hexane phase was again recovered with centrifugation and combined with the first extract. The combined hexane extracts were evaporated under a constant flow of nitrogen to prevent oxidation. The remaining solid lipids were quantified gravimetrically. The lipid solid was then stored under nitrogen at -80 °C for fatty acid analysis.

#### 4.7. Fatty Acids and Sterols

A fatty acid methyl ester (FAME) analysis was performed on the extracted lipids as previously described [54]. The lipid solid was dissolved in hexane and 5.1  $\mu$ g of nondecanoic acid (Sigma-Aldrich, St. Louis, MO, USA) was used as an internal standard (ISTD) to a final concentration of 3.6  $\mu$ g/mL. Saponification, methylation and GC/MS analysis of the lipid mass fraction followed the protocol described in [54]. The software program AMDIS (version 2.64, National Institute of Standards and Technology (NIST), Gaithersburg, MD, USA) was used for the analysis of the fatty acid and sterols. A minimum match factor of 80 and signal threshold of 700 was set for identifying compounds. A FAME library was built using the target ions and retention times of thirty-two known fatty acid standards (Sigma-Aldrich, St. Louis, MO, USA). An alkane (C<sub>7-30</sub>) standard was used as a retention time index. To define compounds important for biomass formation, we used a cut-off of 0.05% of the largest peak in the MS analysis, which means that peaks below those signal intensities would not be reported. For unknown compounds (*i.e.*, that were not identified using the standard library), their fragmentation patterns were compared to the NIST database library (version 2.0, NIST, Gaithersburg, MD, USA). For a range of peaks both the target library as well as the NIST library did not provide accurate hits. Based on manual interpretation of fragmentation

patterns, unknowns that were found consistently in the majority (>75%) of the samples were classified into sterols or fatty acids. From the quantified lipid fraction (g/gDW) the estimated weight of glycerol and phosphate groups was subtracted assuming a glycerolipid to phospholipid ratio of 20:80. It was then assumed that the remainder of the lipid fraction would generate a signal in GC-MS and that the MS response and ionization efficiency for all FA and sterol ions was comparable (due to the unknown character of many FA's this cannot be tested, but individual errors for individual compounds will not impact dramatically on the later modelling). All peak areas were normalized to the total signal generated for that sample. Using the molecular weight of the knowns and an average molecular weight (calculated from all identified FA's and sterols) for the unknowns the individual concentrations were calculated in mol/gDW. A total of 23 separate fractions of biomass were analyzed and the standard deviation was calculated.

#### 4.8. Amino Acids

Amino acid analysis was performed by reversed phase high performance liquid chromatography. 20 samples containing cellular and skeleton components were analysed in addition to 20 samples of skeleton, prepared as above. 5 mL of 6 M HCl was added to each sample and incubated at 105 °C. Hydrolysis times were first optimized and found to be 54 h for the complete biomass samples and 48 h for skeleton samples. Optimization monitored the concentration increase of all amino acids over the time course and 54/48 h was found to be a time at which most amino acids reached the peak concentration. Longer times may favor some compounds but will lead to degradation of others. This compromise was necessary since otherwise individual experiments need to be conducted for all 20 amino acids. Samples were allowed to cool, mixed, and then a 500 µL aliquot was taken and filtered with a 0.22 µm Ultrafree-MC GV centrifugal filter (Merck Millipore, Darmstadt, Germany). The HCl was evaporated by heating to 40 °C under a constant flow of nitrogen. The solid pellet was stored at -80 °C. Derivatisation was performed in a high-performance autosampler (Agilent HiP-ALS SL, G1367C, Santa Clara, CA, USA). 0.5 µL of sample containing 250 µM of internal standards, sarcosine and 2-aminobutyric acid, was added into 2.5 µL of borate buffer (0.4 N, pH 10.2, Agilent PN: 5061-3339, Santa Clara, CA, USA), mixed and incubated for 20 s at 4 °C. 1 µL of OPA reagent (10 mg *o*-phthalaldehyde/mL in 3-mercaptopropionic acid, Agilent PN: 5061-3335, Santa Clara, CA, USA) was then added to initially derivatise primary amino acids. The reaction was mixed and incubated for 20 s at 4 °C. Then 0.4 µL of FMOC reagent (2.5 mg 9-fluorenylmethyl chloroformate/mL in acetonitrile, Agilent PN:5061-3337, Santa Clara, CA, USA) was added, mixed and incubated for 20 s at 4 °C to derivatise the secondary amines proline and sarcosine. 45.6 µL of Buffer A (40 mM Na<sub>2</sub>HPO<sub>4</sub>, 0.02% NaN<sub>3</sub>, pH 7.8) was added to lower the pH of the reaction prior to injecting the 50 µL reaction onto an Agilent Zorbax Extend C-18 column (3.5 µm, 4.6 × 150 mm, Agilent PN: 763953-902, Santa Clara, CA, USA) with a guard column (SecurityGuard Gemini C18, Phenomenex PN: AJO-7597, Santa Clara, CA, USA). Column temperature was kept at 39 °C in a thermostatted column compartment (Agilent TCC, G1316B, Santa Clara, CA, USA). Chromatography was performed using an Agilent 1200-SL HPLC system, equipped with an active seal wash and a degasser (Agilent Degasser, G1379B, Santa Clara, CA, USA). The HPLC gradient was 2%–45% buffer B (45% acetonitrile, 45% methanol and 10%

water) from 0 to 18 min, 50%–60% buffer B from 18.1 to 20 min. 100% buffer B from 20.1 to 24 min, and 2% buffer B from 24.1 to 27 min—using a binary pump (Agilent Bin Pump SL, G1312B, Santa Clara, CA, USA). Flow rate was 2 mL/min. Derivatized amino acids were monitored using a fluorescence detector (Agilent FLD, G1321A, Santa Clara, CA, USA). OPA-derivatized amino acids were detected at 340<sub>ex</sub> and 450<sub>em</sub> nm from 1 to 18 min, and FMOC-derivatized amino acids at 266<sub>ex</sub> and 305<sub>em</sub> nm from 18 to 27 min. Chromatograms were integrated using ChemStation (Rev B.03.02, Agilent, Santa Clara, CA, USA).

#### 4.9. Statistical Analysis

To analyse how the variation between and within individual sponges contributed to the overall variation for each macromolecule separately, the data were fit to a linear mixed effects model using the *nlme* package [55] in R [56].

The amount of macromolecule (g/gDW) was the response variable and Sponge ID (individual) was the random effect. The among-individual variance was divided by the total variance and expressed as the percentage of the overall variability that was due to variation between individuals. To address whether this between-individual variation was significant, we used a likelihood ratio  $\chi^2$  test to compare two models: one with the random effect and one without the random effect.

### 5. Conclusions

As a prerequisite for a systems scale investigation of the metabolic processes responsible for sponge biomass production, we analysed the composition and abundance of the macro-components of *A. queenslandica*. We found the composition to be within the reported ranges for other tropical marine sponges and that there is significant variation in the composition at the population level and notable variation within the biomass of an individual sponge. The skeleton was the most abundant component of the overall biomass, while lipids and protein were the most abundant macromolecules. Further analysis of the fatty acid and amino acids was undertaken. The FAME analysis revealed a diverse and complex fatty acid composition. The composition of the sterols revealed that brassicasterol and an unknown sterol had a higher mean abundance than cholesterol. There was a distinct difference in amino acid composition between the soluble, cellular fraction and the insoluble skeletal component. This highlights the different protein products of metabolism that share the same pool of precursor molecules. This complete analysis of the biochemical composition of *A. queenslandica* provides baseline information that complements the extensive genomic resources available for *A. queenslandica*, a key species for understanding sponge biochemistry and metabolism.

### Acknowledgments

This work was funded by Australian Research Council grants to SMD and BMD in addition to an Australian Postgraduate Award Scholarship to JW. JK was financially supported by the Australian Research Council (No. DE120101549). The authors thank Manuel Plan from Metabolomics Australia for his help with amino acid analysis.

## Author Contributions

JK, SD, and BD initiated the project. JW conducted the fieldwork and performed the macromolecular assays. JW analysed the macromolecular data. TB performed the amino acid and FAME analyses. JW, TB and JK analysed the amino acid and FAME data. JW drafted the initial manuscript. JK, SD and BD edited the manuscript. All authors read and approved the final manuscript.

## Conflicts of Interest

The authors declare no conflict of interest.

## References

1. Blunt, J.W.; Copp, B.R.; Keyzers, R.A.; Munro, M.H.G.; Prinsep, M.R. Marine natural products. *Natl. Prod. Rep.* **2014**, *31*, 160–258.
2. Huyck, T.K.; Gradishar, W.; Kirkpatrick, P. 4 Eribulin mesylate. *Nat. Rev. Drug Dis.* **2011**, *10*, 173–174.
3. Genta-Jouve, G.; Thomas, O.P. *Sponge Chemical Diversity*, 1st ed.; Elsevier Ltd.: Toronto, ON, Canada, 2012; Volume 62, pp. 183–230.
4. Oberhardt, M.A.; Palsson, B.Ø.; Papin, J.A. Applications of genome-scale metabolic reconstructions. *Mol. Sys. Biol.* **2009**, *5*, 1–15.
5. Thiele, I.; Palsson, B.Ø. A protocol for generating a high-quality genome-scale metabolic reconstruction. *Nat. Protoc.* **2010**, *5*, 93–121.
6. Feist, A.M.; Palsson, B.Ø. The biomass objective function. *Curr. Opin. Microbiol.* **2010**, *13*, 344–349.
7. Chanas, B.; Pawlik, J.R. Defenses of Caribbean sponges against predatory reef fish. II. Spicules, tissue toughness, and nutritional quality. *Mar. Ecol. Prog. Ser.* **1995**, *127*, 195–211.
8. Elvin, D.W. The relationship of seasonal changes in the biochemical components to the reproductive behavior of the intertidal sponge, *Haliclona permollis*. *Biol. Bull.* **1979**, *156*, 47–61.
9. Pallela, R.; Koigoora, S.; Gunda, V.G.; Sunkara, M.S.; Janapala, V.R. Comparative morphometry, biochemical and elemental composition of three marine sponges (Petrosiidae) from Gulf of Mannar, India. *Chem. Speciat. Bioavailab.* **2011**, *23*, 16–23.
10. Koigoora, S.; Pallela, R.; Nelakurti, C.R.; Sunkara, M.S.; Janapala, V.R. Morphometric, elemental and biochemical characterisation of three *Haliclona* species (Demospongiae) from the Gulf of Mannar, India. *Chem. Speciat. Bioavailab.* **2013**, *25*, 15–23.
11. Stone, A.R. Seasonal variation in the gross biochemical composition of *Hymeniacidon perleve* (Montagu). *J. Exp. Mar. Biol. Ecol.* **1970**, *5*, 265–271.
12. McClintock, J.B. Investigation of the relationship between invertebrate predation and biochemical composition, energy content, spicule armament and toxicity of benthic sponges at McMurdo Sound, Antarctica. *Mar. Biol.* **1987**, *94*, 479–487.



13. Freeman, C.J.; Gleason, D.F. Chemical defenses, nutritional quality, and structural components in three sponge species: *Ircinia felix*, *I. campana*, and *Aplysina fulva*. *Mar. Biol.* **2010**, *157*, 1083–1093.
14. Hentschel, U.; Piel, J.; Degnan, S.M.; Taylor, M.W. Genomic insights into the marine sponge microbiome. *Nat. Rev. Microbiol.* **2012**, *10*, 641–654.
15. Thomas, T.R.A.; Kavlekar, D.P.; LokaBharathi, P.A. Marine Drugs from Sponge-Microbe Association—A Review. *Mar. Drugs* **2010**, *8*, 1417–1468.
16. Wilson, M.C.; Mori, T.; Rückert, C.; Uria, A.R.; Helf, M.J.; Takada, K.; Gernert, C.; Steffens, U.A.E.; Heycke, N.; Schmitt, S.; *et al.* An environmental bacterial taxon with a large and distinct metabolic repertoire. *Nature* **2014**, *506*, 58–62.
17. Radax, R.; Hoffmann, F.; Rapp, H.T.; Leininger, S.; Schleper, C. Ammonia-oxidizing archaea as main drivers of nitrification in cold-water sponges. *Environ. Microbiol.* **2011**, *14*, 909–923.
18. Srivastava, M.; Simakov, O.; Chapman, J.; Fahey, B.; Gauthier, M.E.A.; Mitros, T.; Richards, G.S.; Conaco, C.; Dacre, M.; Hellsten, U.; *et al.* The *Amphimedon queenslandica* genome and the evolution of animal complexity. *Nature* **2010**, *466*, 720–726.
19. Gross, J.; Sokal, Z.; Rougvie, M. Structural and chemical studies on the connective tissue of marine sponges. *J. Histochem. Cytochem.* **1956**, *4*, 227–246.
20. Fernandez-Valverde, S.L.; Degnan, B.M. *Amphimedon queenslandica* gene reannotation. 2013, Unpublished work.
21. Leys, S.P.; Degnan, B.M. Cytological basis of photoresponsive behavior in a sponge larva. *Biol. Bull.* **2001**, *201*, 323–338.
22. Hooper, J.N.A.; Soest, R.W.M. *Systema Porifera. A Guide to the Classification of Sponges*; Springer US: Boston, MA, USA, 2002.
23. Lehninger, A.; Nelson, D.L.; Cox, M.M. *Lehninger Principles of Biochemistry & eBook*, 5th ed.; W.H. Freeman: New York, NY, USA, 2008; pp. 385–399.
24. Hooper, J.N.; van Soest, R. A new species of *Amphimedon* (Porifera, Demospongiae, Haplosclerida, Niphatidae) from the Capricorn-Bunker Group of Islands, Great Barrier Reef, Australia: Target species for the “sponge genome project”. *Zootaxa* **2006**, *1314*, 31–39.
25. Leys, S.P.; Larroux, C.; Gauthier, M.; Adamska, M.; Fahey, B.; Richards, G.S.; Degnan, S.M.; Degnan, B.M. Isolation of *Amphimedon* Developmental Material. *Cold Spring Harbor Protoc.* **2008**, doi:10.1101/pdg.prot5095.
26. Rodríguez, W.; Osorno, O.; Ramos, F.A.; Duque, C.; Zea, S. Biochemical Systematics and Ecology. *Biochem. Syst. Ecol.* **2010**, *38*, 774–783.
27. Lawson, M.P.; Bergquist, P.R.; Cambie, R.C. Fatty acid composition and the classification of the Porifera. *Biochem. Syst. Ecol.* **1984**, *12*, 375–393.
28. Rod’kina, S.A. Fatty acids and other lipids of marine sponges. *Russ. J. Mar. Biol.* **2005**, *31*, S49–S60.
29. Erpenbeck, D.; Soest, R.W.M. Status and Perspective of Sponge Chemosystematics. *Mar. Biotechnol.* **2006**, *9*, 2–19.

30. Barnathan, G.; Korpnrobt, J.M.; Doumenq, P.; Mirallès, J. New unsaturated long-chain fatty acids in the phospholipids from the axinellida sponges *Trikentrion loeve* and *Pseudaxinella cf. lunaecharta*. *Lipids* **1996**, *31*, 193–200.
31. Carballeira, N.M.; Alicea, J. The first naturally occurring  $\alpha$ -methoxylated branched-chain fatty acids from the phospholipids of *Amphimedon complanata*. *Lipids* **2001**, *36*, 83–87.
32. Christie, W.W.; Brechany, E.Y.; Stefanov, K.; Popov, S. The fatty acids of the sponge *Dysidea fragilis* from the black sea. *Lipids* **1992**, *27*, 640–644.
33. Carballeira, N.M.; Lopez, M.R. On the isolation of 2-hydroxydocosanoic and 2-hydroxytricosanoic acids from the marine sponge *Amphimedon compressa*. *Lipids* **1989**, *24*, 89–91.
34. Nechev, J.; Christie, W.W.; Robaina, R.; de Diego, F.; Popov, S.; Stefanov, K. Chemical composition of the sponge *Hymeniacidon sanguinea* from the Canary Islands. *Comp. Biochem. Physiol. Part A* **2004**, *137*, 365–374.
35. Michal, G.; Schomburg, D. *Biochemical Pathways*; John Wiley & Sons: New York, NY, USA, 2013; pp. 107–122.
36. Erdman, T.R.; Thomson, R.H. Sterols from the sponges *Cliona celata* Grant and *Hymeniacidon perleve* Montagu. *Tetrahedron* **1972**, *28*, 5163–5173.
37. Block, J.H. Marine sterols from some gorgonians. *Steroids* **1974**, *23*, 421–424.
38. Voogt, P.A. Sterols of some echinoids. *Arch. Physiol. Biochem.* **1972**, *80*, 883–891.
39. Haines, T.J. Do sterols reduce proton and sodium leaks through lipid bilayers? *Prog. Lipid Res.* **2001**, *40*, 299–324.
40. Yeagle, P.L. Modulation of membrane function by cholesterol. *Biochimie* **1991**, *73*, 1303–1310.
41. Imhoff, J.M.; Garrone, R. Solubilization and characterization of *Chondrosia reniformis* sponge collagen. *Connect. Tissue Res.* **1983**, *11*, 193–197.
42. Peiz, K.A.; Gross, J. The amino acid composition and morphology of some invertebrate and vertebrate collagens. *Biochim. Biophys. Acta* **1959**, *34*, 24–39.
43. Junqua, S.; Robert, L.; Garrone, R.; Pavans de Ceccatty, M.; Vacelet, J. Biochemical and morphological studies on collagens of horny sponges. *Ircinia* filaments compared to spongines. *Connect. Tissue Res.* **1974**, *2*, 193–203.
44. Schippers, K.J.; Sipkema, D.; Osinga, R.; Smidt, H.; Pomponi, S.A.; Martens, D.E.; Wijffels, R.H. Cultivation of sponges, sponge cells and symbionts: Achievements and future prospects. *Adv. Mar. Biol.* **2012**, *62*, 273–337.
45. Quek, L.; Dietmar, S.; Krömer, J.O.; Nielsen, L.K. Metabolic flux analysis in mammalian cell culture. *Metab. Eng.* **2010**, *12*, 161–171.
46. Freshney, R.I. *Culture of Animal Cells*; Wiley: New Jersey, NJ, USA, 2010; pp. 102–104.
47. Green, M.R.; Sambrook, J. *Molecular Cloning*; Cold Spring Harbor Laboratory: New York, NY, USA, 2012; pp. 68–70.
48. Benthin, S.; Nielsen, J.; Villadsen, J. A simple and reliable method for the determination of cellular RNA content. *Biotechnol. Tech.* **1990**, *5*, 39–42.

49. Fleck, A.; Munro, H.N. The precision of ultraviolet absorption measurements in the Schmidt-Thannhauser procedure for nucleic acid estimation. *Biochim. Biophys. Acta* **1962**, *55*, 571–583.
50. Bradford, M.M. A rapid and sensitive method for the quantitation of microgram quantities of protein utilizing the principle of protein-dye binding. *Anal. Biochem.* **1976**, *72*, 248–254.
51. DuBois, M.; Gilles, K.A.; Hamilton, J.K.; Rebers, P.A.; Smith, F. Colorimetric Method for Determination of Sugars and Related Substances. *Anal. Chem.* **1956**, *28*, 350–356.
52. Rao, P.P.; Pattabiraman, T.N.T. Reevaluation of the phenol-sulfuric acid reaction for the estimation of hexoses and pentoses. *Anal. Biochem.* **1989**, *181*, 18–22.
53. Hara, A.; Radin, N.S. Lipid extraction of tissues with a low-toxicity solvent. *Anal. Biochem.* **1978**, *90*, 420–426.
54. Brennan, T.C.R.; Krömer, J.O.; Nielsen, L.K. Physiological and Transcriptional Responses of *Saccharomyces. cerevisiae* to D-Limonene Show Changes to the Cell Wall but Not to the Plasma Membrane. *Appl. Environ. Microbiol.* **2013**, *79*, 3590–3600.
55. Pinheiro, J.; Bates, D.; DebRoy, S.; Sarkar, D. R Development Core Team. nlme: Linear and Nonlinear Mixed Effects Models. R Package Version 2013. Available online: <http://CRAN.R-project.org/package=nlme> (accessed on 26 October 2013).
56. R Core Team. R: A language and environment for statistical computing. R Foundation for Statistical Computing: Vienna, Austria, 2013. Available online: <http://www.R-project.org/> (accessed on 26 October 2013).

# Type II Collagen and Gelatin from Silvertip Shark (*Carcharhinus albimarginatus*) Cartilage: Isolation, Purification, Physicochemical and Antioxidant Properties

Elango Jeevithan, Bin Bao, Yongshi Bu, Yu Zhou, Qingbo Zhao and Wenhui Wu

**Abstract:** Type II acid soluble collagen (CIIA), pepsin soluble collagen (CIIP) and type II gelatin (GII) were isolated from silvertip shark (*Carcharhinus albimarginatus*) cartilage and examined for their physicochemical and antioxidant properties. GII had a higher hydroxyproline content (173 mg/g) than the collagens and cartilage. CIIA, CIIP and GII were composed of two identical  $\alpha_1$  and  $\beta$  chains and were characterized as type II. Amino acid analysis of CIIA, CIIP and GII indicated imino acid contents of 150, 156 and 153 amino acid residues per 1000 residues, respectively. Differing Fourier transform infrared (FTIR) spectra of CIIA, CIIP and GII were observed, which suggested that the isolation process affected the secondary structure and molecular order of collagen, particularly the triple-helical structure. The denaturation temperature of GII (32.5 °C) was higher than that of CIIA and CIIP. The antioxidant activity against 1,1-diphenyl-2-picrylhydrazyl radicals and the reducing power of CIIP was greater than that of CIIA and GII. SEM microstructure of the collagens depicted a porous, fibrillary and multi-layered structure. Accordingly, the physicochemical and antioxidant properties of type II collagens (CIIA, CIIP) and GII isolated from shark cartilage were found to be suitable for biomedical applications.

Reprinted from *Mar. Drugs*. Cite as: Jeevithan, E.; Bao, B.; Bu, Y.; Zhou, Y.; Zhao, Q.; Wu, W. Type II Collagen and Gelatin from Silvertip Shark (*Carcharhinus albimarginatus*) Cartilage: Isolation, Purification, Physicochemical and Antioxidant Properties. *Mar. Drugs* **2014**, *12*, 385263873.

## 1. Introduction

Type II collagen is a principal component of the extracellular matrix of articular cartilage and constitutes 90%–95% of the total protein content in the cartilage [1]. In the current commercial market, most of the type II collagen is isolated from terrestrial mammalian cartilage due to its high biocompatibility, and it is widely used in the pharmaceutical, food, healthcare, and cosmetic industries [2]. However, the incidences of diseases such as bovine spongiform encephalopathy (BSE) and foot and mouth disease (FMD) have raised concerns about its safety. Alternatively, collagen from fish processing waste may be a suitable substitute. Production of fish collagen and gelatin not only adds significant value to the fish processing sector but also to other pharmacological industries.

Gelatin, a denatured form of collagen, has been extensively studied [3,4]; however, studies related to fish collagen are limited to isolation and characterization [2,5,6]. The functional properties of collagen and gelatin are highly influenced by their molecular structure, amino acid composition and internal linkages, which are affected by the processing conditions.

Recently, several researchers have focused on the oral tolerance of type II collagen to treat autoimmune diseases [1,7]. Oral tolerance is an immunological mechanism by which external agents that enter the body through the digestive system are recognized and ignored by the immune system. The effects of oral administration of type II collagen obtained from bovine, chicken and sheep sources have been evaluated for the treatment of rheumatoid arthritis (RA) [8–10].

The antioxidant activity of collagen is an essential property for the oral tolerance mechanism in autoimmune diseases [11]. Recently, an interest in natural antioxidants has increased because they are widely distributed and safer than synthetic antioxidants. Few studies have been conducted on the antioxidant activity of collagen and gelatin isolated from marine animals, and include sea cucumber skin [12,13], jellyfish skin [14]; squid skin [15] and tuna skin and bone [16]. Recently, Merly and Smith [17] studied the immunomodulatory properties of type II collagen from commercially available shark cartilage capsules. To our knowledge, the physicochemical and antioxidant activities of silvertip shark (*Carcharhinus albimarginatus*) cartilage type II collagen and gelatin have not been examined. Therefore, the present study investigated the physicochemical and antioxidant properties of acid- and pepsin-soluble type II collagens (ASC, PSC) and type II gelatin from silvertip shark cartilage and their potential for further applications.

## 2. Results and Discussion

### 2.1. Biochemical Composition of Shark Cartilage

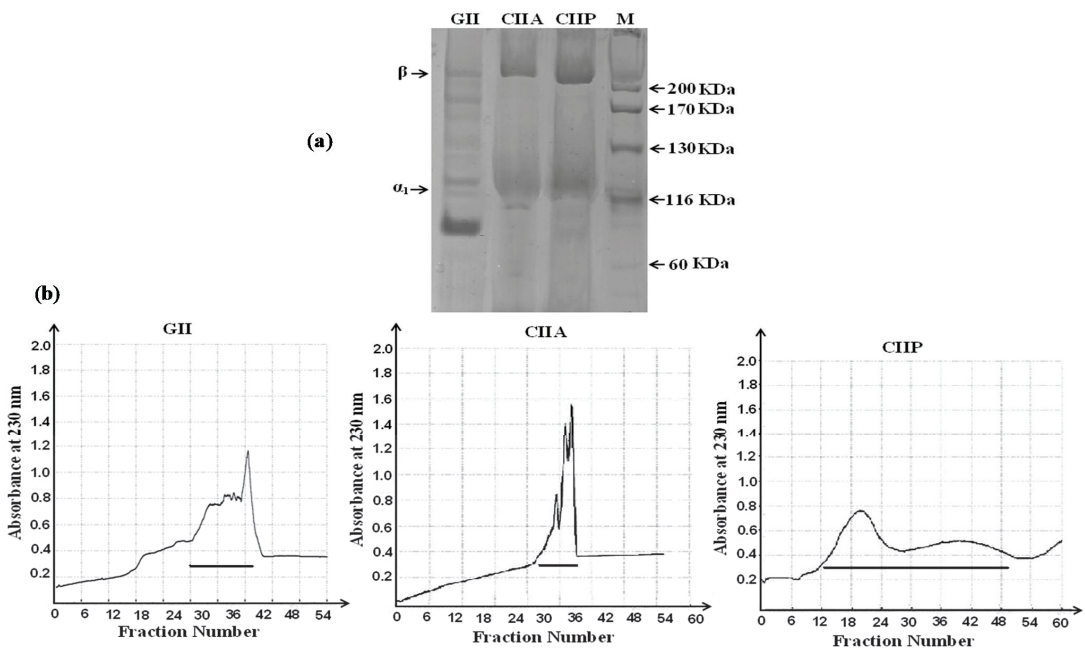
The cartilage ash content was high (25.41%) compared with the protein content (8.95%) (data not shown). This high level of ash was also reported in the cartilage of Amur sturgeon and Nile perch (26.7% and 39.1%, respectively) [18,19]. The generally high ash content of shark cartilage is attributed to its high mineral content [3]. A protein content of 19.2% was reported for another shark species (*Isurus oxyrinchus*) cartilage [20] and was higher than our finding. The moisture and fat content of the silvertip shark cartilage was 63.56% and 1.69%, respectively. Cho *et al.* [20] reported that the fat content of *I. oxyrinchus* shark cartilage was 1.4%, which was lower than in the present report. The moisture, protein, ash and fat contents of cartilage of several species of shark are between 66.84%–78.3%, 14.01%–19.20%, 1.10%–12.09% and 0.21%–1.40%, respectively [20,21]. Fish cartilage generally contains a lower protein content than in skin due to higher ash and fat contents [3].

The hydroxyproline content of shark cartilage was 30.28 mg/g (data not shown), which was lower than that found in CIIA, CIIP and GII. A lower hydroxyproline content of 11.37–13.44 mg/g for shark cartilage was reported by Kittiphattanabawon *et al.* [21]. Variations in the hydroxyproline content among fish species occur because of the differences in their body temperature and seasonal variations. The hydroxyproline content of CIIA, CIIP and GII were 92.7, 113 and 173 mg/g, respectively. Kittiphattanabawon *et al.* [21] reported that hydroxyproline content of PSC and ASC from brownbanded bamboo shark (*Chiloscyllium punctatum*) cartilage was between 103.71 and 104.49 mg/g, which is similar to our findings. Accordingly, silvertip shark cartilage may be a better resource for the isolation of collagen.

## 2.2. Protein Pattern

The degree of purification by gel filtration chromatography and the protein pattern of CIIA, CIIP and GII were evaluated by SDS-PAGE. The purified CIIA and CIIP showed two distinct bands,  $\alpha_1$  and  $\beta$ , with molecular weights of approximately 120 and 210 kDa, respectively (Figure 1a).

**Figure 1.** (a) Electrophoretic pattern of type II collagens and type II gelatin isolated from shark cartilage; (b) Purification of type II collagen and type II gelatin by gel filtration chromatography. The horizontal lines in the chromatograms represent pooled fractions that were analyzed by SDS-PAGE. GII: type II gelatin, CIIA: type II acid soluble collagen, CIIP: type II pepsin soluble collagen.

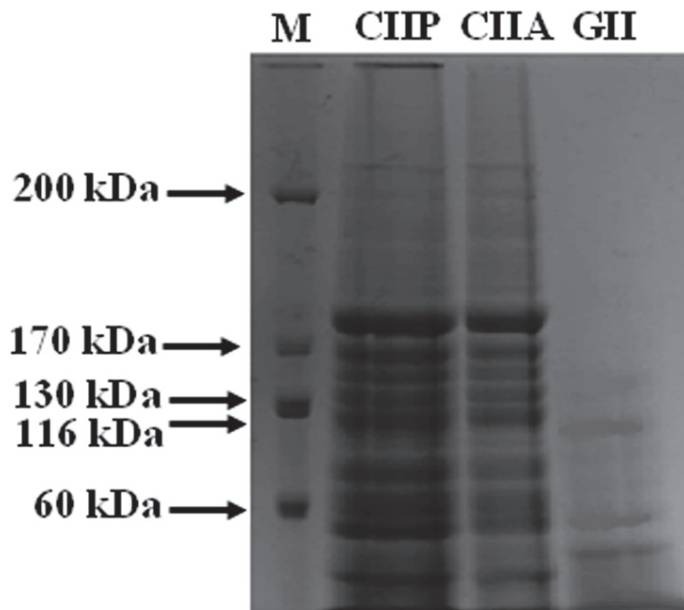


The band intensity of the  $\alpha_1$ -chain was not greater than the  $\beta$  chain in CIIA and CIIP. This may be due to the formation of a  $\beta$  dimer resulting from the inter- and intramolecular cross-linking of the  $\alpha$  component in the collagen structure. A similar protein pattern for type II collagen isolated from the cartilage of sharks and chicks has been reported in several studies [21–23]. When compared with CIIA and CIIP, the mobility of the GII  $\alpha_1$ -chain was lower (approximately 100 kDa) and the band intensity was higher, which may indicate a conversion of the  $\beta$  dimer into the  $\alpha$  component in the heat extraction process. In addition, smaller MW fractions were observed in GII in between the  $\alpha$  component and  $\beta$  dimer, which was attributed to the denaturation of collagen during the isolation process. Therefore, type II collagen isolated from shark cartilage is pure and is composed of two chains, such as  $\alpha_1$  and  $\beta$ , and the secondary structure of collagen was altered by heat extraction.

### 2.3. Peptide Mapping

Shark cartilage type II collagens (CIIA and CIIP) digested by the V8 protease from *Staphylococcus aureus* V8 (EC 3.4.21.19, Sigma–Aldrich, Shanghai, China) exhibited a similar pattern. After hydrolysis, the  $\alpha$  chain and  $\beta$  component of the collagens were degraded into small molecular weight peptides ranging from 180 to 40 kDa (Figure 2). This was in accordance with the peptide pattern for brownbanded bamboo shark cartilage collagen reported by Kittiphattanabawon *et al.* [21]. Peptide mapping revealed that CIIA and CIIP had similar secondary structures. The V8 protease exhibits a high degree of specificity for glutamic acid and aspartic acid residues in proteins [24]. The contents of glutamic acid and aspartic acid residues were higher in CIIP (76.20 and 45.76 residues per 1000 residues, respectively) than CIIA (71.57 and 42.91 residues per 1000 residues, respectively). Therefore, CIIP was more susceptible to hydrolysis by the V8 protease than CIIA, although, a similar pattern of peptide fragments were observed. This result was in accordance with the peptide mapping of ASC and PSC extracted from the skin of the brownstripe red snapper [25].

**Figure 2.** Peptide map of collagen and gelatin isolated form shark cartilage. CIIP: type II pepsin soluble collagen, CIIA: type II acid soluble collagen, GII: type II gelatin, M: Marker.



GII exhibited a different peptide pattern than CIIA and CIIP. The  $\alpha_1$ -chain, as well as high MW cross-linked  $\beta$  components, of GII were completely degraded by the V8 protease and thus more small peptides were observed. This suggests that the  $\alpha_1$ -chain and  $\beta$  components of GII were more susceptible to the V8 protease than CIIA and CIIP. Although GII had lower glutamic acid and aspartic acid contents than the collagens, the degree of hydrolysis was higher in GII. This may be

due to differences in the accessibility of susceptible bonds to the proteinase and to differences in the secondary structure between the collagens and gelatin, which were observed in the FTIR spectra. Hence, the peptide pattern of type II collagens (PSC, ASC) and type II gelatin from shark cartilage may be influenced by internal cross-linking, secondary structure and the composition of amino acids.

#### 2.4. Maximum Absorption

The maximum absorptions of CIIA, CIIP and GII were 238.6, 237.7 and 237.6 nm, respectively (data not shown). The maximum absorption reported for eel skin collagen was similar to our findings [26]. In the present study, shark type II collagens and type II gelatin did not exhibit an absorption peak at 280 nm. This was due to a low tyrosine content (2–8 residues per 1000 residues), which absorbs UV light at 280 nm [27]. Kittiphattanabawon *et al.* [21] stated that no absorption peak of collagen at 280 nm indicates the purity of the collagen and efficacy of non-collagenous protein removal. This indicates adequate efficiency of the collagen and gelatin isolation processes used in this study.

#### 2.5. Amino Acid Composition

CIIA, CIIP and GII extracted from shark cartilage had similar amino acid profiles (Table 1). In general, CIIA, CIIP and GII had high glycine contents (326, 319 and 353 residues per 1000 residues, respectively), which was the primary amino acid followed by alanine and proline. This result was in accordance with other fish collagen studies [18,20,25]. Every third amino acid residue was glycine in the  $\alpha$  chain of collagen, except in the first 14 amino acid residues of the *N*-terminus and the first 10 amino acid residues of the *C*-terminus [28]. Higher contents of glycine, alanine and hydroxyproline were observed in GII compared with CIIA and CIIP. Type II collagens and type II gelatin had low contents of Met, His, Cys and Tyr, which is similar to other fish collagens [2,29,30]. The difference in the amino acid composition between type II collagens and type II gelatin was due to the different isolation processes.

Compared with type II collagens and type II gelatin, shark cartilage contained a lower content of glycine, alanine and proline (310, 122 and 93 residues per 1000 residues, respectively), but a higher amount of glutamic acid, aspartic acid, threonine, tyrosine and cysteine. The removal of non-collagenous protein during the isolation process likely resulted in the changes in the amino acid composition between the raw material and collagens. Imino acid contents of shark cartilage, type II collagens and type II gelatin were from 15.6% to 14.3%, which was relatively lower than that of ASC (21%) and PSC (22%) isolated from brownstripe red snapper skin [25]. CIIA had a lower imino acid content than CIIP and GII. The higher imino acid content of PSC compared with ASC was due to the removal of telopeptides by pepsin digestion [25].



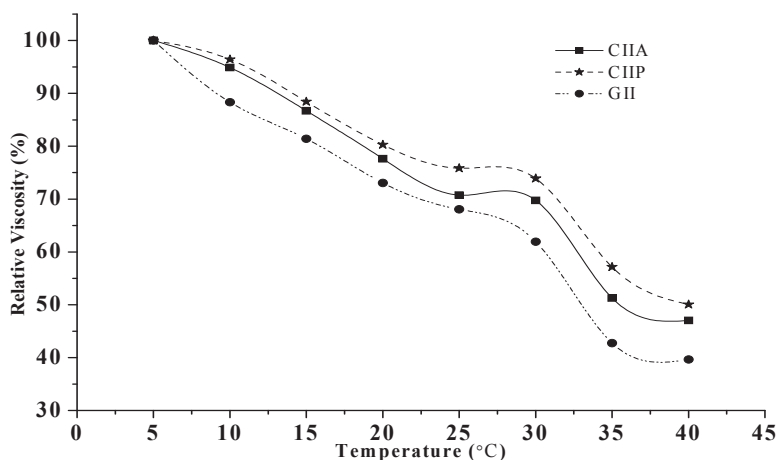
**Table 1.** Amino acid compositions of ASC, PSC and gelatin from shark cartilage (residues/1000 residues). CIIP: type II pepsin soluble collagen, CIIA: type II acid soluble collagen, GII: type II gelatin.

Amino Acids	Shark Cartilage	CIIA	CIIP	GII
Hyp	49.96	47.50	49.25	51.28
Asp	51.84	42.91	45.76	39.84
Thr	27.26	23.54	25.57	21.85
Ser	35.62	36.37	38.27	32.62
Glu	86.45	71.57	76.20	71.70
Pro	93.61	103.30	106.78	102.31
Gly	310.47	326.90	319.69	353.12
Ala	122.87	133.92	132.63	140.45
Cys	5.88	3.93	4.26	3.74
Val	25.63	25.14	25.43	22.65
Met	13.69	10.68	13.54	12.34
Ile	18.55	21.19	21.81	16.94
Leu	40.16	30.01	29.95	25.16
Tyr	15.13	8.75	7.19	2.73
Phe	19.51	18.95	14.97	14.66
Lys	22.34	30.93	29.37	27.35
His	9.98	9.33	9.38	8.15
Arg	50.96	55.05	49.87	53.14
Total	1000	1000	1000	1000
Imino acid	143.58	150.81	156.03	153.59

## 2.6. Relative Viscosity

Relative viscosity is a physicochemical property of collagen. The viscosity of collagen and gelatin decreased continuously with increasing temperature, and this trend was similar for both collagens and gelatin. A sharp decline in the relative viscosity of collagen and gelatin was found above 30 °C (Figure 3). The viscosity observed in this study was similar to that reported for other fish collagens [2,26,31]. The increasing temperature breaks hydrogen bonds between adjacent polypeptide chains of the collagen molecules and transforms intact trimers into individual chains or dimers, and, ultimately, causes the denaturation of the collagen structure. As a result, the helical structure of collagen converts into a random coil with a reduced viscosity. Hence, the viscosity is primarily influenced by the secondary structure of type II collagens and type II gelatin. Viscosity of GII was lower than type II collagens, and this is due to the lower molecular weight and proportion of  $\beta$  chains, as well as to the loss of the triple helical structure of gelatin during the denaturation process [2].

**Figure 3.** Relative viscosity of type II collagens and type II gelatin. The viscosity obtained at 5 °C was considered as 100%. CIIP: type II pepsin soluble collagen, CIIA: type II acid soluble collagen, GII: type II gelatin.



### 2.7. Effect of pH and NaCl Concentration on Solubility

The solubility of CIIA, CIIP and GII increased with increasing pH up to 5 and 6, and above this pH, the solubility decreased (Figure 4A).

**Figure 4.** Effect of pH (A) and salt concentration (B) on the solubility of collagens and gelatin. The highest solubility of collagens and gelatin was considered as 100% solubility. CIIP: type II pepsin soluble collagen, CIIA: type II acid soluble collagen, GII: type II gelatin.

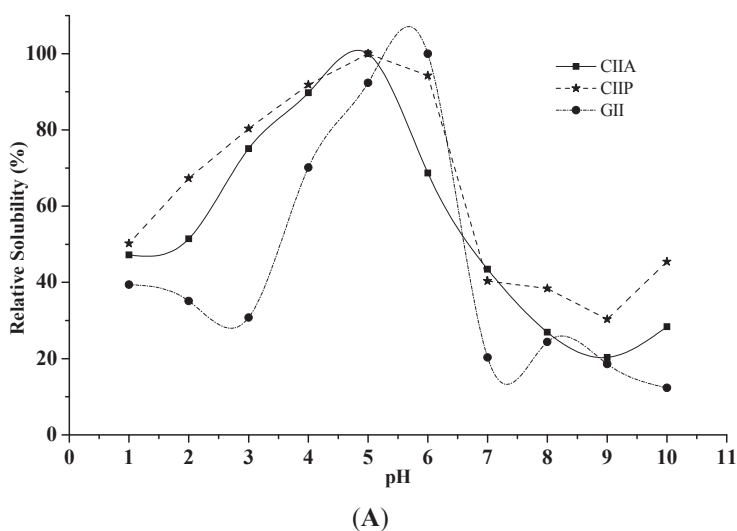
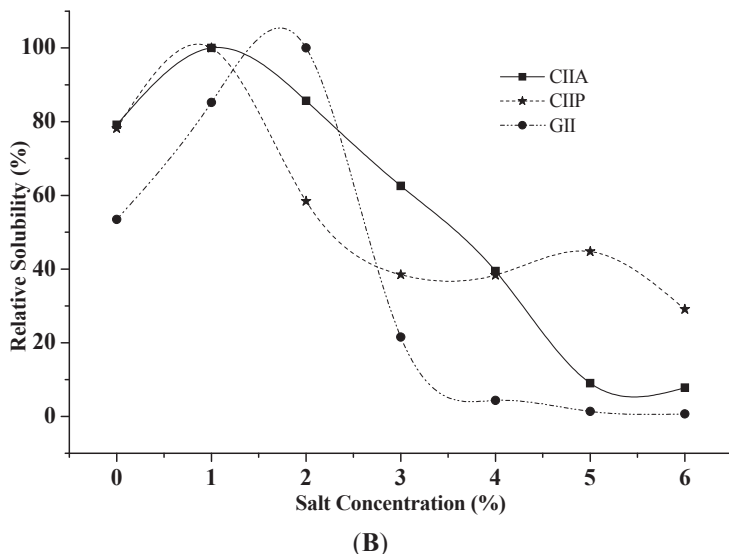


Figure 4. Cont.



Low solubilization of type II collagens and type II gelatin was observed in an alkaline pH from 8 to 9. Bae *et al.* [29] reported that decreased solubility between pH 7 and 9 was due to protein precipitation and the increased relative viscosity of collagen. Moreover, Kittiphattanabawon *et al.* [28] suggested that the variation in solubility at varying pH is attributed to the differences in the molecular conformations of collagen.

Maximum solubility was observed at the salt concentration of 1% for type II collagens and 2% for type II gelatin (Figure 4B). A drastic decrease in solubility was observed between 3% and 4% salt concentration for CIIA and GII and between 1% and 2% for CIIP. The maximum solubility of ASC and PSC from eel skin was reported at 3%–4% salt concentration [26], which is slightly higher than our findings. Jongjareonrak *et al.* [25] explained that the addition of salt decreased the solubility of collagens by increasing the ionic strength and enhancing hydrophobic interactions between protein chains, which leads to protein precipitation. In the present study, CIIP was more soluble than CIIA at 1% salt concentration, which was due to the partial hydrolysis of high molecular weight cross-linked CIIP by pepsin. Variations in the solubility may also be due to differing hydrophobic amino acid contents and the isoelectric point of collagen and gelatin [25].

### 2.8. Thermal Stability

The denaturation ( $T_d$ ) and melting temperatures ( $T_m$ ) of type II collagens and type II gelatin was determined by DSC. Thermal denaturation denotes unfolding of the triple helix to a random coil and leads to a loss of the unique characteristics of collagens. Denaturation and melting temperature of type II collagens and gelatin are shown in Table 2 and Figure 5. Type II collagens and type II gelatin had two endothermic peaks: the first peak occurred with the thermal denaturation of collagen and the second peak with the breakage of peptide chains and the

destruction of the material (melting temperature). According to the DSC spectra, the melting temperature of CIIA, CIIP and GII was observed at 52.04, 58.07 and 66.67 °C, respectively. Wang *et al.* [31] suggested that the difference in thermal stability of ASC and PSC from Amur sturgeon skin may be due to the level of hydration and the number and nature of covalent cross-linkages.

**Table 2.** Antioxidant and thermal transition temperature of type II collagens and type II gelatin. CIIP; type II pepsin soluble collagen, CIIA: type II acid soluble collagen, GII: type II gelatin.

Sample	DPPH Radical Scavenging (%)	Reducing Power (Absorbance at 700 nm)	DSC	
			Denaturation Temp (°C)	Melting Temp (°C)
CIIA	20.08	0.22	30.00	52.04
CIIP	24.77	0.24	31.25	58.07
GII	16.56	0.20	32.50	66.67
BHT	65.72	0.28	-	-

The denaturation temperature ( $T_d$ ) of GII (32.50 °C) was higher than that of CIIP (31.25 °C) and CIIA (30.00 °C). The  $T_d$  of other fish and calf collagen ranged from 19.4 to 40.8 °C [19,23,26,30]. The denaturation temperature may be affected by the degree of hydroxylation of the Pro and the Gly-Pro-Hyp sequence in collagen and gelatin [24]. The pyrrolidine rings of imino acids restrict the polypeptide chain conformation and strengthen the triple helix. Imino acid content is primarily responsible for the thermal stability and the triple stranded helix formation [32]. However, GII had a lower imino acid content than CIIP and a higher denaturation temperature. Similarly, Li *et al.* [6] reported that porcine collagen had higher thermal stability than Amur sturgeon collagen but a lower imino acid content; these authors proposed that the molecular conformation, amino acid sequence and stable covalent intra- and intermolecular cross-linkages may also influenced the thermal stability of collagen. In the present study, we have determined that the changes in the denaturation temperature are due to the different molecular conformations of type II collagens and type II gelatin.

**Figure 5.** DSC thermograms of type II collagens and type II gelatin. CIIP: type II pepsin soluble collagen, CIIA: type II acid soluble collagen, GII: type II gelatin.

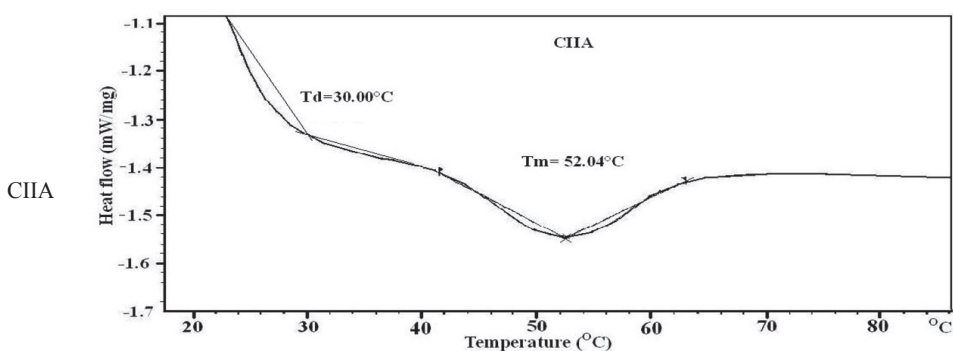
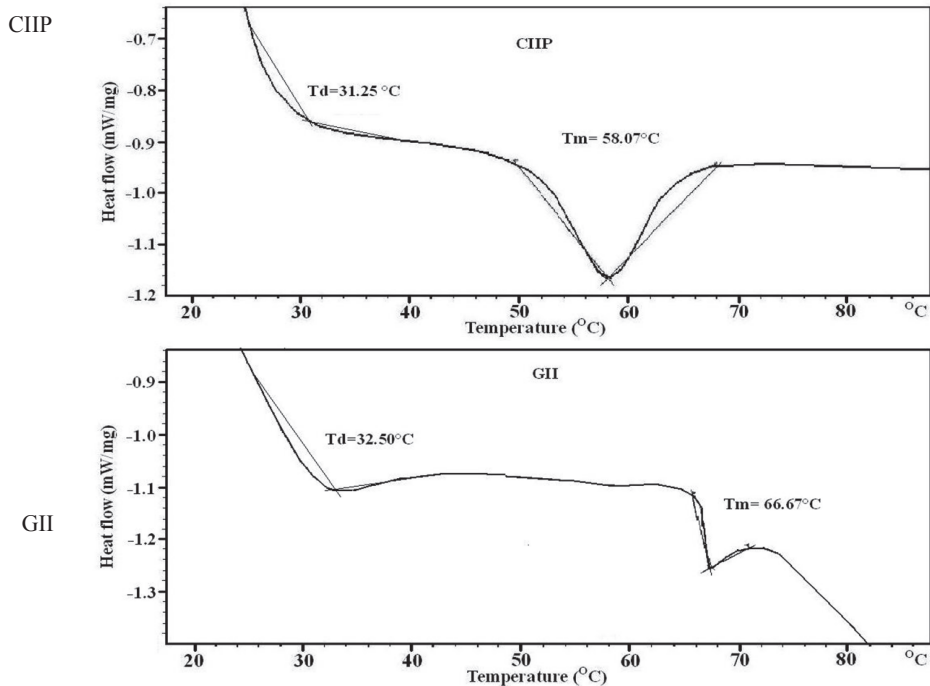


Figure 5. Cont.



Bae *et al.* [29] stated that the Td of fish collagen above 33 °C was considered as high heat resistance. In the present study, the Td of shark type II collagens and type II gelatin indicated higher stability and heat resistance than other reported fish collagens. Although, fish collagen has several important biochemical properties, the lower denaturation temperature of fish collagen than mammalian collagen is a major drawback in practical applications. However, the Td of type II collagens and type II gelatin from silvertip shark is similar to mammalian collagen and therefore may be a suitable alternative source of mammalian collagen.

### 2.9. FTIR Spectra

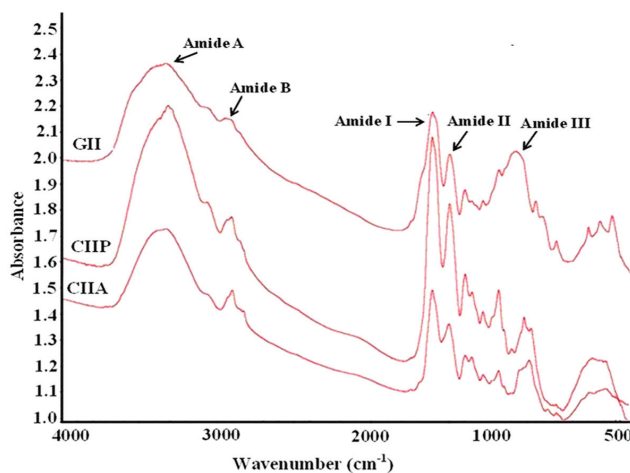
FTIR spectroscopy was employed to monitor the functional groups and secondary structure of type II collagens and type II gelatin. The frequencies at which major peaks occurred for type II collagens and gelatin are given in Table 3. The amide-A peak of CIIA, CIIP and GII appeared at 3340.38, 3331.13 and 3350.73  $\text{cm}^{-1}$ , respectively (Figure 6). This peak is generally associated with N–H stretching coupled with the hydrogen bond of a carbonyl group in a peptide chain.

The amide-B peak was observed at 2927.42, 2932.28 and 2948.13  $\text{cm}^{-1}$  for CIIA, CIIP and GII, respectively. This peak represents the asymmetric stretching vibration of alkenyl C–H, as well as  $\text{NH}_3^+$ . The amide-A and amide-B peaks of type II gelatin appeared at higher wavenumbers than that of type II collagens. The higher wavenumbers of GII are likely due to the increased protein-protein intermolecular cross-linkages through hydrogen bonds of low molecular weight peptides, rather than high molecular weight collagens [19].

**Table 3.** General peak assignments of the FTIR spectra of type II collagens and type II gelatin isolated from shark cartilage. CIIP: type II pepsin soluble collagen, CIIA: type II acid soluble collagen, GII: type II gelatin.

Peak Wavenumber (cm <sup>-1</sup> )			
CIIP	CIIA	GIJ	Assignment
3331.13	3340.38	3350.73	Amide A: NH stretch coupled with a hydrogen bond
2932.28	2927.42	2948.13	Amide B: CH <sub>2</sub> asymmetrical stretch
2882.11	2855.34	-	CH <sub>3</sub> -symmetric stretch: mainly proteins
1796.47	1734.76	-	Carbonyl C=O stretch: lipids
1659.84	1659.77	1657.77	Amide I: C=O stretch/hydrogen bond coupled with COO <sup>-</sup>
1550.67	1554.23	1551.26	Amide II: NH bend coupled with an CN stretch
1452.09	1452.16	1453.79	CH <sub>2</sub> bend
1338.83	1338.22	1338.47	CH <sub>2</sub> wag of proline
1239.69	1240.40	1237.81	Amide III: NH bend coupled with an CN stretch
1157.44	1161.1	1129.96	CO-O-C asymmetric stretch: glycogen and nucleic acids
1079.18	1079.52	-	C-O stretch
876.16	874.26	874.30	Skeletal stretch
616.96	611.58	597.11	Skeletal stretch

**Figure 6.** FTIR spectra of type II collagens and type II gelatin. CIIP: type II pepsin soluble collagen, CIIA: type II acid soluble collagen, GII: type II gelatin.



The amide-I peak was observed at 1659.77, 1659.84 and 1657.77 cm<sup>-1</sup> for CIIA, CIIP and GII, respectively, which was similar to that of other fish collagens [19,27,31]. The amide-I region is mainly used for the analysis of the secondary structure of proteins [19]. The amide-I vibration mode is primarily due to the C=O stretching vibration of the peptide linkages (approximately 80%). The shift of the amide-I peak to a lower wavenumber is associated with the coiled structure of gelatin resulting from the heat denaturation during the isolation process [29].

The characteristic peak of the amide-II region of CIIA, CIIP and GII was observed at 1554.23, 1550.67 and 1551.26 cm<sup>-1</sup>, respectively. The amide-II vibration modes are attributed to the N-H

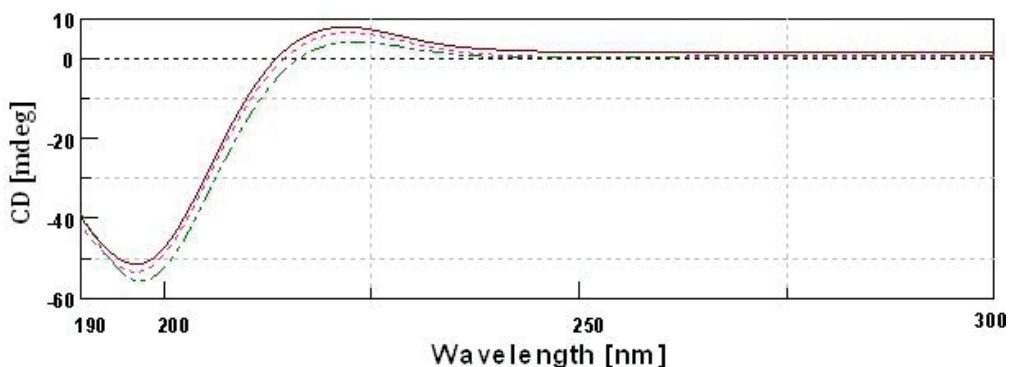
in-plane bend (40%–60%) and the C–N stretching vibration (18%–40%). Muyonga *et al.* [19] also observed the amide II peak at 1540–1558  $\text{cm}^{-1}$  for Nile perch skin collagen. The intensity of the amide peak is associated with the triple helical structure of collagen. In the present study, the intensity of the amide I peak of GII was lower than type II collagens and this indicated the loss of the triple helix structure of collagen during the isolation process. The protein structure of gelatin also confirmed the above statement (Figure 1). Therefore, FTIR spectra clearly indicated that the triple helix structure, molecular order and intermolecular cross-linkages of collagen varied from gelatin.

### 2.10. CD Spectra

The triple helix of collagen consisted of three molecular strands. The prolines are arranged in a left handed polyproline-II-helical conformation, and these helices coil together to form a right handed super helix. Circular dichroism spectroscopy (CD) is used to investigate the molecular order of collagen.

CD spectra of type II collagens and type II gelatin exhibited a rotatory maximum at 221–221.5 nm, a minimum at 196–197 nm and a crossover point at 213.5–215.5 nm (Figure 7), which is characteristic of triple helical protein conformation [33]. The maximum and minimum rotatory CD spectra reported for eel skin collagen were 230 and 204 nm, respectively [26], and those of Adult black drum and sheepshead seabream bone were 220–221 and 197–199 nm, respectively [2]. However, for gelatin that was isolated by heat treatment, the CD spectra was similar to that of collagen. Aewsiri *et al.* [34] reported that after the complete denaturation of collagen, the characteristic triple helical positive peak at 220–230 nm disappeared and only a negative peak at 200 nm remained for gelatin. The triple helical structure of collagen can transform into a random coil when it is heated above its denaturation temperature [19]. The present study showed that the triple helical structures of type II gelatin were not completely destroyed during the isolation process. This is in agreement with the CD spectra of gelatin isolated from Amur sturgeon skin [35].

**Figure 7.** Circular dichroism spectra of type II collagens and type II gelatin. — type II pepsin soluble collagen; - - - type II acid soluble collagen; - · - · GII-type II gelatin.



### 2.11. Antioxidant Activity

In the present study, the protective abilities of type II collagens and type II gelatin against oxidation was examined with the DPPH radical scavenging capacity and the reducing power. Natural or artificial antioxidants scavenge the DPPH radicals by donating a proton to the system. Type II collagens and type II gelatin were capable of scavenging hydroxyl radicals. The DPPH radical scavenging rate is 24%–16% for type II collagens and type II gelatin, which is lower than that of BHT (65%) (Table 2). CIIP exhibited higher scavenging activity than CIIA and GII. Zhu *et al.* [13] reported that the DPPH radical scavenging activity of PSC from sea cucumber was 45.58%, which was higher than our findings. It is thought that collagen can inactivate reactive oxygen species, reduce hydroperoxides, enzymatically eliminate specific oxidants, chelate pro-oxidative transition metals and scavenge free radicals, which may contribute to their antioxidant activities [13]. Moreover, certain specific amino acid residues and their sequences are thought to be responsible for antioxidant activities [15]. Zhong *et al.* [12] suggested that the antioxidant activities of the body wall of sea cucumber may be attributed to collagens. Zhuang *et al.* [14] reported that collagen from jellyfish exhibited improved antioxidant activity in animal mice skin by protecting the endogenous antioxidant enzymes and suggested that the high contents of glycine, proline, and hydrophobic amino acids of the collagen were responsible for the activity. In the present study, higher content of proline and hydrophobic amino acids (valine, leucine, isoleucine, cysteine and methionine) in CIIP than that of CIIA and GII also supports the superior antioxidant activity of CIIP.

The reducing power is determined by the ability of collagen to reduce ferric into ferrous ions. Similar to the DDPH activity, the reducing power was higher in CIIP than in CIIA and GII, with a value of 0.24 at 700 nm (Table 2). The present result was comparable to the porcine protein reducing power of 0.25 [36] and lower than that of the buckwheat protein (0.77–1.24) [37]. The reducing power of BHT was higher than the isolated collagen and gelatin. Li *et al.* [6] reported that the reducing ability increased with increasing concentrations of ASC from 1 to 5 mg/mL. The antioxidant property of proteins is primarily influenced by their size, configuration and amino acid composition [6]. Antioxidant activity of type II collagens and gelatin is one of the important properties for its use as a drug, especially for the treatment of RA. Some researchers have reported the effective inhibitory activity of cartilage type II collagen on rheumatoid arthritis [1,7,22]. There is substantial evidence that the CII-deficiency in transgenic mice results in embryos that die at birth and have skeletal malformations, thus indicating the importance of this protein in bone development [38]. Therefore, further investigations are required to identify specific antioxidant peptides from silvertip shark cartilage collagen and gelatin.

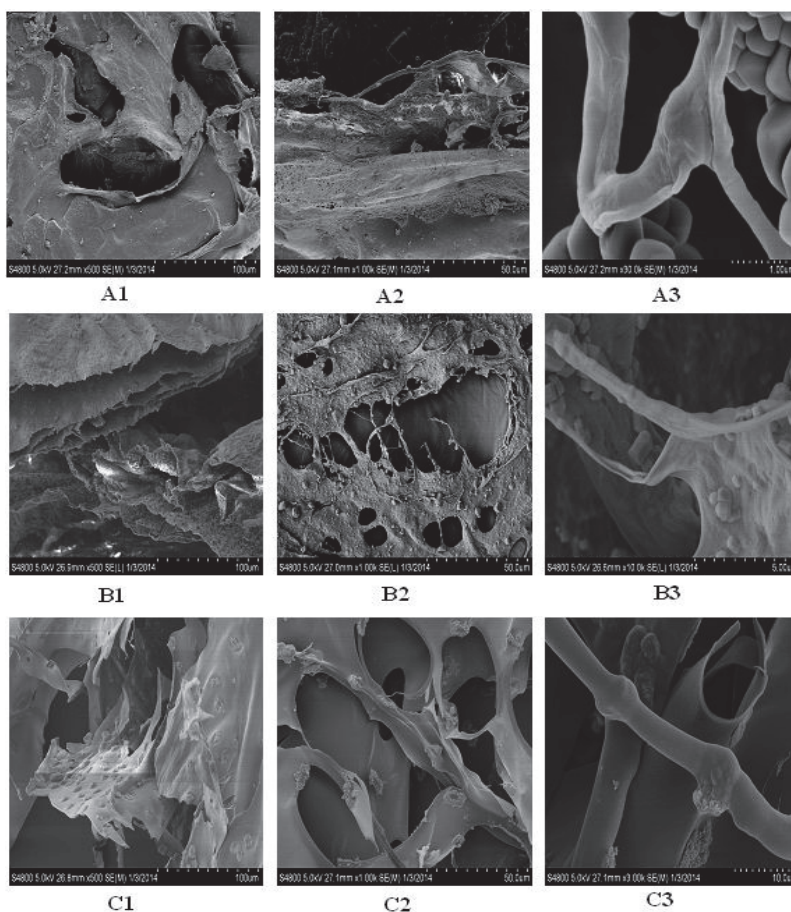
### 2.12. Microscopic Structure

The SEM microscopic structure showed a homogenous, porous, fibrillary and multi-layered structure of collagen and gelatin (Figure 8). The microstructure of CIIA and CIIP was a rough, fibril-dominated network with a coarse structural integrity. Conversely, the surface of gelatin was a smooth, less fibril-dominated network and was partially degraded. This similar structure was



reported for collagen isolated from Amur sturgeon skin [31]. The microstructural changes in the collagen and gelatin are related to the functional properties. At a higher magnification, the collagen and gelatin had a fiber-like structure with an average size of 0.4 to 0.7  $\mu\text{m}$  for CIIP and 0.75 to 1.5  $\mu\text{m}$  for CIAA. An inter-linkage between CIIP and glycoprotein was observed at higher magnification. This structure was similar to the eel skin ASC and PSC structures reported by Veeruraj *et al.* [26]. Accordingly, the surface morphology of collagen greatly differs from that of gelatin due to isolation process.

**Figure 8.** Scanning electron microscopic structure of type II collagens and type II gelatin isolated from silvertip shark cartilage. A1, A2, A3: type II pepsin soluble collagen; B1, B2, B3: type II acid soluble collagen; C1, C2, C3: type II gelatin.



The microstructural changes in collagen are related to the functional properties. The present SEM image showed that the shark collagens and gelatin had a cross-section with an inter-connected network pore configuration. Joseph *et al.* [39] suggested that the moderate pore size of collagen was suitable for *in vivo* studies and that the pore size of collagen was influenced by the water content during preparation. Earlier, Jansson *et al.* [40] reported that the collagen extracted from the

cartilage of horse mackerel and croaker could be used as a biofilm or scaffold for wound healing purposes. In addition, other architectural features, such as pore shape, pore wall morphology and interconnectivity of collagen, have also been suggested for use in cell seeding, growth, gene expression, migration, mass transport, and new tissue formation. Generally, the uniform and regular network structure of collagen as a drug carrier is propitious for a well-proportioned drug distribution [41]. The microscopic structure of type II collagens and gelatin isolated from shark cartilage may provide a suitable biomaterial for a drug carrier system.

### 3. Experimental Section

#### 3.1. Raw Materials

The cartilage (cartilaginous skeleton) of the silvertip shark was used as the raw material for the isolation of fish collagen and gelatin and was obtained from a private fish processing plant, M/s. Yueqing Ocean Biological Health Care Product Co., Ltd. Zhejiang province, Shanghai, China. The cartilage was washed with potable water and cut into small pieces prior to the isolation of collagen and gelatin. Moisture, ash, fat and protein content of the silvertip shark cartilage was determined according to AOAC [42] methods: No. 950.46, 928.08, 960.39 and 920.153, respectively. The sample hydroxyproline content was determined according to the method of Bergman and Loxley [43].

#### 3.2. Isolation of Collagen and Gelatin

##### 3.2.1. Pretreatment of Shark Cartilage

The cartilage was homogenized in a tissue homogenizer using phosphate buffer (pH 6.5; 0.2 mol/L sodium dihydrogen phosphate and 0.2 mol/L disodium hydrogen phosphate heptahydrate). The entire process of collagen isolation was performed at 4 °C. The homogenate was treated with double-distilled water at a ratio of 1:6 (*w/v*) for 24 h to remove water soluble substances. The cartilage was decalcified with 0.5 Methylene diaminetetraacetic acid (EDTA) (pH 7.4) at a ratio of 1:10 (*w/v*) for 48 h. The solution was replaced every 12 h. This pretreated shark cartilage was used for the further isolation of acid soluble collagen (ASC) and pepsin soluble collagen (PSC).

##### 3.2.2. Isolation of ASC and PSC

Type II collagen (CII) was isolated from the shark cartilage according to the method of Kittiphattanabawon *et al.* [21] with modification. The pretreated shark cartilage was soaked into 0.5 M acetic acid (1:6, *w/v*) for 4 days with continuous shaking and the extracts were centrifuged at 10,000 rpm for 30 min at 4 °C. The supernatant was collected and salted out by adding 2 M NaCl. The precipitates were re-dissolved in a minimum volume of 0.5 M acetic acid and dialyzed against distilled water for 2 days until a neutral pH was obtained. The dialyzed sample was lyophilized (Labconco Freezone 2.5, Kansas City, MI, USA) and further referred to as ASC. For the isolation

of PSC, the pretreated shark cartilage was soaked in 0.5 M acetic acid containing 1% pepsin (1:6, w/v) and then followed the above procedure.

### 3.2.3. Isolation of Gelatin

Type II gelatin (GII) was isolated according to Jeevithan *et al.* [4]. Briefly, the shark cartilage was treated twice with 0.2% NaOH at a ratio of 1:6 w/v for 45 min to remove the non-collagenous protein. After thorough washing, cartilage was treated twice with 0.2% H<sub>2</sub>SO<sub>4</sub> at a ratio of 1:6 w/v for 45 min. Samples were then treated with 1% citric acid twice at a ratio of 1:6 w/v for 45 min. The final isolation was carried out with distilled water at a ratio of 1:1 w/v at 45°C for 24 h. The extract was filtered through Whatman No. 4 filter paper under vacuum, lyophilized and used for further characterization.

### 3.3. Purification by Gel Filtration Chromatography

Gel filtration chromatography was performed to purify CIIA, CIIP and GII. In brief, samples (100 mg) were dissolved in 10 mL of a running buffer (20 mM sodium acetate buffer, pH 4.8) and were applied to a Sephadex G-100 (Sigma, Shanghai, China) column (25.0 × 3.0 cm). The column was previously equilibrated with the same buffer until A<sub>230</sub> was less than 0.05 to achieve baseline correction. The elution volume was 200 mL, and the flow rate was 1 mL/min. The protein fractions were identified by UV absorbance spectroscopy and 5 mL fractions were collected. As shown in Figure 1b, the collagen peak was pooled and salted out by addition of 2 M NaCl. The precipitate was dialyzed against distilled water and freeze dried.

### 3.4. Sodium Dodecyl Sulfate-Polyacrylamide Gel Electrophoresis (SDS-PAGE)

The protein pattern was analyzed using sodium dodecyl sulfate poly-acrylamide gel electrophoresis (SDS-PAGE) according to the method of Laemmli [44] with modification. Briefly, the purified samples were dissolved in 5% SDS, kept in a water bath at 60 °C for 20 min and centrifuged at 3500 rpm. The supernatant was mixed with a sample buffer (1:1) containing Tris HCl (pH 6.8; 12.1 g Tris base was dissolved in 80 mL distilled water and the pH was adjusted with concentrated HCl), 1% 2-mercaptoethanol, 40% sucrose, 20% glycerol, 0.02% bromophenol blue and 1% SDS. The mixtures were loaded onto a polyacrylamide gel, composed of 7.5% separating gel and 4% stacking gel, and were subjected to electrophoresis at a constant current of 50 mA. After electrophoresis, gels were fixed with a mixture of 5:1 methanol:acetic acid would be composed of 83.3% and 16.7% methanol and acetic acid, respectively for 1 h. This was followed by staining with 0.5% Coomassie blue R-250 in 150% methanol and 50% acetic acid for 30 min. Finally, the gels were destained with a mixture of 300% methanol and 100% acetic acid for 2 h.

### 3.5. Peptide Mapping

Peptide mapping was performed according to the method of Kittiphattanabawon *et al.* [28] with modification. Samples (5 mg) were dissolved in 1 mL of 0.1 M Tris-HCL (pH 6.8) buffer

containing 0.5% SDS and heated at 100 °C for 2 h. To initiate digestion, 20 µL of the enzyme solution, V8-protease (EC 3.4.21.19, Sigma-Aldrich, Shanghai, China), with a concentration of 5 µg/mL was added to each mixture. The reaction mixtures were then incubated at 37 °C for 1 h and the proteolysis was halted by increasing the temperature to 100 °C for 5 min. Peptides generated by the protease digestion were separated by SDS-PAGE using 10% separating gel and 4% stacking gel as previously described.

### 3.6. Viscosity

Samples (0.03%) were dissolved in 0.1 M acetic acid and the viscosity was measured using a Brookfield LVDV-II+P viscometer (Brookfield Engineering Laboratories Ltd., Middleboro, MA, USA) equipped with an ultra-low viscosity adapter at a speed of 90 rpm. Samples were heated using a rotary water bath from 5 to 40 °C. The sample solutions (20 mL) were incubated for 30 min at each temperature prior to measurement. The relative viscosity was calculated compared with that obtained at 5 °C.

### 3.7. Collagen Solubility Test

Optimum solubility at different pH and salt concentrations was determined according to the method of Jongjareonrak *et al.* [24]. Collagen samples were dissolved in 0.5 M acetic acid with gentle stirring at 4 °C for 12 h to obtain a final concentration of 6 mg/mL.

#### 3.7.1. Effect of pH

The collagen solution (5 mL) was transferred into a series of centrifuge tubes, adjusted to pH values ranging from 1 to 10 by addition of the appropriate amount of 6 M NaOH or 6 M HCl. The resulting sample solution totaled 10 mL with distilled water. The solution was stirred gently for 30 min at 4 °C and centrifuged at 5000× *g* for 30 min. An aliquot (1 mL) of the supernatant was collected from each tube and the protein content was measured by the Lowry method [45]. The relative solubility of collagen was calculated compared with the pH rendering the highest solubility.

#### 3.7.2. Effect of NaCl

The collagen solution (5 mL) was mixed with 5 mL of cold NaCl in acetic acid of various concentrations (0%–12%, *w/v*) to obtain final concentrations of 1%–6% (*w/v*). The mixture was stirred gently at 4 °C for 30 min and centrifuged at 10,000× *g* for 30 min at 4 °C. The relative solubility was calculated compared with that of the salt concentration exhibiting the highest solubility.

### 3.8. UV Absorption Spectrum

UV absorption spectrum of type II collagen samples was measured using a UV spectrophotometer. Samples were dissolved in 0.5 M acetic acid and UV spectra were measured between 190 and 400 nm at a scan speed of 2 nm/s with an interval of 1 nm.

### 3.9. Amino Acid Profiling

The collagen samples were hydrolyzed under reduced pressure in 6 M HCl at 110 °C for 24 h. Amino acid composition was analyzed using an amino acid analyzer (Hitachi L-8800, Tokyo, Japan). The amino acid content is expressed as the number of residues/1000 residues.

### 3.10. Fourier Transform Infrared Spectroscopy (FTIR)

FTIR spectra of the samples were obtained using a Nicolet 6700-Fourier transform infrared spectrometer (ThermoFisher Scientific Inc., Waltham, MA, USA) equipped with a DLaTGS detector. The lyophilized samples (5 mg) were mixed with dried KBr (100 mg), ground in a mortar and pestle and subjected to a pressure of approximately  $5 \times 10^6$  Pa in an evacuated die to produce a  $13 \times 1$  mm clear transparent disk. The absorption intensity of the peaks was calculated using the base-line method. The resultant spectra were analyzed using ORIGIN 8.0 software (Thermo Nicolet, Madison, WI, USA).

### 3.11. Circular Dichroism (CD)

The molecular conformations of collagen and gelatin were assessed by CD using a spectropolarimeter (Jasco J-810, Shanghai, China) according to the method of Cao *et al.* [22] with modification. Briefly, the samples were dissolved in 0.1 M acetic acid to obtain a final concentration of 0.1 mg/mL and were stirred for 6 h. Then, the sample solutions were placed in a quartz cell with a path length of 10 mm. The spectra were recorded between 190 and 300 nm at 25 °C. The acetic acid spectrum was used as a reference and CD spectra of the samples were obtained after subtracting the reference spectrum.

### 3.12. Scanning Electron Microscopy (SEM)

Morphological characteristics of the isolated collagens and gelatin were visualized by SEM-S4800 (Hitachi, Tokyo, Japan). Collagen samples were mounted on specimen stubs with two-sided carbon tape. The sample surface was sputter-coated with a thin layer (~8–10 nm) of gold ions using a sputter-coater. The samples were then introduced into the specimen chamber and examined for surface morphology at a 20 kV accelerating voltage.

### 3.13. Thermal Stability

Differential scanning calorimetry (DSC) was conducted following the method of Rochdi *et al.* [46]. The samples were rehydrated with deionized water at a solid/solution ratio of 1:10 (*w/v*). DSC was performed using a differential scanning calorimeter (Model DSC822e, Mettler-Toledo GmbH, Greifensee, Switzerland). The temperature calibration was conducted using an indium standard. Samples were weighed into aluminum pans and sealed. Subsequently, samples were scanned at 5 °C/min from 20 to 120 °C using ice water as the cooling medium. An empty pan was used as the reference. The denaturation and melting temperatures were estimated from the DSC thermogram.

### 3.14. Antioxidant Activity

#### 3.14.1. DPPH Radical Scavenging Assay

DPPH radical scavenging activity was acquired based on the method of Shimada *et al.* [47]. Briefly, the test sample (500  $\mu$ L) was added to 500  $\mu$ L of 99.5% ethanol and 125  $\mu$ L of 99.5% ethanol containing 0.02% DPPH. The mixture was kept in the dark at room temperature for 60 min before measuring absorbance at 517 nm. In the blank, the sample was replaced with distilled water (500  $\mu$ L) and the above procedure was followed. Butylated hydroxytoluenum (BHT) was used as a positive control. A lower absorbance indicated higher DPPH scavenging activity. Radical scavenging activity was calculated as follows:

$$\text{Radical scavenging activity} = [(\text{blank absorbance} - \text{sample absorbance}) / \text{blank absorbance}] \times 100\%.$$

#### 3.14.2. Reducing Power

Protein solutions (1 mg) were mixed with 2.5 mL of phosphate buffer (0.2 M, pH 6.6) and 2.5 mL of 1.0% potassium ferricyanide and the mixture was incubated at 50°C for 20 min. Trichloroacetic acid (2.5 mL of a 10% solution) was added, and the mixture was centrifuged. The supernatant (2.5 mL) was mixed with water (2.5 mL) and 0.1% ferric chloride (0.5 mL), and the absorbance was measured at 700 nm. Higher absorbance indicated higher reducing power. BHT was used as a reference antioxidant.

## 4. Conclusions

Collagen and gelatin was isolated from shark cartilage using an improved isolation method with a high denaturation temperature. Compared with type II gelatin, CIIP was richer in proline and alanine and lower in hydroxyproline. The homogenous, porous, fibrillary and multi-layered structure of type II collagens and type II gelatin are good characteristics of biomaterials used in cell attachment. In conclusion, the solubility, susceptibility to proteolytic enzymes, high denaturation temperature and efficient antioxidant activities suggest that silvertip shark cartilage type II collagens and type II gelatin have promising potential for use in various practical applications in biomedical industries.

## Acknowledgments

This work received financial support from the National High Technology Research and Development Program of China (No. 2011AA09070109) and the National Natural Science Foundation of China (No. 81341082).

## Conflicts of Interest

The authors declare no conflict of interest.

## References

1. Poole, A.R. Cartilage in Health and Disease. In *Arthritis and Allied Conditions: A Textbook of Rheumatology*, 15th ed.; Koopman, W.J., Moreland, L.W., Eds.; Williams and Wilkins: Baltimore, MD, USA, 2005; pp. 223–269.
2. Ogawa, M.; Moody, M.W.; Portier, R.J.; Bell, J.; Schexnayder, M.A.; Losso, J.N. Biochemical properties of black drum and sheepshead seabream skin collagen. *J. Agric. Food Chem.* **2003**, *51*, 8088–8092.
3. Jeya Shakila, R.; Jeevithan, E.; Varatharajakumar, A.; Jeyasekaran, G.; Sukumar, D. Functional characterization of gelatin extracted from bones of red snapper and grouper in comparison with mammalian gelatin. *LWT Food. Sci. Technol.* **2012**, *48*, 30–36.
4. Jeevithan, E.; Jeya Shakila, R.; Varatharajakumar, A.; Jeyasekaran, G.; Sukumar, D. Physico- functional and mechanical properties of chitosan and calcium salts incorporated fish gelatin scaffolds. *Int. J. Biol. Macromol.* **2013**, *60*, 262–267.
5. Chirita, M. Mechanical properties of collagen biomimetic films formed in the presence of calcium, silica and chitosan. *J. Bionic Eng.* **2008**, *5*, 149–158.
6. Li, Z.R.; Wang, B.; Chi, C.F.; Zhang, Q.H.; Gong, Y.D.; Tang, J.J.; Luo, H.Y.; Ding, G.F. Isolation and characterization of acid soluble collagens and pepsin soluble collagens from the skin and bone of Spanish mackerel (*Scomberomorus niphonius*). *Food Hydrocoll.* **2013**, *31*, 103–113.
7. Chen, L.; Bao, B.; Wang, N.; Xie, J.; Wu, W.H. Oral Administration of Shark Type II Collagen Suppresses Complete Freund's Adjuvant-Induced Rheumatoid Arthritis in Rats. *Pharmaceuticals* **2012**, *5*, 339–352.
8. Zhao, W.; Tong, T.; Wang, L.; Li, P.P.; Chang, Y.; Zhang, L.L.; Wei, W. Chicken type II collagen induced immune tolerance of mesenteric lymph node lymphocytes by enhancing beta2-adrenergic receptor desensitization in rats with collagen-induced arthritis. *Int. Immunopharmacol.* **2011**, *11*, 12–18.
9. Zhu, P.; Li, X.Y.; Wang, H.K.; Jia, J.F.; Zheng, Z.H.; Ding, J.; Fan, C.M. Oral administration of type-II collagen peptide 250–270 suppresses specific cellular and humoral immune response in collagen-induced arthritis. *Clin. Immunol.* **2007**, *122*, 75–84.
10. Garcia, G.; Komagata, Y.; Slavin, A.J.; Maron, R.; Weiner, H.L. Suppression of collagen-induced arthritis by oral or nasal administration of type II collagen. *J. Autoimmun.* **1999**, *13*, 315–324.
11. Youn, J.; Hwang, S.H.; Ryoo, Z.Y.; Lynes, M.A.; Paik, D.J.; Chung, H.S.; Kim, H.Y. Metallothionein suppresses collagen-induced arthritis via induction of TGF-b and down-regulation of proinflammatory mediators. *Clin. Exp. Immunol.* **2002**, *129*, 232–239.
12. Zhong, Y.; Khan, M.A.; Shahidi, F. Compositional characteristics and antioxidant properties of Fresh and Processed Sea Cucumber (*Cucumaria frondosa*). *J. Agric. Food Chem.* **2007**, *55*, 1188–1192.

13. Zhu, B.; Dong, X.; Zhou, D.; Gao, Y.; Yang, J.; Li, D.; Zhao, X.; Rena, T.; Yea, W.; Tana, H.; Wua, H.; Yu, C. Physicochemical properties and radical scavenging capacities of pepsin-solubilized collagen from sea cucumber (*Stichopus japonicas*). *Food Hydrocoll.* **2012**, *28*, 182–188.
14. Zhuang, Y.; Zhao, X.; Li, B. Optimization of antioxidant activity by response surface methodology in hydrolysates of jellyfish (*Rhopilema esculentum*) umbrella collagen. *J. Zhejiang Univ. Sci. B* **2009**, *10*, 572–579.
15. Mendis, E.; Rajapakse, N.; Byun, H.G.; Kim, S.K. Investigation of jumbo squid (*Dosidicus gigas*) skin gelatin peptides for their *in vitro* antioxidant effects. *Life Sci.* **2005**, *77*, 2166–2178.
16. Je, J.Y.; Qian, Z.J.; Byun, H.G.; Kim, S.K. Purification and characterization of an antioxidant peptide obtained from tuna backbone protein by enzymatic hydrolysis. *Process Biochem.* **2007**, *42*, 840–846.
17. Merly, L.; Smith, S.L. Collagen type II, alpha 1 protein: a bioactive component of shark cartilage. *Int. Immunopharmacol.* **2013**, *15*, 309–315.
18. Liang, Q.; Wang, L.; Sun, W.; Wang, Z.; Xu, J.; Ma, H. Isolation and characterization of collagen from the cartilage of Amur sturgeon (*Acipenser schrenckii*). *Process Biochem.* **2014**, *49*, 318–323.
19. Muyonga, J.H.; Cole, C.G.B.; Duodu, K.G. Characterisation of acid soluble collagen from skins of young and adult Nile perch (*Lates niloticus*). *Food Chem.* **2004**, *85*, 81–89.
20. Cho, S.M.; Kwak, K.S.; Park, D.C.; Gu, Y.S.; Ji, C.I.; Jang, D.H.; Lee, Y.B.; Kim, S.B. Processing optimization and functional properties of gelatin from shark (*Isurus oxyrinchus*) cartilage. *Food Hydrocoll.* **2004**, *18*, 573–579.
21. Kittiphattanabawon, P.; Benjakul, S.; Visessanguan, W.; Shahidi, F. Isolation and characterization of collagen from the cartilages of brownbanded bamboo shark (*Chiloscyllium punctatum*) and blacktip shark (*Carcharhinus limbatus*). *LWT Food Sci. Technol.* **2010**, *43*, 792–800.
22. Cao, H.; Shi, F.X.; Xu, F.; Yu, J.S. Molecular structure and physicochemical properties of pepsin-solubilized type II collagen from the chick sternal cartilage. *Eur. Rev. Med. Pharmacol. Sci.* **2013**, *17*, 1427–1437.
23. Helen, E.; Cahir, A. Spatial organization of type I and II collagen in the canine meniscus. *J. Orthop. Res.* **2005**, *23*, 142–149.
24. Vercaigne-Marko, D.; Kosciarz, E.; Nedjar-Arroume, N.; Guillochon, D. Improvement of *Staphylococcus aureus*-V8-protease hydrolysis of bovine haemoglobin by its adsorption on to a solid phase in the presence of SDS: peptide mapping and obtention of two haemopoietic peptides. *Biotechnol. Appl. Biochem.* **2000**, *31*, 127–134.
25. Jongjareonrak, A.; Benjakul, S.; Visessanguan, W.; Nagai, T.; Tanaka, M. Isolation and characterisation of acid and pepsin-solubilised collagens from the skin of brownstripe red snapper (*Lutjanus vitta*). *Food Chem.* **2005**, *93*, 475–484.



26. Veeruraj, A.; Arumugam, M.; Balasubramanian, T. Isolation and characterization of thermostable collagen from the marine eel-fish (*Evenchelys macrura*). *Process Biochem.* **2013**, *48*, 1592–1602.
27. Duan, R.; Zhang, J.; Du, X.; Yao, X.; Konno, K. Properties of collagen from skin, scale and bone of carp (*Cyprinus carpio*). *Food Chem.* **2009**, *112*, 702–706.
28. Kittiphattanabawon, P.; Benjakul, S.; Visessanguan, W.; Nagai, T.; Tanaka, M. Characterisation of acid-soluble collagen from skin and bone of bigeye snapper (*Priacanthus tayenus*). *Food Chem.* **2005**, *89*, 363–372.
29. Bae, I.; Osatomi, K.; Yoshida, A.; Osako, K.; Yamaguchi, A.; Hara, K. Biochemical properties of acid-soluble collagens extracted from the skins of underutilized fishes. *Food Chem.* **2008**, *108*, 49–54.
30. Woo, J.W.; Yu, S.J.; Cho, S.M.; Lee, Y.B.; Kim, S.B. Extraction optimization and properties of collagen from yellowfin tuna (*Thunnus albacares*) dorsal skin. *Food Hydrocoll.* **2008**, *22*, 879–887.
31. Wang, L.; Liang, Q.; Chen, T.; Wang, Z.; Xu, J.; Ma, H. Characterization of collagen from the skin of Amur sturgeon (*Acipenser schrenckii*). *Food Hydrocoll.* **2014**, *38*, 104–109.
32. Ikoma, T.; Kobayashi, H.; Tanaka, J.; Walsh, D.; Mann, S. Physical properties of type I collagen extracted from fish scales of *Pagrus major* and *Oreochromis niloticas*. *Int. J. Biol. Macromol.* **2003**, *32*, 199–204.
33. Usha, R.; Ramasami, T. Structure and conformation of intramolecularly cross-linked collagen. *Colloids Surf. B* **2005**, *41*, 21–24.
34. Aewsiri, T.; Benjakul, S.; Visessanguan, W.; Wierenga, P.A.; Gruppen, H. Improvement of foaming properties of cuttlefish skin gelatin by modification with *N*-hydroxysuccinimide esters of fatty acid. *Food Hydrocoll.* **2011**, *25*, 1277–1284.
35. Nikoo, M.; Benjakul, S.; Bashari, M.; Alekhorshied, M.; Cissouma, A.I.; Yanga, N.; Xu, X. Physicochemical properties of skin gelatin from farmed Amur sturgeon (*Acipenser schrenckii*) as influenced by acid pretreatment. *Food Biosci.* **2014**, *5*, 19–26.
36. Chang, C.Y.; Wu, K.C.; Chiang, S.H. Antioxidant properties and protein compositions of porcine haemoglobin hydrolysates. *Food Chem.* **2007**, *100*, 1537–1543.
37. Tang, C.H.; Peng, J.; Zhen, D.W.; Chen, Z. Physicochemical and antioxidant properties of buckwheat (*Fagopyrum esculentum* Moench) protein hydrolysates. *Food Chem.* **2009**, *115*, 672–678.
38. Aszodi, A.; Hunziker, E.B.; Olsen, B.R.; Fassler, R. The role of collagen II and cartilage fibril-associated molecules in skeletal development. *Osteoarthr. Cartil.* **2001**, *9*, 150–159.
39. Joseph, G.; Jun, O.; Teruo, M. Biodegradable honeycomb collagen scaffold for dermal tissue engineering. *J. Biomed. Mater. Res. Part A* **2008**, *87*, 1103–1111.
40. Jansson, K.; Haegerstrand, A.; Kratz, G. A biodegradable bovine collagen membrane as a dermal template for human *in vivo* wound healing. *Scandinavian J. Plast. Reconstr. Surg. Hand Surg.* **2001**, *35*, 369–375.

41. Zhang, Y.; Liu, W.T.; Li, G.Y.; Shi, B.; Miao, Y.Q.; Wu, X.H. Isolation and partial characterization of pepsin-soluble collagen from the skin of grass carp (*Ctenopharyngodon idella*). *Food Chem.* **2007**, *103*, 906–912.
42. AOAC. *Official Methods of Analysis*; Association of Official Analytical Chemists Inc.: Arlington, VA, USA, 2000.
43. Bergman, I.; Loxley, R. Two improved and simplified methods for the spectrophotometric determination of hydroxyproline. *Anal. Chem.* **1963**, *35*, 1961–1965.
44. Laemmli, U.K. Cleavage of structural proteins during the assembly of the head of bacteriophage T4. *Nature* **1970**, *227*, 680–685.
45. Lowry, O.H.; Rosebrough, N.J.; Farr, A.L.; Randall, R.J. Protein measurement with Folin phenol reagent. *J. Biol. Chem.* **1951**, *193*, 256–275.
46. Rochdi, A.; Foucat, L.; Renou, J.P. NMR and DSC studies during thermal denaturation of collagen. *Food Chem.* **2000**, *69*, 295–299.
47. Shimada, K.; Fujikawa, K.; Yahara, K.; Nakamura, T. Antioxidative properties of xanthan on the autoxidation of soybean oil in cycloextrin emulsion. *J. Agric. Food Chem.* **1992**, *40*, 945–948.

## Pigment Cell Differentiation in Sea Urchin Blastula-Derived Primary Cell Cultures

Natalya V. Ageenko, Konstantin V. Kiselev, Pavel S. Dmitrenok and Nelly A. Odintsova

**Abstract:** The quinone pigments of sea urchins, specifically echinochrome and spinochromes, are known for their effective antioxidant, antibacterial, antifungal, and antitumor activities. We developed *in vitro* technology for inducing pigment differentiation in cell culture. The intensification of the pigment differentiation was accompanied by a simultaneous decrease in cell proliferation. The number of pigment cells was two-fold higher in the cells cultivated in the coelomic fluids of injured sea urchins than in those intact. The possible roles of the specific components of the coelomic fluids in the pigment differentiation process and the quantitative measurement of the production of naphthoquinone pigments during cultivation were examined by MALDI and electrospray ionization mass spectrometry. Echinochrome A and spinochrome E were produced by the cultivated cells of the sand dollar *Scaphechinus mirabilis* in all tested media, while only spinochromes were found in the cultivated cells of another sea urchin, *Strongylocentrotus intermedius*. The expression of genes associated with the induction of pigment differentiation was increased in cells cultivated in the presence of shikimic acid, a precursor of naphthoquinone pigments. Our results should contribute to the development of new techniques in marine biotechnology, including the generation of cell cultures producing complex bioactive compounds with therapeutic potential.

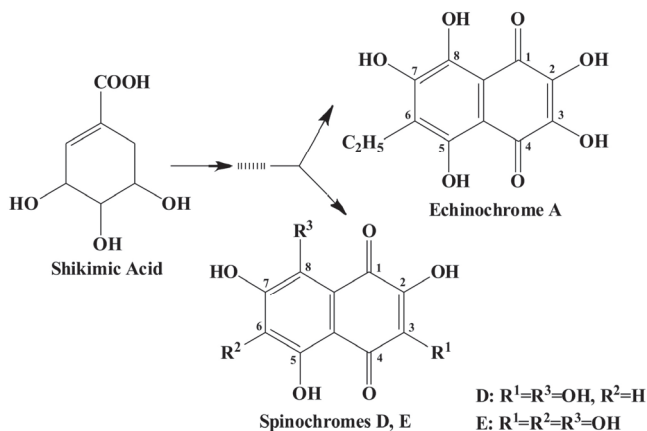
Reprinted from *Mar. Drugs*. Cite as: Ageenko, N.V.; Kiselev, K.V.; Dmitrenok, P.S.; Odintsova, N.A. Pigment Cell Differentiation in Sea Urchin Blastula-Derived Primary Cell Cultures. *Mar. Drugs* **2014**, *12*, 387463891.

### 1. Introduction

Marine inhabitants are the most phylogenetically diverse organisms, demonstrating a significant potential for biodiscovery research [1] and as possible sources of valuable biologically active substances for the pharmaceutical and food industries [2]. For example, sea urchins are a source of pharmacologically important quinone pigments—specifically echinochrome and the spinochromes—that constitute a group of polyketide compounds. Like many marine secondary metabolites, polyketide compounds are known for their highly effective antioxidant, antibacterial, antifungal, and antitumor activities. In addition, these compounds may play decisive roles in the regulation of lipid peroxidation and in immune defense [3–6]. They are generated via a series of enzymatic, oxidative and photochemical reactions from shikimic acid (ShA)—a precursor of naphthoquinone pigments (Figure 1) [7]. Echinochrome is one of these pigments and is synthesized in the sea urchin pigment cells demonstrating a strong bactericidal effect during embryonic and larval development [8,9]. The morphology and behavior of pigment cells are similar to those of macrophages, confirming the involvement of sea urchin pigment cells in the larval immune

system [10]. A drug (Histochrome<sup>®</sup>, Moscow, Russia) with cardiological and ophthalmological activity based on the echinochrome structure has been developed to correct metabolic processes and act as an oxygen transporter [11].

**Figure 1.** The structures of shikimic acid, a precursor of naphthoquinone pigments, and echinochrome and spinochromes in accordance with a previous report [7].



An industrial-scale procurement of echinochrome could lead to the extinction of the organisms that produce this substance. Therefore, cultured sea urchin pigment cells might provide a source of pharmacologically important quinone pigments, as well as help reduce the impact on the adult sea urchin population and pave the way for solving several pharmacological problems.

The aim of our work is to develop a technology for directed-pigment differentiation in sea urchin culture for solving practical tasks in marine biotechnology. Two sea urchin species differing in their number of embryonic pigment cells are chosen: the sea urchin *Strongylocentrotus intermedius* and the sand dollar *Scaphechinus mirabilis*. As shown in [12], the embryos of the sand dollar contain a lot of pigment cells. Previously, Calestani *et al.* [13] revealed three groups of genes expressed in sea urchin pigment cells that play key roles in the biosynthesis of naphthoquinone pigments [14]. The central parts of these genes in *S. intermedius* have been reported to be similar to those of the same genes in the closely related sea urchin *S. purpuratus* [15]. In this study, we evaluated the gene expression associated with the induction of pigment differentiation in cell cultures.

As previously shown, sand dollar embryos transfected with the foreign gene (the yeast *gal4* gene encoding the transcription activator) were dissociated into single cells that produced pigments after one month of cultivation [16]. We then developed an *in vitro* technology for inducing pigment differentiation without transfecting foreign genes into the sea urchin embryos but using the coelomic fluids from sea urchins [15]. Here, to estimate the contributions of the specific components of the coelomic fluids from sea urchins to the pigment differentiation process and the production of naphthoquinone pigments during cultivation, we used matrix assisted laser desorption/ionization (MALDI) time-of-flight (TOF) mass spectrometry and electrospray ionization (ESI) mass spectrometry.

This study has three main results. First, we developed an *in vitro* technology for inducing pigment differentiation in cell culture. Second, our data support the hypothesis that specific components of sea urchin coelomic fluids might act as inductive signals in pigment differentiation through the regulation of genes implicated in naphthoquinone synthesis. Third, echinochrome was produced only in the sand dollar cells, and its maximum level was found in cells cultured in coelomic fluids rather than seawater.

## 2. Results and Discussion

### 2.1. Differentiation of Pigment Cells in a Blastula-Derived Cell Culture

The growth patterns and morphology of cultured cells is often determined by peculiarities of the culture medium. To evaluate the effect of different culture media on the development of pigment differentiation in the cell cultures of both sea urchin species, we tested three types of media (Figures 2 and 3): seawater, the coelomic fluid preparations of control sea urchins and injured sea urchins. Injured sea urchins were obtained by needle pricks in the area of Aristotle's lantern (see the Experimental Section). The first distinctions in the appearance of pigment cells and their pigmentation became obvious after 3–7 days of cultivation. The cells cultivated in seawater were faintly pigmented and not numerous, whereas the pigment cells were more abundant in the coelomic fluid-cultivated cells. This picture was observed both in a short-time culture of the sea urchin *S. mirabilis* and in a long-time culture of the sea urchin *S. intermedius*.

**Figure 2.** Embryonic pigment cells in a blastula-derived cell culture of the sea urchin *Scaphechinus mirabilis* cultivated for 3 days. The cells were cultivated in seawater (A); the coelomic fluid of intact sea urchins (B); or the coelomic fluid of injured sea urchins (C). All culture media were supplemented with 2% fetal bovine serum. Insets in B and C: higher magnifications. Note the change in morphology of the pigment cells depending on the medium tested. Scale bar, 10  $\mu$ m.

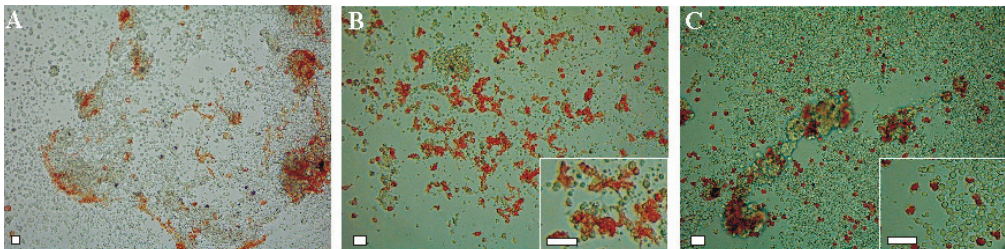
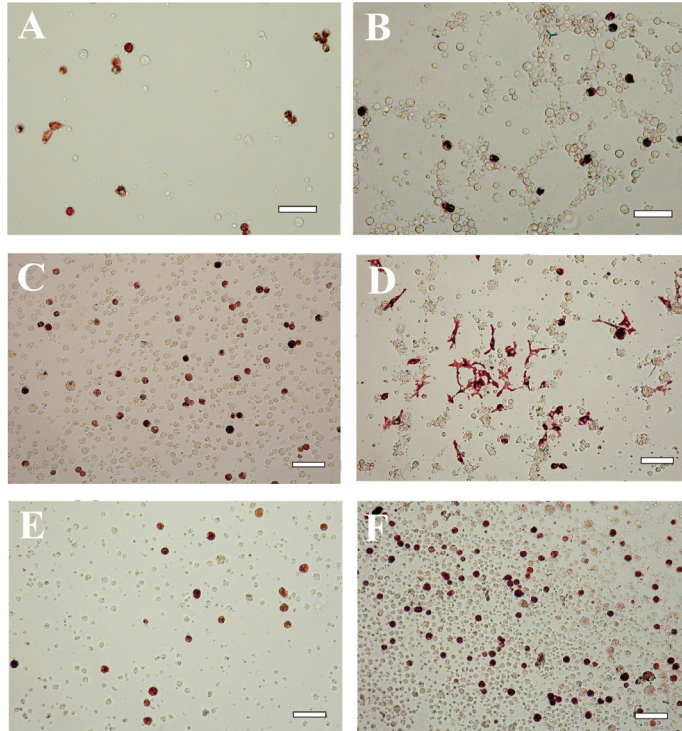


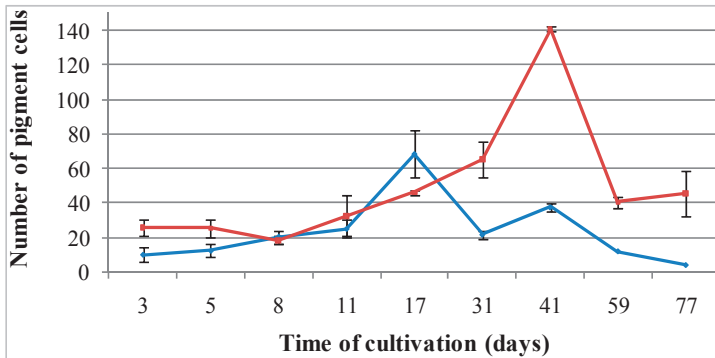
**Figure 3.** Embryonic pigment cells in a blastula-derived cell culture of the sea urchin *Strongylocentrotus intermedius* cultivated for 5 (A,B); 17 (C,D) or 41 days (E,F). A, C, E—cells cultivated in the coelomic fluid of intact sea urchins; B, D, F—cells cultivated in the coelomic fluid of injured sea urchins. The coelomic fluid was supplemented with 2% fetal bovine serum. Note the change in morphology of the pigment cells during cultivation. Scale bar, 10  $\mu$ m.



If the coelomic fluid of intact sea urchins was used as the medium, the pigment cells of *S. mirabilis* were well attached and spread during three days in culture (Figure 2B, insert). However, when the injured sea urchin coelomic fluid was used, most of the pigment cells were rounded and failed to spread (Figure 2C, insert).

The medium-dependent differences in cell morphology were also seen in the sea urchin *S. intermedius*. The pigment differentiation of the cells in the seawater occurred slowly and less extensively (data not shown) than that of the cells in the coelomic fluids. Furthermore, the pigment cells in this species changed their morphology during prolonged cultivation for 20 days in the same medium (Figure 3A–D). When the cells were cultivated in injured sea urchin coelomic fluid, the maximal spreading of the pigment cells was observed on Day 17 of cultivation (Figure 3D). Upon further culture, the cells became rounded (Figure 3E,F) and increased in number up to Day 41 of cultivation (Figure 4). Signs of cell degeneration were still detectable after two months of culturing.

**Figure 4.** Cellular dynamics of pigment cells cultivated in coelomic fluids of intact (blue line) and injured (red line) sea urchins for 2.5 months. At least 500 cells were counted in each tested culture medium.



The maximal number of pigmented cells of *S. intermedius* was detected on Day 17, when the cells were cultivated in the coelomic fluid of intact sea urchins (Figure 4, blue line). When the cells were cultivated in the injured sea urchin coelomic fluid, that maximal number was recorded on Day 41 (Figure 4, red line).

The number of pigment cells was dependent on the coelomic fluid used: twice as many pigment cells were detected in the cells cultivated in the injured sea urchin coelomic fluid as in that from intact sea urchins. In contrast, the number of pigment cells was significantly lower among cells cultured in in seawater (data not shown).

## 2.2. Cell Proliferation in Culture

It is well known that cell proliferation and differentiation are interrelated processes. To compare the contribution of these processes—pigment differentiation (as described above) and cell proliferation—in sea urchin culture, we detected dividing cells with antibodies to phospho-H3-histone, a well-known cell proliferation marker for many organisms [17–19]. At least 300–500 DAPI-stained cells were examined for each experiment with the culture media tested, and the proportion of cells positive for phospho-H3-histone relative to the total number of cells was determined. The number of dividing cells was higher in cells cultured in seawater than in those cultured in the coelomic fluids, where cell division was weak (Figure 5).

A significant difference in the number of dividing cells in the different media after one day of cultivation was found, and this difference increased for three days, when a general decrease in mitotic activity was then detected. In most cases, the cultures survived well, but their proliferation rate was low.

Dividing (phospho-H3-histone+) cells were detected from 6 to 72 h in all media tested, but the maximal number of dividing cells was found in seawater. The decrease in cell proliferation in the coelomic fluids was accompanied by a simultaneous intensification of the pigment cell differentiation. As already noted, the composition of the culture medium affected the rate of appearance of the pigment cells during cultivation. Figure 6A,B arrows, shows dividing cells in both of the coelomic

fluid and seawater after 12 h of cultivation (see details of the immunocytochemical manipulations in the Experimental Section).

**Figure 5.** The number of dividing cells in a blastula-derived culture of the sea urchin *S. intermedius* depending upon culture medium tested. The cells were cultivated for 24–72 h. The proportion of phospho-H3-histone-positive cells among the total number of examined cells (determined by DAPI staining of nuclei) was counted. SW—seawater; CFn—coelomic fluid obtained from intact sea urchins; CFrg—coelomic fluid obtained from injured sea urchins. \*  $p < 0.05$ ; \*\*  $p < 0.01$  versus values of dividing cells cultivated in the sea water (24 h).

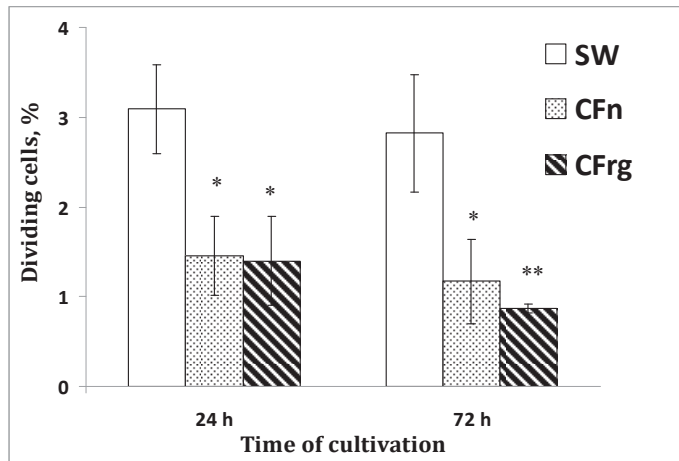
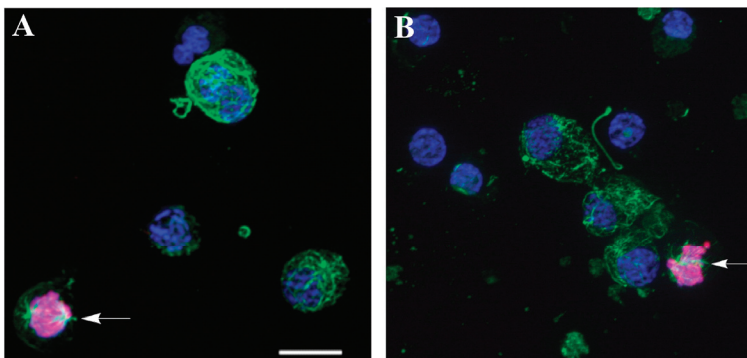


**Figure 6.** Immunofluorescence detection of dividing (phospho-H3-histone-positive) cells in a blastula-derived culture. The preparations were imaged via confocal microscopy. The cells were cultivated on fibronectin-coated coverslips in coelomic fluid obtained from injured sea urchins (A) and in seawater (B) for 12 h and then labeled with Abs against phospho-H3-histone Abs for the detection of dividing cells (red) and tubulin (green) for the detection of microtubules. The nuclei were stained with DAPI (blue). Arrows show ph-H3-histone-positive cells. Scale bar, 10  $\mu\text{m}$ .





### 2.3. MALDI MS Analysis of Coelomic Fluids Obtained from Intact and Injured Sea Urchins

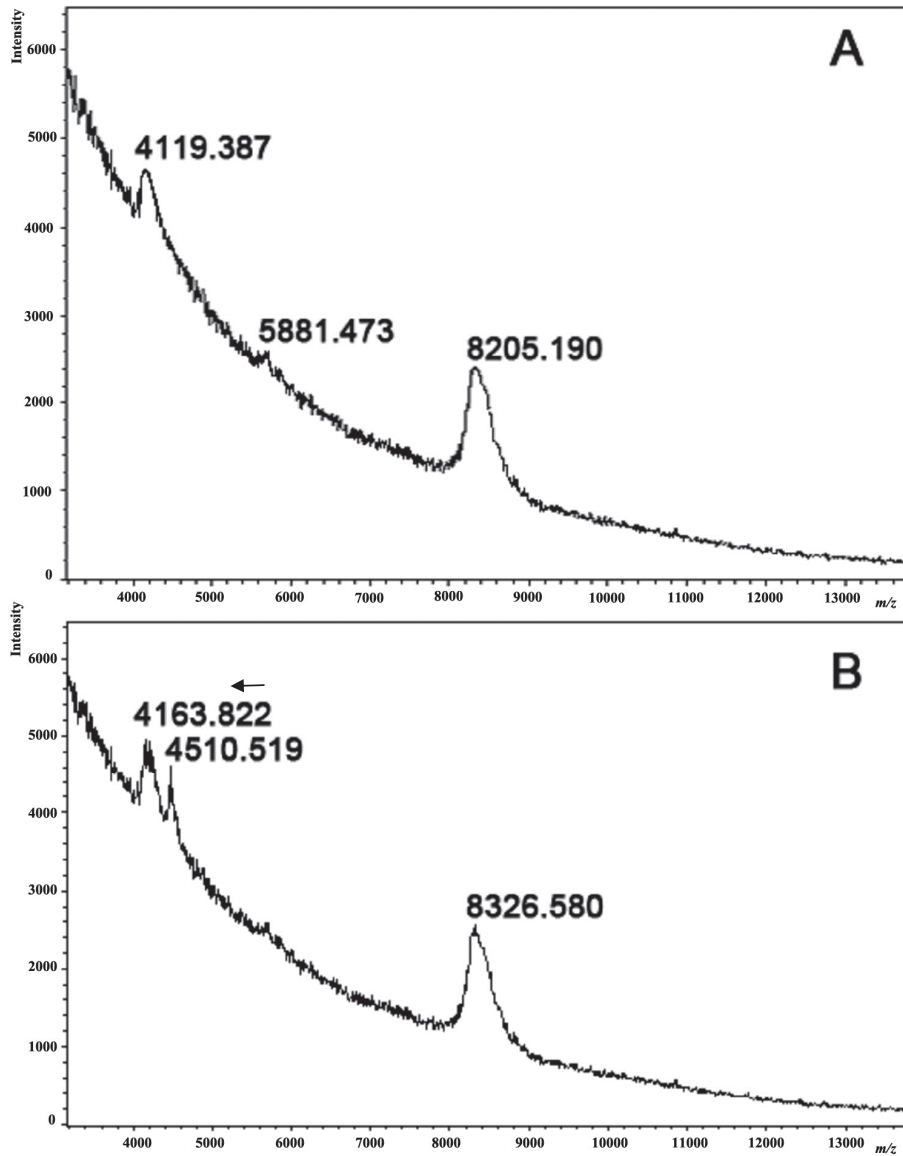
To estimate the contribution of specific components in intact and injured sea urchin coelomic fluids to the cell pigment differentiation process during cultivation and to understand its origin, we conducted MALDI MS analyses of both coelomic fluids of *S. intermedius*. Figure 7 illustrates the MALDI mass spectra obtained for proteins with a molecular mass of 4000–9000 Da. Two well-defined peaks corresponding to proteins of 8205 Da and 4119 Da were detected in the spectrum of the intact sea urchin coelomic fluid (Figure 7A). The spectrum of coelomic fluid obtained from the injured sea urchins exhibited three peaks: 8327 Da, 4511 Da, and 4164 Da (Figure 7B). A comparison of the coelomic fluid profiles revealed a new peak in the coelomic fluid of the injured sea urchins corresponding to a protein with a molecular weight of around 4500 Da and a shift of approximately 40–120 Da from the basic components in the intact sea urchin coelomic fluid, which may be due to a protein modification such as phosphorylation, sulfation, *etc.* The molecular weights of the proteins were measured using MALDI MS with standard precision (0.1%) based on the external calibration programs included (Protein Calibration Mixture II, Bruker Daltonik, Germany). The new peak in the spectrum (4511 Da) indicates a change in the composition of the proteins in the coelomic fluid after injury in comparison to the norm. Although we could not identify the molecular nature of the coelomic fluid proteins, our data clearly demonstrated a qualitative difference in the composition of normal coelomic-fluid proteins and that of coelomic-fluid proteins following injury.

### 2.4. Naphthoquinone Pigment Production in Cultivated Sea Urchin Cells

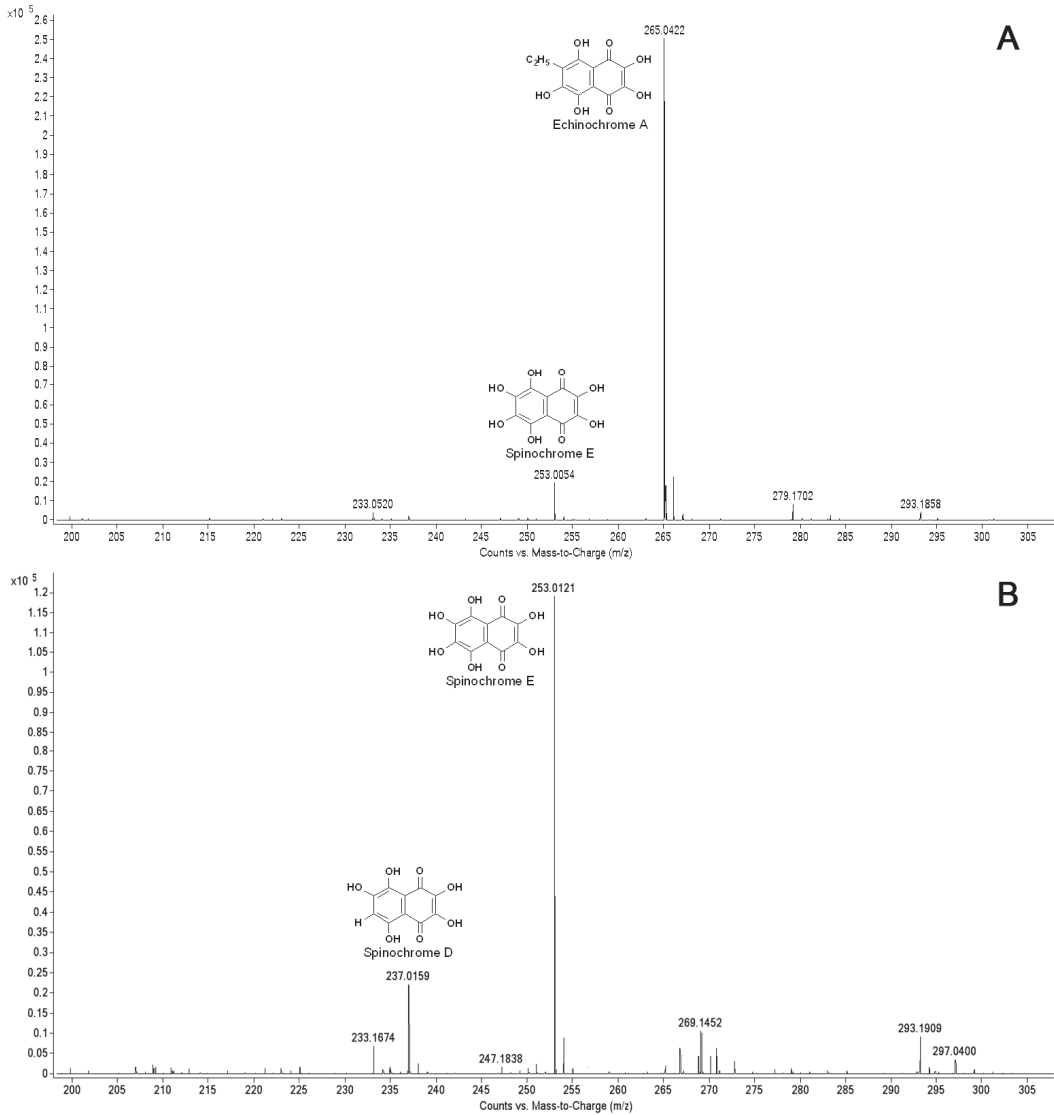
To elucidate the naphthoquinone pigment profile in the cultivated sea urchin cells and the production of pigments during cultivation, we performed ESI MS. As shown in Figure 8A, a significant peak of echinochrome A and a small peak corresponding to spinochrome E were detected in the pigment extracts from the sand dollar *S. mirabilis*, while only the peaks corresponding to spinochromes D and E were recorded in the pigment cell extracts from *S. intermedius* (Figure 8B). Thus, a distinct difference in pigment expression was demonstrated in the cells of the two sea urchin species.

The results of a semi-quantitative measurement (using ESI MS) of the echinochrome and spinochrome production in cells cultivated in the different media are presented in Table 1. Echinochrome A was produced by cultivated *S. mirabilis* cells in all of the tested media, and it was well defined in all of the spectra. The highest level of echinochrome A was detected in the cells cultured in the coelomic fluids as compared to those cultured in seawater. In contrast, no significant differences were seen in the spinochrome D and E levels in the tested media for the cultivated cells of the other sea urchin, *S. intermedius* (Table 1).

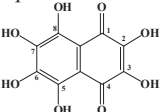
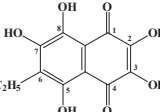
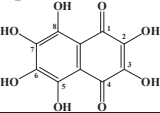
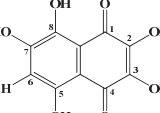
**Figure 7.** The mass spectra of coelomic fluids obtained from intact (A) and injured (B) sea urchins by MALDI TOF MS using a mass spectrometer (Ultraflex-III TOF/TOF, Bruker Daltonics, Germany). Note a new peak in the coelomic fluid of the injured sea urchins, corresponding to a protein with MW near 4500 Da (marked by an arrow), as well as the shift of the basic components of the intact coelomic fluid to approximately 40–120 Da. The coelomic fluids from three independent experiments were analyzed.



**Figure 8.** ESI MS profiles of naphthoquinone pigments from sea urchin cell cultures: (A) the pigment extracts from the cells of the sea urchin *S. mirabilis* after 3-day cultivation in seawater; (B) the pigment extracts from the cells of the sea urchin *S. intermedius* after 6-day cultivation in seawater.



**Table 1.** Naphthoquinone pigment production in sea urchin cultivated cells. Data are presented as the mean  $\pm$  standard error from two independent experiments (ESI MS). SW—seawater; CFn—coelomic fluid obtained from intact sea urchins; CFreg—coelomic fluid obtained from injured sea urchins.

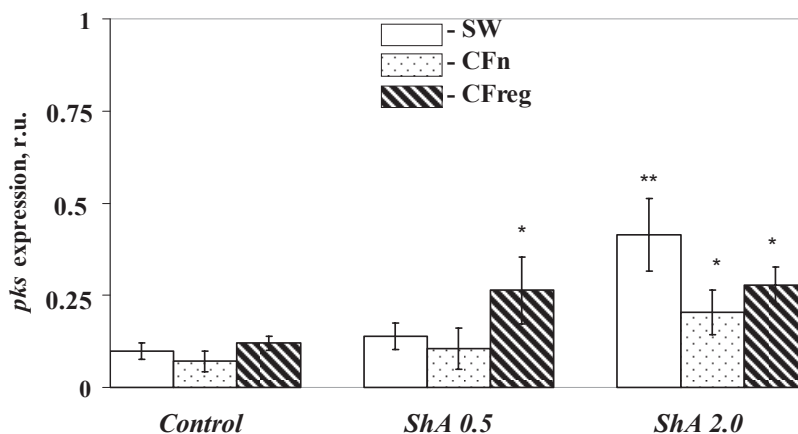
Pigments, mg/g of Fresh Biomass of Cells	M.W.	Cell Culture Medium		
		SW	CFn	CFreg
<i>Scaphechinus mirabilis</i>				
<p><i>Spinochrome E</i></p> 	254.00	0.021 $\pm$ 0.003	0.062 $\pm$ 0.007	0.054 $\pm$ 0.006
<p><i>Echinochrome A</i></p> 	266.04	0.250 $\pm$ 0.026	0.640 $\pm$ 0.061	0.540 $\pm$ 0.055
<i>Strongylocentrotus intermedius</i>				
<p><i>Spinochrome E</i></p> 	254.00	0.024 $\pm$ 0.004	0.013 $\pm$ 0.002	0.015 $\pm$ 0.002
<p><i>Spinochrome D</i></p> 	238.02	0.052 $\pm$ 0.006	0.044 $\pm$ 0.005	0.062 $\pm$ 0.007

### 2.5. Expression of the *pks* Genes in Cultivated Sea Urchin Cells. Experiments with Shikimic Acid, a Precursor of Naphthoquinone Pigments

To understand the molecular mechanisms underlying sea urchin pigment specialization in culture, we evaluated the gene expression associated with the induction of pigment differentiation, particularly the *pks* genes. The expression level of these genes (estimated by quantitative real-time PCR) in sea urchin cells cultivated in different culture media is presented in relative units in Figure 9 (see the Experimental Section). The gene expression in sea urchin cells cultivated in the coelomic fluid of injured sea urchins increased more than 1.2-fold in comparison to the cells cultivated in seawater, whereas the *pks* expression in the cells cultivated in the coelomic fluid from intact sea urchins decreased by almost 1.4-fold; however, these differences were insignificant. The addition of a high concentration of ShA, a precursor of naphthoquinone pigments, (2 mM) to the sea urchin cells resulted in a marked intensification of the gene expression in all media tested (2.3–4.2-fold) compared to the control cells (Figure 9), but the effect was especially significant in seawater. In contrast, adding ShA of a lower concentration (0.5 mM) increased *pks* expression only in the cells cultivated in injured sea urchin coelomic fluid (2.2-fold). No apparent effect on *pks* expression was detected in the cells cultivated with 0.5 mM ShA in seawater or intact sea urchin coelomic fluid.

These data can be explained by the presence of some specific components in the sea urchin coelomic fluids. The marked intensification of the *pks* expression (2.2-fold) in the presence of 0.5 mM ShA only in the cells cultivated in injured sea urchin coelomic fluid is additional evidence of a cellular reaction in response to injury signals. Our findings showing a significant difference between the number of sea urchin pigment cells cultivated in the coelomic fluids of injured and intact sea urchins support this suggestion.

**Figure 9.** Effect of Shikimic Acid (ShA) on the *pks* gene expression in a blastula-derived cell culture of the sea urchin *Strongylocentrotus intermedius*. ShA concentrations tested: 0.5 mM and 2.0 mM. Y-axis—relative units (r.u.). The cells were cultivated with ShA for 4 days in: seawater (SW), coelomic fluid of intact sea urchins (CFn), and coelomic fluid of injured sea urchins (CFreg). After this period, total RNA was isolated from cultivated cells for the following real-time PCR. Control cells are the cells cultivated without ShA. \*  $p < 0.05$ ; \*\*  $p < 0.01$  versus values of *pks* expression in the appropriate control conditions.



## 2.6. Discussion

Marine biotechnology progress is associated with the search, characterization, and development of optimal methods for obtaining new substances from marine organisms with pharmaceutically interesting biological activity, and many are of enormous scientific interest. On the one hand, marine organisms are a source of unique marine secondary metabolites that are the basis for developing new and improved natural products for commercial purposes [2]. On the other hand, they include a variety of phylogenetic groups that are important for understanding the evolutionary history of life. Some, such as the echinoderms, are members of a phylum of deuterostome metazoans and occupy a key position in the early steps in chordate evolution [20,21]. As shown by Evans-Illidge *et al.* [1], the ancestral early-metazoans (Porifera), early eumetazoans (Cnidaria) and some deuterostomes (Echinodermata) have a very high concentration of bioactive compounds.

Here, we have shown that the culture medium composition affects the rate of appearance of pigment cells. In seawater, the number of dividing cells was higher than when the cells were

cultured in the coelomic fluids, but the pigment cell differentiation occurred slowly and less extensively. An increase in cell pigmentation in the coelomic fluids probably leads to a decrease in the number of dividing cells in comparison to the cells incubated in seawater. In the early stages of cultivation, we detected dividing cells and a few pigment cells, but later during the pigment cell differentiation, we observed a decrease in the number of dividing cells and a corresponding increase in the number of pigment cells. This is not surprising: either proliferation or differentiation usually dominates in cell cultures. A significant decrease in the number of dividing cells can be explained by a general reduction of mitotic activity during cultivation that has been previously reported for many invertebrate cells after 7–10 days of cultivation [22,23].

We proposed that a significant difference in the proportion of pigment cells in the cultures grown in the coelomic fluids of intact and injured sea urchins in comparison to those cultivated in seawater was connected to the specific components of coelomic fluids that increase the adhesion of cultivated cells. Recently, approximately 30 proteins that may be involved in adhesion were uncovered by a large-scale proteomic analysis of sea urchin coelomic fluid [24]. Thus, far, a proteomic analysis has only been performed on normal sea urchin coelomic fluid.

In this study, we analyzed the coelomic fluid of both normal and injured sea urchins, and detected qualitative differences in their composition. Our results from the overview of integral MALDI mass spectra of sea urchin coelomic fluids have shown that new peaks appear in the coelomic fluid obtained from injured sea urchins. These new peaks may correspond to stress proteins produced after injury. As recently reported, relatively abundant proteins involved in stress responses were identified in the coelomic fluid of the sea urchin *S. purpuratus* [24]. Homologues of these proteins have been found throughout the animal kingdom and are often used as markers for environmental stress [25]. We have suggested that the new coelomic fluid proteins from the injured sea urchins may be related to stress-response proteins. The MALDI MS data together with the results for *pks* gene expression suggest that the specific components of sea urchin coelomic fluids play a role in pigment differentiation through the regulation of the genes implicated in naphthoquinone synthesis. Analyzing cells cultivated in the presence of 0.5 mM ShA, we showed that *pks* gene expression was two-fold higher in cells cultivated in the injured sea urchin coelomic fluid relative to cells cultivated in that from intact sea urchins. A higher proportion of cells containing naphthoquinones in response to different conditions of stress could be a consequence of a protective reaction and be important as a defense mechanism [26,27].

We found that echinochrome was produced only in the sand dollar cells and its content in cells grown in coelomic fluid was higher than that in cells grown in seawater. This finding suggests the existence of a specific regulatory factor that may induce pigmentation activity and subsequent naphthoquinone production in these coelomic fluids. Our morphological observations of the cultured cells correlated with the semi-quantitative data obtained using ESI MS. Unfortunately, not all of the experiments could be performed on the *S. mirabilis* cell cultures due to the difficulty in obtaining the sand dollar cells free of bacterial contamination.

### 3. Experimental Section

#### 3.1. Animals

Adult sea urchins (*S. intermedius* and *S. mirabilis*, Echinoidea (Agassiz, 1863)), were collected during the breeding season (Vostok Bay, the Sea of Japan), and they were kept in aquaria filled with running, aerated seawater at 16 °C. Before experiments were conducted, the animals were rinsed free of any debris with UV-sterilized filtered seawater. Experiments were performed at the Marine Biological Station «Vostok» (A.V. Zhirmunsky Institute of Marine Biology, Vladivostok, Russia FEB RAS). Gametes and embryos were obtained by the KCl injection method as described before [15]. The embryonic material was placed in tanks with UV-sterilized seawater (18 °C) throughout development and harvested at the mesenchymal blastula (16 h post fertilization, hpf).

#### 3.2. Cell Culture

Developing sea urchin embryos were collected on a fine 30- $\mu$ m nylon mesh and dissociated into single cells with 0.25% collagenase at 17 °C (for 20–30 min) as described earlier [15]. The resulting cell suspension containing all cell types was washed several times in seawater with antibiotics, and then sterile seawater supplemented with 2% fetal calf serum, FCS (Sigma, St. Louis, MO, USA) was added. Cell viability was estimated at different time points by a trypan blue exclusion test. The cells were seeded at the density of  $6 \times 10^6$ – $8 \times 10^6$  cells/mL in plastic Petri dishes (Lux Culture Dishes, MP Biomedicals, Santa Ana, CA, USA), and after two days of cultivation, a subset of cells (after several strokes of gentle pipetting) at the density of  $3 \times 10^6$ – $4 \times 10^6$  cells/mL was transferred into new plastic Petri dishes (Nunc, Nunclon Surface, Roskilde, Denmark) on the coverslips for further culturing. We used three types of the cell culture media (98%) supplemented with 2% FCS: seawater and the coelomic fluid preparations of intact and injured sea urchins (*S. intermedius*) that were obtained as described in [15]. In few, a day after damaging sea urchins, the coelomic fluids from control and injured sea urchins were collected by puncture in the area of Aristotle's lantern. After removal of the clotting of coelomocytes by centrifugation, the supernatant was sterilized by filtration (0.22  $\mu$ m, Millipore, CA, USA). The cell cultures were maintained by replacement of 50% of the medium at 3–5-day intervals for 3–42 days at 17 °C. To observe primary cell cultures during the overall period we used an inverted microscope Axiovert 200M (Carl Zeiss, Jena, Germany).

#### 3.3. Immunohistochemical Analysis

After cultivation on fibronectin-coated or non-coated coverslips for 12–72 h, the cells were fixed in 4% paraformaldehyde (Sigma) in PBS, pH 7.8, for 7–10 min at 4 °C and rinsed three times in cold PBS. The material was stored in PBS with 0.03% NaN<sub>3</sub> at 4 °C until needed. To reduce non-specific binding, the samples were incubated overnight in a blocking solution containing 10% normal goat serum (Sigma), 0.25% BSA, 0.1% Triton X-100, and 0.03% NaN<sub>3</sub> in PBS. The cells were first incubated for 8 h at 10 °C in blocking solution with the following primary antibodies (Abs): mouse monoclonal anti- $\alpha$  acetylated tubulin (Sigma, diluted 1:1000) and rabbit polyclonal

anti-phospho-H3 histone (Merck, Millipore, Germany, diluted 1:500). As secondary Abs, we used goat anti-mouse (GAM) or goat anti-rabbit (GAR) secondary Abs conjugated to Alexa Fluor 488, 546 or 633 (Molecular Probes, Eugene, OR, USA) at a dilution of 1:1000–1:2000 in PBS for 2 h at RT. The specimens were then washed and embedded in the Vectashield mounting medium (Vector Laboratories, Burlingame, CA, USA) containing 0.1  $\mu\text{g}/\text{mL}$  DAPI to reveal the nuclei. For negative controls, primary Abs were omitted from the staining protocol. Specimens were analyzed with a confocal laser scanning microscope (Zeiss LSM 780) equipped with a high sensitivity GaAsP detector (with the 63 $\times$  or 100 $\times$  oil-immersion objectives). For 3D reconstructions, ImageJ software (NIH) was used. The number of dividing cells in each type of culture medium was estimated by calculating the percentage of phospho-H3 histone-positive cells among the total number of examined cells (determined by DAPI staining of nuclei). At least 300–500 DAPI-stained cells were counted in each experiment for each type of culture medium tested.

### 3.4. MALDI and ESI MS

Coelomic fluids obtained from intact and injured sea urchins, as described previously [15] were selected for MALDI-MS analysis. The mass spectra were registered using an Ultraflex-III TOF/TOF mass spectrometer (Bruker Daltonics, Bremen, Germany), equipped with a smart-beam laser (355 nm) having a pulse frequency of 100 Hz and a pulse width of 3 ns (PIBOC, FEB RAS). The mass spectrometer was used in the linear mode with delayed ion extraction and with the matrix alpha-cyano-4-hydroxy-cinnamic acid (Bruker Daltonics). The Protein Calibration Standard I (Bruker Daltonics) (1  $\mu\text{L}$ ) was added as the internal standard.

Metabolites were extracted from cultivated sea urchin cells. Quinone pigments were extracted with 1 mL of acidified ethanol (1 part 25% HCl and 3 parts of 96% ethanol) for 24 h at 4  $^{\circ}\text{C}$ , as described [28]. Diethyl ether was added to supernatants, and an organic layer containing quinones was washed with 5% NaCl until the acid was almost removed. The ether solution was dried over anhydrous sodium sulfate. The extract including the pigments was stored at  $-25^{\circ}\text{C}$  in the dark, and it was then analyzed by ESI-MS using a mass spectrometer Agilent 6510 Q-TOF LC/MS (Agilent Technologies, Santa Clara, CA, USA).

The alcoholic extracts were obtained from cultivated cells ( $5 \times 10^6$  cells/mL) after 3 and 6 days in culture. The sample solution was membrane-filtered (0.45  $\mu\text{m}$ , Millipore), and 2  $\mu\text{L}$  aliquots were used for analysis.

The mass spectra were recorded in the negative-ion detection mode within the  $m/z$  mass range of 100–800 and at mass-to-charge ratio ( $m/z$ ) of 70–500 for MS/MS spectra (scan time 1 s). The quinonoid pigments were identified by exact mass measurement of deprotonated molecules  $[\text{M} - \text{H}]^{-}$  in the MS spectra and by comparisons of the characteristic MS/MS spectra with the MS/MS spectra of pure naphthoquinone standards. The MS/MS spectra were recorded in the MS/MS mode using a collision energy ranging from 20 V to 35 V; the precursor ions were isolated with an isolation width of 1.3  $m/z$ . The mass spectrometer was calibrated using the ESI-L Low Concentration Tuning Mix (Agilent Technologies, USA). A high-resolution MS analysis was performed by adding the Reference Mix (Agilent Technologies, USA) through a reference sprayer



in a Dual-ESI source. The data were analyzed with FlexAnalysis Version 3.0 (Bruker Daltonics, Bremen, Germany).

### 3.5. *Quantitative Real-Time PCR (Q-Real-Time PCR)*

Sterile solutions of ShA (Sigma) in seawater at the desired concentrations (0.5 mM and 2.0 mM) were added in a blastula-derived cell culture of the sea urchin *S. intermedius* after seeding, and the cells were incubated during four days. After this period, total RNAs from cultivated sea urchin cells were extracted with Yellow Solve reagent (Clonogen, St. Petersburg, Russia) and treated with DNase I (Sileks, Moscow, Russia) to remove genomic DNA. The first strand of cDNA was synthesized using 1.5 µg of total RNA as a template with the Reverse Transcription System (Sileks) in a 50 µL reaction volume as described previously [5]. The 0.5–2 µL samples of reverse transcription products were then amplified by PCR on the sea urchin actin gene using the primers 5'CAA CGG ATC CGG TAT GGT GAA GGC and 5'TCC AGA CGG AGG ATG GCG TGG GGA. The PCR reactions were made using iCycler thermocycler (Bio-Rad Laboratories, Inc., Hercules, CA, USA) with the conditions: one cycle of 2 min at 95 °C followed by 40 cycles of 15 s at 95 °C, 15 s at 50 °C and 35 s at 72 °C with a final extension cycle of 10 min at 72 °C. In the following Q-real-time PCR analyses, we used only those reverse transcription reactions that resulted in 500 bp PCR products for the *actin* gene. We discarded those reverse transcription reactions that resulted in both 500 and 700 bp PCR products for the *actin* gene, which indicated DNA contamination.

Quantitative real-time PCR was performed using the established protocol [15]. For TaqMan Q-real-time RT-PCR, cDNAs were amplified in 20 µL of the reaction mixture containing 1× TaqMan Buffer, 2.5 mM MgCl<sub>2</sub>, 250 µM of each deoxynucleotide, 1 U Taq DNA polymerase, 0.5–2 µL cDNA samples, and 0.25 µM of each primer and probe (Real-Time PCR Kit, Syntol, Moscow, Russia). The amplification conditions consisted of one cycle of 2 min at 95 °C followed by 50 cycles of 10 s at 95 °C and 25 s at 62 °C. The TaqMan PCR assays were performed in an iCycler thermocycler supplied with the iQ5 Multicolor Real-Time PCR detection system (Bio-Rad Laboratories, Inc., Hercules, CA, USA) and data were analyzed with the iQ5 Optical System Software v.2.0 as described previously [6] and presented in relative units. The *S. intermedius actin* gene (GenBank accession number DQ229162) and *ubiquitin* gene (LOC754856) were used as an endogenous control to normalize variance in the quality and the amount of cDNA used in each Q-real-time RT-PCR experiment. The data were summarized from five independent experiments. Primers and TaqMan probes for the *actin*, *ubiquitin*, *pks* genes used in Q-real-time PCR were described previously [6,15].

### 3.6. *Statistical Analysis*

The data are presented as mean ± standard error of the mean (SE). Data from the experiments were subjected to a one-way analysis of variance (ANOVA) with Tukey's pairwise comparison test at  $p = 0.05$  with the use of the Microsoft Office Excel 2003 program.

## 4. Conclusions

This study provides evidence for the production of naphthoquinone pigments in cultivated sea urchin cells. Echinochrome A and spinochrome E were produced by cultivated cells from the sand dollar *S. mirabilis* in all tested media, but only spinochromes were recorded in the cultivated cells from the sea urchin *S. intermedius*. Our data support the hypothesis that specific components of sea urchin coelomic fluids might act as inductive signals in pigment differentiation. The differentiation of pigment cells is accompanied by the active expression of genes involved in naphthoquinone synthesis and appears to be important for defense processes. Thus, our findings and the technology developed for directed pigment cell differentiation in culture may be instrumental in solving some practical tasks in marine biotechnology, including the generation of cell cultures producing complex bioactive compounds with therapeutic potential.

## Acknowledgments

This study was supported by the Russian Foundation for Basic Research (12-04-00363a), the Program «Far East» of the Russian Academy of Sciences (11.2.1, 11.2.2), and the Program at the Far Eastern Federal University (11 G34.31.0010). The work was partly performed at the “Far Eastern Cooperative Center of Electron Microscopy” (A. V. Zhirmunsky Institute of Marine Biology, FEB RAS, Vladivostok, Russia). The authors express their thanks to Maria Maiorova for her help in obtaining of confocal microscope images and to the anonymous reviewers for their valuable comments which have improved the manuscript.

## Author Contributions

N.A. and N.O. designed and coordinated the research, took part in the experiments with cell cultures and contributed equally in writing the MS; K.K. and N.A. carried out the real-time-PCR experiments and analyzed the data; P.D. performed the MALDI and ESI MS analysis. All authors read and approved the final manuscript.

## Conflicts of Interest

The authors declare no conflict of interest.

## References

1. Evans-Illidge, E.A.; Logan, M.; Doyle, J.; Fromont, J.; Battershill, C.N.; Ericson, G.; Wolff, C.W.; Muirhead, A.; Kearns, P.; Abdo, D.; *et al.* Phylogeny drives large scale patterns in Australian marine bioactivity and provides a new chemical ecology rationale for future biodiscovery. *PLoS One* **2013**, *8*, e73800; doi:10.1371/journal.pone.0073800.
2. Volkman, J.K. Australiasian research on marine natural products: Chemistry, bioactivity and ecology. *Mar. Freshw. Res.* **1999**, *50*, 761–779.
3. Koltsova, E.A.; Boguslavskaya, L.V.; Maximov, O.B. On the functions of quinonoid pigments in sea-urchin embryos. *Invertebr. Reprod. Dev.* **1981**, *4*, 17–23.

4. Service, M.; Wardlaw, A. Echinochrome-A as a bactericidal substance in the coelomic fluid of *Echinus esculentus* (L.). *Comp. Biochem. Physiol. Part B* **1984**, *79*, 161–165.
5. Castoe, T.A.; Stephens, T.; Noonan, B.P.; Calestani, C. A novel group of type I polyketide synthases (PKS) in animals and the complex phylogenomics of PKSs. *Gene* **2007**, *392*, 47–58.
6. Kiselev, K.V.; Ageenko, N.V.; Kurilenko, V.V. Involvement of the cell-specific pigment genes pks and sult in the bacteria defense response of the sea urchin *Strongylocentrotus intermedius*. *Dis. Aquat. Organ.* **2013**, *103*, 121–132.
7. Thompson, R.H. *Naturally Occurring Quinones*, 2nd ed.; Academic Press: New York, NY, USA, 1971; p. 734.
8. Singh, H.; Moore, R.E.; Scheuer, P.J. The distribution of quinone pigments in echinoderms. *Experientia* **1967**, *23*, 624–626.
9. Smith, L.C.; Rast, J.P.; Brocton, V.; Terwilleger, D.P.; Nair, S.V.; Buckley, K.M.; Majestke, A.J. The sea urchin immune system. *Invertebr. Surviv. J.* **2006**, *3*, 25–29.
10. Gibson, A.W.; Burke, R.D. The origin of pigment cells in embryos of the sea urchin *Strongylocentrotus purpuratus*. *Dev. Biol.* **1985**, *107*, 414–419.
11. Mishchenko, N.P.; Fedoreev, S.A.; Bagirova, V.L. Histochrome: A new original domestic drug. *Pharm. Chem. J.* **2003**, *37*, 48–52.
12. Kominami, T.; Takata, H. Process of pigment cell specification in the sand dollar, *Scaphechinus mirabilis*. *Dev. Growth Differ.* **2002**, *44*, 113–125.
13. Calestani, C.; Rast, J.P.; Davidson, E.H. Isolation of pigment cell specific genes in the sea urchin embryo by differential macroarray screening. *Development* **2003**, *130*, 4587–4596.
14. Beeble, A.; Calestani, C. Expression pattern of polyketide synthase-2 during sea urchin development. *Gene Expr. Patt.* **2012**, *12*, 7–10.
15. Ageenko, N.V.; Kiselev, K.V.; Odintsova, N.A. Expression of pigment cell-specific genes in the ontogenesis of the sea urchin *Strongylocentrotus intermedius*. *Evid.-Based Compl. Altern. Med.* **2011**, *2011*, doi:10.1155/2011/730356.
16. Odintsova, N.A.; Kiselev, K.V.; Bulgakov, V.P.; Koltsova, E.A.; Yakovlev, K.V. Influence of the activator of transcription gal4 on growth and development of embryos and embryonic cells in primary cultures of sand dollar. *Russ. J. Dev. Biol.* **2003**, *34*, 217–222.
17. Hans, F.; Dimitrov, S. Histone H3 phosphorylation and cell division. *Oncogene* **2001**, *20*, 3021–3027.
18. Sharlaimova, N.; Shabelnikov, S.; Petukhova, O. Small coelomic epithelial cells of the starfish *Asterias rubens* L. that are able to proliferate *in vivo* and *in vitro*. *Cell Tissue Res.* **2014**, doi:10.1007/s00441-013-1766-8.
19. Wagenaar, E.B. The timing of synthesis of proteins required for mitosis in the cell cycle of the sea urchin embryo. *Exp. Cell Res.* **1983**, *144*, 393–403.
20. Bromham, L.D.; Degnan, B.M. Hemichordates and deuterostome evolution: Robust molecular phylogenetic support for a hemichordate plus echinoderm clade. *Evol. Dev.* **1999**, *1*, 166–171.
21. Wray, G.A.; Lowe, C.J. Developmental regulatory genes and echinoderm evolution. *Syst. Biol.* **2000**, *49*, 28–51.

22. Peter, R.; Gschwentner, R.; Schürmann, W.; Rieger, R.M.; Ladurner, P. The significance of stem cells in free-living flatworms: One common source for all cells in the adult. *J. Appl. Biomed.* **2004**, *2*, 21–35.
23. Odintsova, N.A. Stem cells of marine invertebrates: Regulation of proliferation and induction of differentiation *in vitro*. *Cell Tissue Biol.* **2009**, *3*, 403–408.
24. Dheilly, N.M.; Raftos, D.A.; Haynes, P.A.; Courtney Smith, L.; Nair, S.V. Shotgun proteomics of coelomic fluid from the purple sea urchin, *Strongylocentrotus purpuratus*. *Dev. Comp. Immunol.* **2013**, *40*, 35–50.
25. Fink, A.L. Chaperone-mediated protein folding. *Physiol. Rev.* **1999**, *79*, 425–449.
26. Branco, P.C.; Pressinotti, L.N.; Borges, J.C.S.; Iunes, R.S.; Kfoury, J.R., Jr.; Silva, M.O.; Gonzalez, M.; Santos, M.F.; Peck, L.S. Cellular biomarkers to elucidate global warming effects on Antarctic sea urchin *Sterechinus neumayeri*. *Polar Biol.* **2012**, *35*, 221–229.
27. Branco, P.C.; Borges, J.C.S.; Santos, M.F.; Jensch, B.E., Jr.; Silva, M.O. The impact of rising sea temperature on innate immune parameters in the tropical subtidal sea urchin *Lytechinus variegatus* and the intertidal sea urchin *Echinometra lucunter*. *Mar. Environ. Res.* **2013**, *92*, 95–101.
28. Kuwahara, R.; Hatate, H.; Chkami, A.; Murata, H.; Kijidani, Y. Quantitative separation of antioxidant pigments in purple sea urchin shells using a reversed-phase high performance liquid chromatography. *LWT Food Sci. Technol.* **2010**, *43*, 1185–1190.

# Lipids and Fatty Acids of Nudibranch Mollusks: Potential Sources of Bioactive Compounds

Natalia V. Zhukova

**Abstract:** The molecular diversity of chemical compounds found in marine animals offers a good chance for the discovery of novel bioactive compounds of unique structures and diverse biological activities. Nudibranch mollusks, which are not protected by a shell and produce chemicals for various ecological uses, including defense against predators, have attracted great interest for their lipid composition. Lipid analysis of eight nudibranch species revealed dominant phospholipids, sterols and monoalkyldiacylglycerols. Among polar lipids, 1-alkenyl-2-acyl glycerophospholipids (plasmalogens) and ceramide-aminoethylphosphonates were found in the mollusks. The fatty acid compositions of the nudibranchs differed greatly from those of other marine gastropods and exhibited a wide diversity: very long chain fatty acids known as demospongiic acids, a series of non-methylene-interrupted fatty acids, including unusual 21:2 $\Delta$ 7,13, and an abundance of various odd and branched fatty acids typical of bacteria. Symbiotic bacteria revealed in some species of nudibranchs participate presumably in the production of some compounds serving as a chemical defense for the mollusks. The unique fatty acid composition of the nudibranchs is determined by food supply, inherent biosynthetic activities and intracellular symbiotic microorganisms. The potential of nudibranchs as a source of biologically active lipids and fatty acids is also discussed.

Reprinted from *Mar. Drugs*. Cite as: Zhukova, N.V. Lipids and Fatty Acids of Nudibranch Mollusks: Potential Sources of Bioactive Compounds. *Mar. Drugs* **2014**, *12*, 457864592.

## 1. Introduction

The molecular diversity of chemical compounds found in marine animals is the result of the evolution of the organisms and their unique physiological and biochemical adaptations and offers a good chance for the discovery of novel bioactive compounds with a variety of unique structures and diverse biological activities [1]. Marine mollusks have become the focus of many chemical studies aimed at isolating and identifying novel natural products [2]. Phylum Mollusca is the second largest phylum of animals. Nudibranch mollusks, which often are very colorful, are not protected by a shell and are named sea slugs, have attracted strong interest for their secondary metabolites, which are active in chemical defenses against predators [3]. These compounds exhibit a large variety of chemical structures [4,5] and have been shown to possess ichthyotoxic, feeding-deterrent and cytotoxic properties, to have antibacterial activity, to act as sexual pheromones [6] and are responsible for various bioactivities, such as antitumor, anti-inflammatory and antioxidant activities. Clearly, dietary sources contribute significantly to the chemical diversity of metabolites found in some mollusks [6]. However, their *de novo* biosynthesis has been reported for several mollusk species [7]. The secondary metabolites isolated from mollusks fall into a wide range of structural classes, with some compounds predominating in certain taxa. In the Gastropoda, terpenes dominate, whereas fatty acid derivatives are relatively uncommon [2].

Mollusks, as well as the invertebrates, in general, constitute a source of lipid bioactive compounds offering a variety of nutraceutical and pharmaceutical applications [2]. Among them, the omega-3 polyunsaturated fatty acids (PUFA), such as eicosapentaenoic acid, 20:5*n*-3, and docosahexaenoic acid, 22:6*n*-3, are known for their beneficial effects on human health [8]. These PUFA *n*-3 fatty acids are widely known for their capacities for cardioprotection; they reduce triacylglycerol and cholesterol levels and have anti-inflammatory and anticancer effects [9]. Numerous experiments on animals confirmed the cancer preventive properties of PUFA *n*-3 fatty acids from marine sources [9,10].

Some other marine lipids also show many potential bioactive properties. Monogalactosyldiacylglycerols and digalactosyldiacylglycerols from the marine microalga, *Nannochloropsis granulata*, have been reported to have a nitric oxide inhibitory activity [11]. The betaine lipid from microalgae *N. granulata*, diacylglyceryltrimethylhomoserine, shows a nitric oxide inhibitory activity, indicating a possible value as an anti-inflammatory agent [12]. The glycolipid, sulfoquinovosyl diacylglycerol, from red alga *Osmundaria obtusiloba* [13] and from brown alga *Sargassum vulgare* [14] exhibits a potent antiviral activity against herpes simplex virus type 1 and 2. This glycolipid from a brown alga, *Lobophora variegata*, possess a pronounced antiprotozoal activity [15]. Studies on glycosphingolipids from marine sponge *Axinyssa djiferi* proved their good antiplasmodial activity [16].

Although interest in the fatty acid composition of mollusks has not been abated, it has become increasingly obvious that phyla of marine invertebrates may be a source of unusual marine lipids, such as plasmalogens, phospholipids, glycolipids and diverse fatty acids.

The aim of the work was to fill a gap in the knowledge of the lipid biochemistry of mollusks. In particular, we consider data on the lipid of the nudibranchs (Mollusca, Gastropoda, Opisthobranchia, Nudibranchia). Herein, we report the investigation of the eight common species of nudibranchs with the use of the high-performance thin-layer chromatography (HPTLC), gas chromatography coupled with flame ionization detection (GC-FID) and gas chromatography coupled with mass spectrometry (GC-MS) methods to elucidate their lipid, phospholipid and fatty acid composition. A suggestion on the origin of the fatty acid variety in nudibranchs and their potential as bioactive compounds is also given.

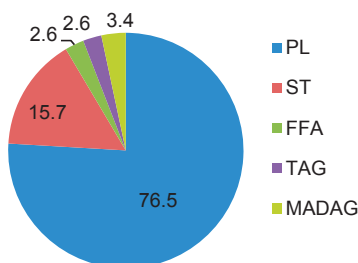
## 2. Results and Discussion

### 2.1. Lipids and Phospholipids

Lipids exert important biological functions as energy storage compounds, structural components of the cell membranes and as signaling molecules. The lipid content of the nudibranchs accounts for 14.2–21.4 mg·g<sup>-1</sup> wet weight. The eight studied species of the nudibranchs appeared to have similar lipid compositions. According to this similarity in the lipid classes of these nudibranchs, the amounts of the lipid classes insignificantly vary depending on species and environmental conditions. Statistical analysis confirmed that lipid class values differed insignificantly among species. Hence, Figure 1 gives the average results for all studied species. The lipid composition of nudibranchs revealed that the major lipid class was phospholipids (PLs) and, to a lesser extent,

sterols (STs) (13.5%–16.1% of total lipids). The PL concentration varied within a range from 73.8% in *Chromodoris geometrica* to 81.7% in *Glossodoris cincta*; this was much more than was found in other mollusks and invertebrates in total [17]. Triacylglycerols (TAGs), monoalkyldiacylglycerols (MADAGs) and free fatty acids (FFAs), which are the storage compounds of the cells, were minor components (2.6%, 3.4% and 2.6%, respectively). The detected distribution was similar to that found in two other tropical species of nudibranchs [18] and confirmed the high membrane phospholipids and low storage lipids in the tissues of these mollusks. The level of the neutral storage lipids is known to be species specific and depends mainly on the life history strategy and food availability [19].

**Figure 1.** Lipid classes (% of total lipids) of nudibranchs. Results are expressed as the mean of eighth species ( $n = 8$ ). PL, phospholipid; ST, sterol; FFA, free fatty acid; TAG, triacylglycerol; MADAG, monoalkyldiacylglycerol.



The PL composition of the studied species was similar, with the dominance of phosphatidylcholine (PC) (up to 62.8% of total PL in *Chromodoris tinctoria*) and further, in descending order: phosphatidylethanolamine (PE), phosphatidylserine (PS), ceramide-aminoethylphosphonate (CAEP), phosphatidylinositol (PI) and diphosphatidylglycerol (DPG) (Table 1). The PL data obtained for the nudibranchs were different from those of other mollusks species by the elevated concentration of PC. The phosphonolipid, CAEP, is relatively abundant in some invertebrates, and it has been detected previously in freshwater and marine mollusks [20].

**Table 1.** Composition of phospholipids in the nudibranchs (mol%). Results are expressed as the mean  $\pm$  SD of four replicates ( $n = 4$ ). PC, phosphatidylcholine; PE, phosphatidylethanolamine; PS, phosphatidylserine; CAEP, ceramide-aminoethylphosphonate; PI, phosphatidylinositol; DPG, diphosphatidylglycerol.

	PC	PE	PS	CAEP	PI	DPG
<i>Chromodoris tinctoria</i>	60.9 $\pm$ 2.1	11.7 $\pm$ 0.9	12.5 $\pm$ 1.1	5.1 $\pm$ 0.4	6.5 $\pm$ 0.8	2.0 $\pm$ 0.6
<i>C. michaeli</i>	53.1 $\pm$ 2.1	21.4 $\pm$ 1.1	13.4 $\pm$ 0.8	5.6 $\pm$ 0.5	4.9 $\pm$ 0.6	1.7 $\pm$ 0.4
<i>C. geometrica</i>	53.8 $\pm$ 1.5	15.4 $\pm$ 0.9	12.6 $\pm$ 0.7	12.2 $\pm$ 1.1	3.7 $\pm$ 1.1	1.2 $\pm$ 0.3
<i>Chromodoris</i> sp.	51.2 $\pm$ 1.1	17.4 $\pm$ 1.3	14.5 $\pm$ 1.2	9.1 $\pm$ 1.9	5.0 $\pm$ 0.6	1.8 $\pm$ 0.4
<i>Glossodoris cincta</i>	56.1 $\pm$ 0.6	16.4 $\pm$ 1.4	15.4 $\pm$ 1.3	5.1 $\pm$ 0.7	4.2 $\pm$ 0.6	1.8 $\pm$ 0.3
<i>G. atromarginata</i>	53.5 $\pm$ 2.3	18.2 $\pm$ 1.9	12.2 $\pm$ 1.4	9.9 $\pm$ 1.7	5.1 $\pm$ 0.6	1.1 $\pm$ 0.2
<i>Risbecia tryoni</i>	49.6 $\pm$ 0.4	18.2 $\pm$ 1.1	13.8 $\pm$ 0.8	10.6 $\pm$ 1.1	4.6 $\pm$ 1.0	3.2 $\pm$ 0.8
<i>Platydorid</i> sp.	50.9 $\pm$ 2.0	21.2 $\pm$ 1.5	10.2 $\pm$ 0.8	8.0 $\pm$ 1.7	5.4 $\pm$ 0.5	2.7 $\pm$ 0.5

Marine invertebrates are known as a rich source of 1-alkenyl-2-acyl glycerophospholipids, commonly called plasmalogens [17,21]. Plasmalogens are particular phospholipids characterized by the presence of a vinyl ether bond at the C1 position of the glycerol skeleton. Plasmalogens are also ubiquitously found in animal cells. In mammals, the brain, heart, lymphocytes, spleen, macrophages and polymorphonuclear leukocytes contain the highest amount of plasmalogen-ethanolamine [22]. Two PLs, PE and PS, were represented as diacyl- and alkenyl-forms, and more than half of these aminophospholipids were plasmalogens (Table 2). 1-Alkenyl-2-acyl-PE made up 50.3%–65.1% of total PE; and 1-alkenyl-2-acyl-PS reached 47.1%–61.3% of total PS. The highest percentage of PE plasmalogens was found in *Risbecia tryoni*, accounting for 65.1% of total PE, and the PS plasmalogen contribution reached 61.3% of total PS in *Platydoris* sp. In contrast to many marine and freshwater mollusks, the nudibranchs contained PC only as a diacyl-form. Earlier, plasmalogens have been detected in PE, PS and PC in common edible mollusk species; the PE fraction is very often composed predominantly of the plasmalogens [23,24].

**Table 2.** Content of plasmalogens (1-alkenyl-2-acyl glycerophospholipids) in the nudibranchs. Expressed as the proportion of the plasmalogen forms relative to the whole of the same class forms; mean  $\pm$  SD of four replicates ( $n = 4$ ).

	1-Alkenyl-2-acyl-PE	1-Alkenyl-2-acyl-PS
<i>Chromodoris tinctoria</i>	60.4 $\pm$ 1.6	47.1 $\pm$ 2.1
<i>Chromodoris michaeli</i>	52.9 $\pm$ 2.4	51.1 $\pm$ 2.4
<i>Chromodoris geometrica</i>	58.8 $\pm$ 2.1	50.6 $\pm$ 1.7
<i>Chromodoris</i> sp.	59.2 $\pm$ 1.8	48.7 $\pm$ 1.1
<i>Glossodoris cincta</i>	61.1 $\pm$ 1.1	47.8 $\pm$ 1.5
<i>Glossodoris atomarginata</i>	60.7 $\pm$ 2.1	48.6 $\pm$ 1.2
<i>Risbecia tryoni</i>	65.1 $\pm$ 1.6	56.5 $\pm$ 1.0
<i>Platydoris</i> sp.	50.3 $\pm$ 1.8	61.3 $\pm$ 1.5

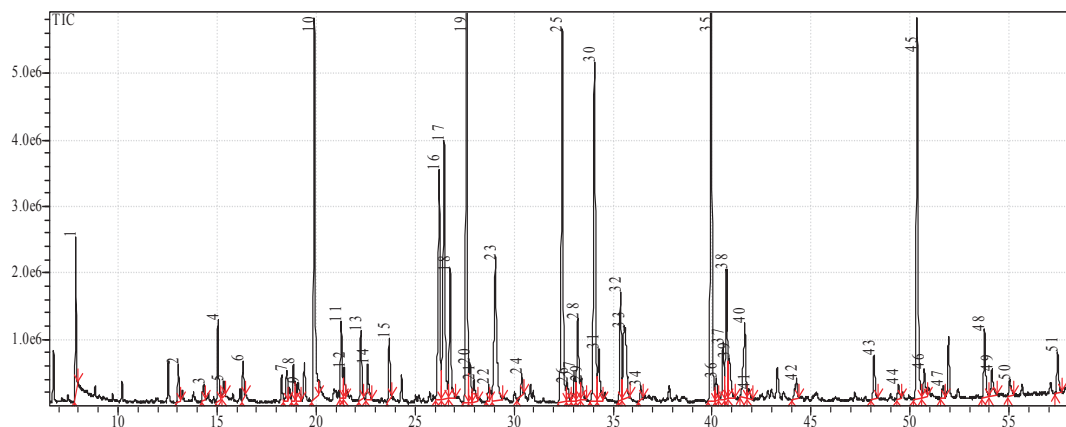
Serving as a structural component of the mammalian and invertebrate cell membrane, plasmalogens are widely distributed in excitable tissues, like heart and brain. Plasmalogens mediate the dynamics of the cell membrane. They provide storage for polyunsaturated fatty acids and can contribute to endogenous antioxidant activity, thus protecting cells from oxidative stress [25]. Plasmalogen phospholipids are suggested to be involved in signal transduction [26]. Plasmalogens are not only components of the plasma membrane and of lung surfactant, they serve as a reservoir for secondary messengers and may be also involved in membrane fusion, ion transport and cholesterol efflux. Low levels of these metabolites have trophic effects, but at a high concentration, they are cytotoxic and may be involved in allergic response, inflammation and trauma. Decreased levels of plasmalogens are associated with several neurological disorders, including Alzheimer's disease, ischemia and spinal cord trauma [27].



## 2.2. Fatty Acids

The fatty acid profiles of the studied species were rather similar and differed only in their qualitative proportions of the fatty acids. Figure 2 shows the GC-MS chromatogram of the 4,4-dimethyloxazoline (DMOX) derivatives from the sea slug, *Chromodoris michaeli*. Table 3 reports the qualitative and quantitative data obtained, respectively, from GC-MS and GC-FID analyses. The components were eluted according to their chain length and the degree of unsaturation in the chain on the MDN-5S capillary column. The chromatographic analyses allowed us to detect and identify about 50 individual fatty acids. The nudibranchs exhibited a wide diversity of fatty acids, including common saturated fatty acids (SFA) (8.6%–16.5% of total fatty acids), monounsaturated fatty acids (MUFA) (22.7%–31.2%) and polyunsaturated fatty acids (PUFA) (15.1%–31.4%), as well as non-methylene-interrupted dioenoic fatty acids (NMID FA) (8.0%–21.5%), very long chain fatty acids (VLCFAs) (7.7%–16.6%) and odd-chain and branched fatty acids (5.0%–17.4%) (Figure 3).

**Figure 2.** GC-MS chromatogram of 4,4-dimethyloxazoline derivatives from *Chromodoris michaeli*.



Marine mollusks are generally characterized by the predominance of essential  $n-3$  PUFA, mainly  $20:5n-3$  and  $22:6n-3$ , which constitute usually almost half of the total fatty acids [17,28]. In contrast, the nudibranchs did not show this property; these two marine PUFA were minor components and constituted in sum about 2% of the total fatty acids (range 1.4%–7.3%) (Figure 4). Nevertheless, sea slugs exhibited some unique features in their fatty acid composition. Their fatty acid profiles were distinguished drastically from those of other mollusks. The differences seem to be more obvious compared with fatty acids of a common marine snail, *Nucella heyseana*, and limpet, *Acmea pallida* [28] (Figure 4).

**Table 3.** Identification of the 4,4-dimethyloxazoline derivatives and fatty acid composition (wt%) of *Chromodoris michaeli*. Results are expressed as the mean  $\pm$  SD of four replicates ( $n = 4$ ).

FA	Molecular Ion ( $m/z$ )	% of Total FA	FA	Molecular Ion ( $m/z$ )	% of Total FA
12:0	253	0.4 $\pm$ 0.1	20:5 <i>n</i> -3	355	0.2 $\pm$ 0.1
14:0	281	0.9 $\pm$ 0.3	20:2 $\Delta$ 5,11	355	1.8 $\pm$ 0.5
<i>iso</i> -15:0	295	1.9 $\pm$ 0.5	20:2 $\Delta$ 5,13	355	1.3 $\pm$ 0.4
<i>anteiso</i> -15:0	295	0.3 $\pm$ 0.1	20:3 <i>n</i> -6	359	0.7 $\pm$ 0.3
15:0	295	1.1 $\pm$ 0.2	20:1 <i>n</i> -11	363	5.6 $\pm$ 0.7
<i>iso</i> -16:0	309	0.5 $\pm$ 0.1	20:1 <i>n</i> -9	363	0.2 $\pm$ 0.1
<i>anteiso</i> -16:0	309	0.7 $\pm$ 0.1	20:1 <i>n</i> -7	363	2.5 $\pm$ 0.6
16:1 <i>n</i> -7	307	1.7 $\pm$ 0.6	21:2 $\Delta$ 7,13	375	0.1 $\pm$ 0.0
16:0	309	5.9 $\pm$ 0.8	<i>iso</i> -21:1	377	0.4 $\pm$ 0.1
<i>iso</i> -17:0	323	1.4 $\pm$ 0.3	21:1 <i>n</i> -7	377	2.0 $\pm$ 0.1
<i>anteiso</i> -17:0	323	0.9 $\pm$ 0.1	21:1 <i>n</i> -5	377	1.3 $\pm$ 0.5
17:1 <i>n</i> -8	321	1.4 $\pm$ 0.4	22:5 <i>n</i> -6	383	0.4 $\pm$ 0.1
17:1 <i>n</i> -6	321	0.4 $\pm$ 0.1	22:6 <i>n</i> -3	381	0.7 $\pm$ 0.2
17:0	323	1.4 $\pm$ 0.1	22:4 <i>n</i> -6	385	10.2 $\pm$ 1.3
18:3 <i>n</i> -6	331	0.2 $\pm$ 0.1	22:5 <i>n</i> -3	383	0.2 $\pm$ 0.1
<i>iso</i> -18:0	337	0.4 $\pm$ 0.2	22:3 <i>n</i> -6	387	0.2 $\pm$ 0.1
<i>anteiso</i> -18:0	337	0.4 $\pm$ 0.2	22:2 $\Delta$ 7,13	389	3.6 $\pm$ 0.7
18:2 <i>n</i> -6	333	7.0 $\pm$ 0.9	22:2 $\Delta$ 7,15	289	1.2 $\pm$ 0.3
18:1 <i>n</i> -9	335	5.4 $\pm$ 0.4	22:1 <i>n</i> -9	391	0.4 $\pm$ 0.2
18:1 <i>n</i> -7	335	3.4 $\pm$ 1.0	22:1 <i>n</i> -7	391	0.1 $\pm$ 0.1
18:0	337	7.4 $\pm$ 1.3	<i>iso</i> -24:2 $\Delta$ 5,9	417	0.2 $\pm$ 0.1
<i>iso</i> -19:1	349	0.1 $\pm$ 0.0	24:2 $\Delta$ 5,9	417	3.1 $\pm$ 0.5
<i>anteiso</i> -19:1	349	0.2 $\pm$ 0.1	<i>iso</i> -25:2 $\Delta$ 5,9	431	4.0 $\pm$ 1.0
<i>iso</i> -19:0	351	0.2 $\pm$ 0.1	<i>anteiso</i> -25:2 $\Delta$ 5,9	431	0.6 $\pm$ 0.2
<i>anteiso</i> -19:0	351	0.2 $\pm$ 0.1	25:2 $\Delta$ 5,9	431	0.1 $\pm$ 0.1
19:1 <i>n</i> -8	349	0.1 $\pm$ 0.0	<i>iso</i> -26:2 $\Delta$ 5,9	445	0.8 $\pm$ 0.3
19:1 <i>n</i> -12	349	2.6 $\pm$ 0.8	<i>anteiso</i> -26:2 $\Delta$ 5,9	445	0.1 $\pm$ 0.0
19:0	351	0.3 $\pm$ 0.1	26:2 $\Delta$ 5,9	445	0.8 $\pm$ 0.3
20:4 <i>n</i> -6	357	10.5 $\pm$ 1.2	<i>anteiso</i> -27:2 $\Delta$ 5,9	459	0.2 $\pm$ 0.1

**Figure 3.** Distribution of fatty acids in nudibranch species. Results are expressed as the mean  $\pm$  SD of eight studied species. OBFA, odd-chain and branched; NMID, non-methylene-interrupted dienoic; VLCFA, very long chain fatty acids.

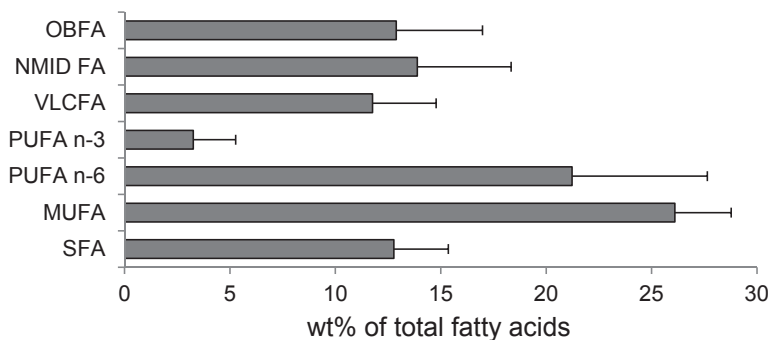
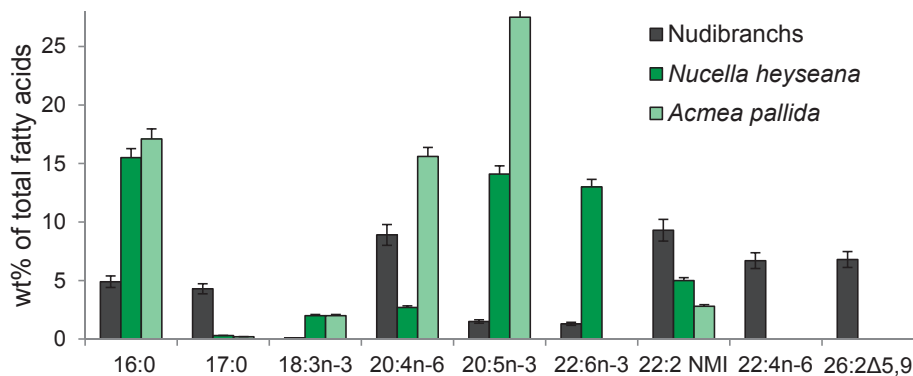


**Figure 4.** Fatty acid composition (wt%) of nudibranchs. Results are expressed as the mean  $\pm$  SD of eight studied species.



In the nudibranchs, a significant amount of VLCFA specific to sponges, so-called demospongiac acids, was found. These nudibranchs are carnivorous and specialized feeders on sponges. Utilization of this food probably is responsible for the high level of the demospongiac acids in these mollusks. It is suspected that the majority of sea slugs feed on certain sponge species, which are known to be distinguished in their fatty acid composition [29]. Indeed, a series of VLCFA with double bonds at  $\Delta 5,9$  positions in the chain was identified in the tropical nudibranchs (Table 4). Concentrations of these components differed among the species. Among VLCFA of *Platydorid* sp., only hexacosadienoic acid 26:2 $\Delta 5,9$  was identified, whereas in *Chromodoris michaeli*, tetracosadienoic 24:2 $\Delta 5,9$  and branched *iso*-25:2 $\Delta 5,9$  were dominant, with some minor VLCFA. Moreover, branched hexacosatrienoic acids, *iso*-26:3 $\Delta 5,9,19$  and *anteiso*-26:3 $\Delta 5,9,19$ , were found only in *Glossodorid cincta*, and *iso*-27:2 $\Delta 5,9$  was identified only in *C. michaeli*. The specific distribution of the VLCFA suggests that these nudibranchs may feed on different sponge species.

**Table 4.** The distribution of very long-chain fatty acids of nudibrans according to the degree of unsaturation and chain length (% of total fatty acids). Results are expressed as the mean  $\pm$  SD of four replicates ( $n = 4$ ).

VLCFA	<i>Chromodoris</i> sp.	<i>C.</i> <i>geometrica</i>	<i>C.</i> <i>tinctoria</i>	<i>C.</i> <i>michaeli</i>	<i>Glossodoris</i> <i>atromarginata</i>	<i>G.</i> <i>cincta</i>	<i>Risbecia</i> <i>tryoni</i>	<i>Platydoris</i> sp.
<i>i</i> -24:2 $\Delta$ 5,9	-	-	-	0.2	0.2	-	-	-
24:2 $\Delta$ 5,9	1.0	4.7	0.4	3.1	1.1	1.2	1.4	-
24:1	-	0.3	0.1	-	-	-	-	-
<i>i</i> -25:2 $\Delta$ 5,9	-	-	-	4.0	-	-	-	-
25:2 $\Delta$ 5,9	4.0	1.6	0.7	0.2	2.3	2.6	0.5	-
25:3 $\Delta$ 5,9	0.5	0.1	-	-	-	1.3	-	-
26:0	-	0.1	-	-	-	0.3	-	-
<i>i</i> -26:2 $\Delta$ 5,9	0.8	0.1	0.8	0.8	-	0.7	-	-
26:2 $\Delta$ 5,9	6.0	3.0	13.6	0.8	6.3	8.4	5.8	10.5
<i>i</i> -26:3 $\Delta$ 5,9,19	-	0.2	-	-	1.2	2.3	-	-
<i>ai</i> -26:3 $\Delta$ 5,9,19	-	-	-	-	-	1.1	-	-
<i>ai</i> -27:2 $\Delta$ 5,9	-	-	-	0.2	-	-	-	-

Thus, this study demonstrated that sponges are not the only source of these  $\Delta$ 5,9 dienoic acids, since they were found also in other marine organisms, such as nudibranch mollusks. Various biological activities have been reported to date for the most encountered VLCFA double bonds at  $\Delta$ 5,9 positions in the chain. The use of an antiparasitic bioassay revealed that fatty acids with 23 to 26 carbon atoms and double bonds in the position  $\Delta$ 5,9 displayed considerable antiprotozoal activity [30]. Thus, these demospongiac fatty acids may be the source of very potent antimalarial drugs. These fatty acids are also potent inhibitors of the enzyme, topoisomerase I; this property could lead to the development of effective anti-cancer drugs. The 14-methyl-5,9-pentadecadienoic acid from phospholipids of the gorgonian *Eunicea succinea* was active against Gram-positive bacteria, such as *Staphylococcus aureus* and *Streptococcus faecalis* [31]. The natural compound, 30:3 $\Delta$ 5,9,23, was isolated from the sponge, *Chondrilla nucula*, and was found to be an elastase inhibitor, which is known to be a potential therapeutic agent in various diseases, such as pulmonary emphysema, chronic bronchitis and several inflammatory disorders. In addition, the C23–C26 $\Delta$ 5,9 fatty acids had almost no cytotoxicity on mammalian L6 cells. Therefore, the  $\Delta$ 5,9 FA may be of use against the parasites without damage to the host [32]. Mixtures of the branched 22-methyl-5,9-tetracosadienoic and 23-methyl-5,9-tetracosadienoic acids showed cytotoxic activity against mouse Ehrlich carcinoma cells and a hemolytic effect on mouse erythrocytes [33].

As referenced above, marine mollusks are probably a unique source of unusual unsaturated fatty acids, the non-methylene-interrupted dienoic fatty acids (NMID FA), as opposed to the common methylene-interrupted PUFA, in that their double bonds are separated by more than one methylene group. These ubiquitous and, in some species, major components of the mollusk lipids [28] have been, to date, extensively studied [34]. The NMID FAs were found in all studied species (Figures 3 and 4); among them, common 20:2 $\Delta$ 5,11, 20:2 $\Delta$ 5,13, 22:2 $\Delta$ 7,13 and 22:2 $\Delta$ 7,15 and a novel isomer, 21:2 $\Delta$ 7,13, were identified. FA 21:2 $\Delta$ 7,13 has been reported earlier in other nudibranch species, *Phyllidia coelestis* [18], in the edible bivalve, *Megangulus zyonensis* [35], and the gonads

of the limpets, *Cellana grata* and *Collisella dorsuosa* [36]. The largest concentration of NMID FA was detected in *Risbecia tryoni* (21.5%). The mollusks are able to synthesize the C20 and C22 NMID FA by a  $\Delta 5$  desaturase acting upon the appropriate precursor, such as 18:1*n*-7 and 18:1*n*-9, and further chain elongation. The potential precursors of 21:2 $\Delta$ 7,13 are 17:1*n*-8 and 19:1*n*-8, which are of bacterial origin and abundant in the nudibranchs (Table 3). It has been recently shown that mollusks expressed a Fad-like gene that encodes an enzyme with  $\Delta 5$ -desaturation activity, which participates in the biosynthesis of NMID FA [37]. Although their biological role and function is not fully understood, it has been suggested that NMID FAs play structural and protective roles in cell membranes, since they are esterified phospholipids and occur in amounts that are often in a reverse relation to 20:5*n*-5 and 22:6*n*-3 [18,34]. The unusual double bond positions in NMID FAs are considered to confer to cell membranes a higher resistance to oxidative processes and microbial lipases than the common PUFA [34]. The introduction of a *trans*-5 double bond into the linoleic acid, 18:2*n*-6, molecule provides a fatty acid, columbinic acid, 18:3 $\Delta$ 5*trans*,9*cis*,12*cis*, with fascinating biological properties [38]. In experiments with essential fatty acid-deficient rats, it has been shown that columbinic acid is effective in maintaining the proper epidermal layer and improves the fertility of the rats, while the inhibition of prostaglandin synthesis has a beneficial effect, since inflammation and the thrombotic tendency are reduced.

Another unique feature of the nudibranchs is associated with an aberrant level of the odd-chain and branched fatty acids (OBFA) that are specific for bacteria and usually named “bacterial fatty acids” (Figure 3). They are normally minor metabolites in most animals, but a high abundance of bacterial acids found in the nudibranchs was extraordinary. The sum of OBFA, predominantly 15:0, 17:0, 17:1*n*-8 and *iso*- and *anteiso*-C15, C16, C17, C18 and C19 fatty acids, reached up to 15.8% in the *Chromodoris geometrica* and 17.4% in *Glossodoris atromarginata*, whereas their concentration in *Platydorid* sp. was the lowest (5.0%). A high level of bacterial fatty acids in the nudibranchs may serve as an indicator that the symbiotic bacteria provide the host with nutrients. Earlier, an abundance of OBFA discovered in *Dendrodoris nigra* allowed us to suggest that symbiotic bacteria may be their source in this nudibranch; transmission electron microscopy (TEM) confirmed the presence of symbiotic bacteria in the cytoplasm of the epithelial cells and the glycocalyx layer covering the epithelium of the notum and the mantle of *D. nigra* [39]. It was found that the bacteria in the glycocalyx sometimes undergo destructive lysis, with their components being utilized by the epithelial cells. The high concentration of typical bacterial fatty acids in the lipids of the nudibranch *D. nigra* agrees well with the results of TEM and confirms that the lysed bacterial cells are utilized by the mollusk tissues [39]. Moreover, some bacterial OBFA, such as 17:1*n*-8 and 19:1*n*-8, evidently serve as potential precursors for the biosynthesis of odd-chain PUFA identified in the nudibranchs, such as 21:2 $\Delta$ 7,13, as well as 21:4*n*-7 isolated from other marine opisthobranch mollusk, *Scaphander lignarius*, and possessed activity against a range of human cancer cell lines (melanoma, colon carcinoma and breast carcinoma) [40].

There is increasing evidence that microbial symbionts are the true source of biologically-active compounds isolated from some species of chemically-rich invertebrates, mainly sponges, bryozoans, isopods and tunicates [41,42]. The symbionts are reported to be producers of the host's secondary metabolites that have defensive and protective functions for their hosts [43,44]. Many

biologically active compounds, including toxic and deterrent secretions, have been isolated from nudibranchs [45]. Interestingly, endobacterial morphotypes have been recently described for twelve of thirteen species of nudibranchs tested [46]. Moreover, the epithelium of the temperate nudibranch, *Rostanga alisae*, rich in OBFA, demonstrated high numbers of symbiont-containing cells (*i.e.*, bacteriocytes) [47]. Taken all together, these results suggest that symbiotic bacteria might be involved in the defense against predators and, so, in production of the bioactive compounds.

### 3. Experimental Section

#### 3.1. Site and Samples

Eight species of nudibranchs, *Chromodoris* sp., *C. geometrica*, *C. tinctoria*, *C. michaeli*, *Glossodoris atromarginata*, *G. cincta*, *Risbecia tryoni* and *Platydoris* sp. (phyla: Mollusca, Class: Opisthobranchia; orders: Nudibranchia, Suborder: Doridina) were collected from the Research Vessel Akademik Oparin by SCUBA divers in Nha Trang Bay of the South China Sea, Vietnam, in January 2005, October 2006, June 2007, and April–May 2013. The nudibranchs collected were placed immediately in tanks under water at the site of collection and transported to the laboratory. Three to five specimens of each species were used for lipid analysis.

#### 3.2. Lipid Analysis

Tissues of mollusks were crushed, and total lipids were extracted by homogenization in a chloroform/methanol mixture (1:2, v/v) [48]. Lipid classes were separated by one-dimensional silica gel thin-layer chromatography (TLC). The Merk Kieselgel 60 G plates (6 cm × 6 cm) were first developed in hexane/diethyl ether/acetic acid (80:20:1, v/v) to resolve nonpolar compounds. After development, the TLC plates were dried under air flow and developed to 20% length in a polar solvent system of chloroform/acetone/methanol/acetic acid/water (50:20:10:10:1, v/v). Lipids were detected on the TLC plates using 10% H<sub>2</sub>SO<sub>4</sub>/methanol with subsequent heating to 180 °C. The TLC plates were scanned using an image scanner (Epson Perfection 2400 Photo) in grayscale mode. Lipid class concentrations were based on band intensity using an image analysis program (Sorbifil TLC Videodensitometer). Units were calibrated using standards for each lipid class.

Polar lipids were separated by two-dimensional silica gel TLC in the solvent systems: chloroform/methanol/28% NH<sub>4</sub>OH, 65:25:4, v/v, for the first direction; chloroform/acetone/methanol/acetic acid/water, 50:20:10:10:1, v/v, for the second one. Lipids were detected on TLC plates using 10% H<sub>2</sub>SO<sub>4</sub>/methanol with heating to 180 °C and by specific reagents for phospholipids [49], amino-containing lipids (0.5% ninhydrin in waterlogged butanol) and choline lipids (Dragendorff's reagent). Phospholipids were quantified with the molybdenum reagent [49].

#### 3.3. Fatty Acid Analysis

Fatty acid methyl esters (FAME) were prepared by a sequential treatment of the total lipids with 1% sodium methylate/methanol and 5% HCl/methanol in a screw-capped vial [50] and purified by

preparative silica gel TLC using benzene as a solvent. 4,4-Dimethloxazoline (DMOX) derivatives were prepared from FAME [51]. The GC analysis of FAME was carried out on a Shimadzu GC-2010 chromatograph (Kyoto, Japan) with a flame ionization detector on a SUPELCOWAX (Supelco, Bellefonte, PA, USA) capillary column (30 m × 0.25-mm internal diameter, 0.25- $\mu$ m film thickness) at 210 °C. Helium was used as a carrier gas at a linear velocity of 30 cm s<sup>-1</sup> (the split ratio was 1:30). Injector and detector temperatures were 250 °C. Fatty acids were identified by a comparison with authentic standards and equivalent chain length values (ECL) [52]. Identification of fatty acids was confirmed by gas chromatography-mass spectrometry (GC-MS) of their methyl esters and DMOX derivatives. The GC-MS analysis of FAME was performed on a model Shimadzu GCMS-QP5050A (Kyoto, Japan) fitted with a Supelco MDN-5S capillary column (30 m × 0.25 mm i.d. Supelco, Bellefonte, PA, USA). Ionization of the samples was performed by an electron impact at 70 eV. The column temperature was programmed from 170 °C, held for 1 min, followed by an increase to 240 °C at a rate of 2 °C min<sup>-1</sup> and then held for 20 min. The temperature of the injector and detector was 250 °C. GC-MS of DMOX derivatives was performed using the same instrument at a column temperature of 210 °C with a 3 °C min<sup>-1</sup> increase to 270 °C, which was held for 40 min. The injector and detector temperatures were 300 °C. Spectra were compared with the NIST library and fatty acid mass spectra archive [53].

#### 3.4. Statistical Analysis

Difference in the mean of lipid concentrations was examined with a one-way ANOVA. In all cases, statistical significance was indicated by  $p < 0.05$ . All data were expressed as mean  $\pm$  SD.

#### 4. Conclusions

Mollusks, as well as the invertebrates in general, constitute a source of lipid bioactive compounds offering a variety of activities. This study has demonstrated for the first time that nudibranchs exhibit a wide diversity of lipids that differed greatly from that of other marine gastropods. Lipids of nudibranchs were composed mainly of phospholipids rich in plasmalogen PE and plasmalogen PS. The nudibranchs exhibited some unique features in their fatty acid composition. They displayed large amounts of VLCFA, various NMID FAs and a high abundance of OBFA. Many of these fatty acids originate in nudibranchs from unusual biosynthetic pathways, specific dietary sources and symbiotic partnerships with bacteria. The results of this study and of previous research suggest that symbiotic bacteria may play an important role in producing bioactive chemicals or their precursors within the host. The current study has shown that these mollusks may be an important resource of a wide range of bioactive compounds.

#### Acknowledgments

I thank Alexey V. Chernyshev for the identification of the nudibranch species. This work was supported by the Government of the Russian Federation (Grant 11.G34.31.0010).

## Abbreviations

CAEP: ceramide-aminoethylphosphonate; DPG: diphosphatidylglycerol; FA: fatty acid; FAME: fatty acid methyl ester; FFA: free fatty acids; GC-MS: gas chromatography-mass spectrometry; MADAG: monoalkyldiacylglycerol; MUFA: monounsaturated fatty acid; NMID FA: non-methylene-interrupted dienoic fatty acids; OBFA: odd-chain and branched fatty acids; PC: phosphatidylcholine; PE: phosphatidylethanolamine; PI: phosphatidylinositol; PL: phospholipids; PS: phosphatidylserine; PUFA: polyunsaturated fatty acid; SFA: saturated fatty acid; ST: sterols; TLC: thin-layer chromatography; VLCFA: very long chain fatty acid.

## Conflicts of Interest

The author declares no conflict of interest.

## References

1. Evans-Illidge, E.A.; Logan, M.; Doyle, J.; Fromont, J.; Battershill, C.N.; Ericson, G.; Wolff, C.W.; Muirhead, A.; Kearns, P.; Abdo, D.; *et al.* Phylogeny drives large scale patterns in Australian marine bioactivity and provides a new chemical ecology rationale for future biodiscovery. *PLoS One* **2013**, *8*, e73800.
2. Benkendorff, K. Molluscan biological and chemical diversity: Secondary metabolites and medicinal resources produced by marine molluscs. *Biol. Rev.* **2010**, *85*, 757–775.
3. Cimino, G.; Gavagnin, M. *Molluscs: Progress in Molecular and Subcellular Biology Subseries Marine Molecular Biochemistry*; Springer-Verlag: Berlin, Heidelberg, Germany, 2006; p. 387.
4. Faulkner, D.J. Marine natural products. *Nat. Prod. Rep.* **2000**, *17*, 7–55.
5. Gavagnin, M.; Fontana, A. Diterpenes from marine opisthobranch mollusks. *Curr. Org. Chem.* **2000**, *4*, 1201–1248.
6. Avila, C. Natural products of opisthobranch molluscs: A biological review. *Oceanogr. Mar. Biol.* **1995**, *33*, 487–559.
7. Fontana, A. Biogenetical proposals and biosynthetic studies on secondary metabolites of opisthobranch molluscs. In *Molluscs: Progress in Molecular and Subcellular Biology Subseries Marine Molecular Biochemistry*; Cimino, G., Gavagnin, M., Eds.; Springer-Verlag: Berlin, Heidelberg, Germany, 2006; pp. 303–328.
8. Simopoulos, A.P. The importance of the omega-6/omega-3 fatty acid ratio in cardiovascular disease and other chronic diseases. *Exp. Biol. Med.* **2008**, *233*, 674–688.
9. Wendel, M.; Heller, A.R. Anticancer actions of omega-3 fatty acids—Current state and future perspectives. *Anticancer Agents Med. Chem.* **2009**, *9*, 457–470.
10. Candela, C.G.; Lopez, L.; Kohen, V. Importance of a balanced omega 6/omega 3 ratio for the maintenance of health: Nutritional recommendations. *Nutr. Hosp.* **2011**, *26*, 323–329.
11. Banskota, A.H.; Stefanova, R.; Gallant, P.; McGinn, P. Mono- and digalactosyldiacylglycerols: Potent nitric oxide inhibitors from the marine microalga *Nannochloropsis granulata*. *J. Appl. Phycol.* **2013**, *25*, 349–357.



12. Banskota, A.H.; Stefanova, R.; Sperker, S.; McGinn, P.J. New diacylglyceryltrimethyl-homoserines from the marine microalga *Nannochloropsis granulata* and their nitric oxide inhibitory activity. *J. Appl. Phycol.* **2013**, *25*, 1513–1521.
13. De Souza, L.M.; Sasaki, G.L.; Villela, R.; Maria, T.; Barreto-Bergter, E. Structural Characterization and anti-HSV-1 and HSV-2 activity of glycolipids from the marine algae *Osmundaria obtusiloba* isolated from Southeastern Brazilian coast. *Mar. Drugs* **2012**, *10*, 918–931.
14. Plouguerne, E.; de Souza, L.M.; Sasaki, G.L.; Cavalcanti, J.F.; Romanos, M.T.V.; da Gama, B.A.P.; Pereira, R.C.; Barreto-Bergter, E. Antiviral Sulfoquinovosyldiacylglycerols (SQDGs) from the Brazilian brown seaweed *Sargassum vulgare*. *Mar. Drugs* **2013**, *11*, 4628–4640.
15. Cantillo-Ciau, Z.; Moo-Puc, R.; Quijano, L.; Freile-Pelegrin, Y. The tropical brown alga *Lobophora variegata*: A source of antiprotozoal compounds. *Mar. Drugs* **2013**, *8*, 1292–1304.
16. Farokhi, F.; Grellier, P.; Clement, M.; Roussakis, C.; Loiseau, P.M.; Genin-Seward, E.; Kornprobst, J.-M.; Barnathan, G.; Wielgosz-Collin, G. Antimalarial activity of axidjiferosides, new beta-galactosylceramides from the African sponge *Axinyssa djiferi*. *Mar. Drugs* **2013**, *11*, 1304–1315.
17. Joseph, J.D. Lipid composition of marine and estuarine invertebrates: Mollusca. *Prog. Lipid. Res.* **1982**, *21*, 109–153.
18. Zhukova, N.V. Lipid classes and fatty acid composition of the tropical nudibranch mollusks *Chomodoris* sp. and *Phyllidia coelestis*. *Lipids* **2007**, *42*, 1169–1175.
19. Gannefors, C.; Boer, M.; Kattner, G.; Graeve, M.; Eiane, K.; Gulliksen, B.; Hop, H.; Falk-Petersen, S. The Arctic sea butterfly *Limacina helicina*: Lipids and life strategy. *Mar. Biol.* **2005**, *147*, 169–177.
20. Hanuš, L.O.; Levitsky, D.O.; Shkrob, I.; Dembitsky, V.M. Plasmalogens, fatty acids and alkyl glyceryl ethers of marine and freshwater clams and mussels. *Food Chem.* **2009**, *116*, 491–498.
21. Sargent, J.R. Ether-Linked Glycerides in Marine Animals. In *Marine Biogenic Lipids, Fats, and Oils*; Ackman, R.G., Ed.; CRC Press: Boca Raton, FL, USA, 1987; pp. 176–193.
22. Magnusson, C.D.; Haraldsson, G.G. Ether lipids. *Chem. Phys. Lipids* **2011**, *164*, 315–340.
23. Dembitsky, V.M.; Rezanka, T.; Kashin, A.G. Fatty acid and phospholipid composition of freshwater molluscs *Anodonta piscinalis* and *Limnaea fragilis* from the river Volga. *Comp. Biochem. Physiol.* **1993**, *105B*, 597–601.
24. Kraffe, E.; Sounant, P.; Marty, A. Fatty acids of Serine, ethanolamine, and choline plasmalogens in some marine bivalves. *Lipids* **2004**, *39*, 59–66.
25. Brosche, T.; Brueckmann, M.; Haase, K.K.; Sieber, C.; Bertsch, T. Decreased plasmalogen concentration as a surrogate marker of oxidative stress in patients presenting with acute coronary syndromes or supraventricular tachycardias. *Clin. Chem. Lab. Med.* **2007**, *45*, 689–691.
26. Latorre, E.; Collado, M.P.; Fernandez, I.; Aragonés, M.D.; Catalan, R.E. Signaling events mediating activation of brain ethanolamine plasmalogen hydrolysis by ceramide. *Eur. J. Biochem.* **2003**, *270*, 36–46.

27. Hartmann, T.; Kuchenbecker, J.; Grimm, M.O. Alzheimer's disease: The lipid connection. *J. Neurochem.* **2007**, *103*, 159–170.
28. Zhukova, N.V.; Svetashev, V.I. Non-methylene-interrupted dienoic fatty acids in mollusks from the Sea of Japan. *Comp. Biochem. Physiol.* **1986**, *83B*, 643–646.
29. Bergquist, P.R.; Lawson, M.P.; Lavis, A.; Cambie, R.C. Fatty acid composition and the classification of the Porifera. *Biochem. Syst. Ecol.* **1984**, *12*, 63–84.
30. Carballeira, N.M. New advances in fatty acids as antimalarial, antimycobacterial and antifungal agents. *Prog. Lipid Res.* **2008**, *47*, 50–61.
31. Carballeira, N.M.; Reyes, E.D.; Sostre, A.; Rodriguez, A.D.; Rodriguez, J.L.; Gonzales, F.A. Identification of the novel antimicrobial fatty acid (5Z,9Z)-14-methyl-5,9-pentadecadienoic acid in *Eunicea succinea*. *J. Nat. Prod.* **1997**, *60*, 502–504.
32. Tasdemir, D.; Topaloglu, B.; Perozzo, R.; Brun, R.; O'Neill, R.; Carballeira, N.M.; Zhang, X.J.; Tonge, P.J.; Linden, A.; Ruedi, P. Marine natural products from the Turkish sponge *Agelas oroides* that inhibit the enoyl reductase from *Plasmodium falciparum*, *Mycobacterium tuberculosis* and *Escherichia coli*. *Bioorg. Med. Chem.* **2007**, *15*, 6834–6845.
33. Makarieva, T.N.; Santalova, E.A.; Gorshkova, I.A.; Dmitrenok, A.S.; Guzi, A.G.; Gorbach, V.I.; Svetashev, V.I.; Stonok, V.A. A new cytotoxic fatty acid (5Z,9Z)-22-methyl-5,9-tetrecosadienoic acid and the sterols from the far eastern sponge *Geodinella robusta*. *Lipids* **2002**, *37*, 75–80.
34. Barnathan, G. Non-methylene-interrupted fatty acids from marine invertebrates: Occurrence, characterization and biological properties. *Biochimie* **2009**, *91*, 671–678.
35. Kawashima, H.; Ohnishi, M. Identification of minor fatty acids and various nonmethylene-interrupted diene isomers in mantle, muscle, and viscera of the marine bivalve *Megangulus zyoensis*. *Lipids* **2004**, *39*, 265–271.
36. Kawashima, H. Unusual minor nonmethylene-interrupted di-, tri-, and tetraenoic fatty acids in limpet gonads. *Lipids* **2005**, *40*, 627–630.
37. Monroig, O.; Navarro, J.C.; Dick, J.R.; Alemany, F.; Tocher, D.R. Identification of a  $\Delta 5$ -like fatty acyl desaturase from the cephalopod *Octopus vulgaris* (Cuvier 1797) involved in the biosynthesis of essential fatty acids. *Mar. Biotechnol.* **2012**, *14*, 411–422.
38. Houtsmuller, U.M.T. Columbionic acid, a new type of essential fatty acid. *Prog. Lipid Res.* **1981**, *20*, 889–896.
39. Zhukova, N.V.; Eliseikina, M.G. Symbiotic bacteria in the nudibranch mollusk *Dendrodoris nigra*: Fatty acid composition and ultrastructure analysis. *Mar. Biol.* **2012**, *159*, 1783–1794.
40. Vasskog, T.; Andersen, J.H.; Hansen, E.; Svenson, J. Characterization and cytotoxicity studies of the rare 21:4n-7 acid and other polyunsaturated fatty acids from the marine opisthobranch *Scaphander lignaris*, isolated using bioassay guided fractionation. *Mar. Drugs* **2012**, *10*, 2676–2690.
41. Proksch, P.; Edrada, R.A.; Ebel, R. Drugs from the seas—Current status and microbiological implications. *Appl. Microbiol. Biot.* **2002**, *59*, 125–134.
42. Schmidt, E.W.; Donia, M.S. Life in cellulose houses: Symbiotic bacterial biosynthesis of ascidian drugs and drug leads. *Curr. Opin. Biotechnol.* **2010**, *21*, 827–833.

43. Lindquist, N.; Barber, P.H.; Weisz, J.B. Episymbiotic microbes as food and defence for marine isopods, unique symbioses in a hostile environment. *Proc. Biol. Sci.* **2005**, *272*, 1209–1216.
44. Haine, E.R. Symbiont-mediated protection. *Proc. Biol. Sci.* **2008**, *275*, 353–361.
45. Wagele, H.; Ballesteros, M.; Avila, C. Defensive glandular structures in Opisthobranch mollusks—From histology to ecology. *Oceanogr. Mar. Biol.* **2006**, *44*, 197–276.
46. Schuett, C.; Doepke, H. Endobacterial morphotypes in nudibranch cerata tips: A SEM analysis. *Helgol. Mar. Res.* **2013**, *67*, 219–227.
47. Zhukova, N.V.; Eliseikina, M.G.; Balakirev, E.S.; Ayala, F.J. A novel symbiotic association of the nudibranch mollusk *Rostanga alisae* with bacteria. Unpublished work, 2014.
48. Bligh, E.G.; Dyer, W.J. A rapid method of total lipid extraction and purification. *Can. J. Biochem. Physiol.* **1959**, *37*, 911–918.
49. Vaskovsky, V.E.; Kostetsky, E.Y.; Vasendin, I.M. A universal reagent for phospholipids analysis. *J. Chromatogr.* **1975**, *114*, 129–142.
50. Carreau, J.P.; Dubacq, J.P. Adaptation of the macroscale method to the micro-scale for fatty acid methyl transesterification of biological lipid extracts. *J. Chromatogr.* **1979**, *151*, 384–390.
51. Svetashev, V.I. Mild method for preparation of 4,4-dimethyloxazoline derivatives of polyunsaturated fatty acids for GC-MS. *Lipids* **2011**, *46*, 463–467.
52. Christie, W.W. Equivalent chain lengths of methyl ester derivatives of fatty acids on gas chromatography—A reappraisal. *J. Chromatogr.* **1988**, *447*, 305–314.
53. Christie, W.W. 2013, Mass Spectrometry of Fatty Acid Derivatives. Available online: <http://lipidlibrary.aocs.org/ms/masspec.html> (accessed on 21 January 2014).

# Effect of *Salicornia herbacea* on Osteoblastogenesis and Adipogenesis *in Vitro*

Fatih Karadeniz, Jung-Ae Kim, Byul-Nim Ahn, Myeong Sook Kwon  
and Chang-Suk Kong

**Abstract:** Bone-related complications are among the highest concerning metabolic diseases in the modern world. Bone fragility and susceptibility to fracture increase with age and diseases like osteoporosis. Elevated adipogenesis in bone results in osteoporosis and loss of bone mass when coupled with lack of osteoblastogenesis. In this study the potential effect of *Salicornia herbacea* extract against osteoporotic conditions was evaluated. Adipogenesis inhibitory effect of *S. herbacea* has been evidenced by decreased lipid accumulation of differentiating cells and expression levels of crucial adipogenesis markers in 3T3-L1 pre-adipocytes. *S. herbacea* treatment reduced the lipid accumulation by 25% of the control. In addition, mRNA expression of peroxisome proliferator-activated receptor (PPAR) $\gamma$ , CCAAT/enhancer-binding protein (C/EBP) $\alpha$  and sterol regulatory element binding protein (SREBP)1c were inhibited by the presence of *S. herbacea*. Bone formation enhancement effect of *S. herbacea* was also confirmed in MC3T3-E1 pre-osteoblasts. The presence of *S. herbacea* significantly elevated the alkaline phosphatase (ALP) activity by 120% at a concentration of 100  $\mu\text{g/mL}$  in differentiating osteoblasts. *S. herbacea* also significantly increased the expression of osteoblastogenesis indicators, ALP, bone morphogenetic protein (BMP)-2, osteocalcin and collagen type I (collagen-I). In conclusion, *S. herbacea* possess potential to be utilized as a source of anti-osteoporotic agent that can inhibit adipogenesis while promoting osteoblastogenesis.

Reprinted from *Mar. Drugs*. Cite as: Karadeniz, F.; Kim, J.-A.; Ahn, B.-N.; Kwon, M.S.; Kong, C.-S. Effect of *Salicornia herbacea* on Osteoblastogenesis and Adipogenesis *in Vitro*. *Mar. Drugs* **2014**, *12*, 513265147.

## 1. Introduction

Natural sources that can be used for the treatment or prevention of diseases have been of much interest during the past decades. In this context, extracts and compounds from plants are among the main targets of studies [1,2]. Several studies in the past reported various biologically active plants with marine plants allocating a large part [3]. Due to the harsh conditions of marine environments and the need for strong protection, marine organisms produce unique substances. Plant extracts and compounds have been intensely studied in order to fully understand their action mechanism against common complications such as oxidative stress and inflammation [4–6], as well as diseases with high morbidity and mortality rates including diabetes, cancer, obesity and AIDS [7–9]. The halophyte *Salicornia herbacea* is endemic to the western coast of the Korean peninsula and a part of folk medicine due to its effect on constipation, diabetes, obesity, *etc.*, [10]. As expected, a number of experiments have credited *S. herbacea* for various bioactivities including antioxidative, antiinflammatory, antihyperglycemic and antihyperlipidemic [11–13]. It was proposed that *S. herbacea*

contained active flavonoids [14–16]. However, very few investigations have been carried out in order to evaluate the effect of *S. herbacea* on osteoporosis.

Bone-related diseases, namely osteoporosis and age-related osteopenia are reported to be associated with bone mass loss due to lack of osteoblastogenesis [17]. Studies showed that glucocorticoid treatment also caused an increase in bone adipocytes, which finally resulted in fractures and osteoporosis [18]. Several mechanisms have been suggested for possible cause of bone mass imbalance. Peroxisome proliferator activated receptor (PPAR) $\gamma$  is confirmed to play crucial roles in the outcome of bone marrow mesenchymal cell differentiation [19]. Both *in vitro* and *in vivo* mechanism studies demonstrated that the activation of PPAR $\gamma$  promotes adipogenesis. Likewise, suppression of PPAR $\gamma$  pathway was shown to inhibit adipogenesis and stimulate osteoblast differentiation depending on the binding ligand [20]. Several diabetic drugs as ligands of PPAR $\gamma$  activate adipogenesis and lower blood glucose. However, this activation also causes problems in bone mass by favoring adipogenesis of bone mesenchymal cells and deteriorating the bone mass balance. Diabetic drugs, obesity-related factors and long chain fatty acids were confirmed to be activating ligands for PPAR $\gamma$  [21]. Overall, in this study *S. herbacea* was tested for its potential effect on adipogenesis of pre-adipocytes and pre-osteoblast differentiation with a possible intervention in PPAR $\gamma$  pathway.

## 2. Results

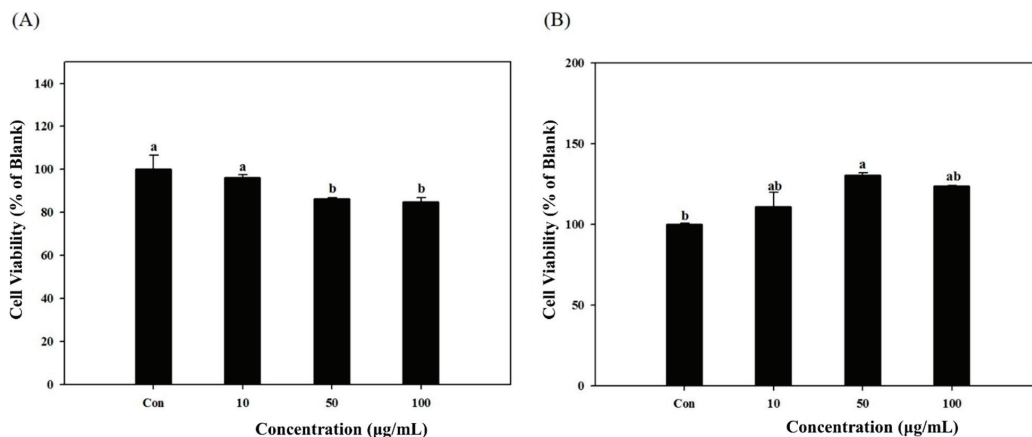
### 2.1. Effect of *S. herbacea* on Differentiation of 3T3-L1 Pre-Adipocytes

Prior to assays, the cytotoxicity of samples was tested *in vitro* using the 3T3-L1 and MC3T3-E1 cells which were used in further experiments. The cytotoxic effect of *S. herbacea* extracts in 3T3-L1 (Figure 1A) and MC3T3-E1 (Figure 1B) cells are presented. At a concentration of 10  $\mu\text{g/mL}$ , there was no cytotoxicity for both cell lines while the two highest concentrations (50 and 100  $\mu\text{g/mL}$ ) caused slight decrease in cell viability of 3T3-L1 cells, indicating a small effect on cell viability at higher concentrations. However, no cytotoxic effect was observed on MC3T3-E1 cells at concentrations of 50 and 100  $\mu\text{g/mL}$ .

In order to evaluate the effect of *S. herbacea* on adipogenesis, 3T3-L1 mouse pre-adipocytes were differentiated into mature adipocytes in the presence and absence of *S. herbacea* extract. Lipid accumulation which is a key indicator of successful maturation into adipocytes was used to analyze the anti-adipogenesis effect. Lipid accumulation is observed by staining of intracellular triglycerides with Oil-Red O. Cell images after staining indicated that the presence of *S. herbacea* decreased the intracellular lipid amount (as red colored areas in cell images) in a dose-dependent manner (Figure 2A). Observable lipid accumulation stained by Oil-Red O was at a minimum compared to all other cases, in the case of the highest concentration treated (100  $\mu\text{g/mL}$ ). Inhibited lipid accumulation was quantified by the elution of accumulated Oil Red O stain. Absorbance values of intracellular accumulated stain are shown in Figure 2B. Quantification of lipid accumulation was in accordance with the cell images. The presence of *S. herbacea* lowered the intracellular stain amount as an indicator of suppressed lipid accumulation. In order to assess the mechanism behind the lowering of lipid amounts, glycerol release into the culture medium was

quantified. Excessive glycerol secretion of adipocytes is a key marker for triglyceride lipolysis. In the presence of *S. herbacea*, glycerol secretion of differentiated cells increased from  $3.09 \pm 0.51$  to  $4.64 \pm 0.62$ ,  $5.26 \pm 0.40$  and  $5.79 \pm 0.32$  at concentrations of 10, 50 and 100  $\mu\text{g/mL}$ , respectively (Figure 2C).

**Figure 1.** Cytotoxicity levels of *S. herbacea* on the viability of 3T3-L1 (A) and MC3T3-E1 (B) cells. Cell viability was observed by MTT assay and presented as percentage value of untreated undifferentiated blank cells. Values are means  $\pm$  SD ( $n = 3$ ). <sup>a,b</sup> Means with different letters are significantly different ( $p < 0.05$ ) by Duncan's multiple range test. (Con: Differentiated untreated cells).



Next, in order to evaluate whether *S. herbacea* affects the expression of key transcription factors for adipogenesis, RT-PCR experiments were carried out. Possible changes in the mRNA expressions of PPAR $\gamma$ , differentiation-dependent factor 1/sterol regulatory element-binding protein (SREBP1c) and CCAAT/enhancer-binding proteins (C/EBP $\alpha$ ) were observed. Different solvent fractions were tested for their ability to suppress PPAR $\gamma$  mRNA expression. Among four tested fractions (*n*Hexane, 85% MeOH, *n*BuOH and H $_2$ O), the *n*BuOH fraction decreased the PPAR $\gamma$  expression most compared to control (Figure 3A). In addition, treatment significantly suppressed the expression of PPAR $\gamma$ , SREBP1c and C/EBP $\alpha$ , compared to fully differentiated control adipocytes (Figure 3B). Hence, *n*BuOH was considered for further activity based-isolation of compounds. Other fractions also showed an observable decrease in mRNA expression, the H $_2$ O extract being the least effective.

**Figure 2.** Effect of *S. herbacea* on adipogenic differentiation as stained cell images following Oil Red O staining of intracellular lipids (A), quantification of lipid accumulation by the absorbance of eluted intracellular stain (B) and glycerol secretion into culture medium during final differentiation (C) of mature 3T3-L1 adipocytes. Values are means  $\pm$  SD ( $n = 6$ ). <sup>a-c</sup> Means with different letters are significantly different ( $p < 0.05$ ) by Duncan’s multiple range test.

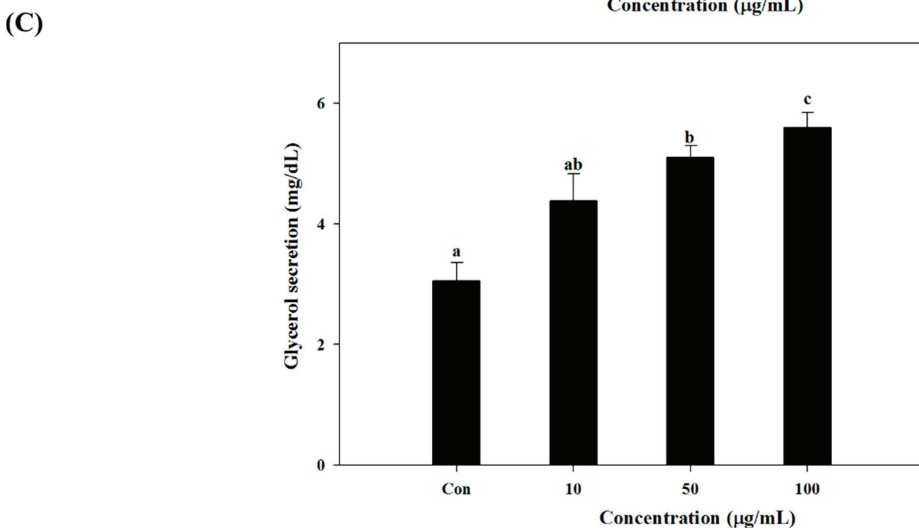
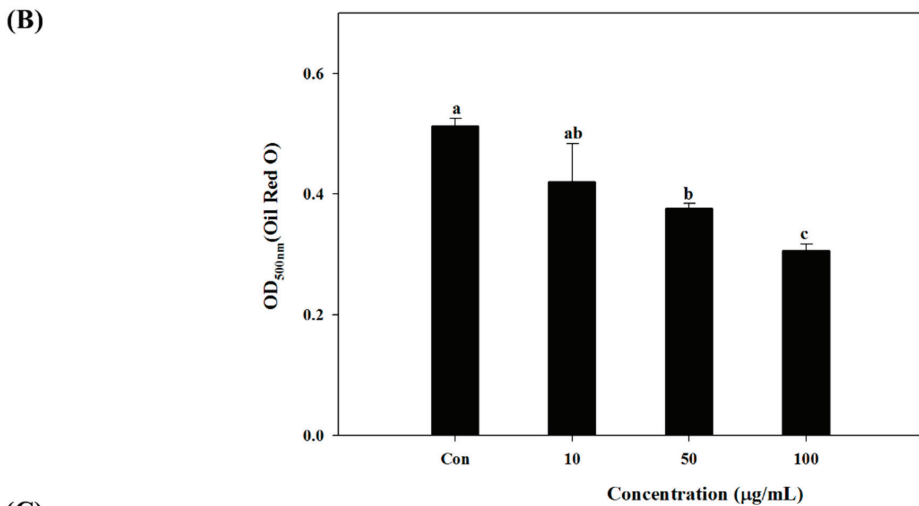
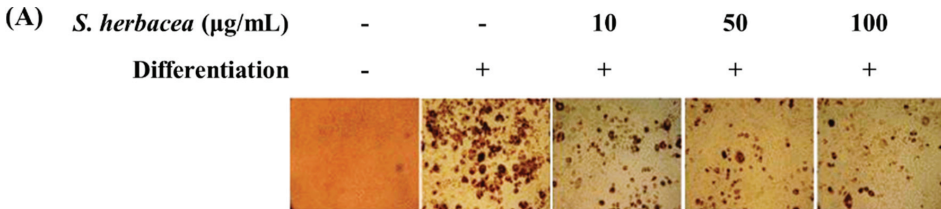
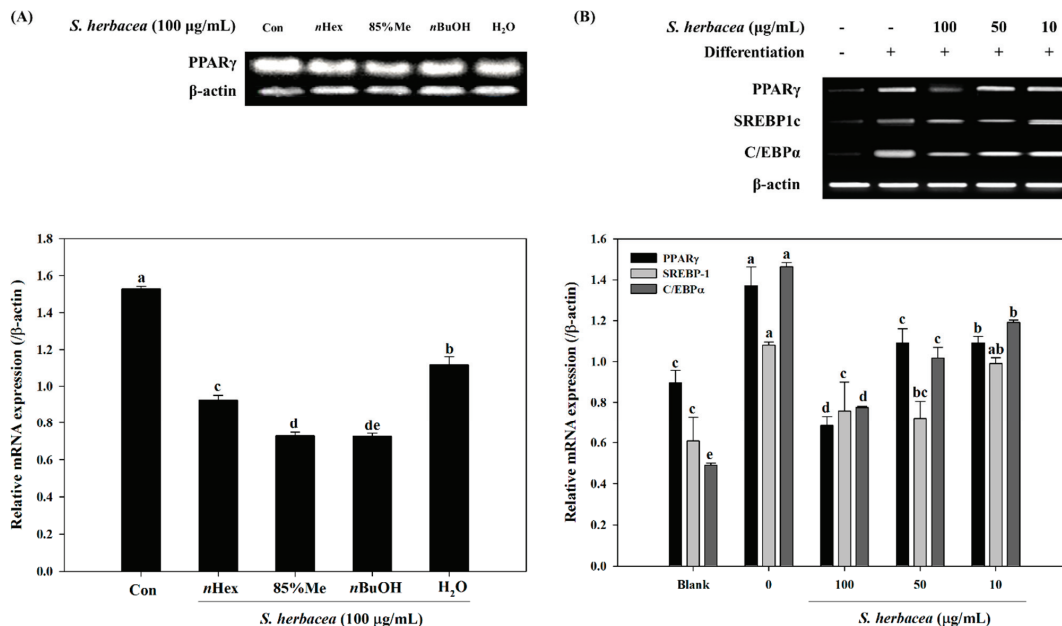


**Figure 3.** Effect of *S. herbacea* extract fractions (A) and the crude extract (B) on the mRNA expression levels of adipogenic target genes in 3T3-L1 adipocytes assessed by RT-PCR and band quantification. Values are means  $\pm$  SD ( $n = 3$ ). <sup>a-c</sup> Means with different letters are significantly different ( $p < 0.05$ ) by Duncan's multiple range test.



## 2.2. Effect of *S. herbacea* on Osteogenic Differentiation of MC3T3-E1 Pre-Osteoblasts

*S. herbacea* was tested for its ability to enhance osteoblast differentiation in mouse MC3T3-E1 pre-osteoblasts. Cells were treated with different concentrations of *S. herbacea* during the differentiation process. Measurement of alkaline phosphatase (ALP) activity of MC3T3-E1 osteoblasts was used as a marker for osteoblastogenesis. Effect of *S. herbacea* on ALP activity was measured by a commercial kit according to the manufacturer's protocol. Results suggested an enhancing ability of *S. herbacea* towards ALP-indicated osteoblastogenesis. Compared to differentiated control cells, *S. herbacea* treatment enhanced the ALP activity by increasing the absorbance values of reaction mixtures from  $0.681 \pm 0.092$  to  $0.814 \pm 0.081$ ,  $0.896 \pm 0.094$  and  $1.049 \pm 0.102$  at concentrations of 10, 50 and 100  $\mu$ g/mL, respectively (Figure 4).

During osteogenic differentiation, MC3T3-E1 pre-osteoblasts were treated with *S. herbacea* extract at concentrations of 10, 50 and 100  $\mu$ g/mL. In order to detect and evaluate the differentiation of pre-osteoblasts, following incubation during 14 days of differentiation, gene expression of key osteogenic markers, namely ALP, BMP-2, osteocalcin, collagen-I, and intracellular levels of ALP and collagen-I proteins were quantified by real-time PCR and Western blotting, respectively. *S. herbacea* enhanced the expression of ALP, BMP-2, osteocalcin and collagen-I mRNA in a dose-dependent manner (Figure 5A). Fractions of extract were shown to enhance the mRNA expression of osteogenesis markers in a similar way to suppressing adipogenesis indicators (Figure 5B). As expected, treatment with *S. herbacea* notably increased



intracellular levels of ALP and collagen-I proteins in a similar fashion to mRNA levels (Figure 6). According to the results, the presence of *S. herbacea* enhanced the expression of osteogenic marker proteins in MC3T3-E1 cells.

**Figure 4.** Effect of *S. herbacea* on alkaline phosphatase (ALP) activity in MC3T3-E1 cells after 14 days of differentiation. Values are means  $\pm$  SD ( $n = 6$ ). <sup>a-c</sup> Means with different letters are significantly different ( $p < 0.05$ ) by Duncan’s multiple range test.

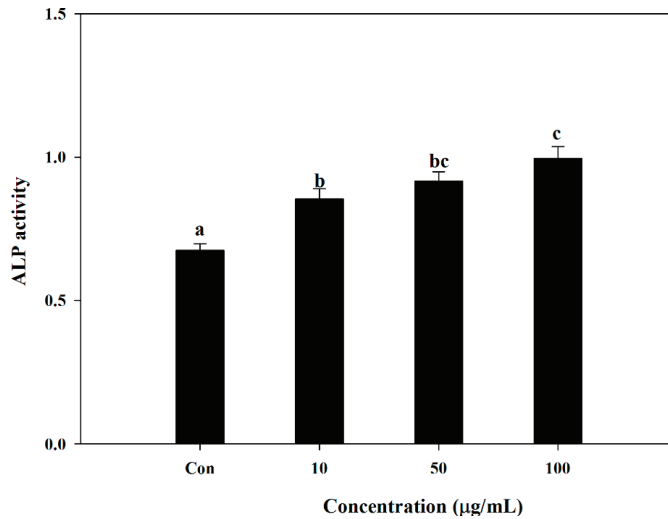


**Figure 5.** Effect of *S. herbacea* extract (A) and fractions (B) on mRNA expression of key osteoblastogenesis markers in MC3T3-E1 osteoblasts according to real time PCR assay. Values are means  $\pm$  SD ( $n = 3$ ). <sup>a-c</sup> Means with different letters are significantly different ( $p < 0.05$ ) by Duncan’s multiple range test.

(A)

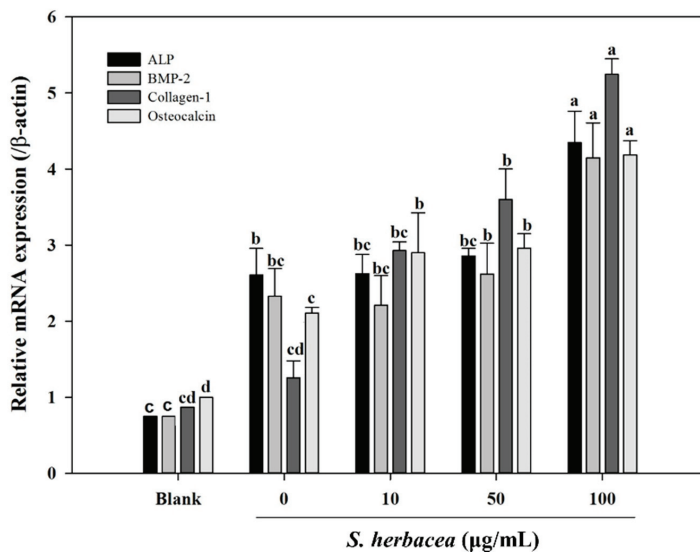
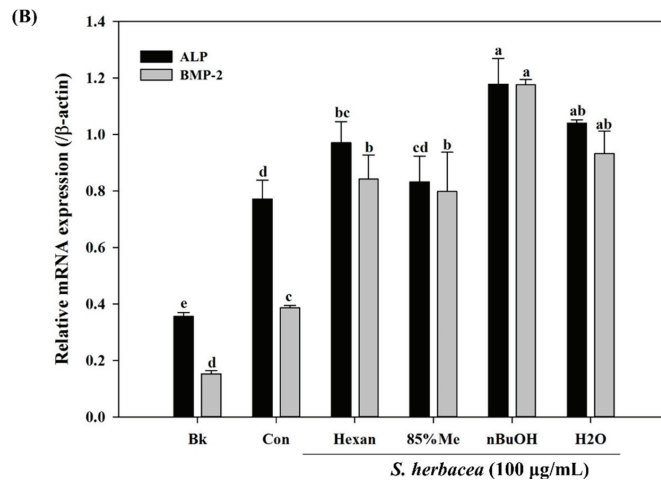
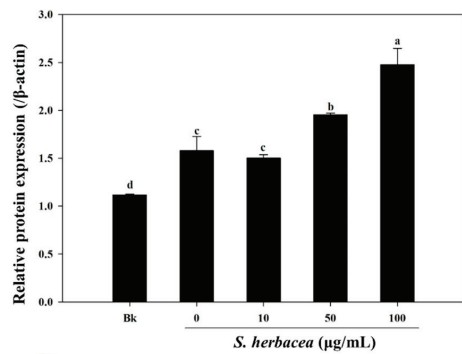
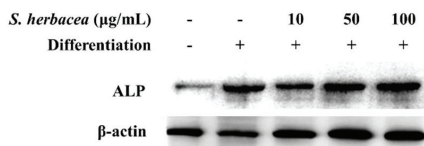


Figure 5. Cont.

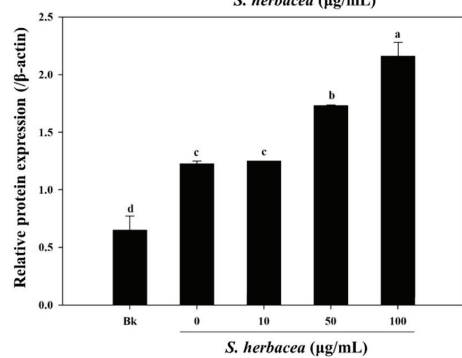
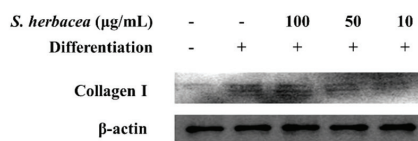


**Figure 6.** Effect of *S. herbacea* extract on protein levels of ALP (A) and collagen (B) in differentiated MC3T3-E1 osteoblasts. Values are means  $\pm$  SD ( $n = 3$ ). <sup>a-d</sup> Means with different letters are significantly different ( $p < 0.05$ ) by Duncan's multiple range test.

(A)

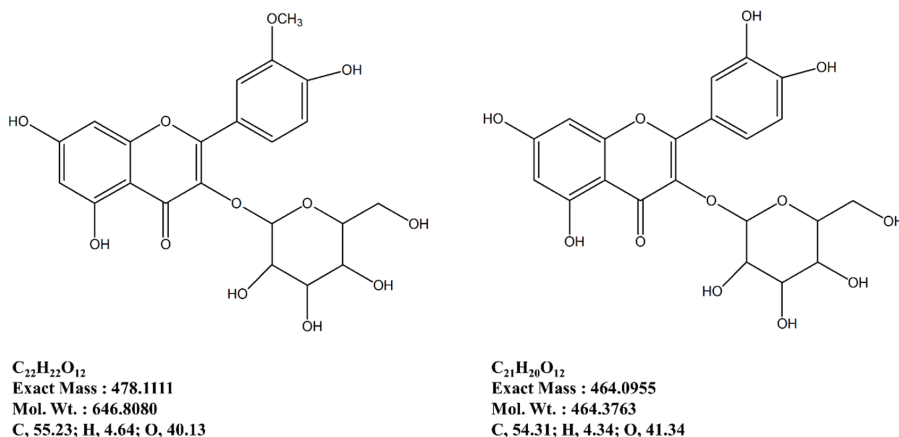


(B)



Following a bioactivity-directed isolation method, two formerly known flavonoid glycosides were isolated from the *n*BuOH fraction of *S. herbacea* as a part of ongoing research (Figure 7). In total accordance with our earlier report, the isolated flavonoid glycosides were confirmed by comparison of basic structural data (data not shown) [15].

**Figure 7.** Isolated flavonoid glycosides as anti-osteoporotic ingredients of *S. herbacea*.



### 3. Discussion

The main age-related metabolic diseases are the major causes of diminished life quality for the elderly. Additionally, recent studies indicate an increasing trend for the younger generation to be diagnosed with obesity, type-2 diabetes and osteoporosis [16,22,23]. Scientists are turning their attention to natural products to use to intervene with the progression of the aforementioned diseases due to bioavailability, biodegradation and fewer side effects. In this context, marine-based organisms are of high interest to pharmaceutical researchers as most marine plants and animals live in extreme conditions, which results in the need for unique compounds for survival. By means of this promising situation, past decades have been fruitful in ways of natural bioactive substance development. Numerous marine plants have been studied intensively in order to discover bioactive chemicals that can act against cancer, tumor growth, oxidative stress, diabetes, obesity and osteoporosis [5,24,25]. Halophytes are also plants that survive under extreme conditions such as high concentrations of salt and harsh climate changes. In this context, the halophyte *S. herbacea* was examined here for possible compounds with health beneficiary effects. Reports had already stated that *S. herbacea* contains flavonoid glycosides and polysaccharides, which are natural antioxidants [15].

In this study, we examined the ability of *S. herbacea* to relieve osteoporosis conditions with a regulatory mechanism towards adipogenesis/osteoblastogenesis imbalance. Uncontrolled inducement of adipogenesis was shown to create a bone mass imbalance which resulted in elevated fragility and susceptibility. Differentiation of both pre-adipocyte and mesenchymal cells is partly regulated by PPAR $\gamma$  signaling [26]. Obesity conditions were recently linked to increased osteoporosis progression in proportional to elevated adipokines [27]. Adipokines and triglycerides trigger in a

similar way an increase in adipogenesis, which is required to be in balance with osteoblastogenesis for healthy bones. Regulation of this imbalance is crucial to prevent and treat osteoporosis, especially when developed under obesity.

Our results showed a strong inhibition on lipid accumulation of differentiated 3T3-L1 adipocytes by *S. herbacea* treatment. Glycerol assay results showed that cells treated with *S. herbacea* released more glycerol to the culture medium. Furthermore, a possible mechanism behind the anti-adipogenic effect of *S. herbacea* was evaluated by assessing expression levels of adipogenesis regulator factors, PPAR $\gamma$ , SREBP1c and C/EBP $\alpha$ . In addition to lowering lipid accumulation, *S. herbacea* also lowered the expression of the aforementioned adipogenesis factors. Results indicated that *S. herbacea* inhibited not only lipid accumulation, but also adipogenesis. In order to be used for further bioactivity-directed isolation, comparison of *S. herbacea* solvent fractions was carried out. Among all fractions, *n*BuOH was found to be the most active to inhibit PPAR $\gamma$  mRNA expression. In addition, Kong *et al.* [14] also reported that two glycosides isolated from *S. herbacea* were shown to possess chemoprotective effect against cancer through matrix metalloproteinase inhibition.

Increase in bone adipocytes is accompanied by severe fragility that defines osteoporosis. In order to relieve the deteriorated stem cell differentiation, inducing differentiating cells towards osteoblastogenesis is considered to be a crucial treatment step. Our results showed that *S. herbacea* inhibited adipogenesis by possible interaction with the PPAR- $\gamma$  pathway and lipolysis. Results also indicated that *S. herbacea* might attenuate the imbalance of bone cell differentiation towards osteoblastogenesis.

In osteoporosis, mesenchymal cell perseverance towards adipogenesis is also accompanied by diminished osteoblastogenesis [28,29]. If an increase in adipogenesis is coupled with a decrease in osteoblastogenesis, bone loses its sturdiness and tends to be more fragile.

We examined the ability of *S. herbacea* extract to enhance osteoblast differentiation in MC3T3-E1 pre-osteoblasts. Differentiating MC3T3-E1 pre-osteoblasts were introduced to *S. herbacea* in different concentrations. Following a full differentiation, alkaline phosphatase (ALP) activity of cell lysates was evaluated. The alkaline phosphatase level is known to be an indicator of successful osteoblast differentiation, as it plays a crucial role in the mineralization of bone [30]. In this regard, results indicated that the presence of *S. herbacea* elevated the ALP activity suggesting a role in the mineralization of osteoblasts at all treated concentrations, indicating an enhancement towards bone formation.

Bone formation is carried out by a distinctive and well-studied pathway of factors and proteins. In this cascade of signaling, bone morphogenetic protein (BMP) 2, 4 and 7 and osteocalcin are some of the key factors elevated at gene expression levels [31]. During osteoblastogenesis, osteocalcin has also been reported to be a cell marker for the final differentiation state. On the other hand, BMPs are known to enhance expression of alkaline phosphatase (ALP), type I collagen (collagen-I) and other non-collagenous bone proteins as indicators for successful osteoblastogenesis [30]. Therefore, mRNA expression of ALP, BMP-2, osteocalcin and collagen-I were assessed in the absence and presence of *S. herbacea*. After full maturation into osteoblasts, RT-PCR experiments suggested an increasing trend towards expression of the aforementioned

markers in cells treated with *S. herbacea*, a result confirmed for ALP and collagen-I by western blot. In the light of these results, it was suggested that *S. herbacea* enhanced osteoblast differentiation while inhibiting adipogenesis in pre-adipocytes. Ha *et al.* [32] also reported that *S. herbacea* might be a potential source of antioxidant agents because of its effect on ovariectomy-induced oxidative stress, which is considered to cause age-related diseases including osteoporosis. Taken together, our results on *S. herbacea* extracts provide evidence for an inhibitory effect on adipogenesis while enhancing osteoblast differentiation. Therefore, *S. herbacea* is proposed as a promising source of bioactive agents for the effective prevention and treatment of osteoporosis.

In this regard, following an earlier reported isolation method adapted for anti-osteoporosis bioactivity-directed flow, two formerly known flavonoid glycosides were isolated [14]. These glycosides, namely isorhamnetin 3-*O*- $\beta$ -D-glucoside and quercetin 3-*O*- $\beta$ -D-glucoside are suggested to be possible bioactive reagents of *S. herbacea*, responsible for relieving the effect of osteoporosis through regulation of adipogenesis/osteoblastogenesis imbalance by inhibiting PPAR $\gamma$  pathway and enhancing bone formation. Isolation of glycosides from the *n*BuOH fraction was expected as this fraction was the most active for inhibiting adipogenesis and enhancing osteoblastogenesis. Several other flavonoid glycosides were isolated and evaluated for their anti-adipogenic activities. Studies also showed the possible absorption and bioactivity mechanisms of dietary flavonoids through the small intestine. Our previous results [14,15] were also in accordance with current assays and suggested that isorhamnetin 3-*O*- $\beta$ -D-glucoside and quercetin 3-*O*- $\beta$ -D-glucoside are strong bioactive substituents of *S. herbacea*. On the other hand, isorhamnetin 3-*O*- $\beta$ -D-glucoside and quercetin 3-*O*- $\beta$ -D-glucoside were also shown to act on inhibition of differentiation of 3T3-L1 cells through AMPK/MAPK pathways. Notoya *et al.* [33] suggested an inhibitory effect of the flavonoid, quercetin, on proliferation, differentiation and mineralization of osteoblasts. However, Kim *et al.* [34] also stated that quercetin was able to inhibit proliferation while elevating the osteogenic differentiation of adipose stromal cells. In such a case, quercetin derivatives might also show the same distinct bioactivity on adipogenesis and osteoblastogenesis as our preliminary results indicated. The isolated derivative of quercetin, quercetin 3-*O*- $\beta$ -D-glucoside has the quercetin backbone with a glucoside side-chain containing -OH branches similar to phloroglucinol derivatives. Considering that phloroglucinol derivatives have been reported to have anti-adipogenesis and pro-osteoblastogenesis activities, it could be suggested that these flavonoids might be responsible for the reported bioactivity of *S. herbacea*. Nonetheless, the *n*BuOH fraction of *S. herbacea* showed strong effects on adipogenesis and osteoblastogenesis and two flavonoid glycosides were isolated from the fraction. However, further studies to reveal the real action mechanisms of isolated compounds and their efficiency on adipogenic and osteogenic differentiation are needed. According to the results, the *n*BuOH fraction of *S. herbacea* might contain other bioactive constituents that are responsible for anti-adipogenic and pro-osteoblastogenic effects. In the future, coupled with *in vivo* assays, results of this study will help to evaluate the true potential of *S. herbacea*, as a potential source of compounds against obesity-related osteoporosis.

## 4. Experimental Section

### 4.1. Plant Materials

The whole plant of *S. herbacea* was briefly dried under shade and kept at  $-25\text{ }^{\circ}\text{C}$  until use. The air-dried sample of *S. herbacea* was chopped into small pieces and extracted for 24 h with  $\text{CH}_2\text{Cl}_2$  ( $3\text{ L} \times 2$ ) at room temperature. After removal of the solvent, the residue was re-extracted for 24 h with MeOH ( $3\text{ L} \times 2$ ) at room temperature.

The combined crude extracts (50 g) were suspended between  $\text{CH}_2\text{Cl}_2$  and water. The organic layer was further partitioned between 85% aqueous MeOH and *n*-hexane and then the aqueous layer was fractionated with *n*-BuOH and  $\text{H}_2\text{O}$ , respectively, to afford the *n*-hexane (3.2 g), 85% aq. MeOH (12.1 g), *n*-BuOH (16.3 g) and water (15.5 g) fractions.

### 4.2. Cell Culture and Adipocyte/Osteoblast Differentiations

Murine 3T3-L1 pre-adipocytes were seeded in 6-well plates at a density of  $2 \times 10^5$  cells/well prior to experiments and grown to confluence in Dulbecco's modified Eagle's medium (DMEM) with 10% fetal bovine serum (FBS) at  $37\text{ }^{\circ}\text{C}$  in a humidified atmosphere of 5%  $\text{CO}_2$ . At 1 day postconfluence (designated "day 0"), a mixture of 3-isobutyl-1-methylxanthine (0.5 mM), dexamethasone (0.25 M) and insulin (5  $\mu\text{g}/\text{mL}$ ) in DMEM containing 10% FBS was introduced into cells in order to induce cell differentiation. After 48 h (day 2), DMEM containing 10% FBS supplemented with insulin (5  $\mu\text{g}/\text{mL}$ ) was introduced to cells following removal of induction medium. While replacing this medium with a fresh one every two days, *S. herbacea* extract was administered to the culture medium from day 0 to day 6 for Oil Red O and RT-PCR experiments and day 6 to day 8 for the glycerol secretion assay.

Murine osteoblast-like MC3T3-E1 cells were seeded in 6-well plates at a density of  $1 \times 10^5$  cells/well and grown to confluence in  $\alpha$ -Modified minimal essential medium ( $\alpha$ MEM) supplemented with 10% heat-inactivated fetal bovine serum (FBS), 1 mM sodium pyruvate, 100 units/L penicillin and 100 mg/L streptomycin at  $37\text{ }^{\circ}\text{C}$  in a humidified atmosphere of 5%  $\text{CO}_2$ . The cells were induced into osteoblastogenesis by adding of ascorbic acid and  $\beta$ -glycerophosphate into medium for five days under the conditions of the earlier report [35]. Following confluence, the cell differentiation was initiated with culture medium containing 50  $\mu\text{g}/\text{mL}$  ascorbic acid and 10 mM  $\beta$ -glycerophosphate for three days. Then, the induction medium was removed and the cell monolayer was washed twice with phosphate buffered saline (PBS). *S. herbacea* extract was administered to the culture medium prior to further incubation of 48 h.

### 4.3. Cytotoxicity Determination Using MTT Assay

Cytotoxic levels of the *S. herbacea* on cultured cells were measured using MTT (3-(4,5-dimethylthiazol-2-yl)-2,5-diphenyltetrazolium bromide) assay, which is based on the conversion of MTT to MTT-formazan by mitochondrial enzyme. The cells were grown in 96-well plates at a density of  $5 \times 10^3$  cells/well. After 24 h, the cells were washed with fresh medium and were treated with control medium or the medium supplemented with *S. herbacea*. After incubation

for seven days while changing the medium and re-treating the samples every two days, cells were rewashed and 100  $\mu$ L of MTT solution (1 mg/mL) was added and incubated for 4 h. Finally, 100  $\mu$ L of DMSO was added to solubilize the formed formazan crystals and the amount of formazan crystal was determined by measuring the absorbance at 540 nm using a GENios<sup>®</sup> microplate reader (Tecan Austria GmbH, Grödigg, Austria). Relative cell viability was determined by the amount of MTT converted into formazan crystal. Viability of cells was quantified as a percentage compared to the control and dose response curves were developed.

#### 4.4. Oil-Red O Staining and Glycerol Release Assay

Fully differentiated cells were fixed with 10% fresh formaldehyde in PBS for 1 h at room temperature and stained with filtered Oil-Red O solution (60% isopropanol and 40% water) for at least 1 h. After incubation, the wells were emptied of Oil-Red O staining solution, washed with distilled water and air dried. Images of lipid droplets in 3T3-L1 adipocytes were collected by an Olympus microscope (Tokyo, Japan). Finally, dye retained in the cells was eluted with isopropanol and quantified by measuring the optical absorbance at 500 nm using a microplate reader (Tecan Austria GmbH, Grödigg, Austria).

The glycerol levels were determined using the enzymatic reagent, free glycerol reagent (Sigma, St. Louis, MO, USA), directed by the protocol of GPO-TRINDER (Sigma, St. Louis, MO, USA).

#### 4.5. Cellular ALP Activity

Cellular ALP activity of *S. herbacea*-treated and control cells was measured following incubation of 14 days. The cell monolayer was gently washed twice with PBS and lysed using 0.1% Triton X-100 and 25 mM carbonate buffer. The lysates were centrifuged at 4 °C 12,000 $\times$  g for 15 min. Enzyme assay buffer (15 mM *p*-nitrophenyl phosphate, 1.5 mM MgCl<sub>2</sub> and 200 mM carbonate buffer) was used to measure the ALP activity of the supernatants. The absorbance of reactive solution was measured at 405 nm.

#### 4.6. RNA Extraction and Reverse Transcription-Polymerase Chain Reaction Analysis

Total RNA was isolated from 3T3-L1 and D1 adipocytes and MC3T3-E1 osteoblasts in the presence/absence of *S. herbacea* using Trizol reagent (Invitrogen Co., Carlsbad, CA, USA). For synthesis of cDNA, RNA (2  $\mu$ g) was added to RNase-free water and oligo (dT), denaturated at 70 °C for 5 min and cooled immediately. RNA was reverse transcribed in a master mix containing 1 $\times$  RT buffer, 1 mM dNTPs, 500 ng oligo (dT), 140 U M-MLV reverse transcriptase and 40 U RNase inhibitor at 42 °C for 60 min and at 72 °C for 5 min using an automatic T100 Thermo Cycler (Bio-Rad, Hertfordshire, UK). The target cDNA was amplified using the following sense and antisense primers: forward 5'-TTT-TCA-AGG-GTG-CCA-GTT-TC-3' and reverse 5'-AAT-CCT-TGG-CCC-TCT-GAG-AT-3' for PPAR $\gamma$ ; forward 5'-TGT-TGG-CAT-CCT-GCT-ATC-TG-3' and reverse 5'-AGG-GAA-AGC-TTT-GGG-GTC-TA-3' for SREBP1c; forward 5'-TTA-CAA-CAG-GCC-AGG-TTT-CC-3' and reverse 5'-GGC-TGG-CGA-CAT-ACA-GTA-CA-3' for C/EBP $\alpha$ ; forward 5'-CCA-CAG-CTG-AGA-GGG-AAA-TC-3' and reverse 5'-AAG-GAA-GGC-TGG-AAA-

AGA-GC-3' for  $\beta$ -actin. The amplification cycles were carried out at 95 °C for 45 s, 60 °C for 1 min and 72 °C for 45 s. Final PCR products were separated by electrophoresis on 1.5% agarose gel for 30 min at 100 V after 30 cycles. Gels were then stained with 1 mg/mL ethidium bromide visualized by UV light using Davinch-Chemi imager™ (CAS-400SM, Wako Co., Osaka, Japan).

#### 4.7. Real-Time RT-PCR Analysis of mRNA Expression

Gene expression was measured by real time RT-PCR in a Thermal Cycler Dice® Real Time System TP800 (Takara Bio Inc., Ohtsu, Japan) following the manufacturer's protocol. Briefly 1.0  $\mu$ L of DNA sample and 12.5  $\mu$ L of Maxima® SYBR Green qPCR Master Mix (Fermentas, Waltham, MA, USA) containing Taq DNA polymerase, dNTP and reaction buffer were mixed. The target cDNA was amplified using the following sense and antisense primers: forward 5'-CCA-GCA-GGT-TTC-TCT-CTT-GG-3' and reverse 5'-CTG-GGA-GTC-TCA-TCC-TGA-GC-3' for ALP; forward 5'-GGA-CCC-GCT-GTC-TTC-TAG-TG-3' and reverse 5'-GCC-TGC-GGT-ACA-GAT-CTA-GC-3' for BMP-2; forward 5'-GCT-GTG-TTG-GAA-ACG-GAG-TT-3' and reverse 5'-CAT-GTG-GGT-TCT-GAC-TGG-TG-3' for Osteocalcin; forward 5'-GAG-CGG-AGA-GTA-CTG-GAT-CG-3' and reverse 5'-TAC-TCG-AAC-GGG-AAT-CCA-TC-3' for Collagen I; forward 5'-CCA-CAG-CTG-AGA-GGG-AAA-TC-3' and reverse 5'-AAG-GAA-GGC-TGG-AAA-AGA-GC-3' for  $\beta$ -actin. The PCR amplification was carried out for an initial denaturation at 95 °C for 10 min, followed by 40 PCR cycles. Each cycle proceeded at 95 °C for 15 s, 60 °C for 60 s. Relative quantification was calculated using the 2<sup>- $\Delta\Delta$ CT</sup> method.  $\beta$ -Actin was used as an internal control.

#### 4.8. Western Blot Analysis

Western blotting was performed according to standard procedures. Briefly, cells were lysed in RIPA lysis buffer (Sigma-Aldrich Corp., St. Louis, MO, USA) at 4 °C for 30 min. Cell lysates (35  $\mu$ g) were separated by 12% SDS-polyacrylamide gel electrophoresis, transferred onto a polyvinylidene fluoride membrane (Amersham Pharmacia Biotech., Amersham, England, UK), blocked with 5% skimmed milk and hybridized with primary antibodies (diluted 1:1000) against ALP and collagen I. After incubation with horseradish-peroxidase-conjugated secondary antibody at room temperature, immunoreactive proteins were detected using a chemiluminescence ECL assay kit (Amersham Pharmacia Biosciences, England, UK) according to the manufacturer's instructions. Western blot bands were visualized using a Davinch-Chemi imager™ (CAS-400SM, Wako Co., Osaka, Japan).

#### 4.9. Statistical Analysis

The data were presented as mean  $\pm$  SD. Differences between the means of the individual groups were analyzed using the analysis of variance (ANOVA) procedure of Statistical Analysis System, SAS v9.1 (SAS Institute, Cary, NC, USA) with Duncan's multiple range tests. The significance of differences was defined at the  $p < 0.05$  level.



## 5. Conclusions

In this study, *Salicornia herbacea* was extracted and experimented with, in order to evaluate its ability as a potential bioactive agent against osteoporosis. Results clearly indicated that, *S. herbacea* was able to inhibit adipogenesis of both pre-adipocytes and bone marrow mesenchymal cells. Inhibiting adipogenesis is important in relieving the fragile bone mass of osteoporosis which is caused by elevated adipogenesis of mesenchymal cells. In addition, results also indicated that *S. herbacea* can enhance osteoblastogenesis which is important to affect the change of fragile bone towards strong bone formation. Finally, following a bioactivity-directed isolation, two flavonoid glycosides were suggested to be responsible for the anti-osteoporosis effect of *S. herbacea* but have yet to be evaluated for their exact mechanism of action. Nonetheless, *S. herbacea* is a promising lead source for bioactive substances that can be utilized against osteoporosis.

## Acknowledgments

This research was supported by Basic Science Research Program through the National Research Foundation of Korea (NRF) funded by the Ministry of Education, Science and Technology (NRF-2012R1A1A3014642). Also, this research was financially supported by the Ministry of Education (MOE) and National Research Foundation of Korea (NRF) through the Human Resource Training Project for Regional Innovation (No. NRF-2013H1B8A2032201).

## Author Contributions

All authors contributed to this report extensively. J.-A.K. and C.-S.K. conceived the idea and designed the experiments and protocols. F.K. interpreted the data and wrote the manuscript. J.-A.K. and F.K. carried out the adipogenesis experiments. Immunoblotting, mineralization and cytotoxicity experiments were performed by B.-N.A. and M.S.K. Finally, C.-S.K. supervised the work.

## Conflicts of Interest

The authors declare no conflict of interest.

## References

1. Qin, G.-W.; Xu, R.-S. Recent Advances on Bioactive Natural Products from Chinese Medicinal Plants. *Med. Res. Rev.* **1998**, *18*, 375–382.
2. Gurib-Fakim, A. Medicinal Plants: Traditions of Yesterday and Drugs of Tomorrow. *Mol. Aspects Med.* **2006**, *27*, 1–93.
3. Rinehart, K.L.; Holt, T.G.; Fregeau, N.L.; Keifer, P.A.; Wilson, G.R.; Perun, T.J.; Sakai, R.; Thompson, A.G.; Stroh, J.G.; Shield, L.S.; *et al.* Bioactive Compounds from Aquatic and Terrestrial Sources. *J. Nat. Prod.* **1990**, *53*, 771–792.

4. Ngo, D.-H.; Wijesekara, I.; Vo, T.-S.; van Ta, Q.; Kim, S.-K. Marine Food-Derived Functional Ingredients as Potential Antioxidants in the Food Industry: An Overview. *Food Res. Int.* **2011**, *44*, 523–529.
5. Mayer, A.M.S.; Rodríguez, A.D.; Berlinck, R.G.S.; Fusetani, N. Marine Pharmacology in 2007–2008: Marine Compounds with Antibacterial, Anticoagulant, Antifungal, Anti-Inflammatory, Antimalarial, Antiprotozoal, Antituberculosis, and Antiviral Activities; Affecting the Immune and Nervous System, and Other Miscellaneous Mechanisms of Action. *Comp. Biochem. Physiol. Part C Toxicol. Pharmacol.* **2011**, *153*, 191–222.
6. Abad, M.J.; Bedoya, L.M.; Bermejo, P. Natural Marine Anti-Inflammatory Products. *Mini Rev. Med. Chem.* **2008**, *8*, 740–754.
7. Tarling, C.A.; Woods, K.; Zhang, R.; Brastianos, H.C.; Brayer, G.D.; Andersen, R.J.; Withers, S.G. The Search for Novel Human Pancreatic  $\alpha$ -Amylase Inhibitors: High-Throughput Screening of Terrestrial and Marine Natural Product Extracts. *ChemBioChem* **2008**, *9*, 433–438.
8. Cragg, G.M.; Grothaus, P.G.; Newman, D.J. Impact of Natural Products on Developing New Anti-Cancer Agents. *Chem. Rev.* **2009**, *109*, 3012–3043.
9. Vo, T.-S.; Kim, S.-K. Potential Anti-HIV Agents from Marine Resources: An Overview. *Mar. Drugs* **2010**, *8*, 2871–2892.
10. Kang, S.; Kim, D.; Lee, B.; Kim, M.-R.; Chiang, M.; Hong, J. Antioxidant Properties and Cytotoxic Effects of Fractions from Glasswort (*Salicornia herbacea*) Seed Extracts on Human Intestinal Cells. *Food Sci. Biotechnol.* **2011**, *20*, 115–122.
11. Im, S.-A.; Kim, G.-W.; Lee, C.-K. Immunomodulatory Activity of *Salicornia herbacea* L. Components. *Nat. Prod. Sci.* **2003**, *9*, 273–277.
12. Lee, K.Y.; Lee, M.H.; Chang, I.Y.; Yoon, S.P.; Lim, D.Y.; Jeon, Y.J. Macrophage Activation by Polysaccharide Fraction Isolated from *Salicornia herbacea*. *J. Ethnopharmacol.* **2006**, *103*, 372–378.
13. Hwang, J.Y.; Lee, S.K.; Jo, J.R.; Kim, M.E.; So, H.A.; Cho, C.W.; Seo, Y.W.; Kim, J.I. Hypolipidemic Effect of *Salicornia herbacea* in Animal Model of Type 2 Diabetes Mellitus. *Nutr. Res. Pract.* **2007**, *1*, 371–375.
14. Kong, C.-S.; Kim, Y.A.; Kim, M.-M.; Park, J.-S.; Kim, J.-A.; Kim, S.-K.; Lee, B.-J.; Nam, T.J.; Seo, Y. Flavonoid Glycosides Isolated from *Salicornia herbacea* Inhibit Matrix Metalloproteinase in HT1080 Cells. *Toxicol. In Vitro* **2008**, *22*, 1742–1748.
15. Kong, C.-S.; Kim, J.-A.; Qian, Z.-J.; Kim, Y.A.; Lee, J.I.; Kim, S.-K.; Nam, T.J.; Seo, Y. Protective Effect of Isorhamnetin 3-*O*- $\beta$ -D-Glucopyranoside from *Salicornia herbacea* against Oxidation-Induced Cell Damage. *Food Chem. Toxicol.* **2009**, *47*, 1914–1920.
16. Lee, Y.S.; Lee, S.; Lee, H.S.; Kim, B.-K.; Ohuchi, K.; Shin, K.H. Inhibitory Effects of Isorhamnetin-3-*O*- $\beta$ -D-Glucoside from *Salicornia herbacea* on Rat Lens Aldose Reductase and Sorbitol Accumulation in Streptozotocin-Induced Diabetic Rat Tissues. *Biol. Pharm. Bull.* **2005**, *28*, 916–918.

17. Muruganandan, S.; Roman, A.A.; Sinal, C.J. Adipocyte Differentiation of Bone Marrow-Derived Mesenchymal Stem Cells: Cross Talk with the Osteoblastogenic Program. *Cell. Mol. Life Sci.* **2009**, *66*, 236–253.
18. Fraser, L.A.; Adachi, J.D. Glucocorticoid-Induced Osteoporosis: Treatment Update and Review. *Ther. Adv. Musculoskelet. Dis.* **2009**, *1*, 71–85.
19. Harsløf, T.; Tofteng, C.L.; Husted, L.B.; Nyegaard, M.; Børglum, A.; Carstens, M.; Stenkjær, L.; Brixen, K.; Eiken, P.; Jensen, J.E.; *et al.* Polymorphisms of the Peroxisome Proliferator-Activated Receptor  $\gamma$  (PPAR $\gamma$ ) Gene Are Associated with Osteoporosis. *Osteoporosis Int.* **2011**, *22*, 2655–2666.
20. Nuttall, M.E.; Gimble, J.M. Controlling the Balance between Osteoblastogenesis and Adipogenesis and the Consequent Therapeutic Implications. *Curr. Opin. Pharm.* **2004**, *4*, 290–294.
21. Spiegelman, B.M. PPAR- $\gamma$ : Adipogenic Regulator and Thiazolidinedione Receptor. *Diabetes* **1998**, *47*, 507–514.
22. Dietz, W.H. Health Consequences of Obesity in Youth: Childhood Predictors of Adult Disease. *Pediatrics* **1998**, *101*, 518–525.
23. Cha, E.; Umpierrez, G.; Kim, K.H.; Bello, M.K.; Dunbar, S.B. Characteristics of American Young Adults with Increased Risk for Type 2 Diabetes: A Pilot Study. *Diabetes Educ.* **2013**, *39*, 454–469.
24. Harvey, A.L. Plant Natural Products in Anti-Diabetic Drug Discovery. *Curr. Org. Chem.* **2010**, *14*, 1670–1677.
25. Newman, D.J.; Cragg, G.M. Natural Products as Sources of New Drugs over the 30 Years from 1981 to 2010. *J. Nat. Prod.* **2012**, *75*, 311–335.
26. De Ugarte, D.A.; Morizono, K.; Elbarbary, A.; Alfonso, Z.; Zuk, P.A.; Zhu, M.; Drago, J.L.; Ashjian, P.; Thomas, B.; Benhaim, P.; *et al.* Comparison of Multi-Lineage Cells from Human Adipose Tissue and Bone Marrow. *Cells Tissues Organs* **2003**, *174*, 101–109.
27. Zhao, L.J.; Jiang, H.; Papasian, C.J.; Maulik, D.; Drees, B.; Hamilton, J.; Deng, H.W. Correlation of Obesity and Osteoporosis: Effect of Fat Mass on the Determination of Osteoporosis. *J. Bone Miner. Res.* **2008**, *23*, 17–29.
28. Rodriguez, J.P.; Astudillo, P.; Rios, S.; Pino, A.M. Involvement of Adipogenic Potential of Human Bone Marrow Mesenchymal Stem Cells (MSCs) in Osteoporosis. *Curr. Stem Cell Res. Ther.* **2008**, *3*, 208–218.
29. Rosen, C.J.; Bouxsein, M.L. Mechanisms of Disease: Is Osteoporosis the Obesity of Bone? *Nat. Clin. Pract. Rheumatol.* **2006**, *2*, 35–43.
30. Rawadi, G.; Vayssière, B.; Dunn, F.; Baron, R.; Roman-Roman, S. BMP-2 Controls Alkaline Phosphatase Expression and Osteoblast Mineralization by a Wnt Autocrine Loop. *J. Bone Miner. Res.* **2003**, *18*, 1842–1853.
31. Ryoo, H.-M.; Lee, M.-H.; Kim, Y.-J. Critical Molecular Switches Involved in BMP-2-Induced Osteogenic Differentiation of Mesenchymal Cells. *Gene* **2006**, *366*, 51–57.
32. Ha, B.J.; Lee, S.H.; Kim, H.J.; Lee, J.Y. The Role of *Salicornia herbacea* in Ovariectomy-Induced Oxidative Stress. *Biol. Pharm. Bull.* **2006**, *29*, 1305–1309.

33. Notoya, M.N.; Tsukamoto, Y.; Nishimura, H.; Woo, J.T.; Nagai, K.; Lee, I.-S.; Hagiwara, H. Quercetin, a Flavonoid, Inhibits the Proliferation, Differentiation, and Mineralization of Osteoblasts *in vitro*. *Eur. J. Pharmacol.* **2004**, *485*, 89–96.
34. Kim, Y.J.; Bae, Y.C.; Suh, K.T.; Jung, J.S. Quercetin, a Flavonoid, Inhibits Proliferation And Increases Osteogenic Differentiation in Human Adipose Stromal Cells. *Biochem. Pharmacol.* **2006**, *72*, 1268–1278.
35. Fatokun, A.A.; Stone, T.W.; Smith, R.A. Hydrogen Peroxide-induced Oxidative Stress in MC3T3-E1 Cells: The Effects of Glutamate and Protection by Purines. *Bone* **2006**, *39*, 542–551.

# Marine Invertebrate Xenobiotic-Activated Nuclear Receptors: Their Application as Sensor Elements in High-Throughput Bioassays for Marine Bioactive Compounds

Ingrid Richter and Andrew E. Fidler

**Abstract:** Developing high-throughput assays to screen marine extracts for bioactive compounds presents both conceptual and technical challenges. One major challenge is to develop assays that have well-grounded ecological and evolutionary rationales. In this review we propose that a specific group of ligand-activated transcription factors are particularly well-suited to act as sensors in such bioassays. More specifically, xenobiotic-activated nuclear receptors (XANRs) regulate transcription of genes involved in xenobiotic detoxification. XANR ligand-binding domains (LBDs) may adaptively evolve to bind those bioactive, and potentially toxic, compounds to which organisms are normally exposed to through their specific diets. A brief overview of the function and taxonomic distribution of both vertebrate and invertebrate XANRs is first provided. Proof-of-concept experiments are then described which confirm that a filter-feeding marine invertebrate XANR LBD is activated by marine bioactive compounds. We speculate that increasing access to marine invertebrate genome sequence data, in combination with the expression of functional recombinant marine invertebrate XANR LBDs, will facilitate the generation of high-throughput bioassays/biosensors of widely differing specificities, but all based on activation of XANR LBDs. Such assays may find application in screening marine extracts for bioactive compounds that could act as drug lead compounds.

Reprinted from *Mar. Drugs*. Cite as: Richter, I.; Fidler, A.E. Marine Invertebrate Xenobiotic-Activated Nuclear Receptors: Their Application as Sensor Elements in High-Throughput Bioassays for Marine Bioactive Compounds. *Mar. Drugs* **2014**, *12*, 559065618.

## Abbreviations

AD, activation domain; AhR, aryl hydrocarbon receptor; BaP, benzo [ $\alpha$ ] pyrene; *BsVDR/PXR $\alpha$* , *Botryllus schlosseri* VDR/PXR orthologue  $\alpha$ ; CAR, constitutive androstane receptor; *CiVDR/PXR $\alpha$* , *Ciona intestinalis* VDR/PXR orthologue  $\alpha$ ; *CiVDR/PXR $\beta$* , *Ciona intestinalis* VDR/PXR orthologue  $\beta$ ; CPRG, chlorophenol red- $\beta$ -D-galactopyranoside; CYP, cytochrome P450 gene; DBD, DNA-binding domain; DDT, 1,1,1-trichloro-2,2-di(4-chlorophenyl)ethane; ER, estrogen receptor; GAL4, yeast DNA-binding transcription factor; GST, glutathione S-transferases; HR96, nuclear hormone receptor 96; LBD, ligand-binding domain; MRP, multidrug resistance-associated protein; NR, nuclear receptor; NR1I, nuclear receptor sub-family 1, class I; NR1J, nuclear receptor sub-family 1, class J; NR1H, nuclear receptor sub-family 1, class H; OA, okadaic acid; PAHs, polycyclic aromatic hydrocarbons; PTX-2, pectenotoxin-2; PCN, pregnenolone 16 $\alpha$ -carbonitrile; PXR, pregnane X receptor; RXR, retinoid X receptor; SRC-1, steroid co-activator 1; TCPOBOP, 1,4-Bis[2-(3,5-dichloropyridyloxy)]benzene; VDR, vitamin D receptor; VP16, viral protein 16; XANR, xenobiotic-activated nuclear receptor; XR, xenobiotic receptor.

## 1. Introduction

A major challenge facing researchers investigating marine natural products, with a view to identify potential drug lead compounds, is the selection and/or development of suitable bioassays. Typically the bioassays selected reflect the researcher's long-term, applied science goals but often they have little ecological or evolutionary rationale. The goal of this review is to promote the idea that chemical detection mechanisms, which adaptively evolve to allow marine animals to detect dietary bioactive chemicals, can be used in bioassays for marine bioactive chemicals. More specifically, we propose that nuclear receptor (NR) proteins may provide "sensor elements" that can be utilized in bioassays. Briefly, in the envisaged bioassays the "sensor element" would be a NR ligand-binding domain (LBD), which binds a bioactive dietary chemical and the resulting conformational change is then transduced into an output signal.

Having stated the overall goal of this review, its limits should also be made explicit. First, the term "xenobiotic receptor" (XR) will be used in this review to denote members of the zinc-finger NR transcription factor super-family that are activated by xenobiotic chemicals (xenobiotic, from the Greek *xenos*: foreigner; *bios*: life). Under this definition we have excluded genuine xenobiotic receptors such as the aryl hydrocarbon receptor (AhR), which are activated by xenobiotics but do not belong to the NR super-family because they bind DNA by a different mechanism [1–3]. In principle, such non-NR xenobiotic receptors could also be utilized in similar high-throughput screens to those proposed here but this is beyond the scope of this review. To remove any ambiguities in terminology, the term "xenobiotic-activated nuclear receptor" (abbreviated XANR) will hereafter be used for the group of xenobiotic receptors considered in this review [4–6].

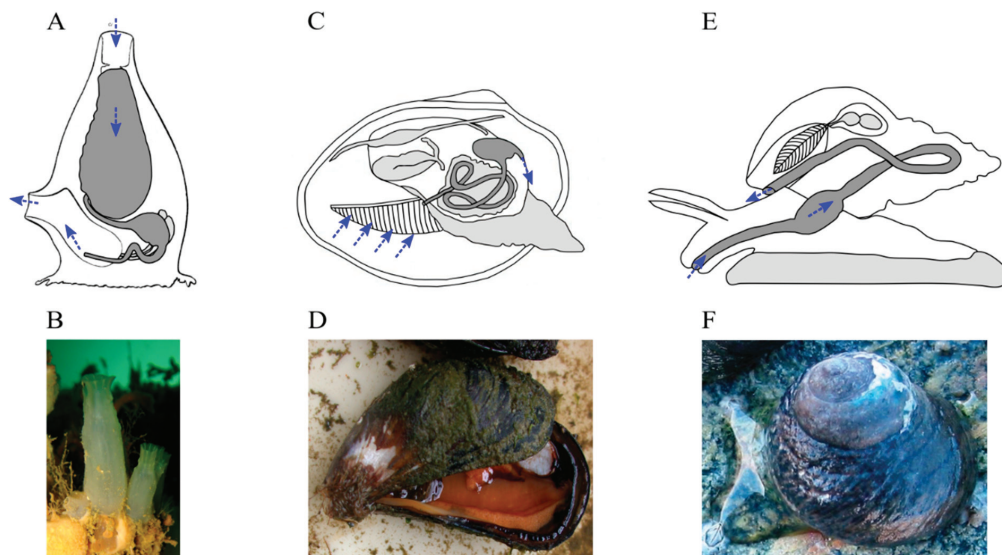
Marine invertebrate XANRs will be the primary focus of this review as such organisms occupy diverse ecological niches and are characterized by great taxonomic diversity. Significantly, this diversity includes both filter-feeders and intense surface-grazers, two foraging behaviors that expose animals to dietary xenobiotics at high concentrations (Figure 1). For example, it is well-established that filter-feeding marine invertebrates clear large volumes of phytoplankton from the water column and consequently bioaccumulate high concentrations of microalgal biotoxins [7,8]. It is to be expected that selective pressures associated with any bioactive compounds, particularly toxic ones, ingested by marine invertebrates may drive adaptive evolution of XANR LBDs that bind these ingested compounds. This idea is explored further in this review.

## 2. Bioactive Chemicals are Naturally Present in Animal Diets

Chemicals in animal diets are often viewed as simply energy sources (e.g., carbohydrates, lipids), building blocks (e.g., proteins), or biochemical pathway intermediates (e.g., vitamins). However, it is apparent that some dietary chemicals have "physiological" roles in the sense that they modulate animal biochemistry and physiology. The biological effects of such dietary chemicals range from influences on reproductive physiology and developmental transitions through to acute poisoning [9–14]. Animal taxa exposed to bioactive dietary xenobiotics evolve both behavioral and physiological traits to minimize any associated deleterious effects [15]. Many animals simply avoid eating plants/prey likely to contain toxins with such avoidance behaviors being both instinctual and

learned [16,17]. For example, vertebrates tend to avoid bitter-tasting plants, as many poisonous phytochemicals (e.g., alkaloids) taste bitter [18–20]. Interestingly, there is evidence that natural selection associated with bitter taste perception may have influenced the evolution of bitter taste receptor gene repertoire sizes in vertebrate genomes [20–22]. In the marine environment, avoidance of toxic/unpalatable prey by coral reef fish is well-documented [23–25], while bivalve molluscs can limit their exposure to toxic compounds using behavioral responses, such as shell closure and restriction of filtration rate [8,26–28]. Despite avoidance behaviors, the diet of many animals will inevitably contain bioactive, and potentially toxic, chemicals that need to be metabolized and eliminated from their bodies [29–33].

**Figure 1.** Examples of filter-feeding and surface-grazing marine invertebrates. Marine invertebrates that filter their diet from seawater are found in a range of taxonomic groups including the phyla *Chordata* and *Mollusca* (A–D). In contrast, grazing gastropods (Phylum *Mollusca*) scour their food from surfaces (E,F). Whatever their ecological niche, marine invertebrates require detoxification mechanisms in order to detect, and effectively metabolize, any potentially deleterious xenobiotics encountered in their diet (A,C,E). Schematic diagrams of the digestive tracts (dark grey) of filter-feeding tunicates (A), filter-feeding bivalve molluscs (C), and grazing gastropod molluscs (E) are shown and the direction of food movement is indicated by blue arrows. Examples of a filter-feeding tunicate (B), *Ciona intestinalis*, Phylum *Chordata*; a filter-feeding bivalve mollusc (D), *Mytilus edulis*, Phylum *Mollusca*; and a grazing gastropod mollusc (F), *Amphibola crenata*, Phylum *Mollusca*.



### 3. Detoxification Pathways and Their Transcription-Level Regulation

Metazoan organisms have specialized biochemical pathways that metabolize and eliminate potentially toxic chemicals, whether endogenously synthesized or exogenously acquired. The complexities of detoxification biochemistry are beyond the scope of this review and are outlined in a number of recent reviews [34–38]. Nonetheless, a brief overview of metazoan detoxification pathways, and the transcriptional control of associated genes, is required to understand the functions of XANRs [39,40].

Detoxification pathways have been classified into three functional stages: oxidation/reduction (Phase I), conjugation (Phase II), and elimination (Phase III) [41,42]. It is to be expected that the genes encoding the functional elements of all three phases may be under both conservative and, at times, adaptive evolutionary pressures reflecting variation in the structures and mode of action of different xenobiotics/toxins associated with different animal diets [33,43]. The cat family (*Felidae*) provides an example of the apparent consequences of relaxation of conservative selective pressures associated with reduced ingestion of phytochemicals. Both domesticated and wild members of the *Felidae* are extremely susceptible to poisoning by phenolic compounds. This sensitivity is associated with a mutation in the feline orthologue of the gene encoding the enzyme UDP-glucuronosyltransferase (UGT) 1A6, a Phase II phenolic compound detoxification enzyme, leading to pseudogenization [44,45]. It is speculated that such UGT1A6 inactivation mutations are tolerated in the *Felidae*, and other hypercarnivores, because of relaxed selective pressures associated with their diet [46], as hypercarnivores are rarely exposed to plant-derived phenolic compounds [45].

In the context of this review, it is the *control of transcription* of detoxification related genes that is of particular interest. Expression of many detoxification pathway genes can be induced by the xenobiotic(s) that the pathway ultimately metabolizes [38,42,47]. Such xenobiotic-mediated induction of gene expression is of medical interest because of its implications for the efficacy, persistence, and side-effects of therapeutic drugs [34,48,49]. Xenobiotic-mediated induction of detoxification gene expression is best characterized for Phase I cytochrome P450 (CYP) enzymes, particularly members of CYP sub-families CYP1-4 that are associated with xenobiotic metabolism [34,48,50,51]. For example, levels of the human CYP enzyme CYP3A4, an enzyme responsible for oxidizing >50% of medicinal drugs, are induced by a range of therapeutic compounds, such as rifampicin, tamoxifen, and hyperforin [49,52], while human CYP1A2 enzymatic activity is induced by polycyclic aromatic hydrocarbons (PAHs) [34,53]. Interestingly, there exists striking inter-taxa variation in inductive responses to some xenobiotics [54]. For example, the steroidal drugs pregnenolone 16 $\alpha$ -carbonitrile (PCN) and dexamethasone are highly efficacious CYP3A enzyme inducers in rodents but not so in humans [55,56]. In contrast, rifampicin is a strong inducer of human and dog CYP3A but not of rodent CYP3A [57,58]. While none of these examples are likely to be of ecological/evolutionary significance, such conspicuous inter-taxa variation in the response to xenobiotics suggests the possibility of adaptive evolution in the genetic elements that control expression of detoxification genes.

Xenobiotic induction of cytochrome P450 enzyme levels has also been reported in several invertebrate phyla, most prominently in the *Arthropoda* in the context of pesticide resistance [59–61]. In insects,



the CYP enzymes induced by xenobiotics mainly belong to the sub-families CYP4, CYP6, and CYP9 [36]. In both *dipteran* and *lepidopteran* insect taxa, the barbiturate phenobarbital induces CYP enzymatic activity in association with transcription level induction of the CYP4, CYP6, and CYP9 genes [62–65]. In the honey bee (*Apis mellifera*), aflatoxin and propolis, ecologically relevant natural xenobiotics, induce CYP gene expression [66,67], while in the “model” arthropod *Drosophila melanogaster* many CYP genes are induced by caffeine and phenobarbital [68–70]. In *Drosophila mettleri* the CYP4D10 gene is induced by primary host plant alkaloids but not by similar alkaloids from a rarely utilized host plant. Clearly this finding suggests adaptive evolution of the associated gene induction mechanism(s) of *Drosophila mettleri* [71]. The soil nematode *Caenorhabditis elegans* (phylum *Nematoda*) displays up-regulated CYP gene expression in response to exposure to multiple xenobiotics [72–74]. For example, beta-naphthoflavone, polychlorinated biphenyl, PCB52, and lansoprazol are all strong inducers of almost all *C. elegans* CYP35 isoforms [72]. Rifampicin, one of the strongest inducers of the human CYP3A4 gene, is also a strong inducer of the *C. elegans* CYP13A7 gene [75]. Amongst marine invertebrates the polychaete *Perinereis nuntia* (phylum *Annelida*) shows increased levels of some CYP gene transcripts after exposure to benzo[ $\alpha$ ]pyrene (BaP) and PAHs [76]. In an ecologically more relevant context, the marine gastropod *Cyphoma gibbosum* (phylum *Mollusca*) is suggested to have adapted to feeding exclusively on highly toxic gorgonian corals by differential regulation of transcripts for two CYP enzymes, CYP4BK and CYP4BL [77].

Whilst most xenobiotic-mediated gene induction research has focused on Phase I CYP genes, Phase II glutathione S-transferases (GST) and Phase III multidrug resistance-associated proteins (MRPs) have also been reported to be inducible by some xenobiotics [35,78]. For example, expression of mouse GSTA1, MRP2, and MRP3 genes is induced by both pregnenolone 16 $\alpha$ -carbonitrile (PCN) and 1,4-Bis[2-(3,5-dichloropyridyloxy)]benzene (TCPOBOP) [79]. In the marine environment, dietary toxins (e.g., cyclopentenone prostaglandins) have been shown to be both inducers and substrates of GST enzymes in three marine molluscs [80–82].

In summary, it is likely, that xenobiotic-mediated *control* of detoxification pathway gene expression may evolve adaptively in response to the differing chemicals to which different animals are exposed to, with diet probably being the main route of exposure [66,67,77,83]. The next section will consider the role of a specific group of ligand-activated transcription factors, the XANRs, in xenobiotic-mediated control of gene expression and speculate how natural selection may influence the adaptive evolution of such XANR genes.

#### 4. Xenobiotic Receptors: Functions, Structures, and Taxonomic Distribution

##### 4.1. Vertebrate Pregnane X Receptor

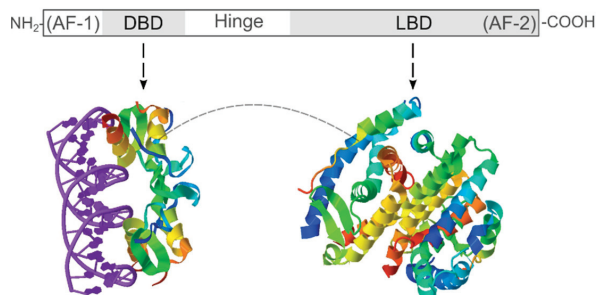
Functional characterization of XANRs is most advanced in a few selected vertebrate taxa [6,84–86]. Mammalian genomes encode two XANRs: constitutive androstane receptor (CAR; NR notation: NR1I3) and pregnane X receptor (PXR; NR notation: NR1I2). Although both CAR and PXR regulate the transcription of genes involved in detoxification of endogenous and exogenous (*i.e.*, xenobiotic) chemicals [85–87], PXR is the better understood with respect to how its LBD

structure relates to ligand-binding and subsequent activation [85]. Therefore, the following sections of this review will focus on PXR and its orthologues.

Mammalian PXR was originally identified in genomic sequence data and designated as an orphan NR as its ligand(s) were then unknown. In 1998, three groups independently reported mammalian PXR activation by both steroids and a range of xenobiotics resulting in three alternative receptor names—with pregnane X receptor (PXR) now the most widely used [88–90]. PXR appears to function much like a standard ligand-activated NR. After ligand-binding within the PXR LBD, the activated PXR protein forms a complex with retinoid X receptor (RXR) before translocating from the cell cytoplasm into the nucleus. The PXR/RXR heterodimer binds to appropriate DNA response elements, thereby influencing transcription of adjacent genes [91–94]. Many of the PXR regulated genes are involved in detoxification. Thus, PXR activation, following xenobiotic-binding to its LBD, provides a mechanistic link between the presence of xenobiotics in a cell and appropriate detoxification gene expression [95].

Vertebrate PXR ligands include a structurally diverse range of endogenously produced molecules (e.g., bile acids, steroid hormones, and vitamins) along with exogenously acquired chemicals (e.g., both synthetic and herbal drugs) [96–101]. Determination of the three dimensional structure of the human PXR protein has helped explain its striking permissiveness with respect to the differing structures of activating ligands. The classic model of NR function proposes that NR ligand specificity arises from the interaction between ligands and a ligand-binding domain (LBD) of the NR protein (Figure 2). In the majority of NRs the LBD cavities have well-defined shapes with restricted mobility, thereby ensuring specificity of ligand—NR LBD interactions [102,103]. In contrast, the human PXR LBD is both larger than is typical of NRs and also displays significant flexibility during ligand binding allowing it to accommodate a wider range of ligand sizes and structures [104,105].

**Figure 2.** Schematic summary of the generic nuclear receptor (NR) structure. The overall structure of ligand-activated NRs is conserved through evolution with five key structural domains: *N*-terminal transcription activation domain (activation function-1, AF-1), DNA-binding domain (DBD), flexible hinge region (Hinge), and ligand-binding domain (LBD), which includes a *C*-terminal activation domain (activation function-2, AF-2). The DBD interacts with DNA while the structurally separate LBD interacts with ligands [106].



Vertebrate PXR display greater inter-taxa variation in LBD sequences than is typical of NRs, along with some evidence of positive selection within the LBD [4,107–109]. From this observation it has been speculated that such inter-taxa PXR LBD sequence differences may reflect adaptive evolutionary changes which enhance PXR binding of those exogenous dietary bioactives/toxins typically encountered by an organism within its particular ecological niche [4,5,107,108,110,111]. Notwithstanding such speculation, it has been shown experimentally that the differential activation of human and rat PXRs by some ligands can be attributed, in part, to specific residues within the PXR LBD [88,89,112–116]. For example, rifampicin is an effective activator of human PXR but has little activity on rat PXR [112] and this difference can be attributed to differences between the two PXR LBDs at a single position: human PXR Leu<sub>308</sub>/rat PXR Phe<sub>305</sub> [117].

#### 4.2. Non-Marine Invertebrate XANRs

Although most advances in our understanding of XANR function and evolution have been within the *Vertebrata*, there has been some progress in characterizing invertebrate XANRs, building on the conceptual foundations provided by the vertebrate PXR studies. It should be noted that phylogenetic approaches to identifying XANR genes within the genomes of non-chordate invertebrate taxa face significant challenges, the biggest being the large evolutionary distances separating the functionally characterized vertebrate query sequences typically used to search invertebrate genomes. The scale of this challenge is reinforced by considering that the split between the deuterostome (includes vertebrates) and protostome (includes most invertebrates) lineages occurred approximately one billion years ago [118–120]. Fortunately, model invertebrate organisms within two protostome phyla, *Arthropoda* (*D. melanogaster*) and *Nematoda* (*C. elegans*), provide the experimental route of using mutant animal phenotypes to assess the functions of putative XANRs initially identified on the basis of sequence homologies [121,122]. A PXR/NR11-like homologue, termed hormone receptor-like 96 (*HR96*), identified in the *D. melanogaster* genome was found to be selectively expressed in tissues involved in the metabolism of xenobiotics [121,123]. *D. melanogaster* flies homozygous for *Dhr96* null alleles displayed increased sensitivity to both phenobarbital and the pesticide 1,1,1-trichloro-2,2-di(4-chlorophenyl)ethane (DDT) along with defects in phenobarbital induction of gene expression [121]. These findings are consistent with experiments, using a combination of RNA interference treatments and *Cyp6d1* promoter reporter assays, that indicate a role for *DHR96* in mediating phenobarbital associated gene induction in *Drosophila* Schneider (S2) cells [123]. In summary, *Dhr96* represents a strong candidate as a *bona fide* arthropod XANR and it may also have roles in cholesterol homeostasis and lipid metabolism [124,125]. A *DHR96* orthologue from a freshwater aquatic arthropod (*Daphnia pulex*), *DappuHR96*, has been shown to be activated by a structurally diverse range of both endogenously produced compounds and xenobiotics, consistent with a role as a lipid and/or xenobiotic sensor [126]. Probable *DHR96* orthologues have also been identified in a range of other arthropod genomes *albeit* with no reports of their functional characterization: beetles [*Tribolium castaneum*] [127], ants [*Camponotus floridabus*] [128], honey bee [*Apis mellifera*] [129], and fall armyworm [*Spodoptera frugiperda*] [130].

The genome of the model nematode *C. elegans* (phylum *Nematoda*) encodes an exceptionally large number of NRs (~284) [131]. Responses of mutant *C. elegans* strains to toxin exposure

indicates that one of these NRs, denoted NHR-8, a homologue of *D. melanogaster* HR96, is involved in the regulation of detoxification enzyme induction which is consistent with NHR-8 functioning as a XANR [122].

From a phylogenetic perspective one useful generalization emerges. To date, all arthropod and nematode putative, and partially functionally verified, XANRs are placed in the NR1J group of the NR super-family [126]. NR1J forms a sister group of the NR1I sub-family, which contains all the chordate XANRs. This grouping is suggestive of a shared ancestral XANR gene being present in the genome of a common ancestor preceding the divergence of the protostome-deuterostome lineage [132].

#### 4.3. Marine Invertebrate XANRs

Over a decade ago, phylogenetic analyses identified two orthologues of vertebrate PXR encoded in the genome of a marine invertebrate chordate; the solitary tunicate *Ciona intestinalis* [133–137]. As the functional characterization of one of these *C. intestinalis* putative XANRs is central to this review, the associated experiments will be described in more detail in Section 5. More recently, two putative PXR/NR1I orthologues have been detected in the genomic sequence of the colonial tunicate *Botryllus schlosseri* [138], while the genome of the pelagic tunicate *Oikopleura dioica* encodes as many as six NR1I clade genes [139].

Although NR encoding genes can be confidently identified in a growing number of publicly available non-chordate marine invertebrate genomic sequences [140], recognizing *bona fide* XANRs within the NR repertoire remains problematic. To date, all functionally characterised XANRs, both deuterostome and protostome, have been placed in the NR1 group of the NR super-family (deuterostome: NR1I; protostome: NR1J) [89,114,121,123,126,141–143]. Therefore, at present, any predicted marine invertebrate NRs placed in the NR1 group may be regarded as potential XANRs. However, such phylogeny-based designations are always highly tentative and only functional data can lead to the confident assignment of a NR1 protein as a functional XANR (Section 5).

Despite the evident phylogenetic/bioinformatic challenges, candidate XANR genes have been identified in sequence data derived from a number of non-chordate marine invertebrates. For example, at least one of the two NRs identified in a demosponge (*Amphimedon queenslandica*, Phylum *Porifera*) genome displays functional characteristics consistent with a role in detecting xenobiotics [144,145]. The genome of the starlet sea anemone (*Nematostella vectensis*, Phylum *Cnidaria*) encodes three NR genes equally related to sub-families NR1 and NR4, while the genome of the Pacific oyster (*Crassostrea gigas*, Phylum *Bivalvia*) encodes as many as 23 NR genes placed in the NR1 sub-family [146,147]. In contrast, the genome of a marine deuterostome, the sea urchin (*Strongylocentrotus purpuratus*, Phylum *Echinodermata*), appears to lack NR1I sub-family genes although three NR1H genes were identified [148]. The apparent absence of NR1I subfamily genes from the *S. purpuratus* genome should be treated with caution as it may simply reflect an incomplete data-set [148].

We suggest that functional characterization of at least one molluscan XANR would be a very useful advance, as both filter-feeding (*Bivalvia*) and grazing (*Gastropoda*) marine molluscs are expected to be exposed to a wide range of bioactive chemicals through their diet (Figure 1) [7,149].

It is also worth noting that molluscs provide a cautionary tale warning against assumptions that sequence homology/orthology necessarily predict shared function. For example, the molluscan homologue of the vertebrate steroid receptors is a constitutive, rather than a ligand-activated, transcription activation factor [150].

In summary, although significant bioinformatic challenges remain, it is clear that the ever increasing nucleotide sequence databases provide an informational resource in which putative marine invertebrate XANRs can be identified with varying degrees of confidence. However, functional characterization of such putative XANRs is always needed, as will be described in the next section.

## **5. Marine Invertebrate Putative XANR LBDs are Activated by Known Marine Bioactive Compounds**

In 2002, the solitary tunicate *Ciona intestinalis* was the first marine invertebrate to have an assembled and annotated genome sequence published [137,151]. Analysis of the *C. intestinalis* genomic sequence, in combination with *C. intestinalis* expressed sequence tag (EST) databases, revealed two genes that phylogenetic analyses placed as orthologous to vertebrate NR11 genes. These two *C. intestinalis* NR11-like genes were denoted “VDR/PXR” reflecting their putative orthology with both the vertebrate PXR and vitamin D receptor (VDR) genes [137,152]. Hereafter, these two *C. intestinalis* genes will be abbreviated as *CiVDR/PXR* $\alpha$  (GenBank accession number: [NM\\_001078379](#)) and *CiVDR/PXR* $\beta$  ([NM\\_001044366](#)) [153,154]. At the time of writing there is no functional data published regarding *CiVDR/PXR* $\beta$  so it will not be discussed further here.

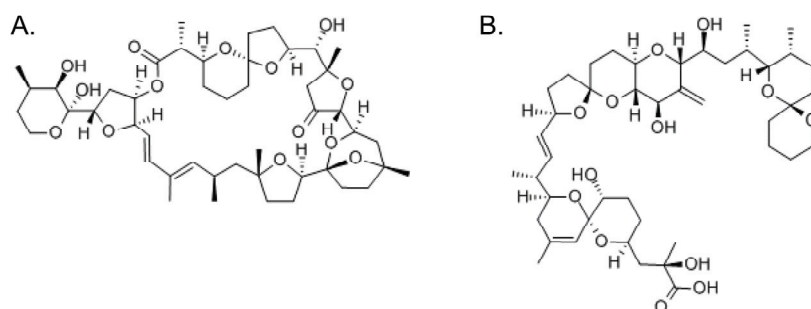
Functional characterization of *CiVDR/PXR* $\alpha$  began with its LBD being expressed, as part of a chimeric protein, in a mammalian cell line. Briefly, the *CiVDR/PXR* $\alpha$  LBD was joined to the generic GAL4 DNA-binding domain (GAL4-DBD) and the resulting chimeric protein was shown to mediate ligand-dependent expression of a luciferase reporter gene in mammalian cells [153,155]. Using this mammalian cell line bioassay, an extensive range of both natural and synthetic chemicals ( $n = 166$ ) were screened for their activity [153,155] and three putative *CiVDR/PXR* $\alpha$  LBD agonists were identified (6-formylindolo-[3,2-b]carbazole:  $EC_{50} = 0.86 \mu\text{M}$ ; *n*-butyl-*p*-aminobenzoate:  $EC_{50} = 16.5 \mu\text{M}$ ; carbamazepine:  $EC_{50} > 10.0 \mu\text{M}$ ). Based on these results a pharmacophore model was tentatively defined which consisted of a planar structure with at least one off-center hydrogen bond acceptor flanked by two hydrophobic regions [153,156]. Note that none of the three *CiVDR/PXR* $\alpha$  LBD agonists identified were strikingly potent, having  $EC_{50}$  values in the  $\mu\text{M}$  range, nor did it seem plausible that these chemicals would have been encountered by *C. intestinalis* over evolutionary time.

Pursuing the hypothesis that the natural ligands of *CiVDR/PXR* $\alpha$  include marine bioactive compounds frequently present in a marine filter-feeder’s diet, four microalgal biotoxins (okadaic acid, pectenotoxin-2 (PTX-2), gymnodimine, and yessotoxin) were tested for activation of the *CiVDR/PXR* $\alpha$  LBD [156] (Figure 3). The four microalgal biotoxins investigated have diverse structures and all came with the caveat that their toxicity towards intact tunicate animals was, and still is, unknown. Of the four biotoxins tested, okadaic acid ( $EC_{50} = 18.2 \text{ nM}$ ) and PTX-2 ( $EC_{50} = 37.0 \text{ nM}$ ) activated the bioassay, while gymnodimine and yessotoxin were inactive [156] (Figure 4). Interestingly, the  $EC_{50}$  values for okadaic acid and PTX-2 are in the low-to-mid nM range

making these ligands two to three orders of magnitude more potent than the three synthetic compounds previously found to be active in the *Ci*VDR/PXR $\alpha$  LBD-based bioassay [153].

**Figure 3.** Structures of four microalgal biotoxins tested for activation of *C. intestinalis* VDR/PXR $\alpha$  LBD-based bioassays. Pectenotoxin-2 and okadaic acid activated bioassays that used the *C. intestinalis* VDR/PXR $\alpha$  LBD as the sensor element while yessotoxin and gymnodimine did not. **(A)** pectenotoxin-2 (CID: 6437385); **(B)** okadaic acid (CID: 446512); **(C)** yessotoxin (CID: 6440821); and **(D)** gymnodimine (CID: 11649137). *Abbreviations:* CID, PubChem compound accession identifier [157].

#### Active in *Ciona intestinalis* VDR/PXR $\alpha$ LBD-based bioassays



#### Inactive in *Ciona intestinalis* VDR/PXR $\alpha$ LBD-based bioassays

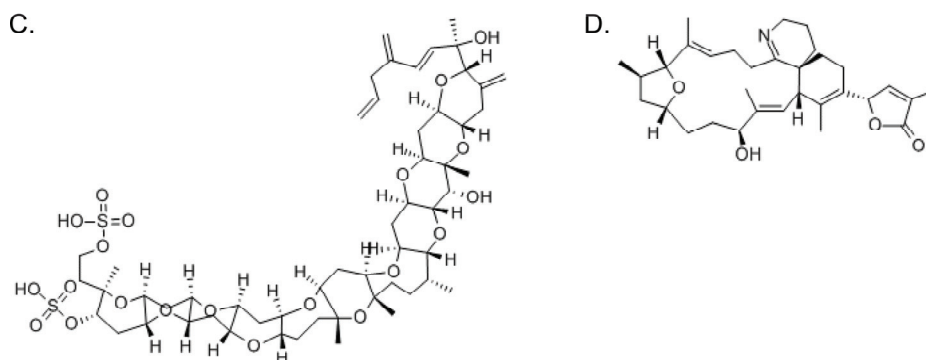
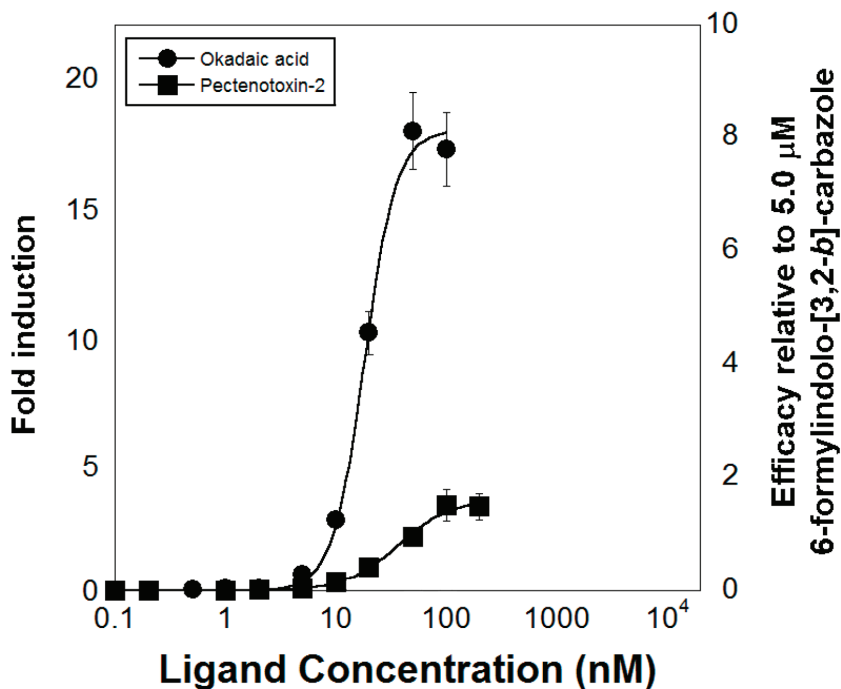


**Figure 4.** Microalgal biotoxin concentration-dependent response curves of luciferase expression induction by cell lines transfected with GAL4-DBD-*Ci*VDR/PXR $\alpha$ LBD fusion genes. The doubly-labelled ordinate axes indicates fold induction compared to vehicle control (left axis) and efficacy relative to 5.0  $\mu$ M 6-formylindolo-[3,2-*b*] carbazole (adapted from Fidler *et al.* [156], with permission from © 2014 Elsevier).



In summary, the combined studies of Ekins *et al.* (2008) and Fidler *et al.* (2012) established that the *Ci*VDR/PXR $\alpha$  LBD displayed xenobiotic/ligand-binding characteristics consistent with *Ci*VDR/PXR $\alpha$  having a role in detecting bioactive marine chemicals naturally encountered by filter-feeding marine invertebrates through their diet [153,156]. Interestingly, the *Ci*VDR/PXR $\alpha$  LBD appears to have rather narrow ligand selectivity when compared to vertebrate, particularly human, PXR $\alpha$ s [153,156]. It is possible that such tunicate VDR/PXR LBD ligand selectivity may reflect tunicate genomes encoding multiple VDR/PXR paralogues, with each paralogue subtype perhaps binding a differing range of ligand structures [138,139]. It should also be remembered that, despite the insights obtained from *Ci*VDR/PXR $\alpha$  LBD functioning in mammalian cell lines, the actual role of VDR/PXR orthologues in intact, living tunicates has not been determined and this represents an important area of future research. Nonetheless, the critical point is that the work of Ekins *et al.* (2008) and Fidler *et al.* (2012) firmly established the feasibility of using marine filter-feeder XANR LBDs as “sensors” in bioassays for marine bioactives. How this basic concept might be developed into cost-effective, high throughput bioassays will be considered next.

## 6. Development of High-Throughput Bioassays Based on Marine Invertebrate XANR LBDs

### 6.1. XANR LBD-Based Bioassays: Technical Considerations and Challenges

As outlined in Section 5, it is established that marine invertebrate XANR LBDs can be utilized as “sensors” in bioassays for marine bioactive chemicals. However, significant technical challenges exist for expanding this simple insight into economically and technically viable bioassays for high-throughput screening of marine compounds. Fortunately, existing NR LBD-based assays provide a strong foundation to build on. This section outlines how well-established NR LBD-based approaches could be applied to marine invertebrate XANR LBDs [158,159].

#### 6.1.1. NR LBD Bioassays Using Recombinant Yeast

Mammalian cell line-based bioassays, as described in Section 5, have the advantage that they provide a cellular/biochemical milieu shared by metazoan cells, which is expected to assist correct folding/functioning of proteins expressed from heterologous genes. However, mammalian cell lines do have significant limitations as they require costly, highly specialized culturing facilities and associated laboratory skills. In contrast, baker’s yeast (*Saccharomyces cerevisiae*) provides a well-established eukaryotic expression system that is inexpensive and suitable for standard microbiology laboratories. Furthermore, the yeast’s nutrient requirements are easily met in a 96-well plate format making *S. cerevisiae*-based bioassays well-suited to high-throughput screening formats [160–162]. In addition, *S. cerevisiae* cells do not contain endogenous NRs to potentially interfere with bioassays based on introduced NRs [163,164]. Finally, *S. cerevisiae* offers the possibility of directed evolution of NRs whereby NR LBD variant sequences, generated by *in vitro* mutagenesis, can be selected for enhancement of growth rates in the presence of a cognate ligand [165]. For example, Chen and Zhao (2003) combined random *in vitro* mutagenesis together with directed evolution to generate novel variants of the human estrogen receptor alpha (ER $\alpha$ ) LBD that had significantly modified ligand-binding properties [165].

Despite the clear attractiveness of *S. cerevisiae* cells for NR LBD-based bioassays, there are aspects of NR functioning that require consideration when designing any associated high-throughput bioassays. Bioassay design needs to address how ligand-induced conformational changes in an introduced metazoan NR LBD will be transduced into a quantifiable output signal. Particular consideration needs to be given to the step in the NR signal transduction pathway selected for activation of the “output signal”. Two ligand-dependent steps in a NR signal transduction pathway have been utilized: (i) ligand-dependent binding of the NR to co-activator protein(s) [166] or (ii) ligand-dependent binding of the NR/co-activator complex to a specific promoter control region [167]. Indeed approach (i) has been successfully used for detecting ligand-dependent interactions between the human PXR and its co-activator protein, human steroid co-activator-1 (hSRC-1) [159,168]. Despite this success with human PXR, it is clear that this approach requires extensive knowledge of a given NR’s co-activator protein, knowledge, which generally will not be available for most marine invertebrate XANRs. Approach (ii) utilizes binding of ligand-activated NRs to control sequences in reporter gene promoters as the mechanism to generate an “output signal” [169,170]. For native,



full-length marine invertebrate XANRs to be used in this approach, both the XANR's co-activators (if any) and the sequences of the cognate DNA elements to which the XANR DBD binds need to be known. Again, for marine invertebrate XANRs such specialized knowledge is unlikely to be available. Even when putative response elements for metazoan XANRs have been identified in marine invertebrate genomes [171], these may not function as required in *S. cerevisiae* cells. Fortunately, such knowledge gaps can be bypassed by exploiting the highly modular structure of NRs (Figure 2). Basically a chimeric protein can be generated in which the XANR LBD is fused to the generic GAL4-DBD, which is native to yeast cells, removing any need for knowledge of the natural heterodimer partners of the XANR or the DNA sequence elements to which the XANR binds through its native DBD.

Following binding to well-characterized DNA control elements, via the GAL4-DBD, the XANR's ligand-dependent activation domain (AF-2) (Figure 2) needs to function within the nuclear milieu of yeast cells. As previous studies have shown that the AF-2 domains of some vertebrate NRs do not function in yeast cells [172,173], a generic transcription activation domain (AD) from the *Herpes simplex* virion protein 16 (VP16) can be added to the C-terminus of the chimeric proteins [173]. In summary, a fusion gene can be generated encoding a chimeric protein that contains the GAL4-DBD, the XANR LBD, and the VP16-AD, with the ligand-binding characteristics of the chimeric protein determined by the XANR LBD.

The reporter gene selected to generate the "output" signal from yeast-based bioassays must combine low background with a clear response signal following activation of the NR LBD. In addition, it is highly desirable that the assay used to quantify reporter gene expression is non-lethal, allowing repeated measurements to be taken over time. Three types of NR-dependent reporter gene assays have been used in recombinant yeast: the *Escherichia coli lacZ* gene, encoding the enzyme  $\beta$ -galactosidase [174], yeast-enhanced green fluorescence protein (yEGFP) [163,175,176], and the luciferase gene [177]. Although the luciferase and yEGFP reporter assays have been shown to be somewhat more sensitive than *lacZ* [178] both have associated complications. For example, luciferase assays require the use of expensive substrates and involve cell lysis [174,179] which can be problematic either due to released cellular proteases [174] or incomplete cell lysis [179]. Although yEGFP assays do not require the addition of substrates, the assays are characterized by a high natural background of green fluorescence [163]. In contrast, *lacZ* assays are inexpensive and, when based on the chromogenic substrate (chlorophenol red- $\beta$ -D-galactopyranoside, CPRG), do not require cell lysis [180]. Such non-lethal measurement of  $\beta$ -galactosidase activity is useful as it means that repeated measurements can be taken over time. This is a significant advantage because the time course of *lacZ* gene transcription induction will vary between ligands due to differences in parameters such as membrane permeability and solubility in the cytoplasm [160].

Notwithstanding the technical challenges many metazoan NRs have been successfully expressed in *S. cerevisiae* in combination with reporter genes [162,166,168,170,181–183]. Furthermore, some of the resulting yeast strains have found application in screening environmental samples for bioactivities—particularly for estrogenic activity [176,180,183–187]. Thus, it is well-established that *S. cerevisiae* provides a suitable expression system for bioassays in which a NR LBD acts as the sensor element that interacts with bioactive chemicals to be detected [183,185,187].

Despite the clear merits of recombinant yeast-based NR bioassays it remains true that all cell-based bioassays face limitations intrinsic to living cells. Such limitations include test compounds being unable to cross cell membranes or being directly toxic to the cells themselves. To address such limitations biosensor techniques have been developed to directly measure physical interactions between macromolecules and their potential ligands.

#### 6.1.2. Biosensors for High-Throughput Screening for NR LBD Ligands

During the past two decades biosensors, which measure a range of physiochemical changes associated with interactions between molecules, have been developed within both industry and academia [188,189]. The main advantage of such biosensors is their cell-free nature thereby removing some of the limitations associated with cell-based bioassays, such as the need for test compounds to cross cell membranes [160]. Biosensors typically consist of a macromolecule immobilized on a surface via either covalent or strong non-covalent bonds [190]. An important consideration is that such attachments should not significantly influence the natural structure of the macromolecule or change its functioning in unpredictable ways [190]. Following immobilization, a wide range of techniques exist to detect and quantify interactions between the immobilized macromolecules and potential ligands—including calorimetric, acoustic, electrical, magnetic, and optical sensing techniques [189].

Numerous NR LBD-based biosensors have been developed, principally in the context of drug development [166,190]. Among the established xenobiotic receptors, the human PXR LBD has been successfully used as the sensor element in a number of differing biosensor formats [111,191,192]. Such biosensors have confirmed previously known human PXR ligands such as hyperforin, clotrimazole, ginkgolide A, SR12813, and 5 $\beta$ -pregnane-3,20-dione [111,112,191]. The successful development of human PXR LBD-based biosensors supports the theoretical feasibility of using marine invertebrate XANR LBDs in biosensor formats to screen for marine bioactive compounds. Furthermore, if routine production of correctly folded and soluble marine invertebrate XANR LBDs can be mastered, then they could be used in affinity chromatography to identify and isolate novel XANR ligands, as has recently been reported for the human PXR LBD [193].

#### 6.2. *XANR LBD-Based Assays: Biological, Ecological, and Evolutionary Considerations*

The application of marine invertebrate XANR LBDs in high-throughput bioassays/biosensors entails some biological, ecological, and evolutionary considerations. The first point to emphasize is the vast taxonomic diversity of marine invertebrates, along with the myriad of ecological niches they occupy. It is expected that this diversity and complexity will be paralleled by the diversity and complexity of the bioactive xenobiotics to which these animals are exposed to during their life-cycles. If dietary bioactive xenobiotics do act as selective agents in shaping the structure of marine invertebrate XANR LBDs, then there exists an effectively unlimited supply of “sensors” in the sea that have been pre-molded by natural selection to facilitate detection of marine bioactive compounds.

If this perspective is correct, then a major decision confronting developers of marine invertebrate XANRs-based bioassays is how to select, from the virtually unlimited options, the marine

invertebrate XANRs to use. We suggest that three considerations should both guide and restrict this decision. The first is the implicit assumption that a bioactive chemical that has acted as a significant selective pressure driving molecular evolution of a given marine invertebrate's XANR LBD may also be active on human cells/tissues. In this context it could be argued that the more closely related an organism is to humans, the more similar would be their susceptibility to marine bioactive chemicals. Whilst doubtless a simplification, this idea does suggest that selecting XANR LBDs from marine invertebrate taxa within the phylum *Chordata* (tunicates, *Urochordata*; lancets, *Cephalochordata*; acorn worms, *Hemichordata*) would be a useful strategy. However, it should be emphasized that there is no *a priori* reason why taxon selection should be restricted to the *Chordata*. For example, at least one marine microalgal biotoxin has acted as a selective pressure in the evolution of bivalves (phylum *Mollusca*) while also being toxic to vertebrates [194,195]. In addition, selections may be restricted simply because promising marine bioactives may exist in contexts/ecological niches to which no marine invertebrate chordate is adapted. This highlights a second consideration in selecting marine invertebrate XANRs for bioassays. The ecological niche occupied by the taxa from which XANR LBDs could be isolated requires careful consideration as such niches restrict the xenobiotics influencing XANR LBD function and evolution. For example, filter-feeding bivalves use a somewhat different mechanism for filtering seawater than do filter-feeding tunicates—and therefore these two groups of filter-feeders ingest somewhat differing profiles/size-ranges of marine microorganisms [196]. It is also important to consider that some bioactive chemicals may be produced by marine organisms that adhere to hard surfaces. For example, benthic microalgae, such as the dinoflagellate *Gambierdiscus toxicus* can produce highly toxic compounds (e.g., ciguatera-associated toxins) [197]. To detect such toxins, XANR LBDs from surface-grazing animals would probably be more suitable for the bioassay than XANR LBDs from filter-feeding animals. A third consideration guiding XANR LBD selection is simply the genomic resources available. Clearly, when a specific marine invertebrate taxon has been selected on evolutionary and ecological grounds, then the required genomic datasets can be generated for increasingly realistic costs. Nonetheless, as discussed earlier in this review, bioinformatic challenges exist when designating a NR as a putative XANR based solely on homology/phylogeny. As a generalization, more reliable predictions of *bona fide* XANRs are likely within those phyla, particularly *Chordata* and *Arthropoda*, for which a number of functionally characterized XANRs exist.

## 7. Future Prospects for Marine Invertebrate XANR LBD-Based Bioassays

The discovery of useful natural marine bioactive compounds, along with the subsequent development of derived pharmaceuticals, faces immense technical challenges [198]. Consequently, despite the enormous number of structurally unique bioactive marine natural products that are now known, to date the associated pharmaceutical pipeline comprises only eight approved drugs, along with twelve natural marine products (or derivatives thereof) in different phases of clinical testing [198,199]. Obviously the natural biological activities of potential drug lead compounds influence their potential medical applications, so bioassay design is a major limiting factor in the detection of useful bioactives [198,200]. In this context we see potential for XANR LBD-based bioassays as their specificities rest on natural evolutionary processes that may have molded the

XANR LBD's structure and its associated ligand-binding properties. Thus, in a sense, these evolutionary processes can provide “creative input” into the bioassay design. Due to the highly modular structure of NRs the XANR LBDs can be combined with generic DNA-binding and transcription-activating domains in various cell-based bioassays or can be used as purified proteins in biosensors. By selecting, on the basis of taxonomy and ecology, the organism to source the XANR LBD from it may be possible to tailor bioassays to search for bioactive compounds from differing sources. As an example, LBDs of potential XANRs identified in the genomes of marine filter-feeding organisms like tunicates and bivalves could be used to test for bioactive compounds associated with the myriad of microorganisms that make up the diet of marine filter-feeders (Figure 1) [7,149].

## 8. Conclusions

This review began with the assertion that, from both an ecological and evolutionary perspective, many bioassays currently used to screen for marine bioactive chemicals are somewhat “arbitrary”, in the sense that they bring together chemicals and biological detection systems that would rarely, if ever, be combined in nature. To address this deficiency, we have proposed that members of a specific group of ligand-activated transcription factors—marine invertebrate xenobiotic-activated nuclear receptors (XANRs)—provide a source of bioassay sensor elements that have been pre-molded by natural selection for detecting bioactive chemicals present in marine invertebrate diets. As a proof-of-concept we outlined recent work showing that mammalian cell lines expressing tunicate XANR LBDs, coupled with an appropriate reporter gene, can detect established microalgal biotoxins. Based on such success with mammalian cell lines we suggest that recombinant yeast strains expressing XANR LBDs may provide low-cost, high-throughput bioassays. Alternatively, it may be possible to entirely remove the need for live cells and adapt biosensor technologies to look for marine chemicals that directly bind to XANR LBDs. Whatever the assay format and technology used, marine invertebrate genomes, each with its own ecological niche and evolutionary history, represent an increasingly accessible informational resource of XANRs that can be harnessed to identify the chemical treasures that are undoubtedly hidden in the sea [198,201].

## Acknowledgments

This work was funded by the New Zealand Ministry of Business, Innovation and Employment (Contract No. CAWX1001). We are grateful to Chris Woods (National Institute of Water and Atmospheric Research, New Zealand) and Rod Asher (Cawthron Institute, New Zealand) for providing photographs used in Figure 1.

## Conflicts of Interest

The authors declare no conflict of interest.

## References

1. Denison, M.S.; Nagy, S.R. Activation of the aryl hydrocarbon receptor by structurally diverse exogenous and endogenous chemicals. *Annu. Rev. Pharmacol. Toxicol.* **2003**, *43*, 309–334.
2. Kewley, R.J.; Whitelaw, M.L.; Chapman-Smith, A. The mammalian basic helix-loop-helix/PAS family of transcriptional regulators. *Int. J. Biochem. Cell Biol.* **2004**, *36*, 189–204.
3. Fujii-Kuriyama, Y.; Kawajiri, K. Molecular mechanisms of the physiological functions of the aryl hydrocarbon (dioxin) receptor, a multifunctional regulator that senses and responds to environmental stimuli. *Proc. Jpn. Acad. Ser. B-Phys. Biol. Sci.* **2010**, *86*, 40–53.
4. Moore, L.B.; Maglich, J.M.; McKee, D.D.; Wisely, B.; Willson, T.M.; Kliewer, S.A.; Lambert, M.H.; Moore, J.T. Pregnane X receptor (PXR), constitutive androstane receptor (CAR), and benzoate X receptor (BXR) define three pharmacologically distinct classes of nuclear receptors. *Mol. Endocrinol.* **2002**, *16*, 977–986.
5. Krasowski, M.D.; Ni, A.; Hagey, L.R.; Ekins, S. Evolution of promiscuous nuclear hormone receptors: LXR, FXR, VDR, PXR, and CAR. *Mol. Cell. Endocrinol.* **2011**, *334*, 39–48.
6. Reschly, E.J.; Krasowski, M.D. Evolution and function of the NR1I nuclear hormone receptor subfamily (VDR, PXR, and CAR) with respect to metabolism of xenobiotics and endogenous compounds. *Curr. Drug Metab.* **2006**, *7*, 349–365.
7. Echevarria, M.; Naar, J.P.; Tomas, C.; Pawlik, J.R. Effects of *Karenia brevis* on clearance rates and bioaccumulation of brevetoxins in benthic suspension feeding invertebrates. *Aquat. Toxicol.* **2012**, *106*, 85–94.
8. Haberkorn, H.; Tran, D.; Massabuau, J.C.; Ciret, P.; Savar, V.; Soudant, P. Relationship between valve activity, microalgae concentration in the water and toxin accumulation in the digestive gland of the Pacific oyster *Crassostrea gigas* exposed to *Alexandrium minutum*. *Mar. Pollut. Bull.* **2011**, *62*, 1191–1197.
9. Forbey, J.S.; Dearing, M.D.; Gross, E.M.; Orians, C.M.; Sotka, E.E.; Foley, W.J. A Pharm-Ecological perspective of terrestrial and aquatic plant-herbivore interactions. *J. Chem. Ecol.* **2013**, *39*, 465–480.
10. Raubenheimer, D.; Simpson, S.J. Nutritional PharmEcology: Doses, nutrients, toxins, and medicines. *Integr. Comp. Biol.* **2009**, *49*, 329–337.
11. Deng, H.; Kerppola, T.K. Regulation of Drosophila metamorphosis by xenobiotic response regulators. *PLoS Genet.* **2013**, *9*, e1003263.
12. Ortiz-Ramirez, F.A.; Vallim, M.A.; Cavalcanti, D.N.; Teixeira, V.L. Effects of the secondary metabolites from *Canistrocarpus cervicornis* (Dictyotales, Phaeophyceae) on fertilization and early development of the sea urchin *Lytechinus variegatus*. *Lat. Am. J. Aquat. Res.* **2013**, *41*, 296–304.
13. Targett, N.M.; Arnold, T.M. Effects of secondary metabolites on digestion in marine herbivores. In *Marine Chemical Ecology*; CRC Press: Boca Raton, FL, USA, 2001; pp. 391–411.
14. Hay, M.E. Marine chemical ecology: Chemical signals and cues structure marine populations, communities, and ecosystems. *Annu. Rev. Mar. Sci.* **2009**, *1*, 193–212.

15. Dearing, M.D.; Foley, W.J.; McLean, S. The influence of plant secondary metabolites on the nutritional ecology of herbivorous terrestrial vertebrates. *Annu. Rev. Ecol. Evol. Syst.* **2005**, *36*, 169–189.
16. Marsh, K.J.; Wallis, I.R.; Andrew, R.L.; Foley, W.J. The detoxification limitation hypothesis: Where did it come from and where is it going? *J. Chem. Ecol.* **2006**, *32*, 1247–1266.
17. Slattery, M.; Avila, C.; Starmer, J.; Paul, V.J. A sequestered soft coral diterpene in the aeolid nudibranch *Phyllodesmium guamensis*. *J. Exp. Mar. Biol. Ecol.* **1998**, *226*, 33–49.
18. Glendinning, J.I. Is the bitter rejection response always adaptive? *Physiol. Behav.* **1994**, *56*, 1217–1227.
19. Chandrashekar, J.; Mueller, K.L.; Hoon, M.A.; Adler, E.; Feng, L.X.; Guo, W.; Zuker, C.S.; Ryba, N.J.P. T2Rs function as bitter taste receptors. *Cell* **2000**, *100*, 703–711.
20. Dong, D.; Jones, G.; Zhang, S. Dynamic evolution of bitter taste receptor genes in vertebrates. *BMC Evol. Biol.* **2009**, *9*, doi:10.1186/1471-2148-9-12.
21. Li, D.; Zhang, J. Diet shapes the evolution of the vertebrate bitter taste receptor gene repertoire. *Mol. Biol. Evol.* **2013**, *7*, 7, doi:10.1093/molbev/mst219.
22. Sugawara, T.; Go, Y.; Udono, T.; Morimura, N.; Tomonaga, M.; Hirai, H.; Imai, H. Diversification of bitter taste receptor gene family in western chimpanzees. *Mol. Biol. Evol.* **2011**, *28*, 921–931.
23. Miller, A.M.; Pawlik, J.R. Do coral reef fish learn to avoid unpalatable prey using visual cues? *Anim. Behav.* **2013**, *85*, 339–347.
24. Long, J.D.; Hay, M.E. Fishes learn aversions to a nudibranch's chemical defense. *Mar. Ecol. Prog. Ser.* **2006**, *307*, 199–208.
25. Ritson-Williams, R.; Paul, V.J. Marine benthic invertebrates use multimodal cues for defense against reef fish. *Mar. Ecol. Prog. Ser.* **2007**, *340*, 29–39.
26. Hegaret, H.; Wikfors, G.H.; Shumway, S.E. Diverse feeding responses of five species of bivalve mollusc when exposed to three species of harmful algae. *J. Shellfish Res.* **2007**, *26*, 549–559.
27. Fdil, M.A.; Mouabad, A.; Outzourhit, A.; Benhra, A.; Maarouf, A.; Pihan, J.C. Valve movement response of the mussel *Mytilus galloprovincialis* to metals (Cu, Hg, Cd and Zn) and phosphate industry effluents from Moroccan Atlantic coast. *Ecotoxicology* **2006**, *15*, 477–486.
28. Wildish, D.; Lassus, P.; Martin, J.; Saulnier, A.; Bardouil, M. Effect of the PSP-causing dinoflagellate, *Alexandrium sp.* on the initial feeding response of *Crassostrea gigas*. *Aquat. Living Resour.* **1998**, *11*, 35–43.
29. Glendinning, J.I. How do predators cope with chemically defended foods? *Biol. Bull.* **2007**, *213*, 252–266.
30. Manfrin, C.; de Moro, G.; Torboli, V.; Venier, P.; Pallavicini, A.; Gerdol, M. Physiological and molecular responses of bivalves to toxic dinoflagellates. *Invertebr. Surviv. J.* **2012**, *9*, 184–199.
31. Fernandez-Reiriz, M.J.; Navarro, J.M.; Contreras, A.M.; Labarta, U. Trophic interactions between the toxic dinoflagellate *Alexandrium catenella* and *Mytilus chilensis*: Feeding and digestive behaviour to long-term exposure. *Aquat. Toxicol.* **2008**, *87*, 245–251.

32. Sotka, E.E.; Gantz, J. Preliminary evidence that the feeding rates of generalist marine herbivores are limited by detoxification rates. *Chemoecology* **2013**, *23*, 233–240.
33. Sotka, E.E.; Forbey, J.; Horn, M. The emerging role of pharmacology in understanding consumer-prey interactions in marine and freshwater systems. *Integr. Comp. Biol.* **2009**, *49*, 291–313.
34. Zanger, U.M.; Schwab, M. Cytochrome P450 enzymes in drug metabolism: Regulation of gene expression, enzyme activities, and impact of genetic variation. *Pharmacol. Ther.* **2013**, *138*, 103–141.
35. Oakley, A. Glutathione transferases: A structural perspective. *Drug Metab. Rev.* **2011**, *43*, 138–151.
36. Li, X.C.; Schuler, M.A.; Berenbaum, M.R. Molecular mechanisms of metabolic resistance to synthetic and natural xenobiotics. *Annu. Rev. Entomol.* **2007**, *52*, 231–253.
37. Nelson, D.R.; Goldstone, J.V.; Stegeman, J.J. The cytochrome P450 genesis locus: The origin and evolution of animal cytochrome P450s. *Philos. Trans. R. Soc. B-Biol. Sci.* **2013**, *368*, doi: 10.1098/rstb.2012.0474.
38. Testa, B.; Pedretti, A.; Vistoli, G. Foundation review: Reactions and enzymes in the metabolism of drugs and other xenobiotics. *Drug Discov. Today* **2012**, *17*, 549–560.
39. Sladek, F.M. What are nuclear receptor ligands? *Mol. Cell. Endocrinol.* **2011**, *334*, 3–13.
40. Baker, M.E. Xenobiotics and the evolution of multicellular animals: Emergence and diversification of ligand-activated transcription factors. *Integr. Comp. Biol.* **2005**, *45*, 172–178.
41. Iyanagi, T. Molecular mechanism of phase I and phase II drug-metabolizing enzymes: Implications for detoxification, In *International Review of Cytology—A Survey of Cell Biology*, 1st ed.; Jeon, K.W., Ed.; Elsevier Academic Press Inc: San Diego, CA, USA, 2007; Volume 260, pp. 35–112.
42. Yang, Y.M.; Noh, K.; Han, C.Y.; Kim, S.G. Transactivation of genes encoding for phase II enzymes and phase III transporters by phytochemical antioxidants. *Molecules* **2010**, *15*, 6332–6348.
43. Sotka, E.E.; Whalen, K.E. Herbivore offense in the sea: The detoxification and transport of secondary metabolites. In *Algal Chemical Ecology*, XVIII ed.; Amsler, C.D., Ed.; Springer: Berlin/Heidelberg, Germany, 2008; pp. 203–228.
44. Court, M.H. Feline drug metabolism and disposition pharmacokinetic evidence for species differences and molecular mechanisms. *Vet. Clin. N. Am. Small Anim. Pract.* **2013**, *43*, 1039–1054.
45. Shrestha, B.; Reed, J.M.; Starks, P.T.; Kaufman, G.E.; Goldstone, J.V.; Roelke, M.E.; O'Brien, S.J.; Koepfli, K.-P.; Frank, L.G.; Court, M.H.; *et al.* Evolution of a major drug metabolizing enzyme defect in the domestic cat and other Felidae: Phylogenetic timing and the role of hypercarnivory. *PLoS One* **2011**, *6*, e18046.
46. Morris, J.G. Idiosyncratic nutrient requirements of cats appear to be diet-induced evolutionary adaptations. *Nutr. Res. Rev.* **2002**, *15*, 153–168.
47. James, M.O.; Ambadapadi, S. Interactions of cytosolic sulfotransferases with xenobiotics. *Drug Metab. Rev.* **2013**, *45*, 401–414.

48. Pinto, N.; Dolan, M.E. Clinically relevant genetic variations in drug metabolizing enzymes. *Curr. Drug Metab.* **2011**, *12*, 487–497.
49. Zanger, U.M.; Turpeinen, M.; Klein, K.; Schwab, M. Functional pharmacogenetics/genomics of human cytochromes P450 involved in drug biotransformation. *Anal. Bioanal. Chem.* **2008**, *392*, 1093–1108.
50. Yamazaki, H. Roles of human cytochrome P450 enzymes involved in drug metabolism and toxicological studies. *J. Pharm. Soc. Jpn.* **2000**, *120*, 1347–1357.
51. Pavsek, P.; Dvorak, Z. Xenobiotic-induced transcriptional regulation of xenobiotic metabolizing enzymes of the cytochrome P450 superfamily in human extrahepatic tissues. *Curr. Drug Metab.* **2008**, *9*, 129–143.
52. Thummel, K.E.; Wilkinson, G.R. In vitro and in vivo drug interactions involving human CYP3A. *Annu. Rev. Pharm. Toxicol.* **1998**, *38*, 389–430.
53. Dobrinas, M.; Cornuz, J.; Pedrido, L.; Eap, C.B. Influence of cytochrome P450 oxidoreductase genetic polymorphisms on CYP1A2 activity and inducibility by smoking. *Pharm. Genomics* **2012**, *22*, 143–151.
54. Martignoni, M.; Groothuis, G.M.M.; de Kanter, R. Species differences between mouse, rat, dog, monkey and human CYP-mediated drug metabolism, inhibition and induction. *Expert Opin. Drug Metab. Toxicol.* **2006**, *2*, 875–894.
55. Vignati, L.A.; Bogni, A.; Grossi, P.; Monshouwer, M. A human and mouse pregnane X receptor reporter gene assay in combination with cytotoxicity measurements as a tool to evaluate species-specific CYP3A induction. *Toxicology* **2004**, *199*, 23–33.
56. Martignoni, M.; de Kanter, R.; Grossi, P.; Mahnke, A.; Saturno, G.; Monshouwer, M. An in vivo and in vitro comparison of CYP induction in rat liver and intestine using slices and quantitative RT-PCR. *Chem.-Biol. Interact.* **2004**, *151*, 1–11.
57. Lu, C.; Li, A.P. Species comparison in P450 induction: Effects of dexamethasone, omeprazole, and rifampin on P450 isoforms 1A and 3A in primary cultured hepatocytes from man, Sprague-Dawley rat, minipig, and beagle dog. *Chem. Biol. Interact.* **2001**, *134*, 271–281.
58. Kocarek, T.A.; Schuetz, E.G.; Strom, S.C.; Fisher, R.A.; Guzelian, P.S. Comparative analysis of cytochrome P4503A induction in primary cultures of rat, rabbit, and human hepatocytes. *Drug Metab. Dispos.* **1995**, *23*, 415–421.
59. Rewitz, K.F.; Styrisshave, B.; Lobner-Olesen, A.; Andersen, O. Marine invertebrate cytochrome P450: Emerging insights from vertebrate and insect analogies. *Comp. Biochem. Physiol. C Toxicol. Pharmacol.* **2006**, *143*, 363–381.
60. Schuler, M.A.; Berenbaum, M.R. Structure and function of cytochrome P450S in insect adaptation to natural and synthetic toxins: Insights gained from molecular modeling. *J. Chem. Ecol.* **2013**, *39*, 1232–1245.
61. Feyereisen, R. Arthropod CYPomes illustrate the tempo and mode in P450 evolution. *Biochim. Biophys. Acta (BBA) Proteins Proteomics* **2011**, *1814*, 19–28.
62. Fisher, T.; Crane, M.; Callaghan, A. Induction of cytochrome P-450 activity in individual *Chironomus riparius* (Meigen) larvae exposed to xenobiotics. *Ecotoxicol. Environ. Saf.* **2003**, *54*, 1–6.



63. Kasai, S.; Scott, J.G. Expression and regulation of CYP6D3 in the house fly, *Musca domestica* (L.). *Insect Biochem. Mol. Biol.* **2001**, *32*, 1–8.
64. Tomita, T.; Itokawa, K.; Komagata, O.; Kasai, S. Overexpression of cytochrome P450 genes in insecticide-resistant mosquitoes. *J. Pestic. Sci.* **2010**, *35*, 562–568.
65. Natsuhara, K.; Shimada, K.; Tanaka, T.; Miyata, T. Phenobarbital induction of permethrin detoxification and phenobarbital metabolism in susceptible and resistant strains of the beet armyworm *Spodoptera exigua* (Hubner). *Pestic. Biochem. Physiol.* **2004**, *79*, 33–41.
66. Johnson, R.M.; Mao, W.; Pollock, H.S.; Niu, G.; Schuler, M.A.; Berenbaum, M.R. Ecologically appropriate xenobiotics induce cytochrome P450s in *Apis mellifera*. *PLoS One* **2012**, *7*, e31051, doi:10.1371/journal.pone.0031051.
67. Niu, G.; Johnson, R.M.; Berenbaum, M.R. Toxicity of mycotoxins to honeybees and its amelioration by propolis. *Apidologie* **2011**, *42*, 79–87.
68. Morra, R.; Kuruganti, S.; Lam, V.; Lucchesi, J.C.; Ganguly, R. Functional analysis of the *cis-acting* elements responsible for the induction of the Cyp6a8 and Cyp6g1 genes of *Drosophila melanogaster* by DDT, phenobarbital and caffeine. *Insect Mol. Biol.* **2010**, *19*, 121–130.
69. Maitra, S.; Dombrowski, S.M.; Waters, L.C.; Ganguly, R. Three second chromosome-linked clustered Cyp6 genes show differential constitutive and barbital-induced expression in DDT-resistant and susceptible strains of *Drosophila melanogaster*. *Gene* **1996**, *180*, 165–171.
70. Misra, J.R.; Horner, M.A.; Lam, G.; Thummel, C.S. Transcriptional regulation of xenobiotic detoxification in *Drosophila*. *Genes Dev.* **2011**, *25*, 1796–1806.
71. Danielson, P.B.; MacIntyre, R.J.; Fogleman, J.C. Molecular cloning of a family of xenobiotic-inducible drosophilid cytochrome P450s: Evidence for involvement in host-plant allelochemical resistance. *PNAS* **1997**, *94*, 10797–10802.
72. Menzel, R.; Bogaert, T.; Achazi, R. A systematic gene expression screen of *Caenorhabditis elegans* cytochrome P450 genes reveals CYP35 as strongly xenobiotic inducible. *Arch. Biochem. Biophys.* **2001**, *395*, 158–168.
73. Menzel, R.; Rodel, M.; Kulas, J.; Steinberg, C.E.W. CYP35: Xenobiotically induced gene expression in the nematode *Caenorhabditis elegans*. *Arch. Biochem. Biophys.* **2005**, *438*, 93–102.
74. Schaefer, P.; Mueller, M.; Krueger, A.; Steinberg, C.E.W.; Menzel, R. Cytochrome P450-dependent metabolism of PCB52 in the nematode *Caenorhabditis elegans*. *Arch. Biochem. Biophys.* **2009**, *488*, 60–68.
75. Chakrapani, B.P.; Kumar, S.; Subramaniam, J.R. Development and evaluation of an *in vivo* assay in *Caenorhabditis elegans* for screening of compounds for their effect on cytochrome P450 expression. *J. Biosci.* **2008**, *33*, 269–277.
76. Zheng, S.L.; Chen, B.; Qiu, X.Y.; Lin, K.L.; Yu, X.G. Three novel cytochrome P450 genes identified in the marine polychaete *Perinereis nuntia* and their transcriptional response to xenobiotics. *Aquat. Toxicol.* **2013**, *134*, 11–22.

77. Whalen, K.E.; Starczak, V.R.; Nelson, D.R.; Goldstone, J.V.; Hahn, M.E. Cytochrome P450 diversity and induction by gorgonian allelochemicals in the marine gastropod *Cyphoma gibbosum*. *BMC Ecol.* **2010**, *10*, 24, doi:10.1186/1472-6785-10-24.
78. Bousova, I.; Skalova, L. Inhibition and induction of glutathione S-transferases by flavonoids: Possible pharmacological and toxicological consequences. *Drug Metab. Rev.* **2012**, *44*, 267–286.
79. Maglich, J.M.; Stoltz, C.M.; Goodwin, B.; Hawkins-Brown, D.; Moore, J.T.; Kliewer, S.A. Nuclear pregnane X receptor and constitutive androstane receptor regulate overlapping but distinct sets of genes involved in xenobiotic detoxification. *Mol. Pharmacol.* **2002**, *62*, 638–646.
80. Whalen, K.E.; Morin, D.; Lin, C.Y.; Tjeerdema, R.S.; Goldstone, J.V.; Hahn, M.E. Proteomic identification, cDNA cloning and enzymatic activity of glutathione S-transferases from the generalist marine gastropod, *Cyphoma gibbosum*. *Arch. Biochem. Biophys.* **2008**, *478*, 7–17.
81. Kuhajek, J.M.; Schlenk, D. Effects of the brominated phenol, lanosol, on cytochrome P-450 and glutathione transferase activities in *Haliotis rufescens* and *Katharina tunicata*. *Comp. Biochem. Physiol. C Toxicol. Pharmacol.* **2003**, *134*, 473–479.
82. Whalen, K.E.; Lane, A.L.; Kubanek, J.; Hahn, M.E. Biochemical warfare on the reef: The role of glutathione transferases in consumer tolerance of dietary prostaglandins. *PLoS One* **2010**, *5*, 0008537.
83. Mao, W.; Rupasinghe, S.G.; Johnson, R.M.; Zangerl, A.R.; Schuler, M.A.; Berenbaum, M.R. Quercetin-metabolizing CYP6AS enzymes of the pollinator *Apis mellifera* (Hymenoptera: Apidae). *Comp. Biochem. Physiol. B Biochem. Mol. Biol.* **2009**, *154*, 427–434.
84. Bainy, A.C.D.; Kubota, A.; Goldstone, J.V.; Lille-Langoy, R.; Karchner, S.I.; Celander, M.C.; Hahn, M.E.; Goksoyr, A.; Stegeman, J.J. Functional characterization of a full length pregnane X receptor, expression *in vivo*, and identification of PXR alleles, in Zebrafish (*Danio rerio*). *Aquat. Toxicol.* **2013**, *142–143*, 447–457.
85. Chai, X.; Zeng, S.; Xie, W. Nuclear receptors PXR and CAR: Implications for drug metabolism regulation, pharmacogenomics and beyond. *Expert Opin. Drug Metab. Toxicol.* **2013**, *9*, 253–266.
86. Xie, W.; Chiang, J.Y.L. Nuclear receptors in drug metabolism and beyond. *Drug Metab. Rev.* **2013**, *45*, 1–2.
87. NR1I2 nuclear receptor subfamily 1, group I, member 2. Available online: <http://www.ncbi.nlm.nih.gov/gene/8856> (accessed on 26 February 2014).
88. Kliewer, S.A.; Moore, J.T.; Wade, L.; Staudinger, J.L.; Watson, M.A.; Jones, S.A.; McKee, D.D.; Oliver, B.B.; Willson, T.M.; Zetterstrom, R.H.; *et al.* An orphan nuclear receptor activated by pregnanes defines a novel steroid signaling pathway. *Cell* **1998**, *92*, 73–82.
89. Blumberg, B.; Sabbagh, W.; Juguilon, H.; Bolado, J.; van Meter, C.M.; Ono, E.S.; Evans, R.M. SXR, a novel steroid and xenobiotic-sensing nuclear receptor. *Genes Dev.* **1998**, *12*, 3195–3205.

90. Bertilsson, G.; Heidrich, J.; Svensson, K.; Asman, M.; Jendeberg, L.; Sydow-Backman, M.; Ohlsson, R.; Postlind, H.; Blomquist, P.; Berkenstam, A.; *et al.* Identification of a human nuclear receptor defines a new signaling pathway for CYP3A induction. *PNAS* **1998**, *95*, 12208–12213.
91. Orans, J.; Teotico, D.G.; Redinbo, M.R. The nuclear xenobiotic receptor pregnane X receptor: Recent insights and new challenges. *Mol. Endocrinol.* **2005**, *19*, 2891–2900.
92. Li, T.G.; Chiang, J.Y.L. Mechanism of rifampicin and pregnane X receptor inhibition of human cholesterol 7 alpha-hydroxylase gene transcription. *Am. J. Physiol. Gastrointest. Liver Physiol.* **2005**, *288*, G74–G84.
93. McKenna, N.J.; Lanz, R.B.; O'Malley, B.W. Nuclear receptor coregulators: Cellular and molecular biology. *Endocr. Rev.* **1999**, *20*, 321–344.
94. Teotico, D.G.; Frazier, M.L.; Ding, F.; Dokholyan, N.V.; Temple, B.R.S.; Redinbo, M.R. Active Nuclear Receptors Exhibit Highly Correlated AF-2 Domain Motions. *PLoS Comput. Biol.* **2008**, *4*, e1000111, doi:10.1371/journal.pcbi.1000111.
95. Tolson, A.H.; Wang, H.B. Regulation of drug-metabolizing enzymes by xenobiotic receptors: PXR and CAR. *Adv. Drug Deliv. Rev.* **2010**, *62*, 1238–1249.
96. Biswas, A.; Mani, S.; Redinbo, M.R.; Krasowski, M.D.; Li, H.; Ekins, S. Elucidating the “Jekyll and Hyde” nature of PXR: The case for discovering antagonists or allosteric antagonists. *Pharm. Res.* **2009**, *26*, 1807–1815.
97. Chang, T.K.; Waxman, D.J. Synthetic drugs and natural products as modulators of constitutive androstane receptor (CAR) and pregnane X receptor (PXR). *Drug Metab. Rev.* **2006**, *38*, 51–73.
98. Hernandez, J.P.; Mota, L.C.; Baldwin, W.S. Activation of CAR and PXR by Dietary, Environmental and Occupational Chemicals Alters Drug Metabolism, Intermediary Metabolism, and Cell Proliferation. *Curr. Pharm. Pers. Med.* **2009**, *7*, 81–105.
99. Manez, S. A fresh insight into the interaction of natural products with pregnane X receptor. *Nat. Prod. Commun.* **2008**, *3*, 2123–2128.
100. Staudinger, J.L.; Ding, X.; Lichti, K. Pregnane X receptor and natural products: Beyond drug-drug interactions. *Expert Opin. Drug Metab. Toxicol.* **2006**, *2*, 847–857.
101. Zhou, C.; Verma, S.; Blumberg, B. The steroid and xenobiotic receptor (SXR), beyond xenobiotic metabolism. *Nucl. Recept. Signal.* **2009**, *7*, e001.
102. Harms, M.J.; Eick, G.N.; Goswami, D.; Colucci, J.K.; Griffin, P.R.; Ortlund, E.A.; Thornton, J.W. Biophysical mechanisms for large-effect mutations in the evolution of steroid hormone receptors. *PNAS* **2013**, *110*, 11475–11480.
103. Eick, G.N.; Colucci, J.K.; Harms, M.J.; Ortlund, E.A.; Thornton, J.W. Evolution of minimal specificity and promiscuity in steroid hormone receptors. *PLoS Genet.* **2012**, *8*, e1003072, doi:10.1371/journal.pgen.1003072.
104. Wu, B.; Li, S.; Dong, D. 3D structures and ligand specificities of nuclear xenobiotic receptors CAR, PXR and VDR. *Drug Discov. Today* **2013**, *18*, 574–581.
105. Wallace, B.D.; Redinbo, M.R. Xenobiotic-sensing nuclear receptors involved in drug metabolism: A structural perspective. *Drug Metab. Rev.* **2013**, *45*, 79–100.

106. Mangelsdorf, D.J.; Thummel, C.; Beato, M.; Herrlich, P.; Schutz, G.; Umesono, K.; Blumberg, B.; Kastner, P.; Mark, M.; Chambon, P.; *et al.* The nuclear receptor superfamily: The second decade. *Cell* **1995**, *83*, 835–839.
107. Krasowski, M.D.; Yasuda, K.; Hagey, L.R.; Schuetz, E.G. Evolution of the pregnane X receptor: Adaptation to cross-species differences in biliary bile salts. *Mol. Endocrinol.* **2005**, *19*, 1720–1739.
108. Krasowski, M.D.; Yasuda, K.; Hagey, L.R.; Schuetz, E.G. Evolutionary selection across the nuclear hormone receptor superfamily with a focus on the NR1I subfamily (vitamin D, pregnane X, and constitutive androstane receptors). *Nucl. Recept.* **2005**, *3*, 2, doi:10.1186/1478-1336-3-2.
109. Zhang, Z.D.; Burch, P.E.; Cooney, A.J.; Lanz, R.B.; Pereira, F.A.; Wu, J.Q.; Gibbs, R.A.; Weinstock, G.; Wheeler, D.A. Genomic analysis of the nuclear receptor family: New insights into structure, regulation, and evolution from the rat genome. *Genome Res.* **2004**, *14*, 580–590.
110. Krasowski, M.D.; Ai, N.; Hagey, L.R.; Kollitz, E.M.; Kullman, S.W.; Reschly, E.J.; Ekins, S. The evolution of farnesoid X, vitamin D, and pregnane X receptors: Insights from the green-spotted pufferfish (*Tetraodon nigriviridis*) and other non-mammalian species. *BMC Biochem.* **2011**, *12*, doi:10.1186/1471-2091-12-5.
111. Moore, L.B.; Parks, D.J.; Jones, S.A.; Bledsoe, R.K.; Consler, T.G.; Stimmel, J.B.; Goodwin, B.; Liddle, C.; Blanchard, S.G.; Willson, T.M.; *et al.* Orphan nuclear receptors constitutive androstane receptor and pregnane X receptor share xenobiotic and steroid ligands. *J. Biol. Chem.* **2000**, *275*, 15122–15127.
112. Jones, S.A.; Moore, L.B.; Shenk, J.L.; Wisely, G.B.; Hamilton, G.A.; McKee, D.D.; Tomkinson, N.C.O.; LeCluyse, E.L.; Lambert, M.H.; Willson, T.M.; *et al.* The pregnane X receptor: A promiscuous xenobiotic receptor that has diverged during evolution. *Mol. Endocrinol.* **2000**, *14*, 27–39.
113. LeCluyse, E.L. Pregnane X receptor: Molecular basis for species differences in CYP3A induction by xenobiotics. *Chem. Biol. Interact.* **2001**, *134*, 283–289.
114. Lehmann, J.M.; McKee, D.D.; Watson, M.A.; Willson, T.M.; Moore, J.T.; Kliewer, S.A. The human orphan nuclear receptor PXR is activated by compounds that regulate CYP3A4 gene expression and cause drug interactions. *J. Clin. Investig.* **1998**, *102*, 1016–1023.
115. Xie, W.; Evans, R.M. Orphan nuclear receptors: The exotics of xenobiotics. *J. Biol. Chem.* **2001**, *276*, 37739–37742.
116. Xie, W.; Barwick, J.L.; Downes, M.; Blumberg, B.; Simon, C.M.; Nelson, M.C.; Neuschwander-Tetri, B.A.; Bruntk, E.M.; Guzelian, P.S.; Evans, R.M.; *et al.* Humanized xenobiotic response in mice expressing nuclear receptor SXR. *Nature* **2000**, *406*, 435–439.
117. Tirona, R.G.; Leake, B.F.; Podust, L.M.; Kim, R.B. Identification of amino acids in rat pregnane X receptor that determine species-specific activation. *Mol. Pharmacol.* **2004**, *65*, 36–44.
118. Wang, D.Y.C.; Kumar, S.; Hedges, S.B. Divergence time estimates for the early history of animal phyla and the origin of plants, animals and fungi. *PNAS* **1999**, *266*, 163–171.

119. Erwin, D.H.; Davidson, E.H. The last common bilaterian ancestor. *Development* **2002**, *129*, 3021–3032.
120. Hedges, S.B.; Dudley, J.; Kumar, S. TimeTree: A public knowledge-base of divergence times among organisms. *Bioinformatics* **2006**, *22*, 2971–2972.
121. King-Jones, K.; Horner, M.A.; Lam, G.; Thummel, C.S. The DHR96 nuclear receptor regulates xenobiotic responses in *Drosophila*. *Cell Metab.* **2006**, *4*, 37–48.
122. Lindblom, T.H.; Pierce, G.J.; Sluder, A.E. A *C. elegans* orphan nuclear receptor contributes to xenobiotic resistance. *Curr. Biol.* **2001**, *11*, 864–868.
123. Lin, G.G.H.; Kozaki, T.; Scott, J.G. Hormone receptor-like in 96 and Broad-Complex modulate phenobarbital induced transcription of cytochrome P450 CYP6D1 in *Drosophila* S2 cells. *Insect Mol. Biol.* **2011**, *20*, 87–95.
124. Palanker, L.; Necakov, A.S.; Sampson, H.M.; Ni, R.; Hu, C.H.; Thummel, C.S.; Krause, H.M. Dynamic regulation of *Drosophila* nuclear receptor activity *in vivo*. *Development* **2006**, *133*, 3549–3562.
125. Sieber, M.H.; Thummel, C.S. Coordination of triacylglycerol and cholesterol homeostasis by DHR96 and the *Drosophila* LipA homolog magro. *Cell Metab.* **2012**, *15*, 122–127.
126. Karimullina, E.; Li, Y.; Ginjupalli, G.K.; Baldwin, W.S. *Daphnia* HR96 is a promiscuous xenobiotic and endobiotic nuclear receptor. *Aquat. Toxicol.* **2012**, *116*, 69–78.
127. Xu, J.; Tan, A.; Palli, S.R. The function of nuclear receptors in regulation of female reproduction and embryogenesis in the red flour beetle, *Tribolium castaneum*. *J. Insect Physiol.* **2010**, *56*, 1471–1480.
128. Bonasio, R.; Zhang, G.; Ye, C.; Mutti, N.S.; Fang, X.; Qin, N.; Donahue, G.; Yang, P.; Li, Q.; Li, C.; *et al.* Genomic comparison of the ants *Camponotus floridanus* and *Harpegnathos saltator*. *Science* **2010**, *329*, 1068–1071.
129. Velarde, R.A.; Robinson, G.E.; Fahrback, S.E. Nuclear receptors of the honey bee: Annotation and expression in the adult brain. *Insect Mol. Biol.* **2006**, *15*, 583–595.
130. Giraudo, M.; Audant, P.; Feyereisen, R.; le Goff, G. Nuclear receptors HR96 and ultraspiracle from the fall armyworm (*Spodoptera frugiperda*), developmental expression and induction by xenobiotics. *J. Insect Physiol.* **2013**, *59*, 560–568.
131. Sluder, A.E.; Mathews, S.W.; Hough, D.; Yin, V.P.; Maina, C.V. The nuclear receptor superfamily has undergone extensive proliferation and diversification in nematodes. *Genome Res.* **1999**, *9*, 103–120.
132. Bertrand, W.; Brunet, F.G.; Escriva, H.; Parmentier, G.; Laudet, V.; Robinson-Rechavi, M. Evolutionary genomics of nuclear receptors: From twenty-five ancestral genes to derived endocrine systems. *Mol. Biol. Evol.* **2004**, *21*, 1923–1937.
133. Delsuc, F.; Brinkmann, H.; Chourrout, D.; Philippe, H. Tunicates and not cephalochordates are the closest living relatives of vertebrates. *Nature* **2006**, *439*, 965–968.
134. Delsuc, F.; Tsagkogeorga, G.; Lartillot, N.; Philippe, H. Additional molecular support for the new chordate phylogeny. *Genesis* **2008**, *46*, 592–604.

135. Singh, T.R.; Tsagkogeorga, G.; Delsuc, F.; Blanquart, S.; Shenkar, N.; Loya, Y.; Douzery, E.J.P.; Huchon, D. Tunicate mitogenomics and phylogenetics: Peculiarities of the *Herdmania momus* mitochondrial genome and support for the new chordate phylogeny. *BMC Genomics* **2009**, *10*, doi:10.1186/1471-2164-10-534.
136. Rowe, T. Chordate phylogeny and development, In *Assembling The Tree of Life*, 1st ed.; Cracraft, J., Donoghue, M.J., Eds.; Oxford University Press: Oxford, UK, 2004; pp. 384–409.
137. Dehal, P.; Satou, Y.; Campbell, R.K.; Chapman, J.; Degnan, B.; de Tomaso, A.; Davidson, B.; di Gregorio, A.; Gelpke, M.; Goodstein, D.M.; *et al.* The draft genome of *Ciona intestinalis*: Insights into chordate and vertebrate origins. *Science* **2002**, *298*, 2157–2167.
138. Voskoboinik, A.; Neff, N.F.; Sahoo, D.; Newman, A.M.; Pushkarev, D.; Koh, W.; Passarelli, B.; Fan, H.C.; Mantalas, G.L.; Palmeri, K.J.; *et al.* The genome sequence of the colonial chordate, *Botryllus schlosseri*. *ELife* **2013**, *2*, doi:10.7554/eLife.00569.
139. DENOEU, F.; HENRIET, S.; MUNGPACDEE, S.; AURY, J.-M.; DA SILVA, C.; BRINKMANN, H.; MIKHALEVA, J.; OLSEN, L.C.; JUBIN, C.; CANESTRO, C.; *et al.* Plasticity of animal genome architecture unmasked by rapid evolution of a pelagic tunicate. *Science* **2010**, *330*, 1381–1385.
140. Bracken-Grissom, H.; Collins, A.G.; Collins, T.; Crandall, K.; Distel, D.; Dunn, C.; Giribet, G.; Haddock, S.; Knowlton, N.; Martindale, M.; *et al.* The Global Invertebrate Genomics Alliance (GIGA): Developing community resources to study diverse invertebrate genomes. *J. Hered.* **2014**, *105*, 1–18.
141. Dussault, I.; Forman, B.M. The nuclear receptor PXR: A master regulator of “homeland” defense. *Crit. Rev. Eukaryot. Gene Expr.* **2002**, *12*, 53–64.
142. Kliewer, S.; Goodwin, B.; Willson, T. The nuclear pregnane X receptor: A key regulator of xenobiotic metabolism. *Endocr. Rev.* **2002**, *23*, 687–702.
143. Timsit, Y.E.; Negishi, M. CAR and PXR: The xenobiotic-sensing receptors. *Steroids* **2007**, *72*, 231–246.
144. Bridgham, J.T.; Eick, G.N.; Larroux, C.; Deshpande, K.; Harms, M.J.; Gauthier, M.E.A.; Ortlund, E.A.; Degnan, B.M.; Thornton, J.W. Protein evolution by molecular tinkering: Diversification of the nuclear receptor superfamily from a ligand-dependent ancestor. *PLoS Biol.* **2010**, *8*, e1000497, doi:10.1371/journal.pbio.1000497.
145. Srivastava, M.; Simakov, O.; Chapman, J.; Fahey, B.; Gauthier, M.E.A.; Mitros, T.; Richards, G.S.; Conaco, C.; Dacre, M.; Hellsten, U.; *et al.* The *Amphimedon queenslandica* genome and the evolution of animal complexity. *Nature* **2010**, *466*, 720–726.
146. Reitzel, A.M.; Tarrant, A.M. Nuclear receptor complement of the cnidarian *Nematostella vectensis*: Phylogenetic relationships and developmental expression patterns. *BMC Evol. Biol.* **2009**, *9*, 230, doi:10.1186/1471-2148-9-230.
147. Vogeler, S.; Galloway, T.; Lyons, B.; Bean, T. The nuclear receptor gene family in the Pacific oyster, *Crassostrea gigas*, contains a novel subfamily group. *BMC Genomics* **2014**, *15*, 369, doi:10.1186/1471-2164-15-369.
148. Sodergren, E.; Weinstock, G.M.; Davidson, E.H.; Cameron, R.A.; Gibbs, R.A.; Angerer, R.C.; Angerer, L.M.; Arnone, M.I.; Burgess, D.R.; Burke, R.D.; *et al.* The genome of the sea urchin *Strongylocentrotus purpuratus*. *Science* **2006**, *314*, 941–952.

149. Gazulha, V.; Mansur, M.C.D.; Cybis, L.F.; Azevedo, S.M.F.O. Feeding behavior of the invasive bivalve *Limnoperna fortunei* (Dunker, 1857) under exposure to toxic cyanobacteria *Microcystis aeruginosa*. *Braz. J. Biol.* **2012**, *72*, 41–49.
150. Bridgham, J.T.; Keay, J.; Ortlund, E.A.; Thornton, J.W. Vestigialization of an allosteric switch: Genetic and structural mechanisms for the evolution of constitutive activity in a steroid hormone receptor. *PLoS Genet.* **2014**, *10*, e1004058, doi:10.1371/journal.pgen.1004058.
151. Satou, Y.; Yamada, L.; Mochizuki, Y.; Takatori, N.; Kawashima, T.; Sasaki, A.; Hamaguchi, M.; Awazu, S.; Yagi, K.; Sasakura, Y.; *et al.* A cDNA resource from the basal chordate *Ciona intestinalis*. *Genesis* **2002**, *33*, 153–154.
152. Yagi, K.; Satou, Y.; Mazet, F.; Shimeld, S.M.; Degnan, B.; Rokhsar, D.; Levine, M.; Kohara, Y.; Satoh, N. A genomewide survey of developmentally relevant genes in *Ciona intestinalis*—III. Genes for Fox, ETS, nuclear receptors and NF kappa B. *Dev. Genes Evol.* **2003**, *213*, 235–244.
153. Ekins, S.; Reschly, E.J.; Hagey, L.R.; Krasowski, M.D. Evolution of pharmacologic specificity in the pregnane X receptor. *BMC Evol. Biol.* **2008**, *8*, doi:10.1186/1471-2148-8-103.
154. Satou, Y.; Kawashima, T.; Shoguchi, E.; Nakayama, A.; Satoh, N. An integrated database of the ascidian, *Ciona intestinalis*: Towards functional genomics. *Zool. Sci.* **2005**, *22*, 837–843.
155. Reschly, E.J.; Bains, A.C.D.; Mattos, J.J.; Hagey, L.R.; Bahary, N.; Mada, S.R.; Ou, J.; Venkataramanan, R.; Krasowski, M.D. Functional evolution of the vitamin D and pregnane X receptors. *BMC Evol. Biol.* **2007**, *7*, 222, doi:10.1186/1471-2148-7-222.
156. Fidler, A.E.; Holland, P.T.; Reschly, E.J.; Ekins, S.; Krasowski, M.D. Activation of a tunicate (*Ciona intestinalis*) xenobiotic receptor orthologue by both natural toxins and synthetic toxicants. *Toxicol.* **2012**, *59*, 365–372.
157. PubChem Compound Database. Available online : <https://www.ncbi.nlm.nih.gov/pccompound?cmd=search> (accessed on 7 September 2014).
158. Pinne, M.; Raucy, J.L. Advantages of cell-based high-volume screening assays to assess nuclear receptor activation during drug discovery. *Expert Opin. Drug Discov.* **2014**, *9*, 669–686.
159. Raucy, J.L.; Lasker, J.M. Cell-based systems to assess nuclear receptor activation and their use in drug development. *Drug Metab. Rev.* **2013**, *45*, 101–109.
160. Norcliffe, J.L.; Alvarez-Ruiz, E.; Martin-Plaza, J.J.; Steel, P.G.; Denny, P.W. The utility of yeast as a tool for cell-based, target-directed high-throughput screening. *Parasitology* **2013**, *141*, 8–16.
161. Hontzas, N.; Hafer, K.; Schiestl, R.H. Development of a microtiter plate version of the yeast DEL assay amenable to high-throughput toxicity screening of chemical libraries. *Mutat. Res. Genet. Toxicol. Environ. Mutagen.* **2007**, *634*, 228–234.
162. Rajasarkka, J.; Virta, M. Miniaturization of a panel of high throughput yeast-cell-based nuclear receptor assays in 384- and 1536-well microplates. *Comb. Chem. High Throughput Screen.* **2011**, *14*, 47–54.
163. Bovee, T.F.H.; Helsdingen, R.J.R.; Hamers, A.R.M.; van Duursen, M.B.M.; Nielen, M.W.F.; Hoogenboom, R.L.A.P. A new highly specific and robust yeast androgen bioassay for the detection of agonists and antagonists. *Anal. Bioanal. Chem.* **2007**, *389*, 1549–1558.

164. An, W.F.; Tolliday, N. Cell-based assays for high-throughput screening. *Mol. Biotechnol.* **2010**, *45*, 180–186.
165. Chen, Z.L.; Zhao, H.M. A highly efficient and sensitive screening method for trans-activation activity of estrogen receptors. *Gene* **2003**, *306*, 127–134.
166. Raucy, J.L.; Lasker, J.M. Current *in vitro* high-throughput screening approaches to assess nuclear receptor activation. *Curr. Drug Metab.* **2010**, *11*, 806–814.
167. Chu, W.-L.; Shiizaki, K.; Kawanishi, M.; Kondo, M.; Yagi, T. Validation of a new yeast-based reporter assay consisting of human estrogen receptors  $\alpha/\beta$  and coactivator SRC-1: Application for detection of estrogenic activity in environmental samples. *Environ. Toxicol.* **2009**, *24*, 513–521.
168. Li, H.; Redinbo, M.R.; Venkatesh, M.; Ekins, S.; Chaudhry, A.; Bloch, N.; Negassa, A.; Mukherjee, P.; Kalpana, G.; Mani, S.; *et al.* Novel yeast-based strategy unveils antagonist binding regions on the nuclear xenobiotic receptor PXR. *J. Biol. Chem.* **2013**, *288*, 13655–13668.
169. McEwan, I.J. Bakers yeast rises to the challenge: Reconstitution of mammalian steroid receptor signalling in *S. cerevisiae*. *Trends Genet.* **2001**, *17*, 239–243.
170. Fox, J.E.; Burow, M.E.; McLachlan, J.A.; Miller, C.A. Detecting ligands and dissecting nuclear receptor-signaling pathways using recombinant strains of the yeast *Saccharomyces cerevisiae*. *Nat. Protoc.* **2008**, *3*, 637–645.
171. Goldstone, J.V.; Goldstone, H.M.H.; Morrison, A.M.; Tarrant, A.; Kern, S.E.; Woodin, B.R.; Stegeman, J.J. Cytochrome P450 1 genes in early deuterostomes (tunicates and sea urchins) and vertebrates (chicken and frog): Origin and diversification of the CYP1 gene family. *Mol. Biol. Evol.* **2007**, *24*, 2619–2631.
172. Berry, M.; Metzger, D.; Chambon, P. Role of the 2 activating domains of the estrogen receptor in the cell-type and promoter-context dependent agonistic activity of the antiestrogen 4-hydroxytamoxifen. *EMBO J.* **1990**, *9*, 2811–2818.
173. Louvion, J.F.; Havauxcopf, B.; Picard, D. Fusion of GAL4-VP16 to a steroid-binding domain provides a tool for gratuitous induction of galactose-responsive genes in yeast. *Gene* **1993**, *131*, 129–134.
174. De Almeida, R.A.; Burgess, D.; Shema, R.; Motlekar, N.; Napper, A.D.; Diamond, S.L.; Pavitt, G.D. A *Saccharomyces cerevisiae* cell-based quantitative beta-galactosidase handling and assay compatible with robotic high-throughput screening. *Yeast* **2008**, *25*, 71–76.
175. Bovee, T.F.H.; Hendriksen, P.J.M.; Portier, L.; Wang, S.; Elliott, C.T.; van Egmond, H.P.; Nielen, M.W.F.; Peijnenburg, A.; Hoogenboom, L.A.P. Tailored microarray platform for the detection of marine toxins. *Environ. Sci. Technol.* **2011**, *45*, 8965–8973.
176. Chatterjee, S.; Kumar, V.; Majumder, C.B.; Roy, P. Screening of some anti-progestin endocrine disruptors using a recombinant yeast-based *in vitro* bioassay. *Toxicol. Vitro.* **2008**, *22*, 788–798.
177. Nordeen, S.K. Luciferase reporter gene vectors for analysis of promoters and enhancers. *Biotechniques* **1988**, *6*, 454–458.
178. Fan, F.; Wood, K.V. Bioluminescent assays for high-throughput screening. *Assay Drug Dev. Technol.* **2007**, *5*, 127–136.



179. Hancock, M.K.; Medina, M.N.; Smith, B.M.; Orth, A.P. Microplate orbital mixing improves high-throughput cell-based reporter assay readouts. *J. Biomol. Screen.* **2007**, *12*, 140–144.
180. Routledge, E.J.; Sumpter, J.P. Estrogenic activity of surfactants and some of their degradation products assessed using a recombinant yeast screen. *Environ. Toxicol. Chem.* **1996**, *15*, 241–248.
181. Miller, C.A.; Tan, X.B.; Wilson, M.; Bhattacharyya, S.; Ludwig, S. Single plasmids expressing human steroid hormone receptors and a reporter gene for use in yeast signaling assays. *Plasmid* **2010**, *63*, 73–78.
182. Chen, Q.; Chen, J.; Sun, T.; Shen, J.H.; Shen, X.; Jiang, H.L. A yeast two-hybrid technology-based system for the discovery of PPAR gamma agonist and antagonist. *Anal. Biochem.* **2004**, *335*, 253–259.
183. Balsiger, H.A.; de la Torre, R.; Lee, W.-Y.; Cox, M.B. A four-hour yeast bioassay for the direct measure of estrogenic activity in wastewater without sample extraction, concentration, or sterilization. *Sci. Total Environ.* **2010**, *408*, 1422–1429.
184. Collins, B.M.; McLachlan, J.A.; Arnold, S.F. The estrogenic and antiestrogenic activities of phytochemicals with human estrogen receptor expressed in yeast. *Steroids* **1997**, *62*, 365–372.
185. Gaido, K.W.; Leonard, L.S.; Lovell, S.; Gould, J.C.; Babai, D.; Portier, C.J.; McDonnell, D.P. Evaluation of chemicals with endocrine modulating activity in a yeast-based steroid hormone receptor gene transcription assay. *Toxicol. Appl. Pharmacol.* **1997**, *143*, 205–212.
186. Passos, A.L.; Pinto, P.I.; Power, D.M.; Canario, A.V. A yeast assay based on the gilthead sea bream (teleost fish) estrogen receptor beta for monitoring estrogen mimics. *Ecotoxicol. Environ. Saf.* **2009**, *72*, 1529–1537.
187. Chen, C.H.; Chou, P.H.; Kawanishi, M.; Yagi, T. Occurrence of xenobiotic ligands for retinoid X receptors and thyroid hormone receptors in the aquatic environment of Taiwan. *Mar. Pollut. Bull.* **2014**, *23*, doi:10.1016/j.marpolbul.2014.01.025.
188. Holdgate, G.A.; Anderson, M.; Edfeldt, F.; Geschwindner, S. Affinity-based, biophysical methods to detect and analyze ligand binding to recombinant proteins: Matching high information content with high throughput. *J. Struct. Biol.* **2010**, *172*, 142–157.
189. Senveli, S.U.; Tigli, O. Biosensors in the small scale: Methods and technology trends. *IET Nanobiotechnol.* **2013**, *7*, 7–21.
190. Fechner, P.; Gauglitz, G.; Gustafsson, J.-A. Nuclear receptors in analytics—A fruitful joint venture or a wasteful futility? *Trends Anal. Chem.* **2010**, *29*, 297–305.
191. Lin, W.; Liu, J.; Jeffries, C.; Yang, L.; Lu, Y.; Lee, R.E.; Chen, T. Development of BODIPY FL Vindoline as a novel and high-affinity pregnane X receptor fluorescent probe. *Bioconjug. Chem.* **2014**, *18*, 18.
192. Hill, K.L.; Dutta, P.; Long, Z.; Sepaniak, M.J. Microcantilever-based nanomechanical studies of the orphan nuclear receptor pregnane X receptor-ligand interactions. *J. Biomater. Nanobiotechnol.* **2011**, *3*, 133–142.
193. Dagnino, S.; Bellet, V.; Grimaldi, M.; Riu, A.; Ait-Aissa, S.; Cavailles, V.; Fenet, H.; Balaguer, P. Affinity purification using recombinant PXR as a tool to characterize environmental ligands. *Environ. Toxicol.* **2014**, *29*, 207–215.

194. Bricelj, V.M.; Connell, L.; Konoki, K.; MacQuarrie, S.P.; Scheuer, T.; Catterall, W.A.; Trainer, V.L. Sodium channel mutation leading to saxitoxin resistance in clams increases risk of PSP. *Nature* **2005**, *434*, 763–767.
195. Bricelj, V.M.; MacQuarrie, S.P.; Doane, J.A.E.; Connell, L.B. Evidence of selection for resistance to paralytic shellfish toxins during the early life history of soft-shell clam (*Mya arenaria*) populations. *Limnol. Oceanogr.* **2010**, *55*, 2463–2475.
196. Roje-Busatto, R.; Ujević, I. PSP toxins profile in ascidian *Microcosmus vulgaris* (Heller, 1877) after human poisoning in Croatia (Adriatic Sea). *Toxicon* **2014**, *79*, 28–36.
197. Parsons, M.L.; Settlemier, C.J.; Ballauer, J.M. An examination of the epiphytic nature of *Gambierdiscus toxicus*, a dinoflagellate involved in ciguatera fish poisoning. *Harmful Algae* **2011**, *10*, 598–605.
198. Martins, A.; Vieira, H.; Gaspar, H.; Santos, S. Marketed marine natural products in the pharmaceutical and cosmeceutical industries: Tips for success. *Mar. Drugs* **2014**, *12*, 1066–1101.
199. Mayer, A.M.S.; Glaser, K.B.; Cuevas, C.; Jacobs, R.S.; Kem, W.; Little, R.D.; McIntosh, J.M.; Newman, D.J.; Potts, B.C.; Shuster, D.E.; *et al.* The odyssey of marine pharmaceuticals: A current pipeline perspective. *Trends Pharmacol. Sci.* **2010**, *31*, 255–265.
200. Imhoff, J.F.; Labes, A.; Wiese, J. Bio-mining the microbial treasures of the ocean: New natural products. *Biotechnol. Adv.* **2011**, *29*, 468–482.
201. Blunt, J.W.; Copp, B.R.; Keyzers, R.A.; Munro, M.H.G.; Prinsep, M.R. Marine natural products. *Nat. Prod. Rep.* **2013**, *30*, 237–323.



MDPI AG  
Klybeckstrasse 64  
4057 Basel, Switzerland  
Tel. +41 61 683 77 34  
Fax +41 61 302 89 18  
<http://www.mdpi.com/>

*Marine Drugs* Editorial Office  
E-mail: [marinedrugs@mdpi.com](mailto:marinedrugs@mdpi.com)  
<http://www.mdpi.com/journal/marinedrugs>





MDPI • Basel • Beijing • Wuhan • Barcelona  
ISBN 978-3-03842-108-5 Volume 1-2  
ISBN 978-3-03842-109-2 Volume 1  
[www.mdpi.com](http://www.mdpi.com)

